STRESS-STRAIN CHARACTERISTICS OF ROCKFILL, AND OF CLAYS UNDER HIGH PORE WATER TENSION

A thesis submitted to the

University of London

(Imperial College of Science & Technology)

for the degree of

Doctor of Philosophy in the Faculty of Engineering

by

Ayad Ali El-Ruwayih, B.Sc. (Eng).

March 1975.

ABSTRACT

This thesis is composed of two separate parts as will be shown in the text. Part I deals with the stress-strain characteristics of rockfill materials. The results of some of the recent research on the behaviour of rockfill under laboratory conditions are critically reviewed. The pre-peak deformations of granular materials are studied with respect to various elastic and plastic models. Several series of drained, undrained and cyclic loading triaxial tests under various stress-density conditions were carried out to investigate the behaviour of rockfill at failure. The results are compared with other published data on rockfill and sands. Agreement is found in some cases and disagreement in others.

For studying the pre-peak deformation behaviour of rockfill a series of constant stress ratio tests was carried out. The elastic and the plastic deformations are examined. A new mathematical equation is suggested for the relationship between the strains and the applied mean normal stresses. This equation is different from that suggested by the Cambridge research group. For a more advanced study, a series of special stress path tests was carried out. For these tests lateral strain measuring devices and a 10 ton load cell were developed. Nitryle rubber membranes were manufactured to resist the deterrent effect of the oil which was used to permit the functioning of the transducers. The results of these tests show that the plastic strain increment vectors along a stress path rotate as the stress level increases which confirms the observations obtained from the constant stress ratio tests. Thus the plastic potentials are not unique and symmetrical about a certain axis. It was also found that the plastic strain increment vectors at a stress point are path-dependent, i.e. they depend on the direction of the stress increment. These observations are in agreement with the findings of some researchers and contrary to those of other workers. Finally analyses of the results showed that the classic behaviour is compatible with the concept of a stress-developed

elastic anisotropy; furthermore the material appears to have only a small "memory" of the previous stresses operating on it.

In the second part of the thesis the stress-strain properties of clays under high pore water tensions were investigated. The release of the confining pressure from fully consolidated, saturated, clay samples produces considerable pore water tensions. The mechanical behaviour (particularly strength and brittleness) is controlled by these pore water tensions.

A theoretical estimate is made of the magnitude of the pore water tensions and the change in strength due to stress release. An experimental programme was carried out in two clays consolidated in the triaxial apparatus under a wide range of pressures. The results indicated that it is the equivalent pore diameter which controls the pore water tension above which the sample ceases to remain fully saturated. The results also showed that above this limit the loss in strength is substantial.

The experimental programme also showed the effect of high pore water tensions on brittleness. A large, undrained, reduction in total stress caused the failure mechanism to change from a plastic failure, with some strain softening, to a brittle failure with sample shattering. Finally, the significance of the results with respect to sampling and testing of soils for engineering purposes is considered.

CONTENTS

NOTATION

D	Diameter of the sample (cylindrical sample)
H	Height of the sample
V	Volume of the sample
d	Particle diameter
e	Void ratio
n	Porosity
n_i	Initial porisity of the sample
subscript i	Refers to conditions as stated above
subscript c	Refers to conditions at the end of consolidation
subscript f	Denotes "at failure"
$\sigma'_1, \sigma'_2, \sigma'_3$	Major, intermediate and minor principal effective stress
$\epsilon_1, \epsilon_2, \epsilon_3$	Principal strains
ϵ_v	Volumetric strains
$\Delta\epsilon_v$	Volumetric strain increment
γ	Shear strain $= \frac{2}{3}(\epsilon_1 - \epsilon_3)$
$\Delta\gamma$	Shear strain increment
p'	Mean principal effective stress $= \frac{1}{3}(\sigma'_1 + 2\sigma'_3)$
q	Principal stress difference $= (\sigma_1 - \sigma_3)$
ϕ'	Angle of shearing resistance
ν	Poisson's ratio
E	Young's modulus of elasticity
R	Stress ratio $= \sigma'_1 / \sigma'_3$
D	Dilatancy factor $= 1 + \frac{d\epsilon_v}{d\epsilon_1}$
K_o	Earth pressure coefficient at rest.

Other symbols will be defined where introduced in the text.

ACKNOWLEDGEMENTS

The research for this thesis was carried out in the Civil Engineering Department of Imperial College of Science & Technology, headed by Professor A.W.Skempton, in the Soil Mechanics Section under Professor A.W.Bishop.

The writer is very greatly indebted to Professor A.W.Bishop and Dr. A.E Skinner, his supervisors, for their help and kindness during the experimental work, and the preparation of this thesis.

The writer expresses his deep graditude to Professor A.W.Bishop who suggested the topic of the second part of the thesis. Throughout the work Professor Bishop provided a great deal of assistance in analysing the results and always took a keen interest. During the present study the writer was a junior author with Professor A.W.Bishop and Dr. N.K.Kumapley in a paper which is being published by the Royal Society, and is now in proof.

Similarly the writer thanks Dr. A.E. Skinner who has at all times done his utmost to help the writer throughout the work. Dr. Skinner suggested the topic of the first part of the thesis, helped in designing the various parts of the apparatus used and read the draft with many constructive comments and suggestions. Also Dr. Skinner helped generously in analysing the results and drawing the conclusions.

Thanks are also due to other members of the academic staff for their help during the work, in particular, Dr. P.R.Vaughan. The writer is also grateful to Mr. D. Evans, the Chief Technician, for his generous help and technical assistance throughout the work especially the kindness and sympathy he gave during the last stages of preparation of the thesis. Also the help and technical assistance of the Soils Laboratory staff, Messrs. E. Harris, L. Spall, F. Evans, C. Gagg and Mrs.E.Gibbs are gratefully acknowledged.

The writer would also like to thank his colleagues, Messrs. J.P. Apted and L.D. Wesley for reading and correcting a large part of the draft. Also Mr. Spouse, Director of DIPCO Ltd., of Slough, is gratefully acknowledged for the technical help and for the material supplied for the nitryle rubber membrane production. The photographic reproductions are by Miss J. Gurr and the writer wishes to thank her for her assistance.

Thanks are also due to the Government of Iraq for the financial assistance provided throughout most of the work. Finally the writer would like to thank Miss E. Niblock who not only typed this thesis, but went to considerable trouble to ensure its correctness.

PART I

STRESS-STRAIN CHARACTERISTICS OF ROCKFILL

CHAPTER I

INTRODUCTION

1.1 Historical Background

Rockfill materials have increasingly been used during the last decade in dam construction, and are now finding uses in road construction and foundation engineering. The reasons behind their use have been widely discussed in the soil mechanics literature, e.g. the 1958 ASCE Symposium on rockfill; Sherard et al, (1963); Pigeon, (1969); Tombs, (1969) and Hirschfeld and Poulos, (1973). In the future the number of earth and rockfill dams being built will be much greater than in the past, due to economic development all over the world, and especially agricultural development to satisfy the need for more and more food. Therefore it is the responsibility of design engineers to rationalise their designs as much as possible to cope with the soaring cost of civil engineering construction. In this thesis it is hoped that some light will be shed on the behaviour of rockfill materials, and to help the design engineers in their decisions. Before reporting the experimental results obtained from this research it is necessary to review the previous work done in this field.

In 1958 the ASCE held a symposium on rockfill dams, at Portland, Oregon, U.S.A. Many of the papers presented there were concerned with settlement and little attention was given to evaluating the angle of shearing resistance.

Generally, up to the time of the ASCE symposium, the angle of shearing resistance ϕ' was estimated from the angle of repose of dumped rockfill. This procedure tends to be too conservative because large pieces of rock usually possess considerable momentum when tipped.

As far as the compressibility of rockfill is concerned, most of the conclusions reached, up to the time of the ASCE symposium, were based on observations of the performance of complete structures. The performance of dams was generally good, due to the design

assumptions, such as a well-graded material is desirable for dam construction and that sluicing the rockfill material with water as it was dumped or placed was a reasonable method for reducing the settlement of the dams. At that time there were few studies concerning the compressibility and strength of coarse materials, e.g. Kjellman and Jakobson (1955).

Terzaghi (1960) presented the first formal stress-strain curves for graded rockfill. These were from observations during the construction of Buo Hanifia Dam, Algeria. Terzaghi showed that the compressibility of rockfill increases in the intermediate range of stress. Of course he was aware of the influence of particle breakage although this subject had not yet been investigated extensively.

Since 1960 many laboratory investigations have been carried out to study the stress-strain characteristics of rockfill. The most important laboratory studies were probably those reported by Kjaernsli and Sande (1963); Billam (1967); Marsal's work (1963 - 1969); Lee and Farhoomand (1967); Fumagalli (1969); Pigeon (1969); Tombs (1969); Marachi et al (1969); Yee (1972) and Charles (1973).

The deformation behaviour of rockfill dams has also been observed in recent years and there are many reported studies in this field, e.g. Pope (1967); Penman et al (1971); Penman and Charles (1971 and 1972); Marsal (1972); Alberro (1972) and Nobari and Duncan (1972).

From this brief historical introduction it can be seen that the study of the properties of rockfill is at an early stage compared with the study of clays and sands. A thorough understanding of the physical properties of rockfill materials is essential both for the use of current methods of design and also for further progress in the field of high dam construction.

For an earth dam the physical properties of the materials can be estimated by testing a soil sample in the laboratory under conditions similar to those existing in the field (e.g. type of material, compaction, saturation, loading conditions and consolidation conditions). In other

words, the laboratory tests should simulate the field conditions.

As far as rockfill dams are concerned, simulation of the field conditions in the laboratory is difficult and sometimes impossible. This is because rockfill materials usually include large particles (sometimes of the order of a few feet in diameter). Under such conditions a very large triaxial cell is required for testing rockfill samples. Therefore, it seems, problems arising from large particle sizes have imposed serious difficulties in simulating field materials in the laboratory.

Alternative methods have been suggested to overcome the above difficulties and to provide a reasonable assessment of the properties of rockfill materials.

One of these methods was suggested by Zeller and Wulliman (1957). This method implies the sieving out of the coarse fractions, then establishing the corresponding grading curves. Drained triaxial tests were carried out on each of the samples having these corresponding gradings at a confining pressure of 0.9 kg/cm^2. The strength versus porosity relationships were established from which curves in the form of strength versus maximum grain size for different porosities were plotted. Then it was possible to estimate approximately the shear strength of the material in the field*.

Another method was suggested by Lowe (1964). This method implies testing model samples which represent prototype materials from the field. Each particle of the model sample was one-eighth the size of the corresponding particle in the prototype material. In other words the gradation curve of the model sample was obtained by shifting the gradation curve of the prototype material parallel to itself to the side which represents the finer particles. Therefore it was assumed that " ... in models of coarse fractions where the only difference between prototype material and model sample is the difference in size of particles, the model sample should closely duplicate the behaviour of the prototype in shear".

---

* Here the gradation and uniformity coefficients for these materials are different.

Lowe justified his assumption by theoretical analysis of the contact stresses for regular packing of ideal spheres. Both the previous methods and their application will be discussed in the next chapter.

Many attempts have been made* to analyse the properties of rockfill and coarse granular materials on the basis of an assembly of ideal spheres made of certain material (e.g. glass, steel, plastic, etc.). Such attempts do not provide a reasonable simulation because the modelled spheres have different elastic properties E and ν, surface texture, crushing strength, size and shape. Besides that, the complexity of the packing of rockfill particles cannot be simulated in the laboratory properly by artificial spheres. Therefore the theoretical analysis of the behaviour of regular and random assemblies of artificial spheres is not applicable directly to rockfill materials.

There have been quite a lot of investigations (as will be seen in the next chapter) into the properties of rockfill materials, but unfortunately most of them were carried out under different conditions; i.e. different apparatus, porosities, grading, particle size, and type of material, as well as stress and testing conditions. Thus it is improper and sometimes impossible to correlate the results and make reasonable conclusions about certain points. There are a few studies which have been carried out under an organised programme (e.g. Tombs, 1969 and Pigeon, 1969), but these need expansion in order to reach clear conclusions. Therefore in this thesis it was thought better to select a material which had been investigated previously under certain conditions and to use apparatus which is widely used in soil mechanics investigations. Hence one can draw wide conclusions, and make correlations of results with others. For these reasons the Granite Gneiss rockfill was chosen to be tested in a triaxial apparatus system.

---

* Farouki and Winterkorn (1964); Mogami (1969); Leussink and Brauns (1969).

1.2 Approaches in Soil Engineering Design

In soil engineering there are mainly two criteria used in the design of earth structures and foundations; these are:

1. Limit Equilibrium Condition. In this case a reasonable factor of safety is taken into consideration to ensure that failure conditions are not reached.

2. Deformations of soils below failure conditions are acceptable within certain limits. In this case the deformations are based on pre-peak stress-strain behaviour.

In the early days of soil mechanics science most of the research and designs were restricted to peak strength and failure criteria. But with advances in research in this subject more emphasis has been placed on deformations of soils at stress levels well below failure. Clays and sands have been under study in the past ten years in many research institutions and various theories have been suggested; some of them agreeing with each other while others are contradictory. Recently the understanding of the stress-strain behaviour of soils at pre-failure conditions has become increasingly important following the rapid development of computers and numerical methods of analysis. In particular the finite-element method seems to be quite useful for soil mechanics analysis, especially for embankment dams. Therefore development of complicated mathematical models to express the deformation of soils at pre-failure conditions became the object of researchers although in the past these had been undesirable and impractical for analysis.

Thus the need for a mathematical model to express the deformation behaviour of soils is obvious; otherwise empirical or semi-empirical methods will be dominant in all design decisions. Due to the wide range of natural soils it would be unrealistic to expect a single model to represent all soils; instead different types of soils may require different types of models. Moreover for one type of soil different models may be needed to express the various stages of

deformation up to post-peak stage.

The study of the yielding of cohesive soils, especially normally consolidated clays, is more advanced than that of cohesionless soils; i.e. sands and silts. The studies on yielding of cohesionless soils are still in their early state. As far as rockfill materials are concerned, such extensive studies are not reported in the literature. The purpose of this thesis is to study some of the fundamental properties and yielding of rockfill materials.

1.3 Outline of the Research Programme

In this part of the thesis (i.e. the part concerning the properties of rockfill materials) two main attempts have been made to investigate the behaviour of rockfill materials:

Firstly to study the strength and deformation of rockfill material at failure conditions; Chapters 2, 6 and 8. This study covers many important points and needs to be expanded in the future to give a clear picture of the behaviour of Granite rockfill.

Secondly to investigate the plastic behaviour of rockfill at pre-failure stages and to examine the applicability of many existing plastic models for rockfill, Chapters 3, 7 and 8. For this study a thorough analysis of the elastic and plastic deformations of rockfill was required. For this purpose the conventional triaxial apparatus was modified to provide proper testing conditions. A new device to measure directly the lateral deformations of triaxial samples was developed. Nitryl rubber membranes were also developed to withstand the detrimental effect of oil, which was used as a cell fluid to permit the functioning of the electrical lateral strain devices. The discussions and conclusions reached will be presented in Chapters 7 and 8.

CHAPTER II

LITERATURE REVIEW OF SHEAR STRENGTH AND DEFORMATION OF ROCKFILL MATERIAL

As far as the properties of rockfill material are concerned there are two types of studies: first, a general study of the properties of rockfill for design and construction purposes, second, a study of the influence of certain factors on the properties of the rockfill material such as sample size, grain strength, grading, etc. In the first three sections of this chapter the general study of the stress-strain characteristics of rockfill will be reviewed and in later sections the factors influencing the properties of rockfill will be discussed.

2.1 The Drained Shear Strength of Rockfill Material Under Triaxial Conditions

Kjellman and Jakobson (1955) reported a series of tests on uniform, fine and coarse gravel and macadam, in both dense and loose states. The gravels were rounded, whereas the macadams were angular materials. The maximum grain size tested was 5 cm and the samples were 50 cm diameter and 100 cm high. The main feature of the apparatus used is that the sample is surrounded by confining rings of mild steel each 5 cm deep and 1.8 cm thick, spaced apart by 2 mm.

In the oedometer tests it was noticed that the angular material compressed approximately 5 - 6 times as much as the rounded material at similar porosities and stresses. Considerable particle breakage occurred and sample compaction induced a state of overconsolidation because Young's Modulus decreased during the first load increments and then increased. Very little rebound occurred on removal of the normal load from a sample of macadam but a more noticeable amount occurred with the pebbles. Because of the creep the load increments had to be applied at two-hourly intervals.

It was concluded that Poisson's Ratio for laterally confined coarse grained materials was constant during the first loading,

irrespective of pressure, grain size or shape and sample density and corresponded to a value of $K_o = 0.44$.

During shearing, the loose samples tended to consolidate, whereas dense samples consolidated and then dilated. The rounded materials dilated more than the angular. It seems that the grain size has little effect on volume changes in the applied stress change although grain shape was an important factor, angular grains deforming more than rounded ones. The range of particle sizes used in the testing programme was insufficient to detect effects due to grain size because the number of contacts and hence the contact forces were not comparable and the stress range was also very limited.

Lewis (1956) carried out a series of drained shear tests on uniform gradings of granite in shear boxes and triaxial apparatus. All the gradings tested were geometrically similar and the particle shapes were also similar. The tests were run wet and all the initial densities were also the same.

The triaxial tests* gave values of ϕ' approximately 3^o higher than the shear box tests. This was attributed to the more uniform distribution of stress in the triaxial tests. Also, the actual state of stress is unknown in the shear box. In the shear box tests the principal stresses are inclined and the usual planes of failure at $45^o - \frac{\phi'}{2}$ to the maximum principal stress do not coincide with the forced failure plane between the two halves of the shear box. During the test the outside edges of the sample failed before the centre and these two effects oppose each other. The actual area being sheared is constantly diminishing during the test and sheared material bears on the end of the shear box.

---

* A number of conclusions were drawn up from the shear box test results which are not included in the subject matter of this thesis.

Zeller and Wulliman (1957) carried out triaxial tests on shell materials for the construction of Geoschenenalp Dam in Switzerland. The maximum particle size was less than 1/5 of the diameter of the sample. The triaxial apparatus was capable of testing samples 505 x 900 mm, 252.5 x 500 mm, 160 x 250 mm and 80 x 150 mm. The large triaxial cell was a vacuum type designed by Bjerrum in 1957 for the design of the Marmorera Dam. The cell was modified so that a confining pressure up to 78 psi could be applied. The deviator stress was assumed equal to

$$\sigma'_1 - \sigma'_3 = \frac{P}{A_o} (1 - \epsilon_1)$$

where P was the applied deviator load, A_o the initial sample area, ϵ_1 the axial strain, and the volume changes were negligible.

The main conclusions of that investigation were:

1. The maximum shear strength for any given porosity was achieved with the grading containing the minimum particle size. The reason for this may be due to:

   a) The unit particle strength is probably greater with small particles because of the smaller incidence of flaws and hence a greater dilatancy takes place rather than breakdown.

   b) With a more uniform grading, the rate of dilatancy is greater at failure. The contact forces are higher with uniform material but the mean applied stresses were quite low so that particle breakdown, in this case, would not have had a predominant influence on the results.

2. For a given grain size distribution the shear strength shows a large increase with decreasing porosity.

3. A decrease in shear strength of 10 - 15% was found in the case of testing saturated samples, and that is probably due to a lubricating effect at the contact surfaces.

4. For a given porosity the differences in shear strength decrease with increasing maximum grain size, Figure (2-1a).

Schultze (1957) described a vacuum triaxial apparatus for testing samples 50 cm diameter by 130 cm high to measure the shear strength of a slatey greywacke material. Lateral strains were recorded from the extension of a circumferential belt at the sample mid height. Six tests were carried out on dense samples (bulk density 1.87 T/m^3) at confining pressures of 0.25, 0.50 and 0.75 kg/cm^2. The Mohr envelope gave an angle of internal friction of 43^o and a cohesion intercept of 0.46 kg/cm^2. Nine tests, carried out on loose samples (bulk density 1.55 T/m^3), indicated an angle of internal friction of 42.2^o and a cohesion intercept of 0.095 kg/cm^2. Field shear tests were carried out and confirmed the above results. In addition samples of gravel and other gravelley soils were tested. The angle of internal friction varied between 45^o to 28^o over a wide range of porosities. Schultze's main conclusions are:

1. Direct and triaxial large shear tests make it possible to investigate materials with coarse particles for earth dams.

2. Whether the Mohr envelope up to 1.5 kg/cm^2 is also accurate enough for higher normal stresses depends on the material tested. In general, the Mohr envelope is not so curved at the beginning, so that larger errors do not appear.

3. The big triaxial apparatus is not suitable for cohesive soils.

4. The coarse fraction in the soils mentioned produced a higher shear strength. Consequently sieving out the coarse fraction and testing the remainder in the small instrument is unrealistic.

5. Density of the soils tested does not affect the angle of internal friction, but it does affect the cohesion intercept and compressibility.

6. Exact details of the relationship between the largest grain diameter and the instrument diameter have yet to be determined by comparative tests in large and small instruments. Up to now, the ratio of the grain size to the instrument diameter has not exceeded 1:5.

Comparison between the results obtained for various sizes of sample is complicated by the use of different types of apparatus as well as various ratios of maximum particle size to sample size. This ratio may well vary for triaxial and shear box samples.

Leslie (1963) tested gravelley soils at confining pressures ranging from 60 - 650 psi to study the effect of particle size, gradation, particle breakdown and confining pressure on the angle of internal friction. Samples tested were 5.9 x 13.8 in., 6 x 12 in. and 12 x 24 in. dia. and height respectively. The 12 x 24 in. sample was later altered to 12 x 27.6 in.

As far as particle size and gradation were concerned, two series of triaxial tests were carried out. In the first series the uniformity coefficient of the gradings were 3.3, 4.7, 6.7 and 9.4. It has been observed that for each grading the angle of internal friction increases with the increase of density. At maximum density the strength increases with the increase in maximum size.

In the second series of tests all gradings held a uniformity coefficient of 3.3. It was found that there is an increase in the angle of internal friction with increase in the density of each gradation. Similarly, as in the first series, the maximum density obtained for each gradation increased with maximum size, but reached a maximum value for the 1 in. and 2 in. maximum sizes. Other gradations were also tested to investigate the shear strength of rockfill.

It was concluded that:

1. Shear strength of alluvial gravelley soils under high confining pressures is in the range of 35^{o} - 40^{o}.

2. Over-size particles did not have as great an effect on shear strength as initially thought.

3. Particle breakage is dependant on the mineral composition, structure, texture, friability, weathering, brittleness, hardness and particle shape.

4. The angle of internal friction decreases with increasing confining pressures. As a result the Mohr envelope is not a straight line over a wide range of confining pressures.

Hall and Gordon (1963) reported a series of tests to obtain the shear strength parameters of sandy gravel material and clayey sand for the construction of the Oroville Dam. Material up to 3 in. maximum size was tested at confining pressure up to 125 psi in a sample 12 in. dia. and 27.6 in. high, and $1\frac{1}{2}$ in. maximum particle size up to 650 psi in a 6 in. diameter by 13.8 in. high sample.

Drained tests were carried out on sandy gravel material with density ranges from 144 - 150 lb/ft^3. The angle of internal friction decreased from 43^o at low pressures to 37^o at high confining pressures. This indicates that the shear strength at high confining pressures is 12 - 15% below that which would be obtained by an extrapolation of the results from tests carried out in the usual range of confining pressure. It is concluded that the decrease in slope of the Mohr envelope is a result of particle breakdown under shearing strains. It is also concluded that particle degradation is a function of the gradation of the individual soils with better-graded soils displaying the least degradation.

Undrained tests on clayey and silty materials were carried out. After consolidation the degree of saturation was approximately 95%. Within the pressure range used, no decrease in the slope of the Mohr envelope was noted as in the previous material.

For the design of the 360 ft. high Shikmen Dam in Taiwan, Lowe (1964) carried out tests on gravel and cobble materials passing a 12 in. sieve. A geometrically similar grading was made up with a

maximum particle size of $1\frac{1}{2}$ in. and drained tests were carried out on samples of 6 in. diameter. Confining pressures used were 50, 100 and 200 psi and a back pressure of 100 psi to ensure full saturation. The Mohr envelope for the loose samples was a straight line with an angle of internal friction of 41^{o}. For the dense samples, the Mohr envelope was also straight and the angle of internal friction was 43^{o}. Therefore it was concluded that the Mohr envelope is approximately a stright line up to 200 psi confining pressure, and it might be curved over a wide range of confining pressures. Finally there was an agreement between results of consolidated drained and consolidated undrained tests.

Marsal (1965a) carried out a testing programme to study the properties of materials involved in constructing El Infiernillo Dam in Mexico. According to Casagrande's recommendations a large triaxial apparatus was constructed capable of testing samples 113 cm diameter and 250 cm high at confining pressures up to 25 kg/cm^2. This apparatus could be used to test plane strain samples 75 x 75 x 180 cm under confining pressures up to 25 kg/cm^2. Another large vacuum triaxial apparatus for testing the same sample sizes but under low pressures has been constructed. In addition, a triaxial apparatus was designed to test samples of 20 cm diameter by 50 cm high at confining pressures up to 50 kg/cm^2.

Two oedometers were also designed, one to test samples 50 cm diameter by 50 cm high at normal stresses up to 32 kg/cm^2, and the other, samples 114 cm diameter by 60 cm high at normal stresses of 100 kg/cm^2. In addition, a direct shear apparatus for testing samples 20 x 30 cm under a maximum normal pressure of 75 kg/cm^2 was designed.

Many conclusions have been drawn from that study, mainly:

1. Triaxial tests on dry sand samples of 113 cm diameter and 250 cm high at 1 kg/cm^2 confining pressure showed that the Mohr envelope was curved.

2. In triaxial tests on dry rockfill samples of 113 cm diameter and 250 cm high, there was a decrease in ϕ'_f from 45^o to 37^o when confining pressures increased from 1 to 25 kg/cm^3. Under high confining pressures, the failure vertical strains are higher. The mode of failure was by bulging, not on single failure planes except in tests where σ'_3 is less than 5 kg/cm^2.

3. There was a dilation in samples tested up to 10 kg/cm^2 confining pressures, while for samples tested under higher confining pressures there was a volume decrease.

4. Tests on gravelley materials gave the same trend in results as tests on rockfill. There was a reduction in ϕ'_f from 53^o to 39^o when confining pressure increased from 0.4 to 25 kg/cm^2.

5. Particle breakage is a function of the mean intensity of the contact forces developed during the test and of the average strength of the particles to compression (q_u). This can be expressed as:

$$B = F\left(\frac{\sigma}{N_s} \quad , \quad \frac{1}{q_u}\right)$$

where B denotes the particle breakage factor

N_s denotes the number of particles

and σ denotes the mean normal stress.

Nitchiporovitch and Rasskazov (1967) tested coarse fragmental materials used in construction of Nurek, Charvak, Sarsang and V.Tobol dams in Russia. The investigation covers laboratory and field tests using both shear box and triaxial apparatus. The main conclusions they arrived at are:

1. The angle of internal friction of coarse fragmental soils depends mainly on the degree of compaction, state of stress and size of the particles being tested.

2. The angle of internal friction of coarse materials decreases with an increase in the stresses which can be explained by particle crushing both during consolidation and shearing.

3. The shear strength of natural soils can be investigated on model mixes with an identical shape and strength of the natural and the modelled particles.

4. Particle size of coarse soil affects the angle of internal friction.

5. There were differences in results between shear box tests and triaxial tests.

The U.S. Army Corps of Engineers (1967) carried out tests on crushed basalt and metavolcanic rockfill. Samples tested were 12 in. and 6 in. diameter depending on the maximum grain size. The dense samples were at a relative density of 95% to 100% and the medium dense at about 70% to 75% relative density. It was concluded that:

1. Both the metavolcanic and basalt rockfill had equal shear strength.

2. The shear strength increased with sample density.

3. The shear strength increased with increasing coefficient of uniformity.

4. The angle of internal friction decreased with increasing confining pressure.

5. There is a considerable increase in strength between the gradings with $\frac{1}{4}$ in. and 3 in. maximum particle sizes.

However, it has not been explained how (3) and (5) above gave that difference in shear strength of rockfill.

Huder and Fetz (1967) described tests on talus materials used for the shoulders of the Goeschenenalp Dam. Maximum particle sizes tested were 100, 30, 10 and 1 mm. The authors suggested that the porosity of the material can be converted to that corresponding to a basic particle size in conjunction with other conditions. The formula for converting the porosity (n) of a sample of particle diameter (d) to that of a larger diameter (D) is:

$$n_D = n_d (1 - P) + P (1 - P_\gamma)$$

where n_D and n_d denote the corresponding porosities

P denotes the percentage of "over size" grains

P_γ denotes a conversion factor that can be read from plot of P_γ vs. maximum particle size.

They concluded that the use of the value of density determined on limited particle-size samples to predict the density of the larger size is only valid when the coarse particles are not in direct contact but are surrounded by finer-grained aggregates. Comparisons between shear strength of such material is possible when the above-mentioned condition was fulfilled.

Tombs (1969) carried out a series of triaxial tests on Silurian Cleaved Mudstone, Granite Gneiss and Chert Gravel. The samples tested were $1\frac{1}{2}$ in. dia. x 3 in. high, 4 x 8 in. and 12 x 24 in. The aim of the investigation was to study the effect of gradation and particle size on the shear strength of rockfill material. Confining pressures used ranged between 10 - 500 psi. It was concluded that a reasonable evaluation of field shear strength of rockfill could be carried out in the laboratory. The detailed conclusions arrived at will be discussed in the following sections of this chapter.

Marachi et al (1969) carried out tests to investigate the stress-strain characteristics of three types of rockfill, Pyramid Dam material (an angular argillite), crushed basalt and Oroville Dam material. Triaxial shear tests were carried out on samples of diameter 2.8 in, 12 in. and 36 in. Gradation of the samples tested is shown in Figure (2.1b). A series of plane strain tests was also carried out on the same materials. The detailed conclusions will be discussed in later sections.

Nash (1971) discussed some of the work which has been done on rockfill in the past few years. The difficulty he encountered was the wide range of materials tested with different equipment and different testing conditions. Nash's work was a review and so presented no new data. There are other investigations which will be discussed in the following sections, e.g. the contributions to Speciality Session No. 13, 7th International Conference SMFE, Mexico 1969; Billam, 1971, etc.

2.2. The Drained Shear Strength of Rockfill Material Under Plane Strain Conditions

Although the drained shear strength of rockfill under plane strain conditions is outside the scope of the experimental programme of this thesis, it is thought that a brief review of the subject will help in understanding the behaviour of the rockfill material. Very limited work has been done as far as rockfill is concerned and usually sand was taken as a guide for design purposes.

Cornforth (1964) carried out the first comprehensive study of the properties of sand under plane strain conditions. Samples of brasted sand 2 in. wide, 16 in. long and 4 in. high were tested in plane strain apparatus. Intermediate principal stresses were estimated by a null mercury meter. It was noted that the angle of internal friction for the dense sand under plane strain conditions was 4^{o} greater than that for triaxial conditions. This difference decreased as the initial porosity increased. For loose sand the difference was only $\frac{1}{2}^{o}$. Similar results have been reported by Sultan and Seed (1967) for tests on Monterey Sand and Ottawa Sand.

Cornforth (1964) also demonstrated that volumetric strains at failure were more dilatant for the triaxial samples than for plane strain samples. This difference between the two decreased as the initial porosity was increased. It was also found that the axial strain at failure was higher for triaxial tests than for plane strain tests, and the difference in this case increased as the initial porosity of sand increased. The residual strength in both triaxial and plane strain tests was found to be approximately the same. The data also indicated that the initial tangent modulus for plane strain was greater than that for triaxial conditions.

To explain the reason for the differences noticed between the shear strength of plane strain and triaxial test samples, Cornforth (1964) considered that "In the plane strain test, the sand grains are least free to move in a random direction in the horizontal plane." Therefore "... the influence of the intermediate stress is through its relationship to the external strain condition acting on the soil. This in turn reflects the internal freedom of movement of the sand grains during shear." He therefore concluded that "The numerical value of the intermediate principal stress has no importance on strength." and that the strain condition during shear is the major factor contributing to strength of sands.

Leussink and Wittke (1963) published results of triaxial and plane strain tests on samples composed of glass and steel balls 1.5 cm in diameter. The plane strain samples were 20 cm wide, 100 cm long and 60 cm high. The triaxial test samples were 20 cm in diameter and 50 - 70 cm in height. The experimental results showed that for a quadratic packing of spheres, there was a slight increase in the maximum principal stress ratio for plane strain conditions over that for triaxial test conditions. For a hexagonal packing with a porosity of 0.26 the angle of internal friction in the triaxial test was 40.7^{o}, while in the plane strain test it was 51.4^{o}.

There are many other research workers who carried out extensive investigations on the behaviour of sand in plane strain conditions (Marachi et al 1969; Green, G.E. 1969 and 1971; and Reades, D. 1972, etc.).

As a summary of the previous work done, it is demonstrated that there are differences in the strength and deformation characteristics of sand when tested under plane strain and triaxial conditions. To compare with triaxial samples, a dense sample of sand when sheared under plane strain conditions will show higher strength, greater initial tangent modulus, smaller failure strain, less dilation, and equal residual strength.

Now after that brief introduction on the behaviour of sand under plane strain conditions, the behaviour of rockfill will be reviewed. To the author's knowledge, there is a very limited amount of work which has been done in this field.

Marsal (1965b) presented details of plane strain apparatus for testing samples 0.75 x 0.75 x 1.80 mrs at a confining pressure up to 25 kg/cm^2. The cell was installed at the laboratories of the Comision Federal de Electricidad in Mexico. Materials tested were

silicified conglomerate from El Fiernillo Dam and granite gneiss rockfill. The cell was at an early stage of construction and few data were published, Figure (2.2). It was noticed that samples tested under plane strain conditions gave angles of internal friction higher than those under triaxial conditions by an average of 13^{o}.

Marsal et al (1967) carried out plane strain tests using the apparatus installed at the laboratory of the Comision Federal de Electricidad in Mexico and which had been designed previously by Marsal (1965b). Prismatic samples 0.75 x 0.75 x 1.8 m of sand gravel from Pinzandaran and sound basalt were tested. The maximum confining pressure was 22 kg/cm^2. The axial and lateral strains that could be reached were 15% and 20% respectively.

From the few tests carried out, it was found that the axial and the volumetric strains are comparable to those recorded in conventional triaxial tests with similar materials. Ratio between principal stresses σ_2/σ_1 and $\frac{\sigma_2}{\sigma_1+\sigma_3}$ resulted approximately constant in the interval $5 \leqslant \sigma_3 \leqslant 15$ kg/cm^2. It was also noted that the failure strains were very large compared with those obtained by Cornforth (1964) on brasted sand.

From the short previous review it appears that the properties of rockfill material need to be investigated thoroughly under generalized stress-strain conditions.

2.3 Undrained Shear Tests on Rockfill Material

There are quite a lot of data on the properties of sand under undrained shear conditions but unfortunately very little work has been done on rockfill material. Ensuring full saturation of rockfill samples is one of the main problems in undrained testing. Sand samples could be set up by deposition under water while rockfill material undergoes segregation if deposited under water. Saturation of rockfill samples

by water percolation might leave some air bubbles between the particles and therefore full saturation cannot be achieved.

Lowe (1964) tested shell materials for the construction of Shihmen Dam, Taiwan. The drained shear tests have been discussed in Section 2.1. A 9^{o} difference in the angle of internal friction was found if the sample was saturated using 100 psi back pressure rather than saturated by percolation of water. A close agreement was found between the consolidated drained and the consolidated undrained tests in terms of angle of internal friction.

Tombs (1969) carried out a series of consolidated undrained tests on silurian mudstone and granite gneiss using samples of 12 in. diameter with maximum particle size of 3 in.

For the consolidated undrained tests on dense silurian mudstone, the angle of internal friction at peak deviator stress was approximately 5^{o} above $\phi'f$ corresponding to zero dilatancy obtained from drained shear tests. The stress path was very similar to that for a dense sand. Tombs believes that membrane effect may have been about 2.2 psi in that test. A loose sample was consolidated then sheared undrained. There was a very high pressure built up at the beginning of the shear stage and the stress path was similar to a loose sand. Again ϕ' at peak deviator stress was greater than that at zero rate of dilatancy for drained shear samples.

For the granite gneiss a dense 12 in. diameter sample of R_d = 85% was tested. The value of ϕ' at peak deviator stress was 46^{o} which is higher than that corresponding to zero rate of dilatancy for a drained sample*. A loose 12 in. diameter sample was also tested which behaved in a similar way to loose sand.

---

* $\phi'f$ corresponding to zero rate of dilatancy was 41^{o}.

Also Tombs (1969) described two consolidated undrained tests on mudstone using 4 in. dia. samples carried out by Dr. Bros at Imperial College. The samples were of medium relative density and consolidated at 75 psi and 25 psi. The stress path of the sample consolidated at σ'_3 = 75 psi was similar to that for a dense sand while the stress path of the sample consolidated at σ'_3 = 25 psi was different to that of loose sand. In both tests the values of ϕ' at peak deviator stress were greater than that at zero rate of dilatancy for corresponding drained shear tests.

The differences in the stress paths between the 12 in dia. sample tested by Tombs and the 4 in. dia. sample tested by Dr. Bros showed that the smaller material was more resistant if subjected to undrained loading. The major difference probably arose because of the finer grading (D/d = 4 in 12 in. dia. sample and D/d = 8 in 4 in. dia. sample) and, hence, much lower interparticle forces. Particle breakage would be less and hence pore pressure build up would also be less with smaller materials.

The same as for silurian mudstone, Dr. Bros carried out consolidated undrained tests on 4 in. dia. samples of granite gneis at a medium density. The first sample was consolidated to 75 psi and gave ϕ' at peak deviator stress of 41.8°. This value of ϕ' was about 5° below that of the denser large sample and coincided with the value of ϕ'f at zero rate of dilatancy in drained shear tests. The second sample was consolidated to 25 psi and again a high angle of internal friction was recorded, along with high effective stresses. The angle of internal friction was somewhat higher than that corresponding to zero rate of dilatancy for samples under drained conditions.

From the previous short review three important points were noticed:

1. The rubber membrane stiffness, penetration and thickness relative to the sample particle size: Application of cell pressure causes considerable membrane penetration then subsequent sample consolidation during shear will build up the pore pressure in opposition to the cell pressure and the membrane penetration will be reduced. The flexibility of the membrane will be equivalent to partial drainage. Therefore small values of D/d* will cause large errors in measuring pore pressures.

2. Particle breakage also has a great influence on pore water pressure. Therefore weak rockfill particles probably result in bigger errors than hard ones.

3. As Lowe (1964) pointed out, using high back pressure to ensure sample saturation causes a reduction in the measured angle of internal friction. Therefore high pore water pressure built up during undrained shearing (specially in loose samples) might cause the same effects.

2.4 Triaxial Cyclic Loading Tests on Granular Soils

It has been thought that the behaviour of soils subjected to cyclic loading and unloading may differ from their behaviour during a single loading. Many investigators have described the results of tests on clayey soils in which repeated loading has been used (e.g. Seed et al 1955; Larew and Leonards 1962; Seed and Chan 1966; Sangrey et al, 1969). These investigations were concerned with the overall stress-strain behaviour, and the general conclusion has been that the repeated loading, at a certain stress level, leads to larger deformations than are obtained for a single cycle of loading. It was also found that for many soils total collapse under cyclic loading occurs at stress levels well below

---

* D and d denote sample and particle diameters respectively.

the maximum that can be resisted in a single cycle test. In addition, it has been shown that there are levels of repeated stress that can be tolerated without causing collapse. Larew and Leonard (1962) called the maximum level of repeated stress that will not lead to failure "the critical level of repeated stress".

Cyclic loading tests on sand were mainly used to investigate the liquefaction phenomenon, (Seed and Lee 1966; Lee and Seed 1967). They tested saturated Sacramento sand under undrained conditions and the loading arrangement allowed the application of pulsating stresses on the samples in compression and extension. The resulting pore water pressure increased and was accumulated with each cycle. It was equal to the cell pressure at the point where the pulsating load was zero upon reaching liquefaction.

Liquefaction of loose sands was defined as the onset of developing the maximum pore water pressure, which was equal to the cell pressure, i.e. zero effective normal stress. This was associated with increase in strains, which reached considerable values after an additional cycle or two.

Failure of dense sands by liquefaction occurred in two stages. The first stage was the onset of liquefaction (partial liquefaction) when the strain started to increase. It occurred when some peaks of the pore water pressure reached the value of the cell pressure. In the second stage, liquefaction might be termed the state when at zero pulsating load the pore pressure was always equal to the confining pressure. Failure was reached when strain became excessive. In loose sands, partial and full liquefaction were reached simultaneously. In dense sand, full liquefaction might come after a large number of additional cycles. In some cases, failure could not be reached as the sample was always able to mobilize the resistance to support the applied stresses.

Seed and Lee (1966) showed that at higher confining pressures, the number of cycles required to cause liquefaction was also higher.

They carried out undrained cyclic loading tests at low and high cell pressures, above and below the critical void ratio line of the Sacramento sand. It was observed that the sample at low confining pressure failed after only 56 cycles, while the sample at higher cell pressure, did not fail even after 10,000 cycles of the same magnitude. In the static test the sample at the high cell pressure should develop high pore water pressure, while the sample consolidated at low pressure has the tendency to dilate, and should develop negative pore water pressure. Lee and Seed (1967) showed that when the relative density increased more cycles were required to cause liquefaction.

Lee and Seed (1967) also concluded that the higher the pulsating load, the fewer the number of cycles required to cause liquefaction. An approximate linear relationship was obtained between the pulsating loads and the logarithm of the number of cycles causing liquefaction in the range of 5 - 200 cycles. This was found to be the case for all densities and all confining pressures.

Koizumi and Ito (1969) carried out cyclic loading tests on Niigata sand. They observed an increase of pore water pressure with the cycles, although at this level of stress in a static test the sand showed a tendency to dilate and develop negative pore water pressure.

Castro (1969) carried out an investigation into the liquefaction of sands using a triaxial cell with a special loading mechanism. He carried out drained, undrained and cyclic loading tests to investigate the concept of critical void ratio and liquefaction. His work and interpretation are far from the purpose of the experimental work of this thesis.

Sha'al (1972) carried out few undrained cyclic loading tests on Ham River sand in an experimental programme to investigate the behaviour of cohesionless soils in simple shear under cyclic loading. Again the study concerned the liquefaction of sand.

Barden et al (1969) carried out a series of cyclic loading tests on sand in an attempt to separate the elastic and plastic components of

the deformation. The study was mainly concerned with the application of the stress dilatancy theory.

There appear to be no reports of work on the behaviour of rockfill material under repeated loading. Therefore a few cyclic loading tests were carried out by the author to investigate and compare the behaviour of granite rockfill material.

2.5 Factors Influencing the Shear Strength and Deformation of Rockfill Material

As has been shown in Chapter I, the most important properties of granular materials are their shear strength and compressibility characteristics. Various shear strength theories were mentioned in Chapter I and will be discussed in a later chapter. Here the Mohr-Coulomb criterion is chosen to express the strength of rockfill throughout the discussion*. Thus the strength of granular soils is often expressed in terms of its angle of shearing resistance at a given normal stress.

Compressibility is generally defined as the amount of volumetric strain caused by a unit increase in pressure, expressed mathematically as

$$C = - \frac{d\epsilon_v}{dp}$$

where C is the compressibility and $d\epsilon_v$ and dp are the increments of volumetric strain of the sample and compressive pressure respectively.

There are many factors which could influence the strength and compressibility of rockfill material. For simplicity these factors could be listed as:-

Influence of the state of stress.

Influence of sample properties - This includes the relative porosity (or density), gradation, grain size and the degree of saturation (or moisture condition).

---

* Mohr-Coulomb criterion is relevant to soils (Bishop, 1966).

Influence of the material properties - This includes the grain shape, coefficient of friction of the material, particle strength and particle breakage.

Other factors such as strain rate of the sample.

The above list is similar to that presented by Anagnosti (1967). The literature contains a lot of data on the influence of some of the above factors but unfortunately the conditions of testing or material properties are different which make the correlation and comparison of results difficult.

2.5.1 Influence of the State of Stress and Confining Pressure

Leslie (1963) tested gravelly soils within a confining pressure range from 60 - 650 psi and noted that the angle of shearing resistance decreases with increasing confining pressure.

Hall and Gordon (1963) carried out tests on dredged tailings, which were composed of sandy gravel soils, at a confining pressure up to 650 psi. The angle of shearing resistance ranged from 43^{o} for low pressure to 37^{o} for high pressure. This shows that the Mohr envelope is not a straight line. They concluded that the decrease in slope of the Mohr envelope is a result of particle breakdown under shearing strains.

Insley and Hillis (1963) tested glacial till material at a confining pressure up to 450 psi and showed that there is a decrease in slope of the Mohr envelope by 2^{o} - 3^{o} over the full range of confining pressure.

Lowe (1964) tested gravelley materials at 50, 100 and 200 psi confining pressures. The Mohr envelope for the loose samples was approximately a straight line with an angle of internal friction of 41^{o}. In the dense state, the Mohr envelope was slightly curved under 50 psi confining pressure, and straight for higher pressures. The angle of internal friction at high pressure was 43^{o}. The difference in the shape of the Mohr envelope was attributed to the higher rate of dilatancy of the dense samples under 50 psi cell pressure than that under 200 psi.

Leussink and Blinde (1964) tested uniform gravel samples of grain sizes of 1.8 - 2.4 cm. It was found that the maximum ratio of principal stresses diminishes when the confining pressure increases. Also the angle of shearing resistance decreases as the confining pressure increases, Figure (2-3). This result has been confirmed again by Leussink, (1965).

Marsal (1965b) noticed during testing silicified conglomerate and granite that the stress ratio σ_1' / σ_3' decreases when the confining pressure was increased from 2 - 25 kg/cm^2, Figure (2-4). He also noticed that the axial and volumetric strains at failure increase with the confining pressure.

Marsal (1965a) tested rockfill material at a confining pressure up to 25 kg/cm^2 for the construction of El Infiernillo Dam in Mexico. It was concluded that:

1. In testing dry rockfill, the angle of internal friction decreased from 45° to 37° when confining pressure was increased from 1 to 25 kg/cm^2. Higher axial and volumetric strains at failure were noticed for higher confining pressure. There was a dilation in samples tested under 10 kg/cm^2 cell pressure, while at high cell pressure there was a volume compression.

2. In testing gravelly materials, the angle of shearing resistance decreased from 53° to 39° when confining pressure was increased from 0.4 to 25 kg/cm^2.

Tombs (1969) carried out a series of tests on Silurian cleaved mudstone, granite gneiss and chert at confining pressure up to 450 psi using $1\frac{1}{2}$, 4, and 12 in. dia. samples. In all cases there was a reduction in the angle of shearing resistance as the confining pressure was increased for all sample sizes tested. For the Silurian cleaved mudstone ϕ'_f reduced from 50° to 34° for values of σ_3' from 10 psi to 500 psi respectively. For granite gneiss ϕ'_f reduced from 60° to 40° over a similar range of cell pressure.

Also as the confining pressure increased, the volumetric and axial strains at failure increased. This trend in behaviour covers all sample sizes and porosities tested. Unfortunately the porosities tested were not consistent* so that comparison of results could be made.

Marachi et al (1969) carried out tests on Pyramid Dam material, crushed basalt and Oroville Dam material at confining pressures from 30 to 650 psi. Samples tested were 2, 8, 12 and 36 in. dia. Again here the angle of shearing resistance decreased with the increase of the confining pressure, Figure (2-5). Also it was noted that both volumetric and axial strains increased as the confining pressures increased. In this piece of work unfortunately the porosities of the samples tested were not indicated and correlation of results is difficult.

Billam (1971) presented results of high pressure tests on granulated chalk, crushed anthracite and limestone sand which show that the principal effective stress ratios at failure (σ_1'/σ_3') decrease as the confining pressure increases**. The deviator loads were measured externally without rotating bushes or load cells.

Yee (1972) tested $1\frac{1}{2}$ in. dia. x 3 in high samples of limestone sand under confining pressure of 100 - 1500 psi. The effects of high confining pressures on the angle of shearing resistance and strains at failure were similar to those presented by Marachi et al (1969). Yee also measured the deviator loads externally without using rotating bushes or load cells and therefore the deviator stress measurements are not accurate enough.

The compressibility of soils as pointed out by Skempton (1960) decreases with increasing pressure, then at pressure high enough to eliminate the voids, it becomes equal to the compressibility of solid particles. The high pressure data on different sands by Terzaghi and Peck (1948); Lee and Farhoomand (1967) and Vesic and Clough (1968) and

---

* There is a large variation in the porosities which are not organised into dense or loose states.

** These tests were carried out by Billam in 1967 as part of a research programme in the University of Birmingham.

also the compression test results on rockfill materials by Kjaernsli and Sande, (1963); Marsal, (1967a) and Pigeon (1969) also show that compressibility decreases as the pressure increases. Roberts and De Souza (1958) defined the critical pressure as the pressure at which the slope of the curve "compression versus log-pressure" increases. And it has been suggested that, at this pressure the crushing of the particles becomes significant. This critical pressure is lower for angular, uniformly graded, loose and weak granular materials than dense, well graded, and rounded particles of hard rocks. It was also noticed that under high pressure all differences in behaviour of granular materials due to variations in initial void ratio, initial grading, or particle shape disappear.

Lee and Farhoomand (1967) studied the influence of varying the ratio of anisotropy on volume changes in standard triaxial equipment. It was found that for ratios of major to minor principal stress varying between 1 and 2.8, the volumetric strain was controlled by the major stress only, for simple stress paths. Similar results have been quoted for clays by Fraser (1957).

From the foregoing short review the effects of confining pressures on shear strength and deformations of rockfill materials can be summarised as follows:

1. The angle of shearing resistance decreases as the confining pressure increases. At very high confining pressures the decrease in the value of the angle of shearing resistance is insignificant. Bishop (1966) showed a clear picture of the variation of ϕ' with cell pressure for sand in a loose and dense state. The angle of shearing resistance, ϕ', starts to increase beyond 1000 psi cell pressure. There is not enough data for rockfill which shows a similar trend in behaviour. Figure (2-6) shows the $\phi' - \sigma_3'$ relationship for some of the work reviewed in this chapter.

2. Volumetric and axial strains at failure increase as the confining pressure increases. This increase would be very small for very high confining pressures. Figure (2-7) shows the variation of ϵ_{1f} with σ_3' for some of the published work.

3. As the confining pressure increases the effects of initial density of the sample decrease and then at very high confining pressure loose and dense soils behave in a similar way.

4. Dense rockfill material sheared at low confining pressure dilate while at high confining pressures volume changes become compressive. This kind of behaviour has been observed for soils and other granular materials by many workers, Hall and Gordon (1963); Bishop (1966); Lee and Seed (1967) and Vesic and Clough (1968). The effects of confining pressure on sample dilatancy will be discussed in detail in another section.

5. As the confining pressure increases, particle breakage increases and this affects the angle of shearing resistance and volume change of the sample. However particle breakage will be discussed in detail in another section.

2.5.2 Influence of Sample Properties

2.5.2.1 Influence of Porosity and Relative Density

One of the important factors influencing the strength and deformation of granular materials is the porosity (Some of the writers use the parameter Λ void ratio). Casagrande (1936) showed that the influence of void ratio is not limited to affecting the value of ϕ' but also the manner in which the shear strains are developed. In dense samples shear strains are accompanied by an increase in volume at failure, while in an initially loose sample the volume decreases at failure. Based on this observation, Casagrande (1936) suggested the concept of critical void ratio, and later it was expanded to arrive at the concept of critical confining pressure by Lee and Seed (1967).

It has been accepted that the shear strength of granular materials increases as porosity decreases on condition that the other factors are the same. This fact has been particularly confirmed for rockfill material by Zeller and Wulliman (1957) in tests on gravelley sand; Leslie (1963) in tests on gravelley soils; Lowe (1964) in tests on gravel; Tombs (1969) in tests on different materials; Marachi et al (1969) in tests on various materials as well, etc.

However when comparing samples with scaled gradings, it is known that constant porosity does not mean identical behaviour because of different particle sizes. Because of that the use of relative density parameters was suggested instead of porosity in comparing the behaviour of rockfill. Unfortunately this suggestion is not successful when data by Tombs (1969) are plotted in Figure (2-8a). It can be seen that the 4 in. dia. samples are the weakest. This may be due to different criteria in determining the maximum and minimum densities of each sample size. Also it can be seen that the 12 in. dia. samples come out stronger than the others when compared on the basis of relative density, while there is little difference when the samples are compared on the basis of porosity.

Density has also a marked influence on the strains at failure. Loose samples fail at axial strains higher than the dense ones. Some very loose samples may not reach failure before the end of the tests.

Loose samples sheared at medium and high confining pressures continue to decrease in volume while dense ones may dilate. At low confining pressures dense samples dilate (Bishop, 1966) while loose ones may dilate or consolidate* at failure.

The influence of density on the dilation of the sample, ϕ' - dilation relationship and particle breakage will be discussed in later sections of this chapter.

---

* This depends on the porosity, confining pressure and type of material.

The compressibility of an initially loose sample is much higher than that of an initially dense sample, Terzaghi and Peck, (1948); Kjaernsli and Sande, (1963); Pigeon, (1969), and many others. Under very high confining pressures, where the effects of initial void ratio vanish, both initially loose and initially dense samples would have almost equal compressibilities.

Kjaernsli and Sande (1963) indicated clearly that loose samples are more compressible than dense ones, Figure (2-9). In this figure samples 5, 6 and 7 show that the relative density is much more relevant here than the porosity. The two samples at 100% relative density have much more similar compressibilities than the two of similar porosities. Similar results have been presented by Fumagalli (1969) for grains of different sizes.

Pigeon (1969) tested different gradings of granite gneiss and mudstone samples at different relative porosities. Results of some of the tests on granite are shown in Figure (2-10). It can be seen that the compressibility decreases as the relative porosity increases for all stress levels.

Therefore from the results presented by Kjellman and Jakobson, (1955); Kjaernsli and Sande, (1963) and Pigeon, (1969) it is concluded that not only the compressibility decreases rapidly with increasing relative density but also that at a given relative density, samples having a lower initial porosity, either due to differences in gradation or grain shape, will deform less, provided that the unconfined compressive strength of the particles is the same for all of them.

2.5.2.2 The Influence of Gradation

Bishop (1948) showed that at a given void ratio the value of the angle of internal friction of a uniformly graded material is higher than that of a well graded soil, but at their maximum densities a well graded soil has a higher angle of internal friction than a uniformly graded soil.

It was also found that the soil gradation has some influence on the curvature of the Mohr envelope. Hall and Gordon (1963) and Insley and Hillis (1963) noticed that the failure envelope for the less well-graded granular materials has a marked curvature, while the envelope for very well-graded soils is often a straight line.

Zeller and Wullimann (1957) in their tests on gravelley sand, concluded that in more uniform grading, the rate of dilatancy is greater at failure. The contact stresses are higher with uniform material but the mean applied stresses were quite low so that particle breakdown would not have had a predominant influence on the results.

Marsal (1967a) tested basalt fragments and granite gneiss. He concluded that the shear strength is higher in well graded materials with a low void ratio, whether of alluvial origin or a product of quarry blasting. He also noticed that materials with similar gradation present an appreciable variation in their strength, probably due to intrinsic characteristics of the particles. Before that, Casagrande (1965) indicated that a well graded rockfill material compacted to its maximum density has higher shear strength and less compressibility.

Leslie, (1969) in tests on Black Butte gravel shows that well graded samples exhibit a higher ϕ' than uniform ones, Figure (2-8b). Unfortunately he has not isolated this variation from the effect of the D/d ratio. Similar results have been presented by Tombs, (1969).

With regard to compressibility Kjaernsli and Sande, (1963) and Pigeon, (1969) showed that a uniformly graded soil is more compressible than a well graded soil, Figures (2-9 and 2-10). Similar results have been presented by Lee and Farhoomand (1967).

However Roberts and De Souza (1958) showed that under pressures as high as 7500 psi, the compressibility of uniformly graded and well graded Ottawa sand are equal. Of course uniform sand would not remain uniform when subjected to such high pressures. For rockfill materials the pressure at which different gradings exhibit the same compressibility may be as low as 500 psi*. This should be investigated in detail.

---

* This depends on the strength of particles.

It can therefore be concluded that well graded material exhibitshigher shear strength, less compressibility and less particle breakage.

2.5.2.3 The Influence of Grain Size

Lewis (1956) in tests on rockfill found that the shear strength increases with increasing particle size. Marsal (1965b) noticed the same trend when testing silicified conglomerate and granite gneiss rockfill, Figure (2-4).

Leussink (1965) in tests on moraine contradicted the above findings and concluded that particle size does not influence the shear strength as long as gradation and ratio of particle diameter to sample diameter were kept the same. He quoted results from Idil, (1960) which are shown in Figure (2-11).

Tests by Marachi et al (1969) show that ϕ' decreases with the increase of particle size. An extrapolation to 24 in particles indicates a further decrease of approximately 2^{o}. All the tests were carried out with the same void ratio and scaled gradings at the same D/d ratios. There is no confirmation of these findings.

Leslie (1969) presented test results on Black Butte gravel showing that changes in particle size for a constant coefficient of uniformity has little effect on ϕ'.

Tombs' test results (1969) show that shear strength is independent of particle size for geometrically similar gradings as long as D/d is kept constant.

With regard to one dimensional compressibility Pigeon (1969) showed that for wide grading material, at a given relative porosity and stress level, the strain is independent of the particle size. Fumagalli (1969) found the same for marly limestone. The reason is probably that particle breakage is limited for a material with wide grading and the deformations are controlled by crushing of the points in contact. For

uniformly graded materials Pigeon, (1969) found that the strains vary with the particle size, it is much larger with larger particles at the same relative porosity*. This variation may be attributed mainly to the increasing interparticle forces with increasing grain size and the consequent particle breakage associated with a uniform grading.

From the previous short review it can be concluded that the effect of particle size on the shear strength is insignificant. This point needs further investigation. The compressibility of well graded rockfill is also independent of the particle size while the compressibility of narrowly graded samples increases with the maximum particle size but that it tends to an upper limit for maximum sizes of approximately 100 mm.

2.5.2.4 The Influence of Sample Size and D/d Ratio

Holtz and Gibbs (1956) and Leslie (1963) indicate that when the sample is sufficiently larger than the particle comprising it, the sample size has no effect on the measured shear strength**. When the ratio of the sample diameter to the maximum particle size becomes small, about 5 - 10, and there is a high percentage of the larger particles present in the sample there is an increase in the measured strength caused by interference between the larger particles.

Data on granite gneiss by Tombs, (1969) were plotted in terms of ϕ' vs. porosity for different D/d ratios, Figure (2-12). It can be seen that D/d ratio has no consistent effects on ϕ' - porosity relationship. A similar conclusion was arrived at from data by Marachi et al (1969).

It can therefore be concluded that if the material gradation is such that the proportion of particles in the maximum sieve size is 30% or less and the ratio of the sample diameter to the largest particle size is 5 or more, there should be no effect of sample size on the measured

---

* Similar findings were presented by Nitchiporovitch, (1964).

**This has been confirmed by Tombs (1969); Marachi et al (1969).

shear strength. In fact most of the writers suggest a minimum D/d ratio of 4 - 5 for well graded soils and approximately 16 for uniform ones.

Pigeon, (1969) and Fumagalli, (1969) found that varying the D/d ratio for wide grading rockfill has insignificant effect on compressibility. For a uniformly graded material, Fumagalli demonstrated that the smaller ψ ($\frac{1}{\psi} = \frac{D}{d}$) the larger the vertical strains.

2.5.2.5 The Influence of Degree of Saturation (Moisture Condition)

Saturation tends to reduce the compressive strength of rock material. Terzaghi (1960) published the following results:

Type of Rock	Average Strength (Dry)	Reduction in Strength due to Saturation.
Austrian granite	21000 psi	12%
Swedish and German granites	35000 psi	6%
Crystalline limestone	14000 psi	10%
Quartz-mica schist	13590 psi	53%
Syenite (Kjaernsli and Sande, (1963))	25500 psi	6% saturated 15% submerged

Pigeon (1969) found 30% reduction in strength due to saturation for the same granite when he crushed irregular lumps.

Horn and Deere (1962) carried out sliding friction tests under different humidity conditions and concluded that as the surface moisture increases, the coefficient of friction increases for massive-structured minerals such as quartz, but decreases for minerals having layer-lattice structures such as mica.

Lowe (1964) applied 100 psi back pressure to ensure the saturation of triaxial gravel samples. A 9^{o} decrease in the angle of internal friction was observed if the sample was saturated using 100 psi back pressure rather than saturated by percolation of water and without back pressure.

As far as the compressibility is concerned Pigeon (1969) carried out extensive investigations to find out if the increase in compression of dry rockfill was due to wetting. For well graded granite an average of 28% increase in compression was observed while for mudstone an average of 100% increase in strain was quite common.

Howkins (1966) suggested that a moisture content of 7% was sufficient for a well graded sample to behave as if it were submerged. This has been confirmed by Pigeon (1969) as well.

In conclusion saturation of rockfill material increases its compressibility during consolidation. Also saturated rockfill samples exhibit lower shear strength than those tested dry.

2.5.3 The Influence of Material Properties

2.5.3.1 Grain Shape

For a given void ratio the angle of shearing resistance of a sample composed of angular particles is higher than that of a sample made of rounded particles. This fact has been confirmed by Chen (1948); Holtz and Gibbs (1956); Casagrande (1965) etc.

Tests on rockfill materials by Kjaernsli and Sande (1963) indicated that compression as well as particle breakage is greater for angular materials than for rounded ones. The same conclusion has been arrived at by Casagrande (1965) who stated that rounded river gravels and cobbles are superior to more angular quarry blast products with regard to compressibility and settlement of an embankment dam.

In conclusion angular materials exhibit higher shear strength and compressibility than rounded ones provided they are at the same void ratios and stress conditions and of the same constituent material.

2.5.3.2 Coefficient of Friction of the Particles

Rowe (1962) suggested that the dilatancy and strength of an assembly of individual particles in contact and subjected to a deviatoric stress system were dependent on the angle of friction, $\phi'\mu$ between the particle surfaces, on the geometry of the packing and on the degree of energy loss during remoulding. The dependancy of shear strength on the angle of friction between the particles has been disputed later by many research workers.

Leussink and Wittke (1963) indicated that in triaxial tests on regular packings of steel and glass spheres, the same strength at failure was obtained even though the $\phi'\mu$ values were different for the two materials.

Borowicka (1963) suggested that the shear strength of soil was a function of interlocking of the packing rather than interparticle friction.

Tombs (1969) in triaxial tests on different types of rockfill material, indicated that the coefficient of friction between particles has no significant effects on the shear strength of rockfill material.

Lately the relationship between shear strength and interparticle friction has been studied extensively by Skinner (1969) who conducted shear box tests on 1 mm glass ballotini, 1/8 in. steelball-bearings, 3 mm lead shot and 3 mm glass ballotini. The experimental results were compared with the theoretical predictions based on Bishop (1954)(1) and Caquot (1934)(2) derivations. It can be seen

---

(1) Bishop (1954) derived approximate solutions

(a) for plane strain conditions taking $\sigma_2' = (\sigma_1' + \sigma_3')/2$

$$\sin \phi'_{cv} = \frac{3}{2}\mu$$

(b) for triaxial compression where $\sigma_2' = \sigma_3' < \sigma_1'$

$$\sin \phi'_{cv} = \frac{15\mu}{(10 + 3\mu)}$$

(2) Caquot (1934) derived the expression for plane strain conditions

$$\tan \phi'_{cv} = \frac{\pi}{2} \tan \phi\mu$$

from Figure (2-13) that the angle of interparticle friction has no influence on the angle of shearing resistance at constant volume ϕ'_{cv}. Skinner related the difference due to the fact that all the theoretical studies exclude particle rolling as a permissible mechanism. Therefore Skinner (1969) concluded that when shearing a random assembly of spherical particles, both the effective angle of shearing resistance at constant volume ϕ'_{cv} and at peak ϕ'_{max} for a given initial porosity do not increase monotonically with increase in the interparticle angle of friction ϕ'_{μ}.

From the previous short review, it can be concluded that interparticle friction has no appreciable effect on the shear strength of rockfill material.

With regard to compressibility, Pigeon (1969) in tests on different types of rockfill material concluded that the coefficient of friction has, if any, only a minor role in the deformation processes of rockfill.

2.5.3.3 Particle Strength

Strength of individual lumps is one of the main factors controlling the shear strength and deformation process of rockfill. Different materials under the same stress system and testing conditions break down by varying amounts. Thus particle breakage is a function of the particle strength.

Tombs (1969) observed that the angle of shearing resistance for granite was higher than that for mudstone. Similar results have been presented by others, Billam (1967); Marachi et al (1969) etc.

At high stresses the contacts fracture and there is a reduction in dilatancy, which is then mainly governed by the particle strength and overall shape. At a very high stress level, the dilation changes to compression and this is a function of the strength of the particles.

With regard to compressibility, Kgaernsli and Sande (1963) concluded that there was a definite relationship between compressibility and particle strength.

Pigeon (1969) in tests on different types of rockfill materials, concluded that the compressibility of rockfill decreases with increasing particle strength, but at an ever decreasing rate. Effects of particle strength on strains are shown in Figure (2-14) for granite and mudstone.

2.5.3.4 Other Factors

There are many factors which affect the shear strength and deformation of rockfill material other than those mentioned earlier, such as strain rate and testing boundary conditions.

It has been found that the rate of strain does not influence the shear strength or the deformation of granular materials significantly.

Tests by Holtz and Gibbs (1956) on free-draining sand and sand-gravel samples showed that variation in rate of axial strain from 1.8 to 0.086% per minute had no significant effect on the shear strength.

The sliding friction tests by Horn and Deere (1962) also showed that when the sliding rate increased from 0.7 to 6 in/minute the coefficient of massive structural minerals such as quartz was unaffected.

Other testing boundary conditions which influence the measured shear strength and deformation of rockfill are free end restraint, rubber membrane penetration, stiffness, etc.

2.6 Shear Strength and Dilatancy of Rockfill Material

Many attempts have been made to try to explain the effects of dilatancy on shear strength of granular materials. Theories proposed in this field managed to explain some facts and failed in others. Bishop (1954) analysed the work done during incremental loading at failure for saturated silts measured in triaxial compression. He concluded that the portion of strength associated with the dilation of the sample is:

$$\sigma_1 - \sigma_3 = \sigma_3 \cdot \frac{dv}{d\epsilon}$$

where σ_1 and σ_3 are the major and minor principal stresses respectively.

dv and $d\epsilon$ are the incremental volumetric and axial strains which are associated with the incremental loading.

Rowe (1962) investigated the behaviour of an assembly of individual particles in contact under triaxial testing conditions. He concluded that the dilatancy and strength of the assembly were dependant on the angle of friction, ϕ'_{μ}, between the particle surfaces, on the geometry of the packing and on the degree of energy loss during remoulding. Rowe suggested that the measured deviator stress should be modified for the effects of rate of dilatancy of the sample. In mathematical terms this modified deviator stress is

$$\sigma'_1/(1 + \frac{d\epsilon_v}{d\epsilon_1}) - \sigma'_3$$

where σ'_1 is the measured effective major principal stress,

σ'_3 is the measured effective minor principal stress,

$d\epsilon_v$ is the volumetric strain increment,

and $d\epsilon_1$ is the axial strain increment.

Hirschfeld and Poulos (1963) reported results of tests on undisturbed Canonsville silt and on a compacted sand obtained by sieving out the material passing a No. 10 sieve from a sandy gravel. Samples tested were 3.58 cm diameter and 8.5 cm high.

At a confining pressure of 60 psi the angles of internal friction for the silt and the sand were both 36°. When the cell pressure increased to 600 psi the angle of internal friction dropped to 33° for the sand and to 26.7° for the silt. It was observed that at high confining pressures the sample tends to consolidate throughout the test, while at low confining pressures there was a consolidation followed by dilation. Therefore the Mohr envelopes were recalculated on the basis of Rowe's modified deviator

stress formula which has been mentioned earlier. The modified Mohr envelope for the sand was straight, passing through the origin and for the silt was with slight curvature. The curvature of the Mohr envelope for the silt was explained by the fact that the sample behaved as an overconsolidated soil below 300 psi confining pressure and as a normally consolidated soil above that pressure. It was concluded that the initial curvature of the Mohr envelope was caused by the volume changes during shear and not by particle degradation.

Rowe (1963b) stated that the modified Mohr envelope for the silt was satisfactory as it yielded, according to the theory, an acceptable angle of interparticle friction of 30.2°. The modified Mohr envelope for sand gave an unacceptably high value of interparticle friction of 37°. This high value was attributed to the membrane penetration and the effect of rigid end platens on the rate of dilatancy at failure.

Vesić and Barksdale (1963) concluded, from high pressure tests on Chatahooche River sand, that dilatancy was a low pressure phenomenon only and at high pressures the Mohr envelopes for dense samples rejoin that for loose ones.

Bishop (1966) pointed out that there exists a relationship between the angle of friction and the rate of dilatancy at failure, which appears to be a property of the material being tested and is less dependant on the test conditions than is the angle of internal friction. Figure (2-15) shows ϕ' - Rate of dilatancy relationship for Ham River sand and indicates that variation of the porosity and of end restraint does not affect the relationship. This makes it helpful when comparing rockfill tests, since variations of density are excluded and attention may be given directly to the effects of particle size and gradation. It also appears from this figure that the effect of increasing the cell pressure at any porosity is to reduce the rate of dilatancy as well as the strength. This reduction is associated with an increase in particle breakage. Figure (2-16) shows how the rate of dilatancy decreases as the cell pressure increases for rockfill material, sand and steel shot. At very high confining pressure

the dilatancy rate of the loose Ham River sand started to increase. Similar findings for granulated chalk have been presented by Billam (1971).

After the previous short introduction, the ϕ' - dilatancy relationship of rockfill material will be examined. The discussion will be limited to the main investigations carried out in the field of rockfill testing.

Hall and Gordon (1963) tested Oroville tailings in the apparatus at the U.S. Corps of Engineers Laboratory, Sausalito. There is considerable scatter in the results, Figure (2-17), and they do not agree well with results by Marachi et al (1969) which are shown in the same figure although the material for the two series of tests was of similar origin and grading.

Marsal et al (1965a) presented results of tests on dry El Infiernillo rockfill material, Malpaso conglomerate and Pinzandaran sand and gravel. Many tests never reached failure. Of the three materials tested, the Pinzandaran sand and gravel is the most self-consistent set of results. In the 44 in. diameter triaxial cell, two rubber membranes with a sand layer in between were used. As has been pointed out by Hillis and Skermer (1968), this might have caused increase or decrease in ϕ' since the sand occupied 17% of the total cross-sectional area of the sample.

Marsal (1967a) has also presented results of tests on Napa basalt and granite gneiss. The volume changes were measured both by water expelled and by extensometer readings (corrected by Marsal 1968). Rates of dilatancy measured by both methods are in reasonable agreement with that presented by the U.S. Army Corps of Engineers Laboratory (1967).

The U.S. Army Corps of Engineers Laboratory, Sausalito, (1967) tested Napa basalt, which is the same type used by Marsal (1967a) Variation of ϕ' with rate of dilatancy at failure is shown in Figure (2-18).

All the results fall within a relatively narrow band, except four tests which indicate abnormally high negative rates of dilatancy.

Marachi et al (1969) presented results of tests on Pyramid Dam material, crushed Napa basalt and Oroville Dam material. The ϕ' - rate of dilatancy relationship is shown in Figure (2-19). For all the three materials the results show little scatter, and the graph shows marked curvature especially below zero rate of dilatancy. The Pyramid material (an angular argillite) and the crushed basalt show almost identical relations. The Oroville material which was associated with the least particle breakage shows the greatest dilatancy.

Tombs (1969) tested granitic gneiss, Silurian mudstone and chert gravel. The ϕ' - dilatancy relationships for the granitic gneiss and the Silurian mudstone are shown in Figure (2-20). The results of the mudstone fall into a narrow band while the granite show much more scatter*. The effects of the D/d ratio in granite is quite clear. One reason for this scatter is that the mudstone particles break up much more than granite and their behaviour in shear was hardly related to their initial packing.

In conclusion, the ϕ' - rate of dilatancy relationships of all the previously mentioned work have been plotted together in Figure (2-21). It can be seen that the strong and rough grained materials show high rates of dilatancy while the mudstone which undergoes heavy breakage cuts right across the others.

2.7 Particle Breakage in Rockfill Material

One of the earliest experimental investigations of particle crushing in granular materials was studied by Roberts and De Souza (1958), when tests on different types of sands were carried out. It was found that at low pressures angular sands crushed more than rounded sands, while at high pressures the compressibility and crushing of both sands were almost

---

* A similar trend in behaviour was observed from tests on crushed chalk, limestone, and anthracite reported by Billam (1971).

the same. It was also observed that a uniformly graded sand crushed more than well-graded sand, whereas this difference disappears under pressures in excess of 8000 psi. The data show that the final gradation of the initially uniform sand after being subjected to a pressure of 8000 psi is very similar to that of well graded sand. Roberts and De Souza considered that when the pressure on the sample becomes sufficiently high, the forces on individual particles become large enough to cause shattering of the particles.

Vesić and Barksdale (1963) and Vesić and Clough (1968) carried out drained triaxial compression tests on uniform medium grained sand under confining pressure up to 10,000 psi. It has been observed that the amount of particle crushing increased with the increase in confining pressure. It was also found that at a certain confining pressure, the amount of particle crushing during consolidation stage is less than that during shear stage. That finding has been confirmed by Bishop et al (1965).

Lee and Seed (1967) presented test results showing that Ottawa standard sand is much more resistant to breakage than fine subangular to subrounded Sacramento River sand. They also showed that particle breakage increases with the increase of the confining pressure.

Bishop et al (1965) carried out drained and consolidated undrained triaxial tests on sand under a confining pressure up to 990 psi. In the drained tests the sample at σ'_3 = 100 psi showed the usual characteristics of an uncompacted sand, while samples at σ'_3 of 500 psi and more showed the volume still decreasing. They related this phenomenon to the structural breakdown of the particles.

Bishop (1965) pointed out that particle damage in granular materials appears to start at quite low stress and major fracturing of the particles occurs in the high stress range, which can lead to dangerous undrained shear characteristics.

The previous investigations and others had given a wide knowledge of the crushing behaviour of sand particles in a qualitative term. Leslie (1963) reported results of triaxial compression tests on gravel materials with maximum particle sizes of $1\frac{1}{2}$ and 3 in diameter. He concluded that the angle of internal friction of soils is reduced in proportion to the increase in particle breakdown, but this cannot be confirmed until the influence of increasing lateral pressure is known.

Hall and Gordon (1963) carried out drained triaxial compression tests on the minus 3 inch portions of the material used in Oroville Dam. They concluded that particle degradation is a function of the individual soil with the better-graded soils undergoing the least degradation.

In the investigation of the settlements of the Venemo rockfill dam in Norway, Holestal, Kjaernsli and Torblaa (1965) carried out oedometer tests on the rockfill material of the dam. They observed that addition of water to both the fill in the field and to the laboratory samples caused an increase in both the amount and rate of the settlement. Similar findings have been presented by Sowers et al., (1965) during investigation of the settlement records of many dams.

The investigations described earlier were devoted mainly to qualitative terms. So far there are three main methods for describing the amount of particle breakage:-

1. Marsal (1965d) proposed a particle breakage parameter (B) defined as the sum of the differences of a given sign (plus or minus) between percentages of material retained on a set of sieves in the original sample and in the sample after testing. On the basis of this experimental work and other theoretical assumptions, he suggested that this factor (B) is dependant on the normal stresses applied to the particles and introduced a mathematical relationship for that. Contact forces between the particles of granular materials were also studied by Marsal (1963a and 1967b).

   Brauns and Leussink (1967) discussed Marsal's work and analysed regular packings of spheres. They concluded that breakage is much more dependant on shear stresses rather than normal ones. Thus one can conclude that particle breakdown should be a function of the principal stress ratio, the stress level and the structural arrangement of the grains as well as their strength.

2. Lee and Farhoomand (1967) introduced the term "relative crushing" to study the influence of breakdown on filter requirements. This term was defined as the ratio of the initial to the final D15 value since it is the "key size criterion" in the design of drains and filters.

3. Pigeon (1969) suggested a graphical index for measuring particle breakage. This index is a measure of the change of area under the grading curves

Marsal (1967a) plotted the principal stress ratio at failure versus the particle breakage factor B, Figure (2-22), for all the rockfill samples tested in the rockfill laboratories of the Comision Federal de Electricidad, Mexico. From the results he concluded that the strength of materials decreases as particle breakage increases. The results also define a lower bound for σ'_1/σ'_3 in terms of B. The scatter of results was attributed to the variations in the type and gradation of the materials and the void ratios of the samples*.

---

* Similar findings have been made by Marachi et al (1969).

Results presented by Lee and Farhoomand (1967) are shown in Figure (2-23). They indicate that for a given consolidation pressure, coarse soils show more particle crushing than fine soils, and also that uniformly graded soils crush more than well-graded soils. It was also found that angular particles crush more than rounded particles and that the greater the principal stress ratio during consolidation, the greater the degree of particle crushing.

Ladanyi (1967) discussed Lee and Farhoomand's findings and pointed out that for a given major principal stress, isotropic consolidation produces very little particle breakage and considerable volume compression of the samples, whereas anisotropic consolidation produces less compression but more crushing. Ladyani also indicated that the finding that large particles crush more than fine ones could be explained by Griffith's theory of brittle fracture which indicates that the probability of occurrence of inherent flaws in the material increases with increase of volume of particles under stress.

From the previous brief review and other published data, it can be concluded that:

1. The amount of particle breakage increases as the confining pressure increases. But the rate of increase in particle breakage decreases with increasing confining pressure.

2. The amount of particle breakage increases as the maximum particle size increases. This is clear during high confining pressure testing.

3. The amount of particle breakage during application of shear stresses (during shear stage) is much more than that during consolidation.

4. There is a unique relationship between the angle of shearing resistance and the particle breakage factor (B).

5. Breakage of particles is influenced mainly by their strength with weak ones undergoing more crushing.

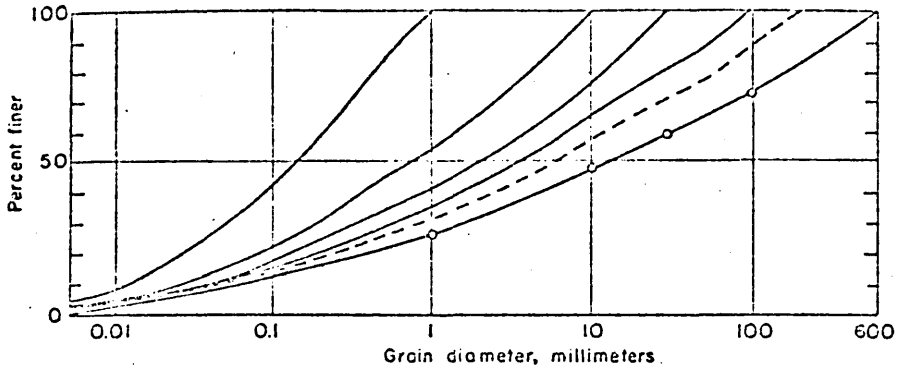

SCALPING ROCKFILL MATERIALS
(AFTER ZELLER, et al, 1957)

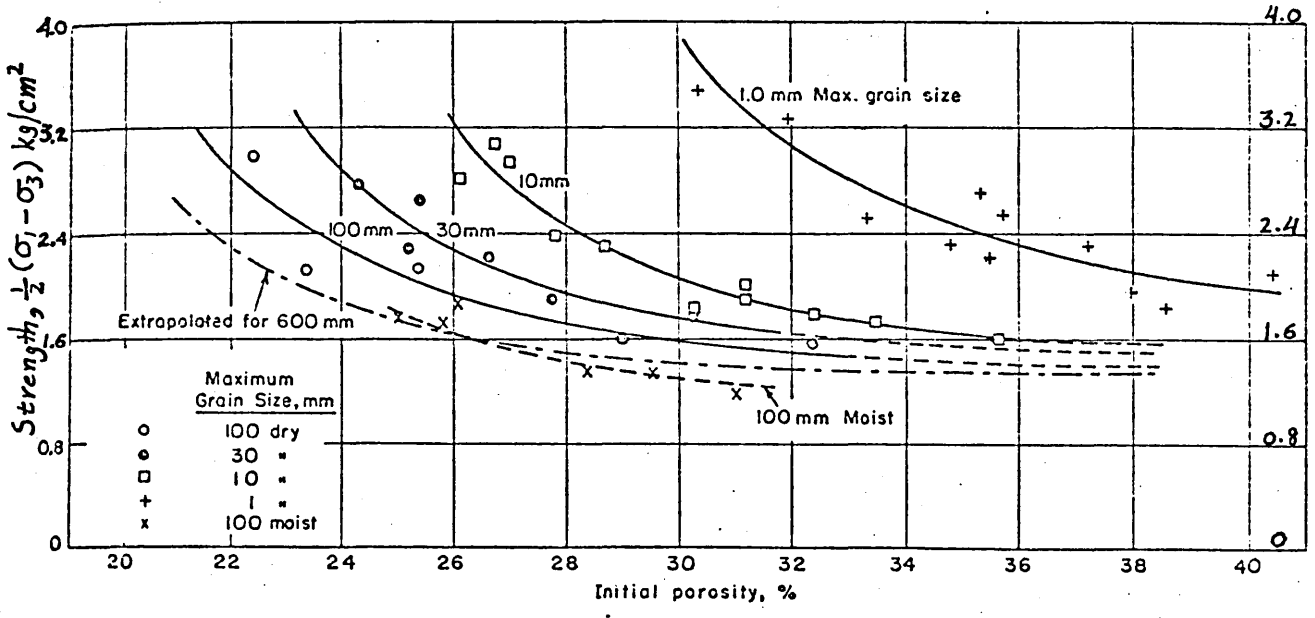

STRENGTH-POROSITY RELATIONS FOR THE SCALPED ROCKFILL MATERIALS
(AFTER ZELLER, et al, 1957)

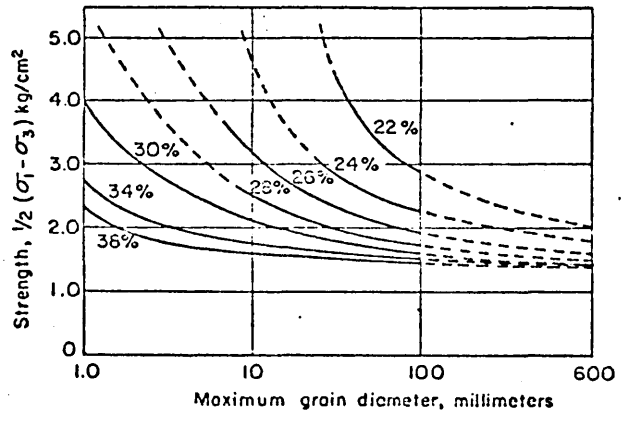

STRENGTH-MAXIMUM SIZE RELATIONS FOR THE
SCALPED ROCKFILL MATERIALS (AFTER ZELLER, et al, 1957)

(After ZELLER & WULLIMANN , 1957)

FIG. 2-1a

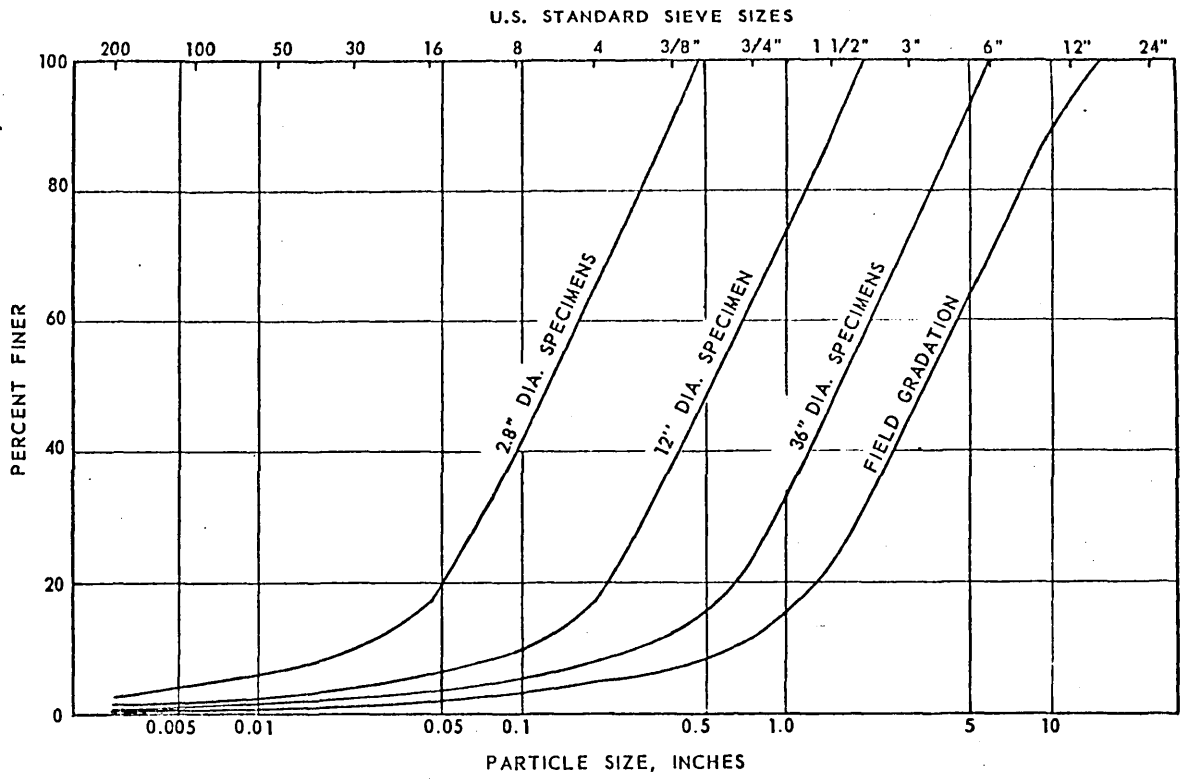

GRAIN SIZE DISTRIBUTION FOR THE MODELED PYRAMID DAM MATERIAL AND CRUSHED BASALT ROCK.

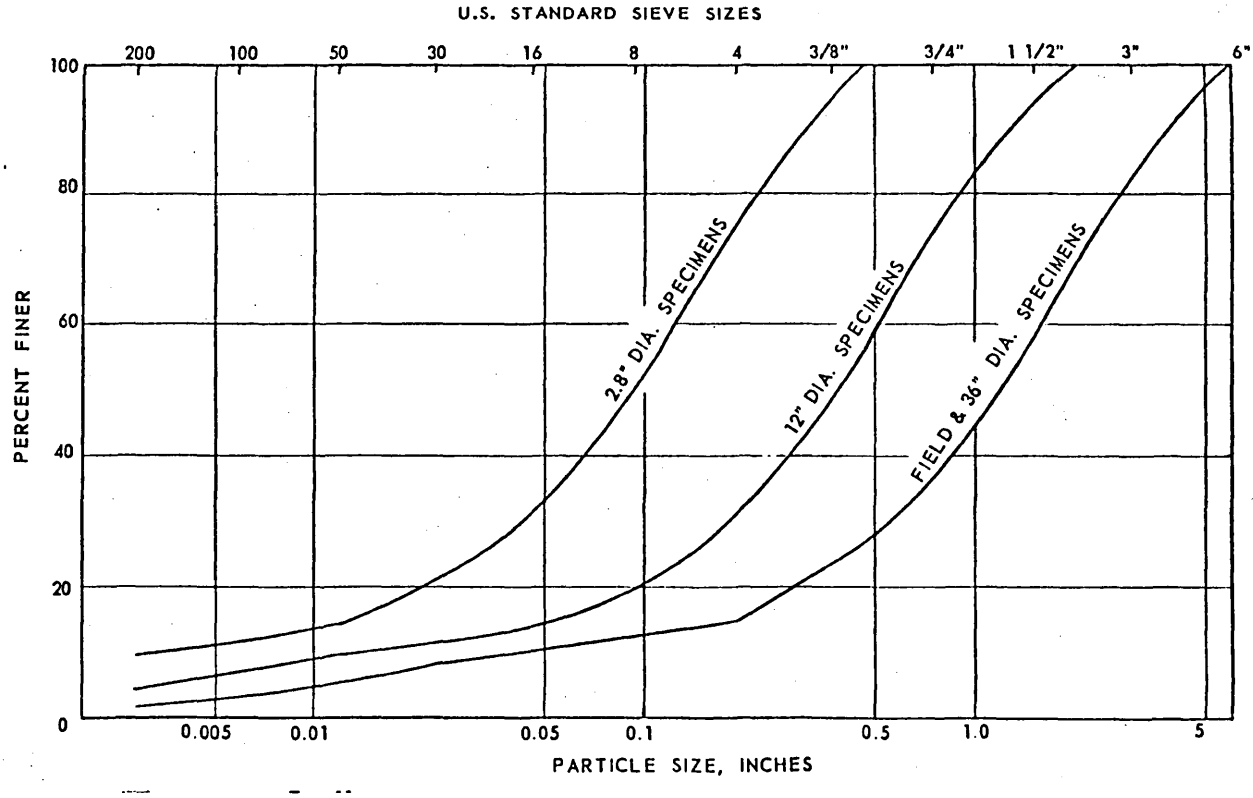

GRAIN SIZE DISTRIBUTION FOR THE MODELED OROVILLE DAM MATERIAL.

After Marachi et al, (1969)

FIG. 2 - 1b

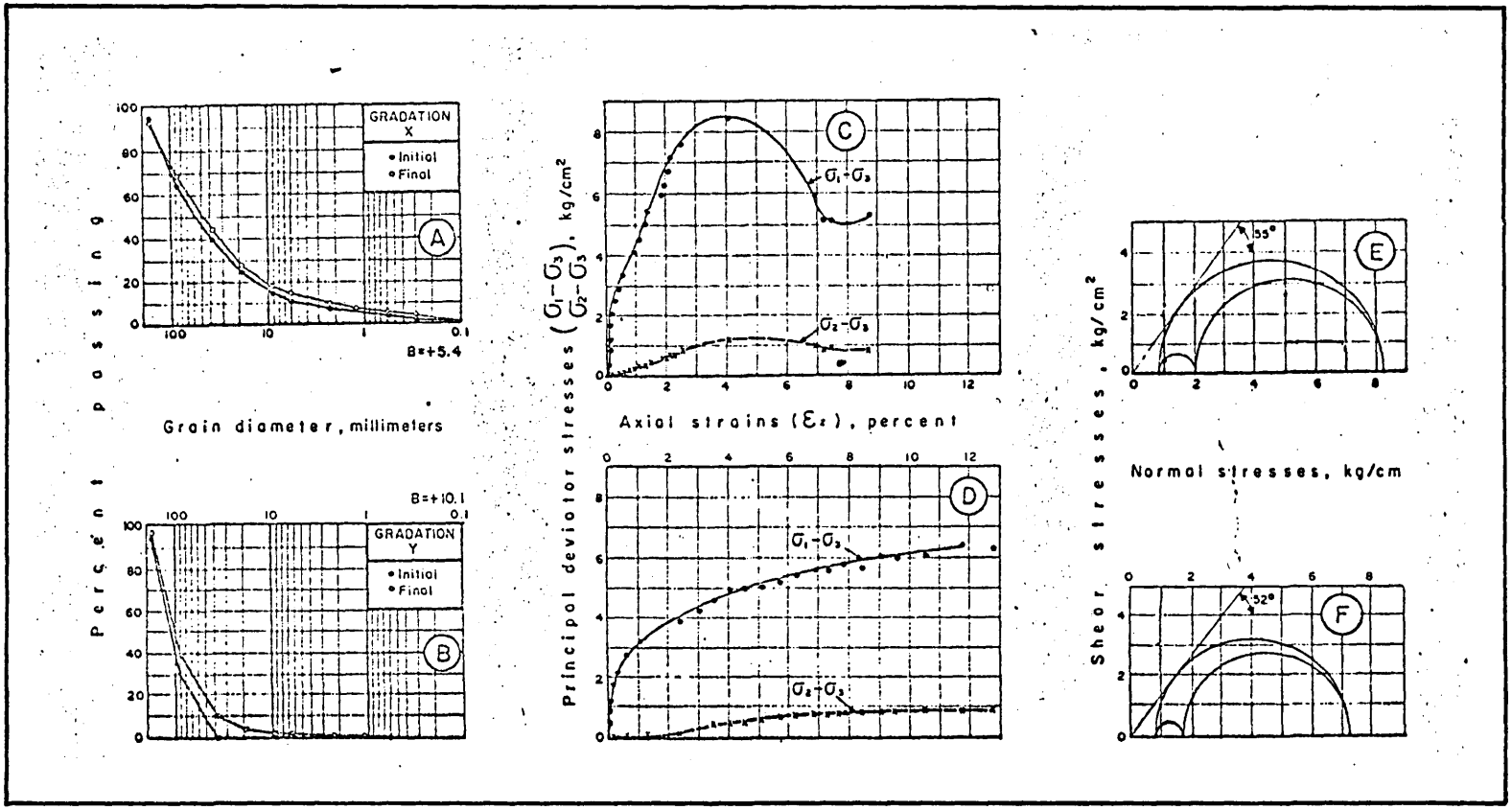

PLANE STRAIN TESTS WITH TWO GRADATIONS OF ROCKFILL ($\sigma_3' = 0.9$ kg/sq. cm.).

(After Marsal, 1965 b)

FIG. 2 - 2

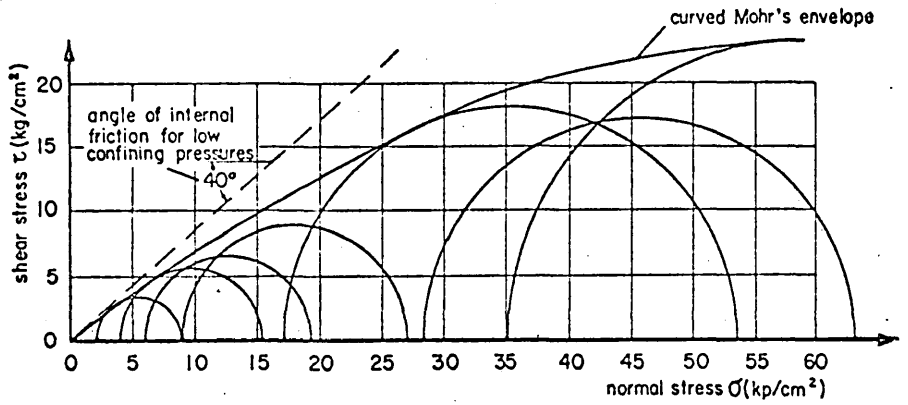

Samples made of uniform gravel, grain sizes of d=1.8 to 2.4 cm

FIG. 2 - 3

DECREASE OF THE ANGLE OF INTERNAL FRICTION WITH INCREASING CONFINING PRESSURES AS MEASURED IN TRIAXIAL TESTS.

(AFTER LEUSSINK AND BLINDE, 1964)

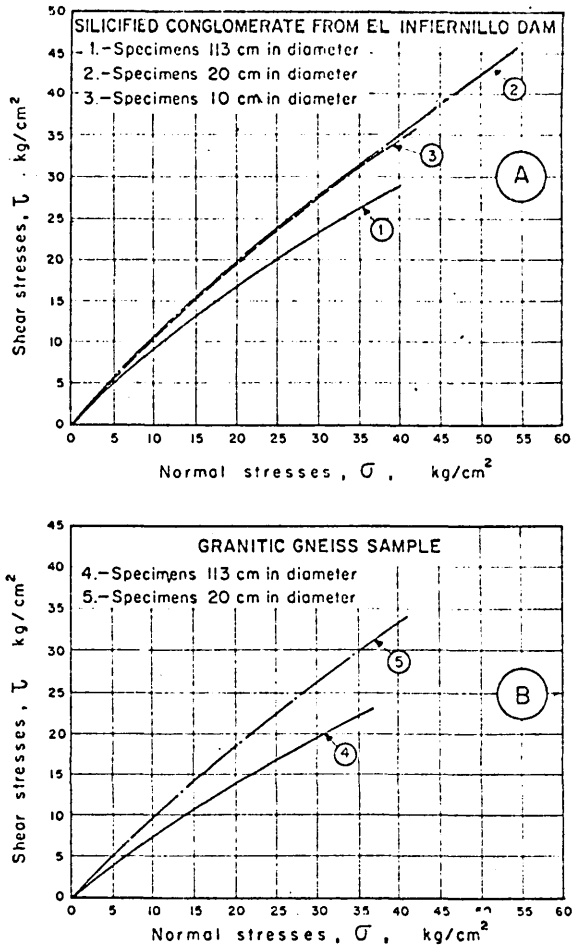

FIG. 2 - 4

MOHR ENVELOPES : A, SILICIFIED CONGLOMERATE FROM EL INFIERNILLO DAM; B, GRANITIC GNEISS;

(AFTER MARSAL, 1965 b)

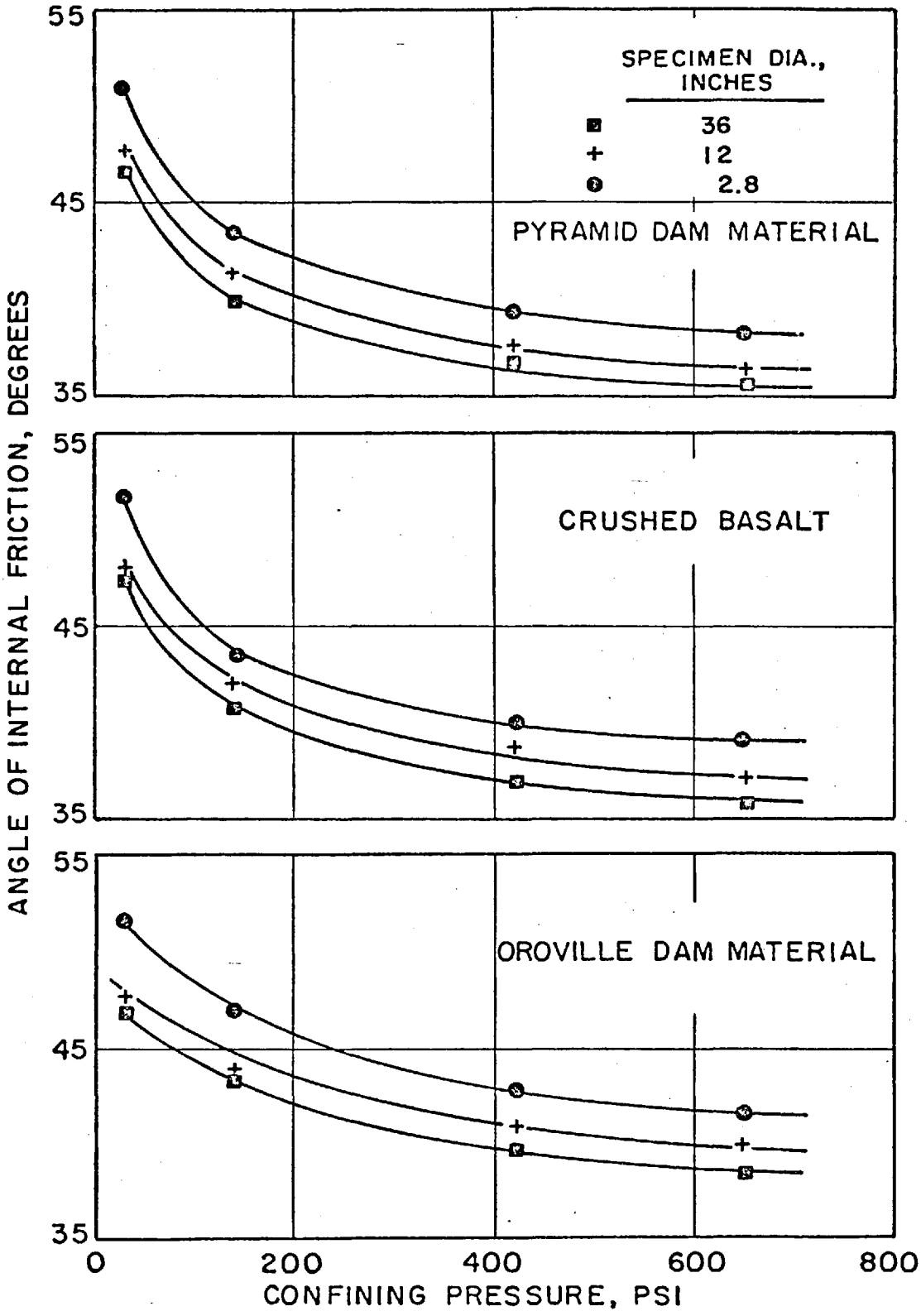

SHEAR TEST RESULTS WITH MODELED ROCKFILL MATERIALS

After Marachi et al (1969)

FIG. 2 - 5

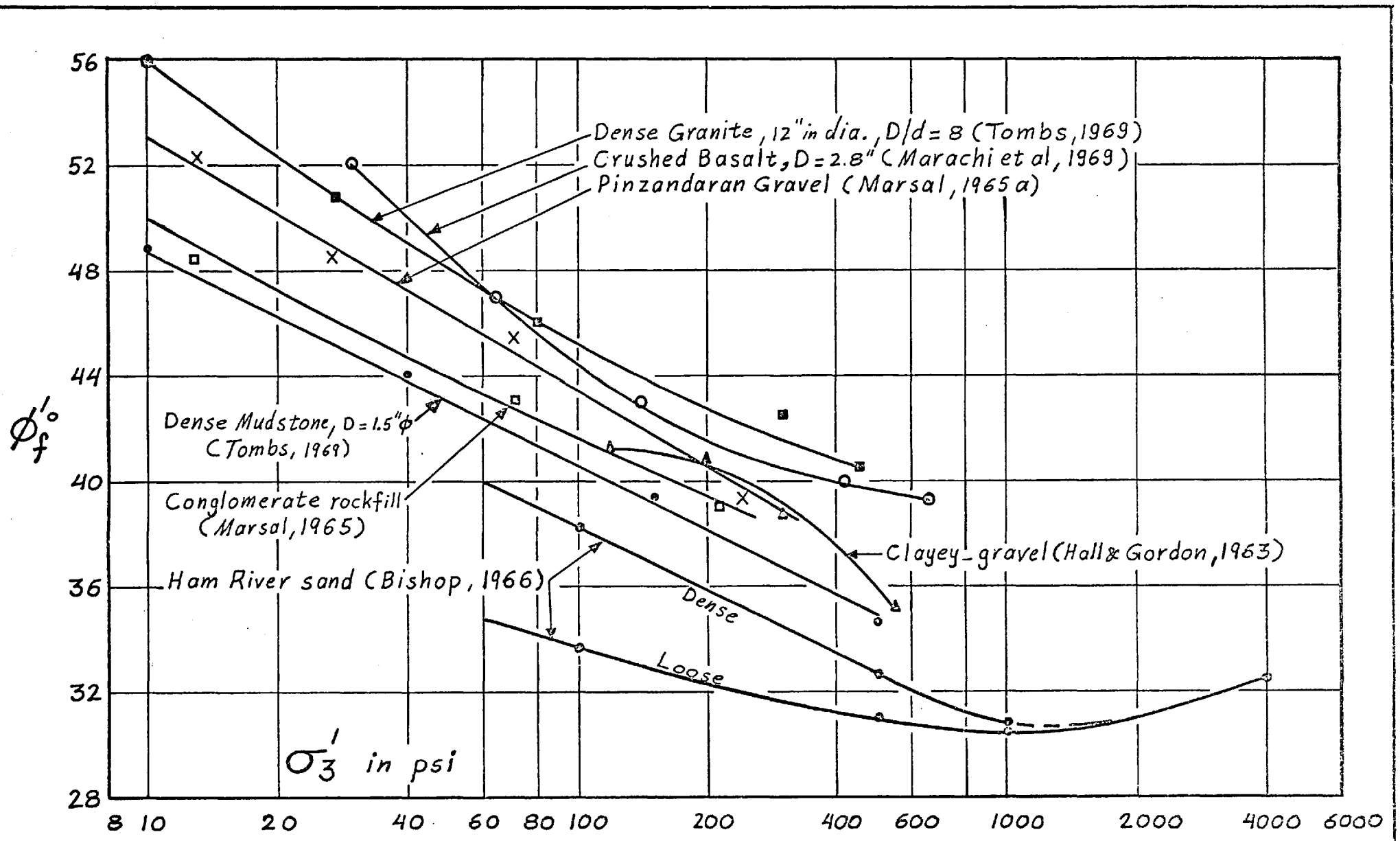

FIG. 2-6

THE VARIATION OF ϕ'_f WITH σ'_3 FOR DRAINED TESTS ON VARIOUS GRANULAR MATERIALS.

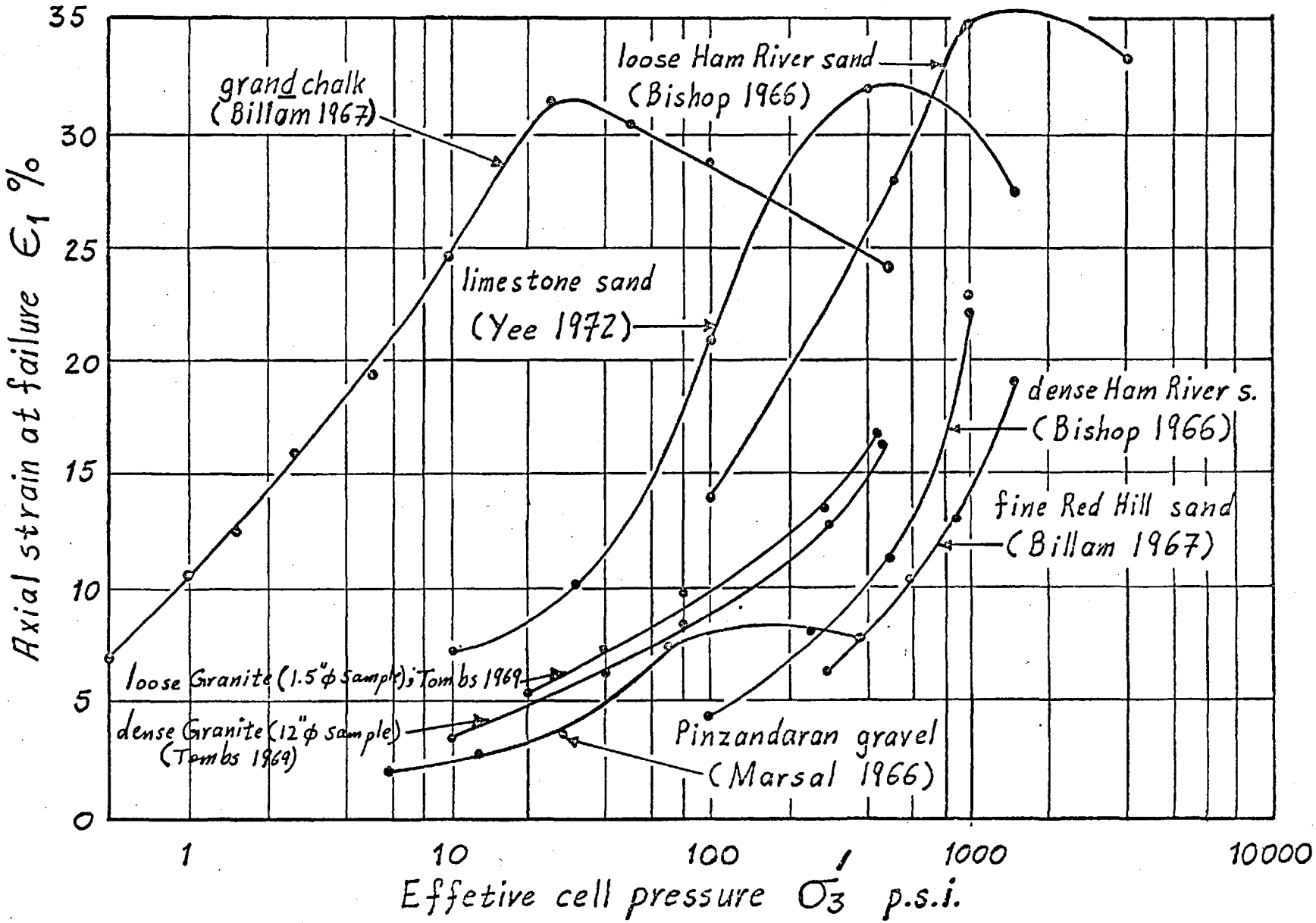

VAPIATION OF AXIAL STRAIN AT FAILURE WITH EFFECTIVE CELL PRESSURE IN DRAINED TRIAXIAL TESTS FOR VARIOUS ROCKFILL MATERIALS.

FIG. 2-7

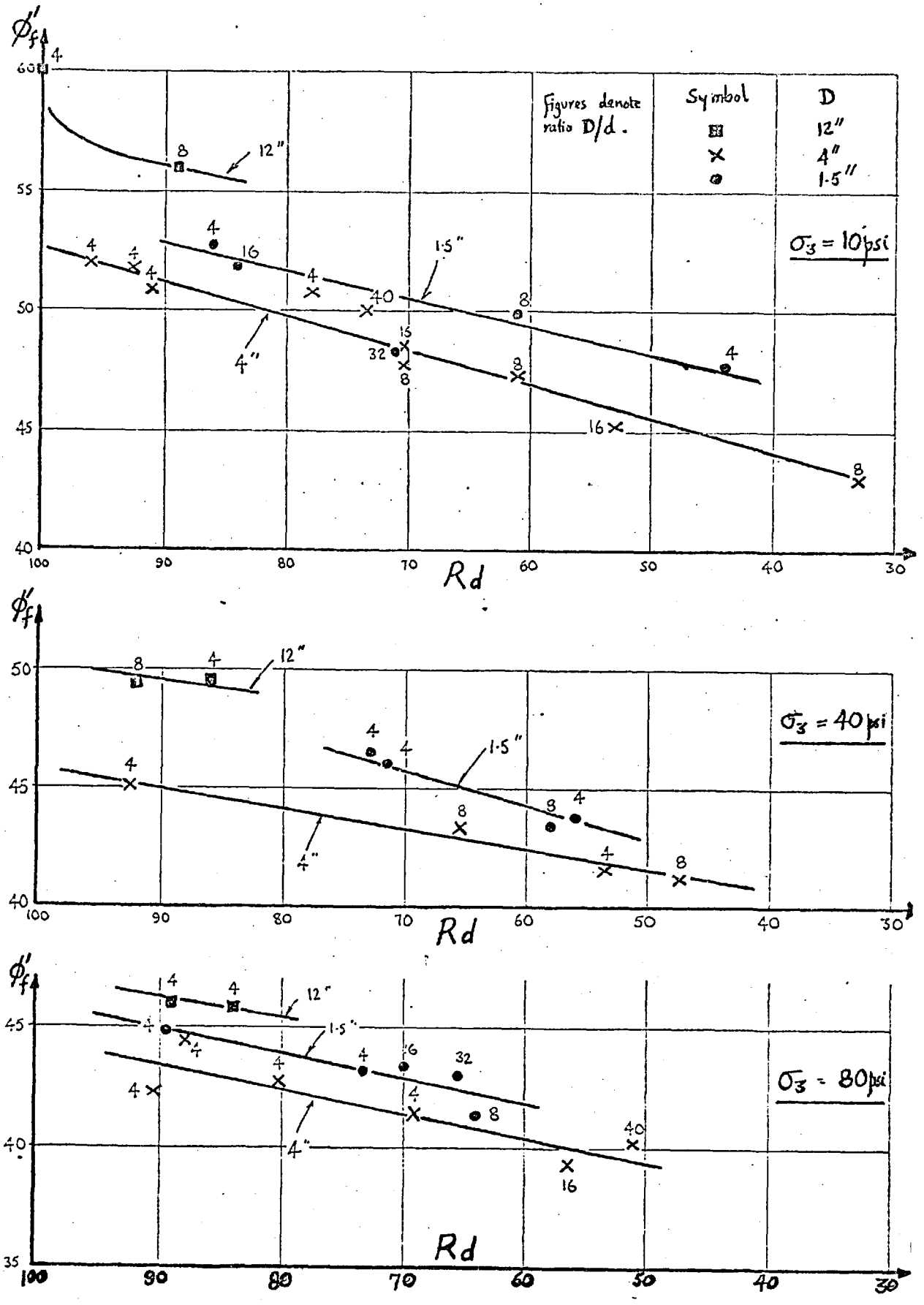

THE RELATION BETWEEN ϕ'_f AND RELATIVE DENSITY FOR DIFFERENT TESTS ON GRANITE ROCKFILL. (AFTER TOMBS, 1969).

FIG. 2 - 8a

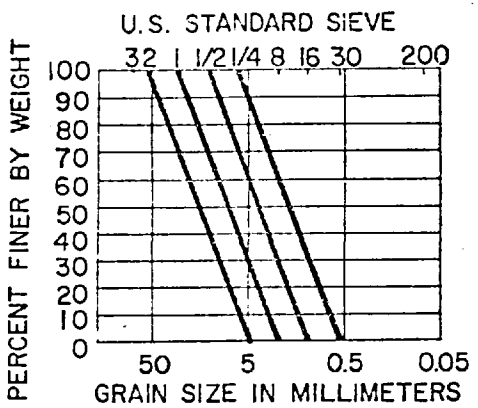

GRADATION OF ALLUVIAL GRAVEL, CONSTANT C_u
(Black Butte Gravel)

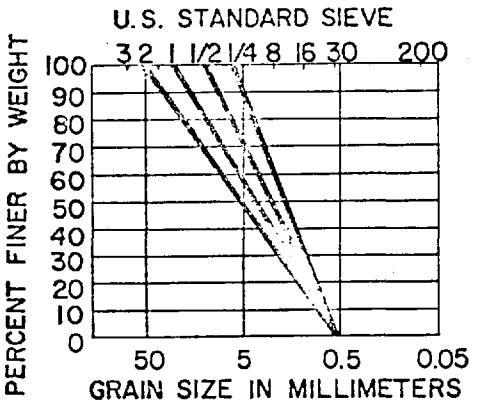

GRADATION OF ALLUVIAL GRAVEL, VARIABLE C_u
(Black Butte Gravel)

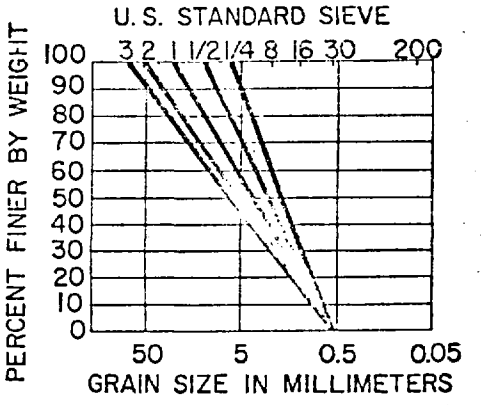

GRADATION OF ALLUVIAL GRAVEL, VARIABLE C_u
(Black Butte Gravel)

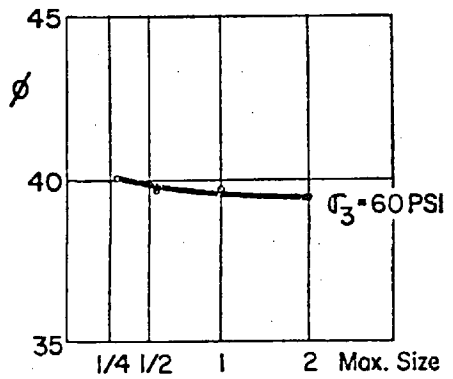

RELATIONSHIP OF SHEAR STRENGTH WITH MAXIMUM PARTICLE SIZE
(Black Butte Gravel)

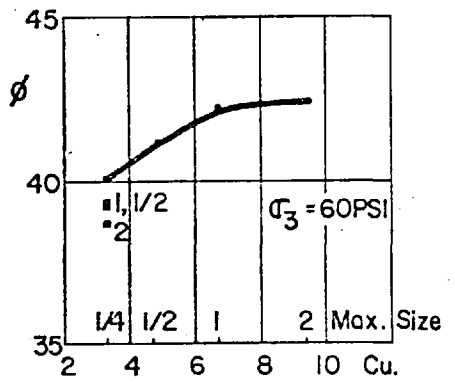

RELATIONSHIP OF SHEAR STRENGTH WITH MAXIMUM PARTICLE SIZE AND C_u
(Black Butte Gravel)

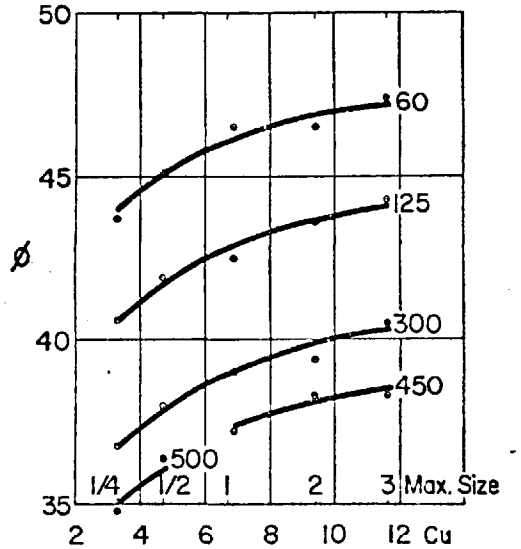

RELATIONSHIP OF SHEAR STRENGTH WITH MAXIMUM PARTICLE SIZE AND C_u
(Black Butte Gravel)

VARIATION OF ϕ'_f WITH GRADATION OF BLACK BUTTE GRAVEL.

(AFTER LESLIE, 1969)

FIG. 2-8 b

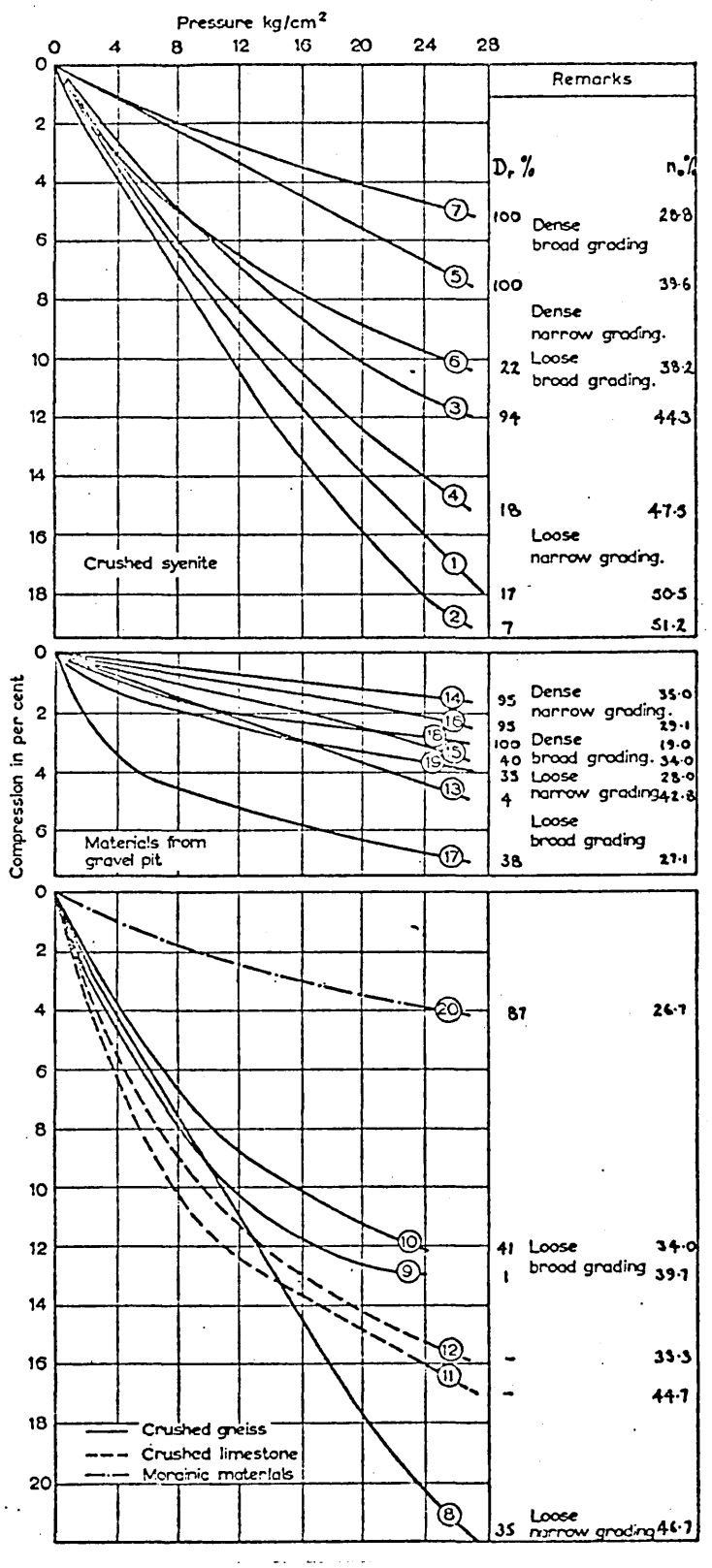

COMPRESSION CHARACTERISTICS OF VARIOUS ROCKFILL MATERIALS

(After Kjaernsli & Sande, 1963)

FIG. 2 - 9

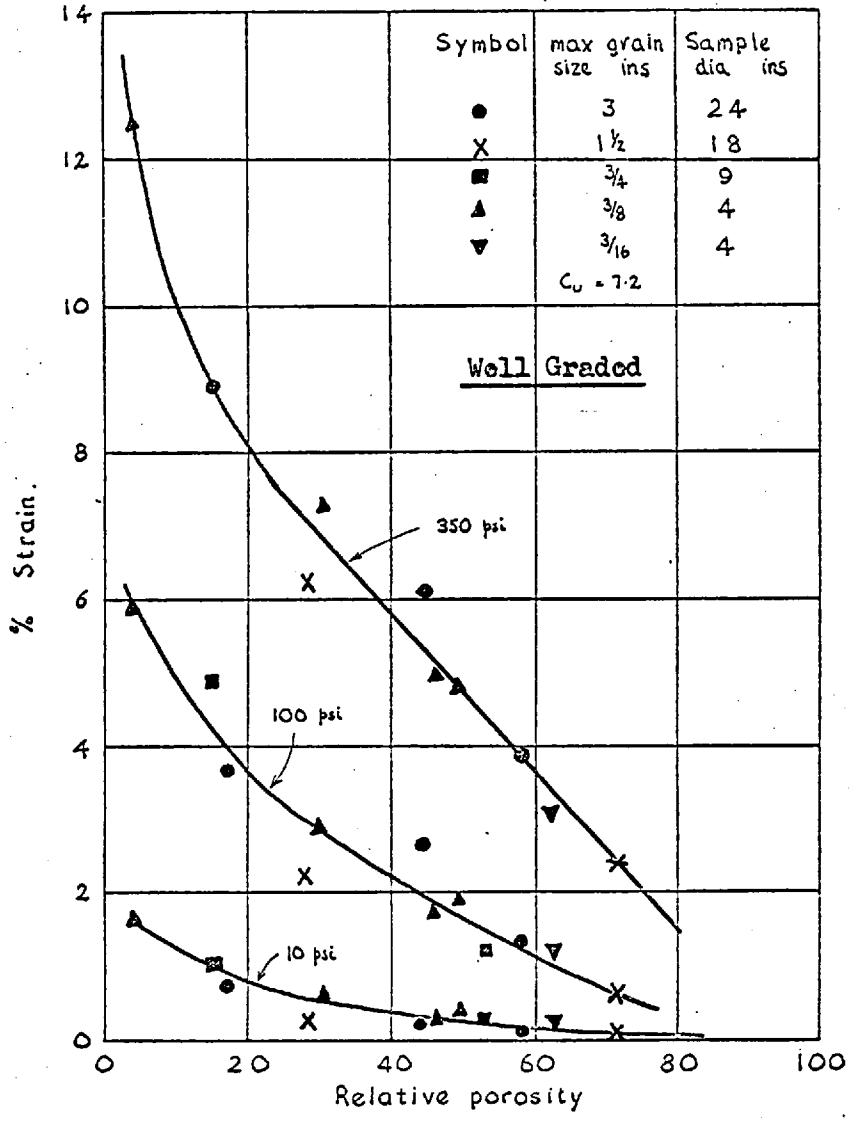

CHANGE IN STRAIN WITH RELATIVE POROSITY FOR SATURATED GRANITE SAMPLES. (AFTER PIGEON, 1969)

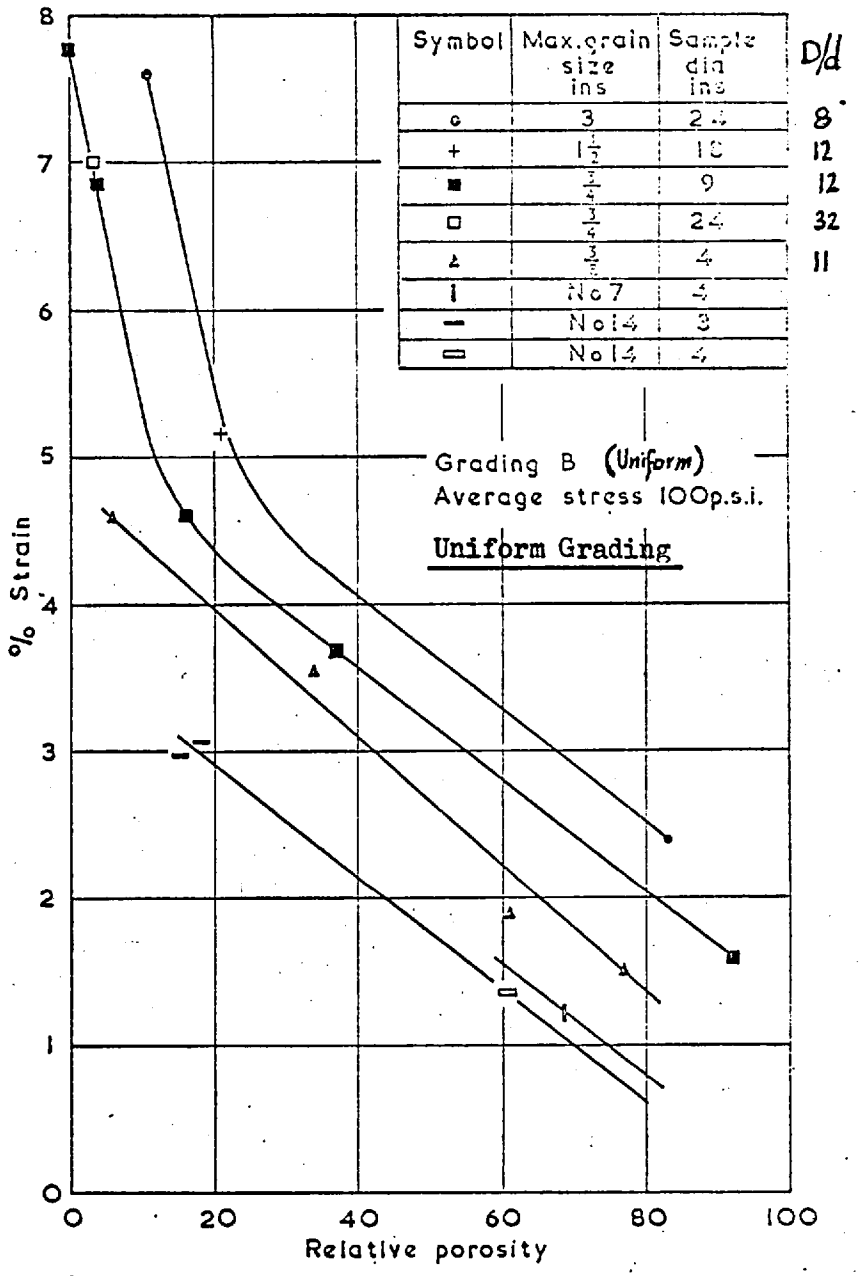

FIG. 2 - 10

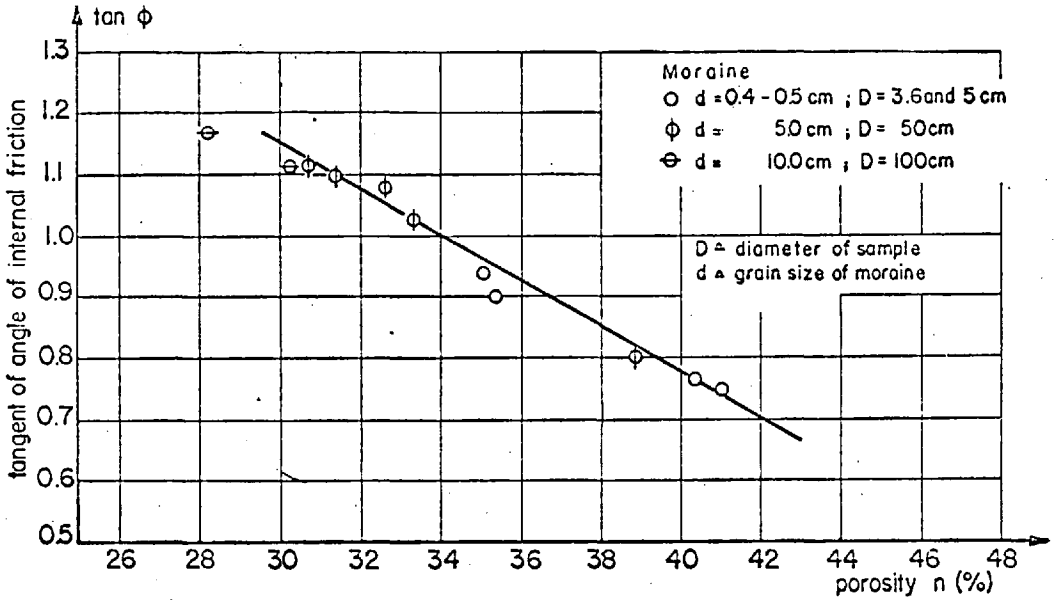

TRIAXIAL TESTS WITH DIFFERENT DIAMETERS OF SAMPLES ON UNIFORM MORAINE (IDEL, 1960).

(AFTER LEUSSINK, 1965)

FIG. 2 - 11

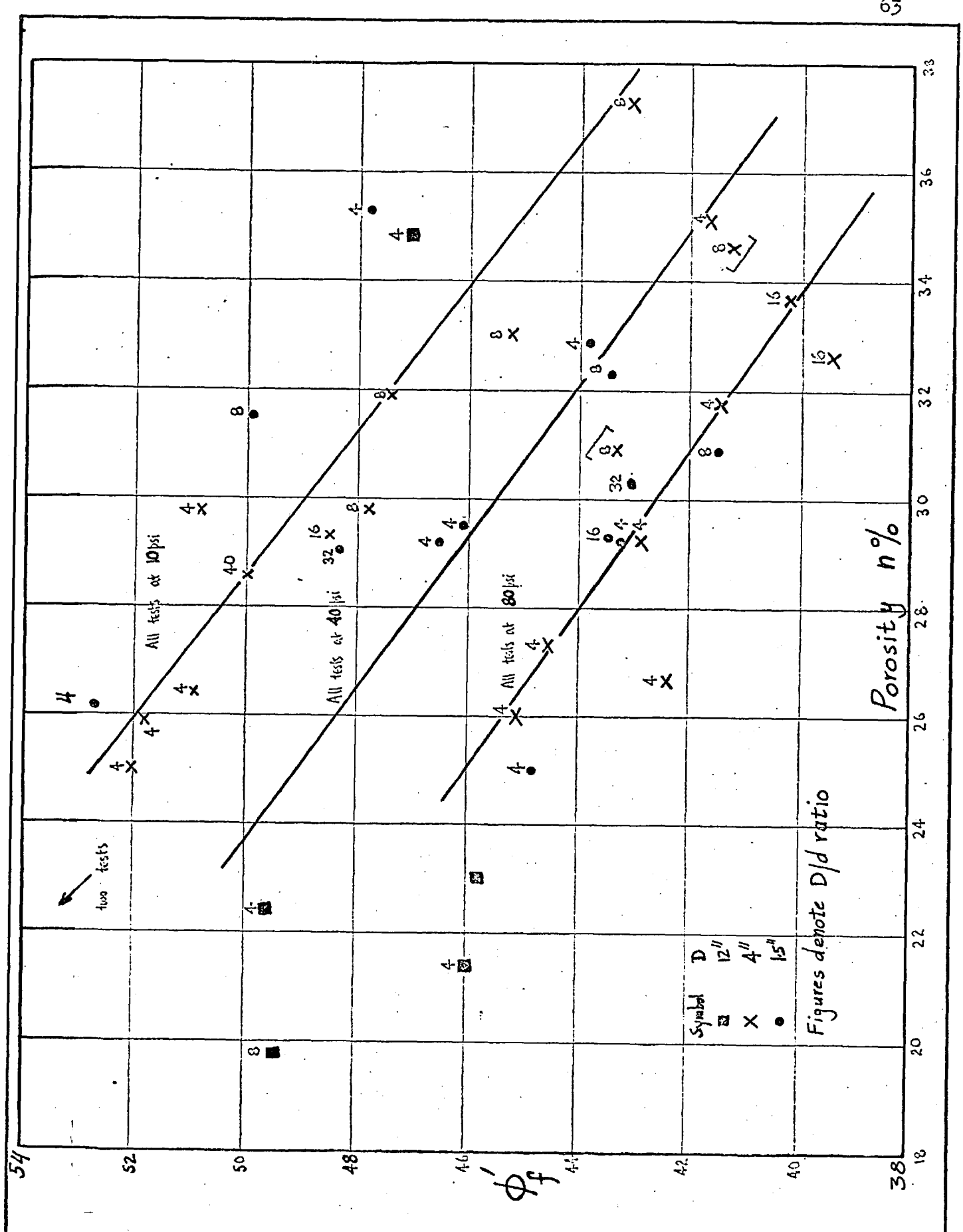

THE RELATION BETWEEN ϕ'_f AND POROSITY FOR TESTS ON SAMPLES OF GRANITE ROCKFILL. (AFTER TOMBS, 1969)

FIG. 2 - 12

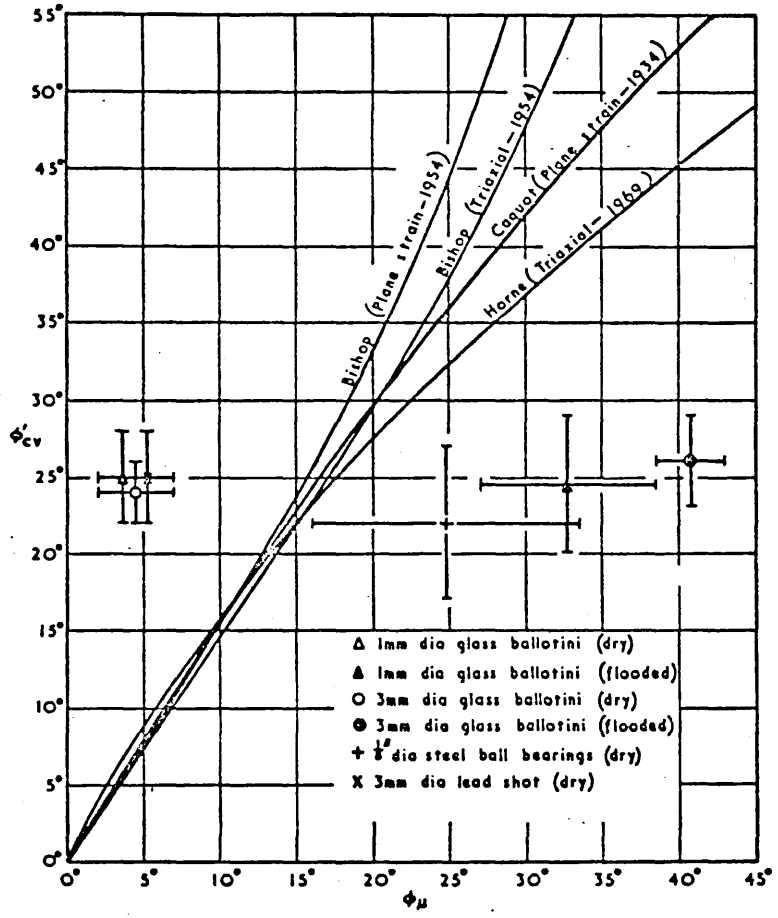

THEORETICAL AND EXPERIMENTAL RELATIONSHIPS BETWEEN ϕ_μ AND ϕ'_{cv}. (After Skinner, 1969)

(FIG. 2 - 13)

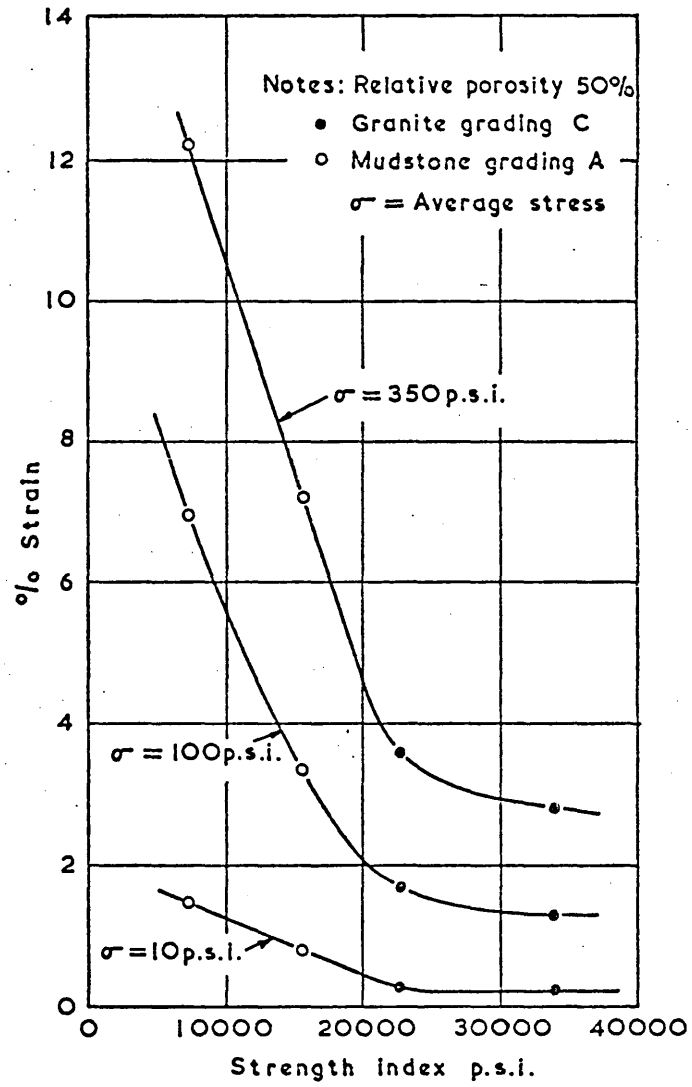

RELATIONSHIP BETWEEN STRAIN & STRENGTH INDEX

(After Pigeon, 1969)

(FIG. 2- 14)

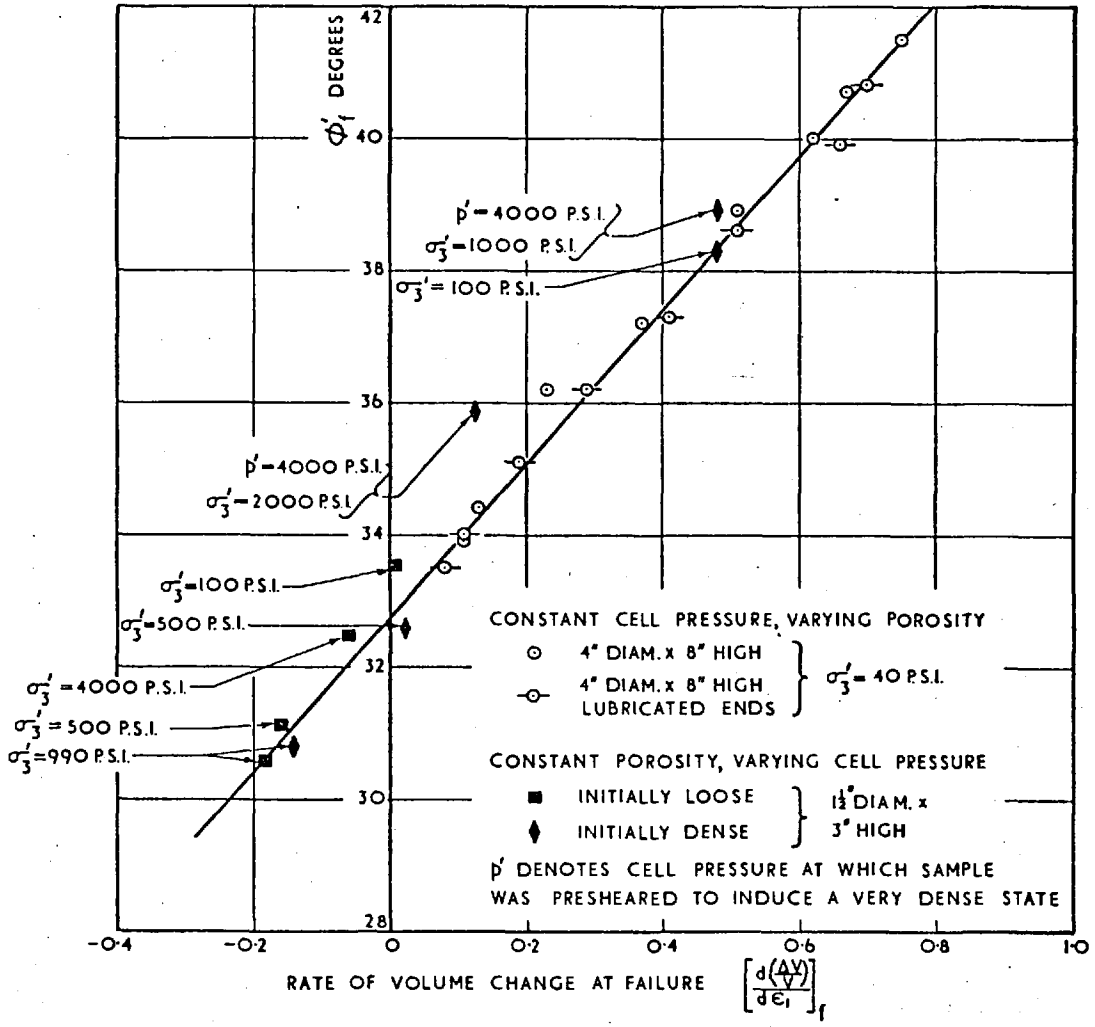

The relationship between ϕ'_f and rate of volume change

$$\frac{d\left(\frac{\Delta V}{V}\right)}{d\epsilon_1}$$

at failure for drained tests on saturated Ham River sand. (Tests by Green and Skinner, 1964-66.)

(After Bishop, 1966)

FIG. 2 - 15

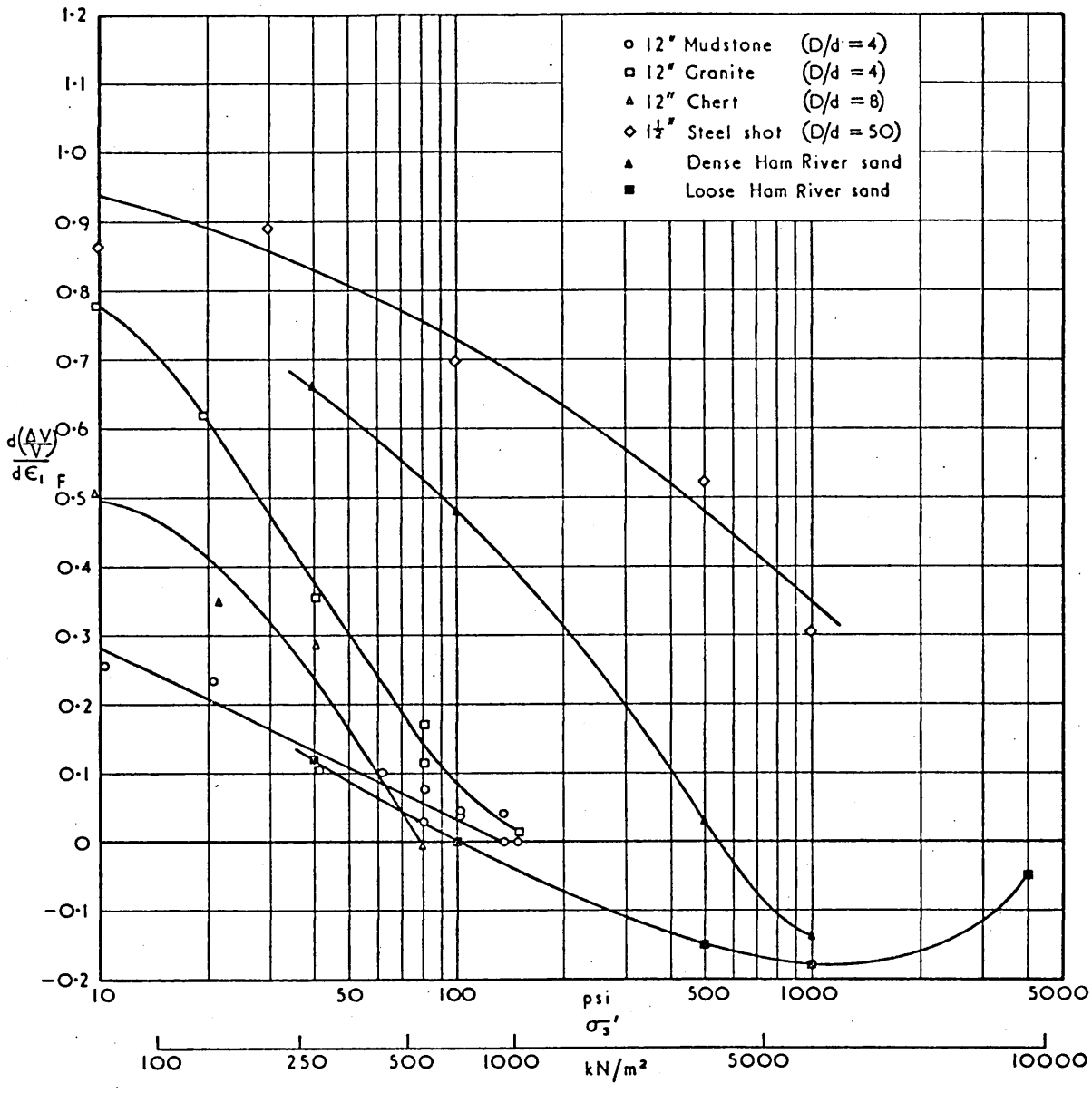

The variation of dilatancy with increase in effective minor principal stress σ'_3 for rockfill, gravel, sand and steel shot. (Data from Tombs, 1967 and from tests by Skinner, 1965-69.)

(After Bishop, 1971)

FIG. 2-16

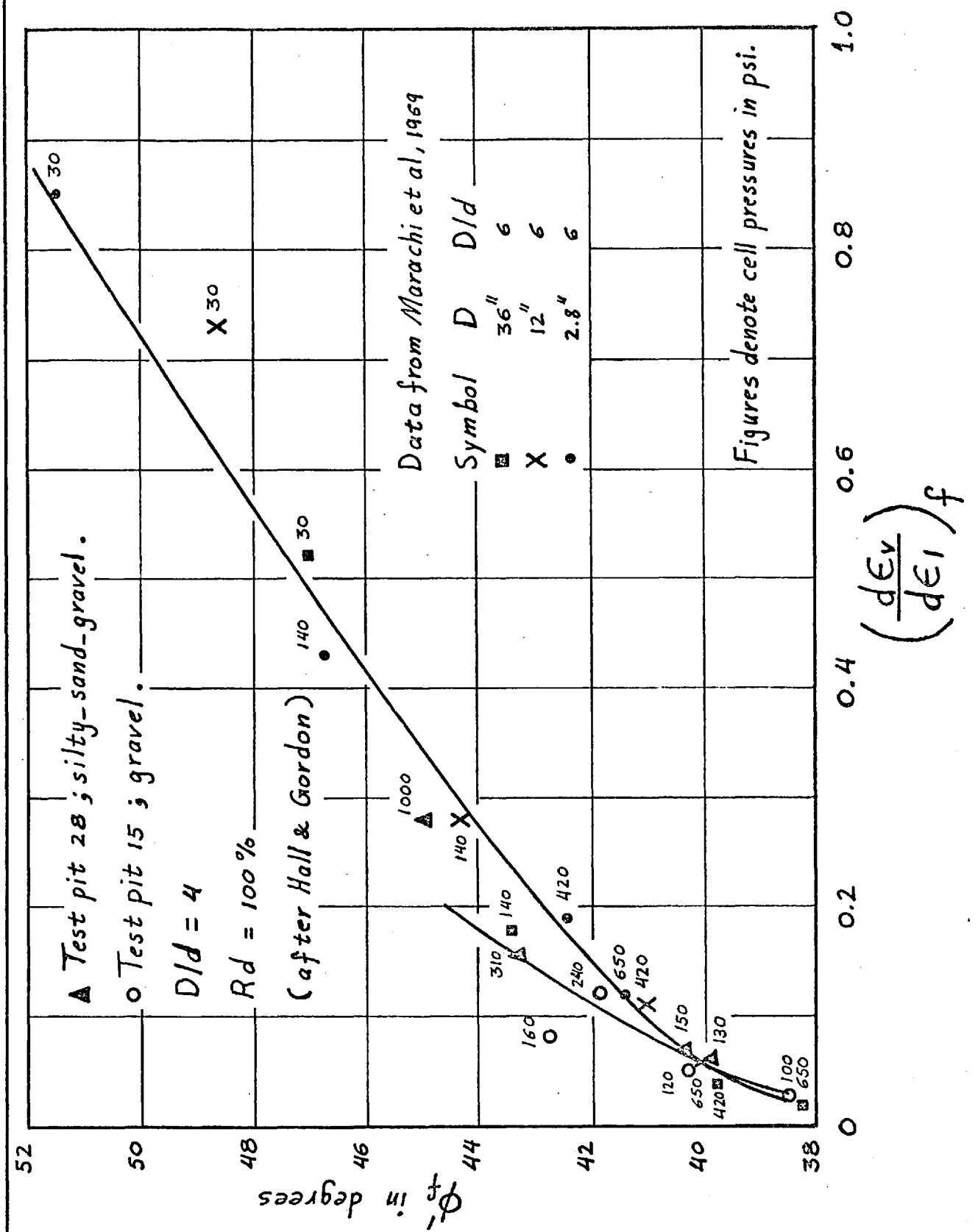

TH RELATION between ϕ'_f AND $\left[\frac{d\epsilon_v}{d\epsilon_1}\right]_f$ FOR OROVILLE DAM MATERIAL

(data from Marachi et al, 1969 and Hall and Gordon, 1963)

FIG 2-17

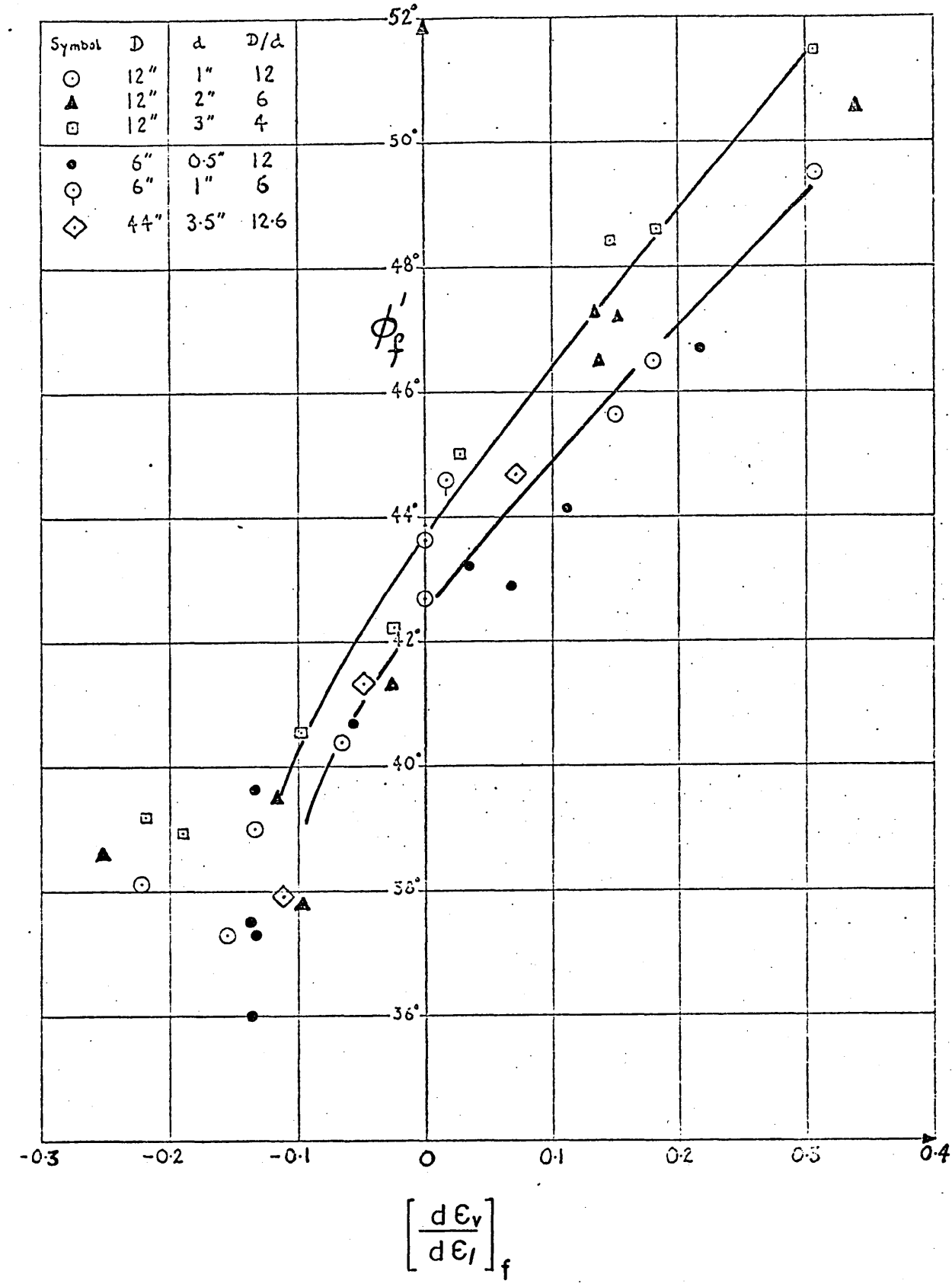

THE RELATIONSHIP BETWEEN ϕ_f' AND $\frac{d\epsilon_v}{d\epsilon_1}$ AT FAILURE FOR VARIOUS TESTS ON NAPA BASALT.

(Reported in Engineering Study 526 : 1967)

FIG 2-18

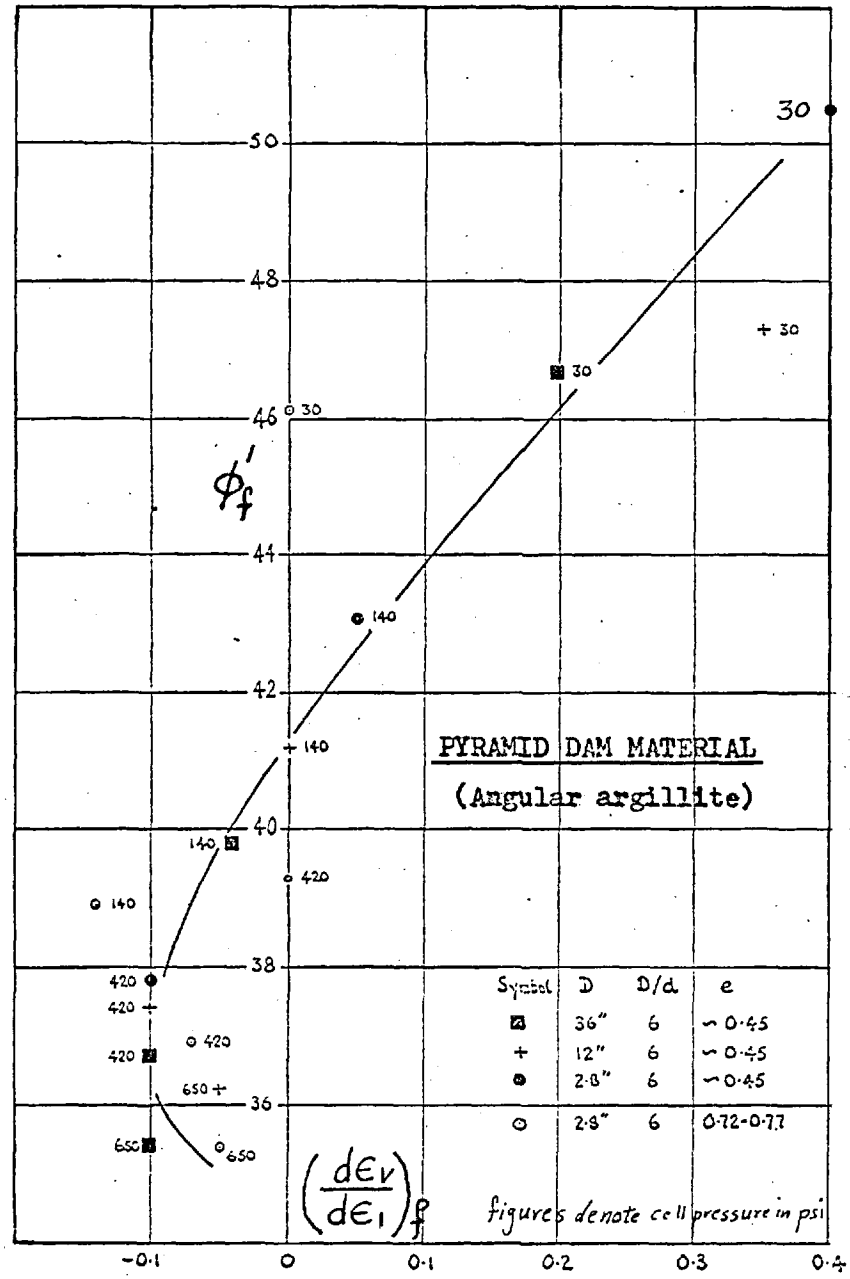

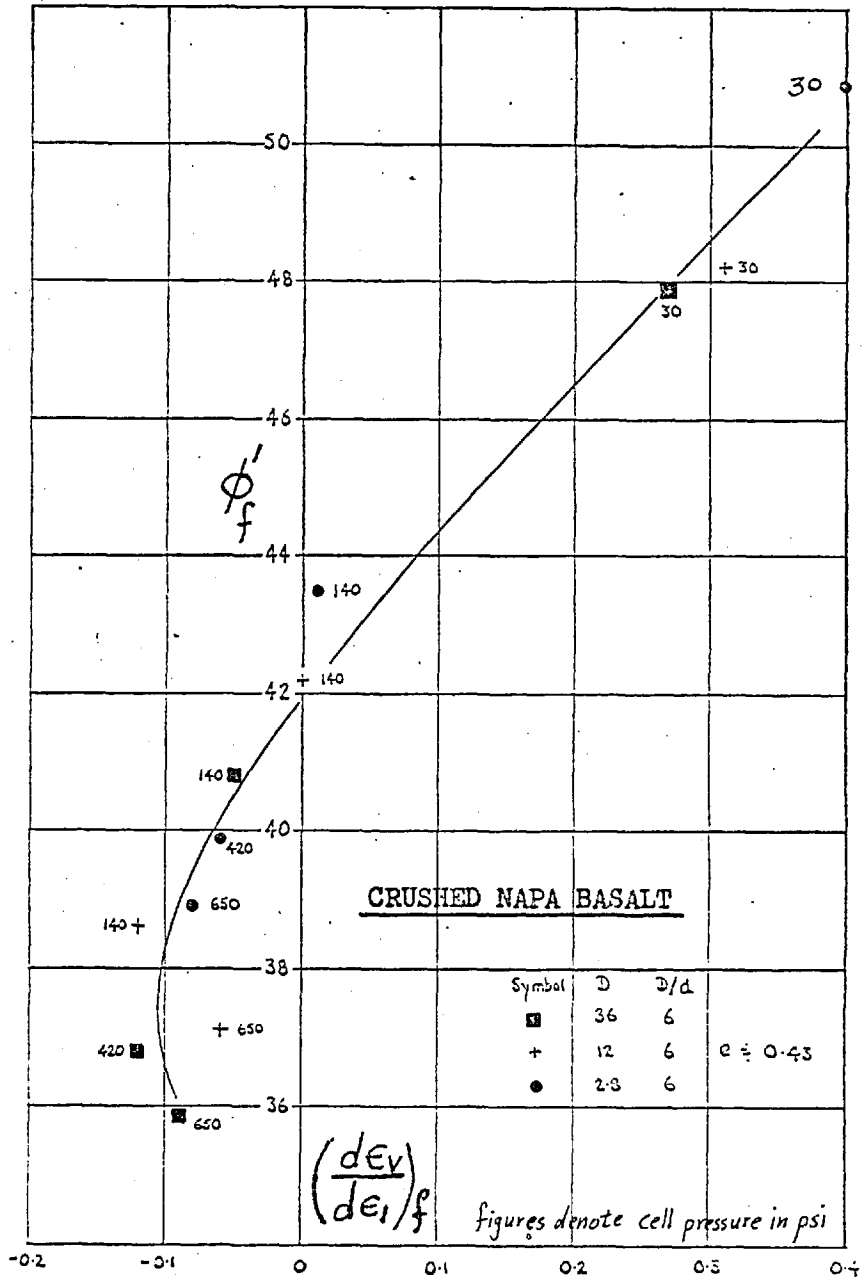

THE RELATIONSHIP BETWEEN ϕ_f' AND $\frac{d\epsilon_v}{d\epsilon_1}$ AT FAILURE FOR PYRAMID DAM MATERIAL AND FOR CRUSHED NAPA BASALT. (DATA FROM MARACHI ET AL, 1969)

NOTE: THE RELATIONSHIP FOR OROVILLE DAM MATERIAL IS SHOWN IN FIG. (2 - 17)

FIG. 2-19

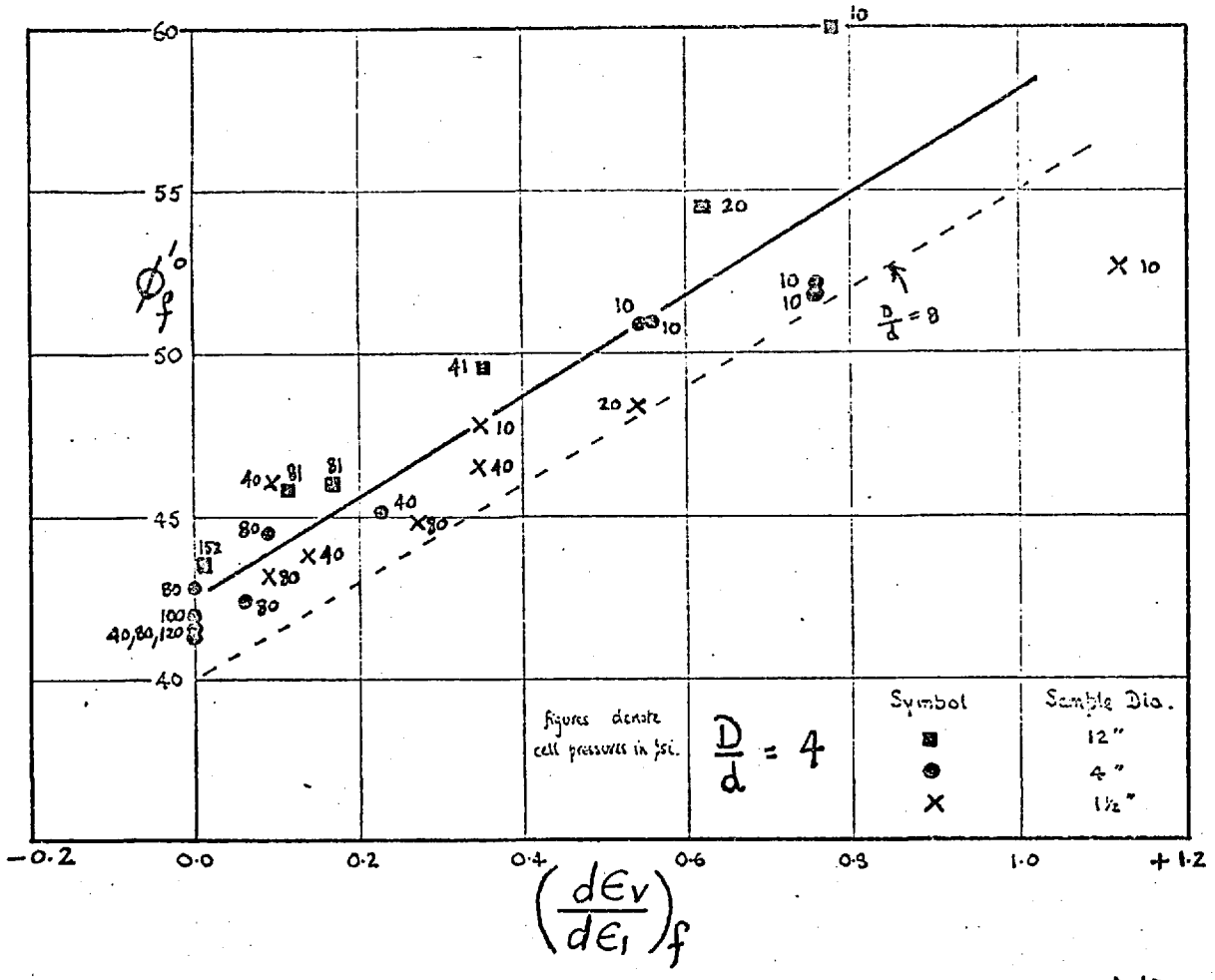

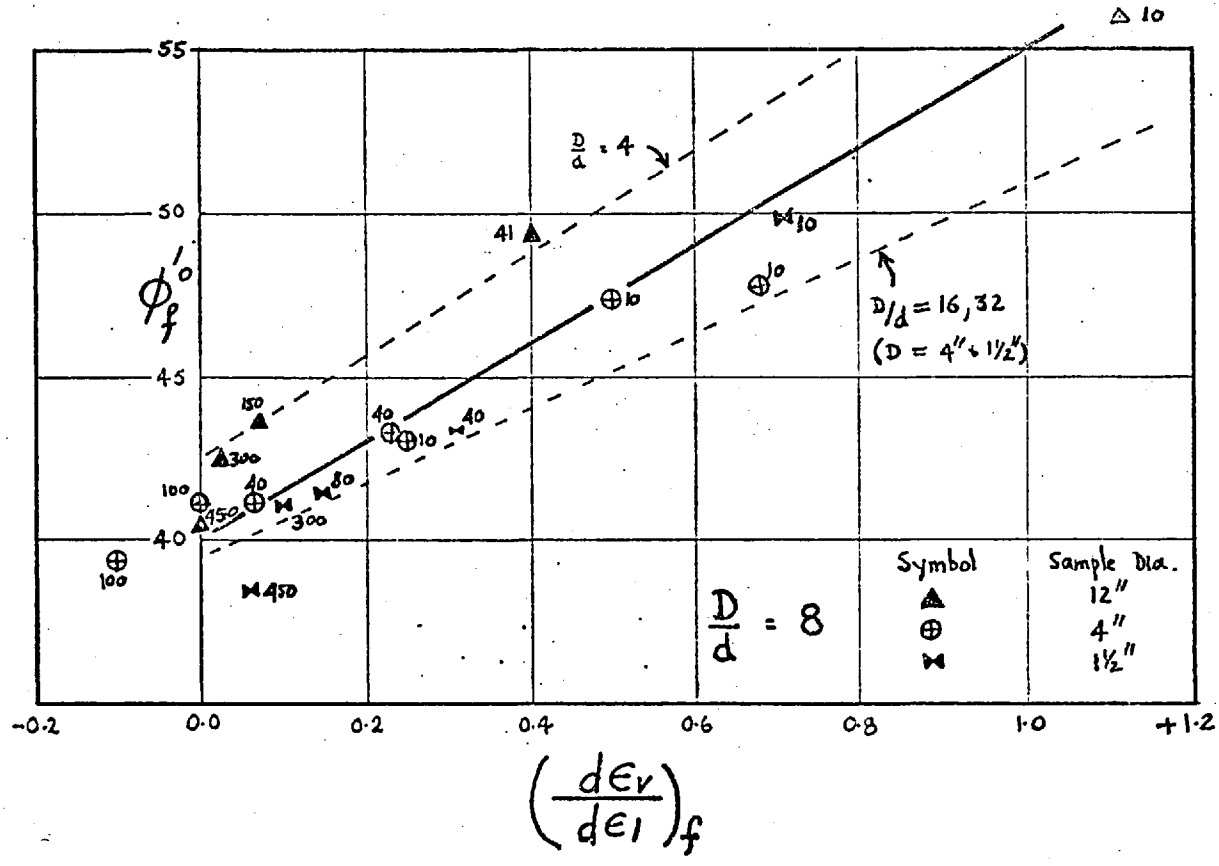

THE RELATIONSHIP BETWEEN ϕ'_f AND $\left(\frac{d\epsilon_v}{d\epsilon_1}\right)_f$ FOR DRAINED TRIAXIAL TESTS ON GRANITE ROCKFILL. (Data from Tombs, 1969)

FIG. 2-20a

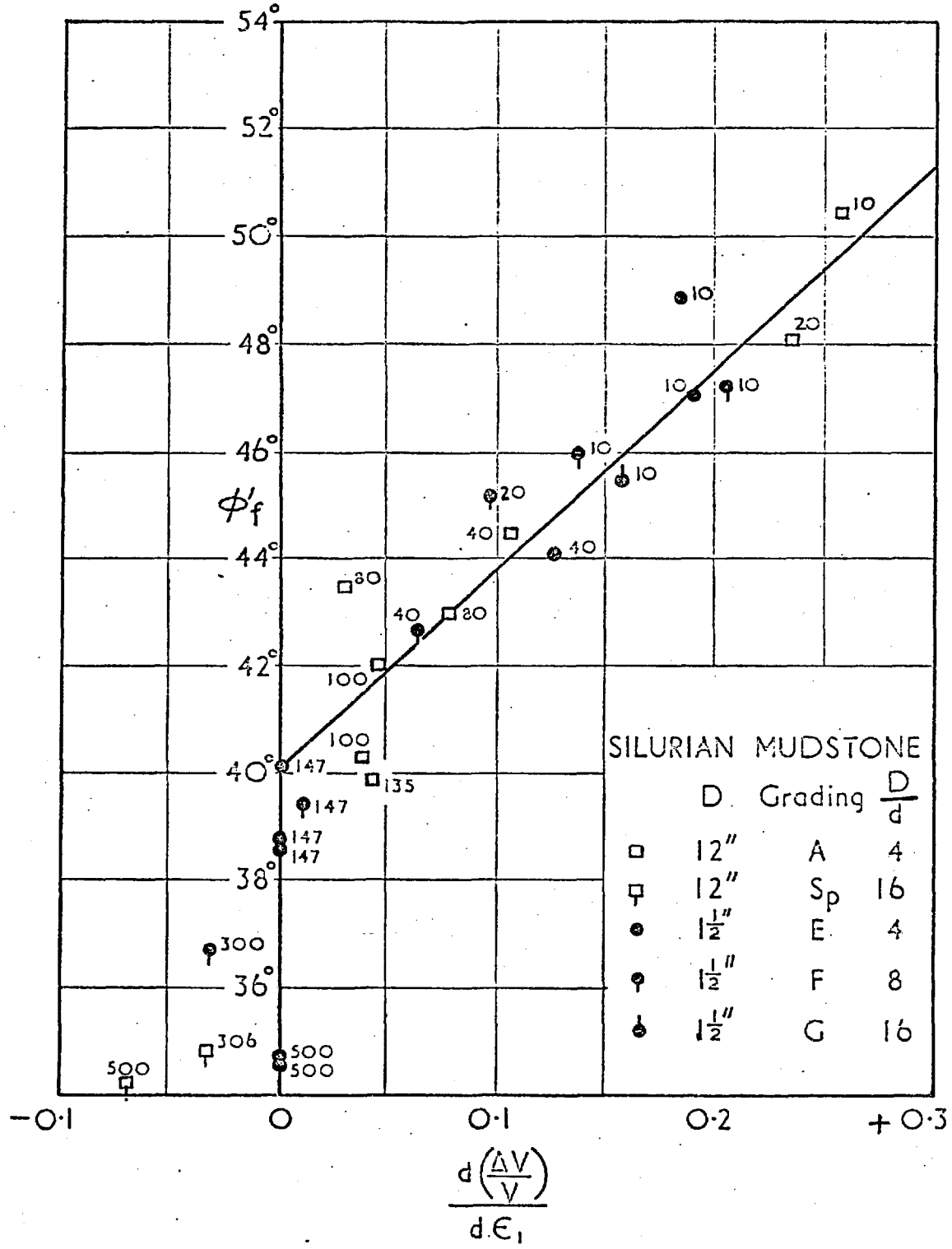

THE RELATIONSHIP BETWEEN ϕ'_f & RATE OF VOLUME CHANGE $d\left(\frac{\Delta V}{V}\right)/d\epsilon_1$ AT FAILURE FOR DRAINED TESTS ON SATURATED ROCKFILL : SILURIAN MUDSTONE FROM LLYN BRIANNE. (Data from Tombs, 1969)

FIG. 2-20b

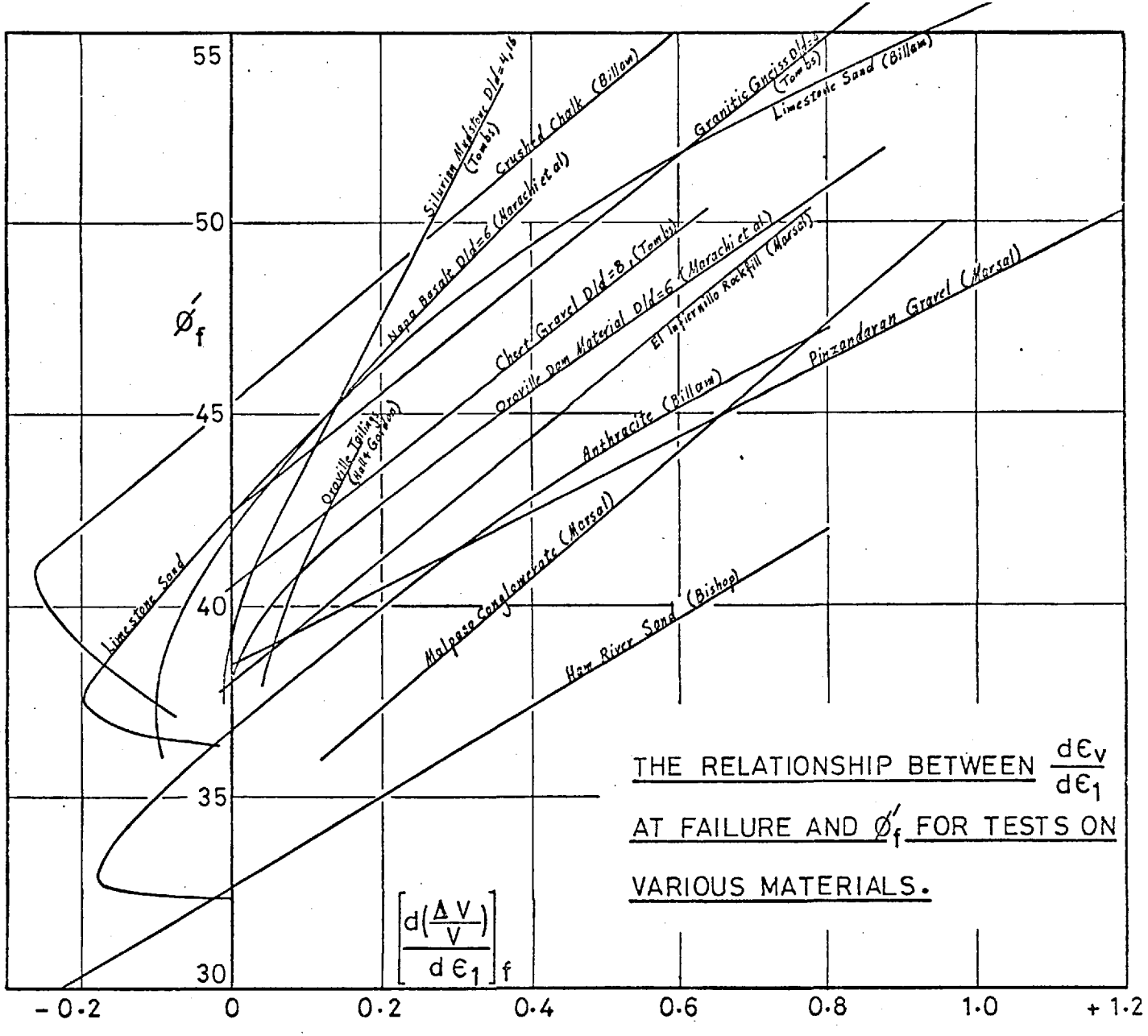

THE RELATIONSHIP BETWEEN $\frac{d\epsilon_v}{d\epsilon_1}$ AT FAILURE AND ϕ'_f FOR TESTS ON VARIOUS MATERIALS.

FIG. 2 - 21

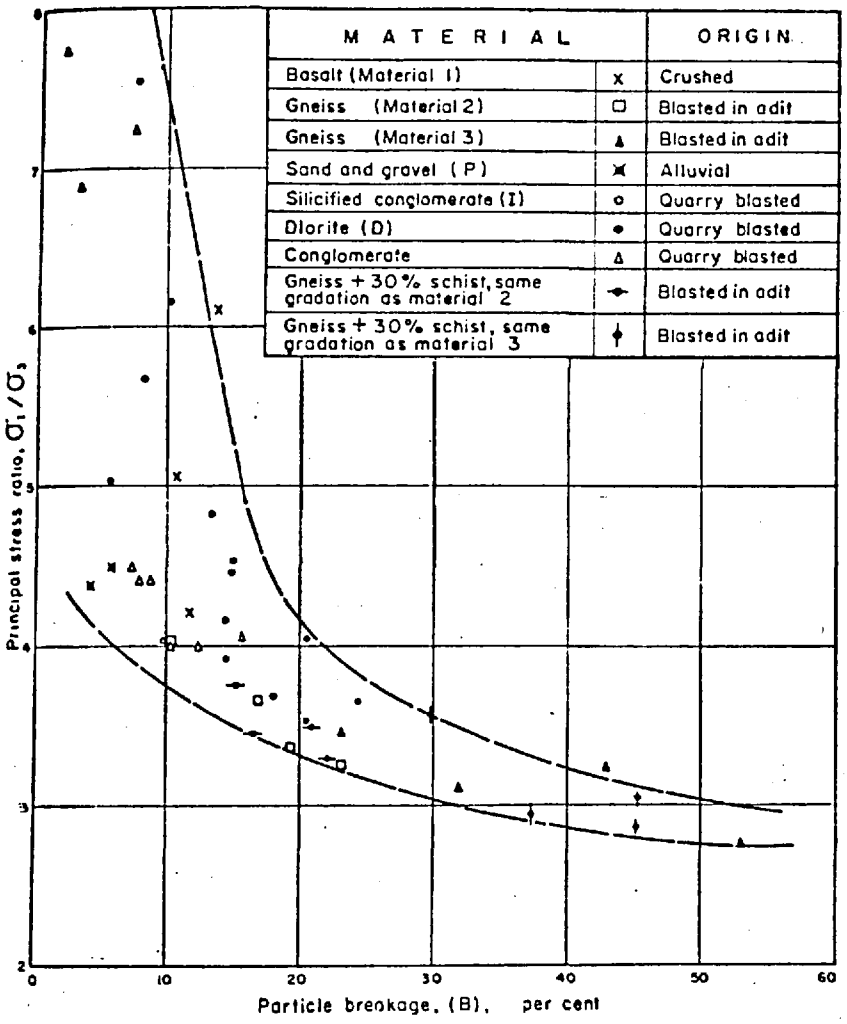

CORRELATION OF THE PRINCIPAL STRESS RATIO AT FAILURE AND PARTICLE BREAKAGE. (AFTER MARSAL 1967a)

FIG 2-22

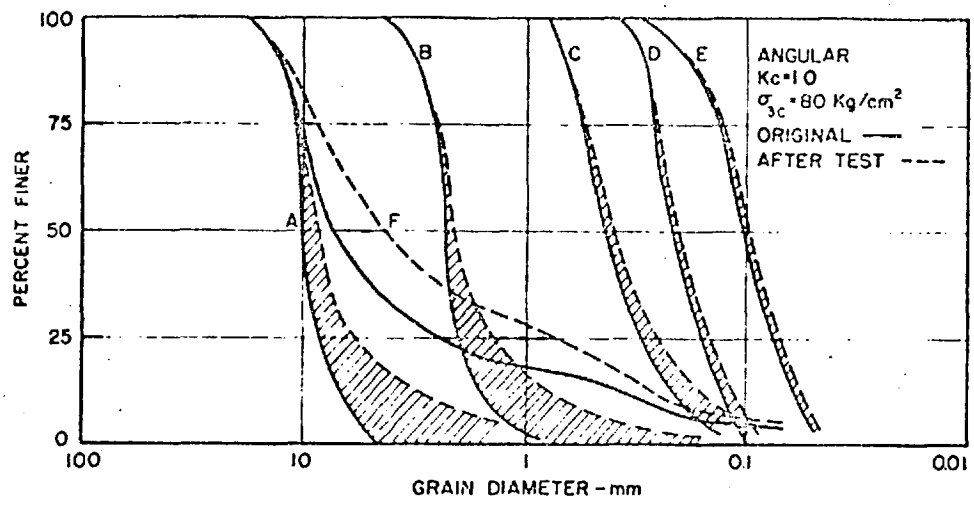

(A)

COMPARISON OF CRUSHING OF SOILS WITH DIFFERENT INITIAL GRAIN SIZES (AFTER LEE & FARHOOMAND, 1967)

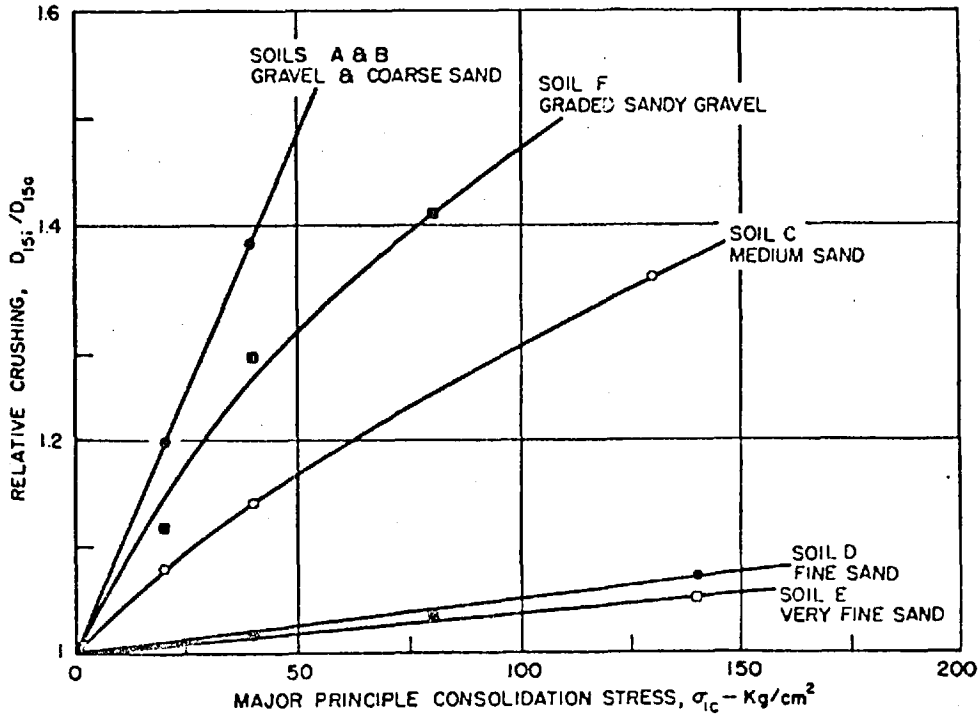

(B)

COMPARISON OF RELATIVE CRUSHING OF DIFFERENT INITIAL GRAIN SIZES: ANGULAR, $K_c = 1.0$ (AFTER LEE & FARHOOMAND, 1967)

FIG. 2 - 23

CHAPTER III

THE STRESS-STRAIN BEHAVIOUR OF GRANULAR MATERIALS

3.1 Introduction

The first extensive study on the yielding of cohesive soils was begun by Rendulic (1936, 1937) and Hvorslev (1937). The difference between the works of Rendulic and Hvorslev is that Rendulic described the process of yielding of a normally consolidated clay, while Hvorslev was concerned with the failure stress condition. The two previous works were not extended or modified until Roscoe started to study Hvorslev's failure criterion in the early 1950s. Then Roscoe, Schofield and Wroth (1958) published the first of a series of papers on yielding of soils at Cambridge University, followed by many other papers by the Cambridge research group.

Henkel (1959, 1960) extended Rendulic's ideas by his extensive research work on saturated remoulded clays at Imperial College. Henkel was mainly concerned with the dependence of water content on stress. Ladanyi (1960, 1964) extended Rendulic's and Henkel's work by using space diagrams which include shear strain as a parameter.

There is another approach to the study of the stress-strain behaviour of soil. This approach is based on the analysis of models of discrete particles and it has mainly been used to study the behaviour of granular materials. One of the authors in this field is Rowe (1962, 1963) who discussed the deformation and failure of a simple arrangement of particles in contact.

In this chapter the fundamental concepts used in studying the yielding of granular soils will be discussed briefly. In subsequent sections the main stress-strain theories and models used for granular soils will be discussed and reviewed.

3.2 Scope of the Review and Discussion in this Chapter

In this chapter the literature review and discussion will be limited to the pre-failure behaviour of granular soils. For the behaviour of granular materials under generalised strain and stress conditions,

especially at failure, there is a considerable amount of published work, e.g. Green, (1969); Reades, (1972); Lade and Duncan (1973) among others.

As far as the application of theory of plasticity in soil mechanics is concerned, there are many ideas and theories in this field. This can be seen clearly in the Proceedings of the Symposium on Plasticity and Soil Mechanics held in Cambridge, 1973. It is not the object of this thesis to discuss all these ideas, but some of them will be referred to in the appropriate place. In this chapter the discussion will be restricted to the main plastic models introduced in soil mechanics, while the elastic ones will be mentioned briefly. Also the discussion will be concentrated on the behaviour of granular materials under drained conditions.

3.3 Components of Strain

3.3.1 General

Elastic, plastic and real deformation of solids have been discussed thoroughly in many text books (Love, 1892; Nadai, 1963; Hill, 1950, etc.) In studying the stress-strain behaviour of soils, it is essential to distinguish between elastic and plastic deformations.

Love (1892) stated that the elastic strain increments are functions of the causative stress increments, while Hill (1950) defined the plastic strain increments as a function of the current stresses and independent of the stress increments*.

Drucker (1964a) stated that during a plastic deformation the energy supplied by the external loads was dissipated within the material while during an elastic deformation the energy was stored and, consequently, was recoverable on unloading. Rowe (1971a) defined a plastic strain as one which is irrecoverable on unloading while Wroth (1971) equated elasticity with linearity of the stress-strain response.

---

* on condition that the stress increments are directed outwards from the current yield surface.

Throughout this thesis the elastic strain will be defined as the recoverable strain during unloading while the plastic strain is irrecoverable. In other words, the definitions of Love, (1892) and Hill (1950) will be adopted. Hence the constitutive equations may be written as:

The Elastic Strain Increment $d\epsilon_{ij} = F(d\sigma'_{kl})$

The Plastic Strain Increment $d\epsilon_{ij} = G(\sigma'_{kl})$

In the case of F = Constant, then the deformation is both linear, reversible and conservative.

3.3.2 Components of the Volumetric Strain

Consider a soil element of any initial void ratio (e) which is subjected to stress increment (dp', dq). The overall volumetric strain may be separated into two components:

$$d\epsilon_v = d\epsilon_v^p + d\epsilon_v^e \qquad \ldots\ldots \qquad (3.3.1)$$

where the superfixes e and p represent the elastic and plastic components respectively*. This could be shown by Figure (3-1) where (AB) is the strain path of the element after it was subjected to the stress increment (dp'). Now if the stresses are removed (on the same stress path as loading) the soil element will expand to point (C). The volume change associated with the unloading is the recoverable volume change and will be called here "The elastic volume change". If $(d\epsilon_v^e)$ is true elastic volumetric strain, then on loading again (on the same stress path), the volumetric strain path will follow the line (CB). Roscoe et al (1963a) and Schofield and Wroth (1968) used the isotropic swelling line to measure the elastic volumetric strain as described above. They assumed the isotropic swelling lines of Cam clay on the e - ln p' plot are parallel and straight. Based on this assumption they derived relationships for the plastic components of both void ratio and volumetric strain in terms of the mean effective normal stress.

---

* Drucker et al (1957) gave a similar equation for a soil element at a state (e, p, q), but in terms of void ratio, $(de = de_e + de_p)$.

Roscoe et al (1958) stated that the elastic volume change is proportional to dp', but it is noted that elastic volume change also occurs with p' constant.

Schofield and Wroth (1968) identify "Granta-Gravel" as having no recoverable strain on unloading. This behaviour has not been observed for real granular soils. For "Wet Clay" Roscoe and Burland (1968) refer to a "Vertical Elastic Wall" in (e, p, q) space. Movement over the wall surface allows a variety of p' - q paths some of which involve varying q/p' ratios. It will be shown that non-elastic strain occurs for those paths which are not admissible in the model. Rowe (1971a) derived equations for the elastic strains and concluded that for general application it is necessary to consider combinations of slip and elastic strains. It can therefore be seen that there are different thoughts about the elastic behaviour of soils.

3.3.3 Components of the Shear Strain

Here the shear strains could be separated into elastic and plastic components in the same way as the volumetric strains were separated. Figure (3-2) shows the strain path of a sample loaded by stress increments (dp' & dq), where AB & BC are the loading and unloading paths respectively. Here also if ($d\gamma^e$) is true elastic shear strain, then on loading again (on the same stress path), the shear strain path will follow the line (CB). Therefore the components of shear strain could be expressed as

$$d\gamma = d\gamma^e + d\gamma^p \qquad \ldots\ldots \qquad (3.3.2)$$

where the superfixes e and p represent the elastic and plastic components respectively. This is the expression that has been adopted by the Cambridge research group.

3.4 Elastic Models for Soils Deformation

3.4.1. Properties of the Elastic Model

The properties of the elastic model were described in detail by Love, (1892). In this section the main properties will be mentioned only.

As has been stated earlier, the constitutive equations for an elastic material whether isotropic or anisotropic are:

$$d\epsilon_{ij} = C_{ijkl}\, d\sigma'_{kl} \qquad \ldots\ldots \qquad (3.4.1)$$

where Cijkl is a 4th order tensor containing 21 independent coefficients; these coefficients may or may not be constants. But the strain increments are unique functions of the stress increments and they occur instantaneously. Since Eqn. (3.4.1) holds for $\mp\, d\sigma'_{kl}$, the strains are fully recoverable on unloading. Hence the energy supplied by the external loads during loading is fully recoverable on unloading and therefore the strains are path independent and the principal of superposition is valid. When all the coefficients in Cijkl are constants over the range of the stress increments under consideration, the model is linear elastic over that stress range.

If a certain symmetry condition is assumed, the number of independent coefficients in Cijkl will be reduced. For the case of an isotropic material the tensor Cijkl contains only two independent coefficients; these may or may not be constants depending on whether or not the condition of linearity is imposed. One of the main consequences of isotropic elasticity is that shear and volumetric strains may be separated and a purely deviatoric stress increment does not cause any volume change. This is in contrast to the case of elastic anisotropy where shear and volumetric strains may no longer be separated and a purely deviatoric stress increment may cause volumetric strains.

For the case of linear elasticity, Eqn. (3.4.1) may be written as

$$\Delta\epsilon_{ij} = C_{ijkl}\, \Delta\sigma'_{kl} \qquad \ldots\ldots \qquad (3.4.2)$$

where the coefficients in Cijkl are constant. For the case of non-linear elasticity total strains may be obtained by analytical or numerical analysis methods.

3.4.2. The Isotropic Elastic Model

Love (1892) stated that the complete stress-strain behaviour of the isotropic elastic model may be obtained from two independent elastic constants: Young's Modulus E' and Poisson's Ratio ν'.

If σ'_1, σ'_2, σ'_3 and ϵ_1, ϵ_2, ϵ_3 are the principal stresses and strains respectively, the stress-strain relations referred to the principal axes for an isotropic elastic material may be written as:

$$d\epsilon_1 = \frac{1}{E'} \left[d\sigma'_1 - \nu (d\sigma'_2 + d\sigma'_3) \right]$$

$$d\epsilon_2 = \frac{1}{E'} \left[d\sigma'_2 - \nu (d\sigma'_3 + d\sigma'_1) \right] \quad \ldots\ldots \quad (3.4.3)$$

$$d\epsilon_3 = \frac{1}{E'} \left[d\sigma'_3 - \nu (d\sigma'_1 + d\sigma'_2) \right]$$

In terms of shear strains* the equations may be written as:

$$\frac{d\epsilon_1 - d\epsilon_2}{2} = \frac{1 + \nu'}{E'} (d\sigma'_1 - d\sigma'_2)$$

$$\frac{d\epsilon_2 - d\epsilon_3}{2} = \frac{1 + \nu'}{E'} (d\sigma'_2 - d\sigma'_3) \quad \ldots\ldots \quad (3.4.4)$$

$$\frac{d\epsilon_1 - d\epsilon_3}{2} = \frac{1 + \nu'}{E'} (d\sigma'_1 - d\sigma'_3)$$

or in a tensor form, the equations will be:

$$d\gamma_{ij} = \frac{1}{G'} (d\sigma'_i - d\sigma'_j) \quad \ldots\ldots \quad (3.4.5)$$

where $$G' = \frac{E'}{2(1 + \nu')} \quad \ldots\ldots \quad (3.4.6)$$

Here G' is called the "shear modulus". In the same way, the volumetric strain increment could be derived as follows:

$$d\epsilon_v = d\epsilon_1 + d\epsilon_2 + d\epsilon_3 \quad \ldots\ldots \quad (3.4.7)$$

---

* For this particular discussion the shear strain is assumed equal to $(\epsilon_1 - \epsilon_3)$.

From equations (3.4.3) and (3.4.7) it follows that

$$d\epsilon_v = \frac{1 - 2\nu'}{E'} (d\sigma'_1 + d\sigma'_2 + d\sigma'_3) \quad \ldots \quad (3.4.8)$$

or in a tensor form as:

$$d\epsilon_v = \frac{1}{K} \cdot d\sigma'_{kk} \quad \ldots \quad (3.4.9)$$

where $$K = \frac{E'}{(1 - 2\nu')} \quad \ldots \quad (3.4.10)$$

Here K is called the "bulk modulus".

For the case of drained isotropic loading $\Delta\sigma'_1 = \Delta\sigma'_2 = \Delta\sigma'_3 = \Delta\sigma'$ and equations (3.4.3) give:

$$d\epsilon_i = \frac{d\sigma'_i}{E'} (1 - 2\nu')$$

and $$d\epsilon_v = \frac{3d\sigma'_i}{E'} (1 - 2\nu')$$

then $$\frac{d\epsilon_v}{d\epsilon_i} = 3 \quad \ldots \quad (3.4.11)$$

Therefore the drained isotropic compression test is a good method to check the isotropy in the material. Also Eqn. (3.4.11) is independent of the elastic constants and it may be written as

$$\frac{\Delta\epsilon_v}{\Delta\epsilon_i} = 3$$

irrespective of the linearity or non-linearity of the elastic constants.

Therefore it seems that the isotropic elastic model is very simple and the two elastic constants may be obtained from a single drained triaxial test.

3.4.3 The Anisotropic Elastic Model

The general stress-strain relationships for an ideal anisotropic elastic model are given in many text books, e.g. Jaeger (1969). There are 36 coefficients which could be reduced to 5 independent elastic parameters if there is an axis of symmetry, i.e. the properties of the material are the same in all directions at right angles to it. If only the principal stresses and strains are considered and the axis of the soil symmetry coincides with one of these, the number of coefficients is reduced to 4, since the shear modulus does not appear. This advantage was taken by some researchers in testing soil samples to avoid complicated testing, Atkinson, (1973). Atkinson tested vertical and horizontal samples only, thus the shear modulus did not appear in the stress-strain relationships. The shear modulus is the relationship between shear strain and shear stress in any plane containing the axis of soil symmetry. For the case of drained isotropic loading of an anisotropic material, Atkinson derived a stress-strain relationship which shows that:

$$\frac{d\epsilon_v}{d\epsilon_i} \neq 3 \qquad \ldots \qquad (3.4.12)$$

This is in contrast to Eqn. (3.4.11) for an isotropic elastic material.

3.5 Plasticity Concepts

3.5.1. The Basic Assumptions of the Theory of Isotropic Plasticity

Many problems in soil mechanics such as stability of slopes, bearing capacity and earth pressures are treated as problems of plasticity. In this approach the soil is assumed as an idealised material where the elastic stresses are ignored and only the limiting equilibrium conditions are considered, i.e. rigid plastic behaviour. The basic assumptions of the theory of isotropic plasticity can be briefly summarised as follows*:

---

* Hill, (1950) gives a detailed study of the theory of plasticity.

1. The elastic deformations are assumed to occur instantaneously and they are time independent.

2. The deformations have two components: an elastic one which is recoverable and a plastic one which is permanent. In tensor form:

$$\epsilon_{ij} = \epsilon_{ij}^{e} + \epsilon_{ij}^{p} \quad \ldots\ldots \quad (3.5.1)$$

where the elastic strains are governed by a generalisation of Hooke's laws:

$$\sigma'_{ij} = C_{ijkl}\epsilon_{kl}^{e} \quad \ldots\ldots \quad (3.5.2)$$

3. The material is assumed to be isotropic and it remains isotropic during loading and unloading.

4. The principal axes of the stress and strain rate tensors are coincident for the plastic strains.

5. No Bauschinger effect is considered. A Bauschinger effect is said to occur if a sample is loaded in extension to a yield stress R, then unloaded and reloaded in compression to a yield stress Q, less than R.

6. The existence of a yield function, such as $f(\sigma'_{ij}) = K^2$, fulfils these conditions: the material behaves elastically if $f(\sigma'_{ij}) < K^2$ and yields for $f(\sigma'_{ij}) = K^2$, if the material is perfectly elastic-plastic.

7. The normality condition is valid.

8. The infinitesimal plastic strain increment can be plotted as a vector, in stress space, normal to the existing yield locus (or to the yield surface if in 3-dimension space). The direction of the plastic strain increment vector is thus unique if the yield stress lies on a smooth portion of the yield locus (or the yield surface if in 3-dimension space) but is indeterminable if the stress point is on a corner of the yield locus. However its direction must lie between adjacent normals at the corner.

9. The direction of the plastic strain increment vector is only a function of the current stress but not of the stress increment.

3.5.2 The Plastic Strain Increment Vectors

The strain increments, obtained as a result of an incremental change of stress, will be expressed in terms of their principal values ($d\epsilon_1$, $d\epsilon_2$, $d\epsilon_3$). Since triaxial compression only is considered in this thesis, $d\epsilon_2 = d\epsilon_3$ and the strain parameters used are:

the volumetric strain increment $d\epsilon_v = d\epsilon_1 + 2d\epsilon_3$

the shear strain increment $d\gamma = \frac{2}{3}(d\epsilon_1 - d\epsilon_3)$

These strain increments are represented by vectors called the "strain increment vectors" whose components are $d\epsilon_v$ & $d\gamma$. In most of the published papers in this field the stress and strain spaces are superimposed on each other. As has been pointed out earlier both total $d\epsilon_v$ and $d\gamma$ have two components, elastic and plastic in the case of loading the soil element beyond the elastic range. The elastic strain increment is calculated from the stress-strain relations.

In the derivation of the stress-strain relationships in metals it is assumed that the inclination of the plastic strain increment vectors is only a function of the current stress but not of the stress increment, (Hill, 1950). This means that if an element of material at a given point is at a given state of stress in which additional loading will produce plastic deformations, the inclination of the resulting plastic strain increment vector will be independent of the direction of the stress increment vector and of the previous loading history of the element.

3.5.3 The Normality Rule

The theory of plasticity requires that the plastic strain increment vector should be normal to the plastic potential curve at a smooth point and between adjacent normals at a corner. This requirement is called the "Normality Rule". This rule is widely accepted in

most of the research work in the field of soil mechanics; Drucker et al, (1957); Schofield and Wroth (1968); Roscoe and Burland, (1968), etc.

Many investigators have presented evidence that the normality rule does not necessarily hold for soils, Poorooshasb, Holubec and Sherbourne, (1966, 1967); Pearce, (1970); Frydman, (1972) and others. This has led to many attempts to modify the conventional plasticity theory to correct the discrepancies created by the use of the normality rule. These attempts are in two forms:

1. Development of yield criteria for which the normality rule is valid (an associative flow rule).

2. Development of yield criteria for which the normality rule is not valid (non-associative flow rule).

3.5.4 Plastic Potential Function

Hill, (1950) defined the plastic potential function as "The function defining the ratios of the components of the plastic strain increment". The gradient of the plastic potential curves is a vector in the stress space. Therefore the normals to these curves at any point gives the inclination of the plastic strain increment vectors. A family of plastic potential curves can be obtained by first plotting plastic strain increment vectors in a stress space and then drawing a set of curves normal to the stress vectors. This family of curves would define the plastic potential function.

For the special case of isotropy and the existence of associative flow rule, the plastic potential curve and the yield curve coincide. Therefore the plastic strain increment vector is normal to both curves. Typical plastic potential curves and plastic strain increment vectors are shown in Figure (3-3).

3.5.5 Yield Loci and Yield Surface

Consider an element of idealised work hardening material under a state of stress 'a' which is defined by stress $(\sigma ij)_a$. Now if the material is tested to determine the various combinations of

principal stress under which it yields, and these states of stress are represented as points in the stress space, the points will define a surface called a "yield surface in principal stress space". Various forms of surface have been presented which correspond to various yield criteria. The representation of the yielding point in two dimensional stress plane is called "Yield Locus".

Now consider that the previous element is within a yield locus G, Figure (3-4). Then any stress path ab, af or abc which is within or on the yield locus gives only elastic strains. If the stress point moves outside the yield locus, cd, elastic and plastic strains will occur simultaneously.

Then a new yield locus will be established which will be followed by another one after a further stress increment. In fact perfect plasticity is a limiting case of work-hardening in which the subsequent yield loci all come closer and closer to the original yield locus. In the limit there is just the one yield surface and the stress point cannot go outside it.

Therefore it can be seen that the yield surface is the boundary of the elastic domain and it is path-independent in the sense that a point on it may be approached by many different stress-paths within the elastic zone.

3.5.6 Work-Hardening Plasticity

Soils are often treated as a perfectly plastic material and the plasticity theory was used as a method of solving some soils problems. Of course, soils are not perfectly plastic, and therefore adopting this approach results in a big difference between the prediction (according to theory) and real behaviour. In real soils the volume change during the shearing process is dependent on the stress history of the soil and this cannot be taken into consideration properly when applying the theory of perfect plasticity.

A strain hardening plasticity model was developed for metals yielding beyond the elastic limit and followed the work of Taylor and

Quinney (1931) on thin-walled metal tubes subjected to combined torsion and tension.

To explain strain hardening plasticity, consider an element of ideal elasto-plastic material. If this element is stressed, it will undergo elastic deformations first, then reaches the yield condition where the stress state will lie on the yield surface. Any stress increment (+ or -) will move the state of stress along the yield surface (if loading) or inside the yield surface (if unloading). Hill, (1950) pointed out that during continual deformation the shape of the yield surface may change, but unfortunately little work has been done in this field. Now consider that this element is a strain hardening material, in a state of stress lying on the initial yield surface. If a stress increment is applied (loading), a new yield surface will be developed which is based on the new stress state. Now on unloading the elastic strains will be recovered, then on reloading to a stress state higher than the first one, a new yield surface will be developed, Figure (3-5). This process may be continued until failure is reached. Hill, (1950) suggested that strain hardening is due only to plastic work done on the material and independent of the strain path followed during plastic deformation.

Drucker, (1951) suggested the theory of work hardening to differentiate between ideal plastic and strain hardening materials on the basis of doing plastic work on them. He stated that for work-hardening to occur, the following conditions should be met:

> "Positive work is done by the external agency during the application of the added set of stress", and "the net work performed by the external agency over the cycle of application and removal is positive if plastic deformations have occurred in the cycle."

Therefore work (or strain) hardening means that for all such added sets of stress, positive work is done, and the net work performed during the load-unload cycle is positive. For ideal elastic material, this latter work is zero and for stable material, it is impossible for the net work

to be negative. Finally, Drucker (1951) concluded that:

1. The yield surface is convex.

2. The plastic strain increment vectors are normal to the yield locus or the ratio of the components of the plastic strain increments are independent of the stress increments.

3. The plastic strain increment vector, at a corner of the yield locus, lies inside the conic surface generated by the normals at the yield locus at that point.

Drucker, Gibson and Henkel (1957) treated soil as a work-hardening material which may reach the perfectly plastic state, Figure (3-5). By accepting the normality concept, they proposed spherical end caps for the end of the yield surfaces and suggested that this should be further examined. The work-hardening plasticity model will be discussed in a later section.

3.5.7. The Yield Criteria

As has been pointed out earlier, the theory of plasticity assumed the existence of a yield function of the stresses. Hill, (1950) defined a yield criterion as "A law defining the limit of elasticity under any possible combination of stresses". Various yield criteria have been extensively discussed in the literature (e.g. Kirkpatrick, 1957; Bishop, 1966; Green, 1969), therefore only a brief definition will be given here.*

1. Tresca Yield Criterion: It states that yielding starts when the maximum shearing stress reaches a certain value k. In terms of principal stresses, it is expressed as:

$$\sigma'_1 - \sigma'_3 = 2k \qquad \ldots\ldots \qquad (3.5.3)$$

where $\sigma'_1 \geqslant \sigma'_2 \geqslant \sigma'_3$

---

* For simplicity the yield criteria are given for cohesionless soils only.

2. Von Mises Yield Criterion: This criterion states that yielding occurs when the second invariant of the stress deviatoric tensor attains a critical value. In terms of principal stresses, it is expressed as:

$$(\sigma'_1 - \sigma'_2)^2 + (\sigma'_2 - \sigma'_3)^2 + (\sigma'_3 - \sigma'_1)^2 = 6K^2 \quad \ldots\ldots \quad (3.5.4)$$

where the parameter (K) is the yield stress in pure shear, ($\sigma'_3 = -\sigma'_1$, $\sigma'_2 = 0$).

3. Mohr-Coulomb Criterion: Although this is a failure criterion, it has been used as a criterion for yielding (e.g. Drucker and Prager, 1952; Drucker et al, 1957).

$$(\sigma'_1 - \sigma'_3) = \sin\phi' . (\sigma'_1 + \sigma'_3)^* \quad \ldots\ldots \quad (3.5.5)$$

which means that yielding occurs when the shearing stress reaches a certain value. It can be seen from Eqn. (3.5.5) that shearing stresses vary linearly with normal stresses. Figure (3-6) shows a schematic section for the three yield criteria across the space diagonal ($\sigma'_1 = \sigma'_2 = \sigma'_3$).

It is important to distinguish between a yield criterion and a failure criterion. A yield criterion relates the stresses during plastic deformation (yielding) while a failure criterion states the limiting stresses that the soil can sustain. However, when the soil is deforming at its limiting state the failure criterion is also the yield criterion. For failure condition the Mohr-Coulomb, extended Von Mises and the extended Tresca failure criteria were suggested as possible failure criteria. These proposed failure criteria presented in (σ'_1, σ'_2, σ'_3) stress space form pyramid-shaped surfaces with the apex at the origin and are symmetrical about the stress-space diagonal. As can be seen from Figure (3-6) the right sections for the three yield surfaces are a regular hexagon (Tresca), a circle (Von Mises), and an irregular hexagon with equal sides (Mohr-Coulomb). Until now no agreement has been reached on the failure criterion which best fits the test results. Bishop, (1966) discussed all of them and concluded that the only satisfactory failure criterion

---

* ϕ is the mobilised angle of shearing resistance.

for soils is Mohr-Coulomb. However, Roscoe et al (1963a) suggest that the variations of test results obtained are due to testing techniques and apparatus and that for the present time the simplest failure criterion should be adopted. They concluded that the extended Von Mises failure criterion should be adopted for the time being as the failure criterion for soils.

In metals it has been found that the yielding is unaffected by the hydrostatic pressure, hence its effect has been neglected in the yield criterion. Also the properties of metals are very uniform while those of soils are a function of the density and particle size distribution. Therefore any yield criterion for soils should take into consideration the mean normal stress and the void ratio.

3.5.8 Flow Rules

A flow rule is defined as a relationship between the plastic strain increments and the current stresses. Mathematically it can be expressed as:

$$d\epsilon_{ij} = G(\sigma'_{kl}) \qquad \ldots\ldots \qquad (3.5.6)$$

Many flow rules have been proposed in soil mechanics literature, but only three groups are important at the present:

1. A flow rule based on the normality condition, e.g. Schofield and Wroth, (1968) this is used in the Cambridge theory.
2. The stress-dilatancy flow rule; Rowe, (1962 and 1963).
3. A simple non-associative flow rule, Davis, (1968).

The first and second flow rules will be discussed in the following sections. The non-associative flow rule is in fact outside the scope of this thesis and will not be discussed. In non-associative flow rule the normality rule does not hold, since the velocity fields and displacement fields do not coincide. This matter has been discussed by many workers, de Josselin de Jong, (1958); Harkness, (1971); apparently without stating specific conclusions.

3.6 Plastic Models for Soils

Hill, (1950) defines the plasticity model as the relationship which describes the deformation of a material during plastic flow after yield. Such a relationship could be expressed in a form of a flow rule which relates the plastic strain increments to the current stresses, as:

$$d\epsilon_{ij} = G(\sigma'_{kl}) \qquad \ldots \qquad (3.5.6)\text{bis}$$

As has been shown at the beginning of this chapter, the strains in a perfectly plastic material are indeterminate and a flow rule containing a relationship between principal stresses and strain invariants is required. In connection with this thesis, three models will be discussed in this section, the work-hardening model, the Cambridge model and the stress-dilatancy model.

3.6.1 Isotropic Work-Hardening Plasticity Model

As mentioned earlier, this model has been introduced by Drucker, Gibson and Henkel (1957) and has been used as the basis of the Cambridge incremental stress-strain theories and the critical-state theory (Schofield and Wroth, 1968). The result of applying the normality rule to a material yielding according to the Mohr-Coulomb criterion, is that the material must increase in volume upon yielding. In fact this kind of behaviour occurs in dense sands but not in loose sands. Drucker et al (1957), from a consolidation test, recognised that hydrostatic pressure induces plastic volume changes and a decrease of hydrostatic pressure induces a non-linear elastic volume change. They concluded that " If this type of behaviour is to be considered, perfect plasticity, with an extended Coulomb criterion for a yield surface, is not suitable. The yield surface must cut the axes of the cone because yielding does occur for a state of stress which is represented by a point on the cone axis. Also this behaviour is work-hardening and not perfect plasticity because continuing plastic volume decrease requires increasing pressure." Drucker et al (1957) suggest a solution to this problem. They proposed that the yield surface with its open end be closed by a spherical cap.

Drucker et al examined the validity of the spherical cap assumption by loading the sample through different stress paths and considered the plastic strain increment vectors are normal to the yield surface. They concluded that "The spherical caps are certainly not the proper shape. Other convex yield surfaces should be tried. The theory of stress-strain relations for work-hardening materials is so general that much more can be accomplished with sufficient thought and much additional experimental information." Based on the previous conclusions, the "Cam Clay" model was developed.

Roscoe et al (1963a) suggested that the yield surfaces for clay approximate to a family of "bullet-shaped" domains; the sharp end of the bullet corresponds to the isotropic virgin-consolidation line. Calladine, (1963) suggested that the yield curves are nearly elliptical instead of bullet-shaped. Roscoe and Burland (1968) in tests on normally consolidated clays confirmed Calladine's suggestion and concluded that the volumetric yield locus is an ellipse with one of its principal axes coinciding with the isotropic consolidation line. Although the normality rule was still applied, the flow rule equation by Roscoe and the others was different from that used by Drucker et al (1957).

As far as the shape of the yield surface is concerned, two main conclusions could be drawn from this model:

1. The plastic strain increment vector is dependent only on the current yield stress σ_{ij}, not the stress increment.

2. The direction of the plastic strain increment vector is independent of the loading history. This will be discussed in detail in Chapter 7.

3.6.2 The Cambridge Model

This model was originally based on the isotropic work-hardening plasticity theory introduced by Drucker et al (1957), then many modifications were applied which will be discussed in the following sections. The basic assumptions of the theory of plasticity are applied here and, in addition, specific assumptions were adopted to develop this

model; these assumptions are:

1. The theory has been applied mainly to triaxial tests, and the results are expressed in terms of p', q, ϵ_v and γ^+.

2. The theory applies mainly to "wet" clay, i.e. normally consolidated or slightly over-consolidated clay.

3. The virgin isotropic and anisotropic consolidation lines (q/p' = constant) form a family of curves which could be approximated to a set of parallel straight lines of slope - λ on a plot of e vs. ln p', as shown in Figure (3-7).

4. The swelling lines form a similar set of parallel straight lines with gradients - k, Figure (3-7).

5. The volumetric elastic strain is a function only of p' and is expressed by

$$d\epsilon_v^e = -\frac{de^e}{1+e} = \frac{k}{1+e}\frac{dp'}{p'} \quad \ldots\ldots \quad (3.6.1)$$

6. The elastic shear strain is negligible.

$d\gamma^e = 0$, therefore $d\gamma^p = d\gamma$

Recently two supplementary assumptions were assumed as fundamental to the theory, these are:

7. The rate at which irrecoverable work is dissipated per unit volume of the soil could be expressed as:

$$\frac{dW}{d\gamma} = Mp' \quad \ldots\ldots \quad (3.6.2)$$

where M is the slope of the critical state* line in (p', q) space.

8. Calladine's definition of the state boundary surface is valid.

---

* The critical state line is defined by Schofield and Wroth (1968).

+ Definitions of these terms are given by Schofield and Wroth (1968).

Calladine, (1963) suggested that "If the curve of the state boundary surface, of which the projection on the (e, p') plane is the elastic swelling curve, is itself projected on the (p', q) plane, then the projection represents a yield locus satisfying the normality condition for the non-linear elastic material formed by isotropic virgin consolidation and subsequent unloading."

3.6.2.1 The Basic Concepts of the Cambridge "Triaxial" Compression Theory

(a) The State Boundary Surface

The state boundary surface in (e, p', q)* space is defined as that surface confining a space between itself and the origin, within which a point can represent a state of a soil element but outside which a point cannot represent such a state, Roscoe and Poorooshasb (1963). The space between the state boundary surface and the origin has been called "the state domain". The state boundary surface in the (e, p', q) space and the state domain for a clay are shown in Figure (3-8). The virgin consolidation line is formed by the intersection of the state boundary surface with the q = 0 plane. The equation of this line is:

$$e = e_a - \lambda \ln p' \qquad \ldots\ldots \qquad (3.6.3)$$

where e_a is the value of e when $p' = 1$ and λ is a soil constant. Now any point lying on the virgin consolidation line represents the state of a normally consolidated sample, while a point on the q = 0 plane which is nearer to the origin than the virgin consolidation line represents the state of an over-consolidated sample.

Poorooshasb and Roscoe (1961) proposed a two-dimensional method of plotting the state boundary surface. They suggested the axes as:

$$\eta = \frac{q}{p'} \qquad \ldots\ldots \qquad (3.6.4)$$

and

$$\xi = \frac{1}{p'} \exp\left(\frac{e_a - e}{\lambda}\right) \qquad \ldots\ldots \qquad (3.6.5)$$

---

* These are defined in the nomenclature page.

With these axes the state boundary surface reduces to a single curve, one end-point of which represents the whole of the isotropic virgin consolidation line and the other end-point the whole of the critical state line.

Many other mathematical formulations have been suggested to define the state boundary surface for various types of soils, e.g. Roscoe and Poorooshasb (1963); Roscoe and Burland (1968) and Schofield and Wroth (1968).

(b) The Critical State

Roscoe, Schofield and Wroth (1958) proposed that an element of soil undergoing uniform shear distortion eventually reaches a critical state condition in which it can continue to distort without further change in void ratio or effective stresses p' and q. This line is shown in Figure (3-8) and its projection on the p', q plane is a straight line with equation:

$$q = Mp' \qquad \ldots\ldots \qquad (3.6.6)$$

and when projected on e - ln p' plane another straight line is obtained where:

$$e = \Gamma - \lambda \ln p' \qquad \ldots\ldots \qquad (3.6.7)$$

where Γ is the critical void ratio when p' = 1 and λ is the slope of the virgin consolidation line. A detailed study of the critical state is presented by Roscoe et al (1958) and Schofield and Wroth (1968).

(c) The Yield Locus

Assume a soil element is in a state (p', q, e) on the boundary surface. The yield locus Y is shown in (p', q) plane, Figure (3-9). If a stress-increment vector (dp', dq) is applied in an outward direction from the yield locus, it will cause a plastic strain increment vector of components ($d\epsilon_v^p$, $d\gamma^p$) normal to the yield locus Y. Many mathematical formulations have been derived to define the yield loci, e.g. Schofield and Wroth (1968). Roscoe and Burland (1968) derived the following equation for the yield loci of normally consolidated clay.

$$\frac{d\gamma^p}{d\epsilon_v^p} = -\frac{dp'}{dq} = \frac{1}{\psi} \quad \ldots\ldots \quad (3.6.8)$$

where $(dq/dp') = -\psi$, is the slope of the current yield locus defined by the current stress parameters p' and q.

3.6.2.2 Modifications to the Basic Cambridge Theory

The following problems are encountered when applying the Cam-Clay Model to predict the behaviour of normally consolidated clays.

1. It underestimates the value of the coefficient of earth pressure at rest Ko.

2. It predicts plastic distortion for the case of isotropic virgin consolidation.

Burland (1965) introduced a generalised plastic strain-increment quantity* which is an invariant of the total plastic strain-increment tensor $d\epsilon_{ij}^p$. He also assumed that: "at all states of yielding (or grain slip) the rate of work dissipation with respect to generalised plastic strain is a constant for a given value of mean normal stress".

Therefore $$dW = p' \sqrt{(d\epsilon_v^p)^2 + (M\, d\epsilon^p)^2} \quad \ldots\ldots \quad (3.6.9)$$

and also $$dW = p' \cdot d\epsilon_v^p + q \cdot d\epsilon^p = \sigma_{ij}\, d\epsilon_{ij}^p \quad \ldots\ldots \quad (3.6.10)\text{†}$$

From Eqns. (3.6.9) and (3.6.10) Burland derived the relationship

$$\frac{d\epsilon_v^p}{d\epsilon^p} = \frac{M^2 - (q/p')^2}{2(2/p')} \quad \ldots\ldots \quad (3.6.11)$$

Based on the previous concepts, Burland, (1965) derived an equation for the yield loci and another for the state boundary surface.** Figure (3-10) shows the yield loci for London clay using the original and the modified models.

---

* This quantity is $\sqrt{(d\epsilon_v^p)^2 + (M \cdot d\epsilon^p)^2}$ (where ϵ is the shear strain).

† This is the increment of work dissipated per unit bulk volume of an isotropic continuum during deformation.

** These equations are available in the original paper.

The equation of the yield locus derived by Burland represents an ellipse in q, p' space. The possibility that the yield locus for wet clay might be nearly elliptical was suggested by Calladine, (1963).

Then Burland, (1965) compared predictions given by this modified theory with results of triaxial compression tests on normally consolidated samples of Kaolin. Excellent agreement was found between the predicted and the observed state boundary surface, but there was under-prediction of both shear and volumetric strains. It was noticed that the disagreement with the observed shear strains was a result of irrecoverable shear distortions below the state boundary surface not taken into consideration in either Cam-Clay or the modified Cam-Clay models.

Roscoe and Burland (1968) revised the modified Cam-Clay model to account for the previous deficiencies. This work was based on Burland's (1965) new equation. Two other assumptions were introduced. First, a new yield locus to take into consideration the shear distortion which occurs, without plastic volume change, for state paths beneath the state boundary surface. Secondly, the Mohr-Coulomb criterion is incorporated in the theory to predict rupture when "wet" clays are subjected to stress paths in three-dimensional stress space.

Still the soil constants M, λ and k are used to predict the mechanical behaviour of wet clays under the new general theory. Also Roscoe and Burland (1968) presented comparison of predicted and observed data for drained and partially drained stress controlled triaxial compression and extension tests on Weald clay and Kaolin. In all cases they claimed good performance of the revised Modified "Cam-Clay" model.

The extension of the Cambridge plasticity models to soils on the dry side of the critical state has received little attention, the emphasis has been directed to other models; e.g. elastic and stress-dilatancy models.

Palmer (1965) examined over-consolidated clays and treated them as unstable plastic materials for which the normality rule might not be valid. He concluded that the limit surface (Mohr-Coulomb) cannot be

an envelope of successive yield surfaces since the plastic strain increment vector is not normal to it. He also derived an expression for the internal energy of a clay system and followed the same assumptions adopted by the Cambridge group to derive his model. He found good agreement between theory and experimental results on Weald clay except the predicted values of $(d\delta/d\epsilon_v)$ were smaller in value than the experimental one.

3.6.3 Rowe's Stress-Dilatancy Model

Rowe, (1962) studied the behaviour of an assembly of particles subjected to a load increment. He derived a relation between the applied stress ratio, the true physical angle of friction ϕ_μ, the geometry of the particle arrangement and the rate of change of unit volume relative to the axial strain for a given particle arrangement. For granular materials this relationship is expressed as:

$$\frac{\sigma'_1}{\sigma'_3} = \left(1 + \frac{d\epsilon_v}{d\epsilon_1}\right) \tan^2 \left(45 + \frac{1}{2}\phi_\mu\right) \quad \ldots\ldots \quad (3.6.12)$$

or in a short form as: $R = D K_\mu$ $\ldots\ldots$ (3.6.13)

and for soils having a cohesion intercept as

$$\frac{\sigma'_1}{1 + \left(\frac{d\epsilon_v}{d\epsilon_1}\right)} = \sigma'_3 \tan^2 \left(45 + \frac{\phi'_f}{2}\right) + 2\, C_\mu \tan \left(45 + \frac{\phi'_f}{2}\right) \quad \ldots \quad (3.6.14)$$

or in a short form as:

$$\frac{R}{D} = Kf \left(1 + \frac{2C_\mu}{\sigma'_3 \sqrt{Kf}}\right) \quad \ldots\ldots \quad (3.6.15)$$

where $Kf = \tan^2 \left(45 + \frac{\phi'_f}{2}\right)$

where the nomenclature is as mentioned at the beginning of the thesis.

There are many methods for measuring the value of ϕ_μ but some of them are questionable; therefore Rowe, (1962) replaced (ϕ_μ) by an empirical parameter ϕ'_f where:

$$\phi_\mu \leqslant \phi'_f \leqslant \phi'_{cv}.$$

Two main assumptions have been used in the derivation of Eqn. (3.6.12). First, the deformations are mainly due to sliding of particles and the deformations due to rolling are negligible. Secondly, the application of the principal of least work to a random mass of irregular particles is valid.

The relationship between ϕf and ϕ_μ has been discussed in Section 2.5.3.2 . In this respect Skinner (1969) concluded that there is no direct relationship between ϕ_μ and ϕ' or $\phi'cv$. The derivation of $\phi' f$ from ϕ_μ has been attributed to the deformations due to rolling of particles not included in the original model which recognised only interparticle sliding; Skinner, (1969); King and Dickin, (1970) and Bishop, (1971). But Horne (1965 a and b), supported Rowe's assumption and concluded that the rotation of particles could be ignored.

These criticisms concerning the use of the ϕ_μ parameter had led Rowe, (1971a) to re-examine the model and propose empirical values for $\phi' f$ as follows:

Triaxial compression $\sigma'_2 = \sigma'_3$ or extension $\sigma'_2 = \sigma'_1$,	
Dense Sand, pre-peak	$\phi' f = \phi_\mu$
Dense Sand, large strains	$\phi' f = \phi' cv$
Loose Sand, all strains	$\phi' f = \phi' cv$
Plane strain, all packings and all strains prior to and including critical state	$\phi' f = \phi' cv$

Indeed the most extensive investigation into the movement and deformation of individual particles has been carried out by Sharma, (1975). Sharma carried out a series of tests on various types and shapes of granular materials and used an X-ray photogrammetric technique to detect the movement of the particles. He observed that the mechanics of deformation involve both rolling and sliding of particles. Thus he contradicted Rowe's first assumption mentioned earlier.

The second assumption concerning the validity of the application of the principal of least work (Rowe, 1962) has been criticised by Gibson and Morgenstern, (1963); Trollope and Parkin, (1963) and Roscoe and Schofield, (1964), while it has been supported by Horne, (1965 a and b, 1969).

Barden, (1969) summarised the concepts on which the stress-dilatancy theory was based as:

1. The minimisation of the energy absorbed in frictional heat loss under certain deformation conditions;

2. The degree of anisotropy induced in the packing geometry.

3. The degree of freedom imposed by the overall strain conditions.

The minimisation of the work done by the major principal stress to that of the minor principal stress is only valid when the assembly can deform with the maximum degree of freedom, as in the axisymmetric deformation where $\phi'f$ approaches ϕ_μ regardless of the initial porosity of the sample; Barden, Khayatt and Wightman (1969). If the degree of freedom is restricted, the above assumption is no longer valid, e.g. in plane strain conditions $\phi'f$ tends to $\phi'cv$, and also during post-peak deformation.

In addition to what has been mentioned, three more interesting points have to be recognised:

1. The dilatancy factor D has been calculated by Horne (1965 a and b) to have a maximum value of 2 (Dmax = 2) for axisymmetric compression with the assumption of no particle crushing, and Barden and Procter, (1971) reported that there is a unique relationship between Dmax and the initial porosity. Rowe (1969) and Barden (1969) concluded that Dmax is not the same for triaxial compression and plane strain conditions.

2. The stress-dilatancy theory would predict failure when the equivalent inter-particle friction angle $\phi'f$ is reached in the

true inter-particle slip direction*. The Mohr-Coulomb criterion is no longer valid when there is volume change during shear.

3. The predictions of the stress-dilatancy theory are only defined but not followed for triaxial extension tests. This has been discussed in detail by Barden and Procter, (1971); Barden, Khayatt and Wightman, (1969); Horne, (1969).

Referring to the stress-dilatancy equation, R = DK, it is seen that the dilatancy factor D expresses some form of the ratio $d\epsilon_3/d\epsilon_1$ (this depends on the condition of loading) and K, is defined by the term $\tan^2(45 + \frac{\phi'_f}{2})$, where $\phi_\mu \leqslant \phi'_f \leqslant \phi'_{cv}$. Therefore the stress-dilatancy relationship, R = DK, is a flow rule because it expresses the relationship between stresses and developed strains. It has been used as a flow rule, and plastic potentials for triaxial compression and plane strain conditions have been predicted, e.g. Barden and Khayatt (1966); Barden, Ismail and Tong, (1969) and Rowe, (1971a).

3.7 The Soil Models and the Behaviour of Real Soils

3.7.1 The Mathematical Soil Models in General

Different elastic and plastic models have been presented and discussed in the previous sections. As has been pointed out, these models assume the soil as an ideal material (linear elastic, plastic, work-hardening or linear elastic-plastic). But natural soils have such a wide range of properties that up to now no model has been able to cope with all these variations of behaviour.

From the general review of the models, it seems there are more fundamental differences between various plasticity models than for the elasticity ones. For example, all the elasticity models predict contractive behaviour as long as Poisson's ratio is kept less than 0.5, and non-linearity in the soil behaviour is accounted for by varying the modulus of elasticity or the shear modulus values. This is in contrast to plasticity

---

* This has been indicated by Rowe, (1971b).

models where volume changes may vary from strongly dilating to strongly consolidating, and non-linearity may be simulated by one of the strain hardening laws. These differences between various elastic and plastic models were also noticed by Audibert, (1972) in a general review of mathematical models used in continuum solution of boundary value problems.

It also appears from the previous review that most of the elastic and plastic models adopt empirical curve approximations or stress-strain relationships in their derivation. For example the Cambridge model described by Schofield and Wroth (1968) and its modifications described by Roscoe and Burland (1968) adopt a linear relationship between the volumetric strains and the logarithm of consolidating pressures; as follows:

$$e = e_o - \lambda \ln p' \quad \ldots\ldots \quad (3.7.1)$$

*

This simple approximation means that the incremental bulk modulus of the soil varies linearly with p'. It will be seen in Chapter 7 that this is not true for rockfill material.

Curve approximation procedure is also used in non-linear elastic models to calculate the modulus at any stress level. For elastic-plastic material the stress-strain curve is assumed elastic up to a certain point then perfectly plastic. Again this is a simple approximation of the real behaviour of soils.

3.7.2. The Elastic and Plastic Behaviour of Soils

In this section the discussion will be limited to the pre-failure stress-strain behaviour of soils. As has been pointed out in the previous sections, the separation of deformation into elastic and plastic components is not easy. It has been suggested that there exists an elastic yield zone at an early stage of the deformation which is then followed by yielding (plastic or a combination of elastic and plastic deformation). This suggestion will be discussed in detail in Chapter 7 together with an experimental investigation. At this stage it is necessary to describe

---

*The nomenclatures were described in the previous sections.

briefly the complete stress-strain curves of two main groups of soils and leave the subject of elastic and plastic zones to Chapter 7.

First, dense granular soils[1] and over-consolidated clays: the stress-strain curves for these materials have a pronounced peak with a clear reduction in strength after peak[2] associated with small or dilatant volume change[3]. The general feature of the stress-strain curves of this group of soils has been thoroughly described by many workers, e.g. Bishop, (1966, 1971).

Secondly, loose granular soils and normally consolidated clays: the stress-strain curves for these materials slowly approach peak at large strains associated, usually, with decrease in volume[3]. According to the critical state theory and its modifications, the first group is on the dry side of the critical and the second group is on the wet side. The critical state theory assumes the deformation of dry soils as elastic while that of wet soils is assumed as plastic and at failure all soils are assumed to reach critical states where the deformations are perfectly plastic. These assumptions have been strongly criticised by many workers, e.g. Bishop, (1971) and Skinner, (1975).

By studying typical stress-strain curves for over-consolidated clays, it can be concluded that a simple linear elastic model could be used to predict stresses and strains up to about 50% of the failure load[4]. This is in contrast to normally consolidated clays and loose sands where the deformation throughout the whole loading is not elastic. For dense granular materials the picture is not clear. However the early deformation characteristics for sand have been discussed by Rowe, (1971a) and Skinner, (1975). It can be concluded that simple elastic models are notaccurate enough to predict stresses and strains in granular materials.

---

1. Dense granular soils will be discussed in detail in Chapter 7.
2. Bishop, (1967) described the post-peak strength reduction by a brittleness index, I_B.
3. This is very much influenced by the stress levels.
4. A similar conclusion has been reached by Atkinson, (1973).

The plastic behaviour of soils is more complicated to investigate than the elastic behaviour. Atkinson, (1973) reviewed briefly many published works and concluded that simple plasticity could reasonably be applied to all soils at the states of limiting equilibrium satisfying the Mohr-Coulomb failure criterion.

Studying the deformation of granular materials at failure and post-peak is outside the scope of this thesis and therefore the discussion will be restricted to pre-failure deformations only. As has been pointed out in the previous section, many models were suggested to define the plastic behaviour of soils; therefore these models will be discussed separately in the following sections.

3.7.3 The Strain-Hardening Plastic Behaviour of Soils

Here the strain-hardening plasticity and Cambridge models will be discussed together since the former theory is the basis for Cambridge work. In Section 3.7.2 it was pointed out that the pre-peak deformations of over-consolidated clays are approximately elastic; hence the discussion in this section will be concentrated on granular materials, normally consolidated clays and lightly over-consolidated clays.

The critical state theory (Schofield and Wroth 1968) defines the deformation of soils at any state below the state boundary surface as elastic while for soils on or outside the state boundary surface the deformations are plastic and the normality rule is valid*. Also the theory assumes that the volumetric and shear strains are unique functions of the octahedral normal and shear stresses respectively. Also the theory indicates that the plastic strain increment vectors are independent of the stress history and the stress increments.

Schofield and Wroth (1968) presented two models to describe the deformation of soils: one the Granta gravel model which assumes only plastic strains, and the other the Cam-Clay model which assumes both elastic and plastic volumetric strains occurring simultaneously.

---

* Pearce, (1970) pointed out that not all Cambridge formulations require normality.

The Cam-Clay model has been used to predict strains for normally and lightly over-consolidated clays. It has been reported that strain fields could easily be predicted by the model and a good agreement was claimed, Burland, (1967, 1971). In contrast to this it appears that the model is not useful in predicting the stress fields in other soils*.

To examine the validity of the strain-hardening plasticity theory experimentally, a soil sample is loaded to a point on the state boundary surface by different stress paths and then stress probes in different directions in stress space are applied. The theory states that the direction of the resulting plastic strain increment vectors is identical for all the stress probes irrespective of their previous stress paths or the stress increments. This kind of test has been reported by Holubec, (1966) and Poorooshasb et al (1966, 1967) for Ottawa sand; Pearce, (1970); Lewin and Burland, (1970) for remoulded slate dust and Namy, (1970) on Newfield clay. Pearce's tests were carried out in the Cambridge true triaxial apparatus while the others used the conventional triaxial apparatus.

Poorooshasb, Holubec and Sherbourne, (1966, 1967) discussed the nature of deformation of Ottawa sand. This paper is a summary of the experimental research programme carried out by Holubec (1966) on the yielding of granular materials. Poorooshasb et al divided the total deformations of a sand sample into elastic and plastic components. The elastic strain components were obtained from special tests and the results were then used to calculate the plastic strain components in other stress paths. The stress paths adopted in this investigations are shown in Figure (3-11). The resulting plastic strain increment vectors corresponding to stress point (a) for all the six paths followed have almost identical gradients. The small variation observed between the gradients of the vectors is due to small experimental errors. A typical plot of the plastic strain increment vectors in a t - s plane is shown in Figure (3-12). The plastic strain potential contours were established by drawing curves normal to the plastic strain increment vectors. These plastic potential contours

---

* Bishop, (1963) noted that the model did not provide a reasonable prediction for Ko values.

trace a family of geometrically similar curves when plotted in a stress space. A flow rule was derived of the form:

$$d\epsilon_{ij} = d\epsilon^{e}_{ij} + \left(\frac{\partial \Phi}{\partial \sigma_{ij}}\right) d\lambda \qquad \ldots\ldots \qquad (3.7.3)$$

and $$\Phi = s f(e \,.\, t/s)$$

where Φ denotes the plastic potential function

$d\epsilon_{ij}$ denotes the total strain tensor increment

$d\epsilon^{e}_{ij}$ denotes the elastic strain tensor increment

σ_{ij} denotes the stress tensor

$d\lambda$ denotes a constant of proportionality which depends on the state of the material and its mode of yielding.

Four main points were observed in this experimental study:

1. The gradient of the plastic strain increment vector is independent of the gradient of the stress increment and the stress path, being a function only of the state of the material. Therefore they established a similarity between the behaviour of the sand and that of plastic material.

2. The yield loci are independent of the void ratio.

3. The plastic potential and the yield surface do not coincide. This is in contrast to the normality rule and therefore the material's behaviour is different from that of a classical plastic body.

4. The plastic strain increment vectors, along any constant stress ratio path, have the same gradients.

Lewin, (1970) carried out tests on remoulded Kaolin and slate dust. He observed small rotation in the plastic strain increment vectors at a common stress point when it was approached by two different stress paths.

Namy, (1970) in tests on Newfield clay, reported different findings from those presented by Holubec, (1966). Namy's main conclusions which are related to this discussion are:

1. The slopes (k and λ) of the consolidation and swelling lines in (p', ϵ v) plane are the same for isotropic and anisotropic consolidation tests. Thus he confirmed the existence of a unique relationship between the incremental plastic volume strains and the incremental octahedral normal stresses.

2. Elastic shear strains can be neglected during consolidation tests, but they are significant when the volumetric strains exceed 20% in isotropic consolidation. This is not valid for shear tests.

3. The elastic volumetric strains are a function of the effective hydrostatic pressure p' only.

4. The plastic strain increment vectors for Newfield clay depend on the stress history and on the stress increment vectors. Also these plastic strain increment vectors are not normal to the yield loci. Figure (3-13) shows the rotation of the plastic strain increment vectors along a certain stress path.

Lewin and Burland, (1970) carried out a series of stress-probe triaxial tests on powdered slate dust. Samples were consolidated anisotropically at constant stress ratios to the same $\acute{p}$-value and stress-probes were then applied at different directions. Isotropic consolidation, drained, undrained and $\acute{p}$-constant tests were also performed as part of the programme. They concluded that the direction of the plastic strain increment vectors resulting from the stress-probe tests was partly dependent on the direction of the stress-probe vectors.

3.7.4 Rowe's Stress-Dilatancy Model and the Behaviour of Soil

The shear strength and dilatancy of soils have been discussed in Chapter 2, while the formulation of Rowe's stress-dilatancy theory was presented in section 3.6.3. In this section the latest modifications will be stated.

The model was originally formulated for an assembly of round frictional particles in order to study the stress-strain behaviour of granular material. In fact the model is merely a flow rule since it expresses the

relationship between stresses and the developed strains. Since the stress-dilatancy model is only a flow rule and no yield function was formulated, it cannot predict the stress fields from the boundary values.

Barden and Khayatt, (1966, 1968) developed a plastic-strain-hardening relationship for sand on the basis of Rowe's stress-dilatancy theory. They disagreed with Poorooshasb et al who divided the deformation into elastic and plastic components as the portions recovered or did not recover from an applied stress state. Barden and Khayatt suggest that the actual elastic deformation occurring during loading is actually much smaller than that indicated from a load-unload cycle; and for practical purposes it is insignificant compared to the plastic deformations. Based on these assumptions Barden and Khayatt derived the following flow rule for the yield locus:

$$\Phi = \frac{\sigma'_1{}^k}{\sqrt{2}\ \sigma'_3} = \text{constant} \qquad \ldots\ldots \qquad (3.7.4)$$

where $k = \tan^2 (45^\circ + \frac{\phi'_f}{2})$ and Φ denotes the strain potential function. It can be seen that Barden and Khayatt's flow rule is simpler than that of Poorooshasb et al (Eqn. 3.7.3). Barden and Khayatt pointed out that their flow rule has the following advantages:

1. It is based on the total strain.
2. It is independent of the initial density, whereas Eqn. (3.7.3) is dependent on the void ratio (e).
3. It is based on the physics of the deformation process.

Application of the stress-dilatancy model to clays and to sand in plane strain conditions is outside the scope of this thesis and the reader could refer to Rowe, (1963); Rowe et al, (1963); Reades, (1972) and Atkinson, (1973).

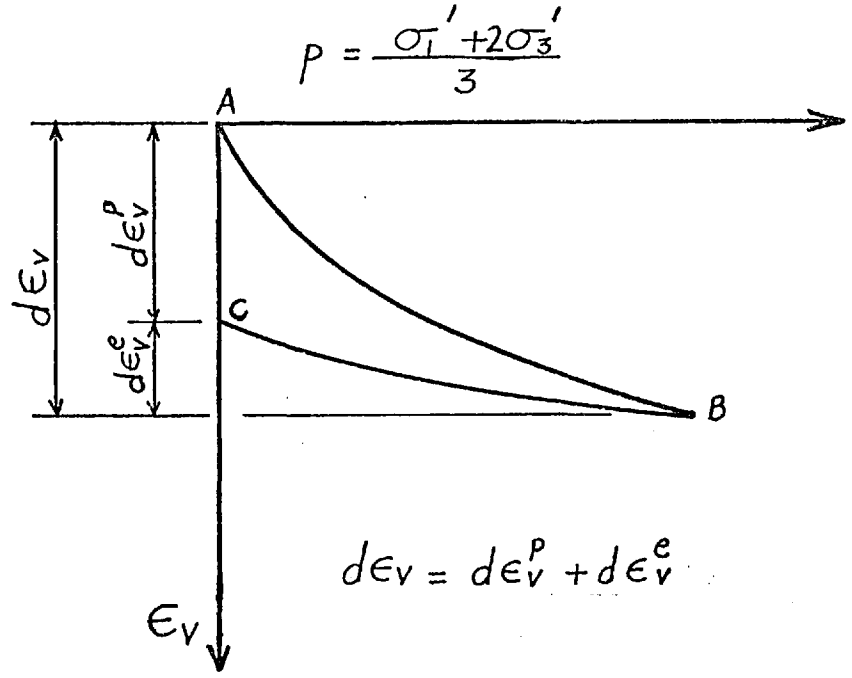

ELASTIC AND PLASTIC COMPONENTS OF THE VOLUMETRIC STRAIN.

FIG. 3 - 1

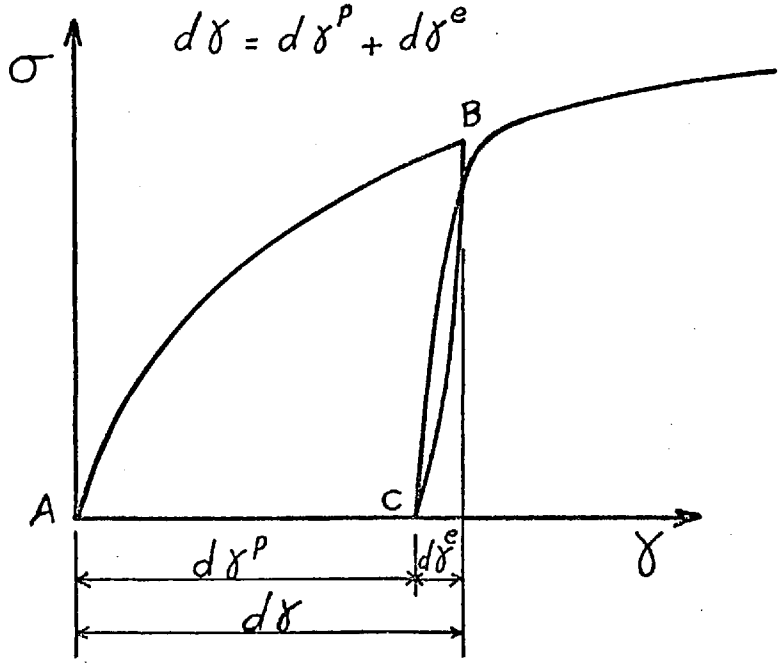

ELASTIC AND PLASTIC COMPONENTS OF THE SHEAR STRAIN

FIG. 3 - 2

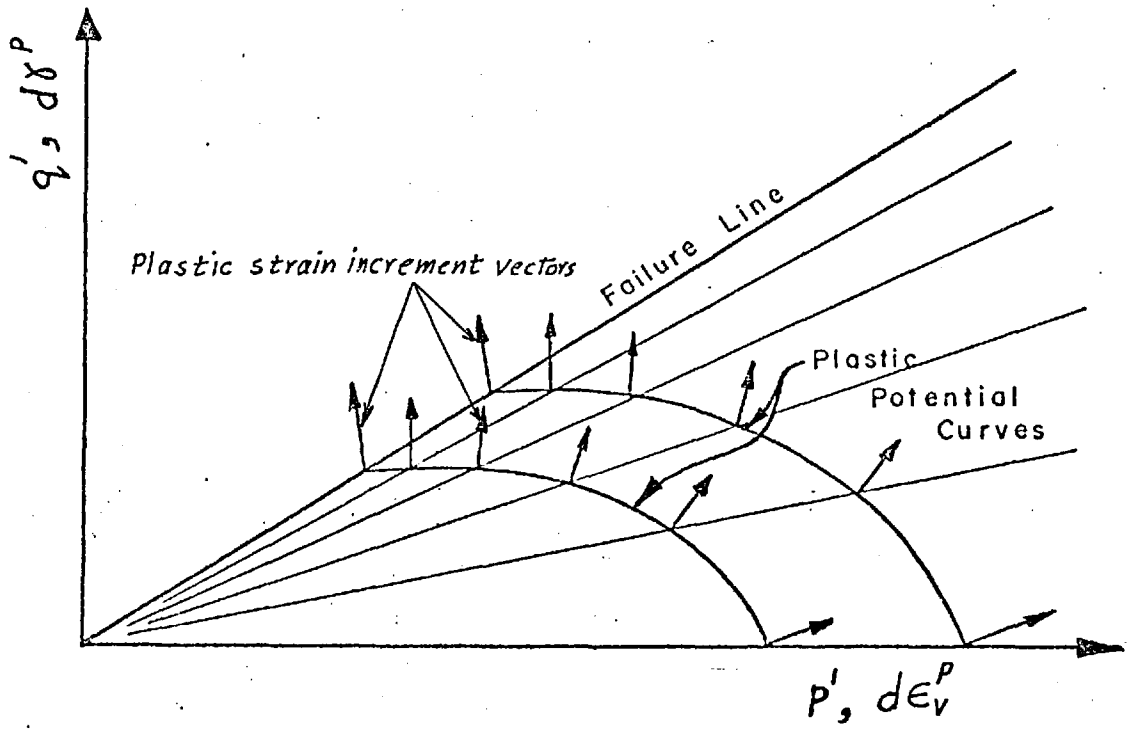

PLASTIC POTENTIAL CURVES IN A CONSTANT VOID RATIO PLANE

FIG. 3 - 3

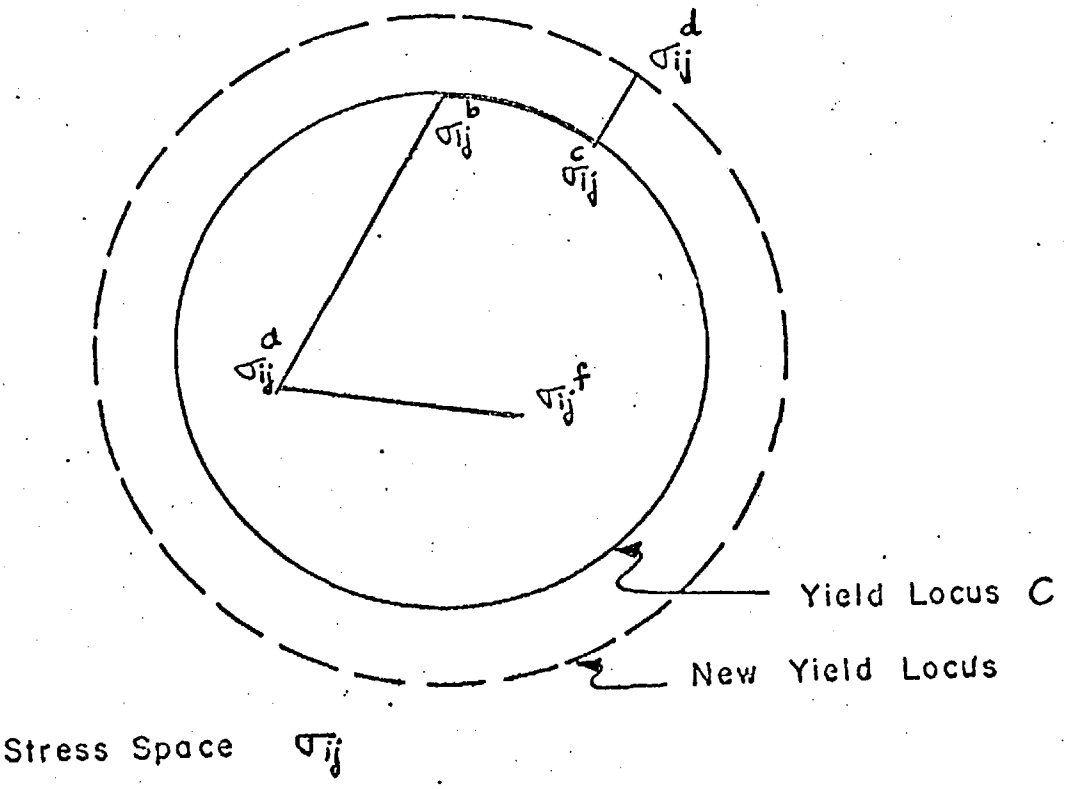

ILLUSTRATION OF A YIELD LOCUS

FIG. 3 - 4

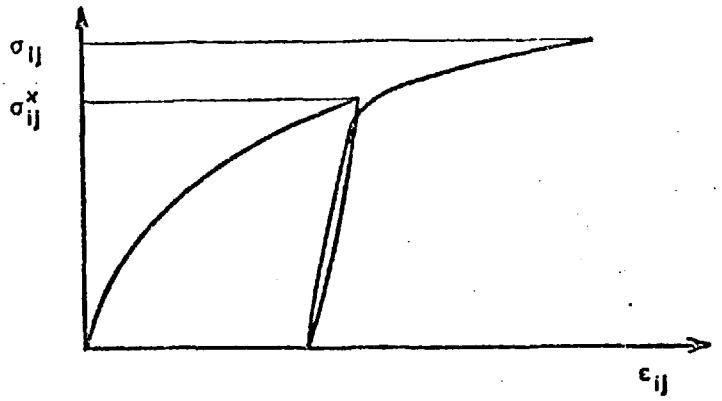

A. Stress-strain curve for a work-hardening material

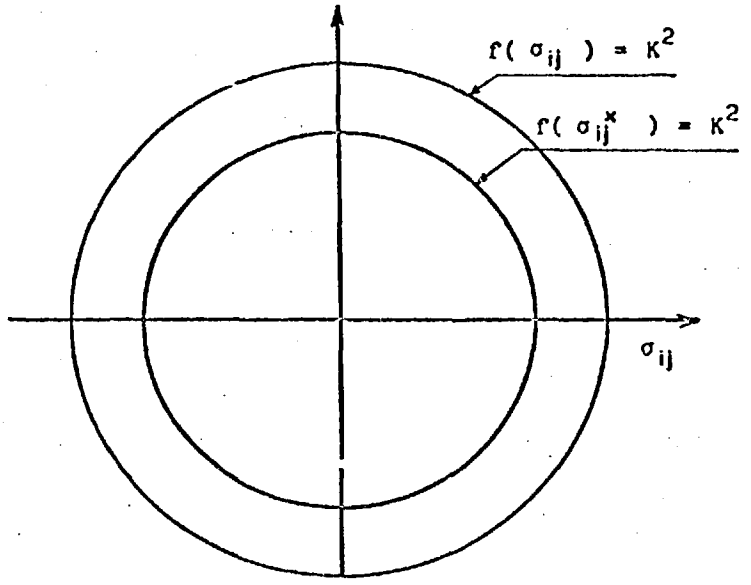

B. Successive yield loci for a work-hardening material

STRESS - STRAIN CURVE AND SUCCESSIVE YIELD LOCI FOR A WORK - HARDENING MATERIAL.

FIG. 3-5

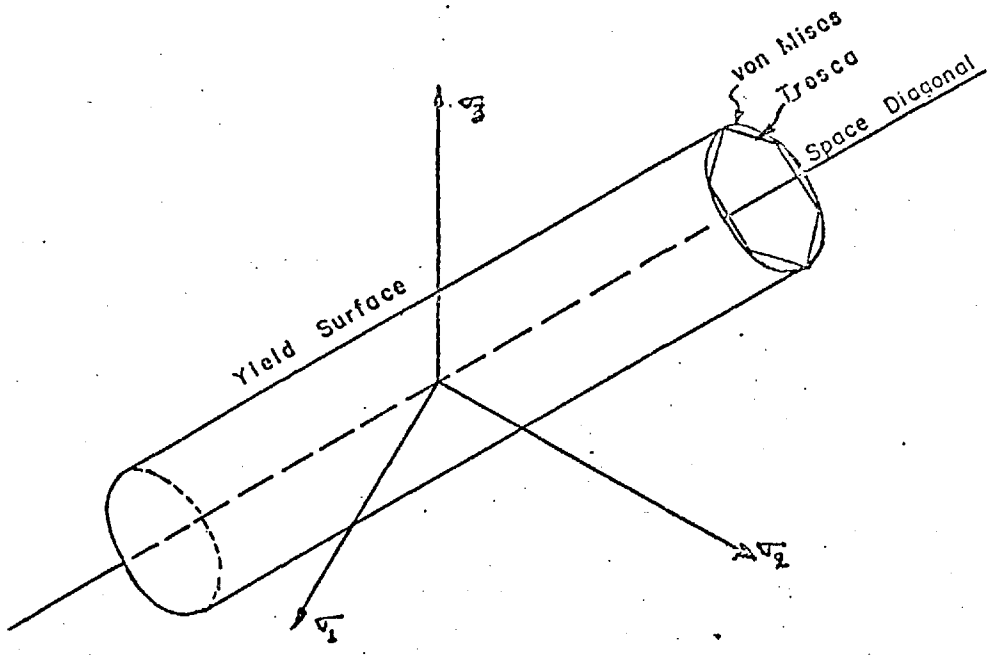

YIELD SURFACES IN METALS

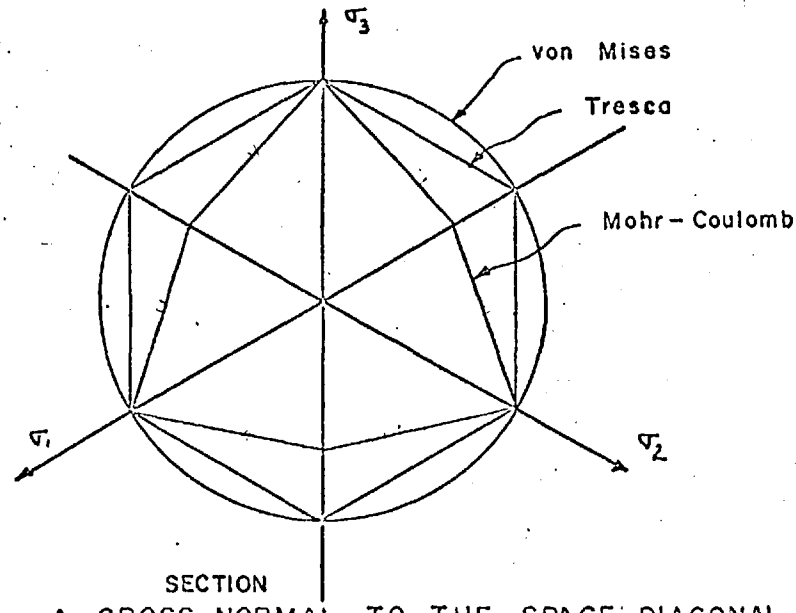

SECTION
A CROSS NORMAL TO THE SPACE DIAGONAL
SHOWING THE DIFFERENT YIELD CRITERIA

REPRESENTATION OF THE YIELD CRITERIA IN PRINCIPAL EFFECTIVE STRESS SPACE

FIG. 3-6

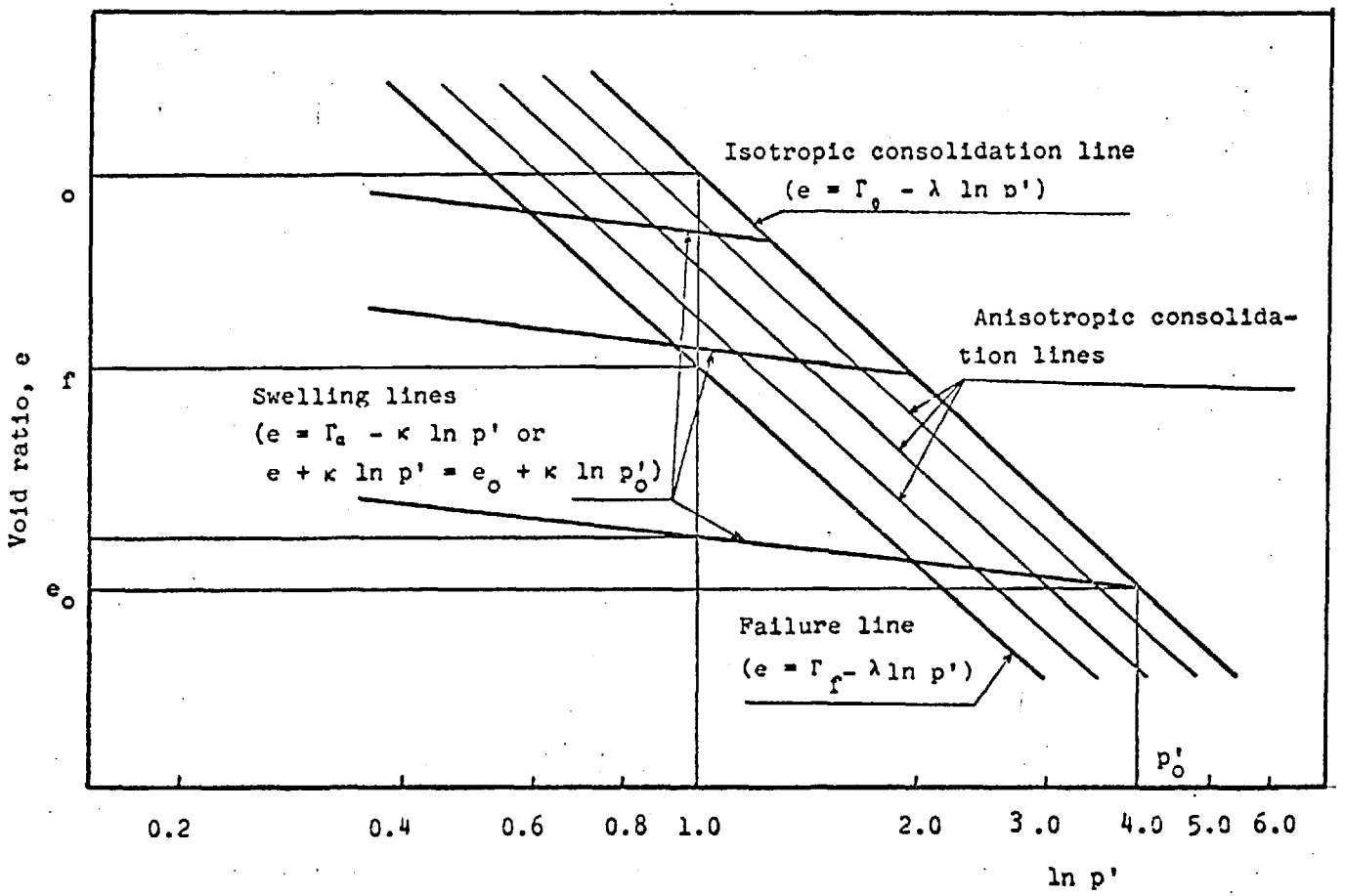

Consolidation and swelling lines

According to Cambridge Model

FIG. 3-7

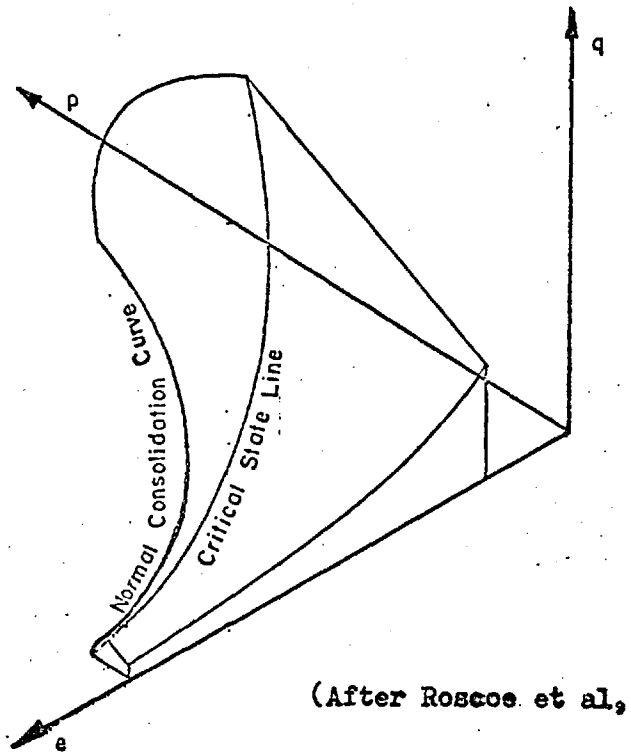

(After Roscoe et al, 1958)

ISOMETRIC VIEW OF A STATE BOUNDARY SURFACE OF A CLAY

FIG. 3 - 8

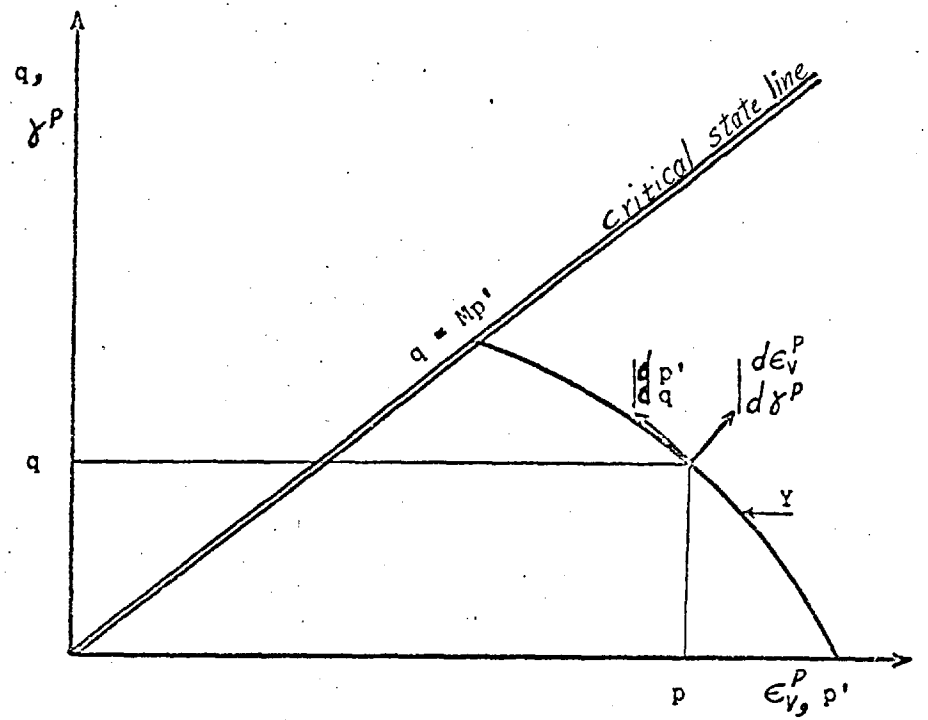

YIELD LOCUS IN (p', q) PLANE

FIG. 3 - 9

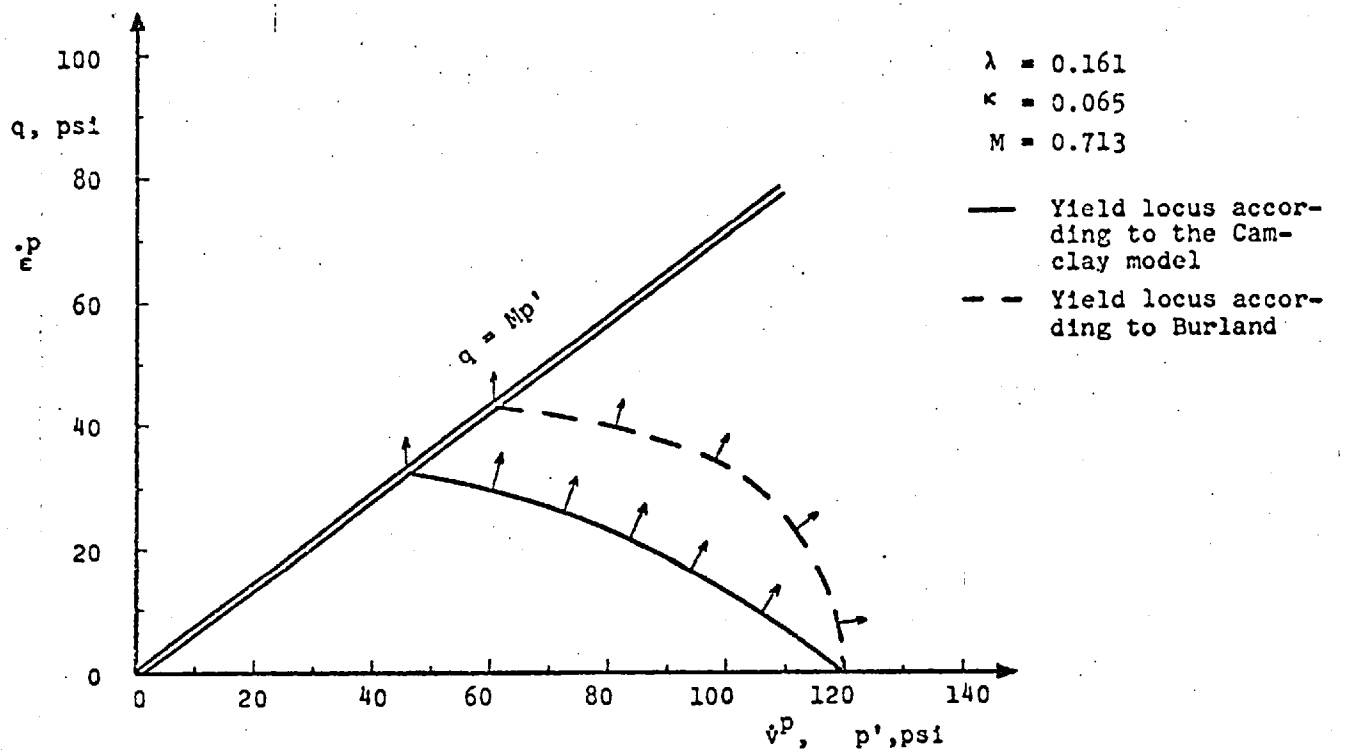

Yield locus for normally consolidated London clay

(After Namy, 1970)

FIG. 3-10

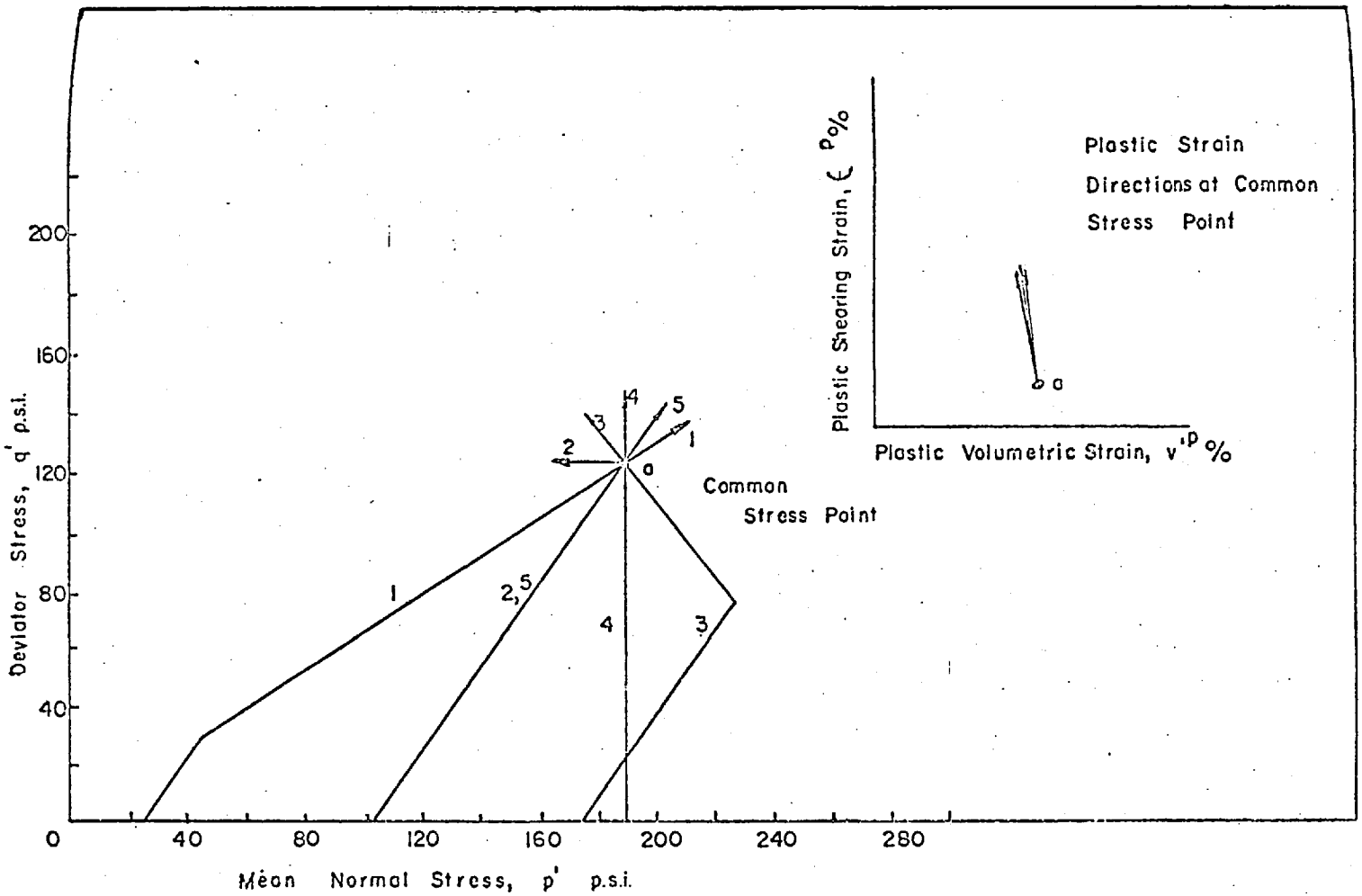

PLASTIC STRAIN DIRECTION AT COMMON STRESS POINT

(AFTER POOROOSHASB ET AL , 1966 & 1967)

FIG. 3-11

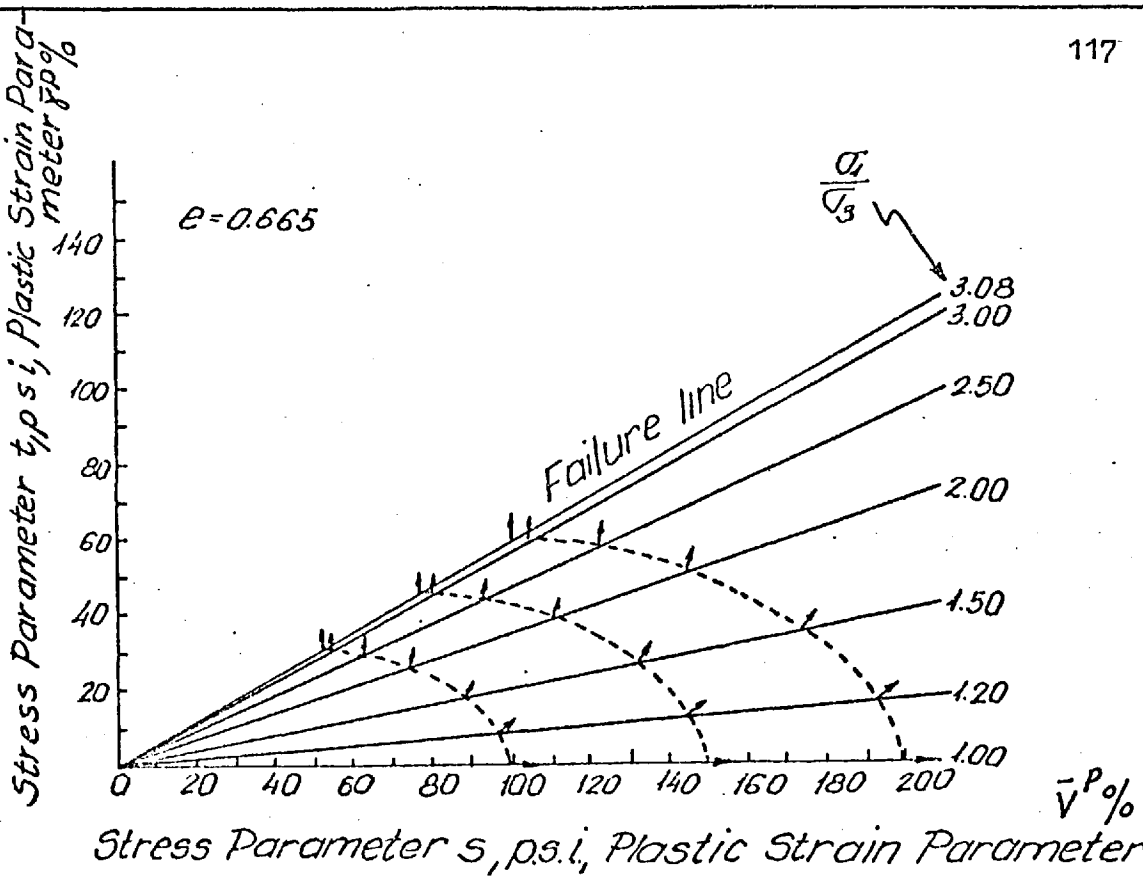

PLASTIC STRAIN INCREMENT VECTORS AND PLASTIC POTENTIAL CURVES OBTAINED FROM TRIAXIAL COMPRESSION TESTS ON SAND.

(After Poorooshasb et al, 1966 & 1967)

FIG. 3 - 12

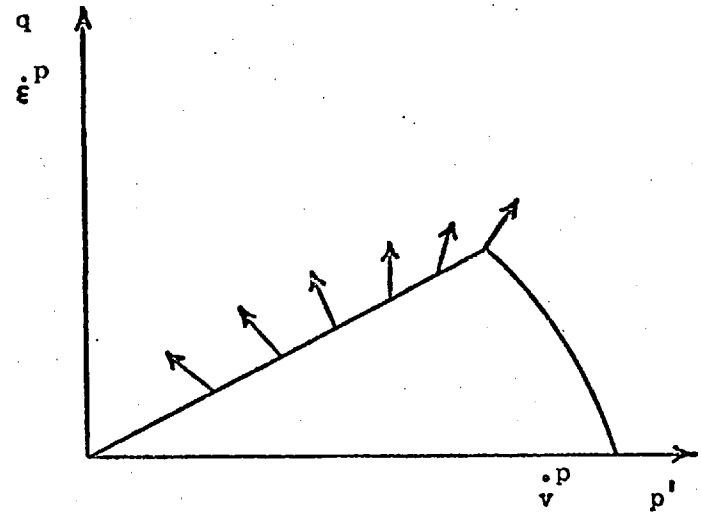

ROTATION OF THE PERMANENT STRAIN INCREMENT VECTOR ALONG THE η_{max} LINE (FOR THE SAME TYPE OF STRESS PATH BUT DIFFERENT OVERCONSOLIDATION RATIO)

(After Namy, 1970)

FIG. 3 - 13

CHAPTER IV

APPARATUS AND TESTING TECHNIQUES

4.1 General Layout and Description of the Triaxial Cell for Testing 1½ in.dia. Samples

The layout of this cell is similar to that of the standard triaxial apparatus described in many soil mechanics text books, e.g. Bishop and Henkel (1962) and Akroyd (1964). A high pressure triaxial cell capable of withstanding a confining pressure range of 0 - 1000 psi was used. The triaxial cell consists of a stainless steel cylinder 4 inches in outside diameter and having a wall thickness of 3/8 in. The axial load is transmitted to the sample by a stainless steel ram running in a bronze bush which is rotated at 2 rpm by a worm drive in order to eliminate the vertical component of friction on the ram. Mechanical details have been given by Bishop, Webb and Skinner (1965). A 1½ inches diameter stainless steel loading plate is fitted to the end of the ram to ensure a uniform load distribution on to the top of the sample.

For tests with cell pressures of up to 150 psi, the sample top cap was a plain perspex disc, 1½ in. dia. x 1 in. high, fitted with two 3.5 mm internal diameter saran drainage leads, retained by Locktite Retaining Compound. Then for the tests at cell pressures in excess of 150 psi, a stainless steel top cap was used. In both cases the top cap was covered with 3/32 in. dia. ball bearings held in place by Vaseline, to transmit the load from the ram to the top cap. Porous stones, 1½ in. dia. and 1/8 in. thick were used for the drainage of the sample. The permeability of these porous stones is 1×10^{-3} cm/second. The deviator loads were measured by stainless steel proving ring which rests on ½ in. dia. ball bearing sitting on the ram. The calibration of the proving rings is given in Appendix A.

The cell pressures less than 150 psi and back pressure were provided by a self-compensating system as described by Bishop and Henkel (1962). The cell pressures in excess of 150 psi (i.e. 150 - 1000 psi) were provided by a hydraulic constant pressure source employing a

spring loaded Amsler bleed valve. Pressures of up to 10000 psi could be provided by this system and over a long period of time (up to six weeks has been tried) without fluctuation.

The other parts of the high pressure apparatus (e.g. sample base, pressure leads, volume gauges, pressure gauges and axial deformation measuring device) are similar to the standard triaxial cell described by Bishop and Henkel, (1962).

4.2 The Triaxial Cell for 4 in. dia. Stress Path Tests

4.2.1 The General Layout

The triaxial cell for testing 4 in. dia. samples was fitted in a compression testing machine supplied by Wykeham Farrance Engineering Ltd. The machine is based on Thyristor controlled motors which are programmed by two sets of digital range switches. These switches indicate the feed rate directly in MM/MIN. The compression machine and the triaxial cell are shown in Plate no. (4-1) and the general layout of the whole apparatus is shown in Figure (4-1).

The cell pressure is applied by means of a self-compensating mercury controlled system as described by Bishop and Henkel (1962). As will be described later, the cell fluid used in the stress path tests is diala oil. An oil/water interface was used to separate the oil in the cell from the water in the mercury pots system. An auxiliary hand pump was used to compensate for the expansion of the perspex cell. The hand pump was filled from time to time from a stand-by oil drum.

The volume changes were measured by three lateral strain devices which will be described in a later section. The amount of water expelled from the sample was also recorded by a glass burette for comparison purposes. The axial deformation was measured with a dial gauge reading to .0005 in. mounted on an arm clamped to the load cell ram and leaning against a stainless steel rod fixed to the cell base.

4.2.2 Details of the Triaxial Cell

A new triaxial cell was designed and built for the stress path tests. In principle it is similar to the other standard triaxial cells but with some modifications. The base of the cell is made of machined stainless steel with a final outside diameter of $13\frac{1}{2}$ in. and it stands on a mild steel ring 7 in. diameter and 4 in. high. Leads are fitted to the base for fluid supply, pressure control, lateral strain transducer wires and drainage.

The top cover is similar to the base in shape and material. The ram of the load cell passes through a bushing bolted to the flat top cover of the cell. An 'O' ring seal is incorporated in the bushing to prevent leakage and as the load is measured internally, any frictional loss in the bushing is of no importance.

The cell is a perspex cylinder of 10 in. in internal diameter, 3/8 in. thick and 18 in. high. The perspex cell is sealed to the base and the top cover by rubber 'O' rings seated in grooves. Six stainless steel tie bars are used to hold the parts of the apparatus together.

The sample pedestal is 5 in. in diameter and 2 in. high. It is made of ground and polished stainless steel (EN 58). The pedestal is a changeable part bolted to the cell base using four top cap screws and is provided with two holes for pore fluid control.

A top cap 5 in. diameter and $1\frac{3}{4}$ in. thick is used on top of the sample and it is also made of ground and polished stainless steel (EN 58). The top cap is covered by $\frac{1}{4}$ in. diameter ball bearings held in place by Vaseline. A hardened stainless steel (EN 57) disc 3/8 in. thick was placed over the ball bearings to allow a proper transmission of the deviator loads. The general details of the cell are shown in Figure (4-2).

The deviatoric loads were measured by a standard Imperial College electrical resistance load cell. The resolution of the load cell, which had a capacity of 6000 lb. was approximately 4.85 microstrains per lb. The load cell consists, in effect, of three triangular cantilevers of uniform

thickness radiating from a common boss and bearing on the edge of a groove in the cylindrical loading cap, Figure (4-3). The load cell is insensitive to the location of the strain gauges and to any horizontal loads. The cylindrical loading cap is filled with oil and sealed with a flexible nitryl rubber cover. Thus the load cell is insensitive to changes of cell pressure.

For high deviatoric loads a 10 ton electrical resistance load cell was designed and built. Its details will be described in a later section. The resolution of this load cell is approximately 0.643 micro-strains per lb. The calibration of both load cells is given in Appendix A.

4.3 Manufacture of Nitryl Rubber Membranes.

As was pointed out earlier, the use of diala oil as cell fluid necessitates the covering of the sample with an oil resistant sleeve. These sleeves or membranes are not available in the size and flexibility required for triaxial testing. Therefore a special process was evolved to manufacture rubber membranes, 4 in. in diameter, 0.010 - 0.020 in. thick and 13 in. long. Fortunately the method was successful and all the required rubber membranes were manufactured in the soils laboratory at Imperial College. The procedure will now be briefly described.

A former is made first, which should be approximately 5% over size in diameter to allow for shrinkage. When the rubber product is dried on the former, it is dried under tension; when removed from the former these tensions will be relaxed and the membrane will therefore be approximately 5% under size, relative to the former.

The material of the former has to be able to withstand a temperature of up to 120^{o}C without splitting or cracking like wood. It can be pvc, or it can be cast aluminium with a core down the middle so that it does not become too heavy, or it could be a piece of stainless steel tube. In this instance a piece of pvc drain-pipe was found to have approximately the right diameter and it has been used as a former after having been fitted with a handle. Three formers were made for the operation to speed up production.

The first operation in the actual manufacture is to coat the former with a coagulant. This is normally a solution of calcium nitrate in industrial methylated spirits with the possible addition of 2 cc per gallon of a 20% solution of non-ionic wetting agent. The problem with wetting agents is to be careful that they do not have an insoluble calcium salt, so commonly a non-ionic wetting agent is used. For example, Vulcastab LW is suitable and available from ICI. A separating agent, that is a powder in suspension, should be added to the coagulant solution in the order of 4 - 5% by weight. This separating agent will facilitate the release of the dipping from the former and stop it from being self-adhesive and forming snag lines as it is pulled off, and there will also be the benefit of the wetting agent giving an even deposit.

The next operation is to allow the alcohol to evaporate, and this could be done by leaving the former in an oven for a minute or two. The former is dried to let it slip into the latex smoothly.

Next the coagulant-coated former is dipped into the latex compound. This compound is carboxylated medium nitryl rubber which contains all the ingredients necessary to ensure that the final rubber product is vulcanisable. It also contains sundry other ingredients depending on the colour required and certain stabilizers which are not necessary in the final product but which are necessary to preserve the colloidal stability of the bath. Having dipped it into the latex, the former should then be re-dipped, the time depending on the thickness required, but it will be of the order of 30 - 60 seconds. The former is then withdrawn slowly, and on withdrawing the residual calcium nitrate coming through the coagulant will ensure that the whole material will set. After having withdrawn the former from the bath, it should be left hanging down and the membrane will then self-set. Then the former, with the coagulated surface which is still soaking wet, but firmly gelled, should be dried at a temperature of $70^{\circ}C$ for an hour.

Then the dried rubber which is still on the former should be vulcanised at a temperature of 110°C for approximately half an hour. After vulcanisation it should be left to cool and then the rubber is pulled off the former. Finally, the surfaces of the finished rubber membrane should be dusted with talcum powder, after which it is ready for use.

All the foregoing remarks are equally applicable to neoprene membranes with the exception that the vulcanising temperature for neoprene should be of the order of 120 - 130°C, and maintained for at least an hour.

Both nitryl and neoprene dipping have been tried and it was found that nitryl was much more suitable for this testing programme. It has been shown that oil has no effects on the nitryl rubber membranes.

4.4 Design, Manufacture and Performance of the Lateral Strain Device.

The volumetric strains are normally measured using a burette in drained triaxial tests. The volume changes measured by this method may not represent the true behaviour of the sample, especially when it is an unsaturated or coarse-grained material, in which case membrane penetration occurs. Therefore special lateral strain devices have been developed which proved to be durable, sensitive and simple to operate.

The lateral strain device is basically a spring stainless steel strip, bent to fit a 4 in. diameter sample. Strain gauges mounted on the strip convert the strains due to the diameter changes, into resistance changes which can be read by a strain balancing unit. Details of this device are shown in Figure (4-4).

The lateral strain device was made out of 0.022 in. thick by approximately 0.350 in. wide bright hard rolled spring stainless steel strip. The spring stainless steel strip has excellent elastic properties. After the required shape had been formed, the ends of the strip were spot welded, then it was heat treated for 20 minutes at a temperature of

400°C and left in the oven to cool. This treatment produced an excellent elastic belt of permanent shape.

After formation of the strip, the outside and inside surfaces of both ends were cleaned, polished and prepared for the mounting of the strain gauges.

Japanese TML foil strain gauges, type FLA-6 were used. The gauge resistance and factor are 120 $\pm$ 0.3 Ω and 2 respectively. Four strain gauges were mounted on the strip, two in compression and two in tension; then they were connected electrically to act as a full bridge configuration. The circuit diagram is shown in Figure (4-4).

Then the lateral strain device was calibrated on a mild steel calibrating cylinder which was specially made for the calibration, Plate no. (4-2). It can be seen from the calibration, that the lateral strain device produced a linear relationship between read-out and diameter change. Furthermore, no visible creep or temperature effects were observed. The lateral strain device was left on the calibrating cylinder for a few days and no significant drifting was registered.

The resolutions for the three devices manufactured were 375, 433 and 474 microstrains per 0.1 in. change in diameter. The detailed calibration is shown in Appendix A. The lateral strain devices were calibrated every two tests and no change was noted. According to the needs of this testing programme, these devices have performed satisfactorily and to an extremely high sensitivity.

4.5 Design, Manufacture and Performance of the 10 ton Load Cell

A 10 ton load cell was designed and manufactured at Imperial College for the compressive deviatoric load measurements. Another 30 ton load cell has been designed for the future but unfortunately has not yet been completed. Details of the design are shown in Figures (4-5), (4-6) and (4-7). The design principals of the 10 ton load cell are similar to those of the Imperial College load cells designed by Dr. A. Skinner.

The main part of the load cell (i.e. the load transducer) consists of three triangular cantilevers of uniform thickness radiating from a common boss and bearing on the edge of a groove in the cylindrical loading cap (diaphragm). As the bending moment and moment of resistance both increase linearly from the apex of each triangular cantilever, the surface strains are almost uniform, and the calibration is therefore insensitive to the location of the electrical resistance strain gauges. This load transducer is made of stainless steel (EN 57) and has been machined, heat treated and tempered before fixing the strain gauges on it.

Twelve strain gauges type (EA-06-125 MG - 120*) are cemented, two in each of the three corners on both the top and bottom surfaces of the element. The strain gauges are connected electrically to act as a full bridge configuration.

The load transducer rests on a mild steel diaphragm with a cylindrical shape. The diaphragm is filled with diala oil and sealed with a flexible nitryl rubber cover which is fixed by a mild steel ring. A change in cell pressure thus has no significant effect either on the zero or on the calibration. The resistance gauges are wired to give complete insensitivity to eccentricity of loading and to the horizontal component of load. Therefore the load cell measures only the force along its stem axis.

A hardened mild steel plate, 4 in. diameter and 3/8 in. thick was screwed to the bottom of the load cell to protect the diaphragm from the effect of ball bearings during loading. The load cell with its base plate is screwed to a 1.5 in. diameter stainless steel ram through which the strain gauge wires pass, Plate (4-3).

The approximate resolution of the load cell is 0.643 microstrains per lb. which is accurate enough for the purpose of the testing. The calibration curve is shown in Appendix A.

---

* These strain gauges are made by "Micro-Measurements, Romulus, Michigan".

4.6 Sample Preparation and Set-up

4.6.1 Sample Preparation

All the size ranges of granite and marble chippings were obtained by crushing bigger particles using crushing machines in the Geology laboratory at Imperial College. No washing or any pre-treatment was carried out on the materials tested.

All the granite and marble chipping samples were prepared by mixing weighed quantities of each size group which consisted of the material passing a given sieve and retained on the following one. The sieve sizes used were 3/16", No. 7, No. 14, No. 25, No. 52 and No. 100.

Knowing the approximate sample dimensions, the required porosity and the specific gravity of the particles, the weight of the material required for each test was calculated. The material required from each size fraction was weighed and thoroughly mixed for each test. This procedure was followed for all the tests in this experimental work. Materials for $1\frac{1}{2}$ in. diameter samples were prepared dry, then saturated after setting up the samples and applying the cell pressures. Materials for the 4 in. diameter samples were prepared saturated right from the beginning, in a way similar to that used for sand, as described by Bishop and Henkel, (1962).

4.6.2 Sample Set-up

For the $1\frac{1}{2}$ in. diameter samples, a 0.020 in. thick latex membrane was first sealed to the sample base with an O-ring. The procedure for assembling the mould was that described by Bishop and Henkel, (1962). Then, the material was placed dry in five layers and each layer was compacted by a 3/8 in. diameter steel rod with a hard plastic disc at the end, of 1.0 in. diameter. The upper layer was arranged by hand to give an even surface. After compaction, the membrane was sealed to the top cap by an O-ring and a suction of 1.0 psi was applied to the sample through the bottom drainage lead. For tests

at confining pressures more than 40 psi, more than one rubber membrane was used. By experience, it was found that using 0.020 in. thick latex membrane, two membranes were required for tests at confining pressures of 80 psi and 120 psi and three for tests at 160 psi. For tests at confining pressures of 300 - 600 psi, a neoprene membrane 0.025 in. thick was used in addition to two 0.030 in. thick latex membranes. Fixing the required porosity and the number of rubber membranes was a matter of trial.

To add more membranes to the sample when under suction, the top drainage tap was closed and the lead disconnected. Then using a membrane expander, the required number of membranes was added to the sample one by one and only after the last one had been put on, were they sealed to the cap and pedestal with two O-rings at each end. Then the top drainage lead was connected again and the cell was assembled and filled with water ready for loading.

For the 4 in. diameter samples, the same procedure was followed except for a few variations. The material was compacted with the water covering the layers during compaction. Thus the sample was initially saturated unlike the small size samples which were compacted dry. The rubber membranes used for the large size samples were as follows: one 0.020 in. thick first to contain the material during compaction, then a second 0.040 in. thick latex membrane. Finally, a third 0.025 in. thick nitryl rubber membrane was added to protect the other latex membranes from the oil in the cell.

For both the small and large size samples, the top caps were covered with ball bearings held in position by Vaseline.

The diameter of each sample was measured at different levels and in perpendicular directions by a vernier caliper to an accuracy of 0.0005 in. The average of eight measurements was taken as the final diameter of the sample after taking into consideration the membrane thickness. The sample height was measured by a dial gauge to an accuracy of 0.0005 in. using the technique described by Bishop and Henkel

(1962). Burette readings were taken before and after measuring up the sample to assess whether there has been any disturbance.

4.6.3 Installation of the Lateral Strain Devices

After the 4 in. diameter sample had been set-up and the top cap fixed, three lateral strain devices were installed, at $\frac{1}{4}$, $\frac{1}{2}$ and $\frac{3}{4}$ of the height of the sample. For safety, the devices were supported by low gauge value wire, to keep them in a horizontal position during testing. These wires had no effect on the movements of the devices. Strain readings of the devices were recorded by a strain balancing unit and there was no significant change in the readings before and after filling the cell with oil. The devices remained horizontal after finishing the test and the sample diameter was measured by a vernier caliper gauge. Plate (4-4) shows the lateral strain devices installed on the sample before assembling the cell. It can be seen that the devices were installed in perpendicular directions so that the average deformations could be recorded.

4.7 Frictionless Ends Arrangement for the 4 in. dia. Samples

A frictionless base and top cap were used for the 4 in. diameter stress path tests. The procedure used for frictionless ends was similar to the one described by Bishop and Green (1965) and Green (1969). The technique used will be described in brief.

A thin layer of silicone grease was applied to the top and base platens and also to one face of each of the four end membranes which were to be used. These membranes were discs cut from standard sample rubber membranes, about 4 in. diameter with central holes in the membranes for the base platen. The end membranes were 0.020 in. thick and the central hole was $\frac{3}{4}$ in. diameter to pass the bottom porous stone.

The first lubricated membrane was placed on each end platen and air bubbles and any remaining surplus grease trapped between the platen and the membrane were removed. The upper face was then

greased with a thin smear, and the second membrane was placed in position. The final upper surface was not greased. The same procedure was adopted for both the top cap and the base in installing the end membranes. When the sample height was measured, the thickness of the end membranes was taken into consideration.

After the end platens were arranged as previously described, the first latex rubber membrane was sealed to the base with an O-ring and the assembled mould was installed on the base. Then the sample build-up was continued as described in the previous section.

The end membranes were changed every test and the end platens cleaned of the grease to prepare them for the next test. The deformations of the sample at the top, middle and bottom and the effect of the free ends will be discussed in a later section.

4.8 Loading Procedure

4.8.1 Axial Strain Rate and Total Strain

All the tests on $1\frac{1}{2}$ in. diameter samples were carried out at a rate of axial strain of 10% per hour. Since the samples tested were of similar height, the rate of axial displacement and the increase of stresses were constant. The total strain reached for this group of tests varied between 18% to 29% because of variations of the failure conditions. However, the amount of strain between the failure and end of the test was approximately the same for all the tests.

A rate of axial strain of 8.5% per hour was adopted for the 4 in. diameter stress path tests on both granite rockfill and marble chippings. The total strains to which the samples were taken were different, depending on the stress path followed.

4.8.2 Loading the Samples

(a) The Drained and Undrained $1\frac{1}{2}$ in. diameter Samples

These samples had been consolidated isotropically then sheared drained or undrained at the rate stated in the previous section. The

consolidation pressure had been applied in increments ranging between 5 - 20 psi depending on the maximum confining pressure required. The sample was left for 20 minutes to consolidate after each pressure increment had been applied. The time 20 minutes was found to be enough to achieve full dissipation of the pore pressures.

At a confining pressure of 20 psi, the back pressure was applied in 5 psi increments and at the same time the cell pressure was also increased by 5 psi increments so that the effective stress would be kept constant at 20 psi level until the maximum back pressure was achieved. The drainage tap was opened from time to time to release the air from the sample and to achieve complete saturation. The water was allowed to circulate for 30 minutes from bottom to top of the sample to get rid of the air inside the sample. The pressure difference used to achieve this water circulation was approximately 1.5 psi.

After the sample had been saturated under a back pressure of 60 psi, the cell pressure was increased in increments to the required level. A back pressure of 60 psi was used in all the $1\frac{1}{2}$ in. diameter tests to ensure full saturation of the samples.

After the required cell pressure had been applied the sample was sheared either under drained or undrained conditions.
The shearing procedure adopted was the same as that described by Bishop and Henkel (1962).

After the failure of the sample had been achieved, the test was continued further to a certain axial strain, then stopped, the drainage leads were closed, the deviator load lifted and the cell pressure released.

(b) The Stress Path Tests on $1\frac{1}{2}$ in. diameter Granite Samples

For these tests a back pressure of 40 psi was applied at an effective stress of 4 psi. Then the samples were consolidated anisotropically at the required stress ratio. The procedure of loading was as follows: the cell pressure was increased by a small increment then the axial load was increased to the required stress ratio. The sample

was left to consolidate under these stresses for 20 minutes during which the axial load was adjusted several times to compensate for reductions due to consolidation and creep of the sample. Once the consolidation of the sample under the required stress ratio had been achieved, a second increment was applied, then a third, and so on. The effective minor principal stresses applied were as follows: 4, 6, 10, 15, 20, 30, 40, 60, 80, 100, 120, 160, 200, 250, 300, 350, 400, 450, 500, 550 and 600 psi.

During the unloading and reloading stages, the same load increments and time intervals were adopted, except that on unloading, the axial stress was reduced first then the cell pressure. This was to ensure that the stress ratio did not approach failure.

Then after the sample had been reloaded to the final stresses, the cell pressure was kept constant and the sample was sheared by increasing the major principal stress under drained conditions.

(c) The Stress Path Tests on 4 in. diameter Samples

The loading procedures used in the previous sections were also used for these tests except that different values of stress increments were applied. The rate of axial strain was 8.5% per hour.

The stress paths followed for each test will be described in detail in Chapter 7. Stated briefly, each of these tests consists of two parts: one part was isotropic loading-unloading and the other was anisotropic loading-unloading. A stress probe, as will be described later, was applied at the end of the loading cycle in each part.

4.9 Sample Dimensions for Results Calculation

4.9.1 Sample Dimensions after Isotropic Consolidation

For the $1\frac{1}{2}$ in diameter samples, the dimensions were corrected for the consolidation process. The amount of vertical and radial strain during isotropic consolidation has been studied by many researchers. The axial strain will be equal to the radial strain provided the sample is

truly isotropic. Whether or not this is the case depends on the technique used in preparing the samples.

Parkin et al (1968) found that a sample may have a greater stiffness in the radial direction than in the vertical direction and vice versa. They reported that samples of Earlston sand set up according to the methods described by Kolbuszewski and Jones (1961), had a vertical stiffness greater than the horizontal by as much as 5 times. Other techniques have given samples a radial stiffness as much as 30% greater than the vertical stiffness.

In general the weaker direction will be the direction of preferred orientation of the particles which results from the type of deposition process and the particle shape.

As has been pointed out earlier in this chapter, extreme care was taken to set up uniform isotropic samples. The condition of uniformity has probably been satisfied, but it is inevitable that in any preparation method involving compaction in layers some anisotropy will result. However, this is believed to be small and therefore during the isotropic consolidation stage it will be assumed that:

the vertical strains = the radial strains

i.e. $$\epsilon_1 = \epsilon_2 = \epsilon_3 \qquad (4.9.1)$$

and $$\epsilon_v = \epsilon_1 + \epsilon_2 + \epsilon_3 \qquad (4.9.2)$$

where the above terms were defined at the beginning of the thesis. Hence dimensions of the $1\frac{1}{2}$ in. diameter samples after isotropic consolidation were calculated on the basis of the above relationships.

For the 4 in. diameter samples in the stress path tests, local measurements of the strains were achieved by the lateral strain devices. Hence the sample dimensions have been calculated on the basis of these measurements.

4.9.2 Cross-Sectional Area Calculations

(a) The $1\frac{1}{2}$ in. diameter samples

The area of each of these samples was calculated at the end of the consolidation stage and during shearing for deviator stress calculations.

Bishop and Henkel (1962) derived an equation for calculating the cross-sectional area during deviatoric stress application. The sample area during shearing is expressed mathematically as:

$$A_s = A_c \frac{(1 - \epsilon_v)}{(1 - \epsilon_1)} \qquad (4.9.3)$$

where A_c is the cross-sectional area of the sample at the end of consolidation. ϵ_v and ϵ_1 are the volumetric and axial strains respectively during the shearing stage.

This equation is based on the assumptions that: the sample is a right cylinder, the end plattens are frictionless and the sample deformation is uniform throughout. It has been found that the equation is accurate up to approximately 15% axial strain and above this limit the errors tend to increase.

There have been other attempts to estimate the sample cross-sectional area during shearing. Barnes (1960) derived an expression to calculate the area of the sample during deformation as

$$A_s = A_c + 2A_c (\epsilon_1 + \epsilon_v) \qquad (4.9.4)$$

where the terms are as those defined for the previous expression.

Billam (1967) modified Bishop's equation of 1962 and suggested an expression which is similar to Barnes'. In this thesis, Bishop and Henkel's equation will be used in all calculations.

(b) The 4 in. diameter samples

As has been pointed out, direct measurement of the strains was achieved, therefore the cross-sectional area of these samples was calculated directly. An average of the three readings at different positions was taken for the area calculation, therefore this area is an average cross-sectional area of the sample.

These 4 in. diameter samples were only strained to well below the failure strain, so the samples were almost cylindrical after testing, unlike the sheared ones which failed by bulging, or along a single line. Therefore the average cross-sectional area is a reasonable approximation.

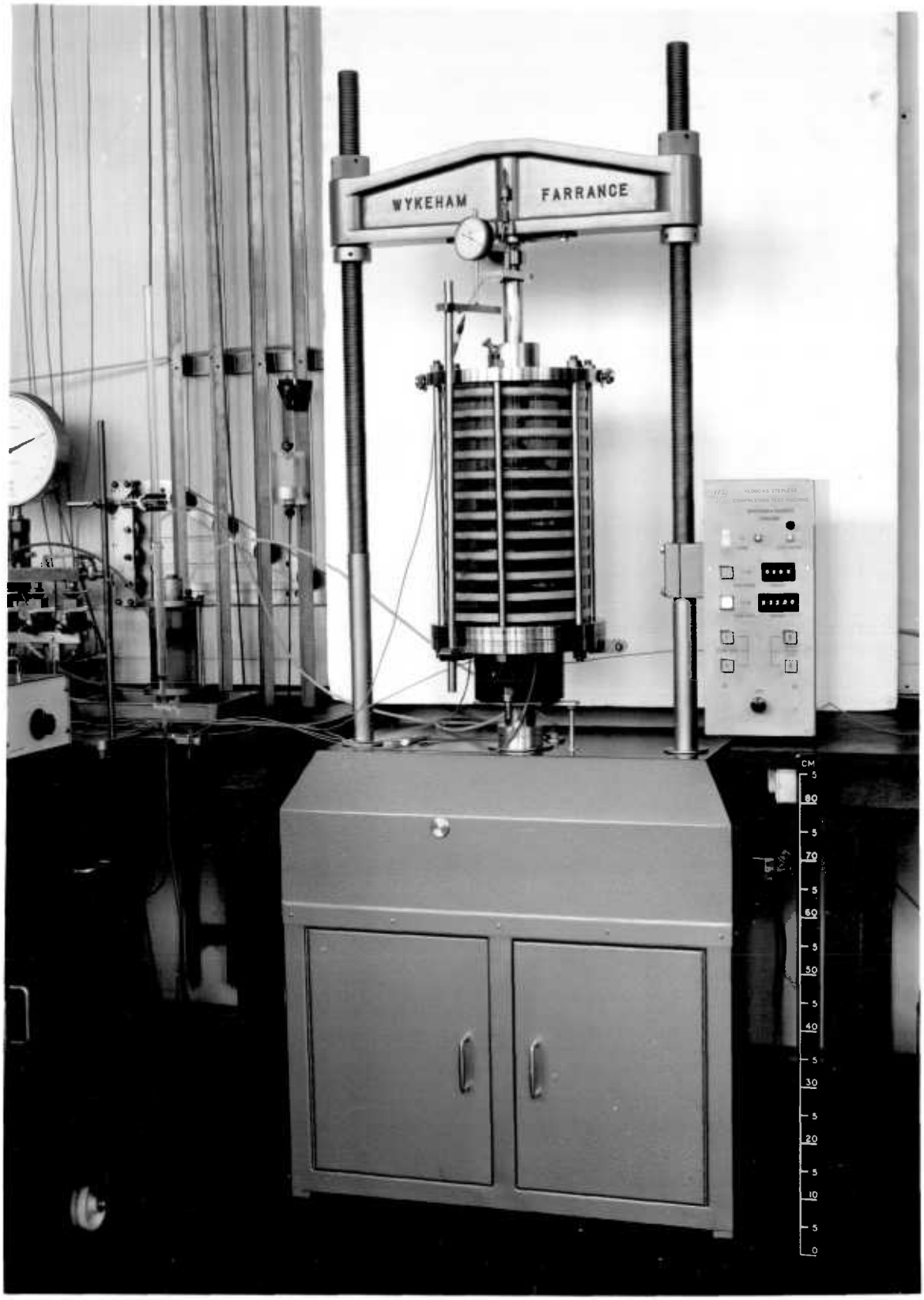

Plate (4-1) The Compression Machine and the 4 in. dia Triaxial Cell for Stress Path Tests.

Plate (4-2): The Lateral Strain Measuring Device and the Calibrating Cylinder

Plate (4-3): The 10-ton Load Cell

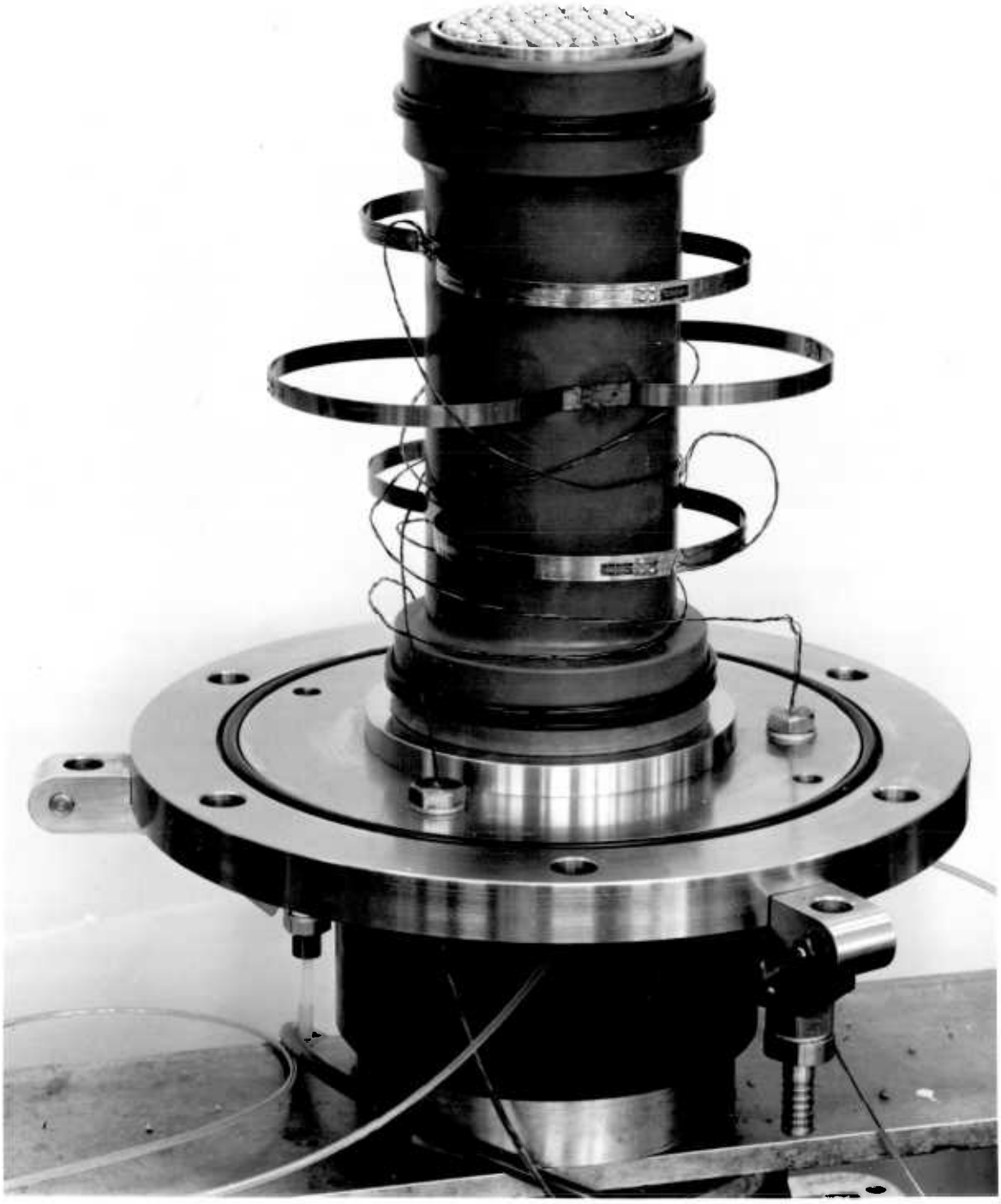

Plate (4-4) The Lateral Strain Devices Installed on 4 in. dia. Sample.

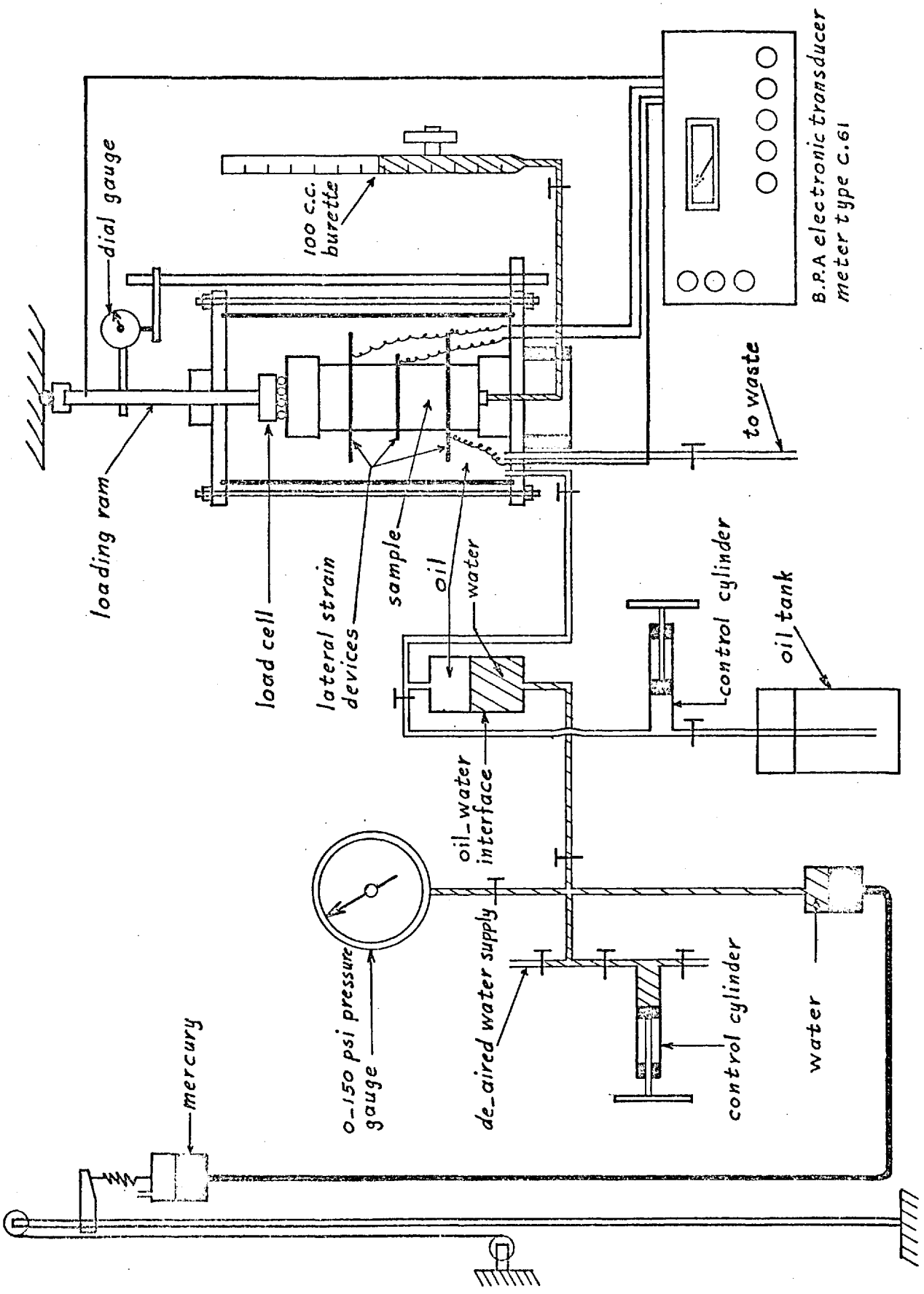

THE GENERAL LAYOUT OF THE TRIAXIAL CELL FOR 4 IN. DIA. STRESS PATH TESTS

FIG 4-1

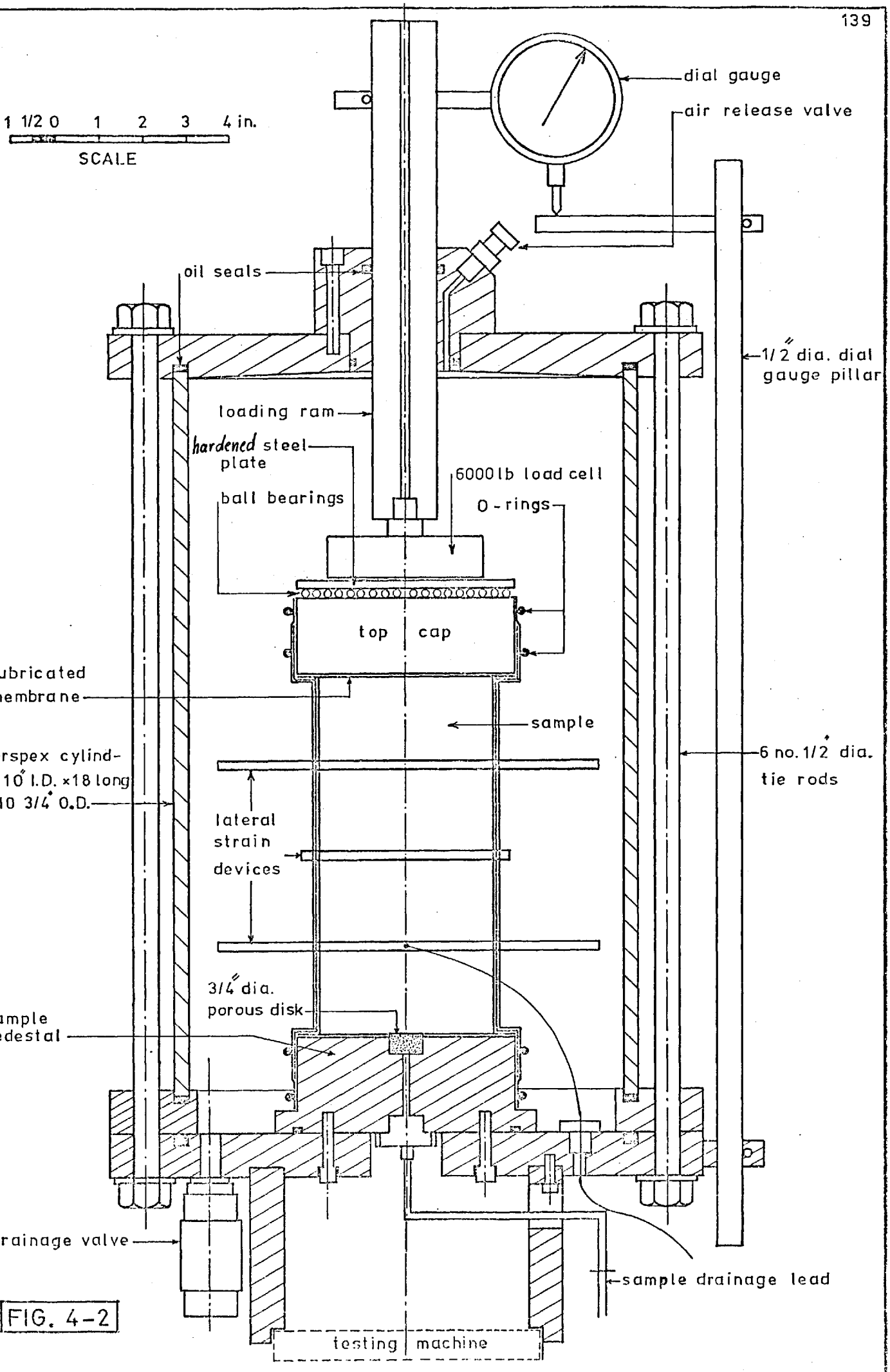

FIG. 4-2

THE TRIAXIAL CELL FOR STRESS PATH TESTS ON 4IN. DIA. SAMPLES

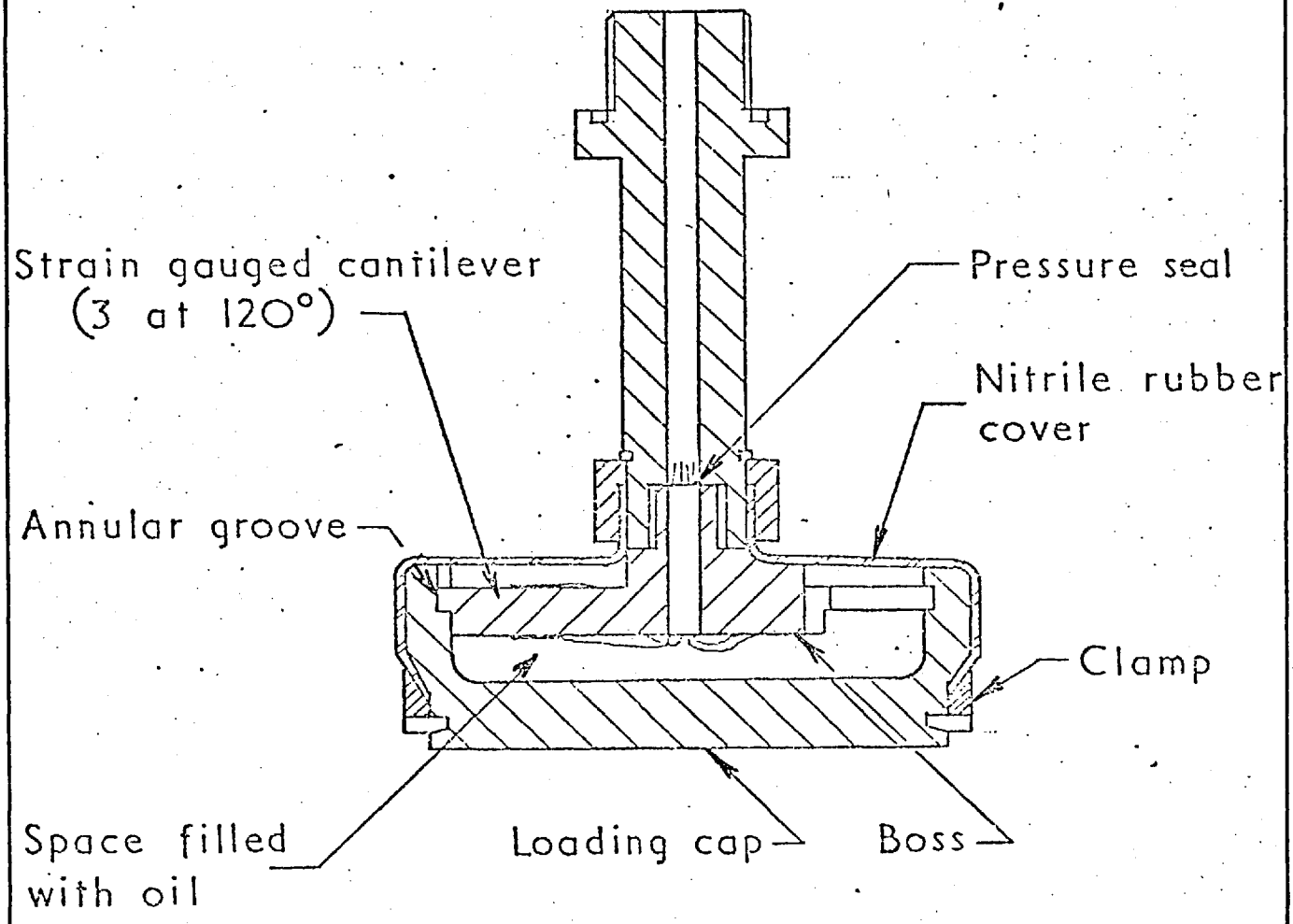

INTERNAL LOAD TRANSDUCER

FIG 4_3

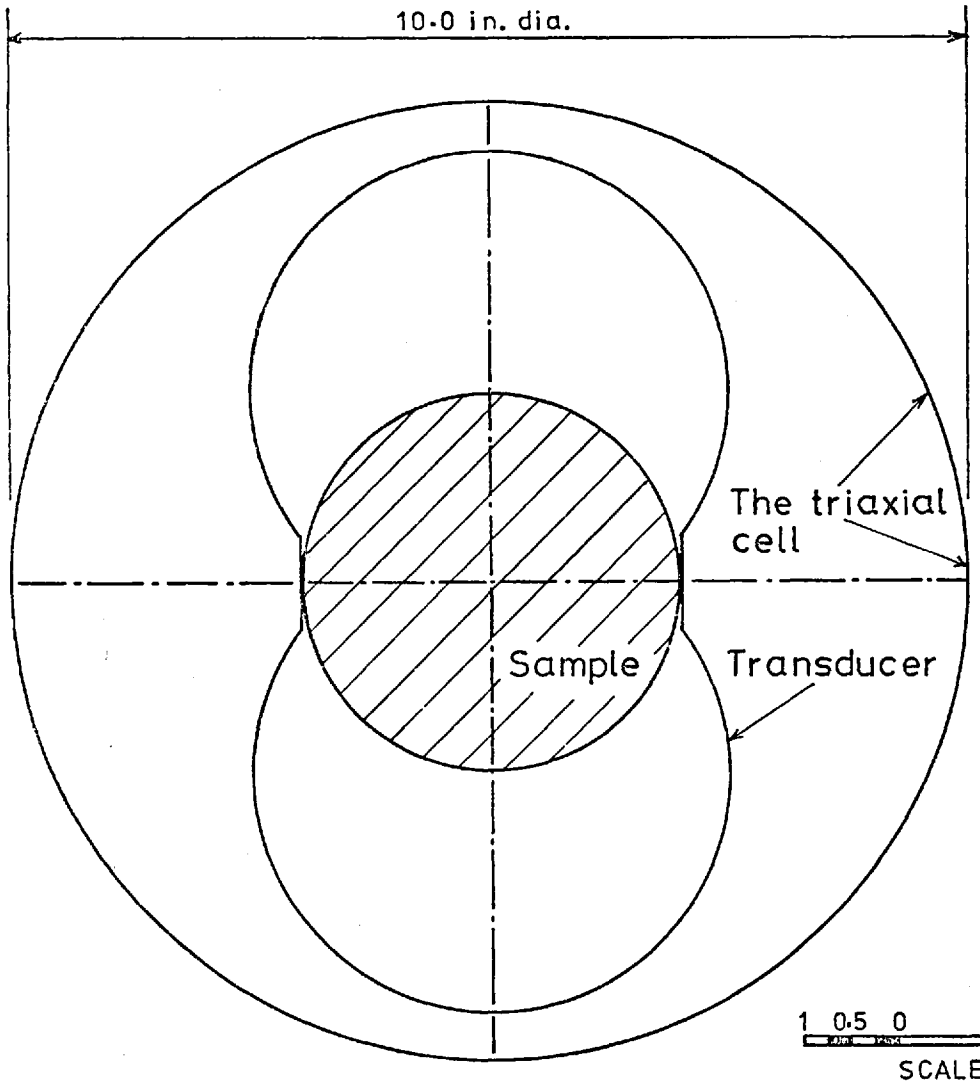

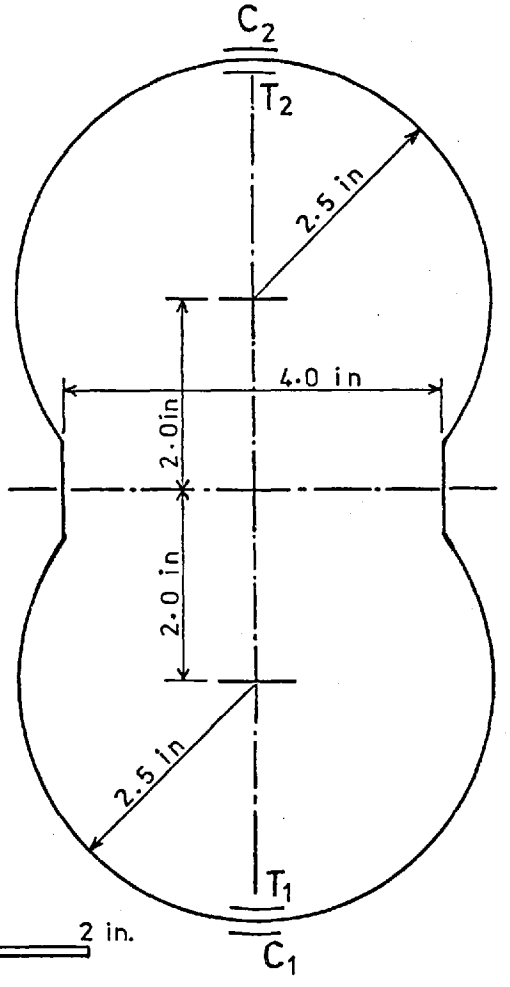

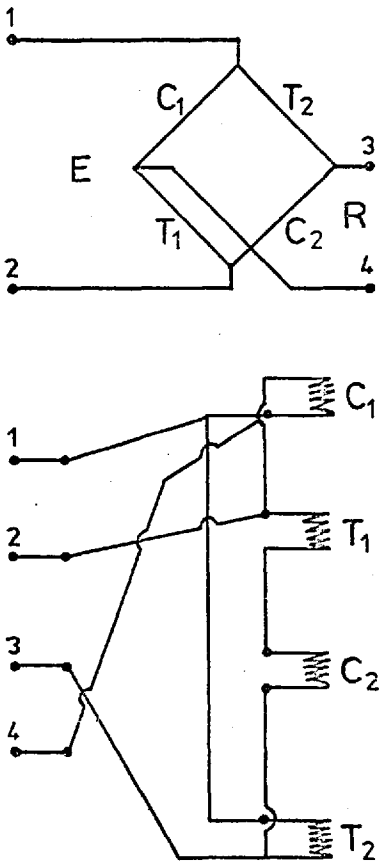

1 0·5 0 1 2 in.
SCALE

GENERAL LAYOUT

SHAPE

CIRCUIT DIAGRAM

LATERAL STRAIN MEASURING DEVICE

FIG. 4-4

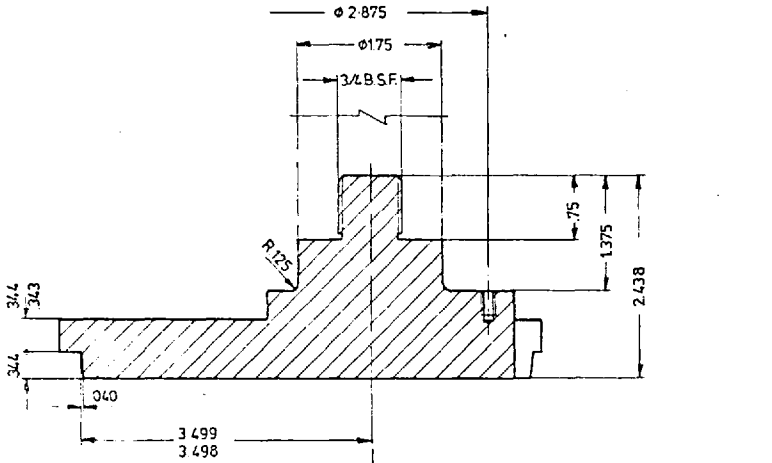

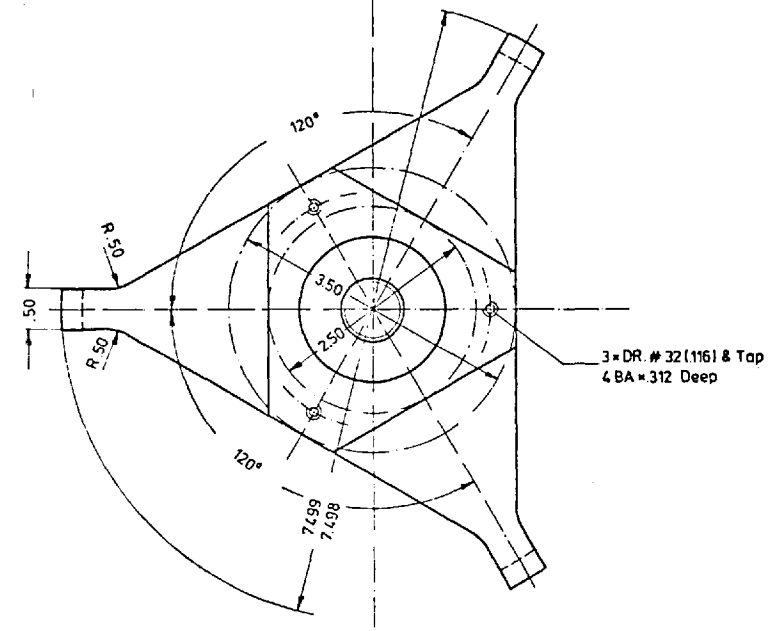

Inside Element

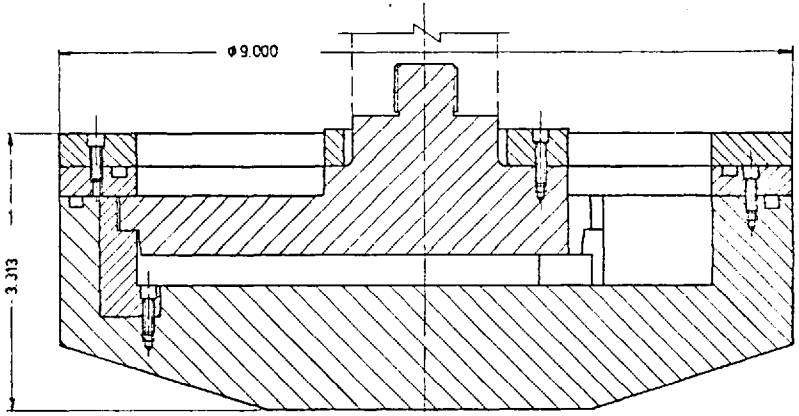

General Assembly

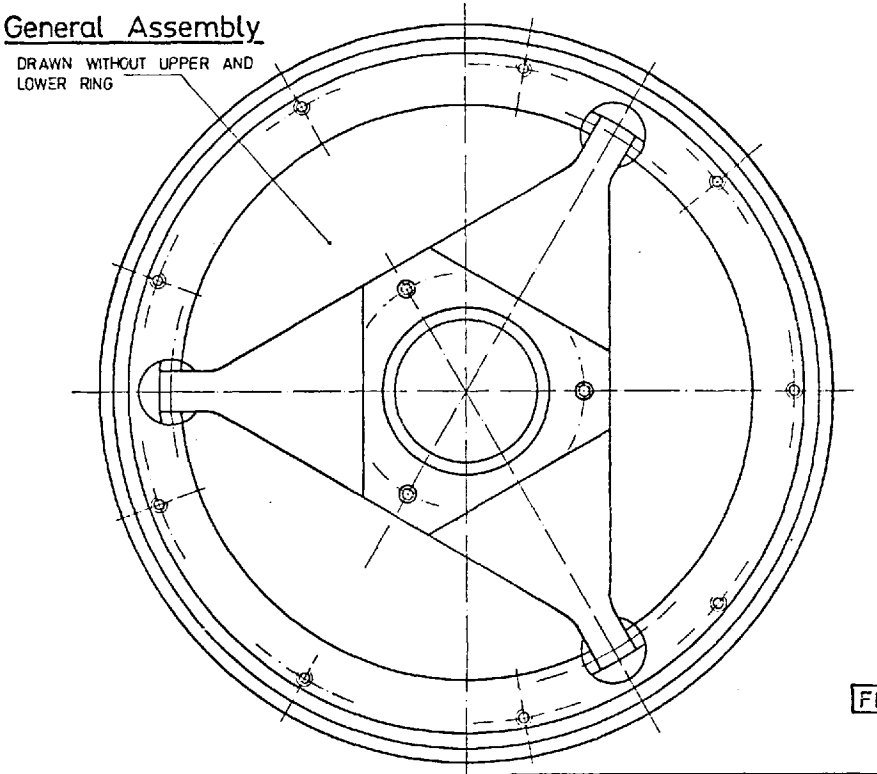

FIG. 4-5

10-TON LOAD CELL			
Designed EL-RUWAITH			GENERAL ASSEMBLY & INSIDE ELEMENT
Scale as shown			
Date	General Limits		
April 1971	Decimal ± 1 DES	Fraction ±	Material Stainless Steel E.N. 24

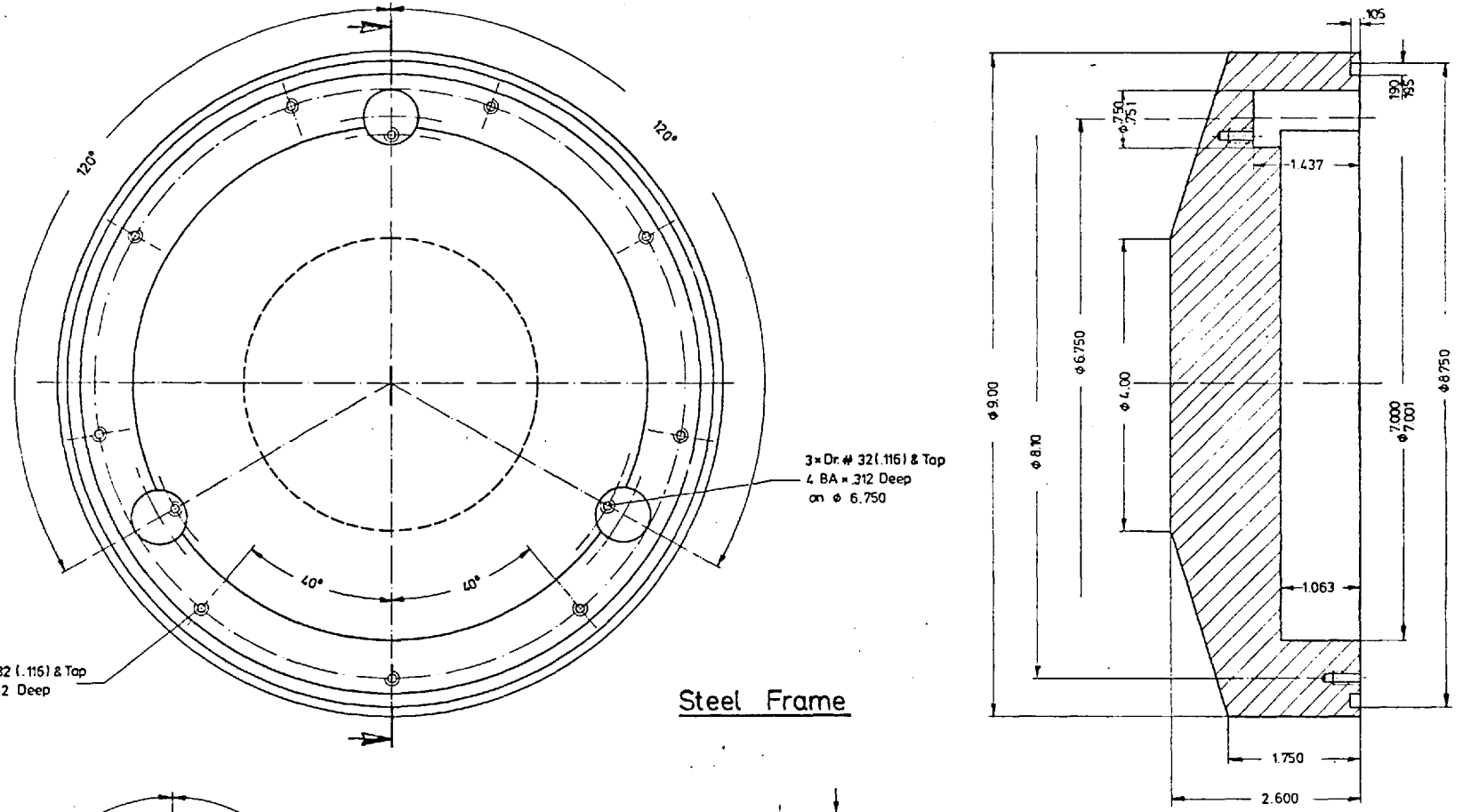

Steel Frame

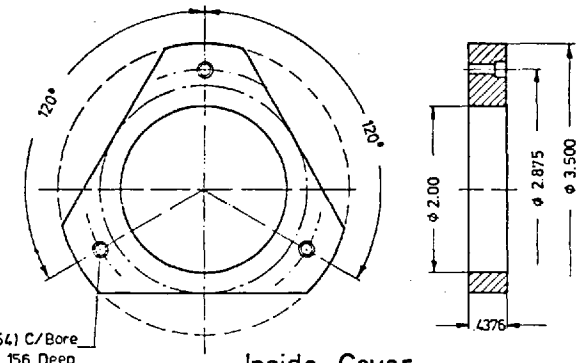

Inside Cover

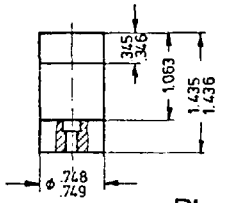

Plug

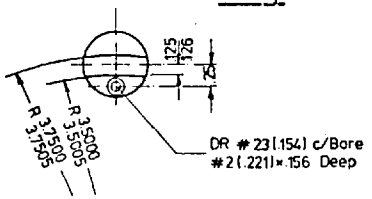

FIG. 4-6

10-TON LOAD CELL			
Designed EL-RUWAYIH			GENERAL DETAILS & STEEL FRAME
Scale as shown			
Date: April 1971	General Limits		Material MILD STEEL
	Decimal ±.005	Fraction /	

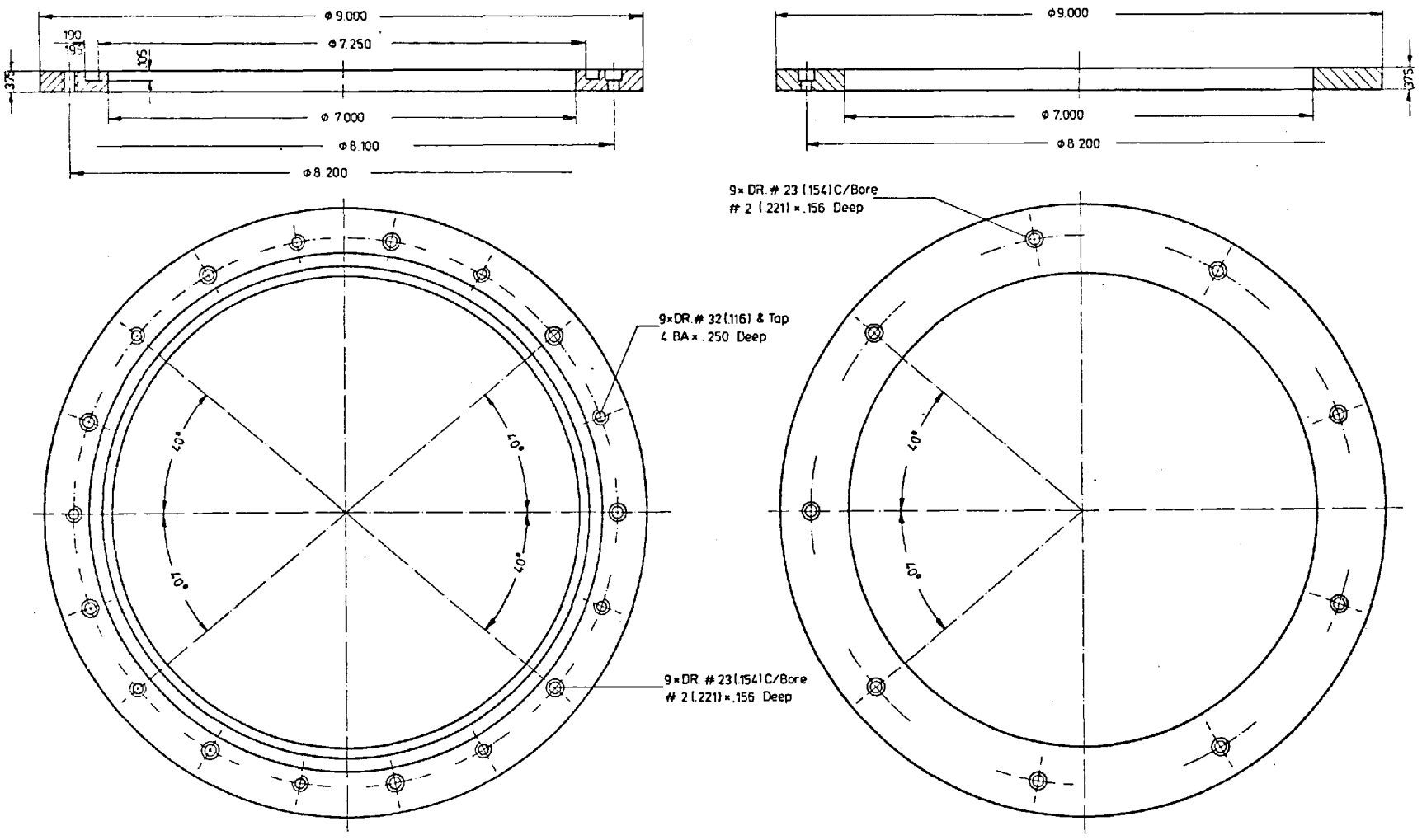

Middle Steel Ring

Upper Steel Ring

FIG. 4-7

10-TON LOAD CELL		
Designed: EL-RUWAYIH	DETAILS OF STEEL RINGS	
Scale: as shown		
Date: April 1971	General Limits: Decimal ± 0.005	Fraction:
	Material: MILD STEEL	

CHAPTER V

THE MATERIALS

5.1 Introduction

Unfortunately many technical papers underestimate the importance of material classification especially those dealing with the behaviour of rockfill materials. In fact a method of soil identification is as important as a soil model or testing techniques.

The main rockfill material investigated in this research work was gneiss alkali granite. From here it will be referred to simply as granite rockfill and the text will mainly concentrate on its description and classification.

The marble chippings and Ham River sand have been tested for comparison purposes only and therefore only a brief description of their properties and classifications will be given.

The granite rockfill investigated in this work is the same material that was studied by Tombs (1969) and Pigeon (1969). Therefore some of the classification tests which were carried out by these authors will not be repeated.

To identify and describe a rockfill material, a petrographic analysis and a set of classification tests are necessary. These classification tests include: grain size and gradation, grain shape, specific gravity, relative density, coefficient of friction and strength of individual grains.

5.2 Mineralogical Analysis

The mineralogy affects the engineering properties of granular materials by controlling the physical properties of each of the rock particles. Horn and Deere (1962) concluded that under similar testing conditions different minerals had different coefficients of friction, but minerals of the same type, though from different origins, had the same frictional characteristics.

The granite used in this work was medium coarse grained and had a mottled, white, gray and black appearance with a gneissose structure. Mica, hornblende, quartz and feldspar are clearly visible in the thin sections. The visual assessment of the primary minerals was supervised by Mr. B. Stimpson of the Rock Mechanics Department at Imperial College. The following composition was recognised:

Orthoclase	27%	
Albite	15%	Feldspar = 57%
Microcline and Microperthite	15%	
Quartz	25%	
Biotite	12%	
Hornblende	4%	
Accessory minerals	2%	

The accessory minerals in descending order are: sphene, ilmenite and its alteration product leucoxene, apatite and zircon.

The texture is described as follows: the feldspathic minerals are interlocked with quartz in a tight mosaic of typical grain size approximately 1 mm. Clearly defined zones of orientated biotite and hornblende alternating with more feldspathic regions give rise to the pronounced gneissose structure.

5.3 Classification Tests

5.3.1 Grain Size and Gradation

The grain size and gradation were both determined by dry sieving. The procedure adopted was that specified by BS 1377: 1967. One grading was used throughout the testing programme and is shown in Figure (5-1). The grading curves are usually described by two parameters: one, a grain size, to locate the curve and the second to describe it. Usually the maximum size is given to locate the grading curve, and this has the advantage of setting an upper limit for a given sample. For other parameters, the geometric mean particle size is adopted taking into account all the sizes of the particles used. Pigeon

(1969) derived a mathematical expression for the calculation of the geometric mean particle size.

The choice of one or more parameters to describe the grading is much more difficult. The coefficient of uniformity is often used in soil mechanics and, so far, it is the best parameter quoted in the soil mechanics literature for describing the grading of granular materials.

However, for samples having similar packings and similar geometrical gradings with the same D/d ratios and the same applied principal stresses, the contact forces between the grains are not equal, this being due to the variation of particle size. Furthermore the larger particles have a larger proportion of flaws and fissures than the smaller particles which, consequently, have a greater unit strength.

In large and small samples with geometrically similar particle distribution, the same mean applied principal stresses, and the same D/d ratios, the greater interparticle loading in the large sample will lead to greater deformation. If, however, the unit shear strength of all the grains is similar, the behaviour of the samples should also be very similar as the shear strength of the particles will be dependent on the square of their nominal size, and hence, proportional to the square of the sample diameter.

The effect of the increase in fines, in a large sample due to the increased breakage because of the higher contact forces, will depend on the initial grading. In a grading short of fines the additional particles may have little or no effect as they may just rest in the voids, leaving larger particles to carry and transmit the applied stresses. Alternatively, if a large proportion of fines already exists, the dilatancy of the sample will be influenced. Therefore a careful selection of the gradation of the rockfill is necessary.

5.3.2 Grain Shape

The most common parameters used to describe the grain shape are "roundness" and "sphericity". Roundness is defined as the ratio of the radius of curvature of the corners of a particle to that of the whole particle. Sphericity is defined as the square root of the ratio of the volume of a grain to that of the circumscribing sphere. These parameters can be estimated visually from charts published by Rittenhouse (1943) and Krumbein (1941). For the granite tested, values of roundness and sphericity are 0.2 and 0.7 respectively. Griffith (1967) showed two main faults in this type of estimation: first it is two-dimensional, and second it is very subjective.

Marsal (1963a) suggested a shape factor which does not have those faults, but whose determination is excessively complicated. It is defined as the ratio of the volume of a grain to that of a sphere having a diameter equal to the grain's average dimensions. This latter value is determined by averaging the grain dimensions in three perpendicular directions and a large number of particles must be measured to obtain a representative value.

Powers (1964) introduced another method avoiding the previous faults and based on data by Loudon (1952). Powers found a direct relationship between the maximum porosity of an assemblage of uniform particles and the angularity factor, Figure (5-2). The angularity factor is defined as the reciprocal of the sphericity factor which is the ratio of the specific surface diameter of a particle to its volume diameter.

The particles of the granite rockfill tested are highly angular and the ratios of length to width remain approximately the same for all the fractions. The following table gives a rough idea of the shape of the particles:

B.S. Sieves		Ratio
Passing	Retained	Length/Width
-3/16"	+ No. 7	1.30
- No. 7	+ No. 14	1.54
- No. 14	+ No. 25	1.36
- No. 25	+ No. 52	1.42

5.3.3 Specific Gravity

The specific gravity was determined on a sample having a grading similar to that used in the testing programme. The procedure followed was that described in the British Standard No. 1377: 1967. The value of the specific gravity of granite was 2.66 which is in good agreement with the values reported by Tombs (1969) and Pigeon (1969).

5.3.4 Relative Density

The state of the compactness of soil samples is usually described by the porosity or void ratio. The term porosity will be used throughout this thesis. The effects of the porosity or the void ratio on the strength and deformation characteristics of rockfill materials have been discussed and reviewed in Chapters 2 and 3 of this thesis.

Methods of measuring triaxial sample dimensions have been reported many times in the soil mechanics literature and will not be repeated here. The sample preparation and the achievement of the required density have been presented in Chapter 4.

The parameter "relative density, D_r" is often used in the soil mechanics literature to define the degree of packing of cohesionless soils. It is defined as:

$$D_r = \frac{e_{max} - e}{e_{max} - e_{min}} \qquad (5.1)$$

where e_{max} and e_{min} are the maximum and minimum void ratios respectively for a given gradation and e is the void ratio at which D_r

needs to be known.

From the relative density definition, it can be seen that the 'loosest' and 'densest' possible states of the granular material should be determined. These limits, the 'densest' and the 'loosest' have been defined by Kolbuszewski (1948); USBR (1963) and others.

On the basis of results by Kolbuszewski (1948) it is suggested that a porosity range, PR, can be defined as:

$$PR = n_{max} - n_{min} \tag{5.2}$$

where n_{max} and n_{min} are the maximum and minimum porosities respectively. This porosity range gives an indication of the shape of the grading curve. Narrow gradings have porosity range values of about 14% (Kolbuszewski, 1948) which may go up to 31% for well graded samples (Felt, 1958). Therefore it is important to determine the 'loosest' and the 'densest' limits of a soil sample and to ensure that no sample looser than the loosest or denser than the densest would be obtained.

Minimum Density

This loose limit has been determined as suggested by the USBR (1963) for coarse cohesionless samples. The results were also compared with those obtained by Kolbuszewski's method (1948), and full agreement was noted. Results of tests in a 4 in. diameter mould are shown in Table (5-1).

Maximum Density

Again the procedure followed here was that described in the USBR (1963). For each test fresh material was used, to limit the influence of particle breakage resulting from the compaction. Results of tests in a 4 in. diameter mould are shown in Table (5-1).

5.3.5 Coefficient of Friction

Horn and Deere (1962) showed that the coefficient of friction between mineral grains varied with the finish of the contact surfaces and the fluid present on those surfaces. They calculated that coefficient of friction increases on saturation for all massive-structured minerals. Later Bromwell (1966) concluded that the coefficients of friction are not influenced by saturation as long as the surfaces are chemically clean.

In view of this, Pigeon (1969) carried out tests on individual lumps of granite without any sort of surface cleaning or polishing. The tests were carried out in a conventional shear box. The rate of displacement was 0.01 in/min and the vertical load was 13.41 lbs. The coefficient of friction was taken as equal to the tangent of the vertical over the horizontal load only when there is no vertical movement, i.e. at zero rate of dilatancy (Hafiz, 1950). Results of such tests on dry and submerged samples are shown in Table (5.2). From these results it can be seen that the interparticle friction for submerged granite is less than that for an air dry one. Similar behaviour has been observed by Tombs (1969) for cleaved Silurian mudstone.

Skinner (1969) carried out friction tests on 1 mm diameter and 3 mm diameter glass ballotini; 1/8 in. diameter steel balls; 3 mm diameter lead shot and 3 mm diameter glass ball sliding on plate glass. He showed that the interparticle friction increased upon flooding the samples. The subject has been discussed further in Chapter 2.

5.3.6 Strength of Individual Particles

The most reliable test to determine rock strength is the unconfined compression test. There are other methods reported in the rock mechanics literature for assessing rock strength*. One of these is the "irregular lump test" (Hobbs, 1963) which is the easiest and quickest test to estimate the strength of rock lumps. The failure mechanism is similar to that occurring in consolidation tests on rockfill: initial crushing

* e.g. Brace, W.F. 1963; Evans and Pomeroy, 1966, etc.

at the contact points followed by complete or partial fracture of the particles when the contacts are not large enough to withstand the applied stresses.

Pigeon (1969) reported sets of tests on granite, where each set consists of 25 lumps of rock weighing between 30 to 34 grams. The results on dry and saturated samples are shown in Table (5.3).

Unconfined compression tests were carried out on dry and saturated $1\frac{1}{2}$ in. diameter x 3 in. height samples of granite by J. Franklin of the Rock Mechanics Department at Imperial College. The average unconfined compression strengths for the dry and saturated granite were 22881 $\pm$ 1200 and 20136 $\pm$ 3358 psi respectively. Detailed results were reported by Pigeon (1969).

Hobbs (1963) suggested a relationship between the irregular lump test and the unconfined compression test. This relationship is expressed as:

$$q = 0.91\ I_A - 3180 \qquad (5.3)$$

where q is the unconfined compression strength, in psi,

I_A is the strength index determined from irregular lump test, in psi.

The standard error of the regression estimate being:

$$\pm 1260 \left[1 + \frac{I_A - 17660}{1105 \times 10^5}\right]^{\frac{1}{2}} \qquad (5.4)$$

The relationship represented by equation (5.3) and the 95% confidence limits calculated by equation (5.4) are shown in Figure (5-3). Pigeon (1969) reported that the test results of granite are within the 95% confidence limits.

5.4 Description of the Marble Chippings

Marble is the name given to limestones that have been completely recrystallized by metamorphic processes during their burial in the earth's crust. The calcium carbonate of shells and finer particles is gradually transformed into crystals of calcite of roughly uniform size. If the limestones were pure they become a white rock after crystallization. On the other hand if the original limestone is not pure, but contains other carbonate minerals such as dolomite and impurities of sand or clay, various chemical reactions take place between the ingredients during the thermal processes of metamorphism resulting in the formation of coloured marbles.

The principal mineral compositions are: calcite and dolomite with minor quantities of wollastonite, amphibole, pyroxene and garnet. Other minor minerals might be present such as olivine and serpentine giving a green colouration to the marble.

The marble chippings tested in this experimental programme were brought from an undertaker in the form of lumps of $1\frac{1}{2}$ in. diameter in size. They were mechanically crushed in the Geology Department of Imperial College to form a mixture with a maximum size passing BS sieve size - 3/16 in. The mixture was then sieved mechanically to separate each size; these being kept in plastic bags.

The final sieved material was coarse grained and had a white appearance. It looked like pure calcite. The particles were angular and had a rough texture similar to that of the granite particles. The fine materials (i.e. material passing sive No. 52 and 100) do not form a paste or adhere to the surface of the larger particles. Unfortunately a mineralogical analysis, similar to that for the granite, was not carried out.

The grading of the marble chippings used throughout this experimental programme is exactly the same as that used for the granite rockfill. Therefore the grading curve shown in Figure (5-1) is representative of both the granite rockfill and the marble chippings.

The specific gravity was measured using the procedure described in the British Standard No. 1377: 1967. The value of the specific gravity measured by the above method was 2.73.

Another procedure for measuring the specific gravity was tried. The reason for this was to measure the specific gravity of the particles under conditions similar to those adopted during the setting up of the triaxial sample for testing. This procedure is similar to that described in the British Standard, except that no deairing of the sample was carried out. The resulting specific gravity was 2.70, which is slightly lower than that obtained using the British Standard method. Therefore it seems that the marble chippings are denser but weaker than the granite rockfill particles.

Other classification tests on marble chippings have not been carried out because it was not intended to study their strength and deformation characteristics. The marble chippings were tested for comparison purposes only.

5.5 Description of the Sand

The sand used throughout these tests was Ham River sand, a medium to fine uniform sand. The material is similar to that used by Green (1969); Shaal (1972) and Reades (1972), although there are slight batch variations. The sand was delivered in 112 lb. bags, and it had not been used in any previous tests. For each test carried out a fresh sample of sand was used.

Particle size analyses of the Ham River sand used in these tests are shown in Figure (5-1). Similar gradings were used by Green (1969) and Reades (1972) in their experimental programme.

The specific gravity was determined according to the British Standard No. 1377: 1967 and the result obtained was 2.677. This is in good agreement with those obtained by Green (1969) and Reades (1972).

The maximum porosity of the sand was determined by Reades (1972) using rapid tilt tests on a dry sample, as described by Kolbuszewski (1948). The result obtained was 48.4%. These are the basic properties required for the experimental programme. For other properties and details, reference should be made to Bishop and Green (1965); Green (1969); Reades (1972) and Skinner (1975).

The method of sample preparation has been presented in Chapter 4. After testing the sand samples were oven dried then sieved for the particle breakage study.

Table (5-1) Granite rockfill - Determination of the maximum and minimum density in a 4 in. dia. Proctor mould.

Maximum particle size (in.)	Maximum density lb/cu. ft.	Minimum density lb/cu. ft.	Porosity range %
-3/16 +No. 7.	129.8	95.2	20.9

Table (5-2) Coefficient of friction for granite on granite (after Pigeon 1969)

Normal load: 13.41 lbs.			
Test No.	Condition	Coefficient of friction	ϕ_μ
1	submerged	0.70	35^o
2	"	0.71	35.3^o
3	"	0.70	35^o
4	"	0.73	36.1^o
5	air dry	0.74	36.4^o
6	" "	0.73	36.1^o
7	" "	0.77	37.7^o
8	" "	0.77	37.7^o

Table (5-3) Irregular lump tests on granite (after Pigeon 1969).

No. of samples tested	Testing conditions	Average load lbs.	Average area in^2	Average strength index psi	Slope of regression line psi.
25	air dry	1171±120			
25	oven dry - air cooled	1078±125	.036±.0056	33884±2310	29940±4550
25	saturated - surface dry	885±75			
25	saturated - submerged	885±115			
25	saturated - submerged	774±75	.0349±.0056	22663±1921	22200±2740

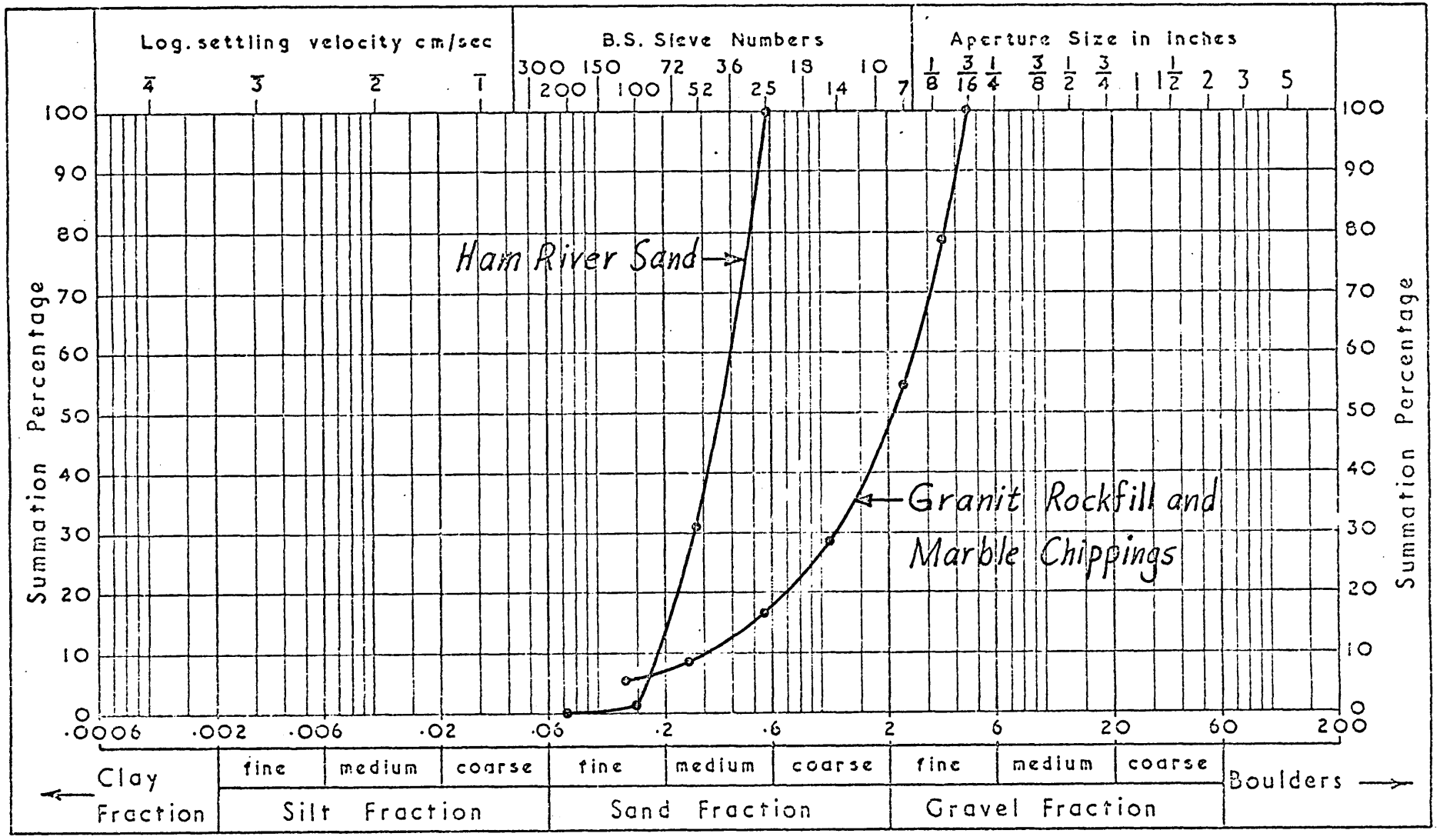

PARTICLE SIZE ANALYSES FOR GRANITE ROCKFILL, MARBLE CHIPPINGS, AND HAM RIVER SAND

FIG. 5 - 1

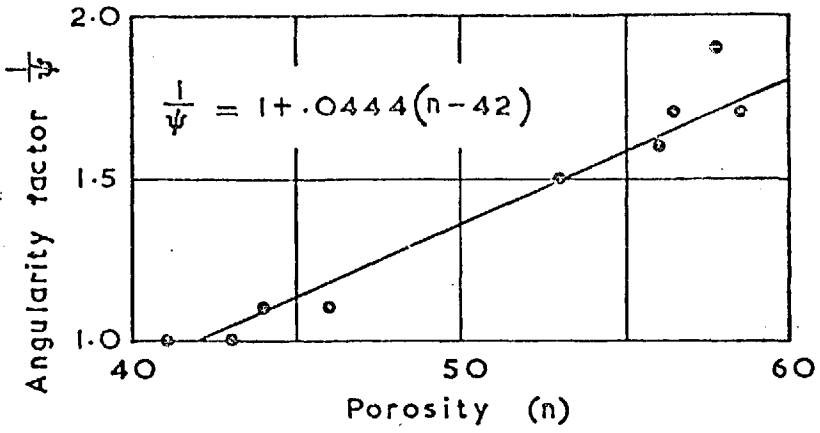

RELATIONSHIP BETWEEN THE ANGULARITY FACTOR AND THE POROSITY FOR THE SIZE GROUP 25-52 MESH SIEVES.

After Powers, 1964

FIG. 5 - 2

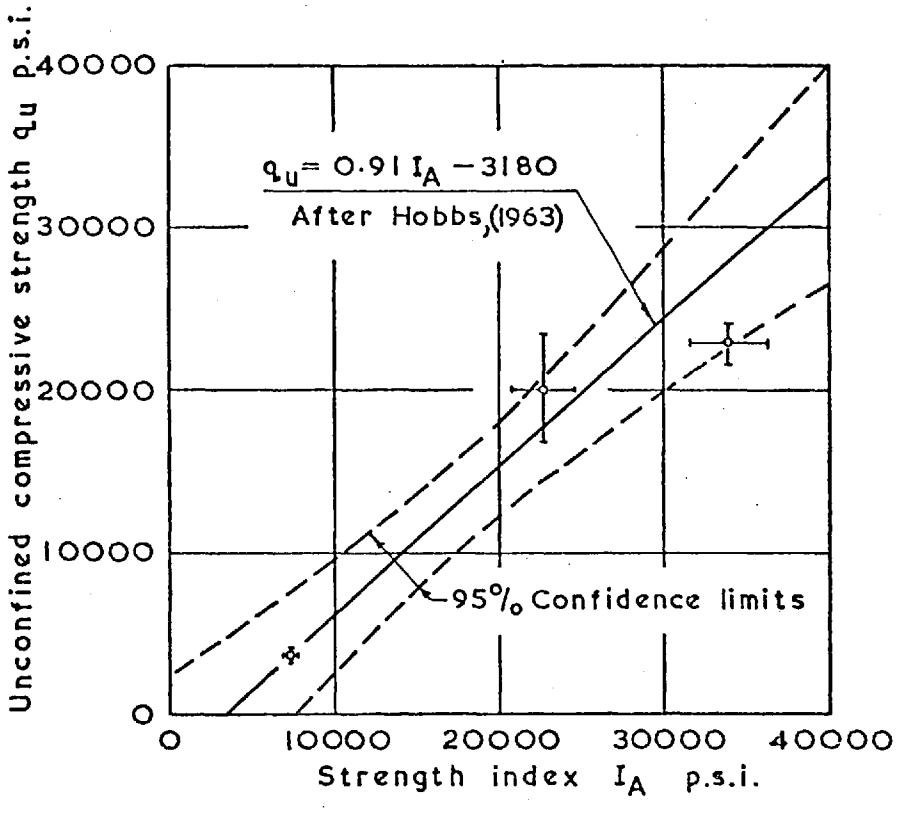

RELATIONSHIP BETWEEN THE AVERAGE APPLIED STRESS AT FRACTURE AND THE UNCONFINED COMPRESSIVE STRENGTH (After Pigeon 1969)

FIG. 5 - 3

CHAPTER VI

EXPERIMENTAL RESULTS AND DISCUSSION OF THE TRIAXIAL STRENGTH TESTS (THE 1½ IN. DIA. SAMPLES)

6.1 Introduction

In this chapter two main factors (the confining pressure and the density) which influence the strength and deformation of rockfill material, have been investigated by five series of drained triaxial tests. Other series of triaxial tests under undrained conditions were also carried out. Finally a series of cyclic loading tests was performed to examine the properties of rockfill under repeated loading. The influence of other factors on the stress-strain properties of rockfill material will be discussed by using results of other tests* together with the present test results. All the results quoted from others are from tests under conditions similar to those carried out here. The initial porosity will be taken as a basis for discussion of results rather than the porosity after consolidation or at failure.†

Before starting the testing programme, tests on Ham River sand were performed to check the equipment and testing technique. Results of such tests are shown in Appendix (B). All data are in reasonable agreement with those published previously (Bishop, 1966; Green, 1969; Skinner, 1975 and others). This means that the procedure adopted and equipment used in this thesis can be used to correlate with other tests on Ham River sand.

6.2 Consolidation of the triaxial samples

The consolidation curves of two isotropically consolidated drained tests at different confining pressures are shown in Figure (6-1). These tests are chosen to represent the dense and the loose states of compaction. The consolidated undrained and the cyclic loading tests

---

*They will be named in the appropriate places.

†Porosities after consolidation or at failure are very critical because the volume changes are influenced by the membrane penetration and the small errors in volume change measurement.

were consolidated in a similar way to that of the drained tests.

From Figure (6-1) it can be seen that the consolidation of a rockfill sample increases as the confining pressure increases. But this relation is not linear and the rate of consolidation decreases as the confining pressure increases. Up to a confining pressure of 850 psi (maximum pressure applied here) there is no evidence that the samples ceased consolidating. Thus the decrease in rate of volume change associated with stress increasewould be related to the increase in sample density.

All drained test samples were consolidated dry up to 30 psi confining pressures then saturated by flushing water through. After flushing water, a back pressure (60 psi) of the same magnitude as an increase of all-round pressure was applied to ensure full saturation, then consolidation was continued to the required maximum cell pressure. During consolidation in the dry state* the dense sample (n = 27.2%) underwent a volume decrease of 1.65% corresponding to 2.7% for the loose sample (n = 38.5%). During subsequent saturation at constant effective stress of 30 psi, a further volume decrease occurred. The amount of this extra volume decrease depends on the density of the sample, it ranges from 19.8% to 30.2% of the volume change which had already occurred before saturation for samples at 27.2% and 38.5% of porosity respectively†. At an effective confining pressure of 850 psi the dense sample consolidated by 8.3% corresponding to 14% consolidation for the loose one. Therefore it can be seen that under the same confining pressures, loose samples consolidated much more than dense ones.

Marachi et al (1969) observed that the consolidation of Pyramid Dam material increases as the particle size increases, while the data for the basalt and the Oroville Dam material were somewhat mixed and did not show a similar trend. Therefore their results concerning the

---

* This is up to σ'_3 = 30 psi.

† Tombs (1969) reported an extra volume change of 49% - 211% of the volume change which had already occurred before saturation for mudstone material.

influence of particle size on the isotropic consolidation behaviour of rockfill material are inconclusive. Tombs (1969) from tests on granite and on cleaved mudstone observed a greater volume change at a given stress, for the samples with greater maximum particle size. This was explained as being due to high contact forces for larger particles and to membrane penetration which is larger for coarser gradings.

The error involved due to penetration of the rubber membrane is unknown, but it is dependent on the confining pressure, membrane thickness and the grading of the material. In fact this error was one of the main reasons behind the development of the lateral strain devices presented in Chapter 4. In Chapter 7 the amount of membrane penetration will be shown.

6.3 The stress-strain behaviour of the samples sheared under drained conditions.

Results of the drained triaxial tests are shown in Tables (6-1) to (6-5) and the final stress-strain curves are plotted in Figures (6-2) to (6-7). Numbers in parenthesis denote the value of the effective minor principal stresses (σ'_3). The curves are presented in five groups depending on the density: very dense ($n \approx 23.0\%$); dense ($n \approx 25.6\%$); medium ($n \approx 30.0\%$); loose ($n \approx 34.2\%$) and very loose ($n \approx 40.7\%$). The density and the relative density of each sample are shown in the tables.

The minimum porosity obtained in the laboratory for the $1\frac{1}{2}$ in. dia. samples was approximately 23.0%. A porosity as low as 20.4% was obtained for test No. (15), but such a high density could only be obtained by excessive compaction and this would create punctures in the rubber membrane which are a serious problem. Therefore it was decided to adhere to approximate minimum porosity of 23% if possible. The maximum porosity of the very loose samples was approximately 40.7% although as high as 41.7% was obtained for test No. (51). It was found that extremely loose samples do not achieve a peak deviator stress and are difficult to set up and keep vertical especially when using a steel top cap and more than one rubber membrane during high confining pressure testing.

The initial slopes of the deviator stress-axial strain curves are very close for the very dense and dense samples while they move apart for loose and very loose samples. This suggests that the stiffness of loose samples varies a lot under a wide range of confining pressures while the difference in stiffness is less for dense samples under the same range of confining pressures. This is more pronounced in the curves of very dense and very loose samples. Behaviour of medium density samples lies between the extreme cases.

The stress-strain curves of the dense samples have a well defined peak which takes place at an early strain stage of shearing, especially at low confining pressure. At intermediate and high confining pressures there is also a marked peak in the stress-strain curves but at higher axial strains. The stress-strain curves of the loose samples show less pronounced peaks than the dense samples and at high confining pressure, as high as 300 psi and 600 psi, the curves level off at the top. At very high confining pressures, as high as 850 psi, the loose samples are similar to the dense samples and show a sharper peak than at lower confining pressures.

In fact the general feature of the stress-strain curves of the loose and dense rockfill samples presented here is similar to that of Ham River sand presented by Bishop, (1966).

The curves of the volumetric-axial strain relationships are shown in Figures (6-2) to (6-5). Again the initial slopes of the curves increase as the confining pressure and density increase. Dense samples under low confining pressures exhibited a little consolidation followed by a high rate of dilatancy, especially at very low cell pressure. As the confining pressure increases, the rate of dilatancy decreases and at σ'_3 of 300 psi the sample was sheared at nearly constant volume. At very high confining pressure, as high as 600 psi and 850 psi, the samples continue to consolidate slowly, indicating a particle crushing process.

Loose samples under low confining pressures consolidated at the beginning of the shear stage, followed by a moderate rate of dilatancy. Again, the rate of dilatancy started to decrease as the confining pressure increased and at σ'_3 = 80 psi the shearing of the samples was associated with approximately constant volume at failure. At high confining pressures, as high as 600 psi and 850 psi, the sample was still decreasing in volume, a rate more than that of the dense sample at the same level of confining pressure. This behaviour is similar to that of Ham River sand presented by Bishop, (1966) although the latter was decreasing in volume,* at a rate much more than that of the rockfill.

In Figure (6-7) some tests at different densities consolidated and sheared at the same cell pressures were plotted. A low confining pressure of 40 psi and a high confining pressure of 850 psi were chosen although the other tests at various confining pressures could have been plotted as well. From this figure it is clear that under the same confining pressure, the stiffness of the sample increases with increase of density both at low and high confining pressures. The main points to be noted from this figure are:

1. Dense samples at low confining pressures show a marked tendency to dilate while at high confining pressures they decrease in volume during shear.

2. Loose samples at low confining pressures consolidate first then dilate moderately while at high confining pressures they continue to decrease in volume during shear.

3. At low confining pressures there is a remarkable difference in the shape of the stress-strain curves, the shear strength and the volumetric strain curves, while at high confining pressures these differences are less pronounced and in fact the stress-strain curves are nearly similar in shape apart from the variation of the stiffness of the sample and the amount of volume change.

---

* Drained tests on Ham River sand, Figure (18), test No. 29.

6.3.1 Variation of the shear strength of the granite rockfill

As has been pointed out in Chapter 2, the shear strength of rockfill will be expressed in terms of the angle of shearing resistance throughout this experimental programme. The relationships between the angle of shearing resistance ϕ' and the initial porosity of the samples for the drained tests are plotted in Figure (6-8). This figure shows how the angle of shearing resistance decreases as the initial porosity increases for the same confining pressure. It is also clear that the angle of shearing resistance ϕ' varies significantly under low confining pressures while at high confining pressures this variation is very small.* Samples tested under low confining pressures gave ϕ' higher than those tested at high confining pressures. The straight line relationship, as shown in the figure, is a matter of approximation only. This figure also shows that the difference in ϕ' for different cell pressures, σ'_3, decreases as the initial porosity increases and approaches a state** where this difference in ϕ' is very small for samples tested at low and high cell pressures.+ Similar trends in the behaviour of rockrill material have been reported by Marachi et al (1969) although the porosity range used was less than that used in this thesis.++ Mangla shale (Burland, 1964) shows large variation in strength with a comparatively small variation in porosity. This is in contrast to Brasted sand (Cornforth, 1964) the shear strength of which is remarkably unaffected by porosity changes.

The Mohr envelopes for loose and dense samples are shown in Figure (6-9). The marked curvature of the envelope at low stresses for the dense samples can be seen. Both Mohr envelopes for dense and loose samples at high stresses tend to converge. Data from Skinner reported by Bishop, (1966) showed that Mohr envelopes for loose and dense Ham River sand converge at high stresses and are nearly coincident at σ'_3 = 1400 psi.

---

* At σ'_3 = 850 psi, ϕ' decreased by approximately 1.3° when the porosity increased from 25% to 35%.

** For very loose samples (n $\approx$ 41%)

+ By extrapolation, the difference in ϕ' is approximately 1.8° between tests at cell pressures of 20 and 850 psi.

++ Marachi et al, (1969) used a porosity range of 32 - 43%.

The curvature of Mohr envelopes can be recognised clearly by studying the values of ϕ' reported in Tables (6-2) and (6-4). The angle of shearing resistance ϕ' for dense samples decreased from 49.8° to 38.6° when the effective cell pressure increased from 20 psi to 850 psi. For loose samples ϕ' decreased from 43.5° to 37.2° for effective cell pressure values of 20 psi to 850 psi. The main reasons for this curvature, as will be seen in the following sections, are particle crushing and dilatancy effects.

The relationships between the angle of shearing resistance ϕ' and the effective cell pressure σ'_3 for all the drained test samples are shown in Figure (6-10). The main discussion and comparison will be concentrated on the loose and dense groups of tests. Here the difference between ϕ' for a dense sample and ϕ' for a loose sample drops from nearly 6.5° at σ'_3 of 20 psi to only 1.4° when σ'_3 is 850 psi. It is apparent that even for loose samples of granite, ϕ' is not independent of the effective stress, but drops about 6° as σ'_3 rises from 20 psi to 850 psi. It will be seen in the following sections that this drop is closely associated with the rate of volume change at failure. This trend in reduction in ϕ' values as σ'_3 increases is similar to the behaviour of Ham River sand reported by Bishop, (1966) except for two points:

1. The magnitude of reduction in ϕ' values of Ham River sand is different from that of granite; this is natural and is due to the properties of both materials

2. At high stresses (as high as σ'_3 of 4000 psi) ϕ' for Ham River Sand increases with cell pressure after it has decreased to a minimum value of about 1000 psi effective cell pressure.

The maximum effective cell pressure used in this thesis is 850 psi and at this stress level the ϕ' value for a dense sample is 1.4° higher than that for a loose sample. From Figure (6-10) there is no evidence that at higher effective cell pressures (higher than 850 psi) the value of ϕ' for both dense and loose samples will be the same nor that they reach a minimum value then increase at higher stresses as

reported by Bishop, (1966) for Ham River sand. Various data by Marsal (1965); Tombs, (1969) and Marachi et al, (1969) support the findings mentioned above for rockfill materials, Fig (6-17).

6.3.2 Variation of the volumetric strain at failure

Figure (6-11) shows the relationship between the volumetric strain at failure and the confining pressure for all the tests. Curves were drawn through the dense and loose samples because of the uniqueness of their initial porosities. This figure indicates that the amount of volumetric strain at failure increases with the increase of the effective cell pressure σ'_3 in the low pressure range, but it shows no significant changes at high pressures* especially the dense samples. The dense sample sheared at σ'_3 of 850 psi showed approximately 0.12% higher† ϵ_v value at failure than that sheared at σ'_3 of 600 psi, while the corresponding increase in ϵ_v value at failure for loose samples is approximately 0.48% for the same pressure range. Very dense samples sheared at high confining pressures showed almost the same ϵ_v at failure. This indicates that particles of loose samples continue crushing significantly during shearing at high confining pressures. But generally speaking, the decrease in volume at failure for both dense and loose samples when sheared at high confining pressures is not significant.

This trend in the variation of ϵ_v at failure as a function of the confining pressure has been observed by Marachi et al, (1969) for tests on different rockfill materials although the initial densities have not been indicated. Tests on crushed basalt material even at 650 psi confining pressure showed ϵ_v at failure less than that at 420 psi confining pressure. It means that ϵ_v at failure increases with confining pressure to a minimum level, then at higher confining pressure starts to decrease. Similar trends in the variation of the volumetric strain at failure as a function of the confining pressure were reported by Vesić and Clough, (1968) for Chattahoochee River sand. Tests on this material showed that ϵ_v value at failure increased as the confining pressure increased, but after reaching

---

* Higher than 600 psi

† $(\epsilon_v)_{850} - (\epsilon_v)_{600} = 0.12\%$

a maximum value it decreased to a more or less constant value. The amount of ϵ_v at failure for a confining pressure of 211 kg/cm^2 was approximately 13%, while for a confining pressure of 633 kg/cm^2 it was only 9%. Here again the porosity was not taken into consideration.

From the volumetric strain-axial strain curves shown in Figures (6-2)to (6-7), it can be observed that up to the confining pressure applied in this testing programme, there is no indication that ϵ_v value at failure is the same for both dense and loose samples. There is still a significant difference in the value of ϵ_v at failure between dense and loose samples tested at σ'_3 of 850 psi. This is shown clearly in Figure (6-11) where ϵ_v at failure for a loose sample was approximately 4.2% more than that for a dense sample sheared at σ'_3 of 850 psi. Tests on Ham River sand by Skinner reported by Bishop, (1966) showed that ϵ_v at failure for loose samples was approximately 7% more than that for dense samples sheared at confining pressure of 990 psi. Thus it can be concluded that the volumetric strain at failure is dependent on the confining pressure and there is little evidence that dense and loose samples may reach the same value of ϵ_v at failure.

The influence of the initial porosity on the ϵ_v at failure can be seen in Figure (6-7) where two series of tests at σ'_3 of 40 and 850 psi were plotted. At a low confining pressure of 40 psi the dense sample was dilating at failure much more than the loose one. It is expected that very loose samples will undergo large volumetric strain at failure because of higher degrees of freedom for particle rearrangement*. As the confining pressure increases the dilation of the sample decreases and at high confining pressure (as high as 300 psi and more) the sample stays at a constant or decreasing volume at failure. This is shown also in Figures (6-2) to (6-7). From Figure (6-7) it appears that the dense sample was at nearly constant volume during shearing, while the loose sample was undergoing a small reduction in volume during and after failure. At this pressure (σ'_3 of 850 psi) the ϵ_v value at failure for loose and dense samples was -9.8% and -5.52% respectively. The effects of particle crushing on the volume changes will be discussed in detail in later sections.

---

* This is at relatively low confining pressure (σ'_3 of 40 psi).

6.3.3 Variation of the axial strain at failure

The axial strains at failure for all the samples are plotted as a function of the effective cell pressure σ'_3 in Figure (6-12). Curves were plotted through the points for the dense and the loose samples because of their unique density while others (very dense, medium and very loose) are scattered. This figure shows that the axial strain at failure increases with the increase of the confining pressure , reaching a maximum value after which it decreases with the increase of the confining pressure.

For dense samples the axial strain at failure increased from about 4.0% at 20 psi effective cell pressure to about 15.5% at 600 psi, then it decreased to about 13.3% at σ'_3 of 850 psi. For loose samples the axial strain at failure increased from about 8.6% at σ'_3 of 20 psi to about 22% at σ'_3 of 600 psi then decreased marginally to 21.5% at σ'_3 of 850 psi. It seems that this decrease in the value of the axial strain at failure at the higher confining stresses for dense samples is more than that for loose ones*.

The axial strain at failure corresponding to a wide range of confining pressures for chalk, limestone sand, Ham River sand and other granular materials is plotted in Figure (6-13). In general there is similarity in $\epsilon_{1_f} - \sigma'_3$ relationships for these various materials and the granite tested in this thesis. All the data show that the axial strain at failure increases as the confining pressure increases, and reaches a maximum value at a certain stress level, above which it decreases. Tests on sand reported by Bishop, (1966) and Vesic and Clough, (1968) showed that for confining pressures beyond 1000 psi the axial strain at failure decreases slightly†. Tests on limestone sand by Yee, (1972) showed that the axial strain at failure starts to decrease after it reaches its maximum value at a confining pressure of 400 psi. Figure (6-13) also shows that the curves are displaced further to the right with increasing

---

* The decrease in ϵ_{1f} were 2.2% and 0.5% for dense and loose samples respectively.

† A similar trend in results was observed by Marachi et al, (1969) for tests on various rockfill materials, although the highest confining pressure applied was 650 psi.

strength which suggests that the relative positions of the curves within the graph are a property of the granular materials. The decrease of the value of the axial strain at failure after it has reached a maximum value may be related to the particle crushing. The curve of Pinzandaran gravel is relatively flat which suggests that this material is relatively incompressible and the particles do not crush easily. This is in contrast to the coarse limestone sand tested by Yee, (1972) which showed a remarkable drop in axial strain value at failure after it had reached its maximum.

In Figure (6-7) the effects of the density on the axial strain at failure are shown. The axial strains at failure for dense and loose samples at σ'_3 of 40 psi are 4.6% and 10.5% respectively. The corresponding values for dense and loose samples at 850 psi are 13.2% and 22.0% respectively. Therefore it can be concluded that for a certain material sheared at a certain level of confining pressure, the axial strain at failure increases with the increase of porosity. A similar trend was observed for tests on Ham River sand reported by Bishop, (1966), on various rockfill materials reported by Marachi et al, (1969) and on limestone sand by Yee, (1972). From Figure (6-12) there is no indication that at high confining pressures loose and dense samples reach failure at the same axial strain.

6.3.4 Rate of dilatancy at failure $(d\frac{\Delta V}{V} / d\epsilon_1)$

The variation of the rate of dilatancy at failure $(d\frac{\Delta V}{V} / d\epsilon_1)$ with the effective cell pressure σ'_3 is shown in Figure (6-14). For both the dense and the loose samples the rate of dilatancy at failure decreased as the effective cell pressure increased. The rate of dilatancy at failure for dense samples decreased from 0.93 at σ'_3 of 20 psi to zero at σ'_3 of 300 psi, then at higher cell pressures it continued to be zero. For loose samples the rate of dilatancy at failure was 0.43 at σ'_3 of 20 psi, then decreased to zero at σ'_3 of 80 psi and continued to decrease at a lesser rate for higher cell pressures until it reached -0.08 at σ'_3 of 850 psi. There is no indication that the rate of dilatancy at failure tends to increase after reaching a minimum value, as reported by

Bishop, (1966) for tests on loose Ham River sand. From Figure (6-14) it can be seen that the general behaviour of granite rockfill is similar to that of Ham River sand except in the following points:

1. Dense samples of Ham River sand reached a minimum value of $(d\epsilon_v/d\epsilon_1)$ of -0.14 at σ'_3 of 1000 psi and it seems there is a tendency to rise at higher cell pressures although no data are available.

2. $(d\epsilon_v/d\epsilon_1)$ values for loose sand samples reached a minimum value of approximately -0.18 at σ'_3 of 1000 psi then increased to -0.05 for σ'_3 of 4000 psi. Tests on granite rockfill did not show such behaviour *within the pressure range tested.*

Within the working range of stresses the dilatancy characteristics of the compacted mudstone tested by Tombs, (1969) are closer to those of a loose sand than those of a dense sand. Other test data on limestone sand, granulated chalk, steel shot and Ham River sand together with those obtained in this thesis are presented in Figure (6-15). From this figure it can be seen that the effect of increasing the cell pressure at any porosity is to reduce the rate of dilatancy at failure as well as the strength. This reduction is associated with an increase in particle crushing as will be discussed in a later section. The relative position and displacement of the curves in Figure (6-15) indicate the nature and strength of the particles. This is clear from the case of dense mudstone where extensive particle crushing takes place and the behaviour is almost close to loose sand*.

The initial porosity plays a significant part at low pressures while at high pressures its significance diminishes and may reach a stage where both dense and loose samples behave the same. At an effective cell pressure of 20 psi the difference in rate of dilatancy at failure between dense and loose samples was about 0.5, while at σ'_3 of 850 psi the difference was only about 0.08. Bishop, (1966) reported a difference in rate of dilatancy at failure of about 0.55 between dense

---

* The behaviour of chalk reported by Yee, (1972) is also a good example of the influence of particle crushing.

and loose sand at σ'_3 of 40 psi while at σ'_3 of 1000 psi the difference was only 0.04*.

It has been known (Bishop, 1966) that there exists a relationship between the angle of shearing resistance ϕ' and the rate of dilatancy at failure, which appears to be a property of the granular material being tested and is rather less dependent on the test conditions than is the angle of shearing resistance. Figure (6-16) shows the relationship between the angle of shearing resistance ϕ' and the dilatancy rate at failure for some of the tests carried out in this experimental programme. A single curve averages all the test results and it is seen how variation of the porosity is excluded from the relationship. In general the departure from the mean curve is about 1.2° only. It can be seen that with increasing cell pressure the test results group around the zero rate of volume change axis, but with progressively lower values of ϕ'. This indicates that the parameter ϕ'_{cv} is substantially more pressure-dependent in this type of rockfill material. The approximate ϕ'_{cv} value in this case is 40.2°.

Tests on Ham River sand by Green and Skinner reported by Bishop, (1966) showed that the relationship between ϕ' and $(d\epsilon_v/d\epsilon_1)$ at failure could be represented by a single straight line for a range of 40 - 4000 psi cell pressure. It was found for Ham River sand that the maximum departure from the mean line is only $1\frac{1}{2}^{\circ}$. The curvature of the failure envelope is thus apparently largely accounted for by the decrease in the rate of dilatancy with increasing stress; the decrease in dilatancy rate is also a function of particle crushing. Tests on Silurian mudstone by Tombs reported by Bishop,(1971) showed a similar trend in the results but with more scattering and that is probably due to the particle crushing. Also a similar trend in the relationship is obtained from tests by Marachi et al, (1969) on Pyramid Dam material and crushed napa basalt. Results of tests on different types of rockfill materials reported by many investigators (e.g. Marsal, 1965 & 1967; Billam, 1967;

---

* Dense samples are more dilatant than loose ones.

Hall and Gordon, 1963; Tombs, 1969; Marachi et al, 1969, etc.) are shown in Figure (6-17). It appears that particle crushing plays a major part in the behaviour of rockfill material during deformation.

6.4 The stress-strain behaviour of the samples under drained cyclic loading

6.4.1 Introduction

A series of five tests has been carried out in this field to study the influence of repeated loading on the behaviour of rockfill material. All the tests will be described separately in the following sections. A conventional drained test (test No. 28)* taken to failure in a single loading cycle will be taken as a reference for comparison purposes and will be called "the reference test". The confining pressure applied in the reference test was 80 psi and the maximum stress difference reached during the test was 364 psi. Samples of the cyclic loading testing were prepared at the same porosity of the reference test sample and consolidated under the same confining pressure of 80 psi. They were subjected to repeated cyclic loading to a maximum stress difference of 82.5 - 86% of the maximum value of 364 psi obtained in the reference test†. A summary of the test results is shown in Table (6-6). In fact this series of tests led to a wider study of the stress-deformation characteristics of rockfill which will be presented in Chapter 7. Particle breakage resulting from repeated loading will be discussed in Section 6.6, but unfortunately these tests are insufficient to provide a wide knowledge of this subject.

6.4.2 The stress-strain behaviour of the sample subjected to 'two' loading cycles

In this test (No. 29) a sample of 25.9% initial porosity, consolidated under an effective all-round pressure of 80 psi, was subjected to two repeated loading cycles to a maximum stress difference of approximately 300 psi. This stress difference is 82.5% of that obtained from

---

* The stress-strain curves of this test are shown in Figure (6-3).

† The exact $(\sigma'_1 - \sigma'_3)$ applied for each test will be mentioned later.

the reference test. The stress-strain and volumetric strain curves are shown in Figure (6-18). On first loading, the point 'a' indicates the axial and volumetric strains reached at the peak stress while the end of the first loading cycle is indicated by the point 'b'. It can be seen from the figure that a considerable amount of irrecoverable axial and volumetric strain remained after the first cycle of loading. Also on unloading from 'a' to 'b' an additional volume decrease had taken place although the sample was unloaded. During the subsequent loading cycle 'bcd' further residual axial deformation was found while the volume was almost constant. Then finally the sample was loaded to failure which was achieved at a maximum stress difference of 367 psi and axial strain of 7.23%. Directly on loading the volume of the sample started to increase and at failure it was dilating at a rate of approximately 0.375. Comparing this test with the reference one (test No. 28) it can be seen that the shear strength, rate of dilatancy at failure and axial strain at failure of both samples are similar. The volumetric strain at failure for the cyclic loading test was 0.24% less than that of the reference test and that is probably due to difference in porosities and membrane penetration. In general the failure behaviour of both the cyclic loading sample and the reference sample was similar.

6.4.3 The stress-strain behaviour of the samples subjected to 'ten' loading cycles

A sample of 25.3% initial porosity consolidated under an effective all-round pressure of 80 psi was subjected to ten repeated loading cycles to a maximum stress difference of 315 psi, (test No. 30). This stress difference is 86.5% of that obtained from the reference test. The stress-strain curves are shown in Figure (6-19). On the first and second loading cycles the sample behaviour was similar to that described in the previous section for test No. 29. Also on the first unloading cycle the volume of the sample increased and on subsequent reloading and unloading, the volume stayed almost constant.

On the third, fourth and fifth loading cycles the volume used to decrease and then increase insiginficantly and the final values of the volumetric strain after loading and unloading were almost the same. There was an increase in the residual axial strain, but in a decreasing rate as the cycles were repeated.

The sixth and seventh cycles were partially unloaded to 160 psi stress difference then reloaded to the previous maximum value of 315 psi. It was noticed that during loading and partial unloading the increase in the residual strain was very small compared to the previous cycles and the portion of the stress-strain curve on loading was almost the same for that on unloading. In general the behaviour of the sample was almost linearly elastic during these two loading cycles.

Then on the subsequent eighth and ninth loading cycles, the amount of the residual axial and volumetric strains increased slightly compared to that during the first few loading and unloading cycles. The stress-strain curve for loading and unloading was almost the same, but not linear. At the tenth loading cycle the sample was taken to failure which was achieved at maximum stress difference of 375 psi and axial strain of 6.5%. During loading to failure the volume change of the sample was similar to that described in the previous section, except here the volumetric strain and rate of dilatancy at failure were zero and +0.423 respectively. There is no evidence from the behaviour of the sample that it was going to fail after a few more repeated loading cycles.

Comparing this test with the reference one (test No. 28), it can be noticed that:

1. The shear strength of thesample after ten loading cycles was approximately 3% more than that of the single loading test.

2. The sample subjected to ten loading cycles failed at an axial strain less than that of the reference sample and the sample subjected to two loading cycles*.

---

*The values of the axial strain at failure are shown in Table (6-6).

3. The volumetric strain at failure of the sample subjected to ten loading cycles was less than that of the reference sample and the sample under two loading cycles.

4. The rate of dilatancy at failure of the sample subjected to ten loading cycles was more than that of the reference sample and the sample under two loading cycles.

The increase in the shear strength, decrease in the axial strain at failure, decrease in volume and the increase in the rate of dilatancy at failure may be attributed to the increase in the density of the sample after so many repeated loading and unloading cycles.

This test (No. 30) was repeated on another sample of 25% initial porosity and the same testing conditions (test No. 32). The only difference here is that the sample was loaded up to 338 psi stress difference which is approximately 92.5% of the failure stress difference of the reference test. The stress-strain curves are shown in Figure (6-19b). It can be seen that the behaviour of this sample is similar to that described previously for test No. 30 except in the following points:

1. The shear strength of the sample in test No. 32 is approximately 14.8% more than that of the reference sample.

2. The axial strain at failure is less than that in test No. 30.

3. In test No. 32 the volume of the sample decreased on loading and unloading cycles more than that of the sample in test No. 30.

4. Here the rate of dilatancy at failure was higher than that of the sample in test No. 30.

These variations may be attributed to the difference in the amount of the applied maximum stress difference in both tests and the variation in the porosities. In general the behaviour of the samples during the two tests was similar.

6.4.4 The stress-strain behaviour of the samples subjected to '139' and '150' loading cycles

A sample of 26.0% initial porosity (test No.35) was set up in order to study the behaviour of rockfill material under a large number of repeated loading and unloading cycles as described in the previous two sections. But unfortunately the rubber membrane burst at the end of the 139th loading cycle. The stress-strain and volumetric strain curves are shown in Figure (6-20). The general behaviour of the sample at the beginning was similar to that of test No.30. This test (No.35) will not be discussed in detail here because it has been repeated.

Another sample of 27.3% initial porosity (test No. 36) was set up under the same conditions used for the tests in this series. A maximum stress difference of 338 psi was applied and the repeated loading and unloading continued to 150 cycles then it was sheared in the usual drained procedure. The stress-strain and the volumetric strain curves are shown in Figure (6-21). The discussion will be concentrated on this test (No. 36) while test No. 35 will be referred to in the appropriate place.

On loading and unloading during the first two cycles, the sample behaviour was similar to that of test No. 29 described in Section 6.4.2. On the first unloading cycle the volume of the sample decreased and on the second loading cycle the volume was approximately constant. There was a considerable residual irrecoverable axial and volumetric strain. These first two cycles are denoted by 'abc' and 'cde' in Figure (6-21). As loading and unloading were repeated again and again, there was still increase in the residual axial strains, but at a decreasing rate. During the first ten cycles after the first unloading, the amount of the residual irrecoverable strain was approximately 0.95%, while that from 50th - 60th cycle was only 0.10%. Then approximately after the 100th cycle or so the stress-strain curves formed nearly closed hysteresis loops with no significant additional axial or volumetric strains. The sample behaviour was approximately linear elastic. In fact it can be

said that the sample was in a state of non-failure equilibrium because no additional changes in axial and volumetric strains occurred with further cyclic loading.

During cyclic unloading the volume of the sample decreased by a small amount. The value of the volumetric strain decreased from approximately -0.745% at the first unloading cycle to approximately -1.70% at the 150th unloading cycle. But as can be seen from the figure, the volumetric strain was decreasing at a slower rate with further load repetition and at the 140th - 150th cycle no noticeable volume change occurred.

Up to this stage the behaviour of this sample (test No. 36) was approximately similar to that exhibited by the sample of test No. 35 except a small difference in the values of the volumetric strain which are due to the difference in porosities of both samples.

After the 150th loading cycle in test No. 36, the sample was loaded to failure, which was achieved at a maximum stress difference of 477 psi and axial strain of 6.52% based on the original sample dimensions. The shear strength exhibited by this sample was 31% higher than that of the reference sample. This is expected because of the increase of the density of the sample after so many loading and unloading cycles. The rate of dilatancy at failure was much higher than that of the reference sample and the other samples of the cyclic loading tests. Here again the high rate of dilatancy at failure is due to the increase of the density of the sample.

In Figure (6-21) consider a horizontal line passing from point A (at maximum stress difference of 338 psi) through point B and extended to intercept the stress-strain curve at point C. If it is assumed that the sample is going to fail due to continuous deformation then it must achieve it at approximately 10.25% axial strain. Therefore many more loading cycles are needed, but as it is seen around the 140th cycle the stress-strain curve formed almost closed hysteresis loops without additional axial strain. There is no evidence that the sample might fail due to excessive

deformation. Also during load repetition the volume of the sample was decreasing to a constant value, hence there is no evidence that failure might occur due to dilatancy effects. In fact cycling loading caused an increase in density and the strength increased, which meant that failure could only be caused by increasing the stress level above the maximum value used during cycling. It can therefore be concluded that the sample had reached a non-failure equilibrium state. Such a state is a function of the sample and material properties, stress level and testing conditions.

6.4.5. Variation of the axial strain under cyclic loading conditions

As has been pointed out in the previous sections, there was an appreciable amount of irrecoverable axial strain during the first loading cycle*. On the second loading and unloading cycle the amount of the residual axial strain+ was much less than that during the first loading cycle. On subsequent loading and unloading the amount of the residual axial strain increased, but at a decreasing rate, until after the 100th cycle the stress-strain curve formed closed hysteresis loops. This is clearly shown in Figures (6-20) and (6-21).

The final axial strains after loading and unloading as a function of the number of cycles for test No. 36 is plotted in Figure (6-22). From this figure it can be seen how the axial strain increases at a decreasing rate and during the 150th cycle the increase in axial strain is almost insignificant compared to that during the first few cycles. By extrapolating these plots to 1000 cycles or more, the amount of the residual axial strain does not exceed 7.0%. It therefore seems that the failure of the sample by excessive deformation is not evident. Two other interesting points can be noticed from this figure:

1. The axial strain-log no. of cycles relationship is linear after the second or third cycle. During the first and second cycles the amount of the irrecoverable strains is very large compared to the subsequent loading cycles. In fact this is very similar

---

* This axial strain ranges from 3.0% - 3.7% for all the tests.

+ In the second cycle the residual axial strain was approximately 0.25%.

to the time dependent behaviour of rockfill under sustained stress where there is a linear relationship between strain and log time; examples of this are shown by Pigeon, (1969).

2. The straight line relationships mentioned above are parallel for loading and unloading cycles.

The axial strain-log no. of cycles relationship for test No. 35 is plotted in Figure (6-23) although the test has not been completed to failure. This relationship is very similar to that described for test No. 36, except at the 29th loading cycle the sample was loaded 25 psi more than the usual maximum stress difference of 325 psi used throughout this test. The deviation seen in the plot was evident up to the 50th cycle, then again a straight line relationship started which is almost parallel to the first portion of the plot. Again the plots for the loading and unloading cycles are almost parallel, which is similar to the previous test No. 36.

6.4.6 Variation of the volumetric strain under cyclic loading conditions

It was pointed out in the previous sections that on the first unloading cycle the volume of the sample used to decrease to a value lower than it was at the end of the first loading cycle. This is in contrast to what was expected that on unloading the volume would increase due to the decrease of the mean effective stress applied on the sample. Tests on Newfield clay under undrained conditions by Sangrey et al, (1969) indicated an increase in the pore water pressure during the first unloading cycle. Similar behaviour has been observed for some tests in Chapter 7 which will be discussed later.

After cyclic loading and unloading the volumetric strain had decreased but the changes for each successive cycle became progressively smaller. At the 100th cycle or so the volumetric strain-axial strain curve formed closed hysteresis loops with insignificant incremental volumetric strains. It indicates that the samples are behaving nearly elastically. This is similar to the results of experiments by Johnson, (1955) on the shear displacements occurring during oscillatory experiments on hard

steel surfaces. Near the end of the tests (Nos. 35 and 36) the volume of the samples was almost constant on loading and unloading.* This is clearly shown in Figure (6-22) where the volumetric strains against the log no. of cycles for unloading and loading cycles of test No. 36 were plotted. It appears that the state of the volumetric strains on loading and unloading depends on the material and sample properties, stress level and testing conditions.

6.4.7 Influence of the cyclic loading on the shear strength and strains at failure

As has been mentioned in the previous sections, the samples under cyclic loading showed higher strengths than under single loading. Unfortunately only a few tests were carried out and therefore the conclusions will be limited in this respect.

Figure (6-23a) shows the variation of the shear strength of the cycled samples with respect to the shear strength of the reference sample under different numbers of loading cycles. It can be seen how the shear strength increases with the increase of loading cycles, but it is not clear with the scatter in the results that the sample strength has reached a maximum value†.

The tests after ten loading cycles gave different shear strengths which indicates that perhaps the samples were not identical at the start of the tests or that different degrees of particle breakage occurred during the cycling stage. The effect of the cyclic loading may be less pronounced than the effect of a slight variation in sample porosity, etc. If this were the case then clearly a number of tests should be performed for a particular number of loading cycles so that a reasonable average may be obtained.

---

* At the beginning of tests Nos. 35 and 36 there was a significant difference between the volume of the samples on loading and unloading, Figure (6-22).

† It would seem reasonable that after a large number of cycles no further increase in strength will occur and the curve will tend to level off.

The axial and volumetric strains at failure decrease significantly with an increasing number of loading cycles, Figure (6-23b). No other definite trend can be seen and the curves fitted to the test data can only at this stage be considered tentative. Therefore more tests need to be done in this field.

6.5 The Stress-Strain Behaviour of the Samples Sheared Under Undrained Conditions

6.5.1 The Shear Strength of the Samples

A series of six consolidated undrained triaxial tests was carried out on $1\frac{1}{2}$ in. dia. samples of granite rockfill. A summary of the test results is shown in Table (6-7). Test 1U gave a relatively low value for the angle of shearing resistance (39.75°) compared to the values obtained from the drained tests carried out under similar stress conditions (T. 17; 49.8°) Thus this test will be ignored during the discussion, as being suspect.

The stress-strain curves for the dense samples (2U, 3U and 4U) are shown in Figure (6-24). The value of ϕ' at peak $(\sigma_1 - \sigma_3)$ obtained from T. 2U (σ'_c = 80 psi)* is 1.9° higher than that obtained from T. 3U (σ'_c = 300 psi). This indicates that ϕ' at peak $(\sigma_1 - \sigma_3)$ decreases as the effective consolidation pressure increases. A similar trend in behaviour can be observed for the loose samples (T. 5U and 6U). The value of ϕ' at peak $(\sigma_1 - \sigma_3)$ obtained from the dense sample 2U is close to the ϕ'f corresponding to zero rate of dilatancy for drained samples (40.2°) while Tests 3U and 4U exhibited lower values.

For test 2U (σ'_3 = 80 psi), at the start of the shearing stage, there was a small build-up of pore water pressure and a large deviator stress was quickly built up. With the continuation of shearing, the pore water pressure started to decrease and at peak $(\sigma_1 - \sigma_3)$ there was a negative pore water pressure. Samples 3U and 4U consolidated at effective cell pressure of 300 psi exhibited different pore water pressure

---

* σ'_c denotes the effective consolidation pressure.

build up during shearing. There was a high pore water pressure built up at the commencement of the shearing stage and at peak $(\sigma_1 - \sigma_3)$ the pore water pressure was nearly constant at about 180 psi. In test 4U (σ'_c = 300 psi) the pore pressure parameter A at peak $(\sigma_1 - \sigma_3)$ is 0.28 which is the highest value obtained from this series of undrained tests. Bishop et al, (1965) reported an A value at peak $(\sigma_1 - \sigma_3)$ of 1.13 for Ham River sand consolidated to an effective cell pressure of 990 psi.

The stress paths for all the dense samples are shown in Figure (6-26). These stress paths showed no tendancy to turn back on themselves, and the samples failed at high effective stresses, thus giving a considerable shear strength. In fact the stress paths of tests 2U and 3U turned down after failure. Sample 4U was looser than samples 2U and 3U and thus its stress path has a different shape at the pre-failure stage. However the sample's behaviour and the stress paths obtained are in agreement with the results reported by Tombs (1969) and Bros (1969) on the same type of material but different sample diameters.

The stress-strain curves for the loose samples are shown in Figure (6-25). Again here the value of ϕ' at peak $(\sigma_1 - \sigma_3)$ decreases as the effective consolidation pressure increases. Also the values of ϕ' at peak $(\sigma_1 - \sigma_3)$ are lower than those obtained from the corresponding dense samples. However, the difference is not large as is shown in Table (6-7).

In the case of sample 5U (σ'_c = 20 psi) the value of ϕ' at peak $(\sigma_1 - \sigma_3)$ is very close to the ϕ'f corresponding to zero rate of dilatancy for drained samples. There was a very small pore water pressure built up at the beginning of the shearing stage, but with continuing shearing the pore water pressure decreased and at peak $(\sigma_1 - \sigma_3)$ the sample exhibited a negative pore water pressure. In the case of sample 6U (σ'_c = 80 psi) there was a large pore water pressure developed at the beginning of the shearing stage, then it continued at a positive

magnitude until the end of the test. Although a high value of ϕ' at peak $(\sigma_1 - \sigma_3)$ was mobilised, the effective stresses and hence the shear strength were only about 42% of that of the dense sample 2U consolidated to the same effective cell pressure. The value of ϕ' at peak $(\sigma_1 - \sigma_3)$ achieved is 1.3^{o} lower than $\phi'f$ corresponding to zero rate of dilatancy for drained samples.

The stress paths for both tests 5U and 6U are shown in Figure (6-26). It is seen in this figure that the stress paths for loose samples have different shape from those for the dense samples. But still none of the stress paths turned back after failure. These results are in agreement with those reported by Tombs (1969) and Bros (1969). However, the stress paths for most of the samples (dense and loose) lie closely to a line which corresponds to $\phi'f$ of 43.8^{o}, Figure (6-26).

6.5.2 Deformation of the Samples

The dense sample 2U consolidated at an effective cell pressure of 80 psi achieved peak $(\sigma_1 - \sigma_3)$ at an axial strain much lower than that of the loose sample 6U consolidated at the same effective cell pressure. A similar trend in behaviour has been observed for samples sheared under drained conditions.

The influence of the effective consolidation pressure on the axial strain at peak $(\sigma_1 - \sigma_3)$ is shown in Figures (6-24) and (6-25). The axial strain at peak $(\sigma_1 - \sigma_3)$ increases with the increase of the effective consolidation pressure for both the loose and dense samples. Tombs (1969) reported the same behaviour for his 12 in. dia. samples of granite while Bros (1969) observed different behaviour. Bros tested 4 in. dia. samples; the first consolidated to 75 psi and the second to 25 psi. The samples reached their peak stress ratios at about the same axial strain though the effective stresses were twice as high in the first sample. A close comparison between the results obtained from the present series of tests and those obtained by Tombs (1969) and Bros (1969) cannot be made due to variations in the testing conditions.

6.6 Particle breakage in granite rockfill

Properties of the material tested and the strength of particles were discussed in Chapter 5. Some of the samples were sieved after testing to assess the degree of particle breakage and its influence on the stress-strain characteristics of granite rockfill. To describe quantitatively the amount of particle breakage associated with each test the method suggested by Marsal, (1965d) was adopted. The values of the particle breakage factor (B) for most of the tests are shown in the tables. The process of particle breakage during various types of loading will be discussed in the coming sections.

6.6.1 Particle breakage during compaction

Tamping was used as a procedure to achieve the required density; it was the best method available at Imperial College Soils Laboratory. To achieve high density samples, repetitive tamping was necessary, which results in significant particle breakage. Gradation curves for two samples compacted dry and wet are shown in Figure (6-27). Porosities of the samples were 30.5 - 31.0% which correspond to medium density samples described previously and the B-factor is about 2.1% for both samples. It is clear from this figure that compaction whether wet or dry causes particle breakage, but it is not very significant in the case of granite material. The marble chippings (as shown in the same figure) undergo more particle breakage. This is obvious because marble chippings are much weaker than the granite particles. Comparison of particle breakage for both materials under different loading paths will be discussed in the next chapter. Four main points could be drawn from the gradation curves in Figure (6-27):

1. There is no significant difference between dry and wet compaction during sample preparation.
2. Weak particles undergo breakage more than strong ones during compaction.
3. To achieve high density samples more compaction is required which results in more particle breakage.

4. Coarse particles undergo crushing more than fine ones.

6.6.2 Particle breakage during isotropic consolidation

Loose and dense granite rockfill samples consolidated at 600 and 850 psi effective cell pressures were sieved after isotropic consolidation. The B-factor values for these tests are shown in Table (6-8) and the grading curves for the loose and dense samples consolidated at σ'_3 of 850 psi are plotted in Figure (6-28). It appears that particle breakage is relatively small* during isotropic consolidation, although the confining pressure is high. Similar results presented by Marachi et al, (1969) on different types of rockfill material show that particle breakage during isotropic consolidation is small compared to that during shearing. Bishop, (1966) reported results of tests on Ham River sand and pointed out that at high stresses the particle breakage during the shear stage is much more than that during the consolidation stage. Data presented by Marachi et al (1969); Tombs, (1969) and others confirmed Bishop's finding but did not separate the particle breakage due to compaction from that due to application of the consolidation pressures. From the results presented in this section and the previous one, it appears that the particle breakage resulting from compaction is as much as or more than that resulting from application of the confining pressure. Of course particle breakage resulting from consolidation at low confining pressure is almost insignificant. From Table (6-8) it appears that loose samples undergo particle breakage less than dense samples. But it is not clear whether this is due to the compaction or due to the process of consolidation.

6.6.3 Particle breakage during drained shearing to failure

The original and the final gradings for all the dense, loose and very loose samples are shown in Figure (6-29). It is obvious from the figure that the particle breakage has increased with the increase of the

---

* The B-factor resulted from consolidation of the dense sample at 850 psi effective cell pressure was 3.8, which is fairly low compared to other drained shear tests.

confining pressure. This is also clear from the B-factor values shown in Tables (6-2)(6-4) and(6-5). For loose samples the B-factor has increased from 3.9% at σ'_3 = 20 psi to 24.5% at σ'_3 of 850 psi, and for dense samples the B-factor increased from 3.1% to 25.4% for the same range in cell pressure increase. It seems that the density has little influence on the amount of particle breakage during the shearing stage. Comparing this figure with Figure (6-28) it appears that the amount of particle breakage during shearing is substantially larger than that during consolidation. This is shown clearly in Figure (6-30) where the grading curves after consolidation and shearing stages for tests at 850 psi confining pressures are plotted.

This behaviour is similar to that observed previously by Vesic and Barksdale, (1963); Bishop, (1966); Vesic and Clough, (1967) and Marachi et al (1969).

By examining the B-factor calculations and the grading curves it will be noted that the loss of grains in the coarse fractions and the gain in the fine fractions are clearly evident. Marachi et al (1969) from tests on various rockfill materials with sample size up to 36 in diameter concluded that the particle breakage factor B increased as the maximum particle size of the samples increased*.

Values of the particle breakage factor (B) for the dense and loose samples are plotted as a function of the confining pressure in Figure (6-31). The figure shows that the amount of particle breakage increases as the confining pressure increases; however the increase is more rapid at low confining pressures than at high confining pressures. At high confining pressure (approximately 700 psi) it seems that the particle breakage of loose and dense samples is approximately the same. This trend in behaviour is in agreement with data presented by Vesic and Clough, (1968); who showed that particle degradation for samples of sand sheared under a confining pressure of 633 kg/cm^2 was only slightly greater than that of the samples sheared under a confining pressure of 211 kg/cm^2.†

---

* A similar trend in results was observed by Tombs (1969).

† A similar trend in results was observed by Marachi et al, (1969) in tests on various rockfill materials.

The values of the angle of shearing resistance (ϕ') for all the dense and loose samples are plotted against the corresponding values of the particle breakage factor (B) in Figure (6-32). It is clear that there is a unique relationship between the angle of shearing resistance ϕ' and the particle breakage factor B. There is a scatter in the results due to the variation of the porosity of the samples, especially for the loose ones. From this figure it can be seen that the angle of shearing resistance decreases as particle breakage increases. This is in agreement with Leslie's (1963) conclusion, stating that the angle of shearing resistance is reduced in proportion to the increase in particle breakdown. A similar conclusion has been arrived at by Marsal, (1967a) who plotted the principal stress ratio (σ'_1/σ'_3) at failure against the particle breakage factor B for all the rockfill samples tested in the Soils Laboratories of the Comision Federal de Electricidad, Mexico. The scatter in the results is due to type and gradation of the materials, density, sample size and testing conditions. Similar findings have been reported by Marachi et al (1969) for various rockfill materials.

Figure (6-33) shows that there is a unique relationship between the particle breakage factor B and the rate of dilatancy at failure. It can be seen that the rate of dilatancy at failure decreases as the particle breakage increases and at zero volume change the particle breakage factor rises considerably. Of course there is a considerable difference between dense and loose samples, but in general the relationship is still the same.

It can therefore be concluded that the behaviour of a rockfill material in shear may be described by the parameters ϕ', rate of dilatancy at failure and particle breakage factor B for first loading. These parameters appear to be directly interrelated, and for any material the choice of such other variables as density, particle size and stress level only define their value.

6.6.4 Particle breakage during drained cyclic loading

Samples sheared under cyclic loading were sieved and the particle breakage factor values are presented in Table (6-6). The B-factor values of the conventional drained tests are approximately equal to those of 2 - 10 cycles under the same porosity and stress level. It seems that few cycles (less than ten cycles) do not cause excessive particle breakage compared to the one cycle loading tests provided they are under the same testing conditions. The grading curves after shearing for 10 and 150 cyclic loading tests are plotted in Figure (6-34). As the number of loading cycles increases, the particle breakage increases. This is also clear from the values of the particle breakage factor reported in Table (6-6). The angle of shearing resistance ϕ' for the 150 cycle test is 4.4^{o} more than the two cycle test, although the particle breakage factor for the first is more than the second. This is explained as being due to the increase in density of the sample after repeated loading. Therefore the expected decrease in ϕ' value due to increase in particle breakage was countered by the increase in density of the sample after cyclic loading, which resulted in an increase in the angle of shearing resistance. Hence the relationship shown in Figure (6-32) is not applicable here.

6.6.5 Particle breakage during anisotropic consolidation and shearing

As will be discussed in the next chapter a series of samples consolidated anisotropically under different principal stress ratios then sheared drained as part of a programme to study the stress-strain characteristics of rockfill material was tested. Some of the samples were sieved after testing and the grading curves are plotted in Figure (6-35). A summary of B-factor calculations is shown in Table (6-9). It can be seen from this figure that samples consolidated at σ'_1/σ'_3 of 2.04 underwent particle breakage more than those consolidated at lower stress ratios. But when the stress ratio (σ'_1/σ'_3) was increased to 3.0 the particle breakage was smaller than that when σ'_1/σ'_3 was at 2.04. This is clear from the grading curves and B-factor values shown in the

table. El-Sohby, (1969) presented results of constant stress ratio tests on dense and loose sand. Data showed that the compressibility of loose sand increases as the stress (σ'_1/σ'_3) increases from 1.0 to 2.0. When the stress ratio increased to more than 2.0 the compressibility decreased. The explanation is that loosely packed samples tend to collapse when the shear stresses are increased at low stress ratios, while at higher stress ratios dilatancy occurs and consequently the compressibility decreases. On the other hand, the compressibility of dense samples decreased as the stress ratio was increased from 1.0 to 4.5.

Comparing the grading curves in Figure (6-35) with those of conventional drained samples, it can be seen that the amount of particle breakage caused by anisotropic consolidation is substantially different from that caused by isotropic consolidation. Particle breakage caused by loading samples through other stress paths will be discussed in the next chapter.

6.6.6 Particle breakage during undrained shearing to failure

Samples sheared undrained were sieved after testing and the grading curves are plotted in Figure (6-36) while values of B-factor are shown in Table (6-7). Although the undrained shearing of samples is usually associated with zero volume change, a process of particle breakage is expected to take place during the shearing stage. This has been indicated by Bishop et al, (1965); Kumapley, (1969) and others. This is clear in Figure (6-36) where dense and loose samples underwent particle crushing. The main points which can be concluded from this figure are:

1. Particle breakage increases as the effective consolidation pressure increases for both dense and loose samples.
2. Dense samples undergo particle breakage more than loose ones.
3. Loose samples sheared undrained at low confining pressure (as low as σ'_3 = 60 psi) show insignificant particle breakage.
4. Samples consolidated to the same effective pressure show less particle breakage when sheared undrained than when sheared drained.

Table (6-1)

Drained Triaxial Tests on $1\frac{1}{2}$ in. dia. Samples of Very Dense Granite Rockfill

Test No.	14	15*	16	21
Effective Cell Pressure (σ'_3) psi	40	80	80	450
Back Pressure psi	40	40	40	60
n_i%	22.9	20.4	23.0	22.74
Rd	.961	1.05	.957	.968
γ_d (lb/ft^3)	128.1	132.1	127.8	128.3
$\phi'_f{}^o$	48.9	47.8	45.70	39.7
$(\sigma'_1 - \sigma'_3)_f$	244.3	459.1	404.7	1595
$(\sigma'_1 + \sigma'_3)_f$	324.3	619.1	564.7	2495
σ'_{1f}	284.3	539.1	484.7	2045
ϵ_1% @ failure	4.75	4.67	6.4	13.7
ϵ_v% @ failure	+2.19	+.85	+1.22	-4.45
$(d\epsilon_v/d\epsilon_1)_f$	+.772	+.54	+.47	0
Final Strain %	9.5	12.45	11.1	22.6

* More than very dense.

Table (6-2)

Drained Triaxial Tests on $1\frac{1}{2}$ in. dia. Samples of Dense Granite Rockfill

Test No.	13	17	18	19	20	22	27	28	33	58
Effective Cell Pressure (σ'_3) psi	40	20	120	160	300	160	602	80	300	850
Back Pressure psi	40	60	60	60	60	60	60	60	60	60
n_i %	25.7	25.6	25.0	24.8	26.0	25.9	26.0	26.0	25.5	25.8
Rd %	85.6	86.0	88.3	89.0	84.5	84.7	84.5	84.5	86.5	85.2
γ_d(lb/ft^3)	123.3	123.35	124.5	124.84	122.84	123.15	122.85	122.9	123.5	123.2
ϕ_f^o	47.3	49.8	43.1	42.4	38.5	41.8	39.0	44.0	39.8	38.6
$(\sigma'_1 - \sigma'_3)_f$	222.1	132.5	518.0	662.0	988.9	640.9	2048	363.9	1069	2838
$(\sigma'_1 + \sigma'_3)_f$	302.1	172.5	758.0	982.0	1588.9	960.9	3252	523.9	1669	4542
σ'_{1f}	262.1	152.5	638.0	822	1288.9	800.9	2650	443.9	1369	3688
ϵ_1% @ failure	4.66	3.85	7.38	7.27	9.5	7.98	14.70	8.0	11.6	13.2
ϵ_v% @ failure	+2.10	+2.50	-.15	-1.21	-3.82	-1.46	-5.40	+.6	-4.01	-5.52
$(d\epsilon_v/d\epsilon_1)_f$	+.666	+.93	+.222	+.148	0.0	+.162	0	+.35	0	0
Final Strain %	9.32	11.22	15.1	16.15	12.67	19.15	23.1	17.6	17.74	19.8
B-Factor	4.2	3.1		10.9		10.9	22.2	7.3	15.3	25.4

Table (6-3)

Drained Triaxial Tests on $1\frac{1}{2}$ in. dia. Samples of Medium Density Granite Rockfill

Test No.	45	46	47	48	49	61
Effective Cell Pressure (σ'_3) psi	80	40	20	162	300	602
Back Pressure psi	60	60	60	60	60	60
n_i%	30.84	29.4	29.2	29.2	29.6	30.8
Rd %	64.3	70.5	71.4	71.4	69.7	64.3
γ_d(lb/ft^3)	114.8	117.2	117.6	117.5	116.9	114.8
ϕ'_f °	41.8	44.8	47.1	41.0	39.25	38.25
$(\sigma'_1 - \sigma'_3)_f$	316.6	190.4	109.6	616.1	1032	1959
$(\sigma'_1 + \sigma'_3)_f$	476.6	270.4	149.6	940.1	1632	3163
σ'_{1f}	396.6	230.4	129.6	778.1	1332	2561
ϵ_1% @ failure	9.0	7.71	4.53	10.54	12.66	18.95
ϵ_v% @ failure	-1.33	+1.01	+1.71	-2.98	-3.84	-7.78
$(d\epsilon_v/d\epsilon_1)_f$	+.126	+.388	+.625	+.059	0	-.059
Final Strain %	19.28	19.29	16.17	19.46	27.0	24.12

Table (6-4)

Drained Triaxial Tests on $1\frac{1}{2}$ in. dia. Samples of Loose Granite Rockfill

Test No.	37	38	40	42	43	59	60	62
Effective Cell Pressure (σ'_3) psi	20	40	80	302	160	852	600	302
Back Pressure psi	60	60	60	60	60	60	60	60
n_i%	33.1	34.4	34.8	34.3	33.7	35.2	35.0	32.6
Rd %	53.5	47.3	45.2	47.7	50.8	43.2	44.3	55.9
γ_d(pcf)	111.2	108.9	108.3	109.1	110.1	107.4	107.9	111.75
$\phi'_f{}^o$	43.5	41.5	40.0	38.2	39.6	37.2	37.5	38.8
$(\sigma'_1 - \sigma'_3)_f$	88.6	156.7	288.6	979.2	562.1	2602	1864	1014
$(\sigma'_1 + \sigma'_3)_f$	128.6	236.7	448.6	1583.2	882.1	4306	3064	1614
σ'_{1f}	108.6	196.7	368.6	1281.2	722.1	3454	2464	1314
ϵ_1% @ failure	5.90	10.50	12.39	17.88	14.7	21.58	22.0	20.0
ϵ_v% @ failure	+1.32	-.13	-2.1	-8.55	-5.56	-9.8	-9.32	-7.54
$(d\epsilon_v/d\epsilon_1)_f$	+.43	+.147	0	-.095	-.063	-.088	-.08	-.070
Final Strain %	16.34	16.15	22.83	29.26	29.4	25.18	28.85	27.32
B-Factor	3.9	6.0	5.2		13.1	24.5	23.2	17.0

Table (6-5)

Drained Triaxial Tests on $1\frac{1}{2}$ in. dia. Samples of Very Loose Granite Rockfill

Test No.	50	51	63	64	65
Effective Cell Pressure (σ'_3) psi	20	40	300	160	80
Back Pressure psi	60	60	60	60	60
n_i%	40.7	41.7	40.0	40.5	40.0
Rd %	12.5	6.2	16.6	13.5	16.6
γ_d(pcf)	98.5	96.8	99.7	98.8	100.08
$\phi'_f{}^o$	38.0	37.7	35.6	35.6	37.8
$(\sigma'_1 - \sigma'_3)_f$	64	125.6	837.4	445.2	253.0
$(\sigma'_1 + \sigma'_3)_f$	104	205.6	1437.4	765.2	413
σ'_{1f}	84	165.6	1137.4	605.2	333
ϵ_1% @ failure	11.67	13.39	22.56	17.14	15.6
ϵ_v% @ failure	-.618	-2.89	-9.88	-7.15	-5.19
$(d\epsilon_v/d\epsilon_1)_f$	+.072	-.040	-.12	-.075	-.07
Final Strain %	20.0	20.08	26.5	21.65	24.3
B-Factor	2.8	2.8	17.9	10.25	

Table (6-6)

Drained Triaxial Cyclic Loading Tests on $1\frac{1}{2}$ in. dia. Samples of Granite Rockfill

Test No.	28	29	30*	32*	35	36
Effective Cell Pressure (σ'_3) psi	80	80	80	90	90	80
Back Pressure psi	60	60	60	60	60	60
n_i%	26.0	25.9	25.3	25.0	26.0	27.3
Rd %	84.5	84.7	87.1	88.3	84.5	79.1
γ_d(pcf)	122.9	123.0	124.0	124.5	122.8	120.7
ϕ'_d	44.0	44.1	44.5	46.3		48.5
$(\sigma'_1 - \sigma'_3)_f$	363.9	366.7	374.8	417.8		476.9
$(\sigma'_1 + \sigma'_3)_f$	523.9	526.7	534.8	577.8	Sample failed (burst)	636.9
σ'_{1f}	443.9	446.7	454.8	497.8		556.9
ϵ_1% @ failure	8.0	7.23	6.5	5.14		6.52
ϵ_v% @ failure	+.6	+.36	0	-1.93		-1.33
$(d\epsilon_v/d\epsilon_1)_f$	+.35	+.375	+.423	+.74		+1.10
Final Strain	17.6	17.68	16.0	19.3		23.6
No. of Cycles	1	2	10*	10*	139	150
B-Factor	7.3	6.8	7.6	7.2		10.5

* Eight complete loading-unloading cycles and two partial ones.

Table (6-7): Consolidated-Undrained Triaxial Tests on $1\frac{1}{2}$ in. dia. Samples of Granite Rockfill

Test No.	2U	3U	4U	5U	6U
Effective Concolidation Pressure $\acute{\sigma}_c$ psi	80	300	300	20	80
Back Pressure psi	100	50	40	60	60
n_i %	23.1	22.3	24.5	36.3	32.9
Rd %	95.5	98.3	90.1	37.4	54.6
γ_d (lb/ft^3)	127.68	128.97	125.27	105.72	111.4
ϕ' at peak ($\sigma_1 - \sigma_3$)	40.3°	38.4°	38.5°	40.1°	38.9°
peak ($\sigma_1 - \sigma_3$)	364.0	614.5	516.0	107.2	152.0
$\acute{\sigma}_1$ at peak ($\sigma_1 - \sigma_3$)	463.5	801.5	672.0	136.8	197.0
ϵ_1% at peak ($\acute{\sigma}_1 - \acute{\sigma}_3$)	10.8	15.5	13.0	11.0	19.0
u at peak ($\sigma_1 - \sigma_3$)	-19.5	+113	+144	-9.6	+35.0
Final Strain%	23.6	24.3	15.5	18.0	21.8
B-factor	7.3		11.2	4.8	6.1

Table (6-8)

B-Factors for Granite Samples Under Isotropic Consolidation

State of Density	n_i	σ'_3	B-Factor
Loose	34.0	600	2.20
Dense	26.0	600	2.65
Loose	35.0	850	2.79
Dense	26.0	850	3.8

Table (6-9)

B-Factor Values for Granite Rockfill Samples Consolidated Anisotropically then Sheared Drained

State of Density	n_i%	σ'_3 psi	σ'_1 / σ'_3	B-Factor
Dense	26.2	610	1.42	8.35
Dense	25.7	610	2.04	19.04
Dense	26.0	600	3.0	14.93
Loose	33.2	600	1.42	9.53
Loose	33.0	600	2.04	17.84
Loose	33.4	600	3.0	15.70
Very loose	39.0	600	1.42	9.6
Very loose	40.2	600	2.04	19.24
Very loose	38.0	600	3.0	12.97

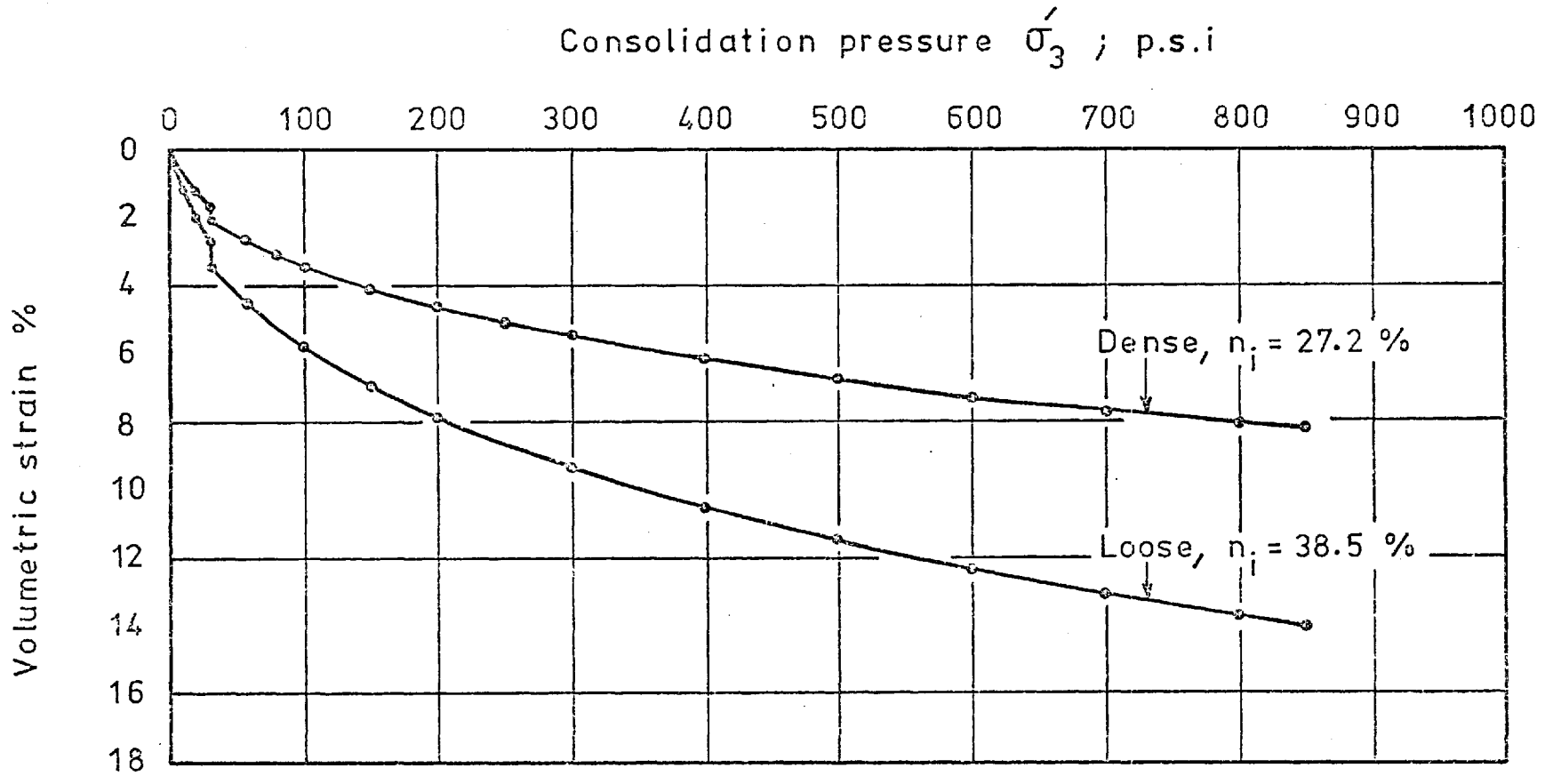

ISOTROPIC CONSOLIDATION OF GRANITE ROCKFILL

FIG 6-1

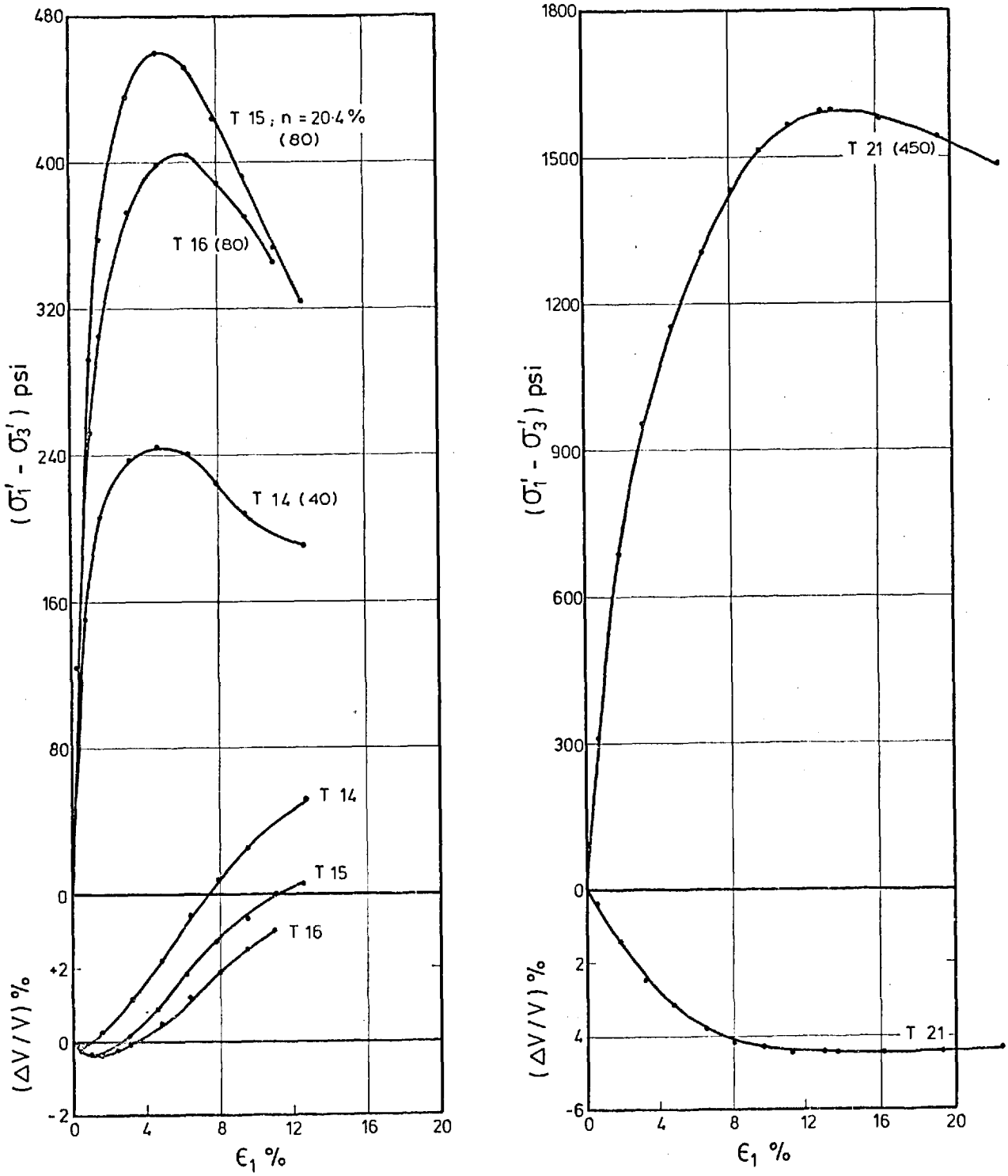

GRANITE ROCKFILL - VERY DENSE (n ≈ 23 %)

Fig. (6-2)

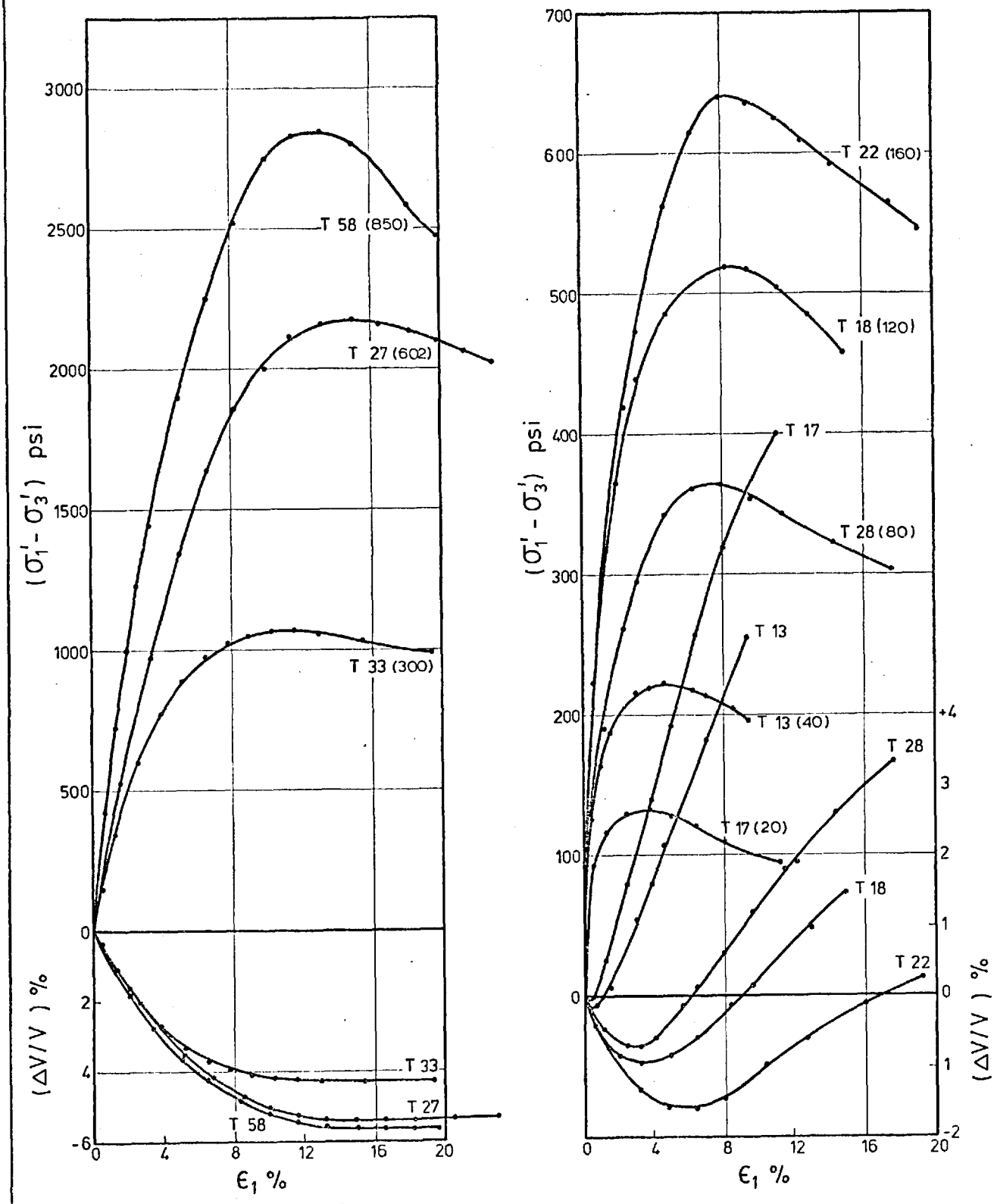

GRANITE ROCKFILL - DENSE ($n \approx 25{\cdot}6\%$)

Fig. (6-3)

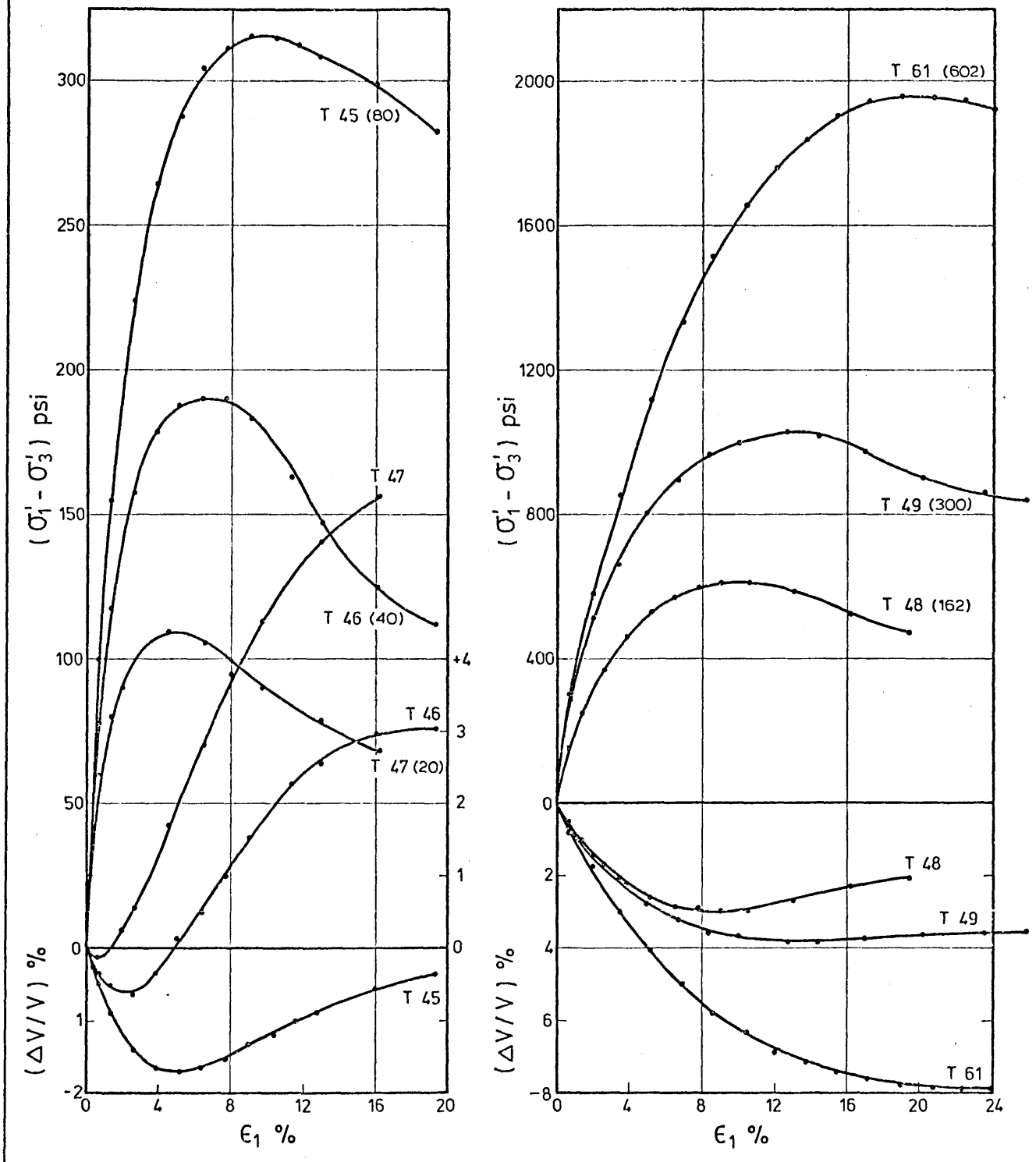

GRANITE ROCKFILL - MEDIUM DENSE ($n \approx 30\%$)

Fig. (6-4)

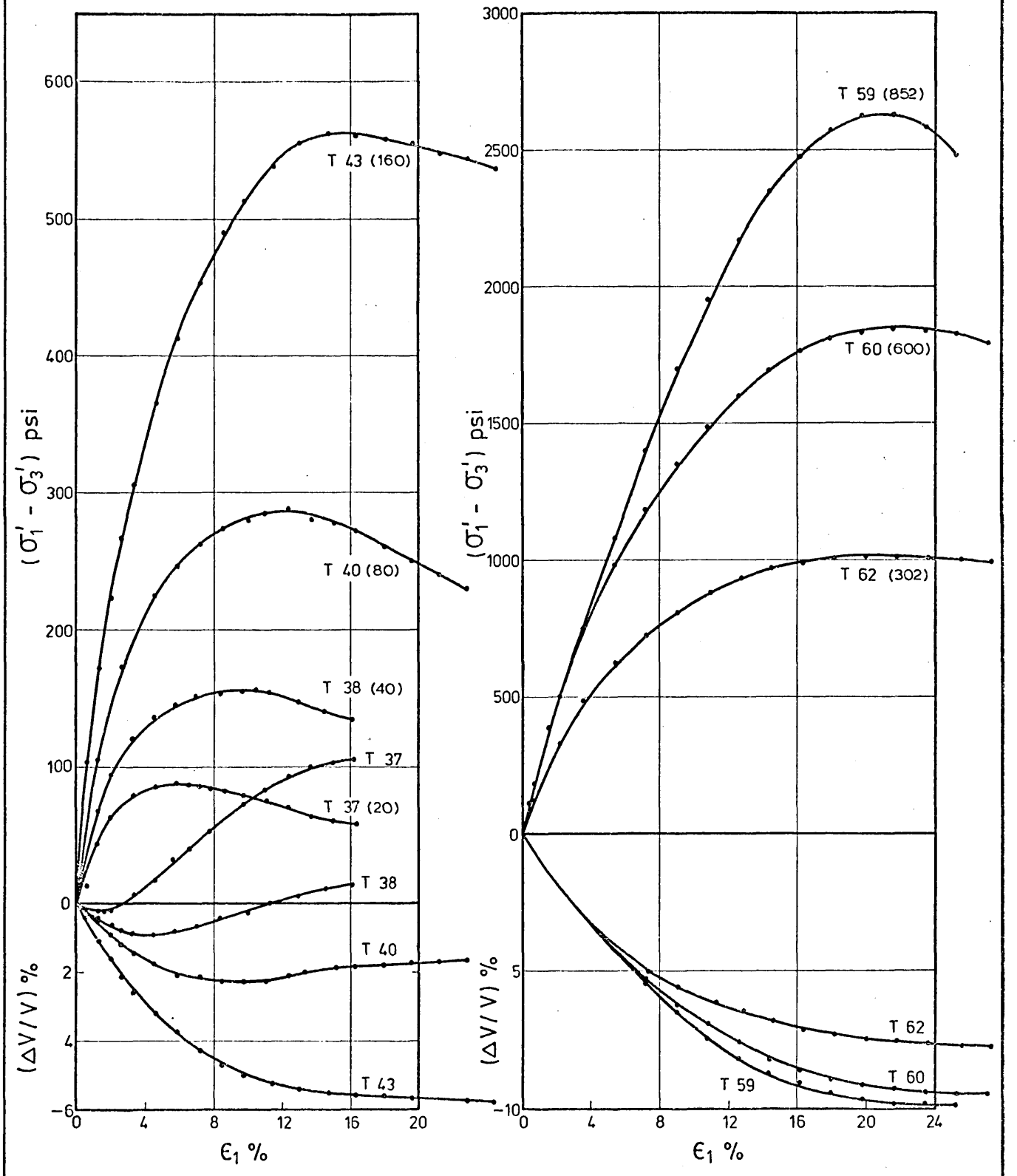

GRANITE ROCKFILL - LOOSE ($n \approx 34{\cdot}2\%$)

Fig.(6-5)

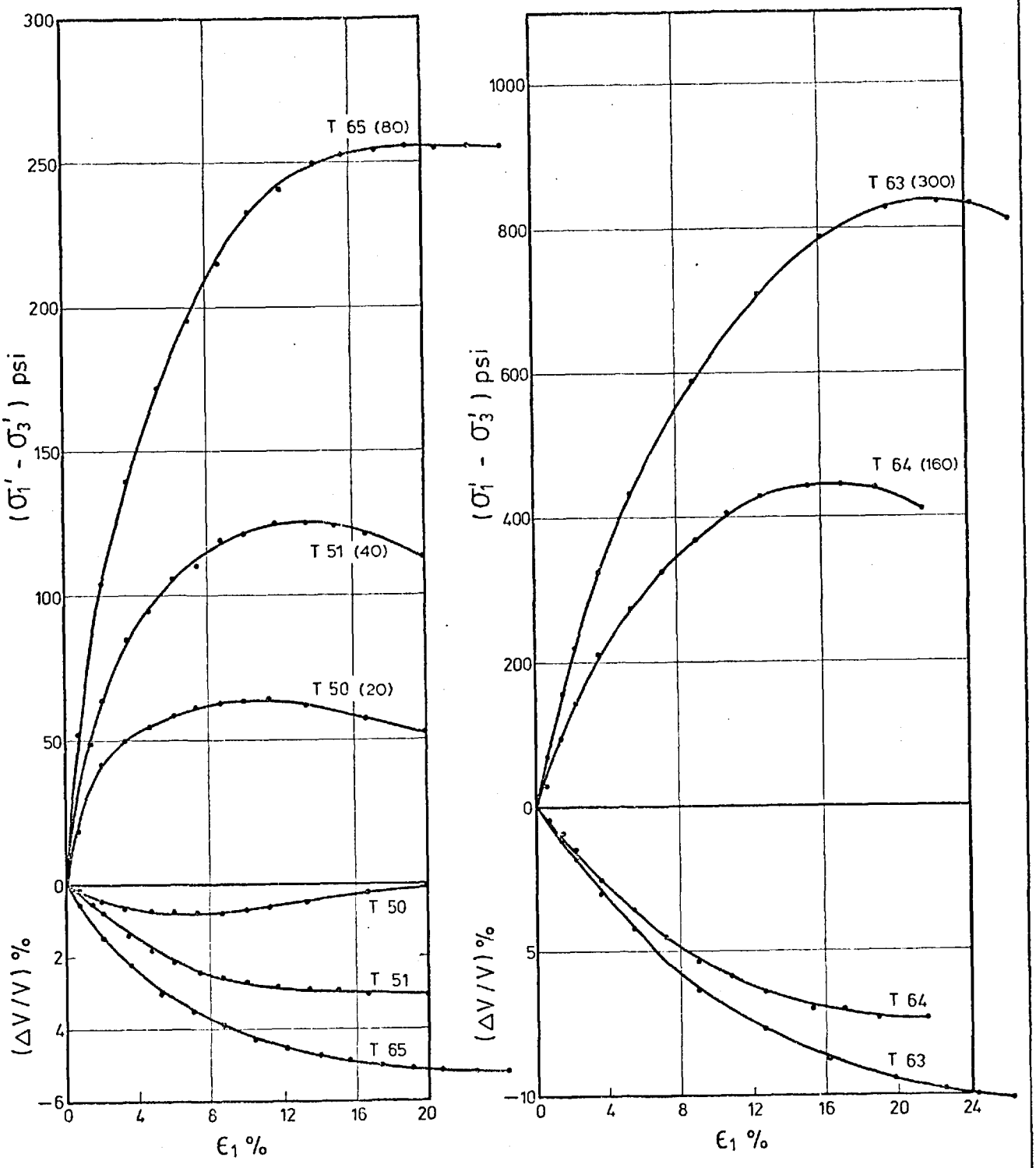

GRANITE ROCKFILL - VERY LOOSE (n ≈ 40·7%)

Fig.(6-6)

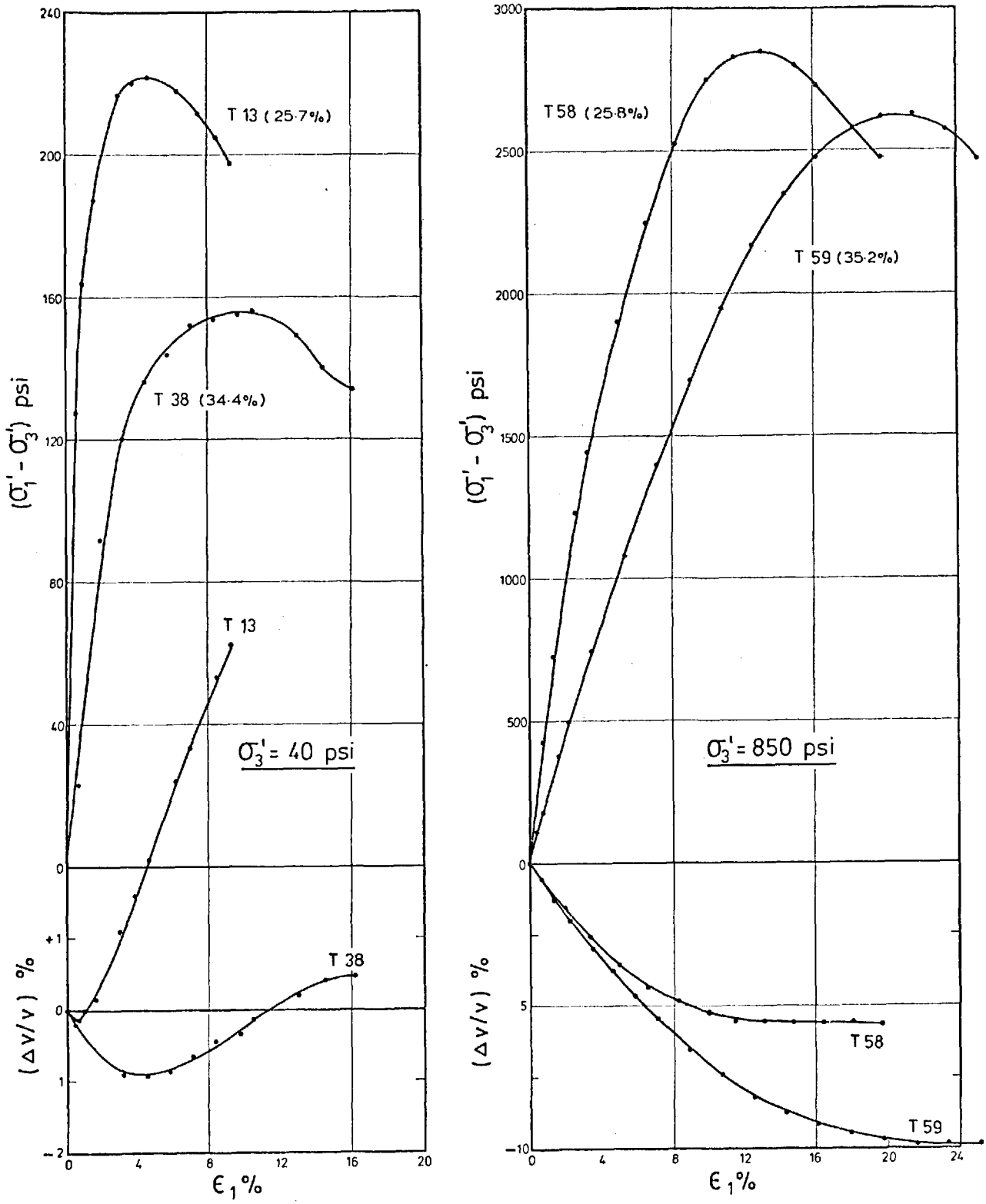

Granite Rockfill Samples Sheared at σ_3' = 40 & 850 psi

Fig.(6-7)

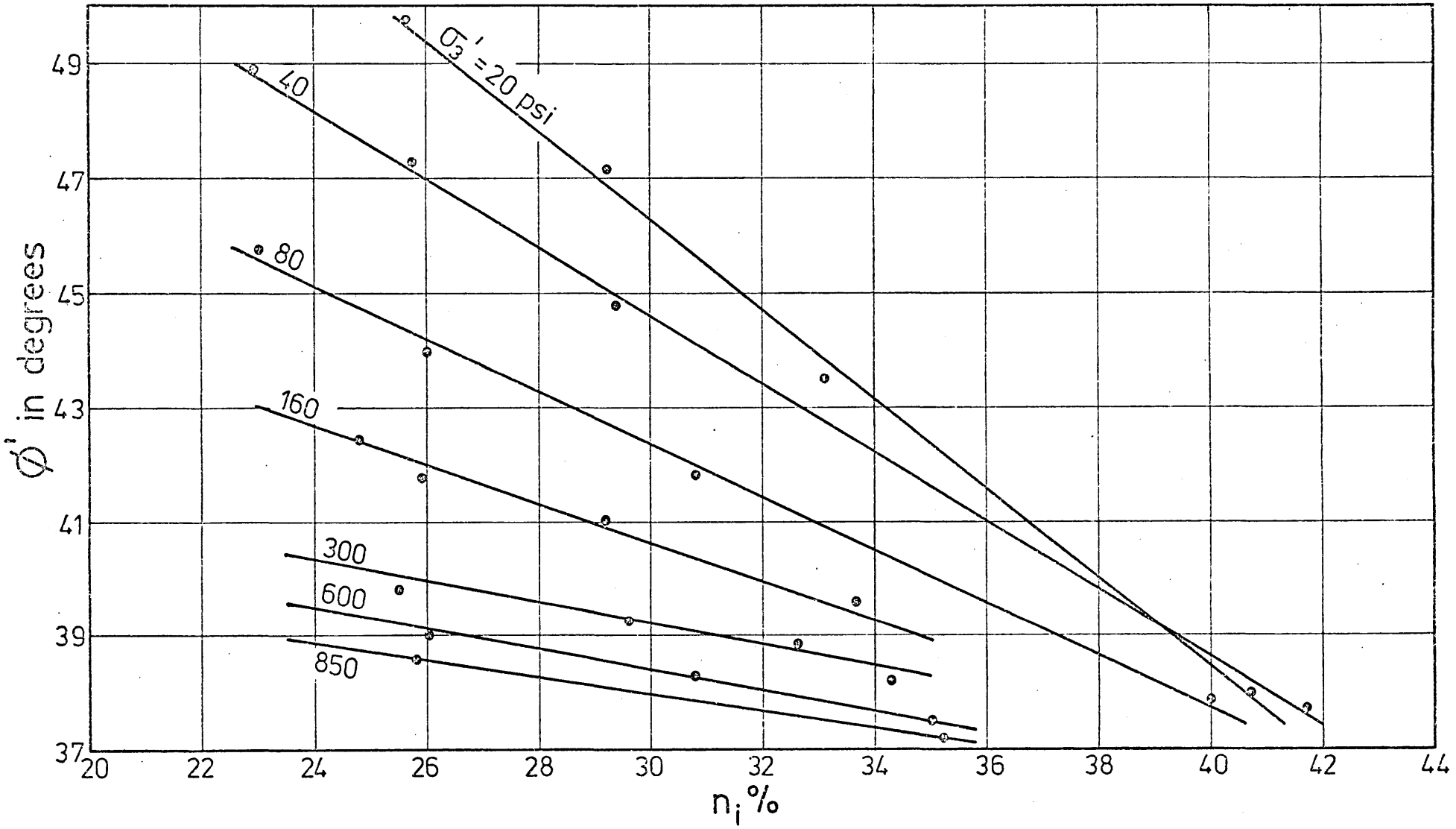

GRANITE ROCKFILL - VARIATION OF Ø' WITH INITIAL POROSITY IN DRAINED TESTS.

Fig. 6-8

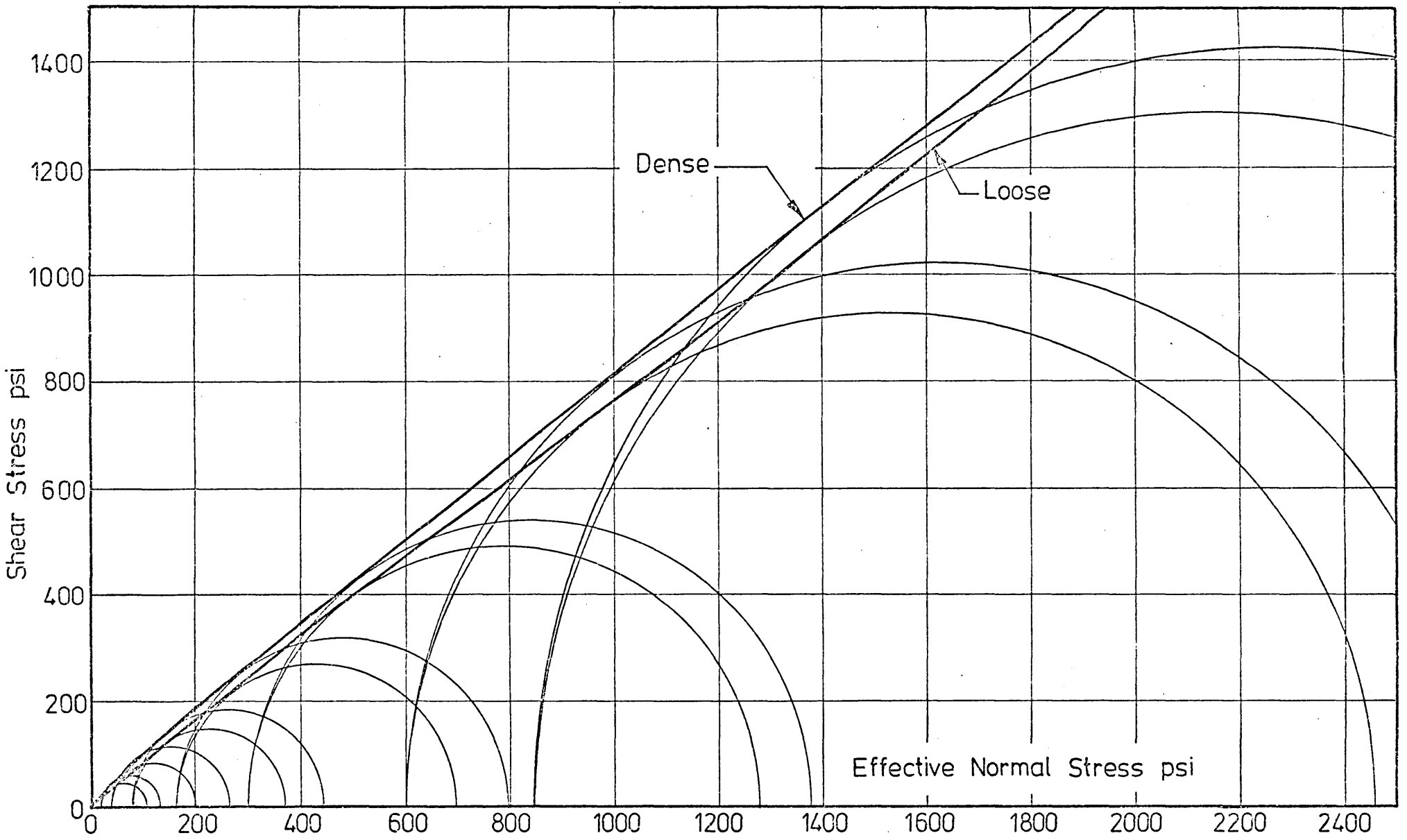

GRANITE ROCKFILL-MOHR ENVELOPES FOR DRAINED TESTS ON LOOSE AND DENSE SAMPLES.

Fig. 6-9

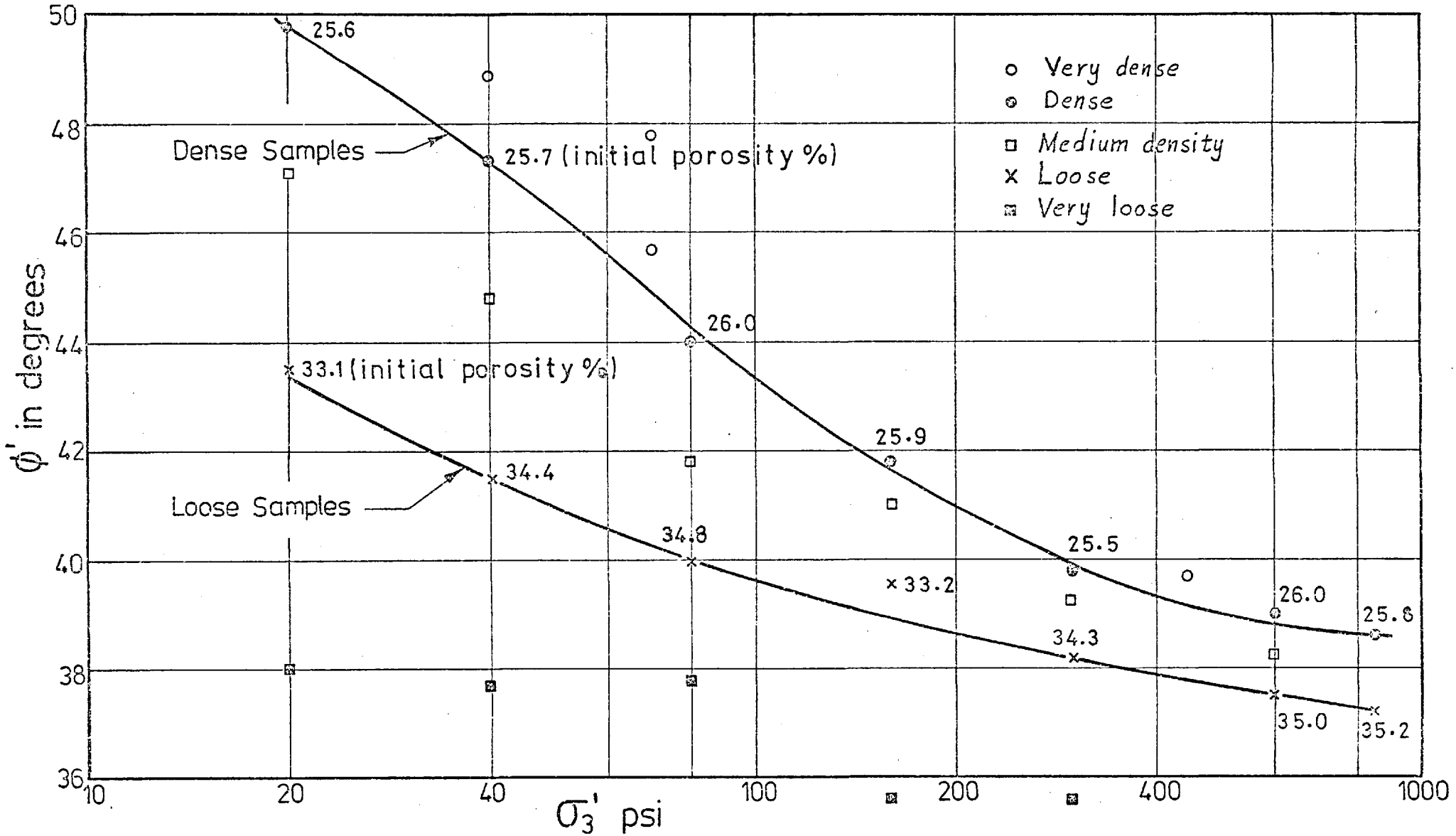

GRANITE ROCKFILL - VARIATION OF ϕ' WITH σ_3' IN DRAINED TESTS.

Fig. 6-10

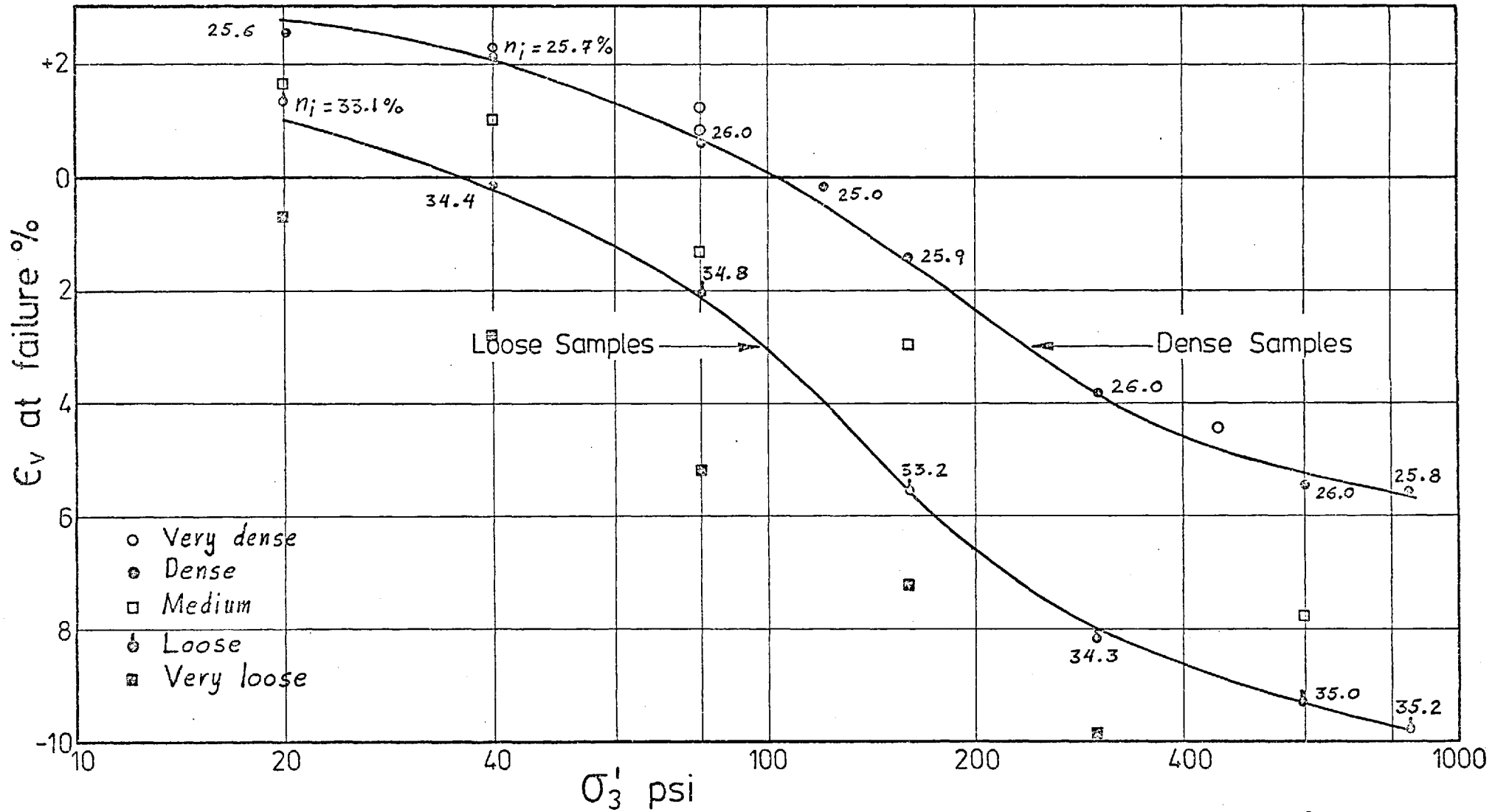

GRANITE ROCKFILL - VARIATION OF VOLUMETRIC STRAIN AT FAILURE WITH σ_3' IN DRAINED TESTS.

Fig. 6 - 11

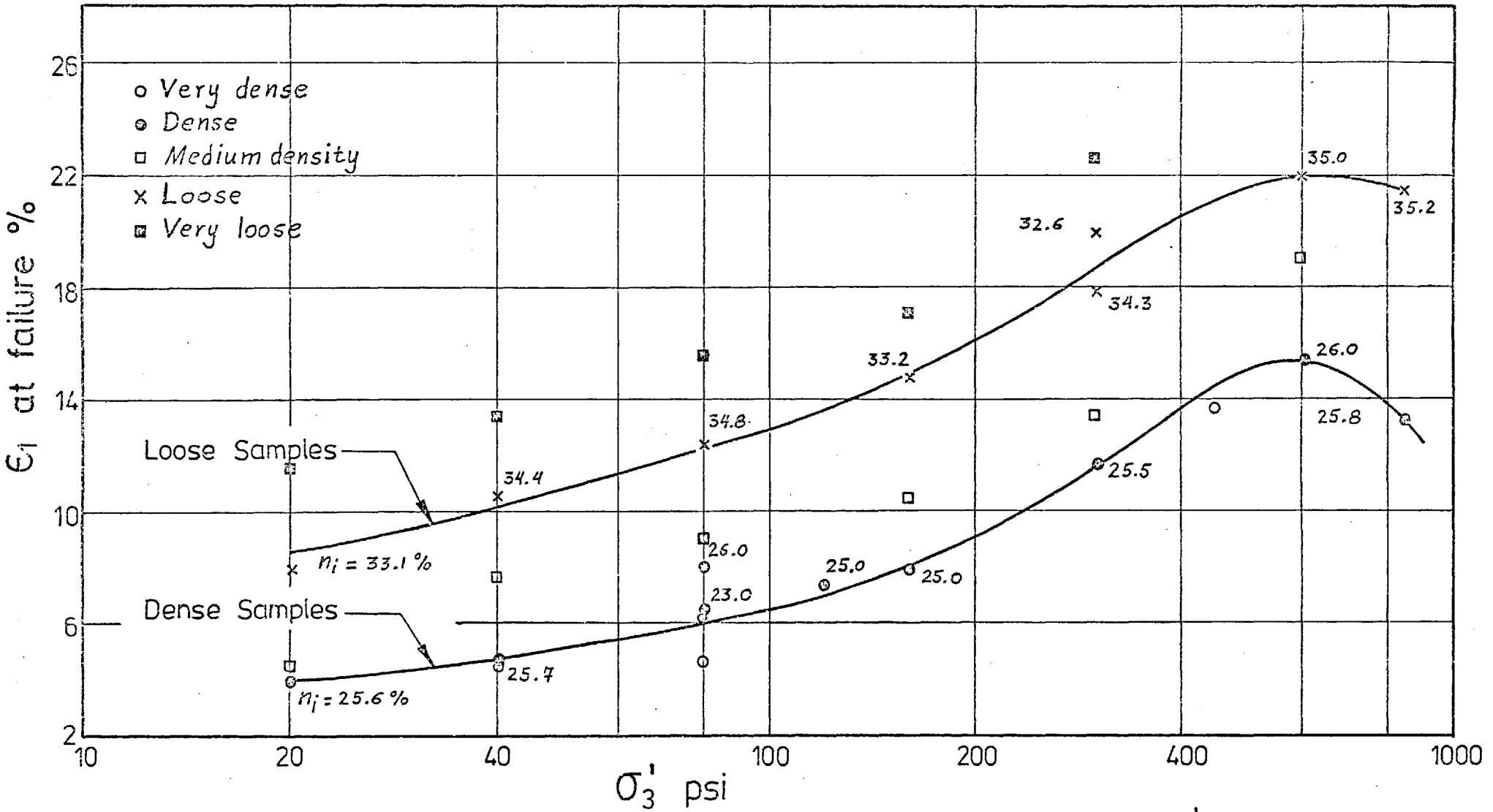

GRANITE ROCKFILL - VARIATION OF AXIAL STRAIN AT FAILURE WITH σ_3' IN DRAINED TESTS.

Fig. 6-12

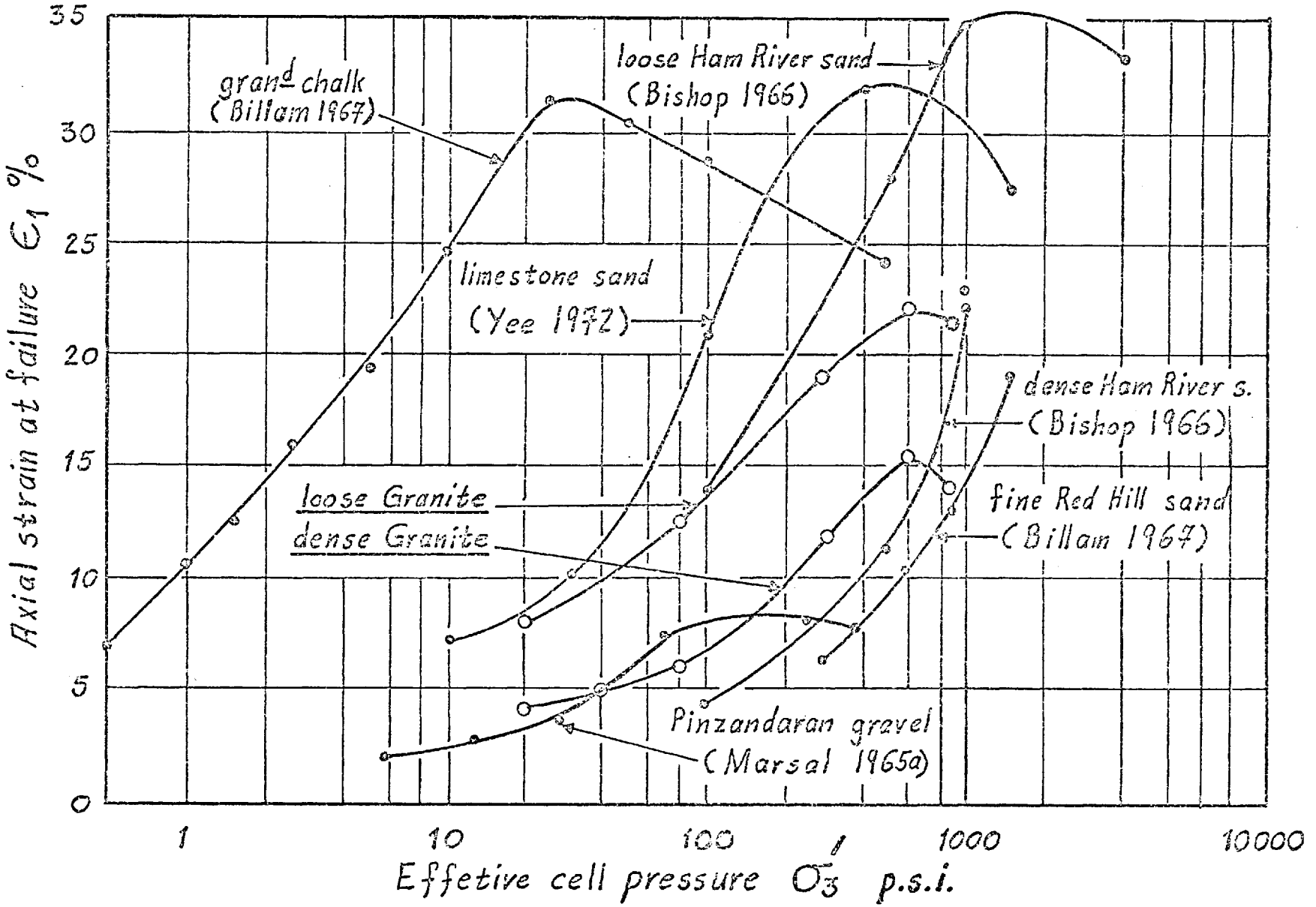

VARIATION OF ϵ_1 AT FAILURE WITH σ_3 IN DRAINED TRIAXIAL TESTS FOR VARIOUS ROCKFILL MATERIALS.

FIG 6—13

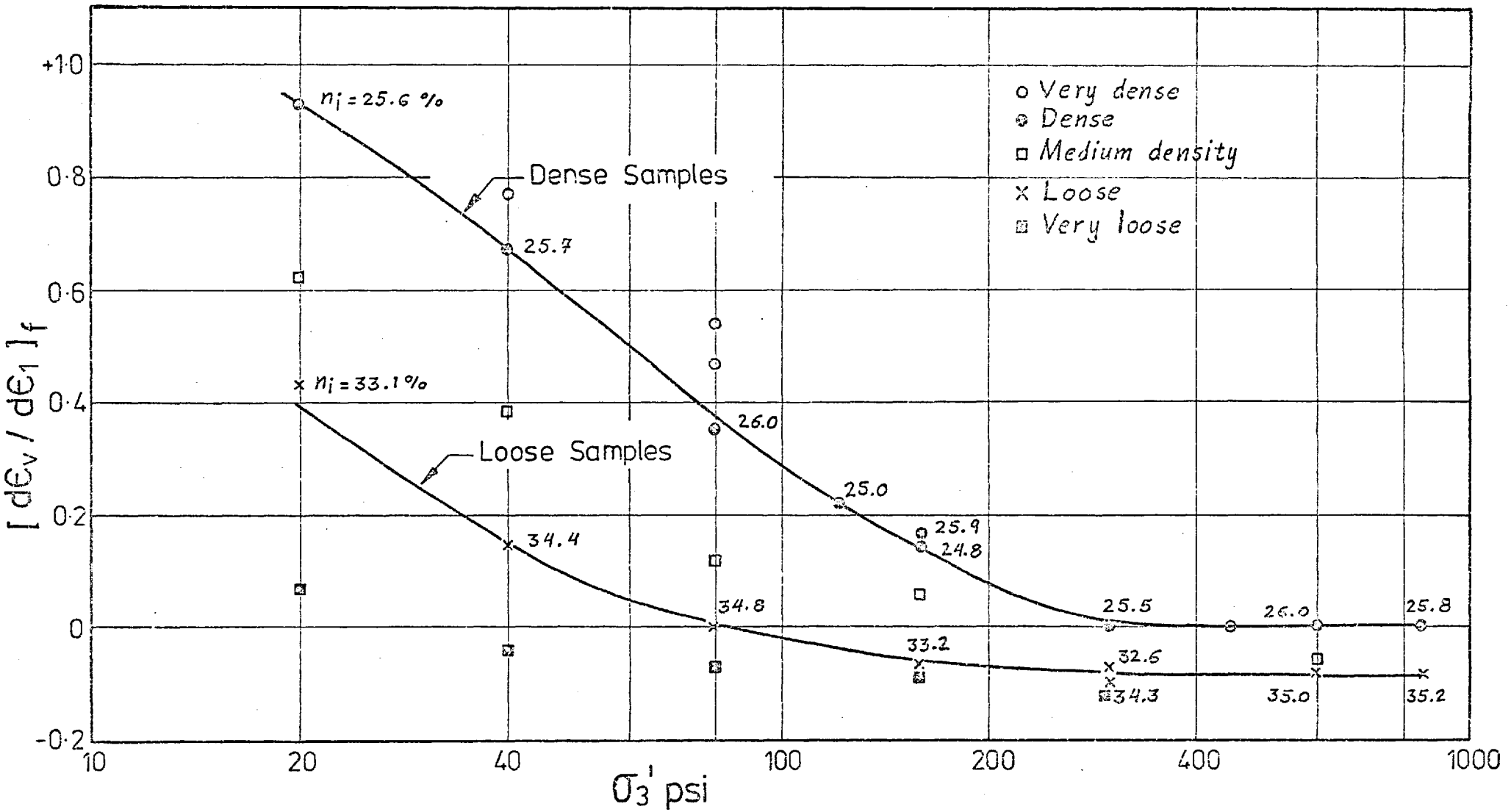

GRANITE ROCKFILL - VARIATION OF RATE OF DILATANCY AT FAILURE WITH σ_3'.

Fig. 6-14

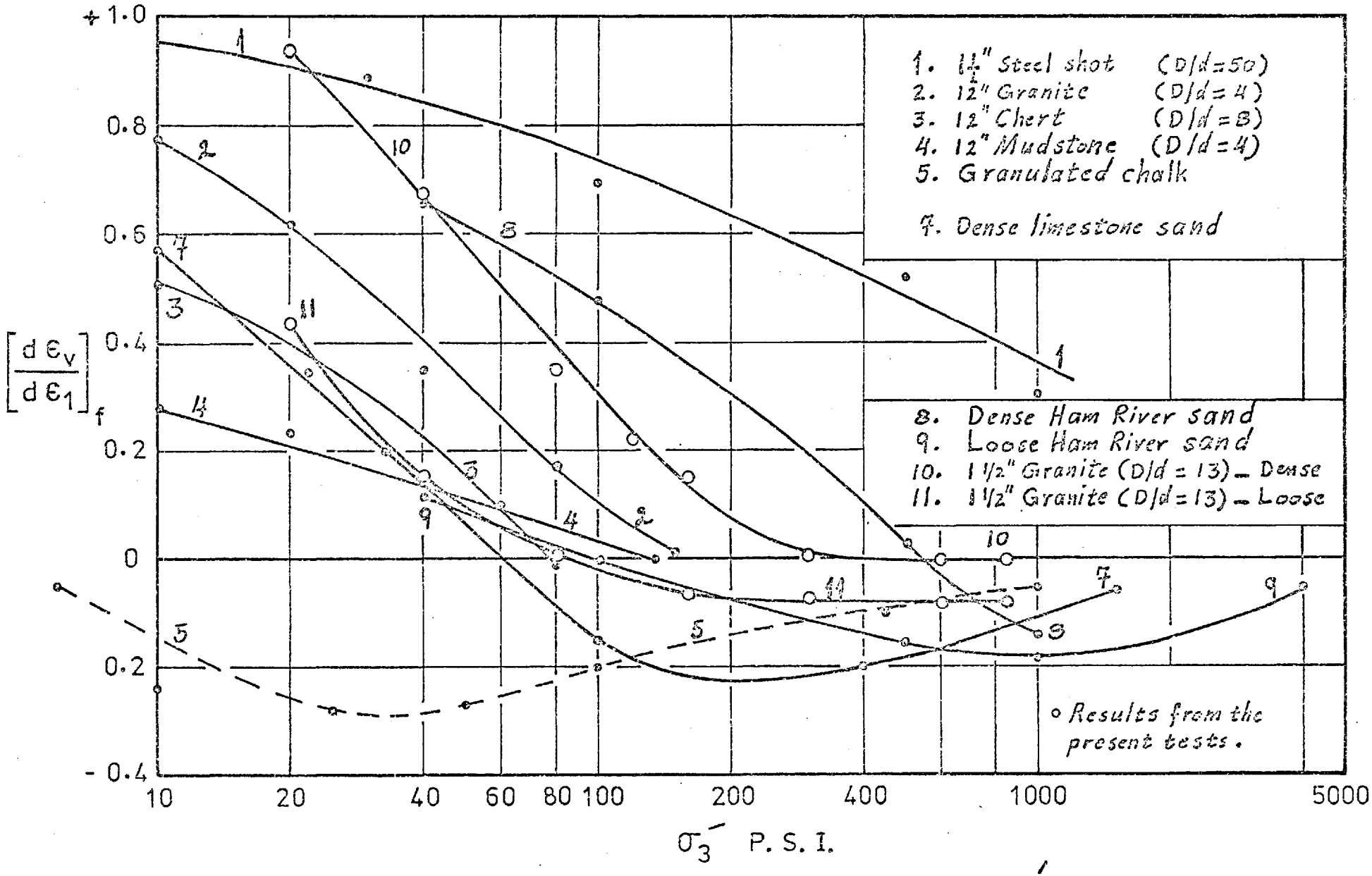

THE VARIATION OF RATE OF DILATANCY AT FAILURE WITH σ_3' FOR VARIOUS ROCKFILL MATERIALS.

FIG 6-15

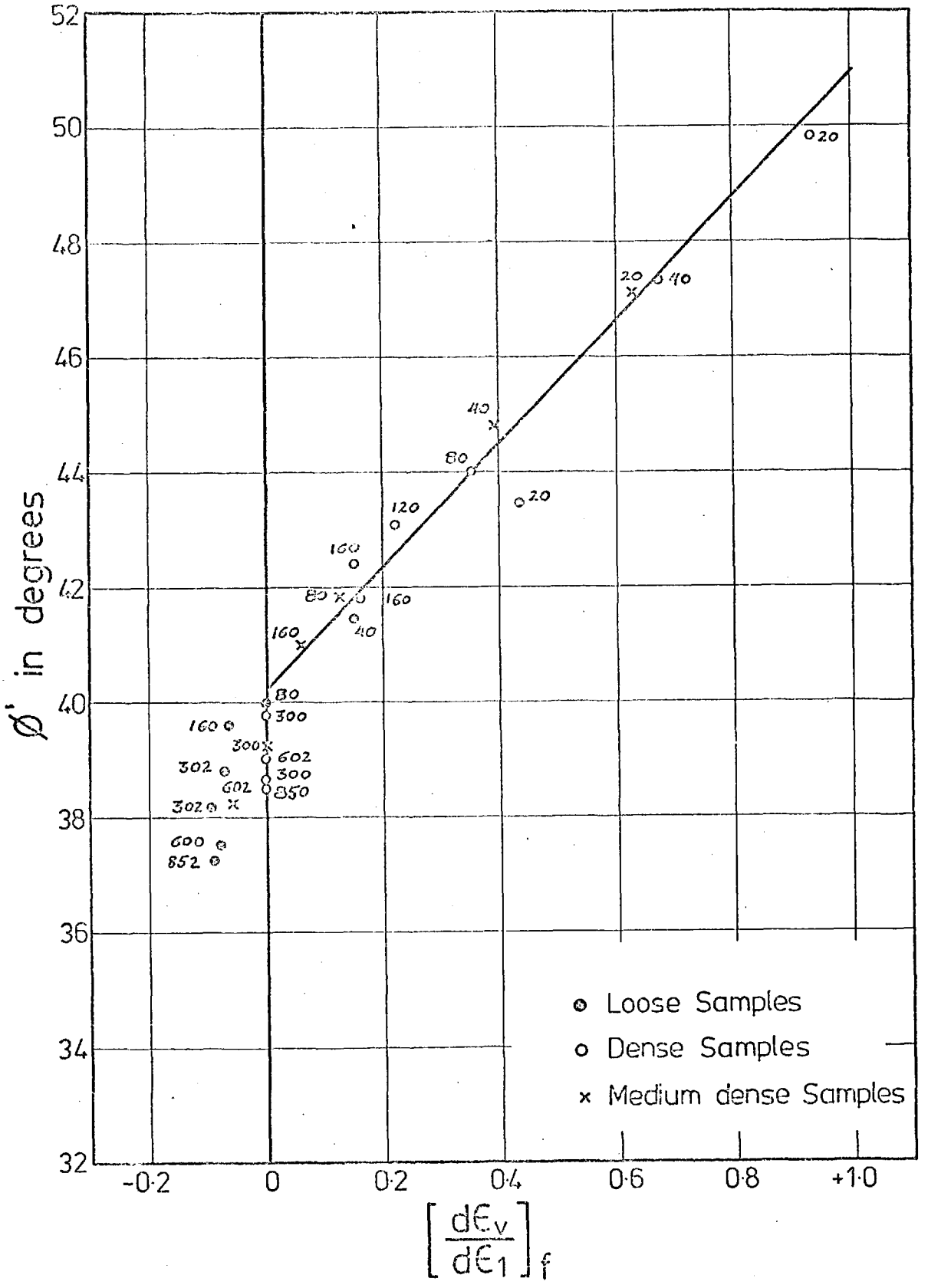

GRANITE ROCKFILL - THE RELATIONSHIP BETWEEN Ø' AND RATE OF VOLUME CHANGE $\left[\frac{d\epsilon_v}{d\epsilon_1}\right]_f$ AT FAILURE.

Fig. 6-16

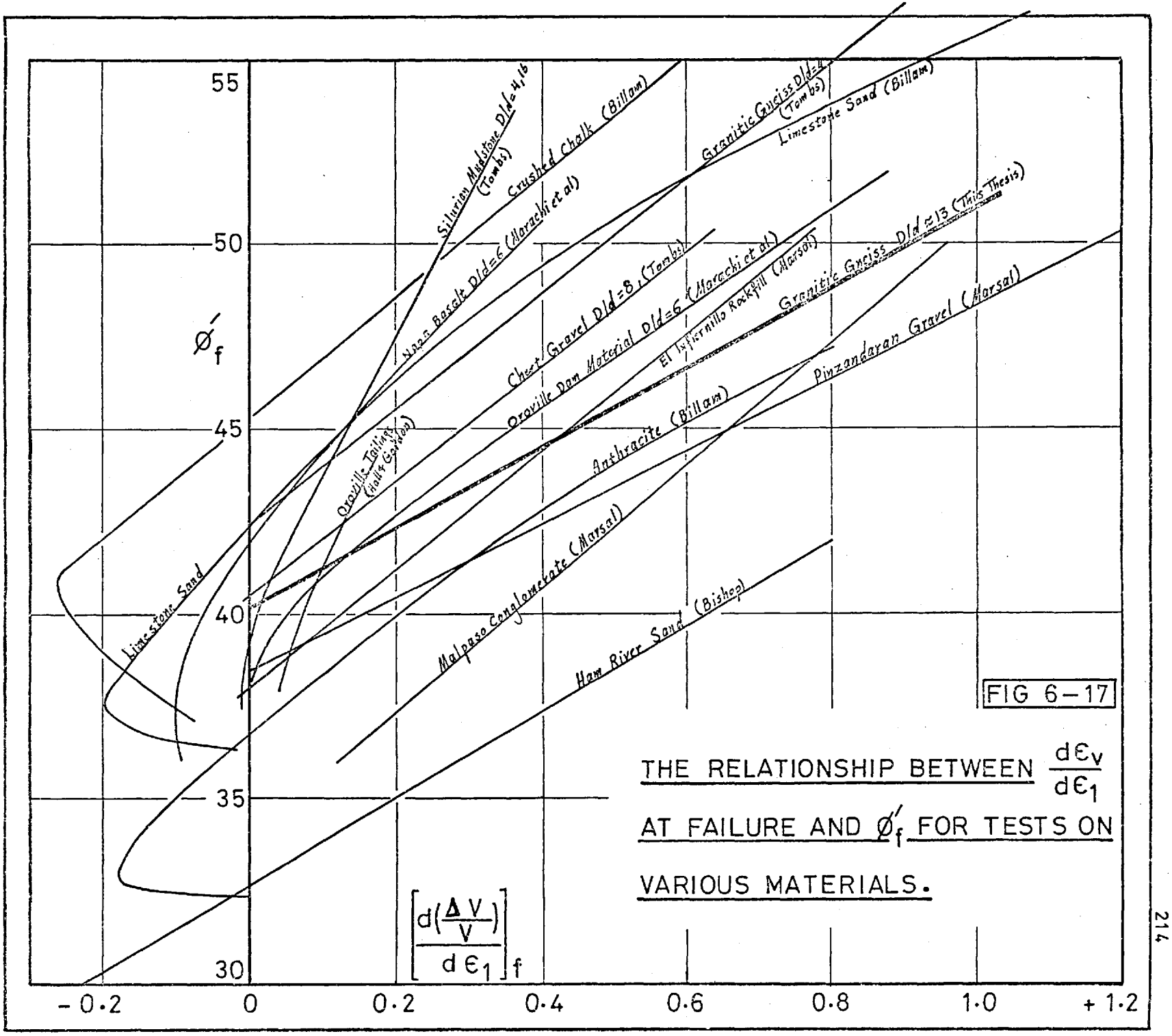

FIG 6–17

THE RELATIONSHIP BETWEEN $\frac{d\epsilon_v}{d\epsilon_1}$ AT FAILURE AND ϕ'_f FOR TESTS ON VARIOUS MATERIALS.

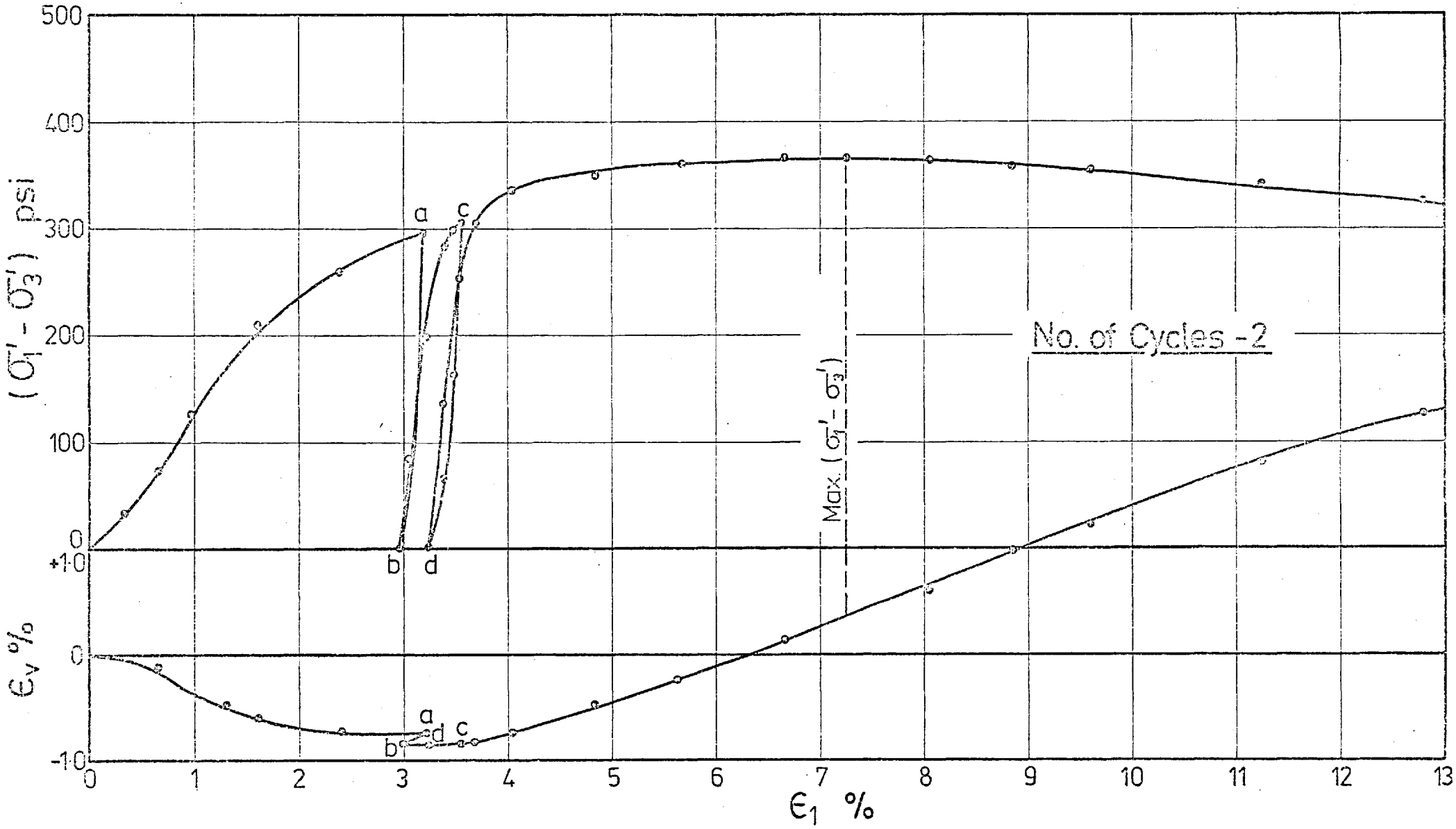

GRANITE ROCKFILL - CYCLIC LOADING TEST NO. 29.

Fig. 6-18

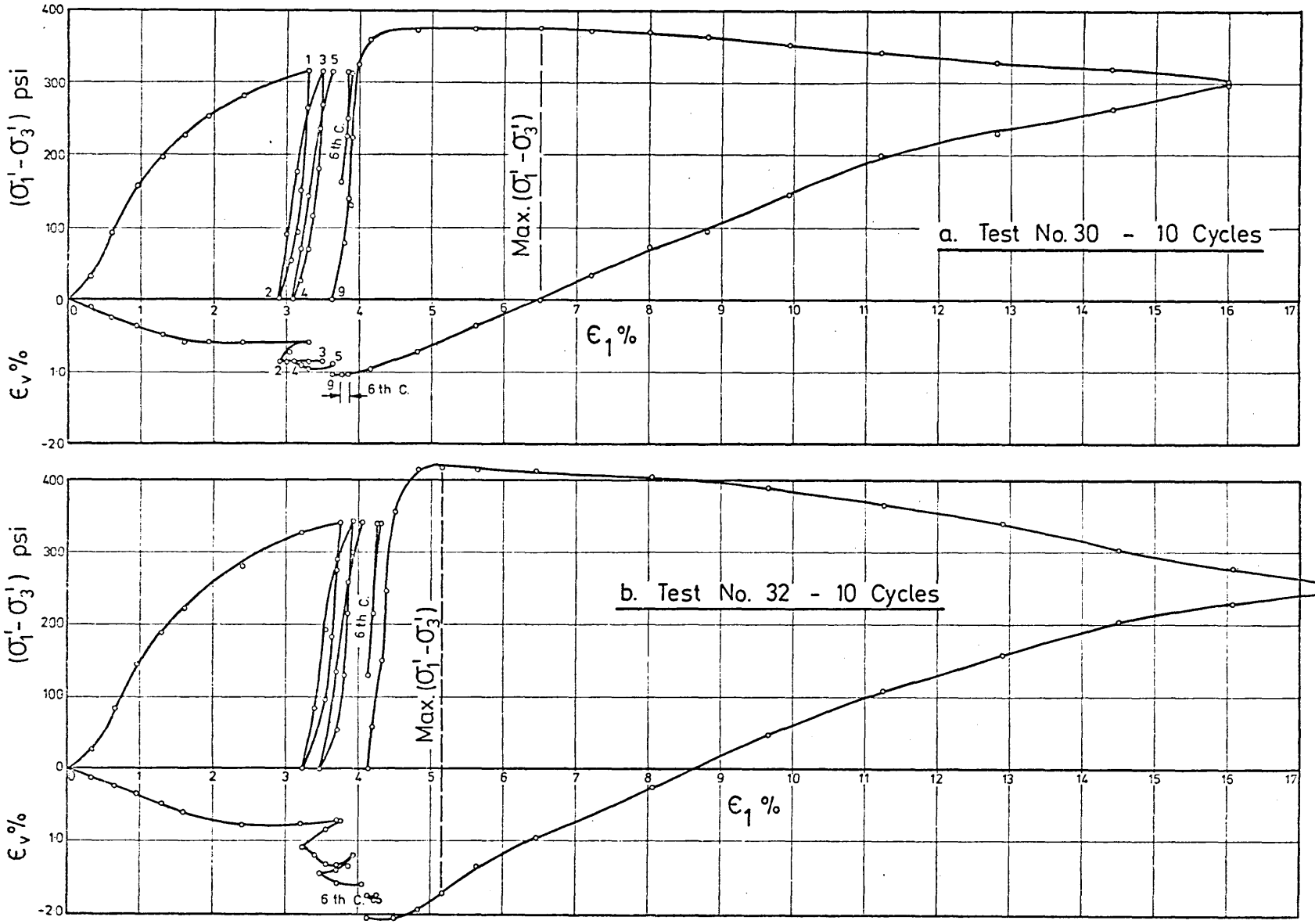

GRANITE ROCKFILL - CYCLIC LOADING TESTS NOS. 30 & 32

Fig. (6-19)

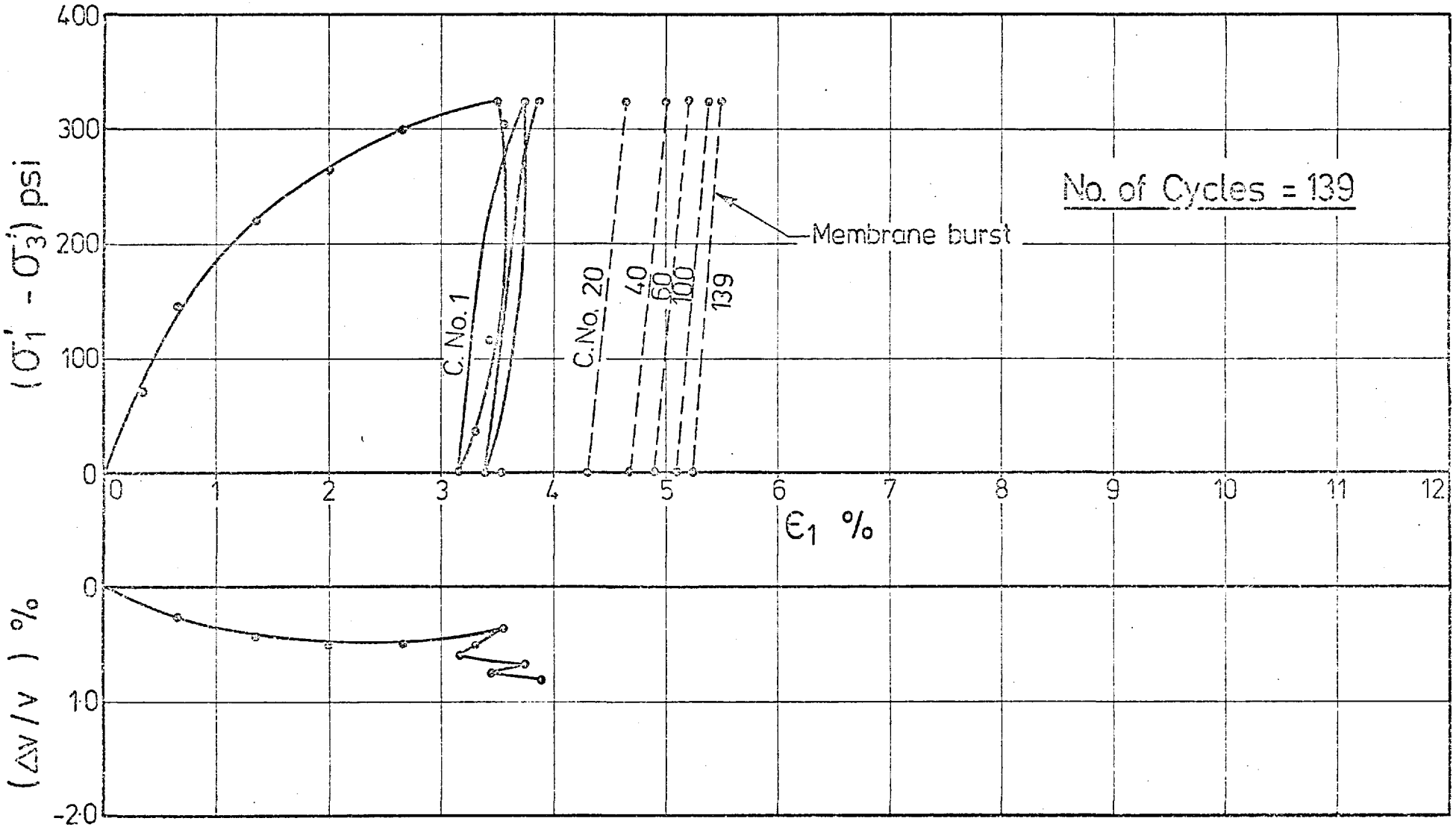

GRANITE ROCKFILL - CYCLIC LOADING TEST NO. 35

Fig. 6-20

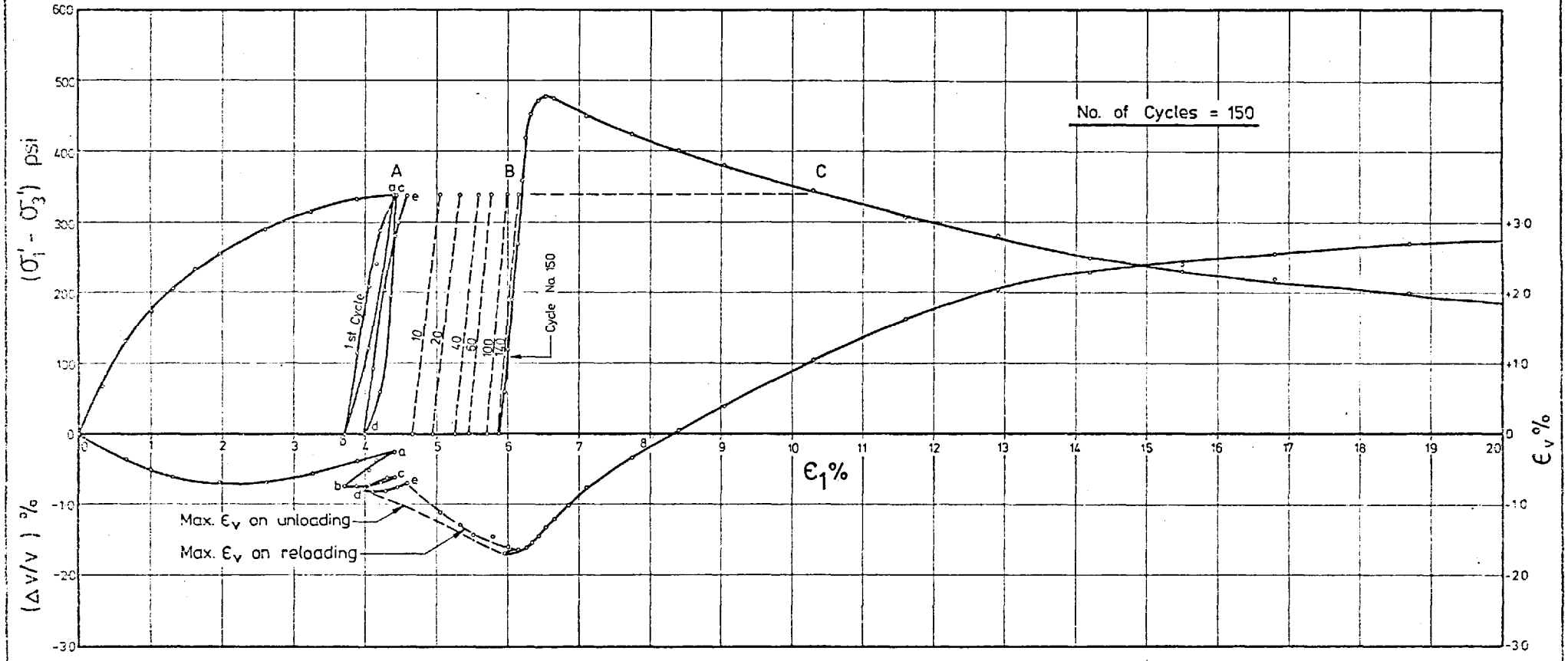

Granite Rockfill - Cyclic Loading Test No. 36

Fig.(6-21)

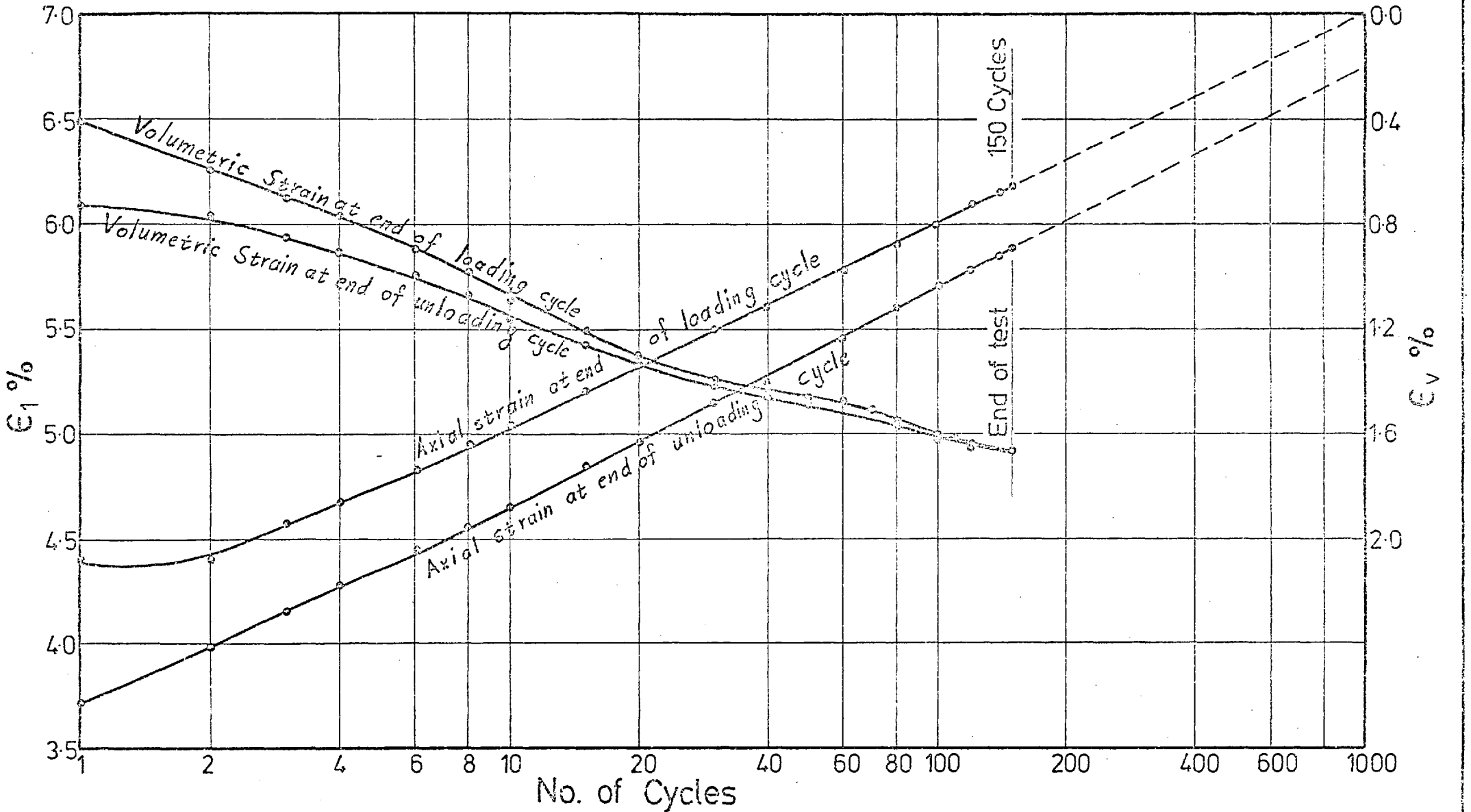

TEST No. 36 - STRAINS AT END OF LOADING AND UNLOADING.

Fig. 6-22 a

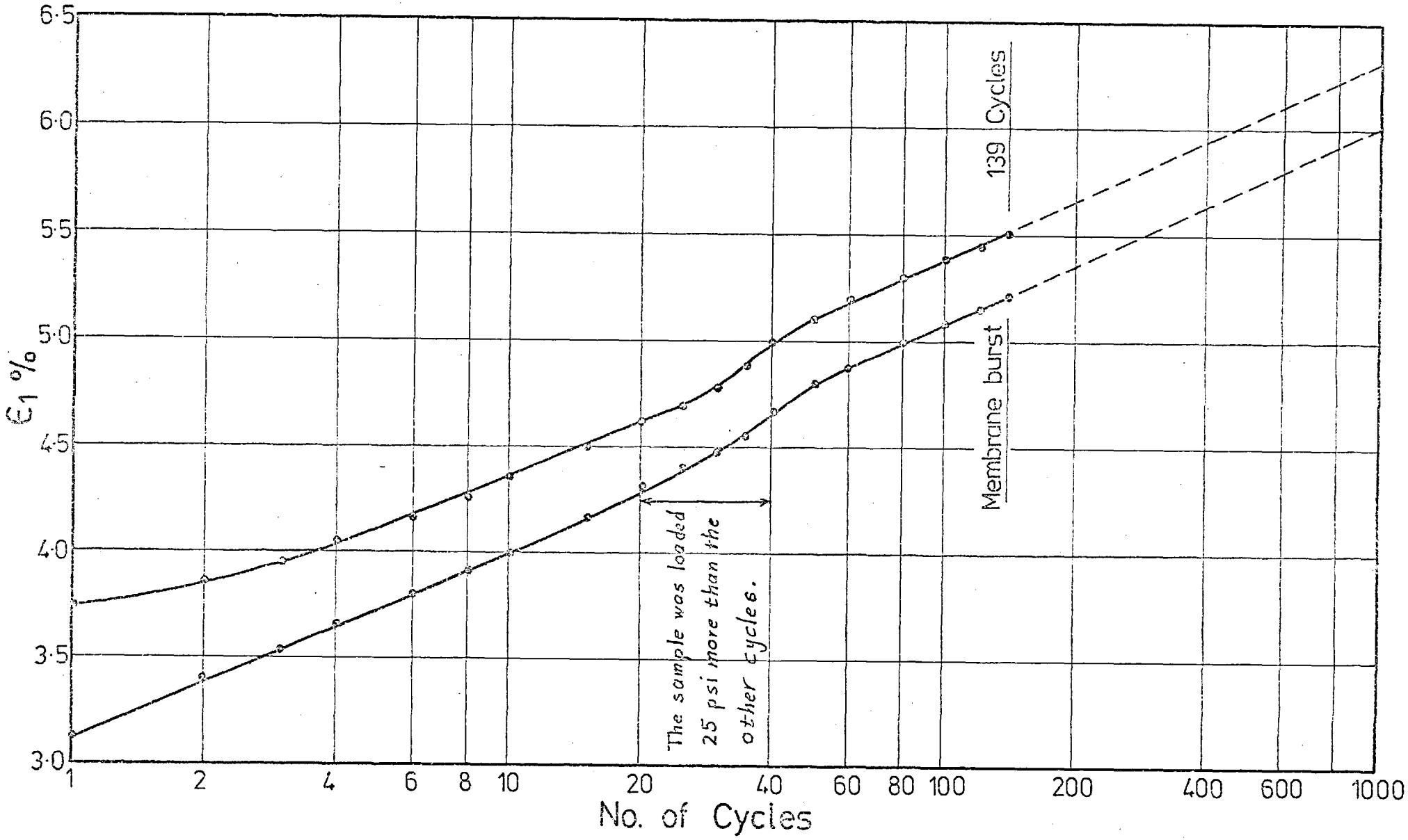

TEST No. 35 - THE AXIAL STRAIN AT END OF LOADING AND UNLOADING CYCLES.

Fig. 6-22b

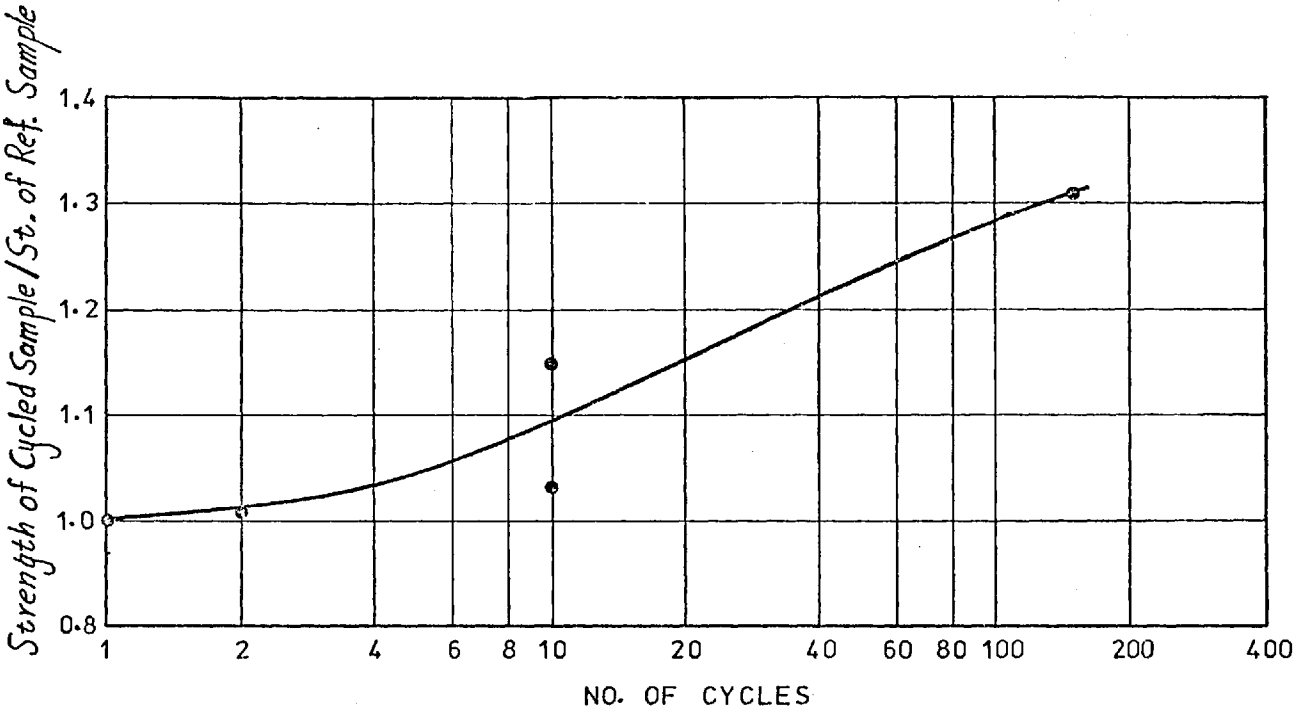

INFLUENCE OF DRAINED CYCLIC LOADING ON THE SHEAR STRENGTH OF ROCKFILL.

FIG 6-23 a

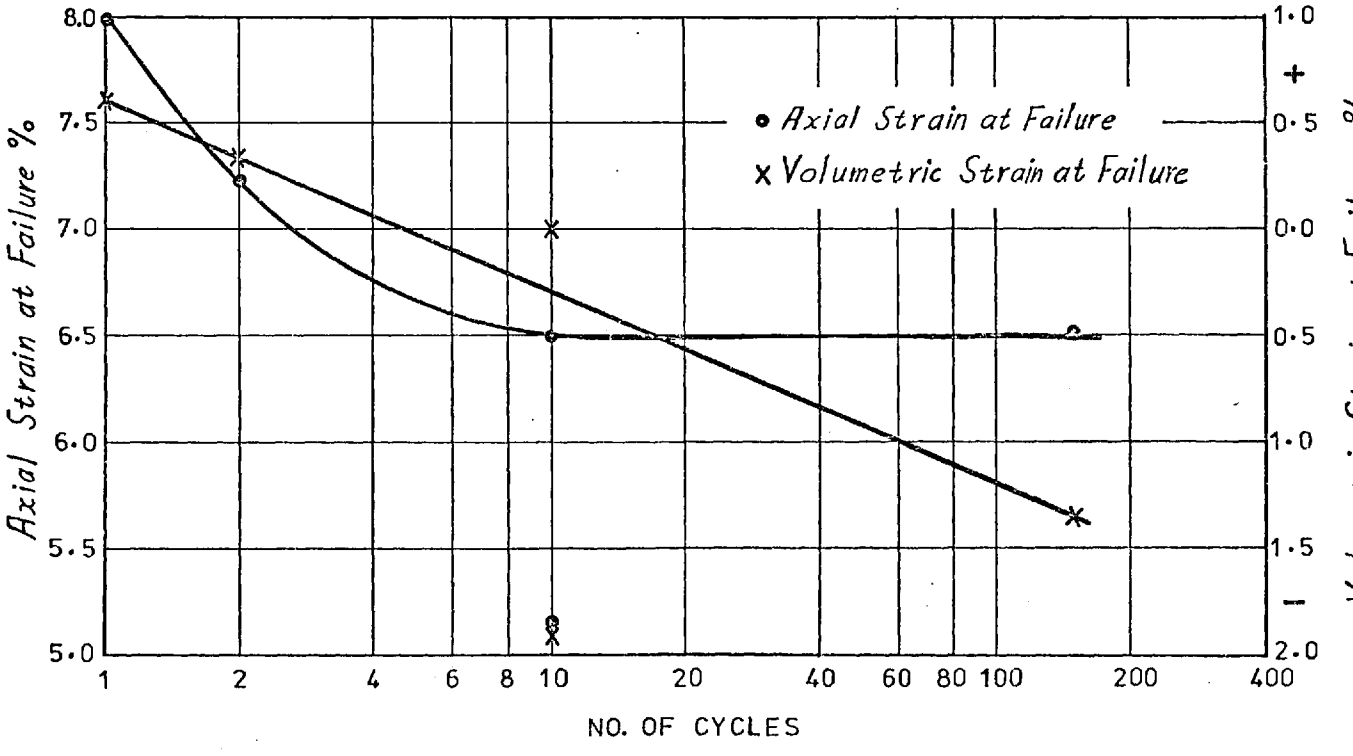

INFLUENCE OF DRAINED CYCLIC LOADING ON THE VOLUMETRIC & AXIAL STRAINS AT FAILURE.

FIG 6-23 b

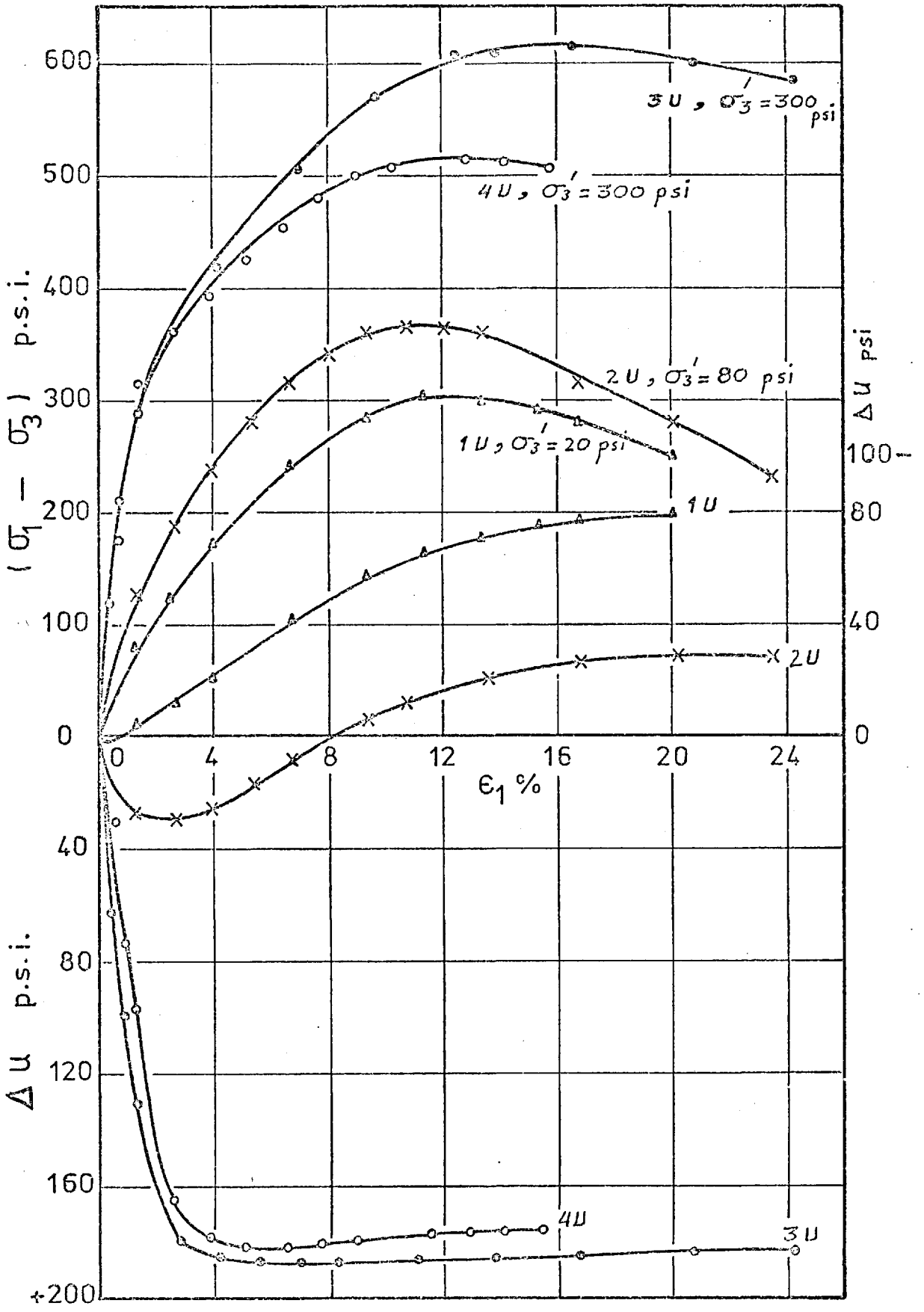

CONSOLIDATED UNDRAINED TESTS ON DENSE GRANITE ROCKFILL

FIG. 6 – 24

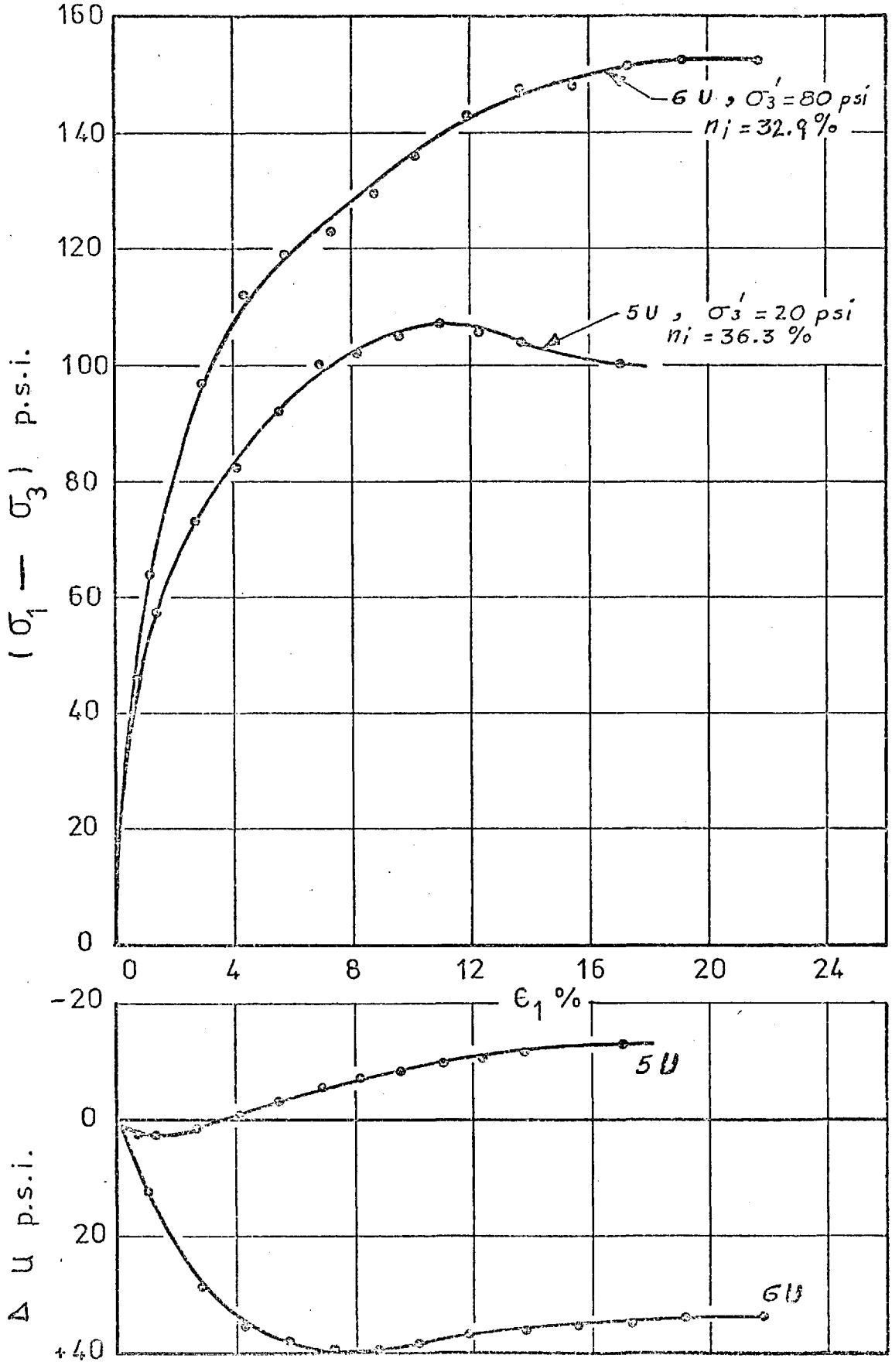

CONSOLIDATED–UNDRAINED TESTS ON LOOSE GRANITE ROCKFILL

FIG. 6–25

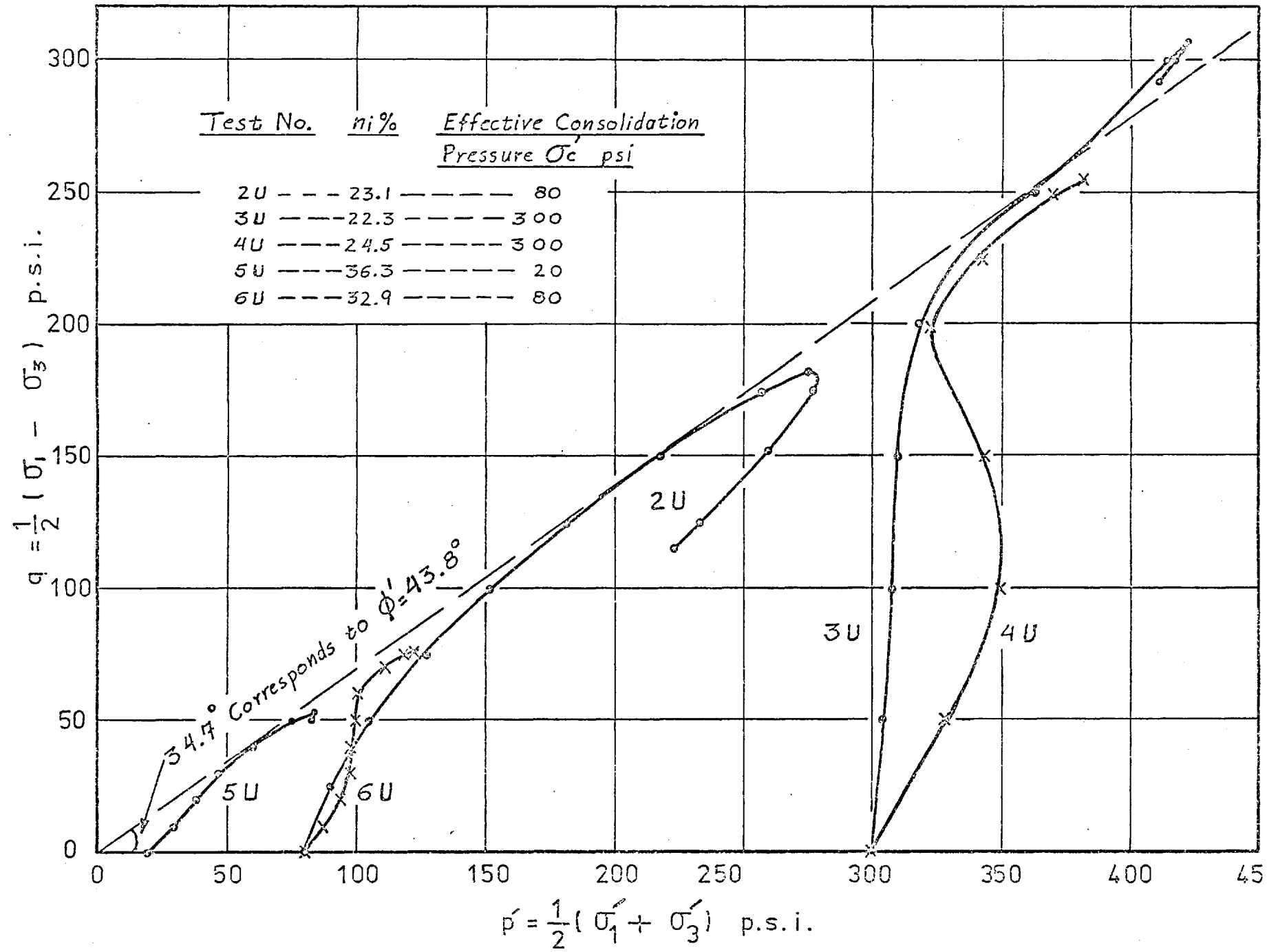

STRESS PATHS FOR CONSOLIDATED UNDRAINED TESTS ON GRANITE ROCKFILL

FIG. 6-26

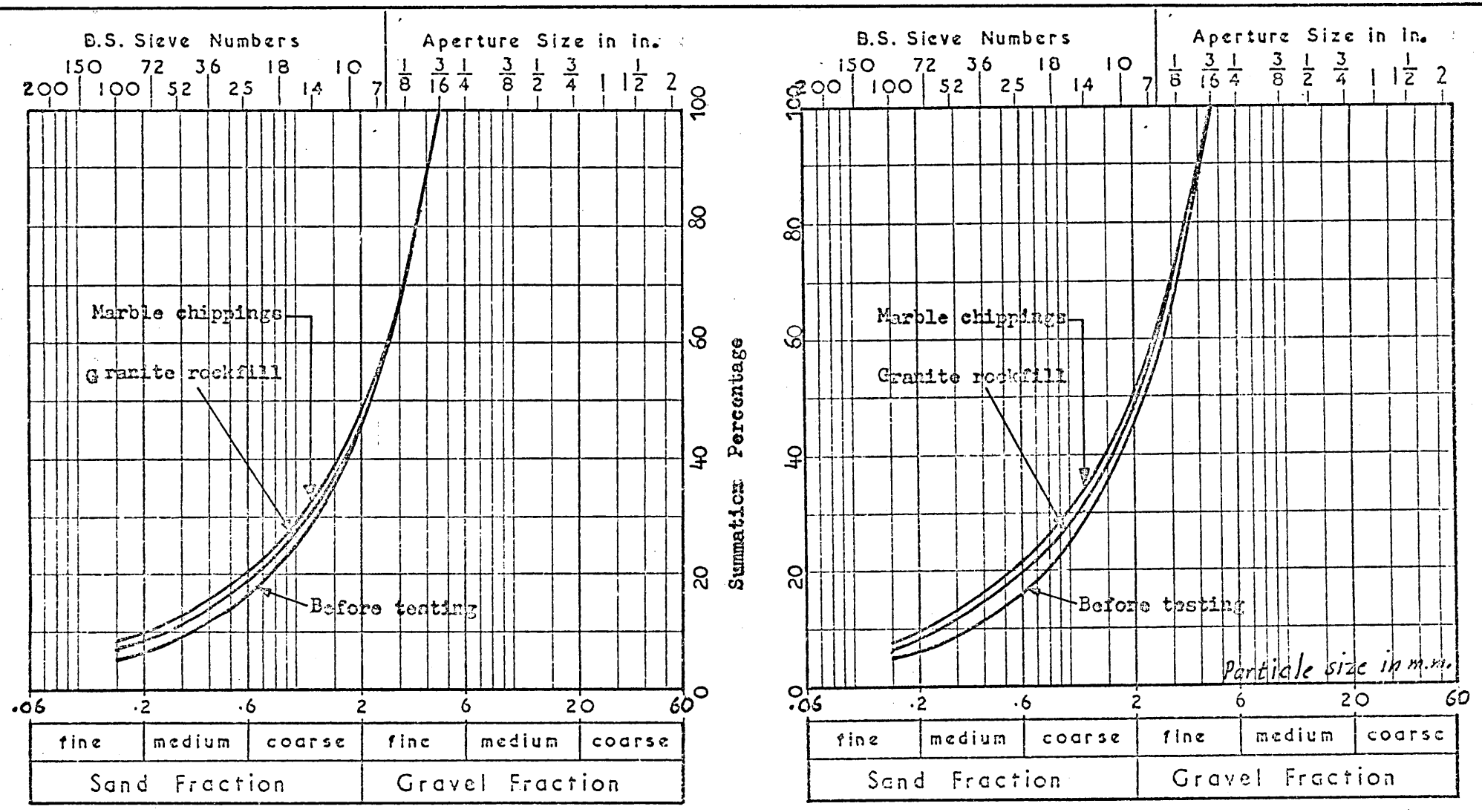

WET COMPACTION - n= 30.3%

DRY COMPACTION - n= 31.0%

GRANITE ROCKFILL & MARBLE CHIPPINGS. GRADINGS AFTER COMPACTION.

FIG 6-27

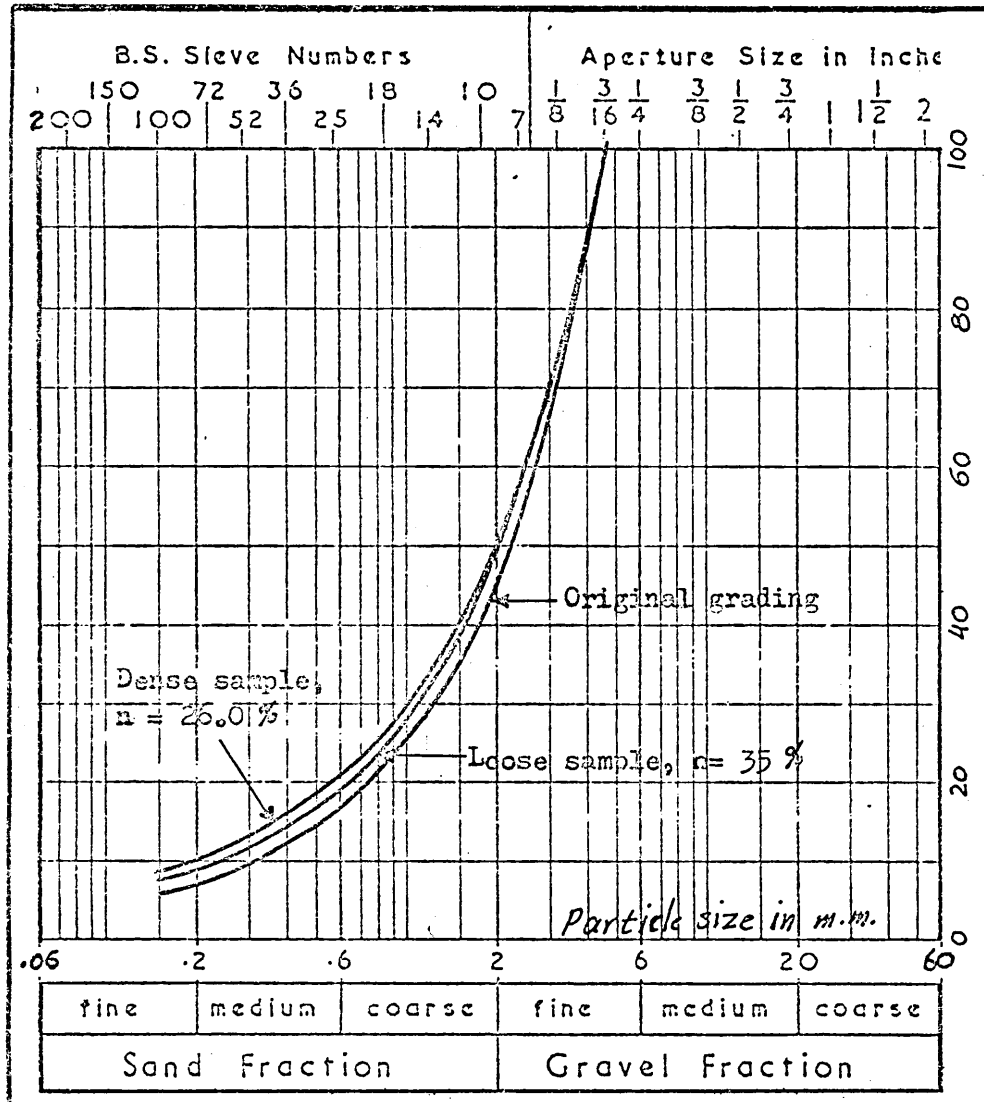

GRANITE ROCKFILL - GRADING AFTER CONSOLIDATION AT $\sigma_3' = 850$ psi.

FIG. (6 - 28)

Summation Percentage

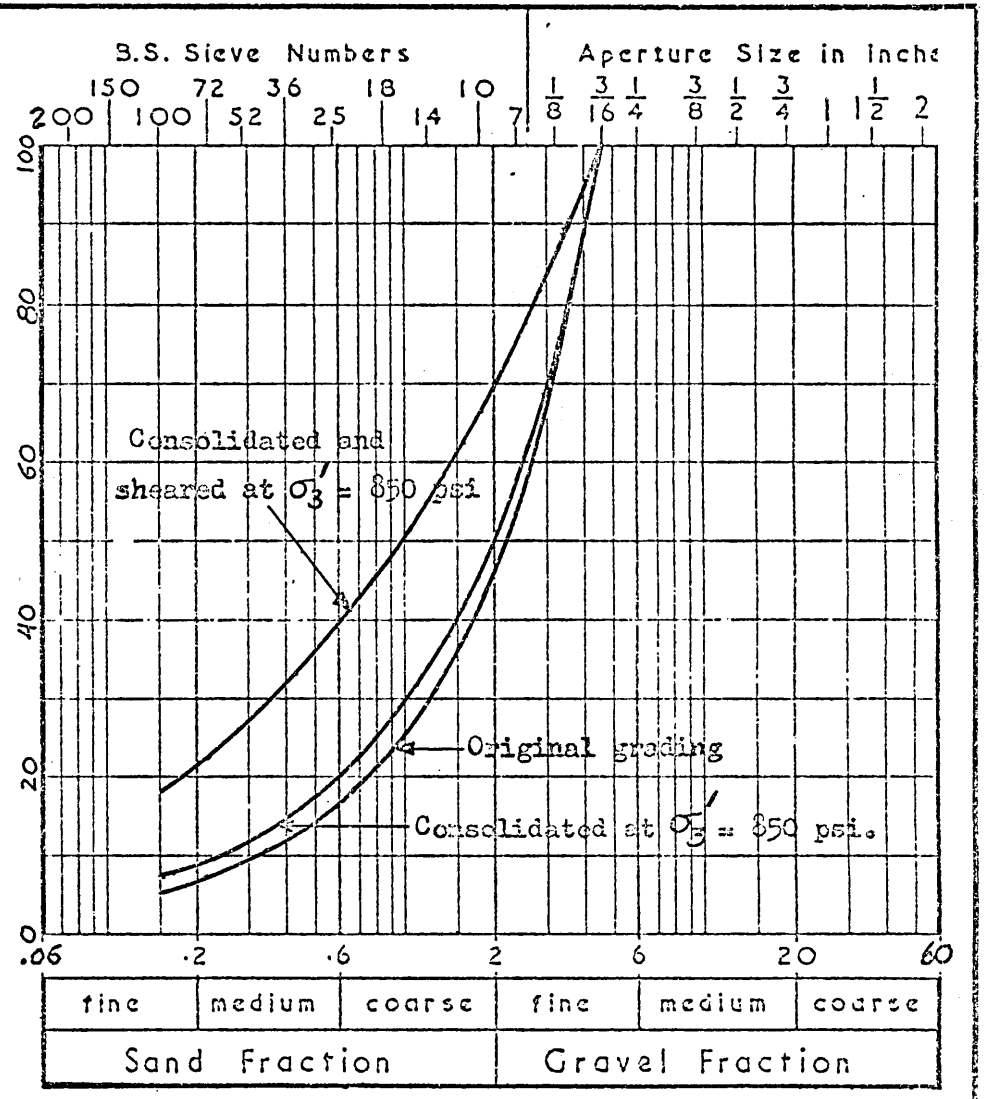

GRANITE ROCKFILL - COMPARISON OF PARTICLE BREAKAGE DURING CONSOLIDATION AND DRAINED SHEARING.

FIG. (6 - 30)

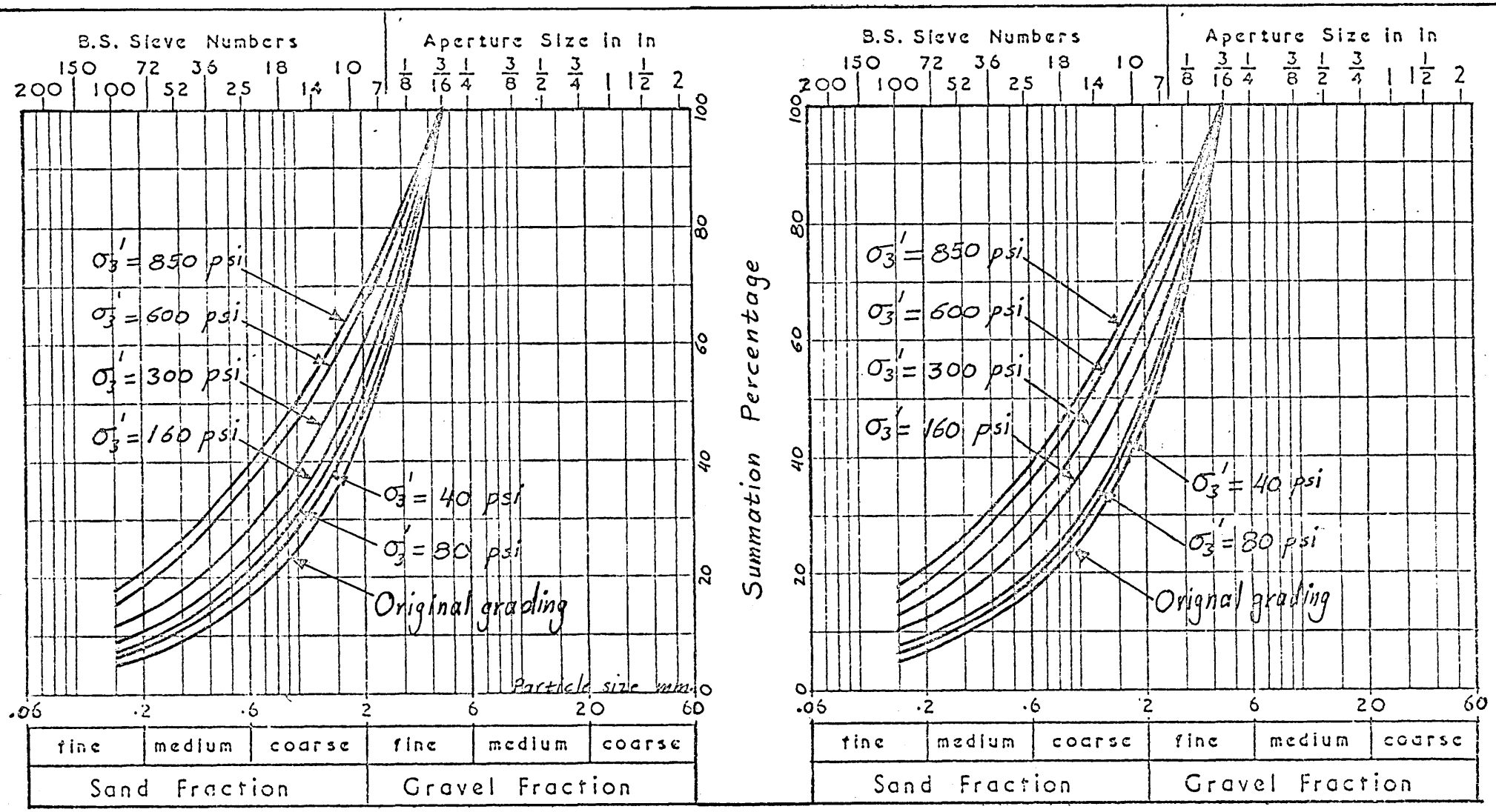

a. Dense Samples

b. Loose Samples

GRANITE ROCKFILL- GRADINGS AFTER TRIAXIAL DRAINED SHEARING.

FIG 6-29

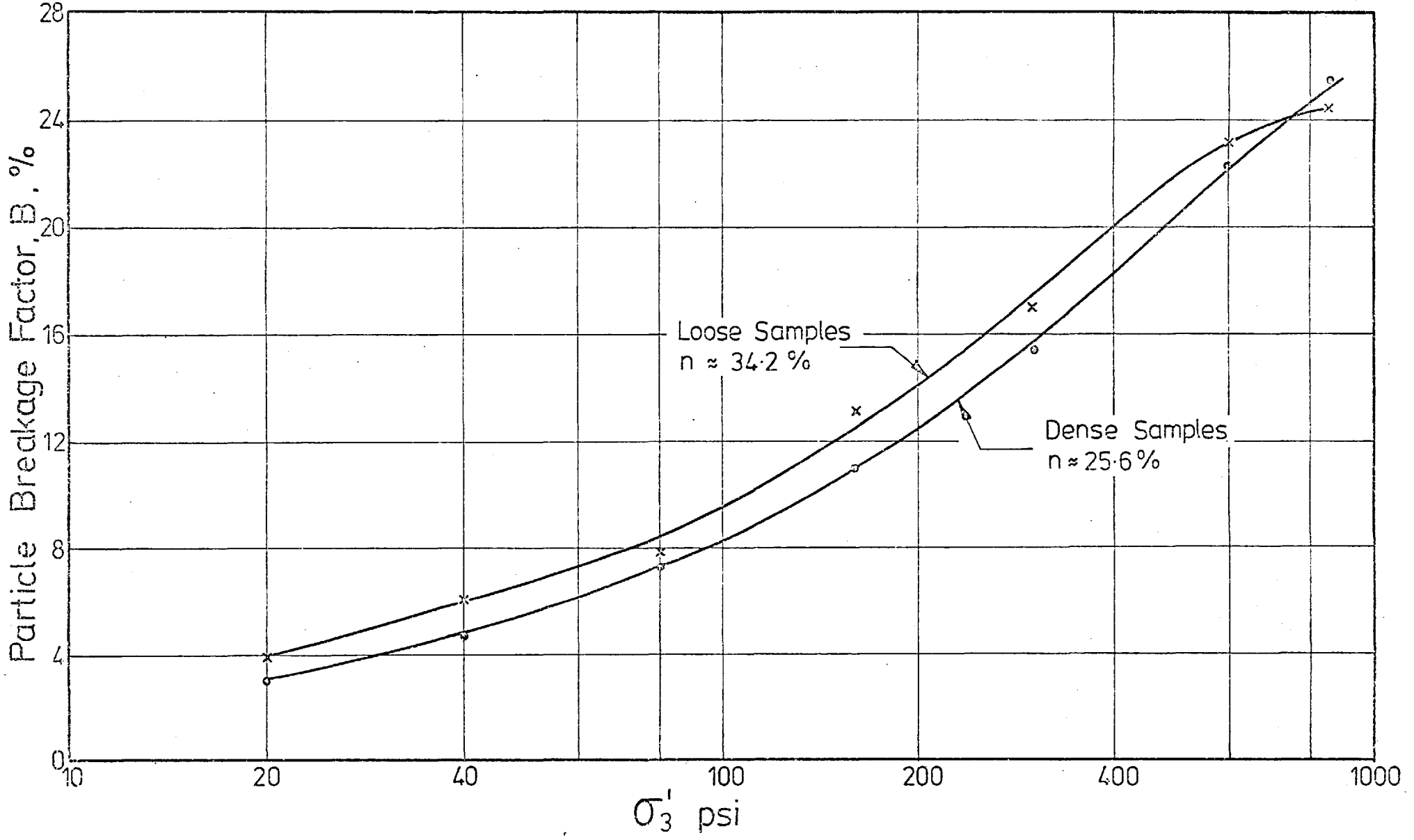

GRANITE ROCKFILL - VARIATION OF PARTICLE BREAKAGE FACTOR, AFTER DRAINED SHEARING, WITH σ_3'.

Fig. 6-31

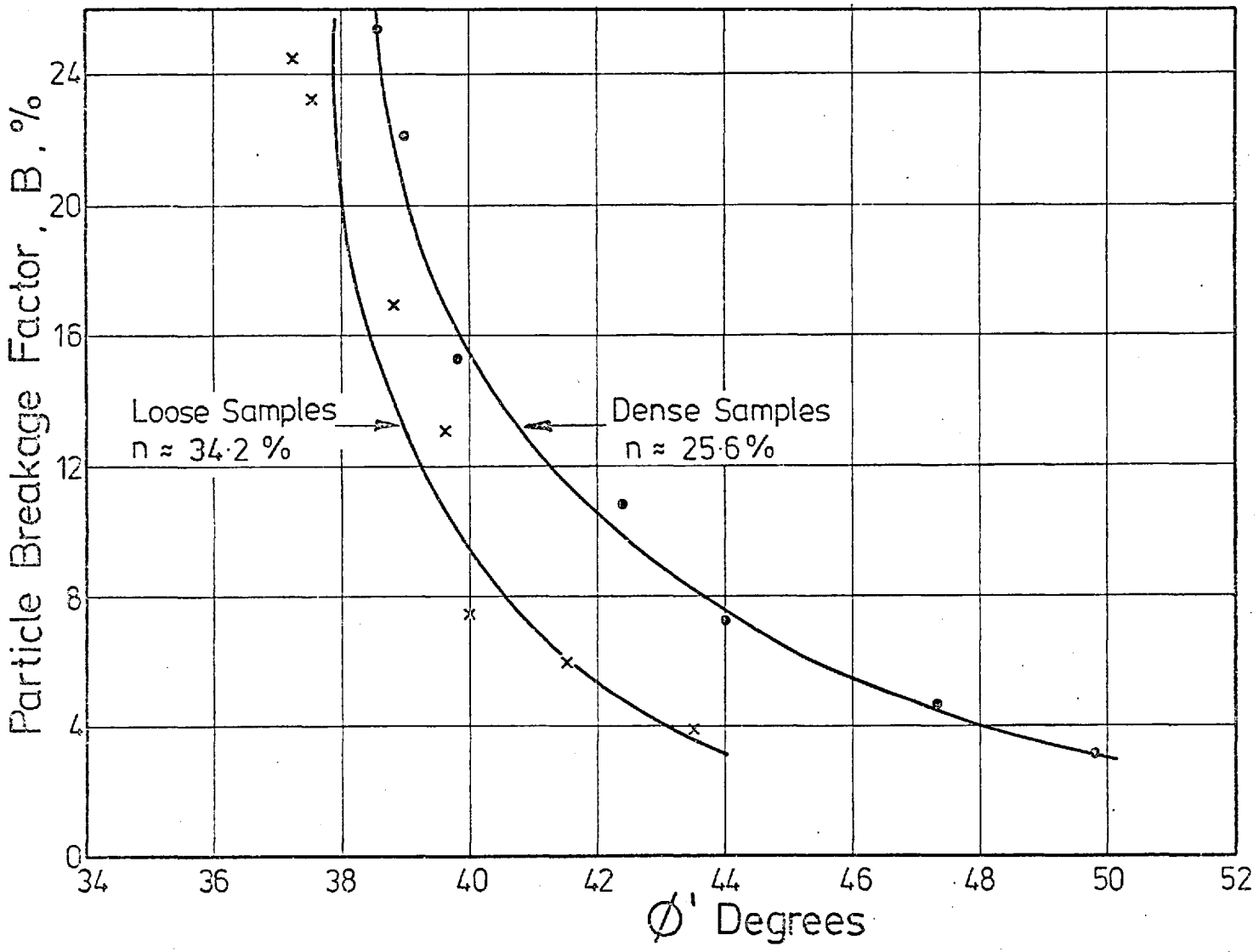

GRANITE ROCKFILL-RELATIONSHIP BETWEEN THE PARTICLE BREAKAGE FACTOR AND THE ANGLE OF SHEARING RESISTANCE.

Fig. 6-32

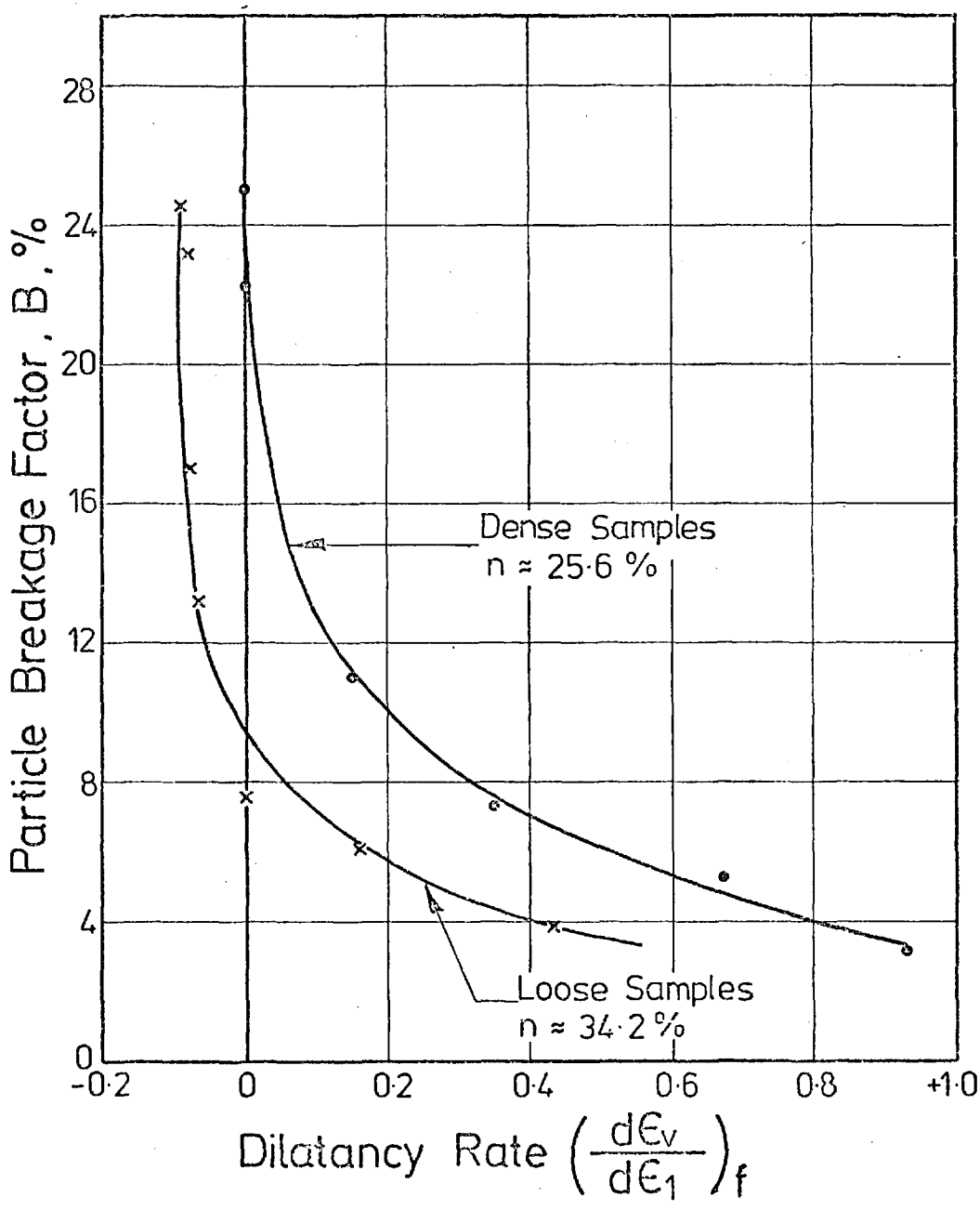

GRANITE ROCKFILL-RELATIONSHIP BETWEEN PARTICLE BREAKAGE FACTOR B AND DILATANCY RATE AT FAILURE.

Fig. 6-33

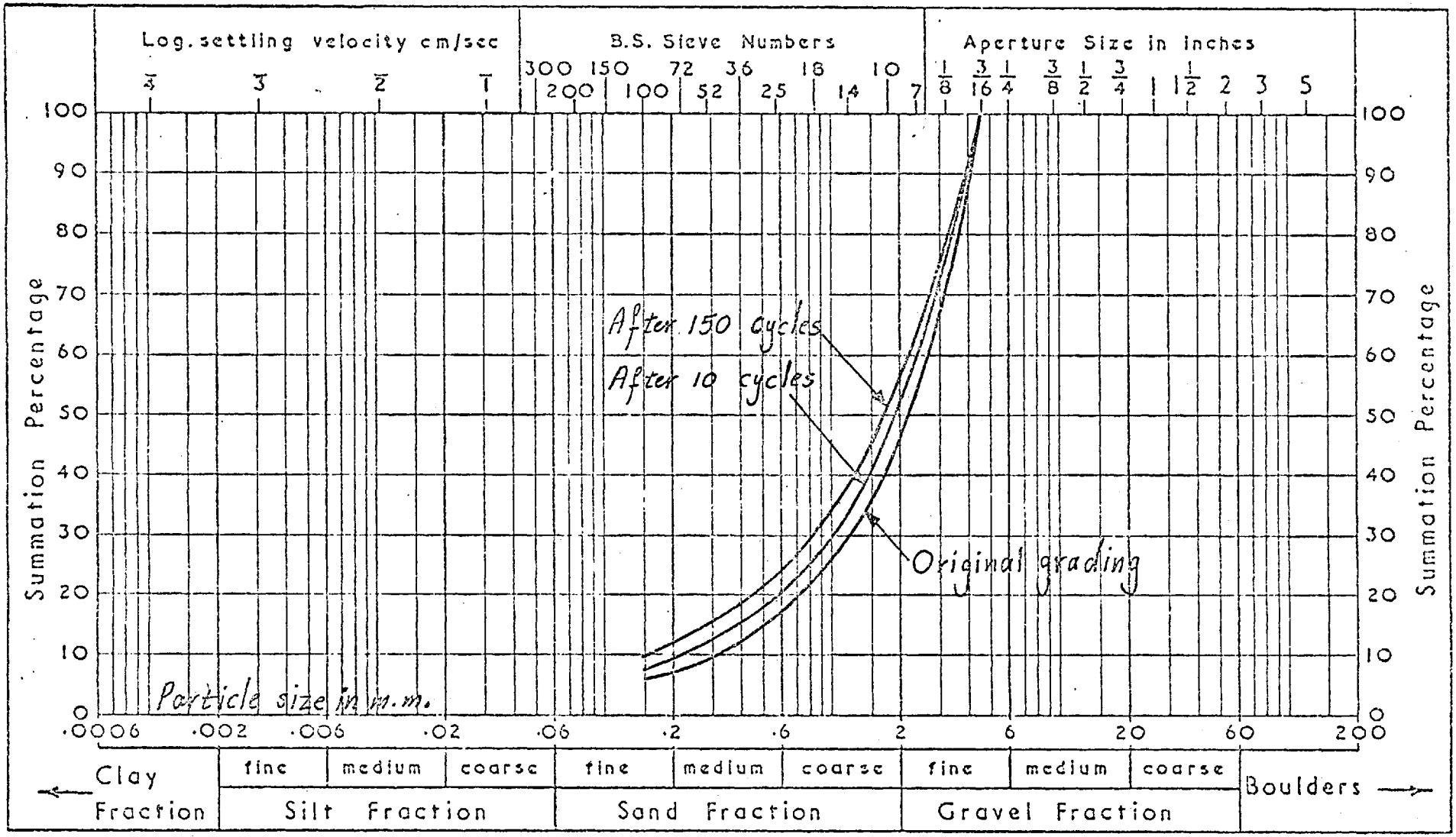

GRANITE ROCKFILL - GRADING AFTER DRAINED CYCLIC LOADING AND SHEARING UNDER DRAINED CONDITIONS.

(THE 10 & 150 CYCLE TESTS).

FIG 6—34

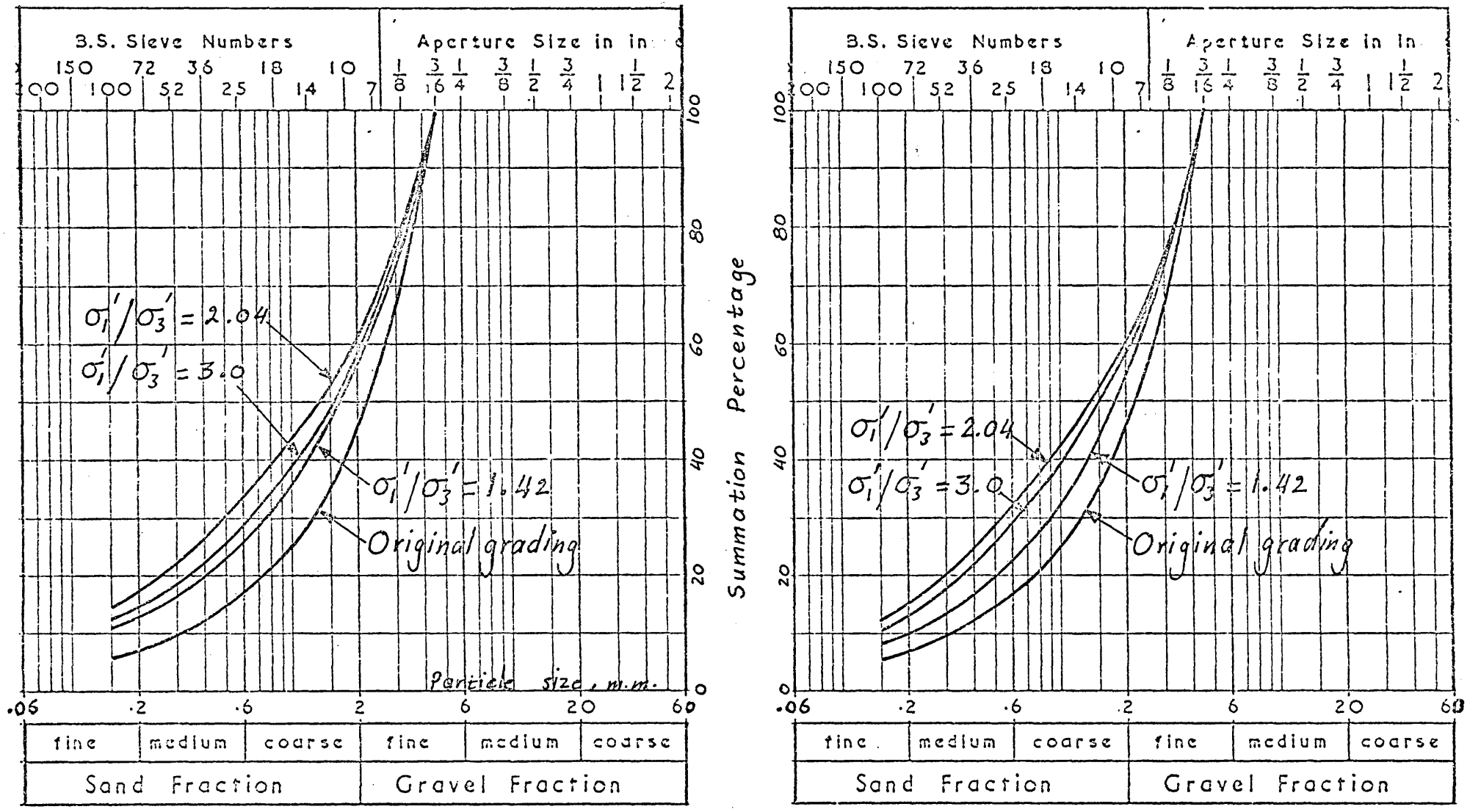

DENSE SAMPLES

LOOSE SAMPLES

GRANITE ROCKFILL - GRADINGS AFTER CONSTANT STRESS RATIO CONSOLIDATION AND DRAINED SHEARING.

FIG 6-35

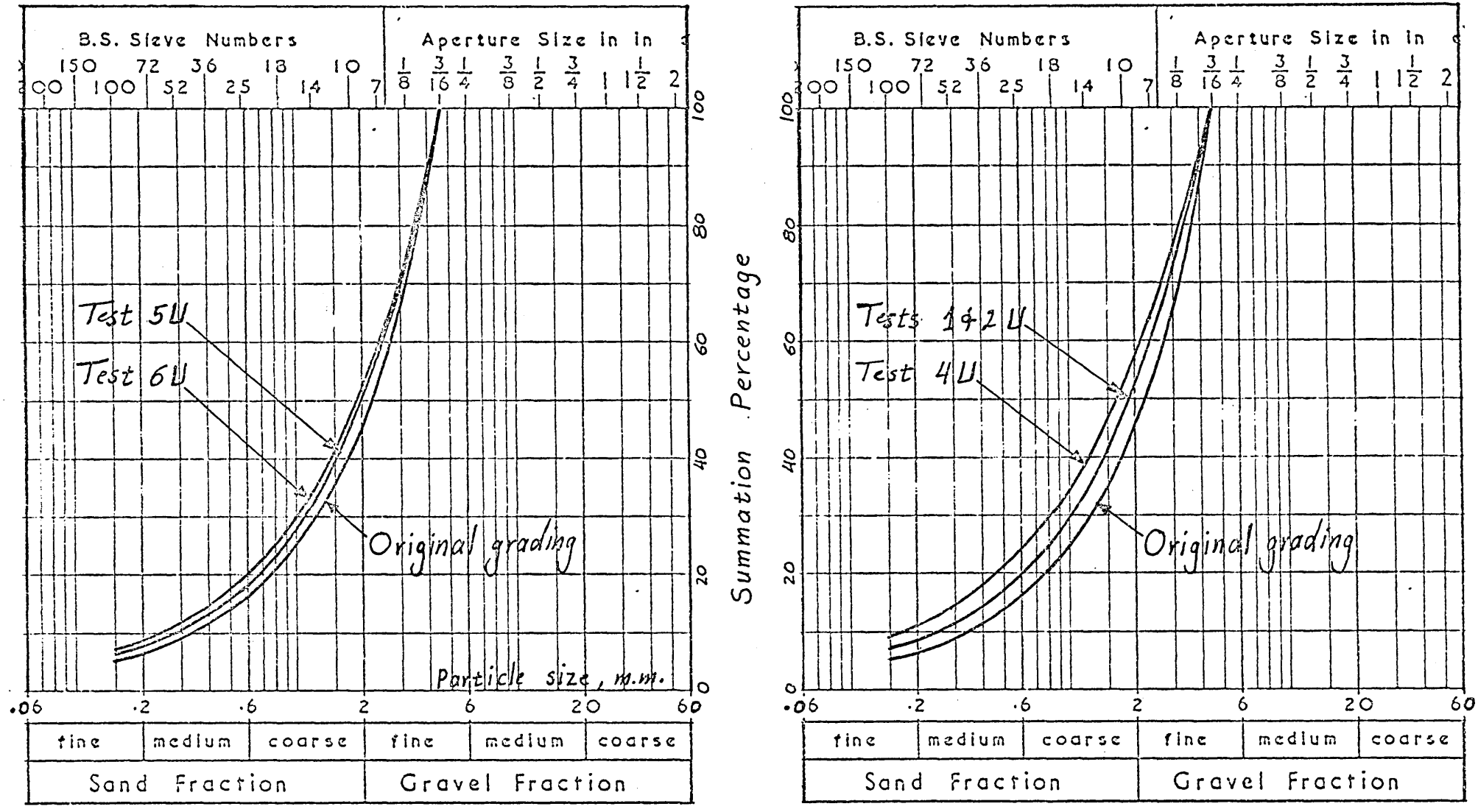

LOOSE SAMPLES

DENSE SAMPLES

GRANITE ROCKFILL - SAMPLES SHEARED UNDER UNDRAINED CONDITIONS.

FIG 6-36

CHAPTER VII

EXPERIMENTAL RESULTS AND DISCUSSION OF THE STRESS PATH TESTS

7.1. Introduction

7.1.1 The Aim of the Investigation

The main purposes of the experimental investigation in this chapter are summarized in the following points:

1. To study behaviour of granite rockfill subjected to various constant stress ratio (σ'_1/σ'_3) loadings and unloadings in the triaxial apparatus, and to try to find out what kind of relationship exists between the applied stresses and the volumetric strains.

2. To study the influence of the stress paths followed and the stress history of the rockfill material on their elastic and plastic deformations.

3. To investigate the influence of applying various stress probes on the plastic deformation of rockfill material.

4. To try to establish whether an elastic domain exists for granular materials.

7.1.2 Brief Layout of the Experimental Work

The experimental work carried out and discussed in this chapter is divided into two main parts. First, the investigation of the properties of granite rockfill under different constant stress ratios on loading and unloading, then shearing the samples to failure. Three levels of constant stress ratio were applied; these are 1.4, 2.04 and 3.0. Data for granite rockfill under constant stress ratio of 1.0 (i.e. isotropic loading) are available in Chapter 6. Three states of sample density were examined, dense, medium and loose, and the procedure of testing was that described in Chapter 4. Secondly, investigation of the deformations of granite rockfill under different stress paths, then applying stress probes.

Volumetric changes were calculated from strains accurately measured by a strain transducer developed specially for this purpose. The apparatus and testing technique have been described in Chapter 4. Similar tests have been carried out on marble chippings and Ham River sand to compare their behaviour with that of granite rockfill. Marble particles are weaker and Ham River sand particles are stronger than those of granite material.

7.1.3 Parameters Used in the Interpretation of the Test Results

The basic parameters used to interpret and discuss the data obtained from the triaxial stress path tests in this chapter are;

the mean effective principal stress $p' = \frac{1}{3}(\sigma'_1 + 2\sigma'_3)$

the stress difference $q = (\sigma'_1 - \sigma'_3)$

the volumetric strain $\epsilon_v = \frac{\Delta V}{V_o} = (\epsilon_1 + 2\epsilon_3)$

the shear strain $\gamma = \frac{2}{3}(\epsilon_1 - \epsilon_3)$

where compressive stresses and strains have been considered positive. In fact these parameters have been adopted by Cambridge research group and the reason for this choice has been explained in detail by Schofield and Wroth (1968).

7.2 The Anisotropic Consolidation Tests on Granite Rockfill

7.2.1 Test Programme and General Description

The term anisotropic consolidation used here will refer to consolidation under constant stress ratio σ'_1/σ'_3. A set of nine tests was carried out in this series. Three states of densities were examined and each state of density was tested under three different constant stress ratios of 1.4, 2.04 and 3.0, Figure (7-1). The stress paths are also shown in a triaxial plane (i.e. $\sigma'_2 = \sigma'_3$) plotted on $\sigma'_1 : \sqrt{2}\ \sigma'_3$ diagram. It is seen that the stress paths tested lie above the space diagonal ($\sigma'_1 = \sigma'_2 = \sigma'_3$) which means that all the

tests are in compression (i.e. $\sigma'_1 > \sigma'_2 = \sigma'_3$). To extend the present work it is necessary to test stress paths below the space diagonal as well, i.e. extension tests where $\sigma'_1 < \sigma'_2 = \sigma'_3$.

To avoid repetition, one test will be described in detail which represents the other nine tests. For such a test a sample of granite rockfill was set up as described in Chapter 4 and the cell was assembled ready for loading the sample. The cell and back pressures were increased simultaneously in small increments keeping an effective minor principal stress of 4 psi until the back pressure reached a value of 40 psi; this was done to ensure full saturation. Water was flushed through the sample using a pressure difference of 1.5 psi between the top and bottom of the sample to get rid of all the air bubbles from inside the sample. Then the sample was consolidated anisotropically using a strain controlled loading arrangement where the stresses were increased by 5 psi increments to ensure uniform stress distribution. After achieving the maximum required stress level,* the sample was unloaded anisotropically, on the same stress path followed during loading, back to the initial starting point.

Then the sample was reloaded anisotropically on the same stress path to the maximum stress level reached in the first loading cycle. Finally the cell pressure was kept constant and the sample was sheared to failure under drained conditions with a constant back pressure as mentioned earlier. Sets of records have been taken for the stress differences, axial deformations and volume changes.

7.2.2 The Behaviour of the Samples Under Anisotropic Loading and Unloading

7.2.2.1 The Volumetric Strains

The volumetric strain-mean normal stress relationships for all the three densities tested are plotted on natural log scale in Figures (7-2), (7-3) and (7-4) and a summary of the test results is shown in Table (7-1).

---

* In all tests the maximum stress level was achieved when the applied cell pressure reached 650 psi.

The isotropic consolidation and swelling lines (i.e. $\sigma'_1 / \sigma'_3 = 1$) are shown for the dense and loose samples only. On reloading the samples, on the same stress path as the first loading cycle, the volumetric strains followed lines which are nearly identical with those of unloading. The volumetric strain lines on reloading are not plotted in the figures to avoid confusion but they will be discussed in a later section.

For each density state, the volumetric strain lines on first loading are parallel and straight, lying close to each other for the range of stress ratio considered. At low values of mean normal stress there are discrepancies in the results, because of the influence of the rubber membrane penetration and variation in the porosities. For each state of density, the maximum volumetric strain obtained at the end of the consolidation stage varies from one test to another. This is because of the varying maximum mean normal stress ($\acute{p}$) applied during consolidation of the samples.

It was observed that the difference in ϵ_v values of various constant stress ratio tests increases as the porosity increases. But still this difference in ϵ_v values does not change the general feature of the volumetric strain lines either on loading or on unloading. Therefore it can be concluded that the volumetric strain lines on first loading for constant stress ratio consolidation tests are straight and parallel to one another. This may not be valid for stress ratios more than 3.0. A mathematical expression could be derived for the volumetric strains during first consolidation as follows:

$$\ln \epsilon_{v2} - \ln \epsilon_{v1} = \bar{\lambda} (\ln p'_2 - \ln p'_1) \tag{7.1}$$

after rearrangement

$$\epsilon_{v2} = \epsilon_{v1} \left(\frac{p'_2}{p'_1} \right)^{\bar{\lambda}} \tag{7.2}$$

or in short form as:

$$\epsilon_v = D_1 (\acute{p})^{\bar{\lambda}} \tag{7.3}$$

where D_1 is the volumetric strain which corresponds to mean normal stress of 1 psi and ($\bar{\lambda}$) is the slope of the volumetric strain path (on natural log. scale); both (D_1) and ($\bar{\lambda}$) are on first loading.

On unloading, the volumetric strain lines do not lie close to each other as in the loading case, because the maximum mean normal stress from which the unloading started varies from one test to another. It can be seen here that the volumetric strain lines on unloading for constant stress ratio tests are straight and parallel to one another. Again, this statement may not be valid for stress ratios more than 3.0. A mathematical relationship for the volumetric strains on unloading could be derived in the same way as for the loading stage. This expression in its final form is:

$$\epsilon_{v2} = \epsilon_{v1}\left(\frac{p'_2}{p'_1}\right)^{\overline{K}} \qquad (7.4)^*$$

or in a short form as

$$\epsilon_v = D_2\,(p')^{\overline{K}} \qquad (7.5)$$

where D_2 is the volumetric strain which corresponds to mean normal stress of 1.0 psi and $(\overline{K})$ is the slope of the volumetric strain path (on natural log. scale); both (D_2) and $(\overline{K})$ are on unloading or reloading.

The volumetric strain lines on loading and unloading for the tests at each state of density are averaged by a single curve which is replotted in Figure (7-5). It is seen from the figure that the volumetric strain lines on loading and unloading form a family of parallel straight lines for all states of density.

Values of the coefficients D_1 and D_2 which represent the volumetric strains at $p'_1 = 1.0$ psi on first loading and on unloading respectively were obtained from this Figure (7-5) and are plotted against the corresponding porosities in Figures (7-6a) and (7-6b). Therefore with the aid of these figures and knowing the parameters $\overline{\lambda}$ and $\overline{K}$, the volumetric strains on loading and unloading could be predicted.

For this granite material and up to the maximum stress ratio examined the values of the parameters $\overline{\lambda}$ and $\overline{K}$ are 0.441 and 0.122 respectively; these are estimated from Figure (7-5).

---

* Note that the values of the terms in this expression are different from those in eq. (7.2) although the same suffixes are used.

7.2.2.2 The Shear Strains

It has been pointed out at the beginning of this chapter that the shear strains for this series of tests are defined as:

$$\gamma = \frac{2}{3}(\epsilon_1 - \epsilon_3)$$

or $$= (\epsilon_1 - \frac{\epsilon v}{3})$$

where ϵ_v values have been recorded from volume change measurements using a burette. Errors due to rubber membrane penetration have not been eliminated from ϵ_v values which influenced the shear strain calculations. Therefore the shear strain values will not be accurate enough for a quantitative analysis in this section, especially at low constant stress ratios for loose samples. At low values of mean normal stress (lower than 60 psi) the influence of the rubber membrane penetration was significant, therefore γ values have not been plotted in the figures. At higher stress levels the rubber membrane penetration decreases, hence the γ values become more reliable.

The variations of the shear strains with the mean normal stresses on loading, unloading and reloading for each state of density tested are plotted in Figures (7-7) through (7-9). For comparison and analysis purposes, these relationships for all the samples tested are replotted in Figure (7-10).

The shear strain lines on loading are not all straight and parallel as was the case with volumetric strains. The slopes of the shear strain lines change as the stress ratio during consolidation changes. In fact the shear strains during isotropic consolidation (i.e. stress ratio of 1.0) are equal to zero and they should increase with the increase of the stress ratio during consolidation. Actually the shear strains are a function of the shear stresses.

An interesting point to be noted from Figure (7-10) is that the shear strain lines of tests consolidated at the same constant stress ratio but at different densities are parallel to each other*.

---

* Tests 3A, 6A and 9A are consolidated at constant stress ratio of 3.0 and tests 2A, 5A and 8A are consolidated at constant stress ratio of 2.04.

The influence of the porosity on the shear strains is quite clear in Figure (7-10). Loose samples underwent shear strains larger than dense ones consolidated under the same constant stress ratio.

At low values of mean normal stress negative shear strains have been observed; these have not been plotted in the figures. There are two explanations for measured negative shear strains. One is that the diameter of the sample is contracting at a greater rate than its length is contracting, therefore the term $(\epsilon_1 - \epsilon_3)$ will be negative. Another, is that the volume changes recorded are larger than the true values due to membrane penetration which in turn gives negative values of $(\epsilon_1 - \frac{\epsilon_v}{3})$. For this reason accurate volume change measurements or direct lateral deformation measurements are necessary.

Therefore at this stage of the experimental investigation no attempt will be made to present mathematical formulations for the shear strains on loading as was the case with the volumetric strains.

On unloading the shear strains for all the tests have been plotted in Figures (7-7) through (7-10). The shear strains on unloading are so small that they are too sensitive to the variations of the volume changes. Here the influence of the rubber membrane penetration is less than during the loading stage because after the first loading the rubber membrane had taken the shape of the sample surface and filled most of the voids between the particles near the surface. From Figure (7-10) it can be seen that the shear strain lines on unloading are nearly straight parallel lines for all the tests.

A mathematical relationship between the shear strains and the mean normal stresses could be formulated in a similar way to that for the volumetric strains on unloading. In its final form this expression is:

$$\gamma_2 = \gamma_1 \left(\frac{p'_2}{p'_1}\right)^{\alpha} \qquad (7.6)$$

or in a short form as:

$$\gamma = S\,(\acute{p})^{\alpha} \qquad (7.7)$$

where S is the shear strain on unloading which corresponds to mean normal stress of 1.0 psi for each constant stress ratio test and α is the slope of the shear strain line on unloading. In this formulation the influences of the stress ratio and the density are quite clear.

7.2.3 Analysis of the Elastic (recoverable) Deformations

7.2.3.1 The Elastic Volumetric Strains

It has been pointed out in Section (7.2.2.1) that the volumetric strain lines on reloading are identical with those on unloading. Hence it can be assumed that the volumetric strains on unloading and reloading are elastic since all the strains are recoverable. Variations of the volumetric strains on reloading with the mean normal stresses are plotted in Figure (7-11). It is clear from this figure that the volumetric strain lines of all the tests are nearly straight lines and parallel to each other. They are similar to those on unloading which are shown in Figure (7-5). Therefore equation (7.5) which was suggested for the unloading paths, could be applied here for the reloading paths, in other words it could be used to represent the elastic volumetric strains of the material. Hence the elastic volumetric strains will be:

$$\epsilon_v^{\,e} = D_2\,(\acute{p})^{\bar{K}} \qquad (7.8)$$

where D_2 is as defined in equation (7.5). The assumption of representing the volumetric strain lines of different constant stress ratio tests at a certain density by a single curve is also valid here. From Figure (7-11) a $\bar{K}$-value of 0.122 is estimated to represent the slopes of the volumetric strain lines of all the tests. This relationship between the elastic volumetric strains and the mean normal stresses for rockfill materials is different from the previous relationships suggested by other researchers, e.g. Cambridge research group; Namy (1970); Holubec (1966 and 1968).

Holubec (1966) from tests on Ottawa sand suggested that the elastic volumetric strains versus $\acute{\sigma}_3$ plots for various stress ratios

form closely spaced curves of parabolic shape. He suggested a mathematical expression in the form of:

$$\epsilon_v^e = d\,(\sigma_3' - 3)^{\frac{1}{2}} \qquad (7.9)$$

where the constant d is a function of the initial void ratio and the stress ratio of the particular anisotropic consolidation test.

Cambridge research group and Namy (1970) suggest that the relationship between the elastic volumetric strains and log. mean normal stresses for isotropic and anisotropic consolidation tests on clays form a family of straight parallel lines. These conclusions are different from what was observed for rockfill material in this thesis.

The last point which will be examined here is whether the elastic volumetric strain is a function of the mean normal stress or the confining pressure. To discuss this point, it is necessary to refer to Section (6.4) where cyclic loading tests under constant cell pressure were described. It was observed that the sample behaviour under repeated loading was not elastic after the first loading cycle, and that the volume changes of the sample were insignificant whereas ϵ_1 continued to rise. Here in this series of anisotropic consolidation tests the mean normal stress is varying due to change of the cell pressure and the axial stress to keep the stress ratio constant. Significant volume changes were observed during loading-unloading, in contrast to what was noted in the cyclic loading tests under constant cell pressure. Therefore it appears that the elastic volumetric strain is better defined along constant stress ratio path rather than constant cell pressure path.

7.2.3.2 The Elastic Shear Strains

It has been shown in Figures (7-7) through (7-9) that the shear strain lines on reloading are nearly identical with those on unloading except at the end of the consolidation stages where they start to move apart. During the last few stress increments the samples start to yield, i.e. they exhibit plastic deformations and if loading exceeded the previous maximum mean normal stress, larger deformations will take place.

This point will be discussed later on in Section (7.2.7). At this stage it can be stated that the samples' behaviour on unloading and reloading up to the previous maximum mean normal stress is nearly elastic. The shear strain lines on reloading for all the tests are replotted together in Figure (7-12). They are nearly straight and parallel. Some of the data are missing due to bursting of the rubber membranes; hence the shear strain paths are represented by broken lines. Equation (7.7) which was derived for the shear strains on unloading could be adopted here to represent the elastic shear strains as follows:

$$\gamma^e = S\,(p')^{\alpha} \qquad (7.10).$$

where the coefficient S is the same as was defined in equation (7.7). From Figure (7.12) the α value is estimated by 0.088 to represent all the tests in the series.

Another interesting point which can be seen in Figure (7-12) is that the shear strain lines do not lie close to each other as was the case of the volumetric strain lines. Therefore a single value of S to represent various constant stress ratio tests at a certain density cannot be suggested here.

Many conclusions have been stated concerning the significance of the elastic shear strains. Schofield and Wroth (1968) suggested that the elastic shear strains for Granta-gravel and Cam-clay models are equal to zero. Most of Cambridge research group agree on this assumption and apply it in their stress-strain formulations*. Namy (1970) for anisotropic consolidation tests on Newfield clay observed that the elastic shear strains are insignificant compared to the total shear strains. Lewin and Bursland (1970) from tests on powdered slate dust concluded that the elastic shear strains are negligible.

From this series of tests and the tests on other materials presented in the following sections, it can be stated that the elastic shear strains are really insignificant compared to the shear strains which occur during the first loading.

---

* For example, Roscoe, Schofield and Thurairajah (1963a) and Roscoe and Poorooshasb (1963).

7.2.4 The Plastic Strain Increment Vectors

7.2.4.1 Basic Considerations

In this section the stress space will be represented by the parameters p' and q which have been defined earlier. To plot the plastic strain increment vectors, the components of the strain space ϵ_v^p and γ^p are plotted on the stress space for each stress point under consideration. Therefore for each stress increment a strain increment vector could be plotted on the same plot. The plastic strain increment vectors for various constant stress ratio tests will be presented in the next section.

It has been shown in Chapter 3 that the plastic components of the strain increments are expressed by the following equations:

$$d\epsilon_v^p = d\epsilon_v - d\epsilon_v^e$$

and

$$d\gamma^p = d\gamma - d\gamma^e$$

It has also been shown in the previous section that the elastic component of the shear strain is very small compared to the total shear strain occurring during the first loading. Besides that there are errors due to membrane penetration. For these reasons the plastic component of the shear strain will be assumed equal to the total shear strain, i.e

$$d\gamma^p = d\gamma \qquad (7.11)$$

This assumption is similar to that suggested by Schofield and Wroth (1968) for Granta-gravel and Cam-clay models and also similar to that accepted by other workers as pointed out in the previous section.

With regard to the elastic component of the volumetric strain increment, the problem is more difficult than that for the shear strain increment. It has been shown in Section (7.2.3.1) that there are considerable elastic volumetric strains. But more than this they are small in comparison to the overall volume changes and the effect of the rubber membrane penetration is more significant than the elastic

strains and so in the following analysis the elastic volumetric strains will be discounted.*

This assumption is similar to that proposed by Schofield and Wroth (1968) for Granta-gravel model. Actually, such an assumption will only cause a small decrease in the slope of the plastic strain increment vectors throughout the constant stress ratio path†. Therefore such an assumption seems not unreasonable for the present discussion; the direction of the plastic strain increment vectors. Also in this section of the thesis the strain vectors above p' of 50 psi will only be discussed to avoid the influence of the membrane penetration. Hence the plastic component of the volumetric strain increment will be expressed as:

$$d\epsilon_v^p = d\epsilon_v \qquad (7.12)$$

The assumptions proposed here, i.e. $d\epsilon_v^e = d\delta^e = 0$, will be used only in this section of the thesis, while direct measurement of the elastic components will be attempted in the following sections.

7.2.4.2 Test Results

The plastic strain increment vectors (PSIVs) along the constant stress ratio paths and along the shearing paths for all the tests are plotted in Figures (7-13) through (7-15). The PSIVs form acute angles with both the constant stress ratio paths and the drained shearing stress paths.

Along the constant stress ratio paths the angles (i.e. the angles between the PSIVs and the stress path) are larger at the beginning of the anisotropic consolidation stage, then they become smaller gradually as the stress level, p', increases. In other words the PSIVs rotate anti-clockwise along every anisotropic consolidation line for all states of

---

* Influence of the rubber membrane decreases with the increase of the cell pressure.

† Because the consolidation and swelling lines have gradients of the same sign.

density. Also along all the anisotropic consolidation lines the PSIVs remain on the right hand side without crossing to the other side. The variation of the slopes of the plastic strain increment vectors along every constant stress ratio consolidation path, with the mean normal stress for all the tests has been plotted in Figure (7-16). It can be seen from this figure that the magnitude of the angle between the PSIV and the stress path decayed smoothly as the stress level increased.

Along the drained shear paths the PSIVs are also larger at the beginning of the shearing stages then as the shearing continues they rotate anticlockwise until the samples reach the failure stage. At failure (or just before failure) the PSIVs become coincident with the direction of the shearing paths. This was observed for all the states of density. Direction of the PSIVs at failure is outside the scope of this thesis but willbe referred to briefly during the discussion.

The PSIVs along the various stress paths for each state of density are plotted together, Figures (7-17) through (7-19). For each state of density the drained shearing paths of various tests converge and meet at a common point then continue on one path until failure. These common points are denoted by N_1, N_2 and N_3 for all the three densities tested. At each of these common points the PSIVs, due to different stress paths*, have different directions. But along each common drained shear path (i.e. the path after various drained shear paths had met at a common point) the direction of the PSIVs of various stress paths became nearly identical until failure where all the PSIVs are coincident with the direction of the shearing path.

7.2.4.2 Discussion of Results

In this section the discussion will be concentrated on the direction of the plastic strain increment vectors in five positions along the stress paths followed in this series of tests.

---

* Each common point is approached by three drained shear paths. Unfortunatel a few paths are not plotted due to the bursting of the rubber membranes.

(a) Along various constant stress ratio paths

Test results presented in the previous section show that the plastic strain increment vectors rotate in an anticlockwise direction along every stress path as the stress level increases. This unique rotation is a function of the mean normal stress, Figure (7-16). This observation contradicts Holubec's (1966) findings for Ottawa sand which indicate that the plastic strain increment vectors have a constant gradient along the constant stress ratio paths. It should be remembered that Ottawa sand particles are much stronger than those of granite rockfill and the maximum mean normal stress applied by Holubec was up to 220 psi only.

Most of the other workers in this field of study were concerned with the plastic strain increment vectors at a certain stress point approached by different stress paths and neglected the feature of the plastic strain increment vectors along these paths. Lewin (1972, 1973) in tests on powdered slate dust assumed that the PSIVs along constant stress ratio paths have constant slope, thus he formulated a relationship between the direction of the PSIVs and the directions of the stress paths. Namy (1970) in tests on overconsolidated Newfield clay observed a rotation of the PSIVs along the constant stress ratio paths while such behaviour has not been observed on normally consolidated clay.

From Figure (7-16) it seems there is no relation between the rotation of the plastic strain increment vectors of various constant stress ratio paths. In other words construction of plastic potentials, as suggested by some researchers*, seems unreasonable for rockfill materials.

(b) At points where the stress paths rotate from the constant stress ratio direction to the shearing direction.

These points are denoted by M_2 to M_9 in Figures (7-13),(7-14) and (7-15). Actually loading a sample along the drained shear path corresponds to applying a stress probe in that direction. It is seen

---

* e.g. Roscoe and Poorooshasb (1963); Holubec (1966); Lewin (1972, 1973).

from Figures (7-13),(7-14)and (7-15) that the resulting plastic strain increment vector from a drained shear loading increment has a direction different from that of the last strain increment along the constant stress ratio path. Therefore it can be concluded that rotation of the stress increment vector causes rotation of the resulting plastic strain increment vector. Or in other words, the direction of the plastic strain increment vector is dependent on the direction of the stress increment vector.

These findings are in agreement with those observed by Lewin and Burland (1970) in tests on powdered slate dust, although they used small magnitude stress probes compared to the drained shear stress path used in this thesis. The magnitude of the stress probe is an important factor in determining the direction of the plastic strain increment vectors. However, contradictory findings have been reported by Holubec (1966) in tests on Ottawa sand. He observed that the direction of the plastic strain increment vector is independent of the direction of the stress increment and is dependent only on the current stress. The stress probes applied by Holubec were in directions which form continuation of the main stress paths leading to the point under consideration. In this thesis the stress increments have directions different from those of the main consolidation stress paths. However, these points will be discussed in detail in the second stage of this experimental study.

(c) At points where various drained shear paths meet.

These points are denoted by N_1, N_2 and N_3 in Figures (7-17), (7-18) and (7-19) respectively. Another set of points could have been obtained at lower stress levels but unfortunately tests No. 1A and 4A were stopped because of bursting of the rubber membranes. The plastic strain increment vectors at each point, resulting from stress increments along various stress paths, have different directions. In fact each of these points N_1, N_2 and N_3 represented a stress point approached by different stress paths. Therefore it can be concluded that the plastic strain increment vectors at these stress points are path dependent.

Similar behaviour has been observed by Lewin and Burland (1970) in powdered slate dust and by Namy (1970) in Newfield clay. However Holubec (1966) and Poorooshasb et al (1966 and 1967) observed contrary behaviour in Ottawa sand. They concluded that the plastic strain increment vector at a certain stress point, in Ottawa sand, is path independent. It should be noted that there are four main differences between Holubec's tests and the tests of this project; these are: type of material tested, stress paths followed, magnitude of the stress increments applied, and the stress level of the points under consideration.

(d) Along the common drained shear paths beyond points N_1, N_2, N_3

It is seen from Figures (7-17), (7-18) and (7-19) that the drained shear paths of tests consolidated at σ'_1/σ'_3 of 2.04 and 3.0 at each state of density had converged and met at points N_1, N_2 and N_3, then they continued together till failure. The plastic strain increment vectors of various tests along this common drained shear path have nearly the same direction. This is shown clearly in Figures (7-17) and (7-18). It seems that the stress history of the samples had little effect on these plastic strain increment vectors along this part of the stress path. This is in the case of the present simple stress path but it is not known what the situation would be if complicated stress paths were followed.

(e) At failure stages

The direction of the plastic strain increment vectors at failure for all the tests becomes nearly identical with the direction of the corresponding drained shear paths irrespective of the stress history or the density of the samples. Lade and Duncan (1973) carried out tests on Monterey sand in a cubical triaxial apparatus. Their test results showed that the directions of the strain increment vectors at failure form acute angles with the failure surfaces in the triaxial plane for both dense and loose sand. Also it was found that the projections of the plastic strain increment vectors on the octahedral plane are perpendicular to the trace of the failure surface in that plane.

7.2.5 Errors Involved in Strain Measurements

Deformations of the samples during pre-failure stage were the main purpose of the investigation carried out in this chapter. Therefore accurate measurement of the deformations was essential for the analysis and discussion here.

Axial deformations were measured by a dial gauge to an accuracy of $\pm$ .0005 in., which is accurate enough for this investigation. Calculations of the axial strains were based on the assumption that the samples were deforming uniformly throughout the tests. Actually the axial strains are not uniform throughout the height of the sample because of the restraint at the ends of the sample, rubber membrane and other factors.

The triaxial apparatus for testing $1\frac{1}{2}$ in. diameter samples available in the Imperial College soils laboratory is not fitted with a device to measure directly the radial deformations. Hence shear strains were calculated on the basis of the volume changes and axial deformations measurements. Volume changes were measured by a glass burette connected to the sample and the amount of the expelled water was taken as a basis for calculation. Such measurements are liable to an error due to rubber membrane penetration. Many methods have been suggested to assess the amount of membrane penetration but all these methods are approximate and are based on extrapolations which involve errors.

Accurate strain measurements were needed to analyse the results discussed in the following sections, therefore a new apparatus and testing technique were developed. A device to measure directly the radial deformations was developed and a free end restraint arrangement was used. They are described in Chapter 4. Therefore the errors involved in the deformation measurements presented in the following sections are small. However, the conclusions arrived at in the previous sections are still valid and will not be affected by the errors involved in the deformation measurements.

7.2.6 Shearing the Samples to Failure

It has been pointed out that the aim behind carrying out the anisotropic consolidation tests is to investigate the deformations during pre-failure stage and shearing the samples to failure came as a secondary aim. Some of the samples failed to reach failure due to bursting of the rubber membranes and have not been repeated. The available results at failure will be discussed in the following sections.

After the samples were reconsolidated to the previous maximum mean normal stress reached in the first loading cycle, the cell pressure was kept constant at that level then the samples were sheared to failure under drained conditions. A summary of the test results is shown in Table (7-1) and the stress-strain curves are plotted in Figures (7-20) through (7-22). It should be noted here that the stress history of these samples is different from those discussed in Chapter 6, therefore the discussions and conclusions reached in that chapter are not valid here.

7.2.6.1 The Shearing Strength

In this series of tests there are two variable factors which are influencing the shear strength and deformation characteristics of the samples. The first is the stress ratio (σ'_1 / σ'_3) under which the samples were consolidated and the second is the initial density of the samples.

For the dense state* the angle of shearing resistance of sample No. 2A consolidated under a stress ratio of 2.04 was 2.1 degrees higher than that of sample No. 3A consolidated under a stress ratio of 3.0. In the loose state+ the corresponding difference was approximately 1.7 degrees. It seems that the angle of shearing resistance decreases as the constant stress ratio, at which the sample was consolidated, increases.

---

* n = 26.0% - 26.6%

\+ n = 32.4% - 35.2%

This is shown clearly in Figure (7-23a) where the values of the constant stress ratio during consolidation are plotted against the corresponding values of the angle of shearing resistance. Values of the angle of shearing resistance corresponding to constant stress ratio of 1.0 are taken from Chapter 6.

Inspecting the stress-strain curves plotted in Figures (7-20), (7-21) and (7-22) it can be seen that with the samples consolidated under the same constant stress ratio and to the same maximum mean normal stress, the dense ones exhibit higher angle of shearing resistance than the loose ones. To show such a relationship clearly, the values of the angle of shearing resistance against the corresponding porosities for samples consolidated under constant stress ratios of 1.0, 2.04 and 3.0 are plotted in Figure (7-23b). There is an indication that a similar trend in behaviour during shearing exists for both isotropically and anisotropically consolidated samples. However, it is not known whether such a relationship is valid or not for samples consolidated at constant stress ratios more than 3.0.

7.2.6.2 The Volumetric Strains at Failure

Values of the volumetric strains at failure for various constant stress ratio tests are reported in Table (7-1). It should be noted that those volumetric strains were calculated on the basis of the initial dimensions of the samples, while those reported in Chapter 6 are based on sample dimensions after consolidation.

For the dense samples the value of the volumetric strain at failure decreased from -13.9% to -12.3% when the constant stress ratio during consolidation increased from 2.04 to 3.0. The volumetric strain at failure for dense samples consolidated isotropically (i.e. stress ratio of 1.0) at σ'_3 of 600 psi then sheared drained was -16.8% *. Therefore the value of the volumetric strain at failure for the dense samples decreases as the stress ratio during consolidation stage increases.

---

* This figure has been obtained from Test No. 27 in Chapter 6, after recalculation on the same basis adopted for the anisotropic tests.

Similar behaviour was observed for the loose samples. The value of the volumetric strain at failure decreased from -22.2% to -18.6% when the constant stress ratio during consolidation increased from 2.04 to 3.0. The value of the volumetric strain at failure for a loose sample consolidated isotropically at σ'_3 of 600 psi then sheared drained was -22.7%*. Therefore it seems that the value of the volumetric strain at failure for loose samples decreases as the stress ratio during consolidation stage increases.

Figure (7-24a) shows the variation of the volumetric strains at failure with the stress ratios during consolidation for both the dense and the loose samples. The straight lines plotted in this figure are just an approximation for the results and more tests need to be done in this field.

As far as the influence of the porosity is concerned, it seems its influence is similar to that described for the tests in Chapter 6. The volumetric strain at failure increases with the increase of the porosity for any stress ratio applied during consolidation stage within the stress range tested. However, it is not clear what the behaviour would be if lower confining pressures were used.

7.2.6.3 The Axial Strains at Failure

For the dense samples the value of the axial strain at failure decreased from 14.8% to 12.4% when the stress ratio during consolidation increased from 2.04 to 3.0. The axial strain at failure for the dense sample consolidated isotropically then sheared drained at σ'_3 of 600 psi was 18.1%†. Loose samples also showed a similar trend in behaviour. Values of the axial strain at failure decreased from 21.2% to 19.3% when the stress ratio during consolidation increased from 2.04 to 3.0. The ϵ_{1f} value for a loose sample consolidated isotropically then sheared drained at σ'_3 of 600 psi was 25.5%+.

---

* This is obtained from Test No. 60, Chapter 6, and recalculated as pointed out for the dense samples.

† Test No. 27, Chapter 6.

+ Test No. 60, Chapter 6.

Figure (7-24b) shows the variation of the axial strain at failure with the stress ratio during consolidation stage for dense and loose samples. It can be seen from this figure how the ϵ_{1f} values for both loose and dense materials decrease as the stress ratio during consolidation stage increases. But it is not clear what the behaviour would be at higher stress ratios especially near the failure lines.

The influence of the density on the axial strain at failure is similar to that described in Chapter 6. The axial strain at failure increases with the increase of the porosity for all values of the stress ratio applied during consolidation stage within the range tested.

7.2.6.4 Rate of Dilatancy at Failure

Both dense and loose samples consolidated anisotropically then sheared drained at constant cell pressure exhibited approximately similar rate of dilatancy at failure. Values of the rate of dilatancy at failure range from -0.143 to -0.151 with an average of -0.15. Within the ranges of density and pressure tested it seems that the stress ratio during consolidation stage has insignificant influence on the rate of dilatancy at failure.

Dense and loose samples consolidated isotropically then sheared drained at σ'_3 of 600 psi gave values of dilatancy rate at failure of zero and -0.08 respectively. At this stress level (i.e. σ'_3 = 600 psi) particles undergo heavy breakage and values of dilatancy rate at failure obtained from all the tests ranged from zero to -0.15. Therefore at this high stress level it is difficult to investigate the influence of the stress ratio during consolidation on the dilatancy rate at failure. Such behaviour is better investigated at lower confining pressures.

7.2.7 Conclusions

The deformations of samples consolidated at various constant stress ratios have been described and discussed in the previous sections. The results of these tests show that first loading produces large irrecoverable volumetric and shear strains while unloading and reloading give reasonable strain recovery, i.e. this path is nearly elastic in behaviour. However, the shear strain values are less reliable than the volumetric strain values due to the errors pointed out in a previous section. Thus there is obvious need for better lateral strain (ϵ_3) measurements to investigate properly the deformations of soils.

However, these constant stress ratio tests are considered as pilot tests in this programme. These pilot tests give an indication that a linear relationship between the void ratio (e) and $\ln p'$ with slope independent of the constant stress ratio (R) is not applicable here for granite rockfill. An alternative relationship has been suggested for rockfill material; this is in the form of:

$$\epsilon_v = D_1 (p')^{\bar{\lambda}} \qquad (7.3)\text{ bis}$$

where $\bar{\lambda}$ is the slope of the $\ln \epsilon_v$ vs. $\ln p'$ line which is independent of the density and the range of stress ratio used in this programme, and D_1 as defined earlier.

For the shear strains the case is more complicated. A relationship similar to that represented by Eq. (7.3) may not be valid.

It has been shown that unloading and reloading give good repeatability, i.e. all the strains are nearly recoverable. Therefore the sample behaviour is nearly elastic, and for this elastic behaviour, relationships have been suggested in the following form:

Elastic Volumetric Strains $\epsilon_v^e = D_2 (p')^{\bar{K}}$ (7.8) bis

Elastic Shear Strains $\gamma^e = S (p')^{\alpha}$ (7.10) bis

where the terms in the equations have been defined in earlier sections.

However, these conclusions might not be valid for stress ratios more than 3.0. For example El-Sohby (1969) observed that the compressibility of dense and loose sand samples increased as the stress ratio during consolidation increased. Then as the stress ratio increased further, the compressibility decreased and at R = 4.5 dense samples exhibited negative compressibilities (i.e. dilatancy). To clarify this point further the volumetric strains of the granite samples tested in this thesis are plotted against the mean normal stress in a plot similar to that of El-Sohby, Figure (7-25). From this figure it appears that up to the stress ratio tested, some of the samples were dilating during the anisotropic consolidation. But it is not known what the case would be at stress ratios higher than 3.0.

In conclusion, the Cam-clay model type is not obeyed here in rockfill material, i.e. the $e - \ln \acute{p}$ linear relationship is not valid. However $\ln \grave{e}$ varies linearly with $\ln \acute{p}$ and a nearly elastic behaviour is achieved for constant stress ratio unloading and reloading paths. If the remainder of the Cam-clay type of model is to remain intact then there must be an elastic domain which can be defined. The pilot tests showed that the behaviour of the rockfill samples on unloading and reloading under constant stress ratio paths is nearly elastic. What must now be established is the behaviour under other compound or complicated stress paths. This will be discussed in the following sections.

The plastic strain increment vectors along the constant stress ratio paths rotate in an anticlockwise direction as the stress level increases. Therefore the plastic potentials are not expanding symmetrically as the stress level increases. It appears that the plastic potentials are path dependent and do not form surfaces of revolution about any stress axis, as suggested by the Cambridge research group; Holubec (1966); Lewin (1972). This point can also be noted from the slopes of the volumetric and shear strain lines. Actually there is no relation between the slopes of the volumetric strain lines and the shear strain lines neither in magnitude nor in direction. Thus the direction of the resulting plastic

strain increment vectors may vary along the constant stress path as the pressure increases.

Another interesting point which has been concluded in this part of the programme is that the direction of the plastic strain increment vector at a certain stress point is dependent on the stress path and direction of the stress increment. This is in agreement with the findings of Lewin and Burland (1970) and in contradiction to that of Holubec (1966). This will be discussed in more detail in the following sections.

7.3. The Special Stress Path Tests

7.3.1 Testing Programme

In this part of the experimental programme three series of tests have been carried out, the first on granite rockfill, the second on marble chippings and the third on Ham River sand. The stress paths followed were similar for all three materials. Each series consists of three tests and each test has two separate parts. The programme of the tests is described as follows:

Granite Rockfill

Test No. 1G First Part

1. The sample was consolidated isotropically to a maximum cell pressure of 120 psi, then unloaded, also isotropically, to a zero cell pressure. The cell pressure was applied at levels of 0, 5, 10, 15, 20, 30, 40, 60, 80, 100 and 120 psi. Then the sample was reloaded isotropically to the previous maximum cell pressure of 120 psi using the same pressure increments.

2. The sample was sheared under drained conditions at a constant cell pressure of 120 psi to a maximum stress ratio, σ'_1/σ'_3, of 3.0. At this stress level, point A in Figure (7-26), the mean normal stress was 200 psi.

3. The stress difference ($\sigma'_1 - \sigma'_3$) was kept constant and the cell pressure was increased by two increments to 140 psi. This increase in the mean normal stress while the stress difference is constant will be called "stress probing". The 140 psi cell pressure is the maximum pressure for the perspex cell. Then the sample was unloaded on the same stress path to point A where $\sigma'_1 = 3\sigma'_3$; i.e. the stress probe was removed.

4. The sample was then unloaded on the same drained shear path described in step (2) to an equal all round pressure of 120 psi.

5. Finally the sample was unloaded isotropically to zero cell pressure.

Test No. 1G Second Part

1. The sample was consolidated anisotropically at a stress ratio of 3.0 to a mean normal stress of 200 psi. Then it was unloaded anisotropically to zero cell pressure on the same loading path.

2. The sample was reloaded anisotropically as described in the previous step to a mean normal stress of 200 psi, point A in Figure (7-26).

3. The stress difference ($\sigma'_1 - \sigma'_3$) was kept constant and the cell pressure increased to 140 psi. Then the sample was unloaded along the same stress path to point A where $\sigma'_1 = 3\sigma'_3$. This stress probing is the same as described in step (3) of part 1.

4. Finally, the sample was unloaded anisotropically on a stress path of $\sigma'_1 / \sigma'_3 = 3.0$ to zero cell pressure.

Test No. 2G First Part

The loading and unloading steps followed in this part are exactly the same as those of the second part of Test No. 1G i.e. steps (1), (2), (3) and (4).

Second Part

In general this part is similar to the first part of Test No. 1G.

1. The sample was consolidated isotropically to a maximum cell pressure of 120 psi using stress levels as described in step (1) of part 1, Test No. 1G. Then it was sheared under drained conditions at a constant cell pressure of 120 psi to a maximum stress ratio of 3.0. At this stress level, point A in Figure (7-26), the mean normal stress was 200 psi.

2. The sample was unloaded on the same stress path described in the previous step to zero cell pressure.

3. The sample was loaded isotropically to a maximum cell pressure of 120 psi then sheared at constant cell pressure to a maximum stress ratio of 3.0, exactly as described in the first step.

4. The stress difference ($\sigma'_1 - \sigma'_3$) was kept constant and a stress probe of 20 psi was applied, as described in step (3) of part 1, Test No. 1G. Then the sample was unloaded on the same stress path to point A where $\sigma'_1 = 3\,\sigma'_3$.

5. Finally the sample was unloaded on a drained shear path to an all round pressure of 120 psi where the unloading continued isotropically to zero cell pressure.

Test No. 3G First Part

1. The sample was consolidated to a maximum cell pressure of 120 psi, unloaded to zero cell pressure then subsequently reloaded to the previous maximum cell pressure; the stress path being isotropic throughout.

2. σ'_1 was kept constant at a level of 120 psi and the cell pressure was reduced to a stress ratio of 3.0; i.e. point D in Figure (7-27). Then the cell pressure was increased on the same path to 120 psi; i.e. $\sigma'_2 = \sigma'_3 = 120$ psi.

3. The unloading-loading path described in the previous step was repeated once more. At the end of this stage the sample was under an all round pressure of 120 psi.

4. Finally the sample was unloaded isotropically to zero cell pressure.

Second Part

1. The sample was consolidated anisotropically at a constant stress ratio of 3.0 to a mean normal stress of 66.7 psi, i.e. point D in Figure (7-27). This is the same point to which the sample was unloaded anisotropically in part 1 of this test. From point D the sample was unloaded anisotropically to zero cell pressure.

2. Finally the loading-unloading path described in step (1) was repeated to the same previous maximum mean normal stress of 66.7 psi.

Marble Chippings

Test No. 1M

This test is the same as Test No. 1G, except in a few points. Therefore the stress path of this test will not be described in detail.

First Part

1. The sample was loaded, unloaded then reloaded isotropically to a maximum cell pressure of 120 psi.

2. The sample was sheared under drained conditions at a constant cell pressure of 120 psi to a maximum stress ratio of 3.0. Then it was unloaded on the same stress path to an all round pressure of 120 psi.

3. The sample was reloaded along the drained shear path to point A where the mean normal stress was 200 psi. The stress difference was kept constant and a 20 psi stress probe was applied, as described in step (3), part 1 of Test No. 1G. Then the sample was unloaded to point A.

4. The sample was unloaded on the same drained shear path described in step (2) to an all round pressure of 120 psi.

5. Finally the sample was isotropically unloaded to zero cell pressure.

Second Part

This part is similar to the second part of Test No. 1G. Briefly, it is anisotropic loading-unloading in the first cycle, then anisotropic loading followed by a stress probe and finally unloading on the same path as that for loading.

Test No. 2M First Part

This part is exactly the same as the first part of Test No. 2G and is also similar to the second part of the previous test, No. 1M.

Second Part

1. The sample was loaded, unloaded then reloaded isotropically to a maximum cell pressure of 120 psi, then it was sheared drained at this constant cell pressure to a stress ratio of 3.0. Then it was unloaded to

an all round pressure of 120 psi and reloaded on the same drained shear path to the previous stress ratio of 3.0.

2. A stress probe of 20 psi was applied, as explained in the previous tests. Then the sample was unloaded to point A where the stress ratio is equal to 3.0.

3. Finally the sample was unloaded along the drained shear path to an all round pressure of 120 psi, then subsequently unloaded isotropically to zero cell pressure.

Test No. 3M

This test is exactly the same as Test No. 3G.

Ham River Sand

Test No. 3S

This has not been carried out due to reasons which will be explained later. The results of such a test are expected to be the same as those of tests 3G and 3M.

Schematic diagrams for all the tests carried out are shown on the volumetric strain versus mean normal stress plots at the end of the chapter.

7.3.2 The Total Deformation of the Samples Tested

7.3.2.1 Deformation of the Granite Rockfill Samples

Test No. 1G

The volumetric strains are plotted against the mean normal stresses in Figure (7-28). During the first isotropic loading cycle to a maximum mean normal stress of 120 psi the sample volume decreased by 2.28% on a non-linear strain path. On unloading, the volume stayed nearly constant at the beginning then increased non-linearly to a volumetric strain of 1.03%. On reloading, the sample volume decreased non-linearly with p' on a strain path close to that on first unloading. The value of the volumetric strain on reloading at maximum mean normal stress was 2.4% compared to 2.28% at the end of the first loading. Therefore it seems that the

volumetric strain of the sample at the end of the second loading cycle was nearly the same as at the end of the first loading cycle.

At this mean normal stress of 120 psi the cell pressure was kept constant and the sample was sheared under drained conditions to a maximum stress ratio of 3.0. As the shearing started there was a large sudden decrease in the volume of the sample compared to the isotropic consolidation stage. This indicates that a large distortion occurred due to the change of the stress path direction. At mean normal stress of 200 psi, the deviator stress was kept constant and a stress probe of 20 psi was applied. There was a small volume decrease at the beginning of the application of the stress probe then the volumetric strain curve started to level off at the end of the stress probing. The value of the volumetric strain at mean normal stress of 220 psi was 3.67%. On unloading on the same loading path, there was a small volume increase and at mean normal stress of 120 psi, the volumetric strain was 3.36%. During unloading isotropically, the shape of the volumetric strain curve was almost similar to that of the first isotropic unloading cycle. The volumetric strain attained by the sample at the end of the unloading stage was 1.84%.

In the second part of the test, the sample was consolidated anisotropically at a stress ratio of 3.0 to a maximum mean normal stress of 200 psi. All the volumetric strain values during the anisotropic consolidation were higher than those during the unloading stage of the first part of the test. On unloading, the sample volume started to increase at a small rate up to a mean normal stress of 80 psi, after which the rate of the increase was higher. At the end of the unloading stage the volumetric strain was 1.92% which is slightly less than that at the beginning of the anisotropic loading. On the second anisotropic loading cycle the volumetric strains followed a path which falls below the first loading path and almost parallel to it up to mean normal stress of 200 psi. The volumetric strain value at this stress level was just 0.05% higher than the value attained by the sample at the end of the first anisotropic loading cycle. Then the deviator stress was kept constant and a

stress probe of 20 psi was applied. There was a very small volume decrease and it is less than that which occurred during the first stress probe. The volumetric strain value at 220 psi maximum mean normal stress was 3.38%. On subsequent unloading, the volumetric strains followed a path parallel to the unloading path of the previous unloading cycle. The final volumetric strain value at the end of the unloading was only 0.06% less than that at the end of the first loading cycle. In fact the volumetric strain paths of the second part of the test were close to each other.

The shear strains are plotted against the mean normal stresses in Figure (7-29). On the first loading cycle the shear strains were zero and on the first unloading cycle there was small accumulated shear strain measured at the end of the unloading stage. This may be due to anisotropy during setting up the sample. Measuring the changes of the sample height by lowering the load cell on top of the sample causes some disturbance which might influence the shear strain measurements. And since no device has been developed for measuring the sample height internally, the axial strains were taken as equal to the lateral strains during the isotropic consolidation and swelling stages. The experimental data showed that this assumption is not unreasonable. After the isotropic reloading cycle, the sample was sheared drained as described earlier. Large shear strains occurred which reached 1.28% at p' of 200 psi. During the application of the stress probe, a further 0.25% shear strain occurred. On unloading no shear strains were recovered until p' reached 180 psi, where gradual shear strain recovery started to occur. At p' of 120 psi the shear strain value was 1.15% and during isotropic unloading, the change in the shear strain was zero.

On the first anisotropic loading-unloading cycle, the irrecoverable shear strains were much less than those during the first part of the test. Up to mean normal stress of 50 psi there were large shear strains and above that stress level the shear strains increased, but at a slower rate. During the subsequent loading-unloading cycle the shear strain paths were nearly parallel to those of the first cycle. Actually the reloading shear

strain path of the second cycle was quite close to that of the unloading path of the first cycle. The final shear strain after the ending of the test was 1.5%.

The amount of the irrecoverable shear strain occurring during the application of the stress probe in the second part of the test was very small compared to that occurring during the application of the stress probe in the first part of the test.

Test No. 2G

The volumetric strains are plotted against the mean normal stresses in Figure (7-30). On the first anisotropic loading at a stress ratio of 3.0, the volumetric strains followed a non-linear path up to the maximum mean normal stress of 200 psi. On unloading anisotropically part of the volumetric strain was recovered and at complete unloading the ϵ_v value was 0.94%. On reloading, the volumetric strain path was close to that for the first unloading cycle which indicates that no additional plastic deformations are taking place. At 200 psi mean normal stress, the ϵ_v value was only 0.06% higher than the value attained by the sample on first anisotropic loading cycle. Then the deviator stress was kept constant and a stress probe was applied. A significant volumetric strain occurred (1.7%) which indicates a distortion of the sample due to the stress probing. On unloading, the volumetric strains due to the stress probe were recovered and on subsequent anisotropic unloading, the volumetric strains followed a path parallel to that of the first unloading cycle. The final ϵ_v value was 1.23%.

In the second part of the test the sample was first consolidated isotropically. The volumetric strains followed a path nearly parallel to that of the second anisotropic unloading cycle. On shearing at a constant cell pressure of 120 psi, a distortion occurred and the volumetric strains followed a path different from that of the anisotropic loading cycle. At a maximum mean normal stress of 200 psi, the sample was unloaded and part of the volumetric strains were recovered. Then the sample was unloaded isotropically and the final ϵ_v value after complete unloading was

1.62%. In the second loading-unloading cycles the volumetric strains followed paths parallel to the paths of the first cycle. The only difference is that during shearing at a constant cell pressure the sample dilated at the beginning then consolidated. The reason for this is not clear, but may be due to sudden distortion of the sample on shearing. However this does not influence the general trend of the strain paths. During application of the stress probe in this part of the test, very small volumetric strains occurred. All the volumetric strains during the stress probe application were recovered on unloading. The loading and unloading volumetric strain paths of the last cycle were close to each other. It is of interest to note that on shearing at a constant cell pressure, a yielding occurred although the sample had been loaded and unloaded previously at a stress ratio of 3.0 to a maximum mean normal stress of 200 psi.

The shear strains are plotted against the mean normal stresses in Figure (7-31). On the first anisotropic loading, large shear strains occurred, especially at the beginning of the loading. On unloading a small part of the shear strains was recovered. The shear strain path was almost horizontal up to $\acute{p}$ of 45 psi where large shear strains recovery started. On the second anisotropic loading cycle, the shear strains followed a path close to the previous unloading one. This indicates that no additional shear distortions occurred due to the second anisotropic loading cycle, except when the loading reached the previous maximum mean normal stress value a further shear distortion occurred. During the application of the stress probe no further shear strains occurred. The unloading shear strain path was nearly parallel to that of the first cycle.

In the second part of the test the shear strains on loading and unloading along the isotropic stress path were insignificant. After the isotropic consolidation stage the sample was sheared at a constant cell pressure and significant shear strains occurred, although the sample was consolidated anisotropically at a stress ratio of 3.0 and to $\acute{p}$ of 200 psi. During the application of the stress probe small shear strains occurred and on unloading only part was recovered.

Test No. 3G

The volumetric strains are plotted against the mean normal stresses in Figure (7-32). During the isotropic loading, unloading and reloading paths the deformation behaviour of the sample was similar to that described for Test No. 1G, first part. Therefore the description will not be repeated here. Then σ'_1 was kept constant at 120 psi and σ'_3 reduced to a level where the stress ratio (σ'_1/σ'_3) is equal to 3.0. Part of the volumetric strains were recovered during this unloading stage and on reloading to the previous maximum stress level of $\sigma'_1 = \sigma'_2 = \sigma'_3 = 120$ psi, further volumetric strains occurred. But these volumetric strains were small compared to the first isotropic loading cycle. The last loading-unloading cycle was repeated and all the resulting volumetric strains were recovered. Then the sample was unloaded isotropically and the volumetric strains followed a path which is parallel to the first isotropic unloading path.

In the second part of the test the sample was loaded then unloaded anisotropically twice to a maximum mean normal stress of 66.7 psi. The volumetric strain paths on loading and unloading are close to each other and in the second cycle they are almost identical. The amount of the irrecoverable volumetric strains are very small.

The shear strains are plotted vs. the mean normal stresses in Figure (7-33). Here the shear strains on isotropic loading, unloading and reloading were insignificant and assumed to be equal to zero as explained in Test No. 1G, first part. Then when the sample was unloaded anisotropically ($\sigma'_1/\sigma'_{3_a} = 3$) with $\sigma'_1 = 120$ psi, large shear strains occurred; they followed non-linear path. On loading again to the previous maximum mean normal stress of 120 psi, then unloading and reloading, all the shear strains were recovered. The shear strain paths are almost straight and nearly identical. On unloading isotropically from p' of 120 psi to zero, the shear strain path followed a horizontal line.

In the second part of the test there were small irrecoverable shear strains after the anisotropic loading and unloading, although the maximum mean normal stress attained was only 66.7 psi.

7.3.2.2 Deformations of the Marble Chipping Samples

Test No. 1M

In section (7.3.1) it has been shown that the stress path of this test is similar to that of Test 1G. Therefore the description will be concentrated on the differences between the two tests only.

The volumetric strains of the sample are plotted against the mean normal stresses in Figure (7-34). In general, the shape of the volumetric strain curves are similar to those of Test No. 1G, apart from the differences in the absolute values of the volumetric strains. This is not surprising as they are different materials.

During the application of the stress probes, volume changes occurred as in Test No. 1G, but with different values, in spite of small differences in the stress paths followed before the stress probing. At the end of the test the final volumetric strain value was 4.42% compared to 2.0% for Test No. 1G.

The shear strains are plotted against the mean normal stresses in Figure (7-35). Here again, the shear strain curves are similar to those of Test No. 1G except in the absolute values of the strain. The shear strains which occurred during the application of the first stress probe are much less than those of the stress probe of Test No. 1G. This is because the stress probe of Test No. 1M was applied after reloading, while that of Test No. 1G was applied as continuation of the first shearing stage. Two other interesting points are noted here. One, the shear strains associated with the first drained shearing stage in Test No. 1M are much greater than the corresponding shear strains of Test No. 1G. Secondly, the shear strains that occurred during the second part of the test are similar to those of the second part of Test No. 1G. The final shear strain value at the end of Test No. 1M is 2.5% compared to 1.49% for Test No. 1G.

Test No. 2M

The volumetric strains are plotted against the mean normal stresses in Figure (7-36). The general shapes of these volumetric strain curves are similar to those of Test No. 2G. And of course the values are different because they are different materials. It has been observed that sample No. 2G was dilating at the beginning of the second shearing stage then it continued to consolidate; such behaviour has not been noted for sample No. 2M. The value of the volumetric strain at the end of the test is 4.04% compared to 1.73% for test No. 2G.

The shear strains are plotted versus the mean normal stresses in Figure (7-37). Here the shear strain curves are also similar to those of Test No. 2G. The shear strain paths of Test No. 2M during the isotropic loading and unloading stages are horizontal and straight lines while those of Test No. 2G have a small curvature at the end of the unloading stages. Of course the absolute values of the shear strain of the two samples are different, as would be expected. The value of the shear strain at the end of Test No. 2M is 2.92% compared to 1.45% for Test No. 2G.

Test No. 3M

The stress path of this test is exactly the same as that followed in Test No. 3G. The volumetric strains are plotted versus the mean normal stresses in Figure (7-38). It can be seen from this figure that the shape of the volumetric strain curves and the general trend of the sample behaviour is similar to sample No. 3G. The value of the volumetric strain at the end of the test is 2.32% compared to 1.18% for Test No. 3G.

The shear strains against the mean normal stresses are plotted in Figure (7-39). Again the shear strain paths of the sample are similar to those of sample No. 3G, except a difference in the absolute values of the strains. The shear strain value at the end of Test No. 3M is 0.26% compared to 0.58% for sample No. 3G.

7.3.2.3 Deformations of the Ham River Sand Samples

Test No. 1S

The volumetric and shear strains are plotted against the mean normal stresses in Figure (7-40) and Figure (7-41) respectively. The trend in the deformation behaviour of this sample is similar to that described for samples 1G and 1M. The differences are only in the absolute values of the strains.

The scatter in the experimental results of this sample is much less than those of the granite and marble chippings because sand samples can be set up more uniformly than other coarse granular materials like rockfill. Besides that, breakage of sand particles is less than granite particles or marble chippings. The strain curves of this test, 1S, are smooth and well defined compared to those of the granite and marble chippings.

Test No. 2S

The volumetric and shear strains are plotted against the mean normal stresses in Figure (7-42) and Figure (7-43) respectively. It has been pointed out that the stress path of this test is similar to those of Test Nos. 2M and 2G. It can be seen from these figures that the deformation behaviour of this sample (2S) is similar to that described for samples 2M and 2G, except in the strain values. Again in this sample the scatter in the experimental results is much less than those of the granite or the marble chippings. The reasons have been given during the description of Test No. 1S.

7.3.3 Analysis of the Elastic (Recoverable) Deformations

7.3.3.1 The Elastic Volumetric Strains

Isotropic Consolidation

Tests Nos. 1G, 3G, 1M, 3M and 1S were isotropically loaded, unloaded then reloaded at the beginning of the first part of the tests. The unloading and reloading volumetric strain paths are denoted by the numbers

(2) and (3) respectively in Figures (7-28), (7-34) and (7-40). It can be seen from these figures that the unloading and reloading strain paths are nearly parallel to each other and in the case of the granite they are close to each other. This indicates that the behaviour of the three materials is nearly elastic on reloading. At maximum mean normal stress of 120 psi the values of the volumetric strains on reloading are higher than those at the end of the first loading cycle. These differences are due to accumulated distortions and crushing of particles. Anyway these differences are not significant when calculating the values of the volumetric strain for the stress increments which will be used in the analysis of the plastic deformations. There are two main differences between the strain curves of these three materials. First, the shapes of the strain curves vary from one material to another, which indicates that each material has elastic parameters different from the others. Secondly, the value of the volumetric strain for each stress increment varies also from one material to another.

Tests Nos. 2G, 2M and 2S were isotropically loaded, unloaded then reloaded after the samples had been anisotropically consolidated to a maximum p' of 200 psi, i.e. the samples were overconsolidated. Here the strain curves are also parallel and close to each other; more so than those of the first parts of the tests. This may be due to the increase in the density of the samples after the first loading cycle. Also the value of the volumetric strain for each stress increment varies from one material to another.

Therefore it can be concluded, for these isotropic consolidation tests, that the elastic volumetric strain is a function of the material type, confining pressure and porosity. And the sample behaviour on unloading and reloading is nearly elastic.

Drained Shearing at Constant Cell Pressure

In tests Nos. 1G, 1M and 1S the shearing of the samples at constant cell pressure had commenced after the isotropic consolidation stages. In these parts of the tests the samples were sheared drained

at a constant cell pressure of 120 psi to a maximum stress ratio of 3.0 then stress probes were applied with $\Delta q = 0$. The amount of the volumetric strains recorded on unloading are very small, to such a degree that the strain paths are nearly horizontal.

On reloading the volumetric strain paths are close to the unloading paths except near the maximum mean normal stress where the two paths diverge. But still the slopes of the unloading and the reloading volumetric strain paths are nearly the same.

In tests Nos. 2G, 3M and 2S the shearing of the samples at constant cell pressure was carried out in the second part of the tests. Here the samples had been anisotropically loaded-unloaded in the first part of the tests up to a maximum p' of 200 psi, i.e. the samples were overconsolidated. In these tests the volumetric strain curves during loading, unloading and reloading along the drained shear path are very close to each other specially on unloading and reloading stages. Therefore it can be assumed that the volumetric strains on unloading and reloading are nearly elastic for the three materials tested.

Anisotropic Consolidation

The behaviour of granite rockfill under anisotropic consolidation have been discussed in Section (7.2). In this section only a constant stress ratio of 3.0 will be discussed. For Tests 2G, 2M and 2S, where the anisotropic loading and unloading were performed first, the volumetric strain paths on unloading and reloading are close to each other except where the reloading approaches the previous maximum mean normal stress. For the other tests, i.e. Tests Nos. 1G, 3G, 1M, 3M and 1S, similar behaviour has been observed except at very low mean normal stresses. At low stress levels it is expected that the rubber membrane expands and distortional movements may take place. Therefore it can be concluded that the volumetric strains on unloading and reloading along this stress path are nearly elastic. This conclusion is in agreement with the findings reported in Section (7.2) for various constant stress ratio tests.

σ'_1 constant and σ'_3 decreasing

This path is illustrated in Tests 3G and 3M. The volumetric strain paths on unloading and reloading are close to each other, especially in the second loading-unloading cycle. In fact if a third cycle was performed, the unloading and the reloading strain paths would be identical, i.e. all the volumetric strains are recoverable. Therefore it can be concluded that the unloading and reloading volumetric strains along this stress path are nearly elastic.

7.3.3.2 The Elastic Shear Strains

Isotropic Consolidation Stages

In this type of triaxial test it was observed that there were small shear strains accumulated at the end of each loading-unloading cycle. In an ideal isotropic material loaded or unloaded isotropically the shear strains should be zero, i.e. $\epsilon_1 = \epsilon_3$. Also for such material the shear strains are a function of the shear stresses and not the confining pressure.

The shear strains observed in these tests may be due to anisotropy of the samples during setting up or due to non-uniform testing conditions, i.e. end restraint and rubber membrane influence. For this particular investigation no device has been developed to measure accurately the changes in height of the samples without causing any disturbance. Therefore it will be assumed that the shear strains during isotropic loading and unloading are zero, Figures (7-28)to(7-43).

Shearing at Constant Cell Pressure

For Test No. 1G only the unloading shear strain path is shown in Figure (7-29) because the sample has not been reloaded. For Tests 1M and 1S the unloading and reloading shear strain paths form closed hysterises loops. At the maximum mean normal stress of 200 psi nearly all the shear strains were recovered.

For Tests No. 2M and 2S the unloading and reloading shear strain paths are also very close to each other and all the shear strains

were recovered on unloading.

Therefore it can be concluded that the shear strains on unloading and reloading along this stress path are nearly elastic.

Anisotropic Consolidation

The shear strains on loading and reloading along this stress path for Tests Nos. 2G, 2M and 2S are very small compared to those which occurred during the first loading in the first parts of the tests. The shear strain paths on unloading and reloading are nearly horizontal up to mean normal stress of 20 psi. This is in agreement with the findings reported in Section (7.2.3) where samples of granite rockfill have been consolidated under various constant stress ratios then unloaded anisotropically.

For Tests Nos. 1G, 1M, 1S, 3G and 3M the shear strain paths on unloading and reloading are more close to each other than those of Tests 2G, 2M and 2S and nearly all the shear strains were recovered. Therefore it can be concluded that the shear strains on unloading and reloading along the anisotropic stress path are nearly elastic.

7.3.3.3 Discussion of the Elastic Deformations

In this analysis the term 'elastic' will be used to express the recoverable or reversible strains. On the other hand the irrecoverable strains will be called 'plastic'. It has been observed in the tests described in the previous sections that both elastic and plastic deformations occur during loading the samples. In fact these granular materials have the characteristics of strain hardening materials which were described in Chapter 3. A reasonable assessment of the elastic strains is essential for studying the yielding of soils but unfortunately all the methods are questionable. Various mathematical formulations have been suggested to assess the value of the elastic strains, and most of these formulations are either empirical or based on graphical approximations. For comparison some of the main studies in connection with this work will be mentioned briefly.

Holubec (1966) suggested an approximate mathematical relationship of a parabolic form for the elastic strains of Ottawa sand under different triaxial stress conditions. This is expressed as:

$$\epsilon_v^e = a\,(\dot{p})^n \qquad \ldots\ldots \quad (7.13)$$

where (a) is a constant depending on the void ratio and type of test and (n) ranges from $(\frac{1}{2})$ for isotropic consolidation to $(\frac{2}{3})$ for anisotropic consolidation tests. A similar expression has been suggested for the elastic axial strains. Other expressions of similar form have also been suggested for constant cell pressure and constant mean normal stress tests.

Also Holubec (1966 and 1968) tried to separate the elastic axial strains due to mean normal stresses from those due to shear stresses. Holubec's conclusions have been criticised by Merkle and Merkle (1969); Coon and Evans (1969) and Rowe (1971a).

Ko and Scott (1967 a and b) noted sand to be non-linearly elastic and isotropic but they found that a complete separation between hydrostatic and deviatoric components had not been achieved because an elastic volume change occurred during shearing at constant mean normal stress.

Schofield and Wroth (1968) suggested that 'Granta-gravel' has no elastic strains. Roscoe, Schofield and Wroth (1958) stated that the elastic volume changes are proportional to $d\dot{p}$ but it has been observed that elastic volume changes occur in constant mean normal stress tests.

There are many other researchers in this field who proposed various relationships, e.g. Chen (1948); Wilson and Sutton (1948); Jackobson (1957); Makhlouf and Steward (1965); Wroth and Bassett (1965); Roscoe and Burland (1968); Rowe (1971a) among others. In Section (7.2.3) of this thesis new mathematical formulations were suggested for the elastic stress-strain relationships for constant stress ratio loading-unloading tests which are based on the shape of the strain curves over a wide range of mean normal stresses.

It can be concluded from the above brief comments that there are different opinions concerning the assessment of the elastic strains and none of them can be adopted to analyse the results of the special stress path tests in this section. In these special stress path tests compound types of stress path were followed; i.e. isotropic consolidation, constant stress ratio, drained shearing and stress probing at constant deviator stress. Therefore it was decided to study each part of the stress path separately and the recoverable strains will be taken as elastic. This is the reason for the detailed description of the strains on unloading and reloading presented in the previous sections which will be used in the analysis of the plastic deformations.

7.3.4 Analysis of the Plastic (Irrecoverable) Deformations

7.3.4.1 Results of the Tests on Granite Rockfill

The PSIVs Along the Stress Paths

The first and second parts of Test No. 1G are represented by the lines OCAB and OAB respectively in Figure (7-44). Point 'A' is the common point approached by the two stress paths and 'AB' is the stress probe. The PSIVs along the stress paths CAB and OAB are denoted by V_1 and V_2 respectively, as shown on Figure (7-44). No PSIVs are plotted along the isotropic consolidation path OC because, as was explained previously, $\Delta \delta$ is assumed zero, and therefore the vectors are horizontal, i.e. coincident with the stress increments direction. The PSIVs along the stress path CA form acute angles with the direction of the stress path on the right hand side and are rotating in an anticlockwise direction as the stress level increases, i.e. as the shearing continues. The rotation is smooth up to point 'A' before applying the stress probe. Therefore these PSIVs suggest that yielding is taking place due to shearing the sample at constant cell pressure.

In the second part of the test the PSIVs also form acute angles with the direction of the stress path OA on the right hand side and are rotating in an anticlockwise direction as the stress level increases. This suggests that the material is yielding due to loading at constant stress ratio although the sample was loaded previously to point 'A'.

For Test No. 2G the PSIVs are shown in Figure (7-45) where various parts of the stress path are marked in the same way as Test No. 1G. In the first part of the test the PSIVs form acute angles with the stress path OA on the right hand side and are rotating in an anticlockwise direction as the stress level increases. Yielding is occurring as the loading continues along this constant stress ratio path. In the second part the sample was sheared under drained conditions at constant cell pressure. Yielding also took place although the sample was anisotropically consolidated to point 'A' in the first part of the test. This is

indicated by the PSIVs along the stress path CA. These PSIVs also form acute angles with the stress path CA and rotate in an anticlockwise direction as the shearing continues.

In fact the general behaviour of sample No. 2G is similar to that of sample No. 1G. Of course the angles between the PSIVs and the stress paths are different from one test to another.

For Test No. 3G the PSIVs are plotted in Figure (7-46). Along the stress path CD the PSIVs are also rotating in an anticlockwise direction as the shear stress, q, increases although the mean normal stress is decreasing. Here the rotation is small compared to that along the paths OA and CA of the other tests. This is probably because the investigation is in the low stress level range where the maximum applied shear stress was only 80 psi. Thus it can be concluded that yielding takes place as the sample is unloaded along the path CD.

In the second part of the test the PSIVs also form acute angles with the direction of the path OD and rotate in an anticlockwise direction as the stress level increases. The behaviour is similar to that of the second part of test No. 1G.

The PSIVs at the Common Stress Points 'A' and 'D'

The stress point 'A' is the common point where the two stress paths of each test meet each other. At point 'A' of each test, i.e. Test 1G and Test 2G, there are two PSIVs generated from the two stress probes applied at the end of each stress path, Figures (7-44) and (7-45). Each PSIV has a direction different from the other PSIV because of the difference between the stress path followed. This difference between the directions of the PSIVs is not so small that it might be attributed to experimental errors, but is a fundamental difference in behaviour. The PSIVs at point 'A' of each test are marked by (1) to distinguish them from the previous vectors along the stress paths. It should be remembered here that the PSIVs along the stress paths are generated from the first loading cycles while those at point 'A' were generated during the second cycles due to the application

of the stress probes. It will be shown in the following sections that four PSIVs could be drawn at point 'A' of each test.

The stress point 'D' in Test No. 3G was approached by the stress paths CD and OD but no stress probe was applied. There are two PSIVs at point 'D' where each is related to one stress path, Figure (7-46). The PSIVs at point 'D' are plotted parallel to the last strain increment along each stress path. This is equivalent to applying a stress increment in the same direction of the stress path under consideration. It can be seen from Figure (7-46) that the PSIVs at point 'D' have different directions. Here also the difference between the directions is fundamental and not within the range of experimental error.

Magnitude of the Plastic Strain Increment Vectors

Values of the PSIVs are shown between parenthesis on Figures (7-44), (7-45) and (7-46). They are calculated to correspond to equal stress increments $\Delta p'$ of 10 psi. It can be seen that there is no unique relationship between the magnitude and directions of the PSIVs as the stress level increases. The magnitudes of the PSIVs are influenced by the plastic deformation of the sample. The plastic deformation is a result of particle crushing, rolling, sliding, fracture and collapse of the weak zones inside the sample. Therefore the PSIVs are not expected to be of unique magnitudes. However, the magnitudes of the PSIVs are immaterial to the present investigation of the plastic deformation of rockfill. The shapes of the plastic potentials and yield locus are dependent on the direction of the PSIVs, not on their magnitudes.

7.3.4.2 Results of the Tests on Marble Chippings

The plastic strain increment vectors of Tests Nos. 1M, 2M and 3M are shown in Figures (7-47), (7-48) and (7-49) respectively. The stress paths are denoted in the same way as that used for granite rockfill with the stress points 'A' and 'D' as common points.

The PSIVs along the various stress paths are denoted by V_1 and V_2 to represent the first and second parts respectively of each test. All the PSIVs form acute angles with the direction of the stress paths on the right hand side and rotate in an anticlockwise direction as the stress increases, i.e. as the shearing continues. The rotation is smooth up to point 'A', before the application of the stress probes. This trend in behaviour has been observed for all the stress paths adopted in these tests.

At the common stress point 'A' of each test, i.e. Test 1M and Test 2M, there are also two PSIVs generated from the two stress probes applied, Figures (7-47) and (7-48). Here the PSIVs also have different directions as was the case for granite rockfill.

At stress point 'D' in Test 3M, the PSIVs have also different directions due to different stress paths followed, Figure (7-49). The trend of the behaviour is similar to that described for Test No. 3G, with the exception that there is no relation between the two tests from a quantitative point of view.

As far as the magnitudes of the PSIV are concerned, the brief description stated for the granite is applicable here for marble chippings, and will not be repeated.

7.3.4.3 Results of the Tests on Ham River Sand

The plastic strain increment vectors of Tests Nos. 1S and 2S are shown in Figures (7-50) and (7-51) respectively where the common stress point is denoted by 'A'. The PSIVs along the various stress paths are denoted by V_1 and V_2 to represent the first and second parts respectively of each test.

The PSIVs form acute angles with the direction of the stress paths and rotate in an anticlockwise direction as the stress increases. The rotation is quite smooth up to point 'A'. The general trend of behaviour is similar to those of granite rockfill and marble chippings.

At the common stress point 'A' of each test there are also two PSIVs generated from the two stress probes applied. These vectors at point 'A' have different directions but the difference is not large as was the case for the granite rockfill and marble chippings. The difference is still outside the range of the experimental error.

7.3.4.4 Discussion of the Results

It has been assumed in the theory of isotropic work-hardening plasticity and subsequently in derivation of the Cam Clay model that the plastic strain increment vector is independent of the stress increment vector, (i.e. the stress increment corresponding to any stress path), and is independent of the stress history, (i.e. the stress path followed to bring the soil element to the state point p', q, e). In other words the plastic strain increment vector is a function of the state of stress and is path independent. This assumption has been examined experimentally for sand and clay and contradictory results were reported. These were reviewed briefly in Chapter 3.

The stress point 'A' in the granite rockfill tests (i.e. Tests 1G and 2G), has been approached by two different stress paths in each test. A plastic strain increment vector corresponding to the last stress increment of each stress path could be plotted at this point 'A'. Such PSIVs for Tests 1G and 2G are shown in Figures (7-52 a and b). It can be seen that the PSIVs of each test have different directions; each vector depends on the stress path followed. Similar findings were obtained for marble chippings and Ham River sand, and the results are plotted in Figures (7-52 c to f).

The PSIVs at the stress point 'D' for both granite rockfill and marble chippings tests (i.e. Test 3G and Test 3M) are shown in Figures (7-52 g and h). Again the PSIVs of each test have different directions. It should be noted here that the stress level at point 'D' is lower than that at point 'A'. Besides that, point 'A' and 'D' have been approached by different types of stress paths.

Therefore it can be concluded that the plastic strain increment vector is path dependent and not as assumed previously in the theory of isotropic work-hardening plasticity. As a result of that a unique plastic potential cannot be established here. Similar findings have been reported by Namy (1970) for Newfield clay although the stress paths he adopted are different from those used here. However, contradictory results have been observed by Holubec (1966) for Ottawa sand. Furthermore, Holubec reported that the PSIVs along any constant stress ratio path have constant slope, therefore he constructed a family of plastic potentials for constant void ratios. But it is not clear what the slope of the PSIVs along his special stress paths would be. There are two unsatisfactory points Holubec used in his analysis. These are:

1. The mathematical approximation he used of elastic strain curves having parabolic form, does not agree with observed experimental behaviour of rockfill. Then the separation of the elastic axial strains into two components, one due to deviator stress and one due to the mean normal stress is inappropriate; Rowe (1971a). Holubec's approach has also been strongly criticised by Merkle and Merkle (1969) and Coon and Evans (1969). For rockfill it was observed in this thesis that a parabolic approximation of the elastic strain leads to an error in the analysis of the plastic deformation.

2. The lateral strains were based on results of pilot tests carried out at the beginning of the programme and from them the influence of the rubber membrane was obtained.

The plastic strain increment vectors generated from applying the stress probes are also shown in Figures (7-52 a to f). For each of the materials tested the PSIVs at point 'A' have different directions. Therefore it can be concluded that the plastic strain increment vector is a function of the stress increment vector. Again this finding contradicts

the assumption used in the theory of isotropic work-hardening plasticity. Similar findings have been reported by Lewin and Burland (1970) for tests on remoulded, saturated, powdered slate dust and Tatsuoka and Ishihara (1974) for tests on sand. Rotation of the plastic strain increment vector due to the rotation of the stress increment vector has also been reported for tests involving undrained, conventional drained and constant stress ratio paths by Le Lievre and Poorooshasb (1967) for Kaolin; Calabresi (1968) for a silty clay. However Holubec (1966) and Poorooshasb et al (1966 and 1967) in tests on Ottawa sand found that the plastic strain increment vectors resulting from various stress increment vectors are closely spaced, i.e. they are nearly pointing in the same direction. Therefore they established a unique plastic potential function for Ottawa sand.

7.3.5 Yielding of Coarse Granular Materials

It has been assumed for the Cam-clay model, Granta-gravel model and most of the Cambridge researchers' theories that there exists an elastic domain outside which soils deform plastically. From the special stress path tests and the previous constant stress ratio tests an attempt will be made in this section to examine the validity of the above assumption in respect to the material tested in this thesis.

In the constant stress ratio tests (Section 7.2) the granite rockfill samples exhibited an elastic behaviour on reloading along all the stress paths examined; this includes the isotropic loading path. However reloading along the drained shearing path the samples showed non-elastic behaviour. This is also clear from the cyclic loading tests described in Section 6.4. In Figure (7-53 a and b) the constant stress ratio paths and the drained shear path are plotted for comparison.

The domain around the stress point 'A' described in the special stress path tests will now be examined. At point 'A' for each material

tested five stress probes could be considered acting in different directions as shown in Figure (7-53 c). These stress probes are described briefly as follows:

No. 1. Along a drained shear path on loading. Plastic deformations occur on the application of such a stress probe. This has been observed for all the drained triaxial tests and the special stress path tests.

No. 2. Along the constant stress ratio path on loading. Plastic deformations occur also along this path on first loading. This has been observed for all the constant stress ratio tests and the special stress path tests.

No. 3. Described in the special stress path tests. It has been shown in Section 7.3.4 that plastic deformations occur on application of such a stress probe even if the sample is overconsolidated.

No. 4. Along the drained shear path on unloading. The deformations along this path are, in many cases, nearly elastic. The cyclic loading tests described in Section 6.4 showed that this path required many loading-unloading cycles to stabilize, but always involved hysteresis. The behaviour was strongly influenced by the stress ratio from which unloading occurred, the confining pressure and the density of the sample. A similar trend in behaviour was observed for the special stress path tests.

No. 5. Along the constant stress ratio path on unloading. The pilot tests, i.e. the constant stress ratio tests, showed that the behaviour of the samples was nearly elastic.

It seems, from the above brief description that the deformations within the zone enclosed between probes (4) and (5) are nearly totally recoverable, i.e. nearly elastic. This does not mean that all the zone OCA, Figure (7-53 c), is elastic. To clarify this point Tests 3G and 3M will be examined. Samples 3G and 3M underwent irrecoverable defor-

mations on loading after the isotropic consolidation stage although this path is within the zone OCA, Figure (7-46).

It seems it is not possible to have completely elastic behaviour enclosed in a defined domain but we can say that there is some domain within which strains are nearly recoverable and outside this domain large irrecoverable strains will occur. This kind of behaviour has been observed for the three materials tested; granite, marble chippings and Ham River sand. Now, the question is where can the boundary of this domain be drawn? To do so the deformations along the various stress paths tested will be examined here.

1. Deformations along the isotropic consolidation path in the first part of each test are nearly elastic on reloading, Figure (7-54 a). On application of any stress probe at maximum consolidation pressure, as shown in the figure, yielding occurred.

2. Deformations on loading along any path after the isotropic consolidation in the second part of each test are nearly elastic within a narrow zone outside which yielding occurs, Figure (7-54 b). Such samples are overconsolidated due to the loading in the first part of each test.

3. Deformations along a constant stress ratio path in the first part of each test are nearly elastic on reloading and the application of any stress probe along this path will cause irrecoverable strains, Figure (7-54 c). Thus the elastic zone is limited to a narrow strip around this constant stress ratio path.

4. Deformations along a constant stress ratio path in the second part of each test are elastic within a zone wider than that mentioned in the third point. The samples here are overconsolidated and the case is similar to that described in the second point.

Hence it seems that there are narrow elastic zones which depend on the stress path and the stress history of the samples. There is no one elastic domain with definable boundaries.

Therefore it is clear that these granular soils tested do not comply with simple isotropic plastic model behaviour such as that postulated in the Cam-clay and Granta-gravel models. Nevertheless yield zones can be defined provided past stress history is taken into account. Past stress history can give rise to the non-unique plastic strain increment directions at the same stress point such as those 'A' and 'D' described earlier. Even on first loading the plastic strain increment vectors along simple stress paths, such as the constant stress ratio paths, do not have the same slopes, which is in contradiction to the model presented by Holubec (1966) and Poorooshasb et al (1966 and 1967).

7.3.6 Particle Breakage During the Special Stress Path Tests

All the granite rockfill, marble chippings and Ham River sand samples were sieved after testing. A summary of the B-factor values is shown in the following table:

Material	Test No.	B-factor Value
Granite Rockfill	1G	5.06
	2G	4.56
	3G	2.14
Marble Chippings	1M	9.00
	2M	9.45
	3M	6.60
Ham River Sand	1S	2.15
	2S	2.35

It can be seen from this table that the values of the B-factor for the first and second tests of each material are close to each other. This indicates that the amount of particle breakage after finishing the tests is similar (except in Tests 3G and 3M). This similarity may be due to the samples being loaded along the same stress paths. The grading

curves for tests 1G, 1M and 1S are plotted in Figure (7-55) together with the grading curves for the materials before testing. The grading curves of the other tests 2G, 2M and 2S lie close to those shown in the figure and therefore have not been plotted.

As far as tests 3G and 3M are concerned the values of the B-factor are much less than those for the previous tests. This means that the amount of particle breakage is less during tests 3G and 3M. This is due to the lower stress levels to which these samples were loaded. From the data obtained from these tests it can be concluded that:

a) Particle breakage during loading along the drained shear path with σ'_3 constant is more than that during loading along any constant stress path.

b) Particle breakage increases with the increase of the stress level to which the samples are loaded.

c) The amount of particle breakage increases with the decrease of particle strength.

d) When samples are loaded successively along two stress paths, these two stress paths being the same for all samples, the order in which the two samples are followed has only a small effect on the final amount of particle breakage.

e) The phenomenon of particle breakage has a marked influence on the direction of the plastic strain increment vectors. The increase in breakage of particles during loading tends to cause increase in rotation of the plastic strain increment vectors. This can be noted clearly from Figures (7-44) to (7-51) of various materials tested in this programme.

Table No. (7-1): Summary of the Anisotropic Consolidation Tests on $1\frac{1}{2}$ in. dia. Samples of Granite Rockfill.

Test No.	1A	2A	3A	4A*	5A	6A	7A≠	8A	9A+
σ'_1 / σ'_3	1.42	2.04	3.0	1.42	2.04	3.0	1.42	2.04	3.0
n_i%	25.4	26.6	26.0	32.4	35.2	33.4	38.8	40.2	38.7
Rd %	86.9	82.1	84.5	57.0	43.2	52.0	23.7	15.5	24.3
γ d pcf	123.9	121.9	122.9	112.2	107.7	110.7	101.6	99.3	101.8
σ'_3 during shearing	612	613	612	600	600	600	600	602	600
Back Pressure psi	40	40	40	40	40	40	40	40	40
ϕ'_f		38.6°	36.5°		36.4°	34.7°		34.3	
$(\sigma'_1 - \sigma'_3)_f$		2034	1793		1752	1588		1555	
σ'_{1f}		2647	2405		2352	2188		2157	
ϵ_1 % at failure		14.75	12.43		21.2	19.29		23.81	
ϵ_v % at failure		-13.92	-12.32		-22.17	-18.66		-25.3	
$(d\epsilon_v/d\epsilon_1)_f$		-.149	-.151		-.151	-.143		-.152	
Final Strain%		20.65	19.00	3.68	27.0	27.78	10.94	28.57	17.7

* Membrane burst after the reconsolidation

≠ Membrane burst before reaching failure

\+ Membrane burst after the consolidation stage

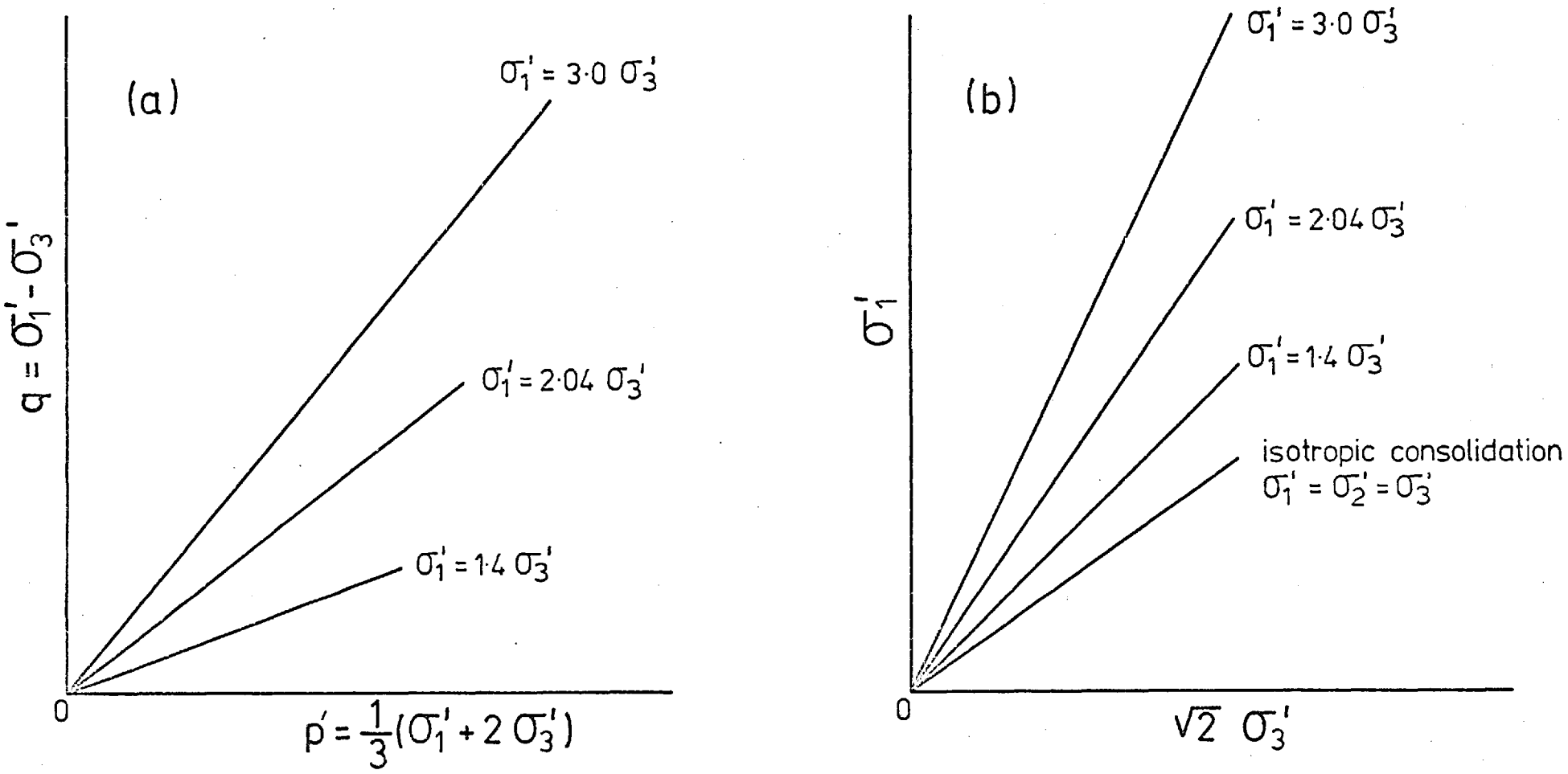

PATHS USED IN CONSTANT STRESS RATIO TESTS

Fig. 7-1

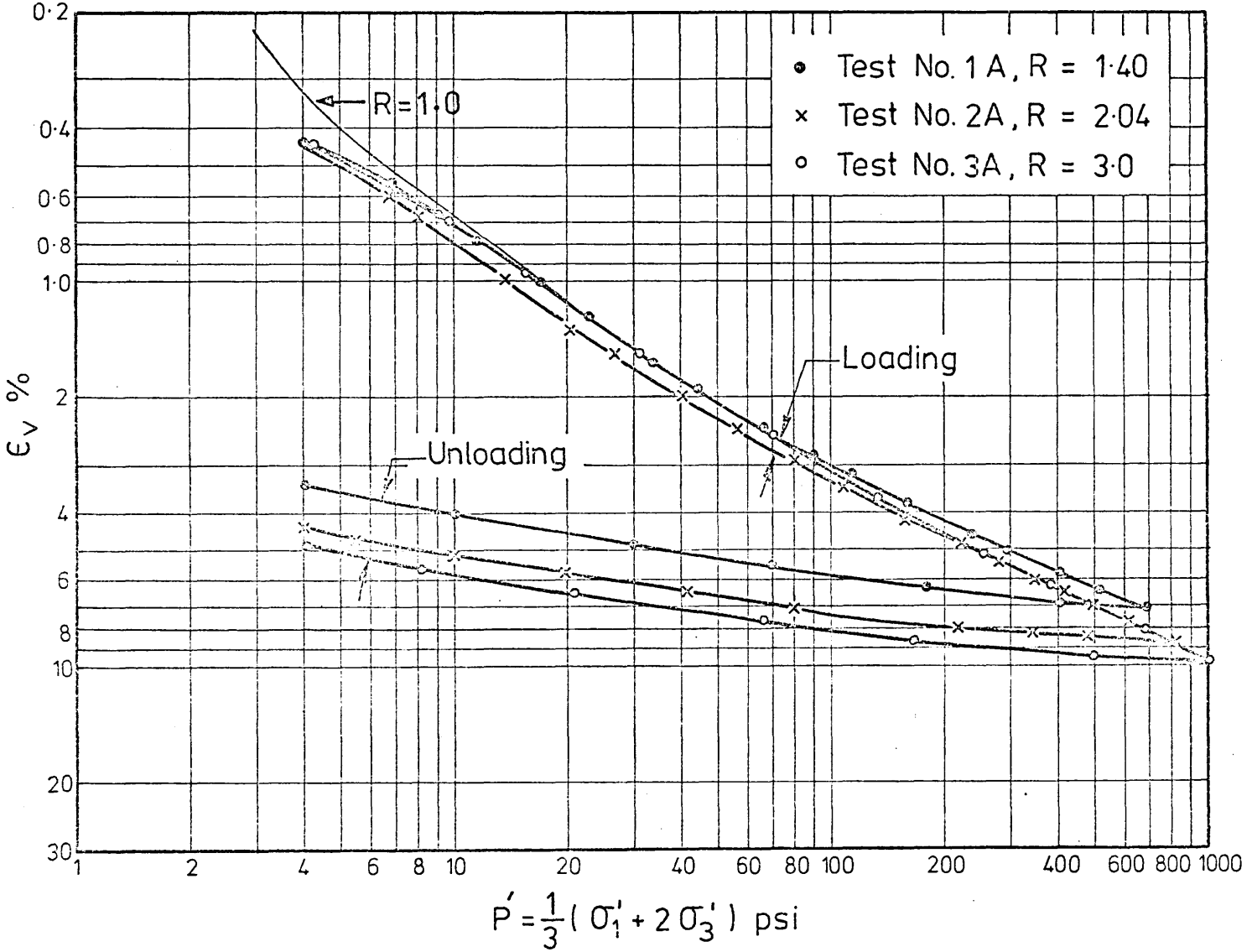

GRANITE ROCKFILL - Anisotropic Consolidation Tests on Dense Samples

Fig. 7-2

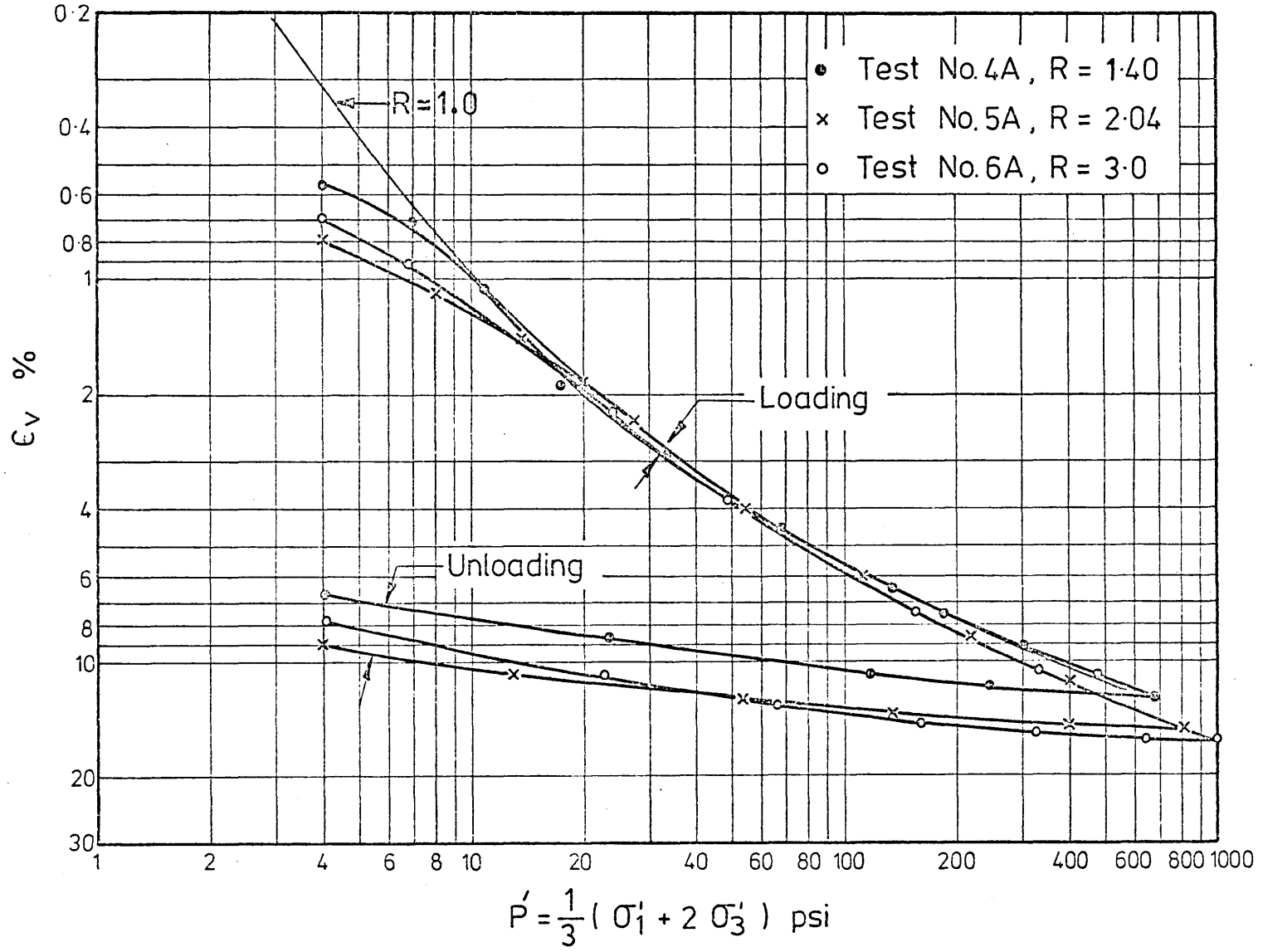

GRANITE ROCKFILL - Anisotropic Consolidation Tests on Loose Samples

Fig. 7-3

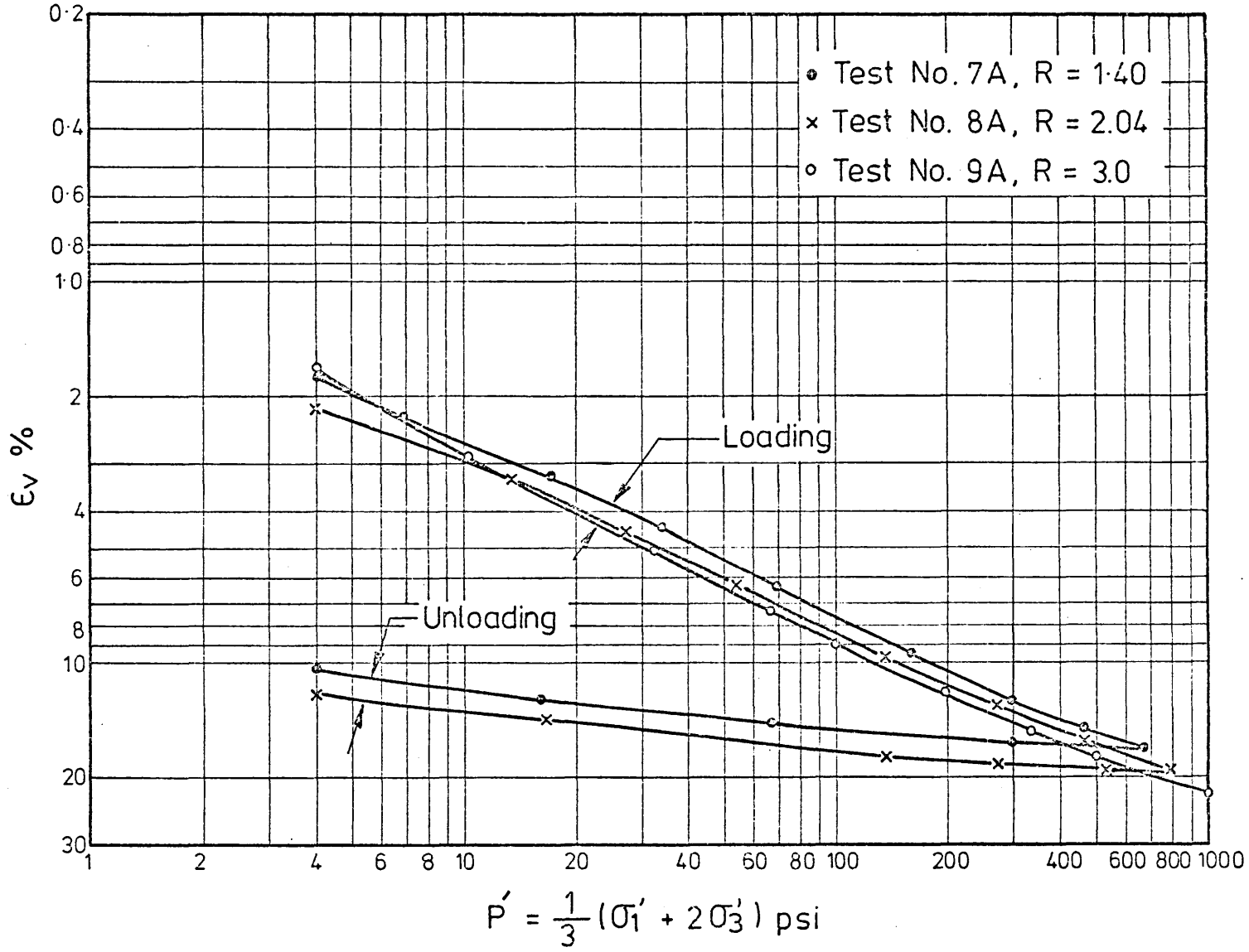

GRANITE ROCKFILL - Anisotropic Consolidation Tests on Very Loose Samples

Fig. 7 - 4

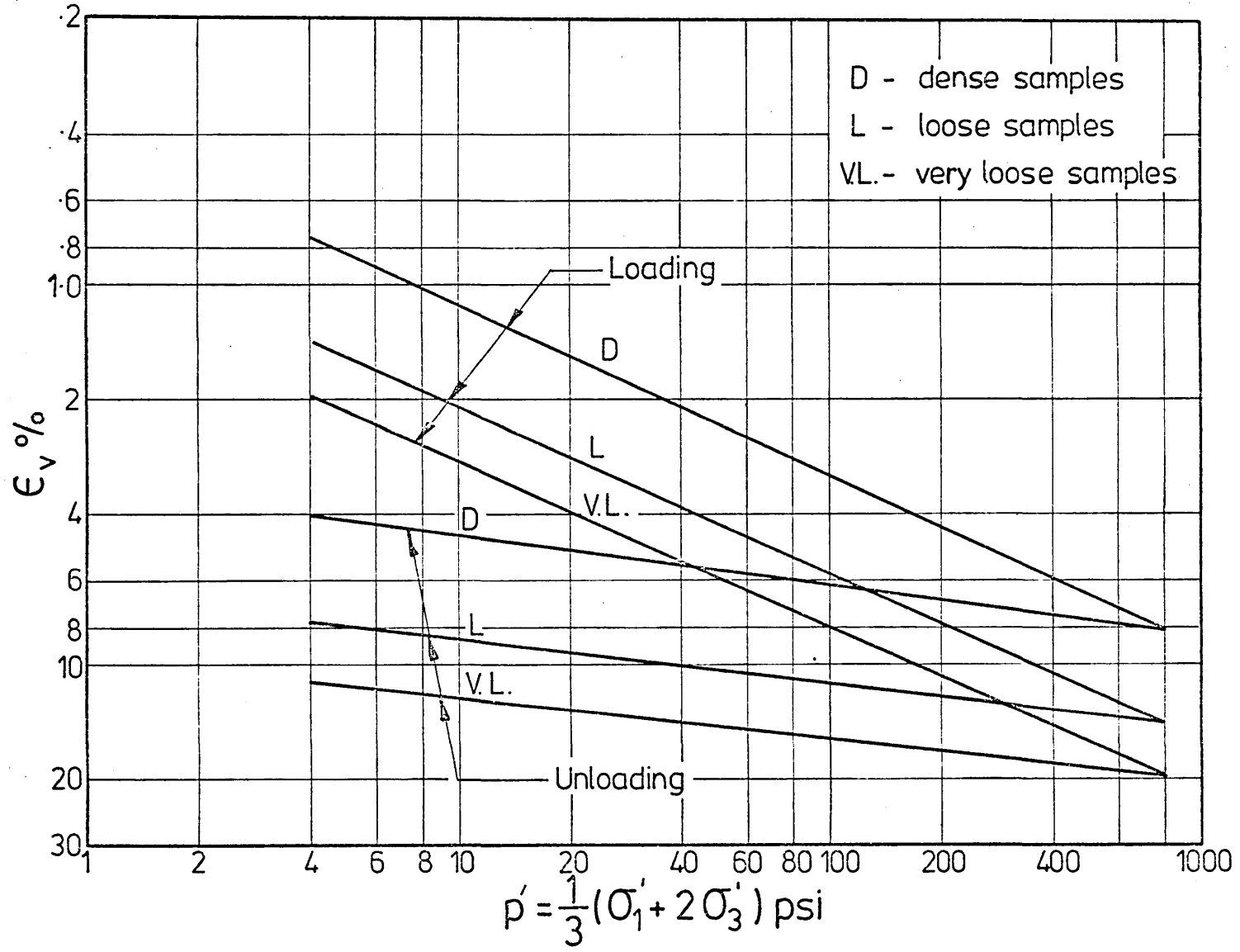

THE AVERAGE VOLUMETRIC STRAIN CURVES FOR ANISOTROPIC CONSOLIDATION AT VARIOUS DENSITIES.

Fig. 7-5

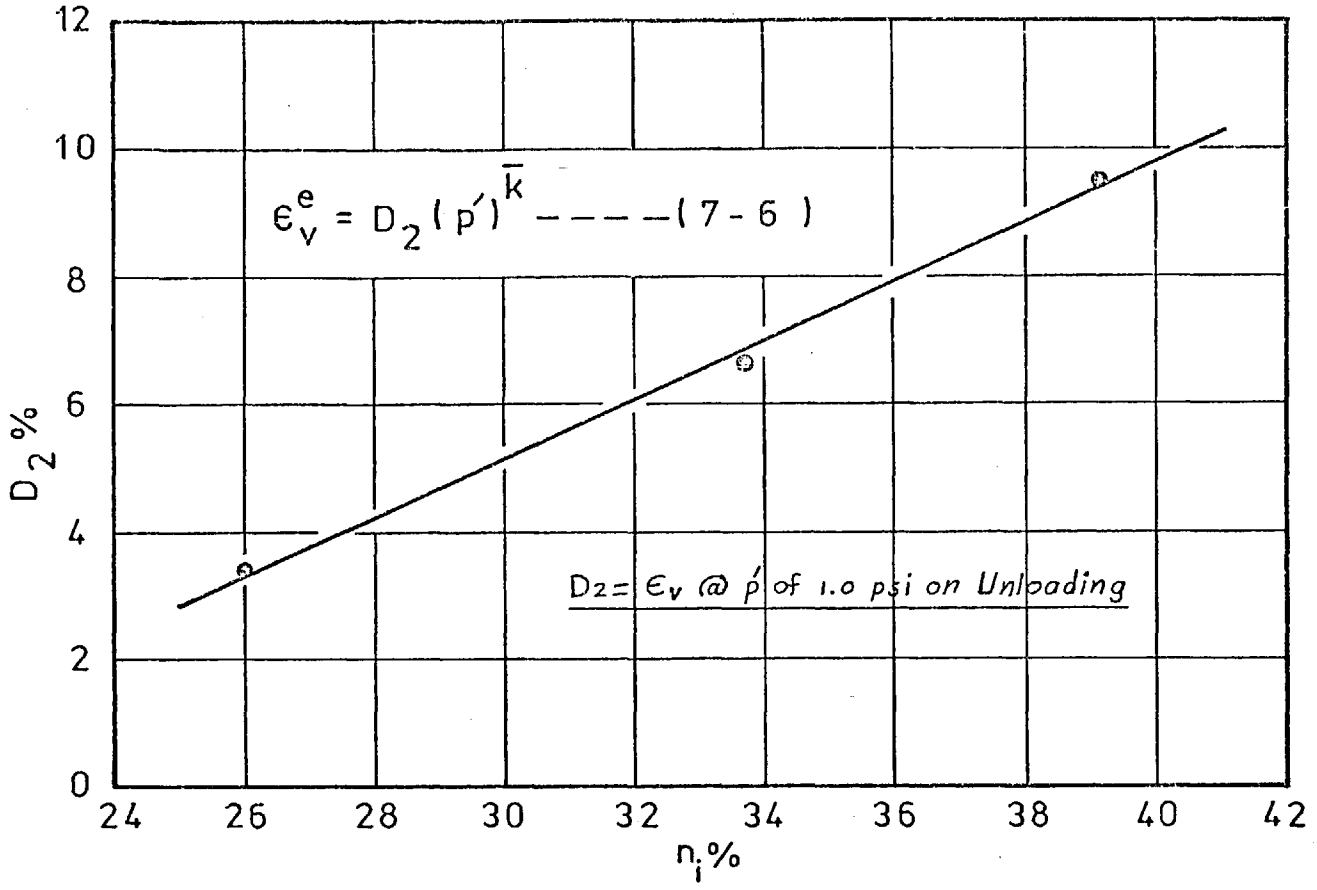

B. COEFFICIENT D_2

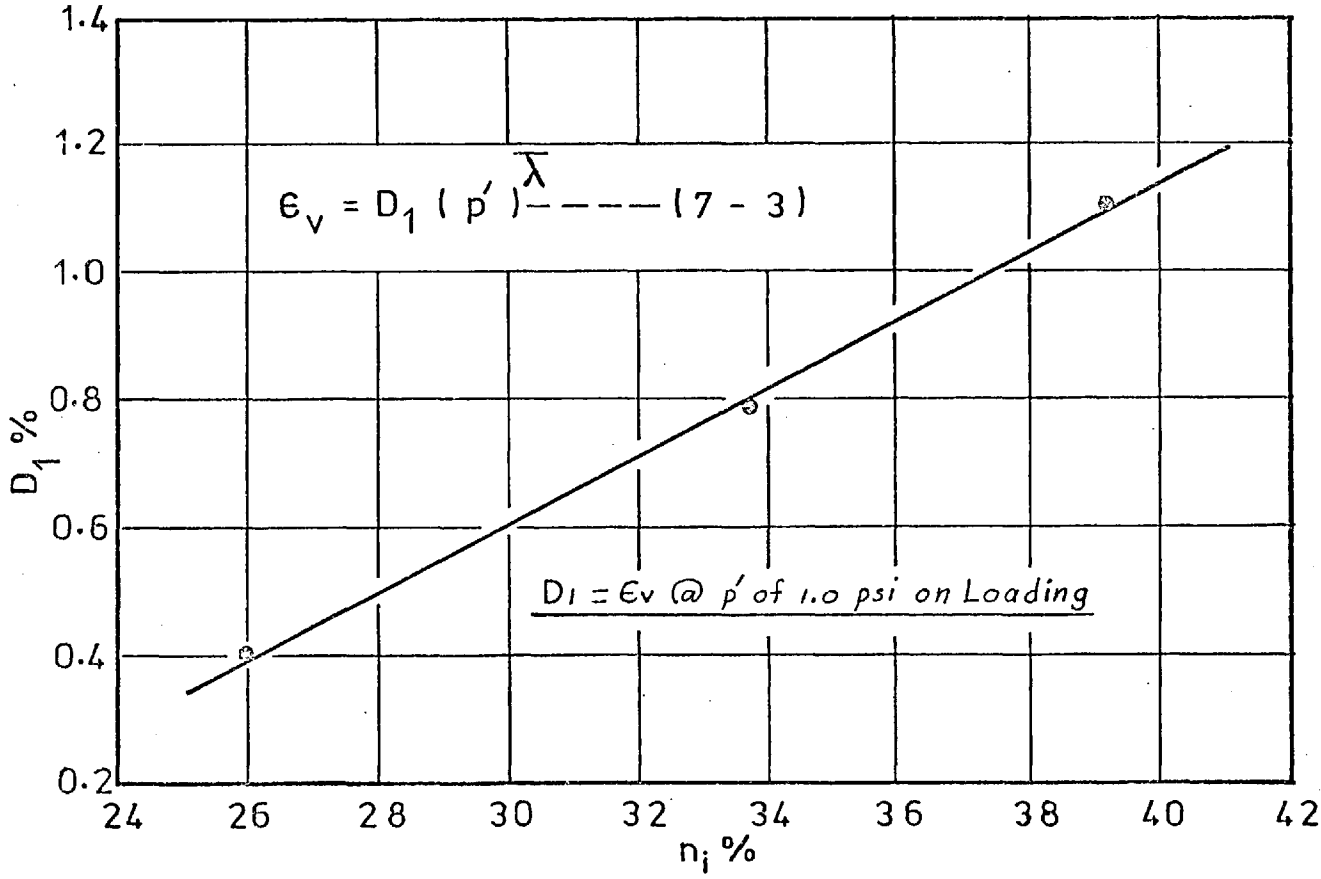

A. COEFFICIENT D_1

VARIATION OF THE COEFF'S. D_1 & D_2 WITH THE INITIAL POROSITY OF THE SAMPLES

FIG 7-6

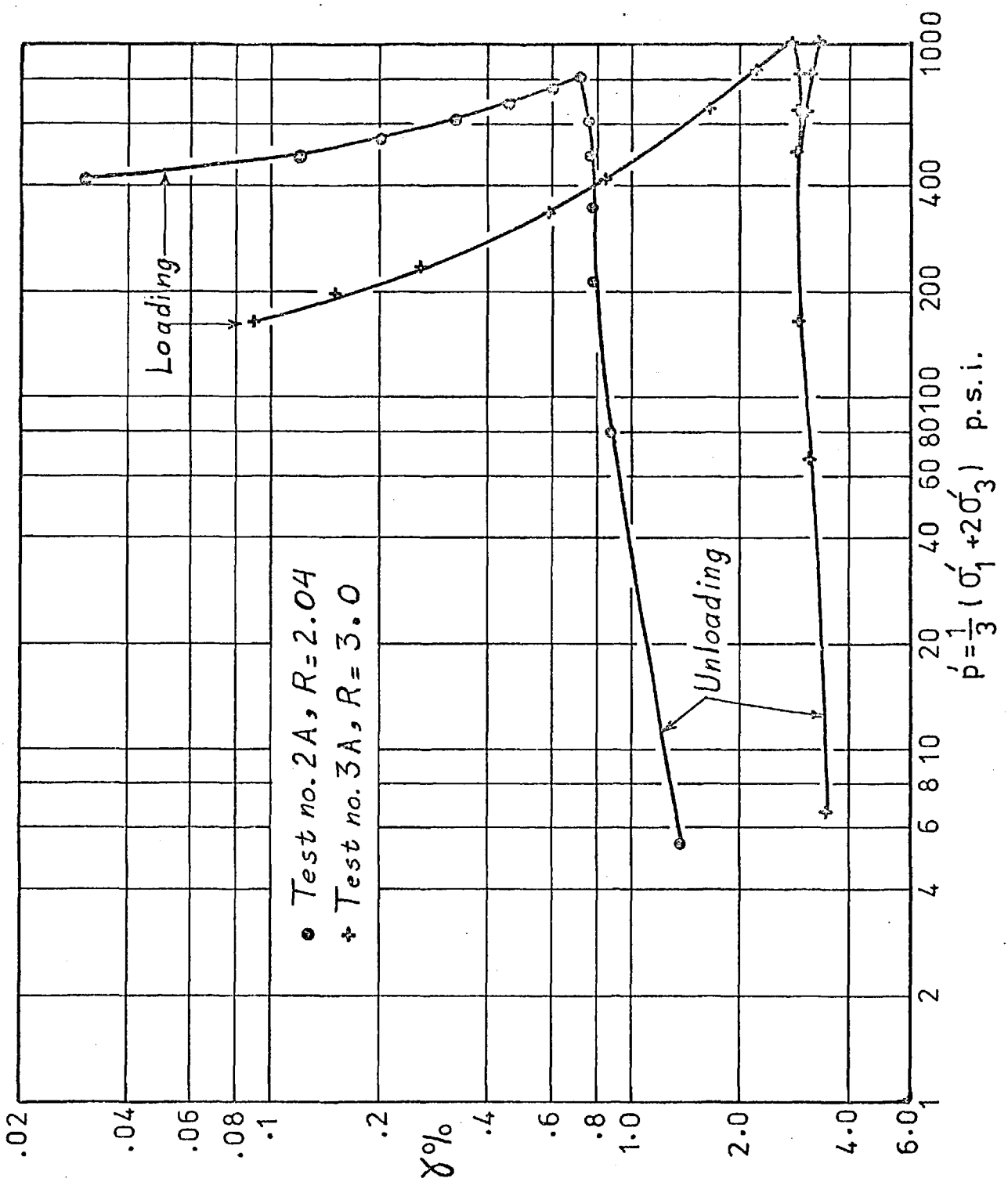

SHEAR STRAIN VS. MEAN NORMAL STRESS FOR DENSE SAMPLES

FIG 7-7

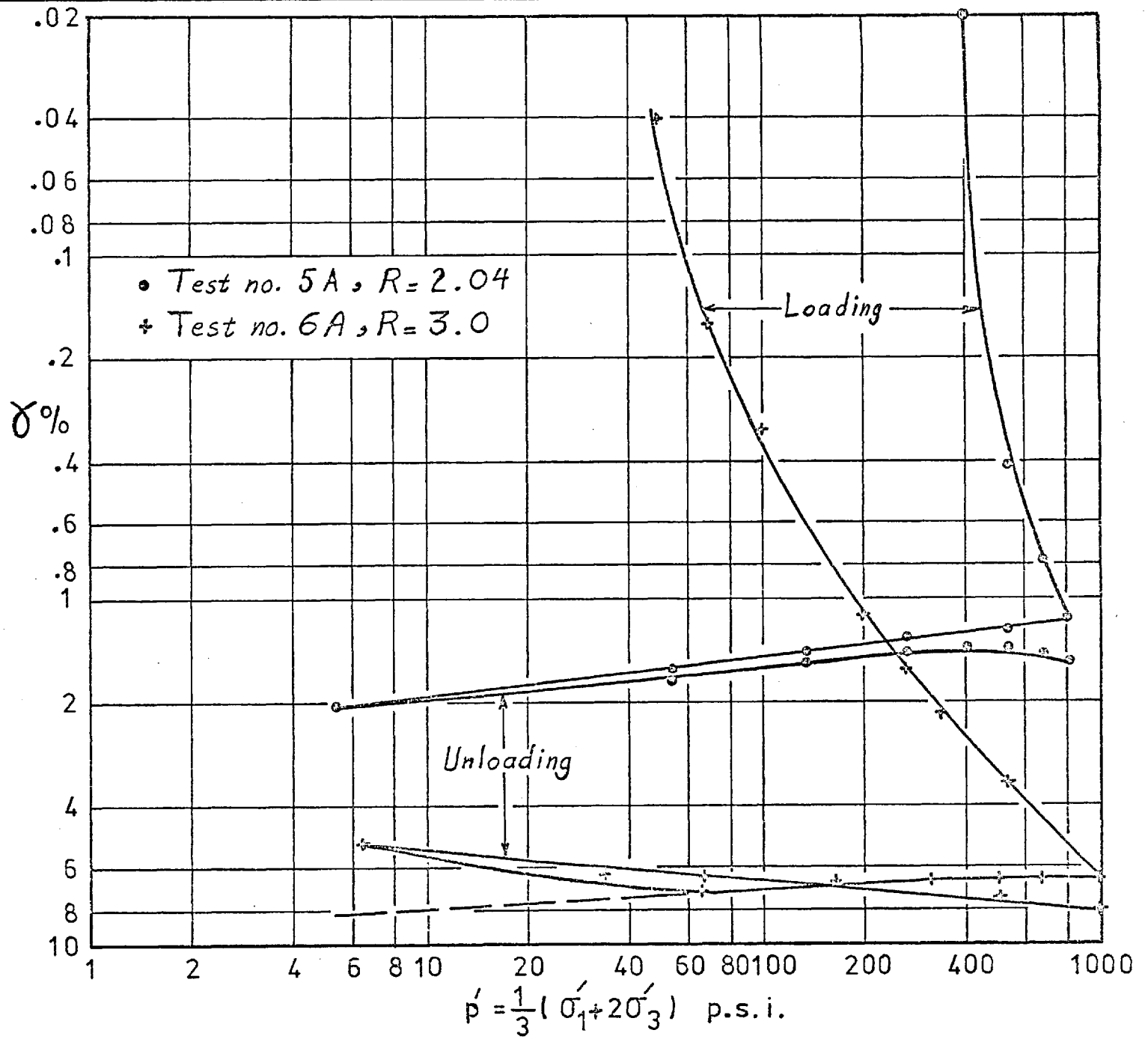

SHEAR STRAIN VS. MEAN NORMAL STRESS FOR LOOSE SAMPLES

FIG 7—8

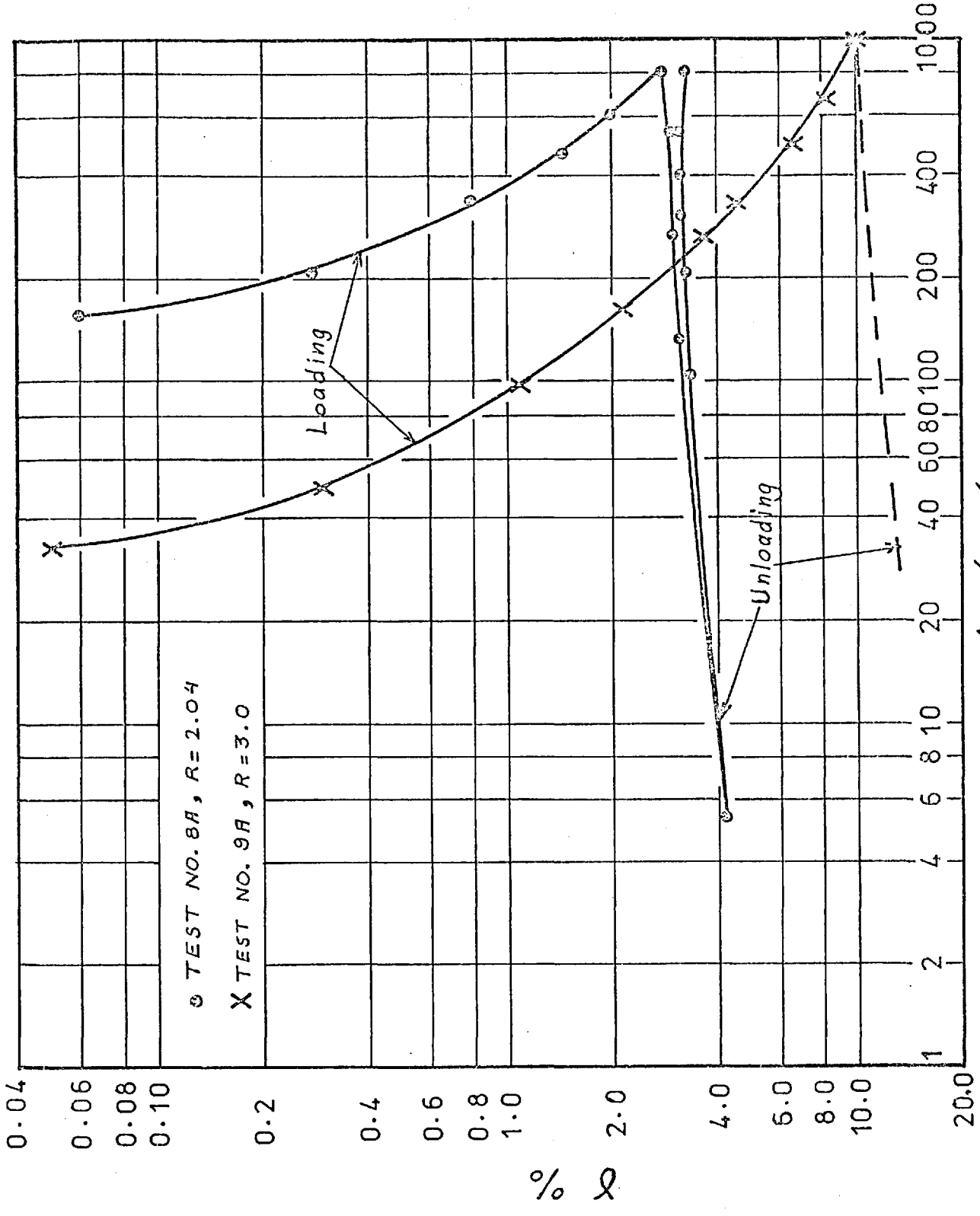

SHEAR STRAIN VS. MEAN NORMAL STRESS FOR VERY LOOSE SAMPLES

FIG 7-9

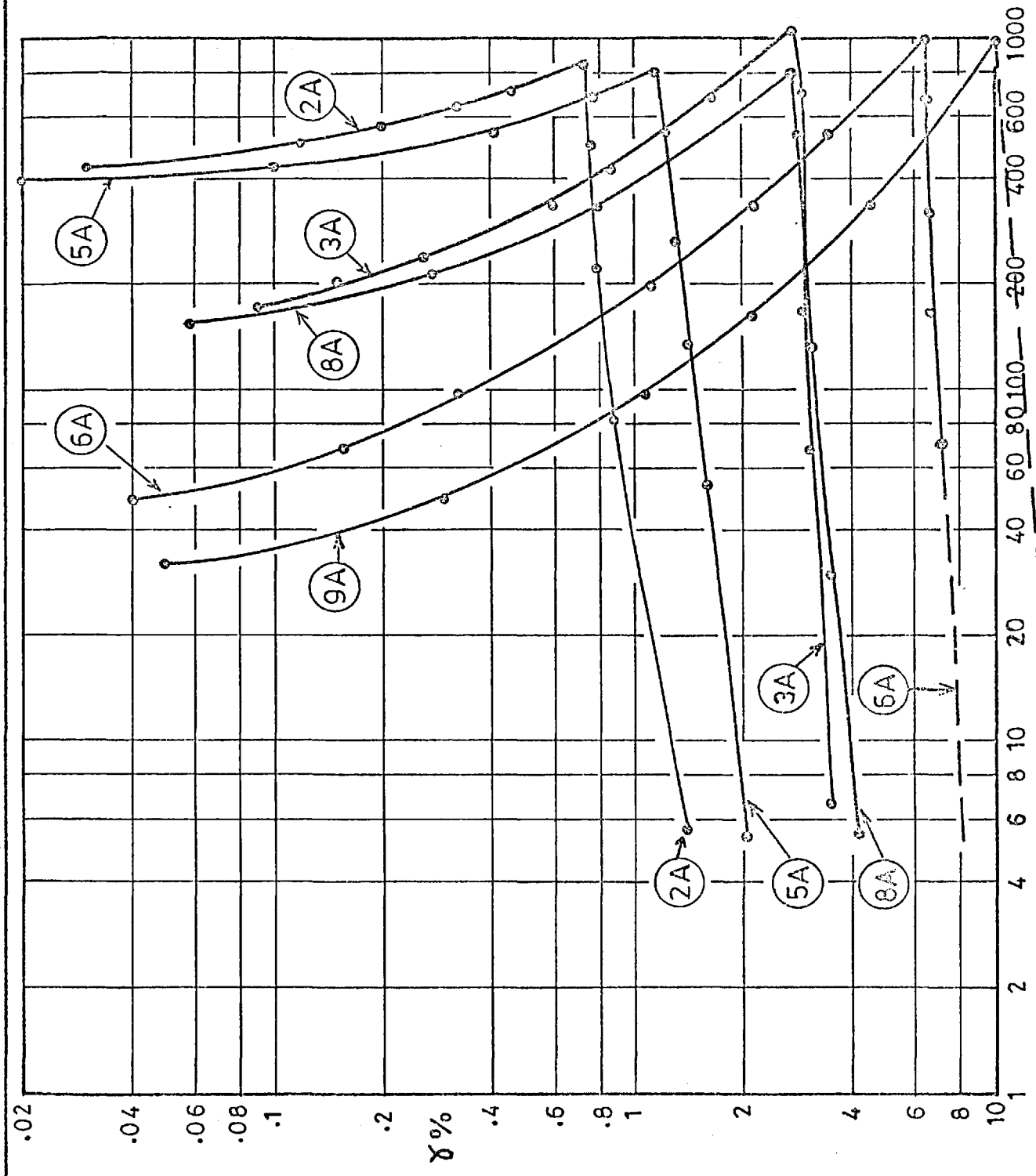

SHEAR STRAIN VS. MEAN NORMAL STRESS FOR ALL THE ANISOTROPIC CONSOLIDATION TESTS.

FIG 7-10

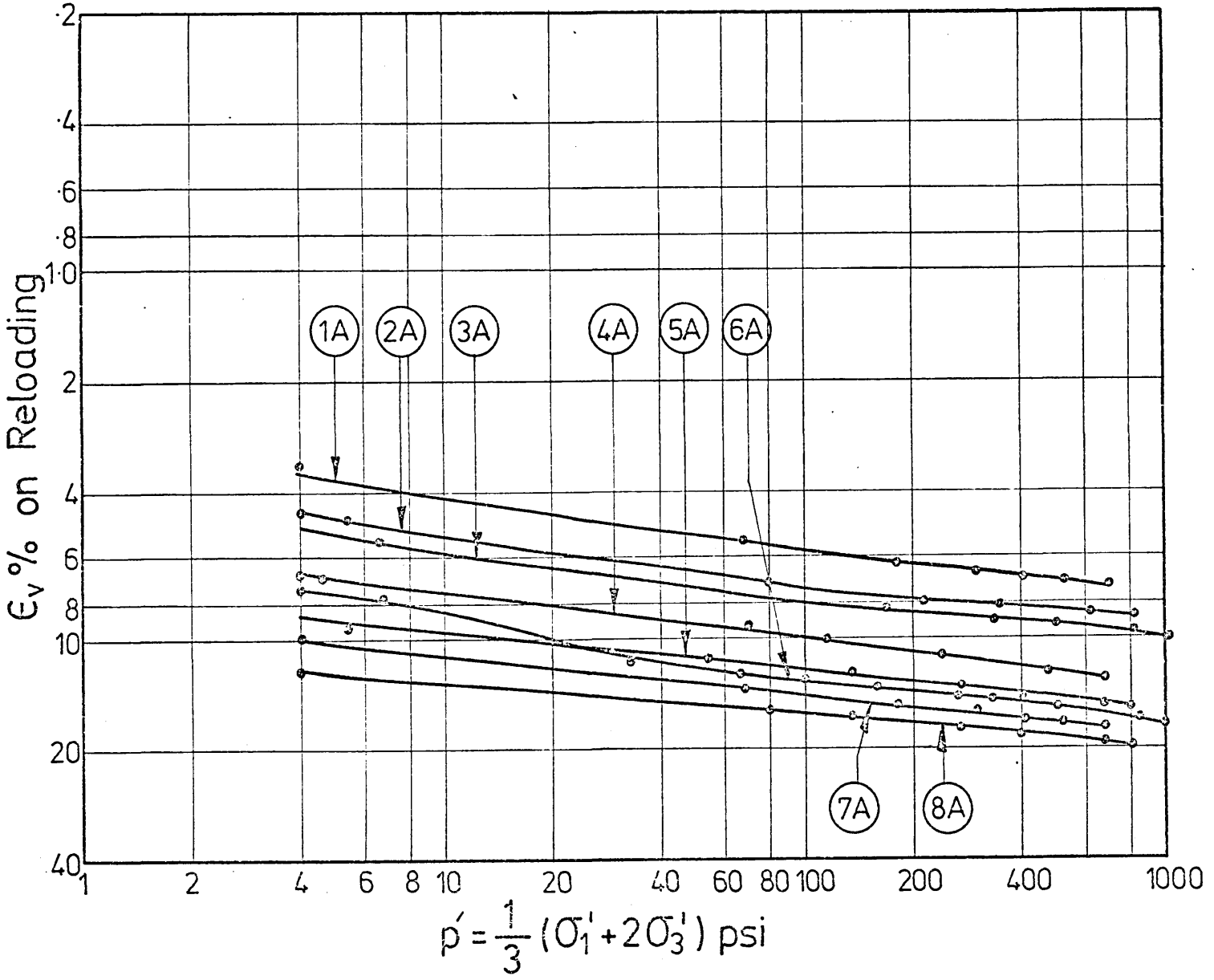

VOLUMETRIC STRAIN VS. MEAN NORMAL STRESS ON RELOADING FOR ALL THE ANISOTROPIC CONSOLIDATION TESTS.

Fig. 7-11

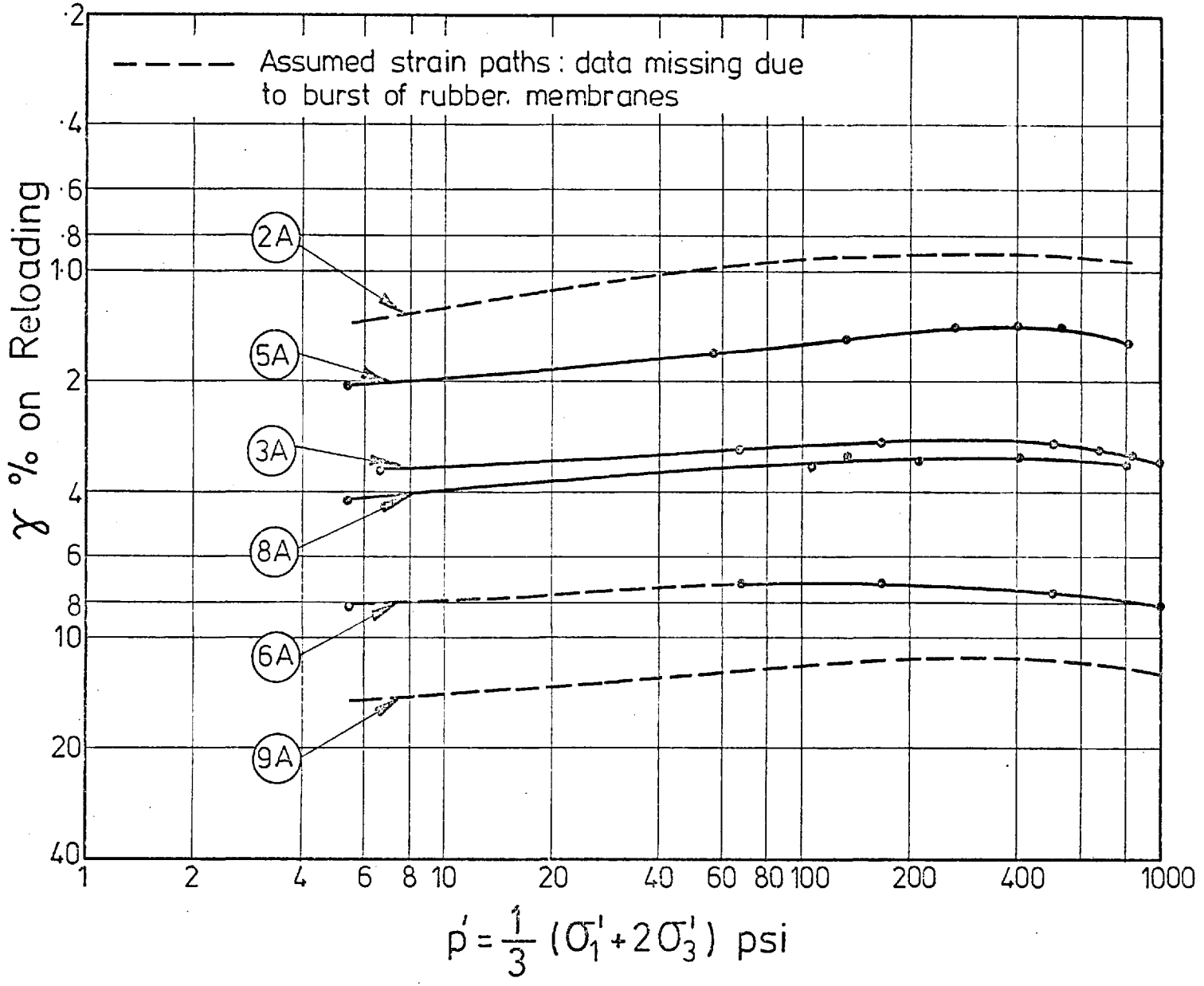

SHEAR STRAIN VS. MEAN NORMAL STRESS ON RELOADING FOR ALL THE ANISOTROPIC CONSOLIDATION TESTS.

Fig. 7-12

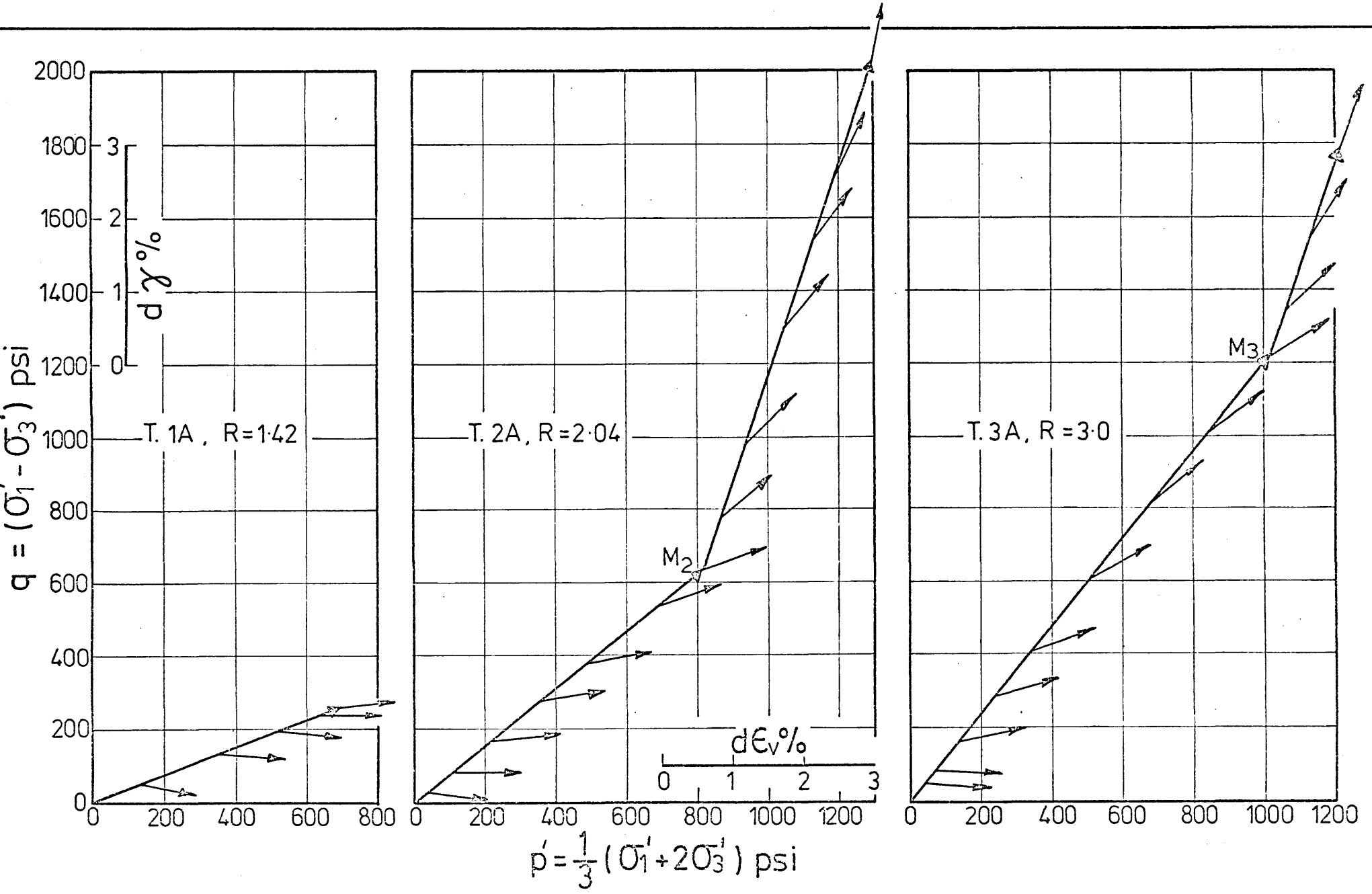

PLASTIC STRAIN INCREMENT VECTORS FOR THE DENSE SAMPLES No. 1A, 2A AND 3A.

Fig. 7-13

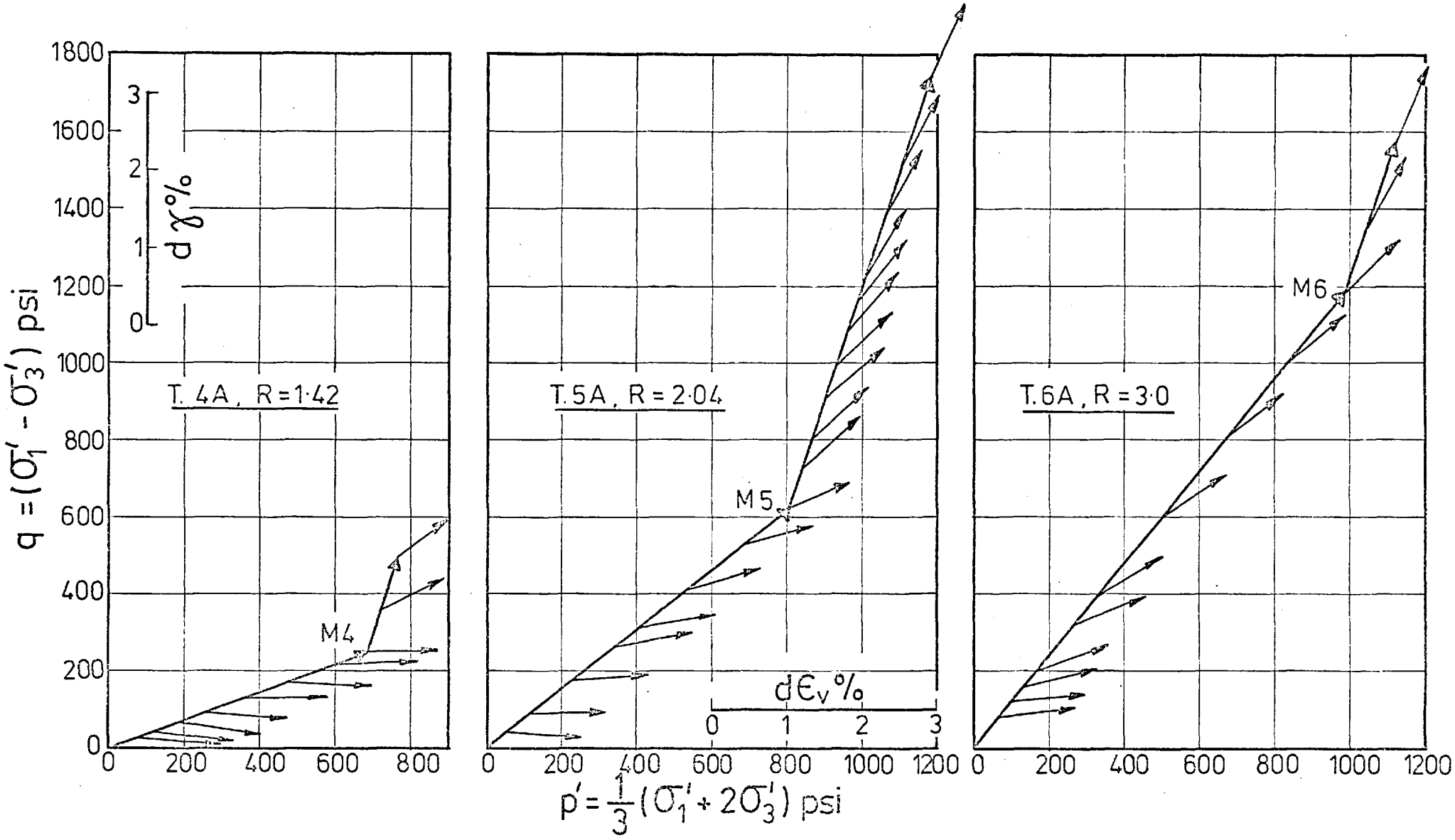

PLASTIC STRAIN INCREMENT VECTORS FOR THE LOOSE SAMPLES No. 4A, 5A AND 6A.

Fig. 7-14

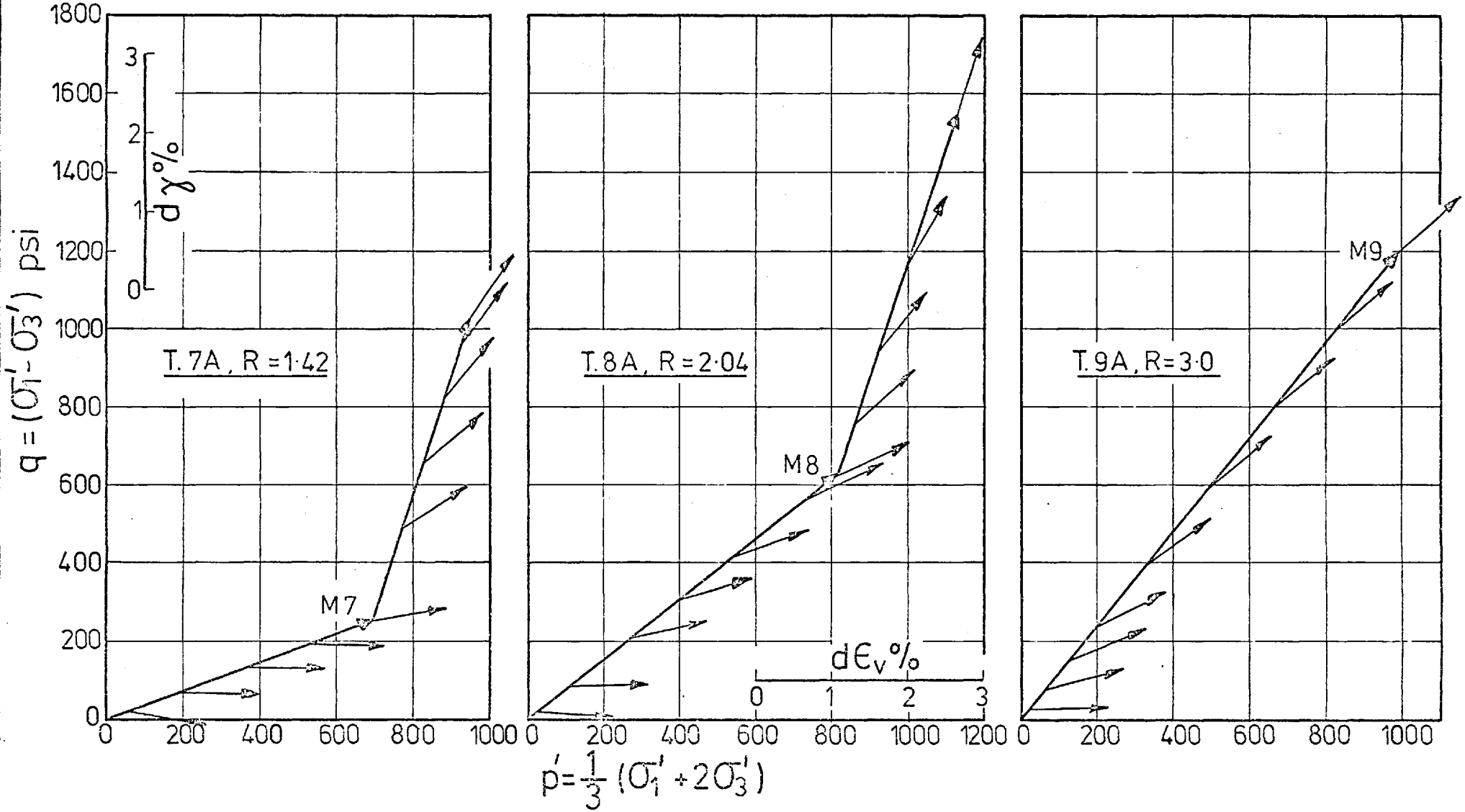

PLASTIC STRAIN INCREMENT VECTORS FOR THE VERY LOOSE SAMPLES No. 7A, 8A AND 9A.

Fig. 7-15

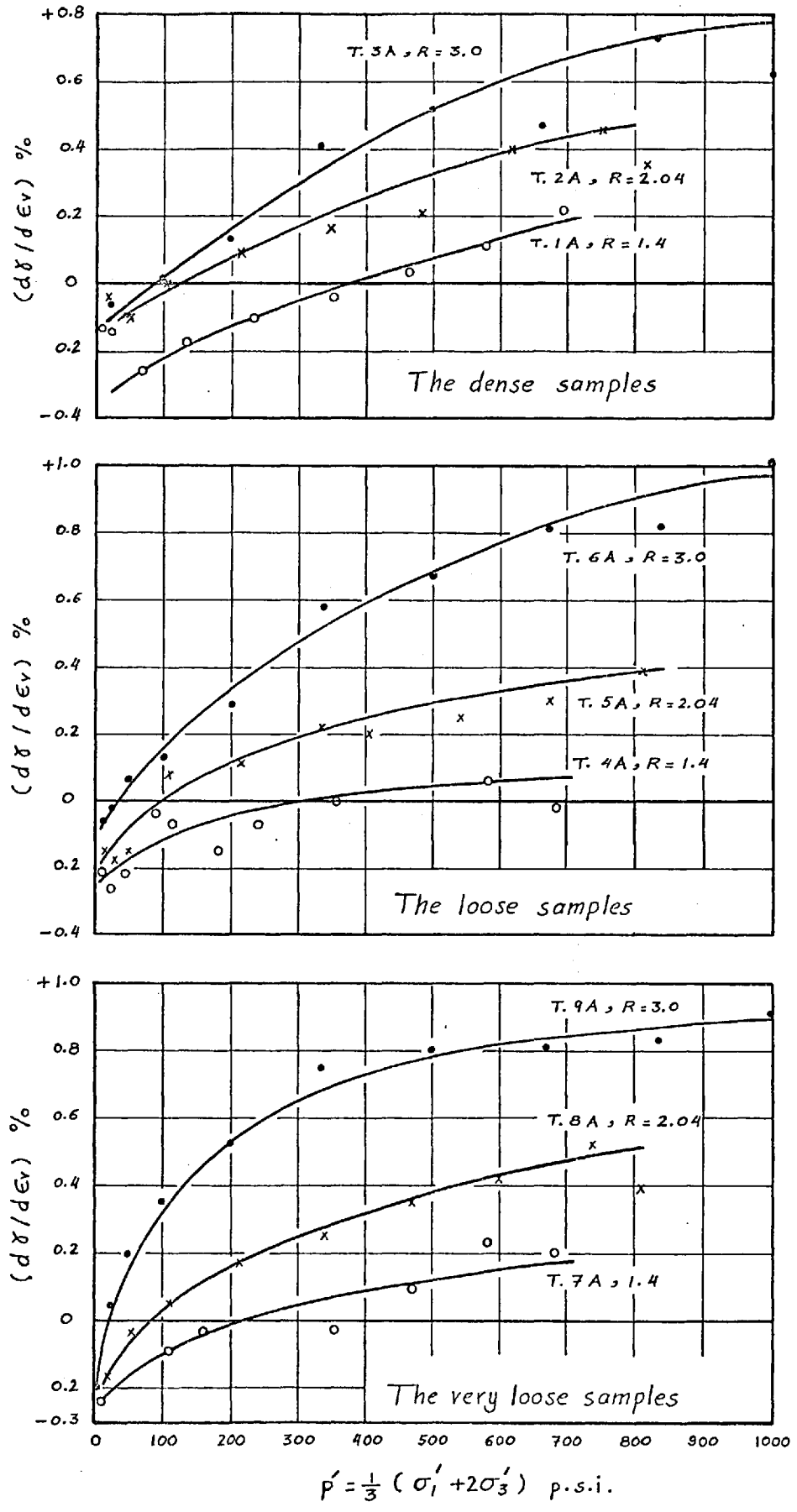

VARIATION OF THE SLOPES OF THE PLASTIC STRAIN INCREMENT VECTORS ALONG THE CONSTANT STRESS RATIO CONSOLIDATION PATHS, WITH THE MEAN NORMAL STRESS.

FIG 7–16

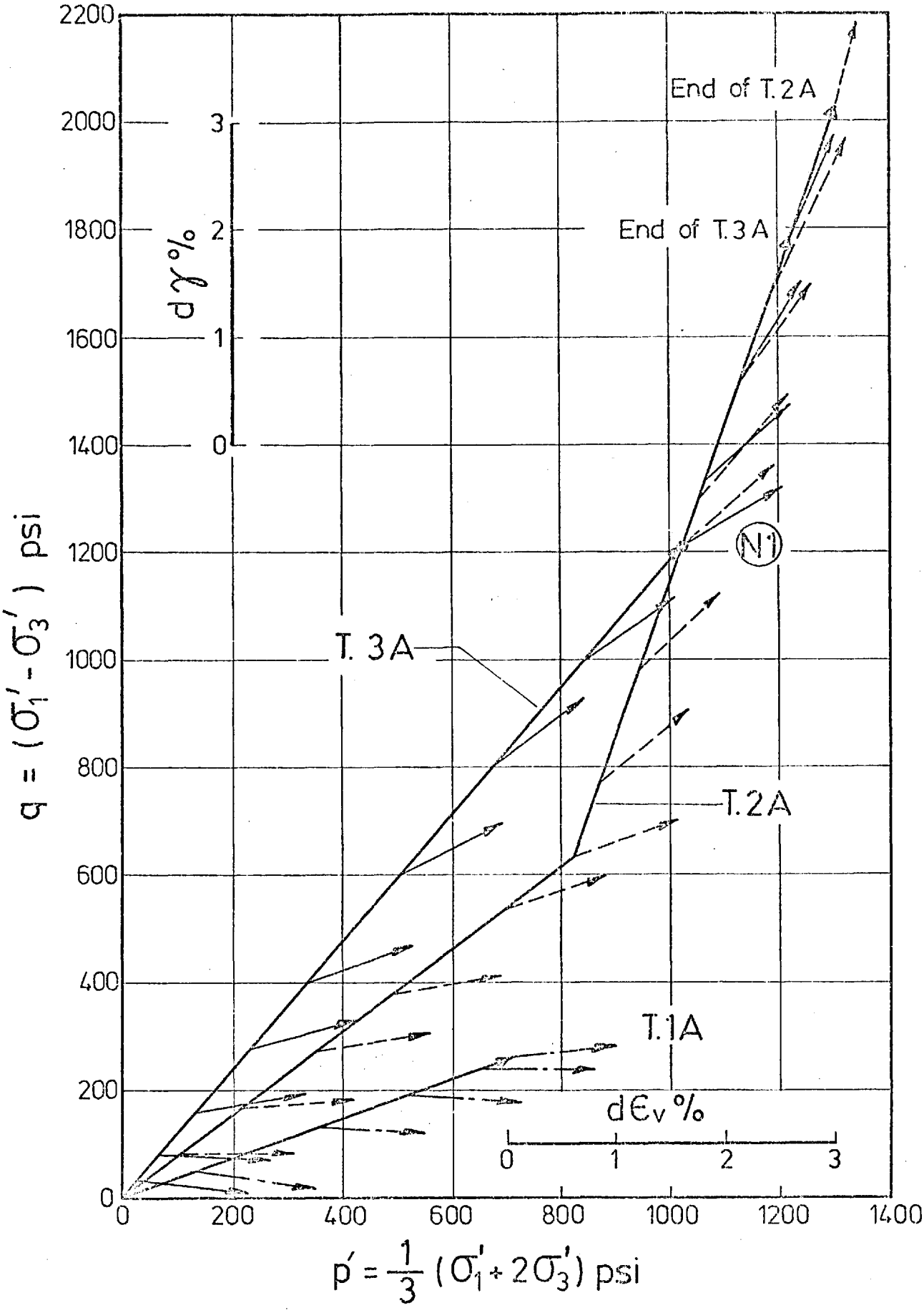

PLASTIC STRAIN INCREMENT VECTORS FOR DENSE SAMPLES.

Fig. 7-17

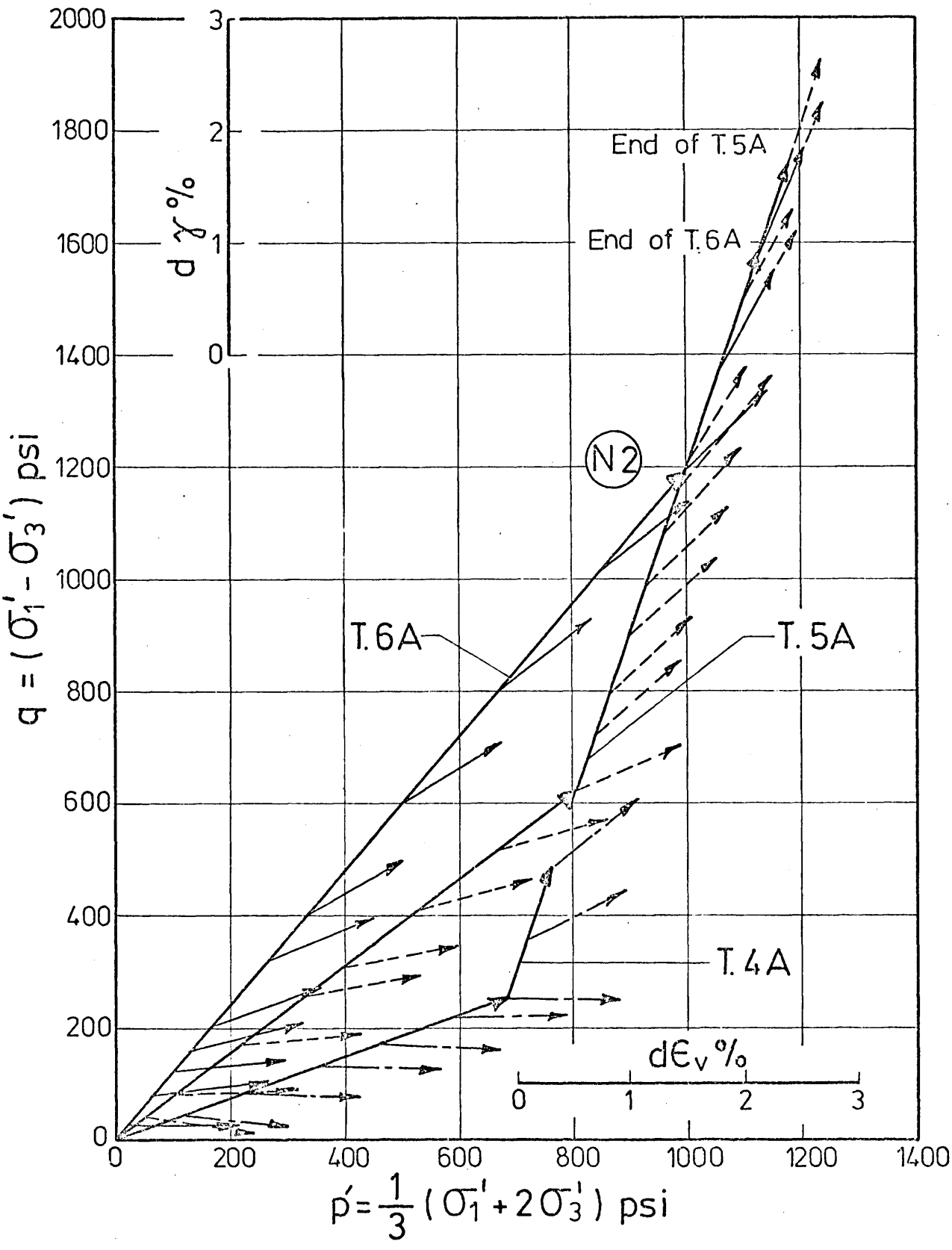

PLASTIC STRAIN INCREMENT VECTOR FOR LOOSE SAMPLES.

Fig.7-18

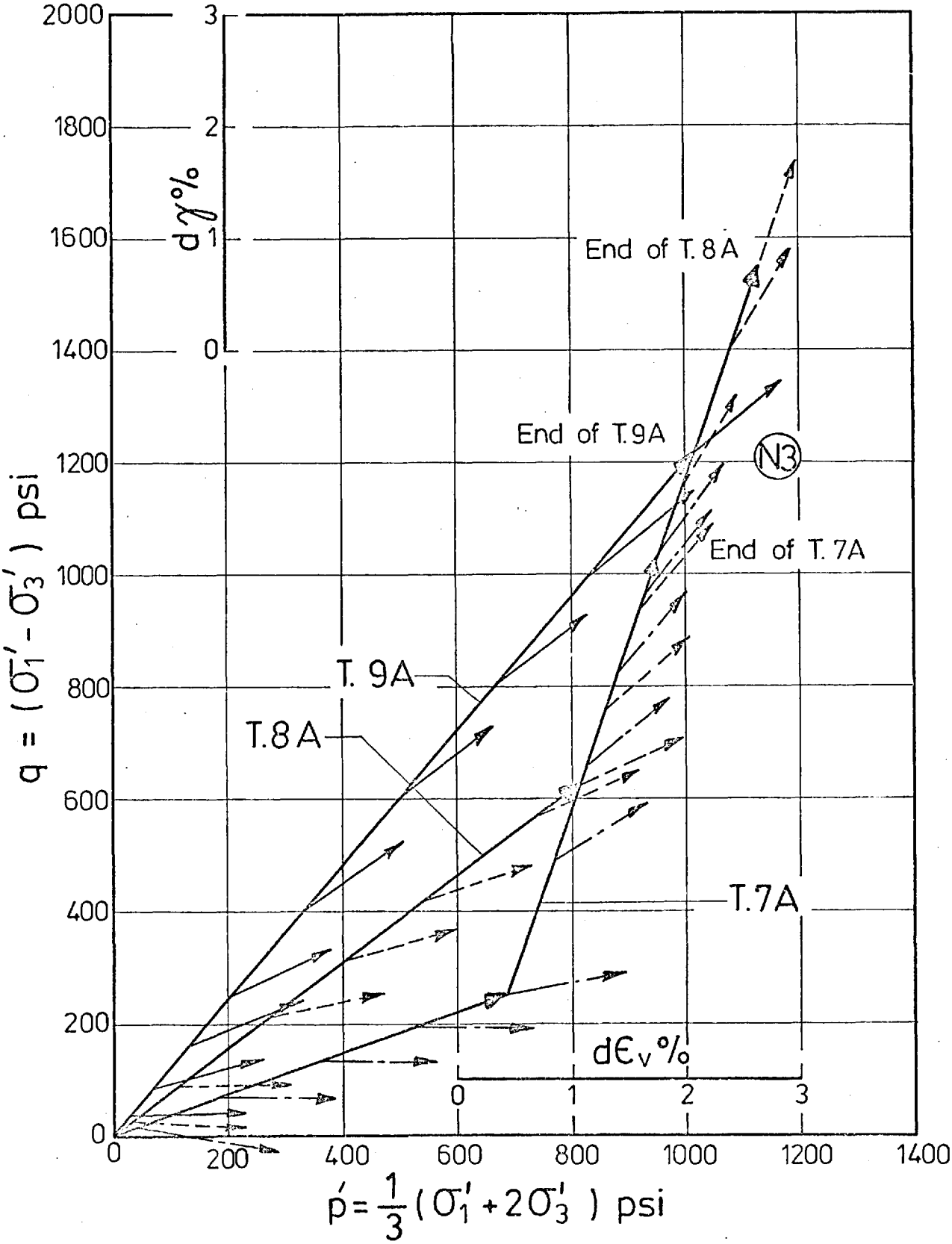

PLASTIC STRAIN INCREMENT VECTORS FOR VERY LOOSE SAMPLES.

Fig. 7-19

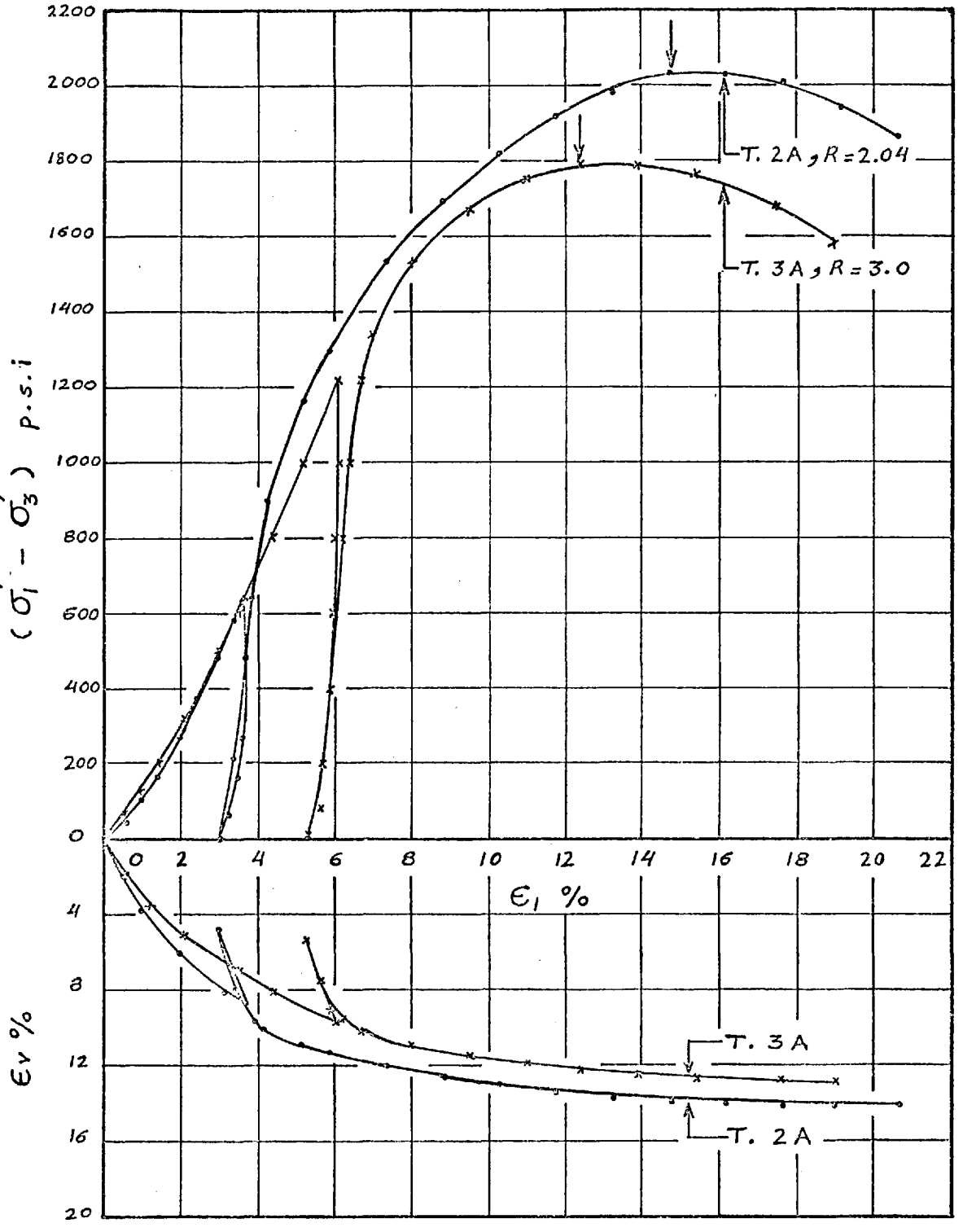

GRANITE ROCKFILL – DENSE SAMPLES CONSOLIDATED ANISOTROPICALLY THEN SHEARED DRAINED.

FIG. 7 – 20

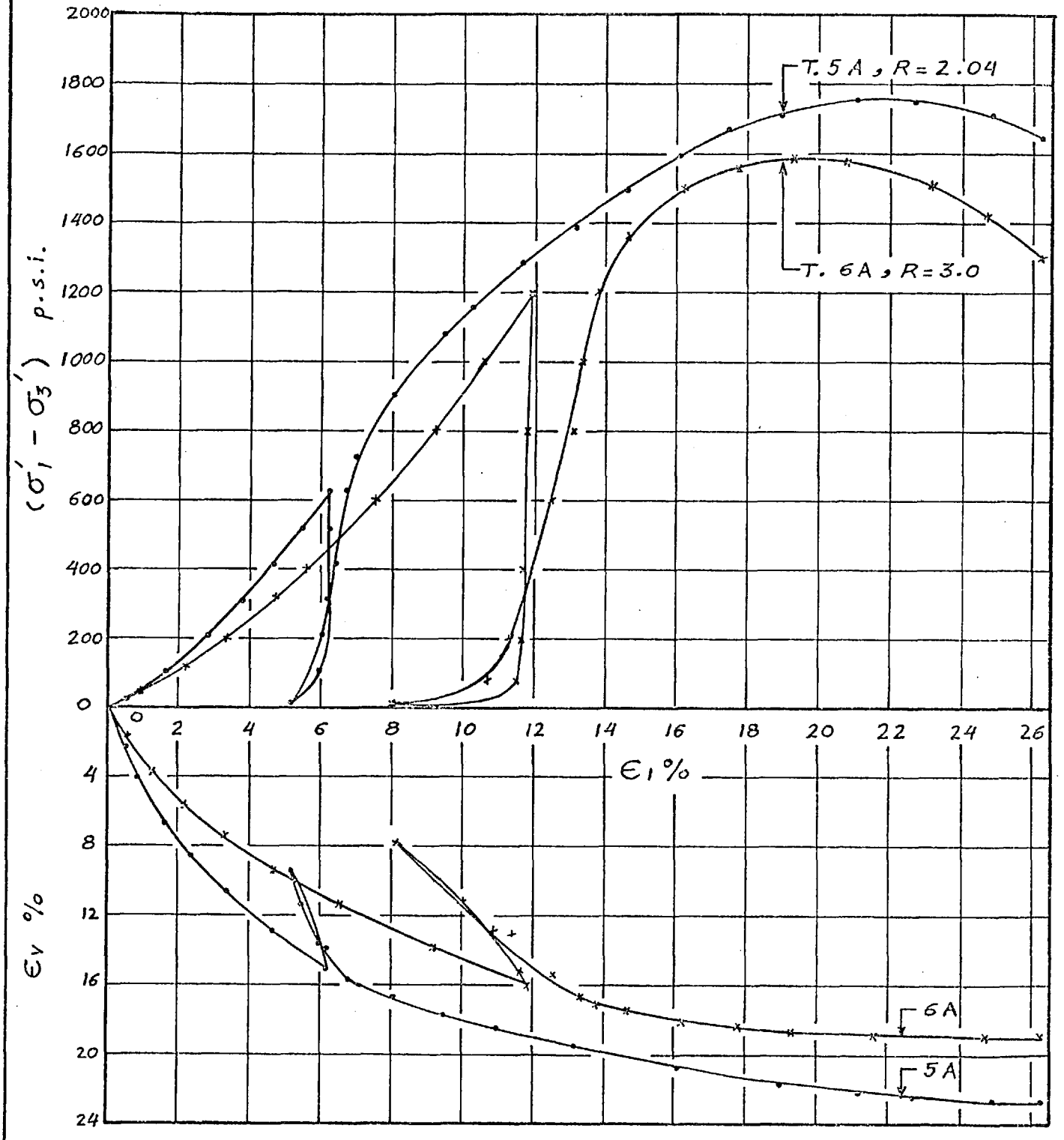

GRANITE ROCKFILL — LOOSE SAMPLES CONSOLIDATED ANISOTROPICALLY THEN SHEARED DRAINED.

FIG. 7 – 21

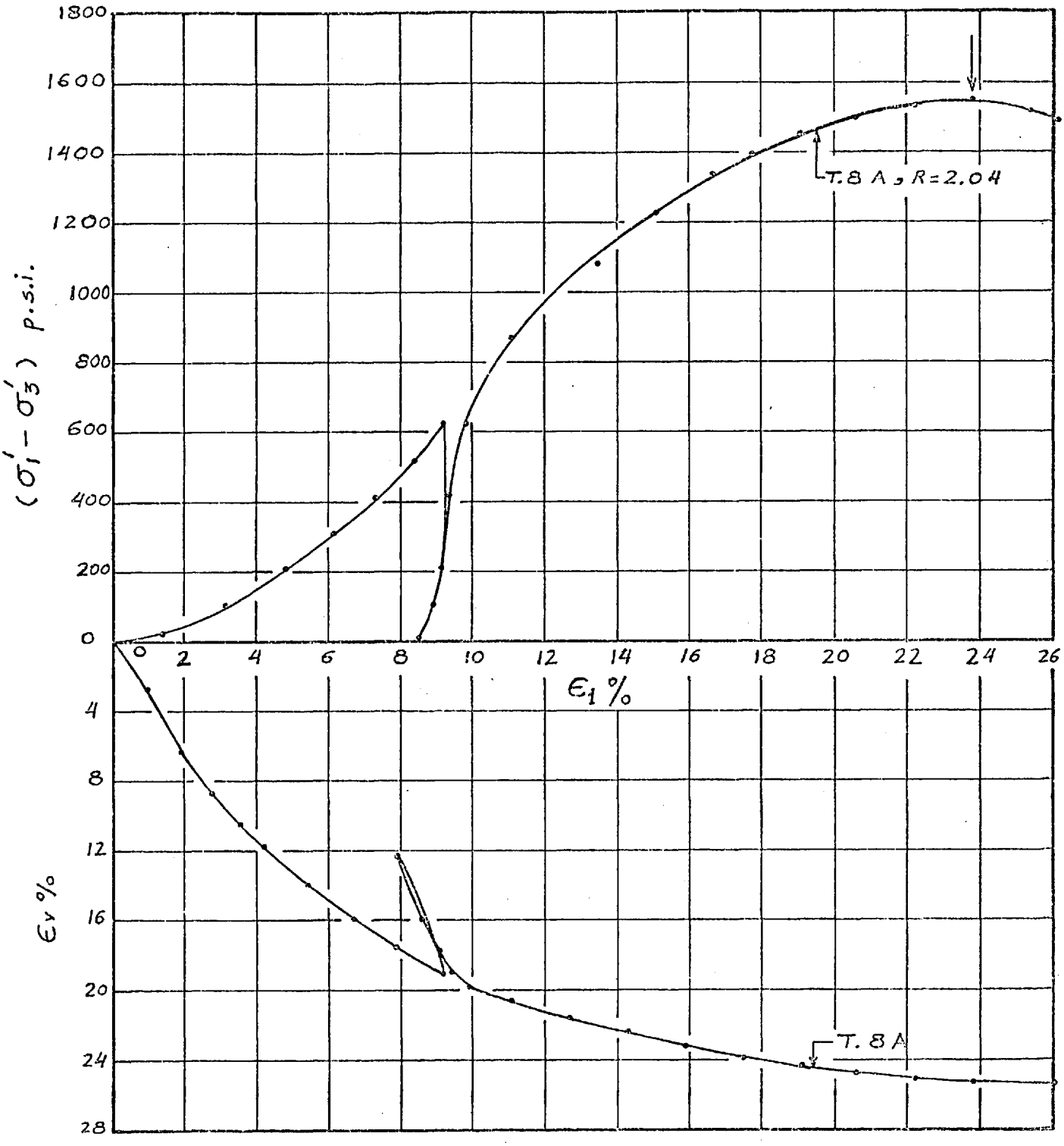

GRANITE ROCKFILL—VERY LOOSE SAMPLE CONSOLIDATED ANISOTROPICALLY THEN SHEARED DRAINED.

FIG. 7—22

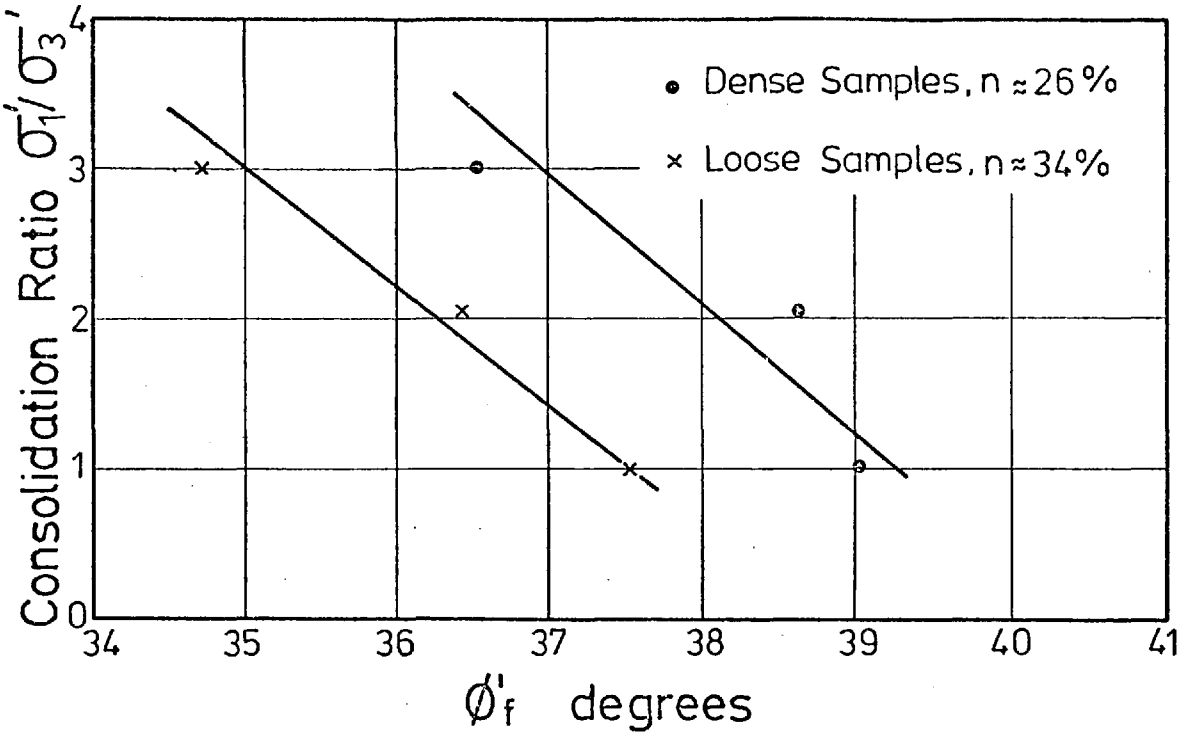

A) CONSOLIDATION RATIO σ_1'/σ_3' vs. ϕ_f'

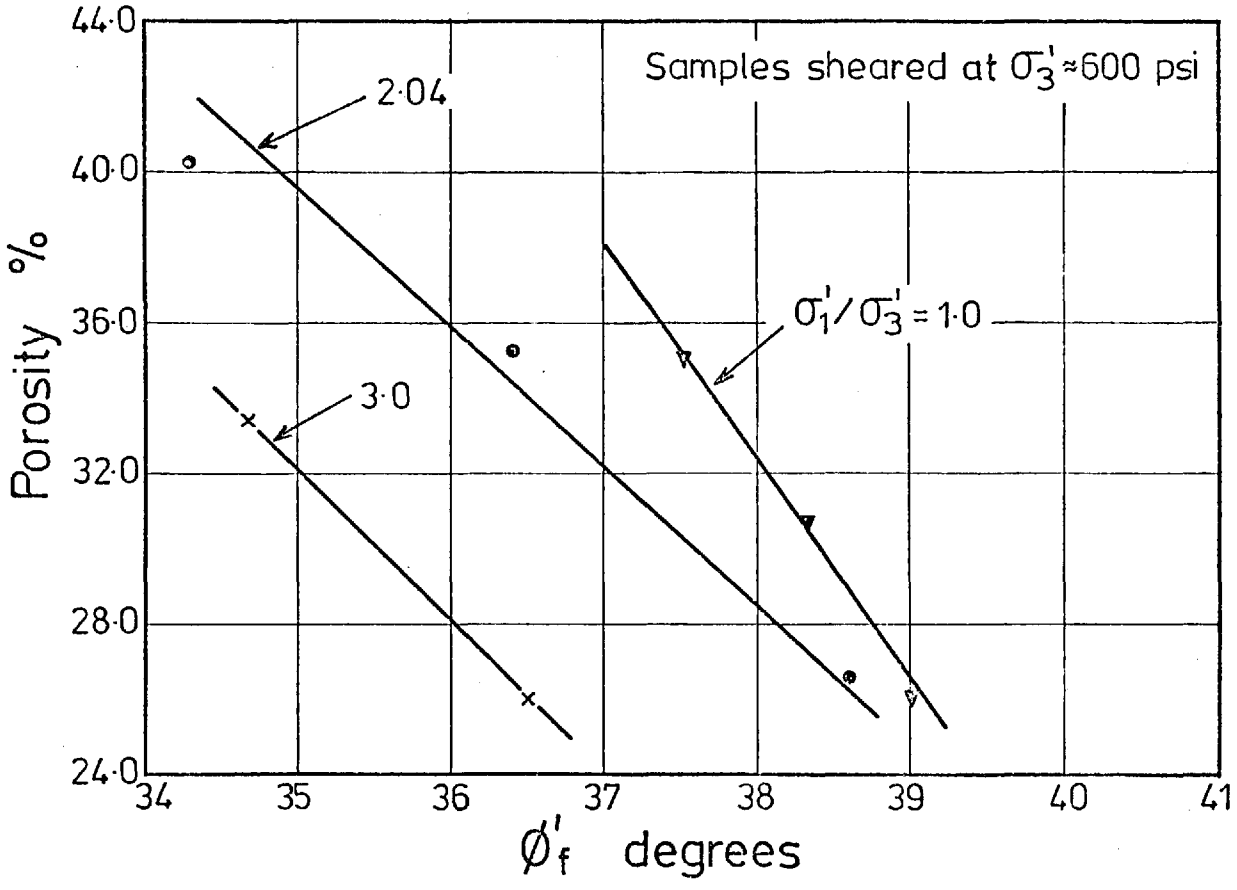

B) INITIAL SAMPLE POROSITY vs. ϕ_f'

Fig. 7-23

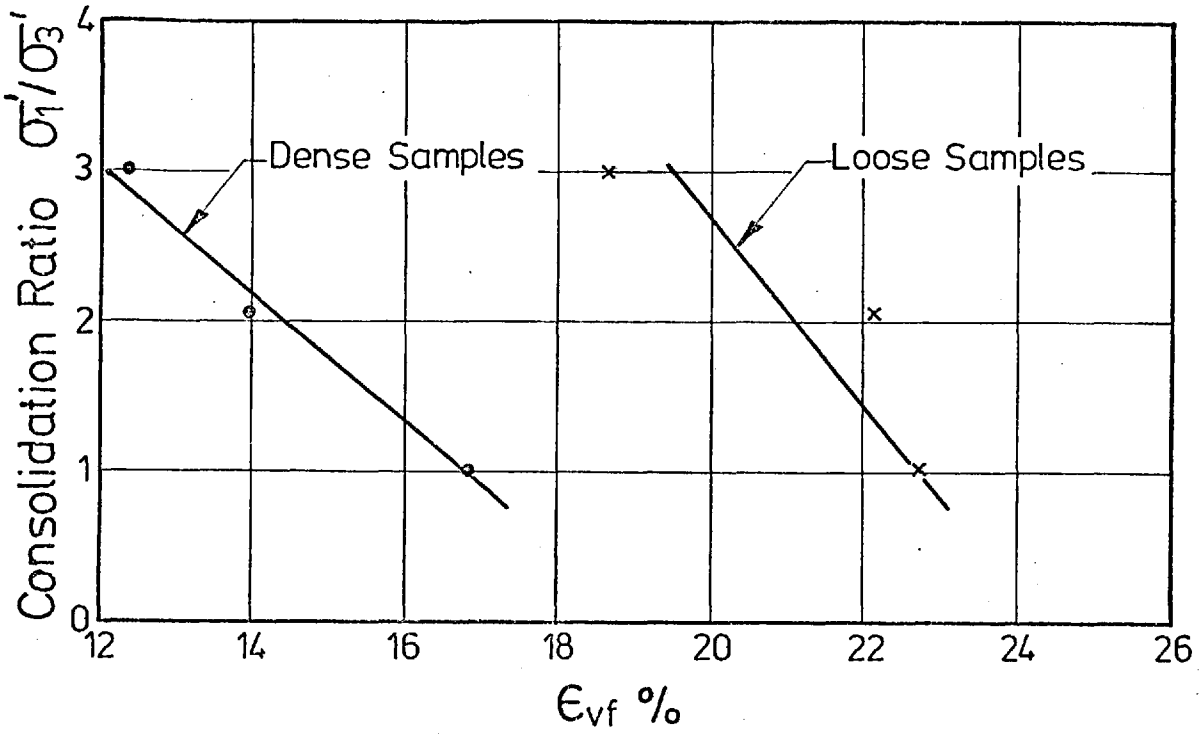

A) CONSOLIDATION RATIO σ_1'/σ_3' vs. ϵ_{vf} %

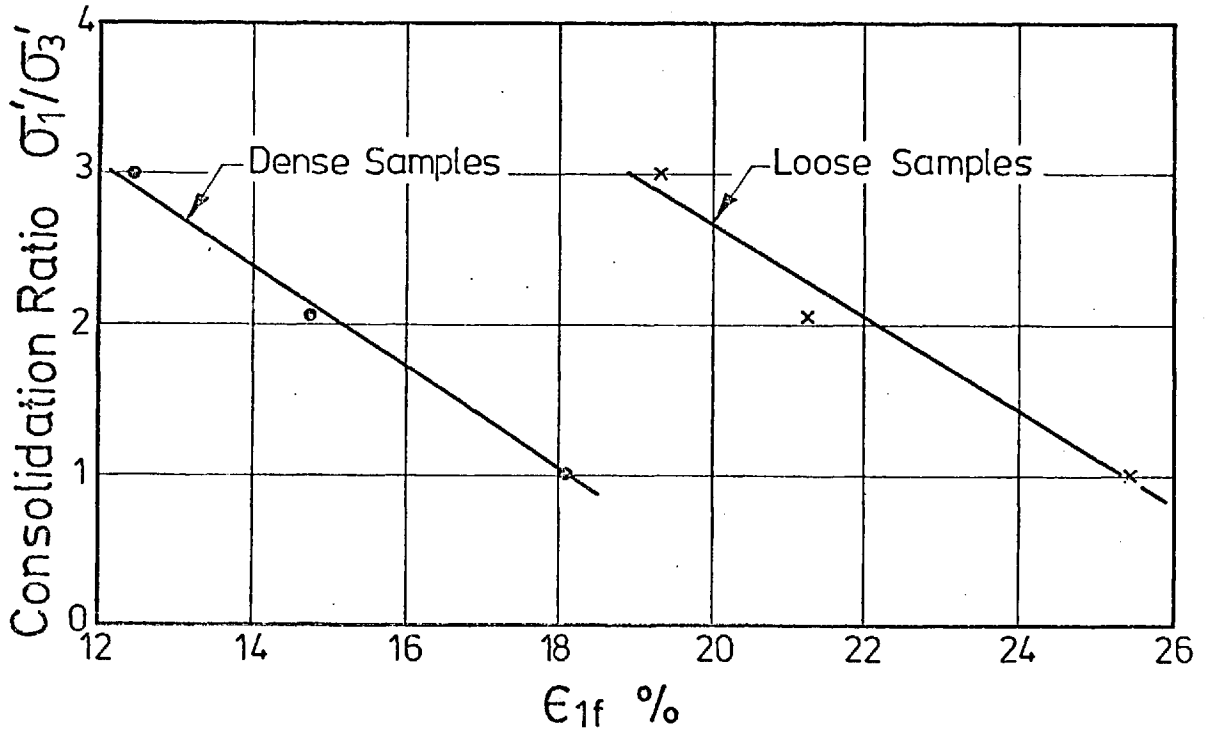

B) CONSOLIDATION RATIO σ_1'/σ_3' vs. ϵ_{1f} %

Fig. 7-24

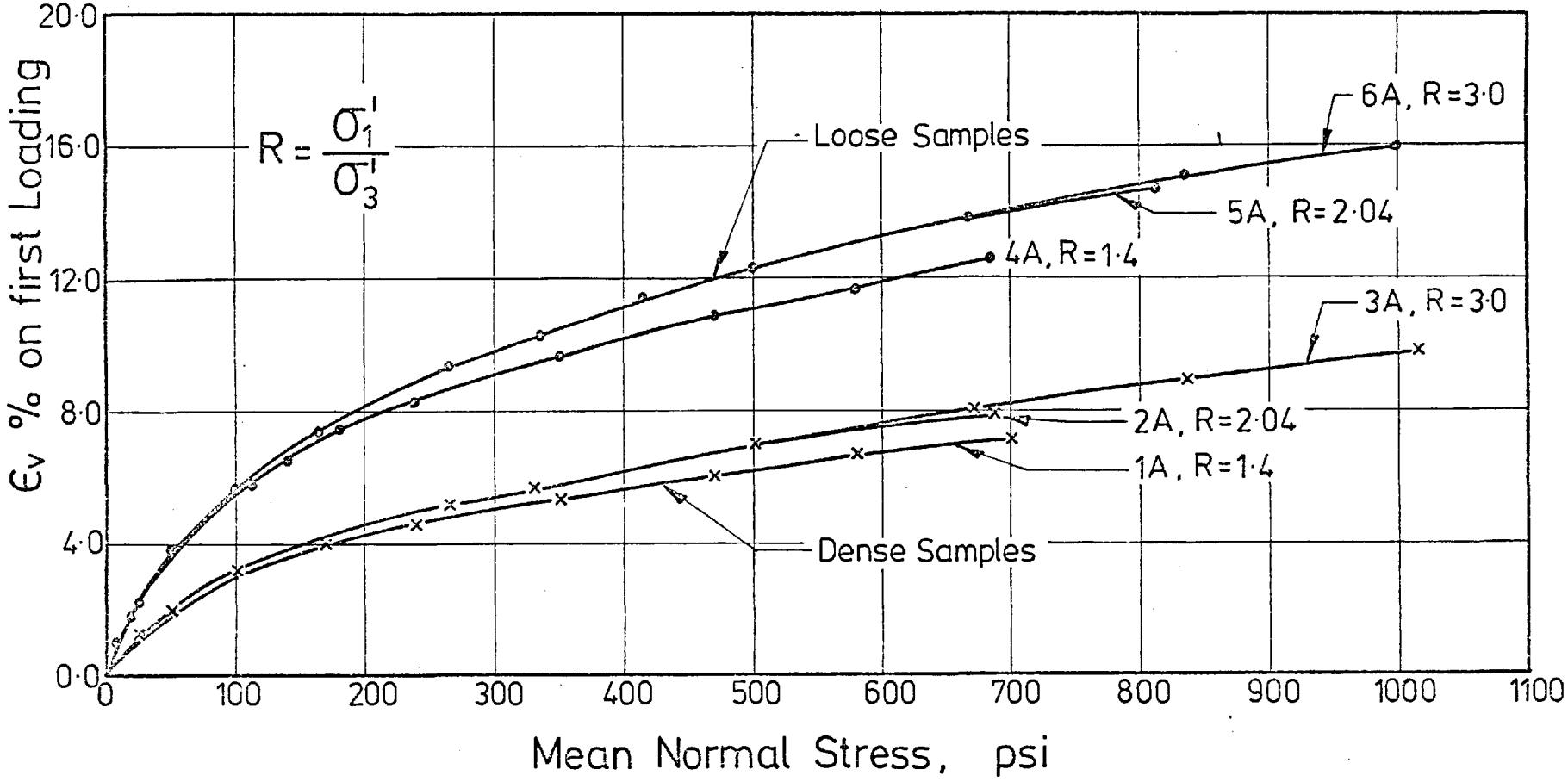

VOLUMETRIC STRAIN vs. MEAN NORMAL STRESS FOR THE ANISOTROPIC CONSOLIDATION TESTS.

Fig. 7-25

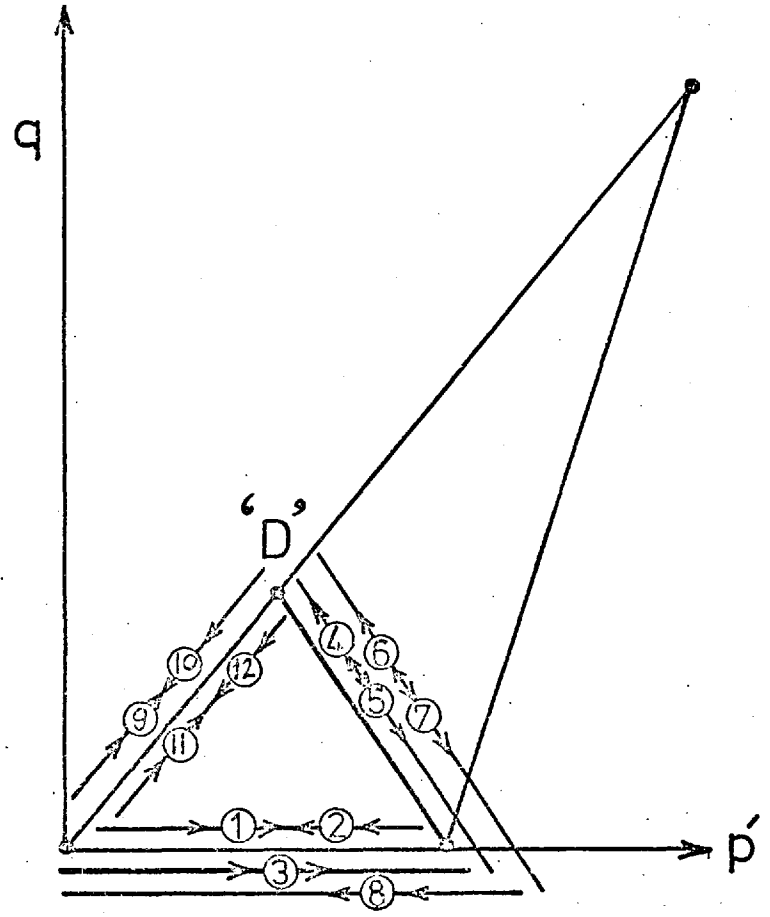

TEST 3G

FIG (7-27)

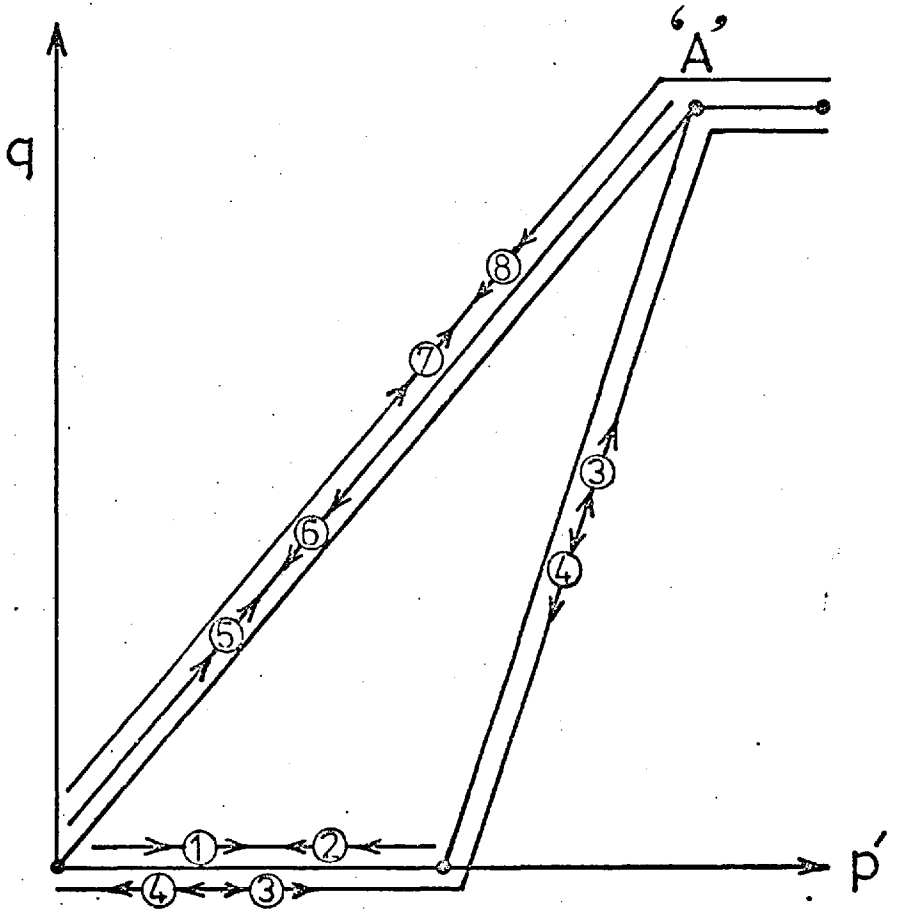

TEST 1G

FIG (7-26)

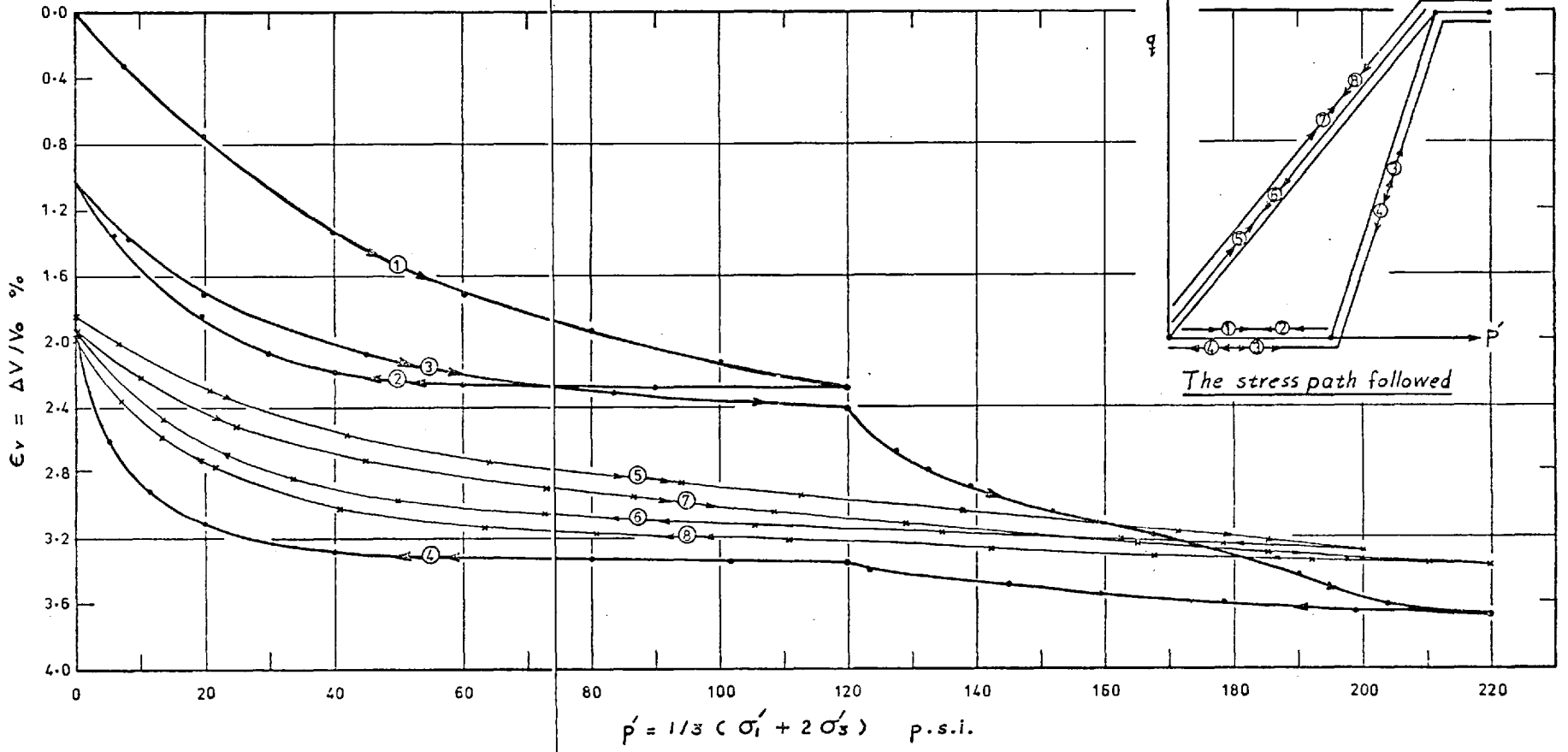

GRANITE ROCKFILL-VOLUMETRIC STRAIN VS. MEAN NORMAL STRESS FOR TEST 1G

FIG 7 - 28

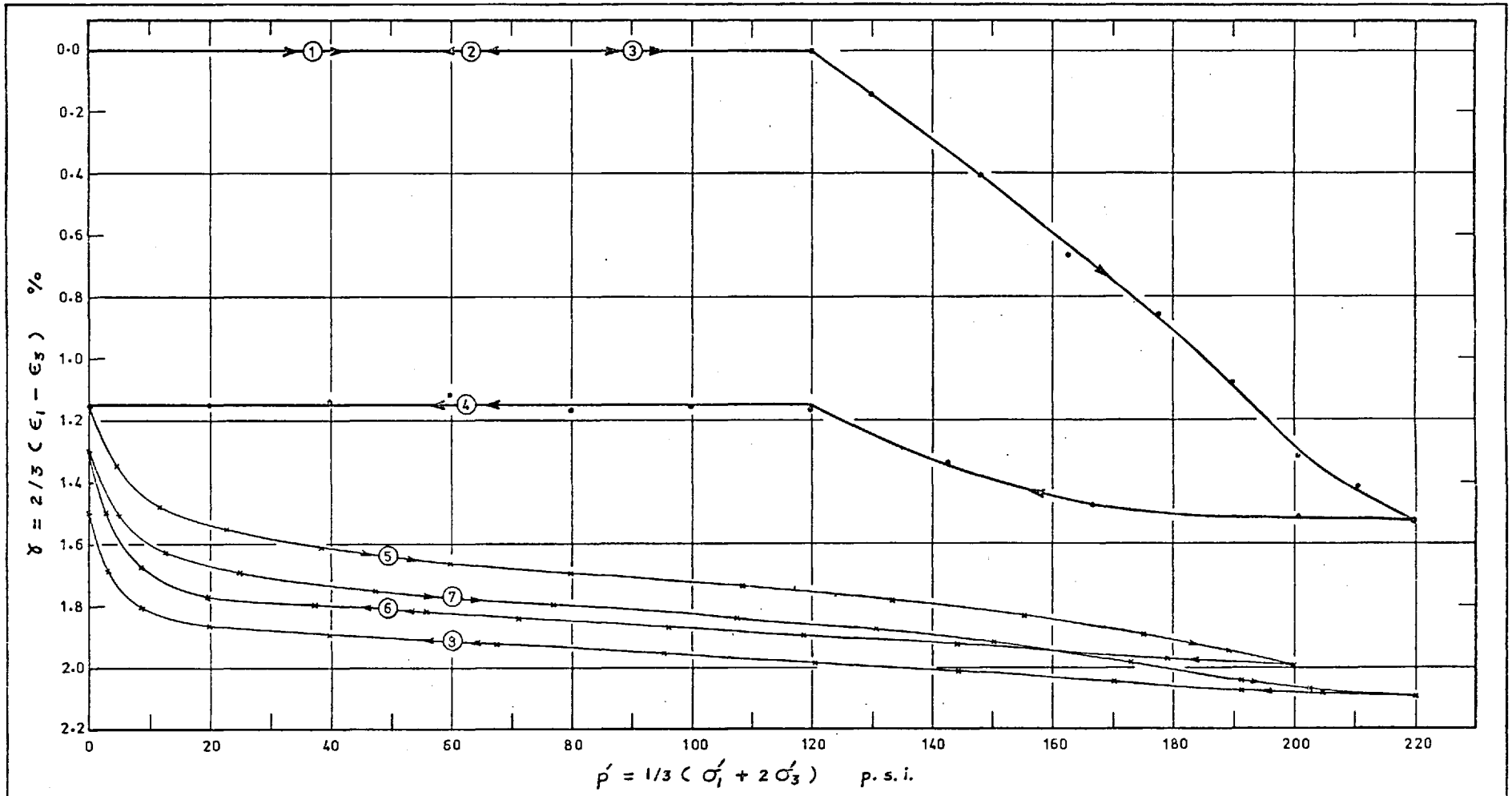

GRANITE ROCKFILL-SHEAR STRAIN VS MEAN NORMAL STRESS FOR TEST 16

FIG 7 - 29

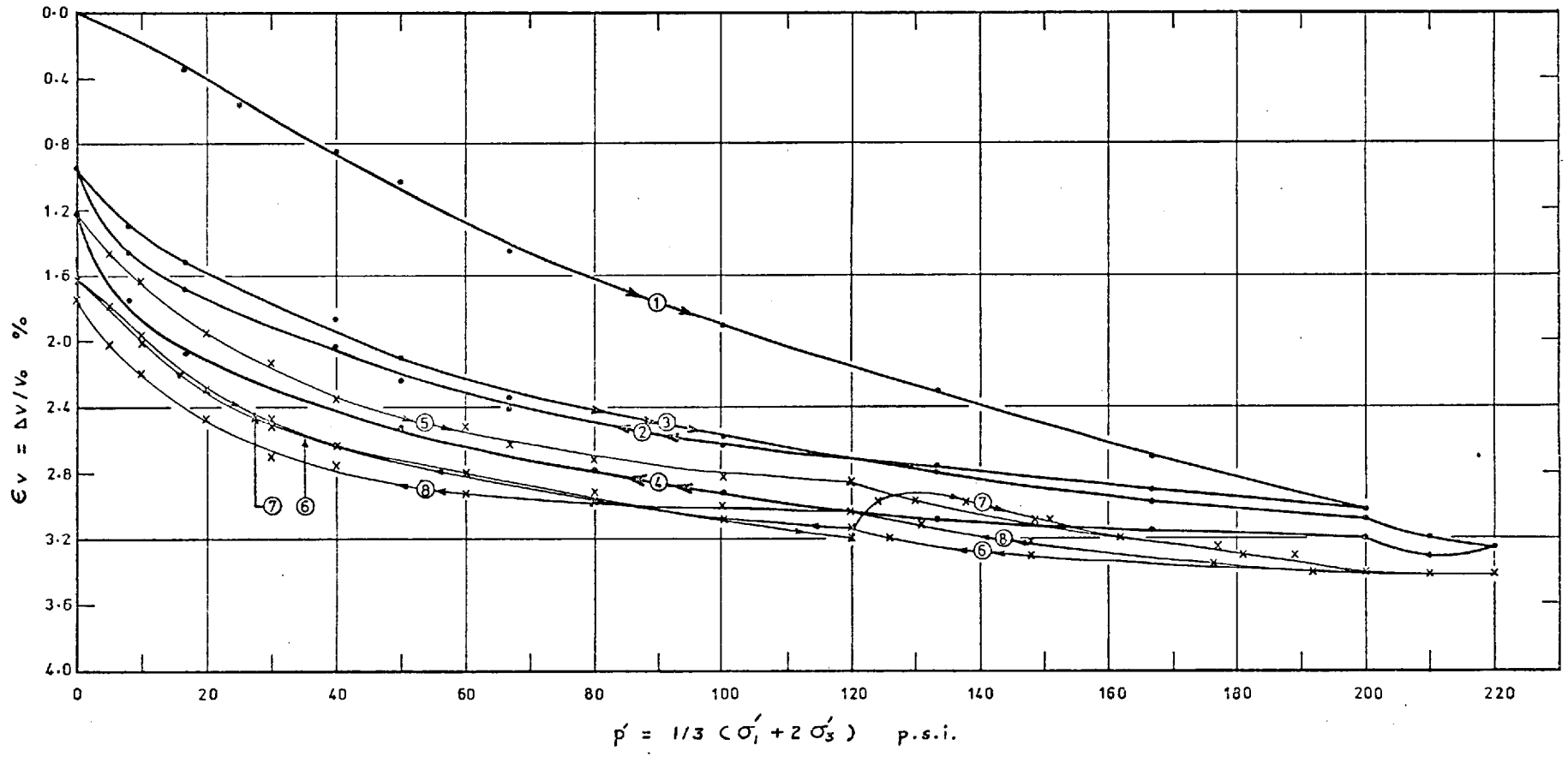

GRANITE ROCKFILL - VOLUMETRIC STRAIN VS. MEAN NORMAL STRESS FOR TEST 2G

317

FIG 7 - 30

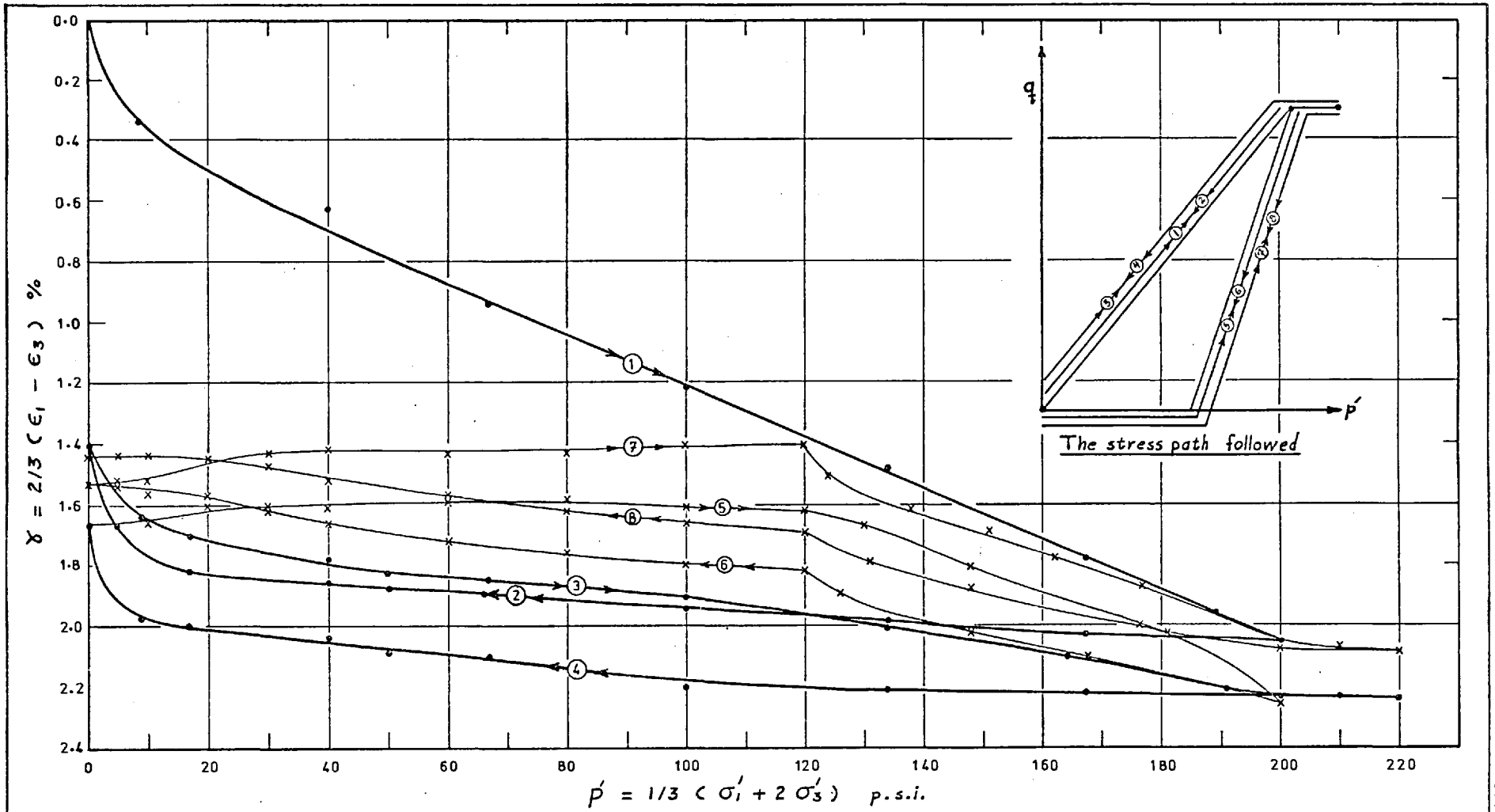

GRANITE ROCKFILL-SHEAR STRAIN VS. MEAN NORMAL STRESS FOR TEST 2G

FIG 7 - 31

318

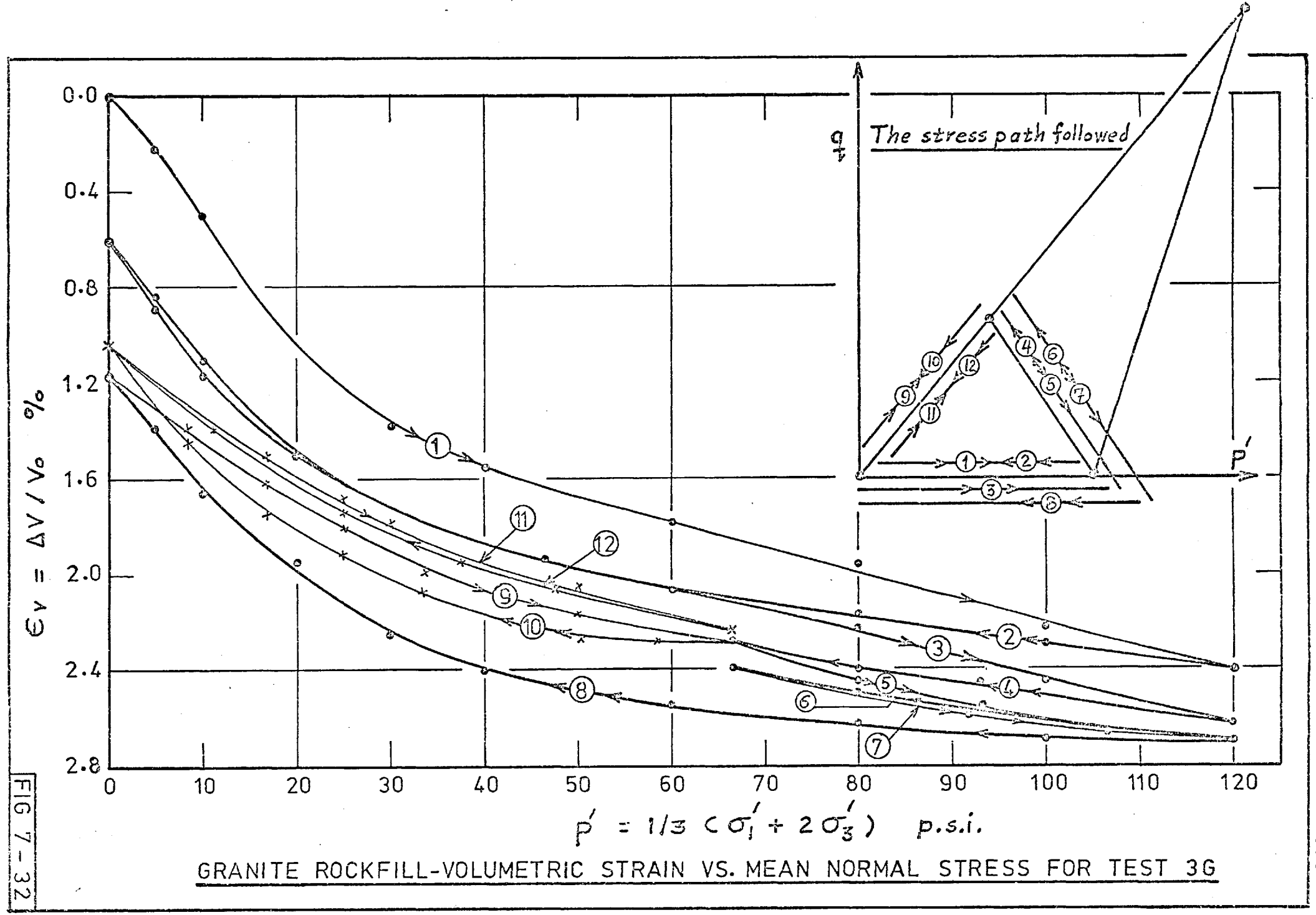

FIG 7-32

GRANITE ROCKFILL-VOLUMETRIC STRAIN VS. MEAN NORMAL STRESS FOR TEST 3G

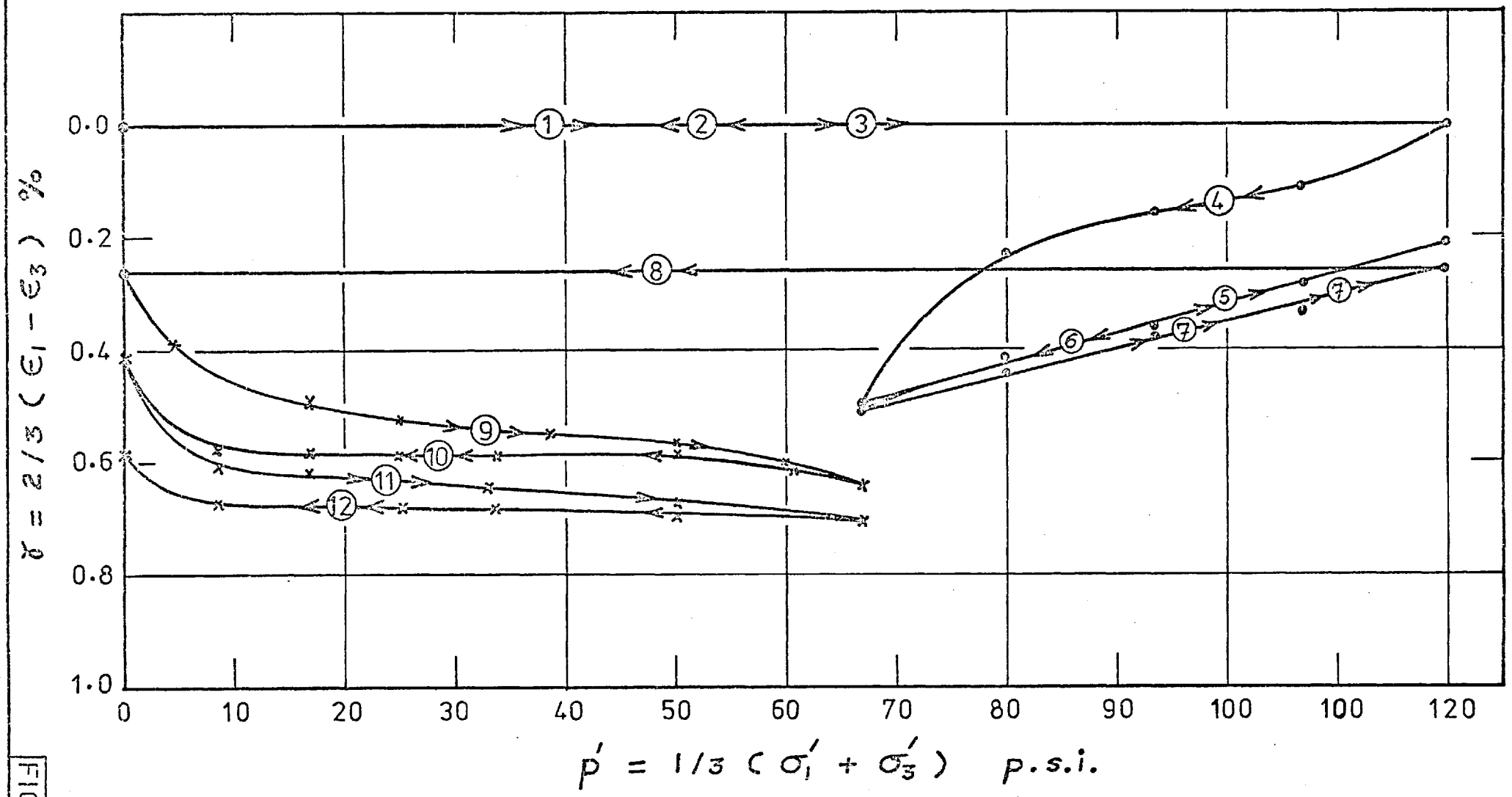

FIG 7-33

GRANITE ROCKFILL - SHEAR STRAIN VS. MEAN NORMAL STRESS FOR TEST 3G

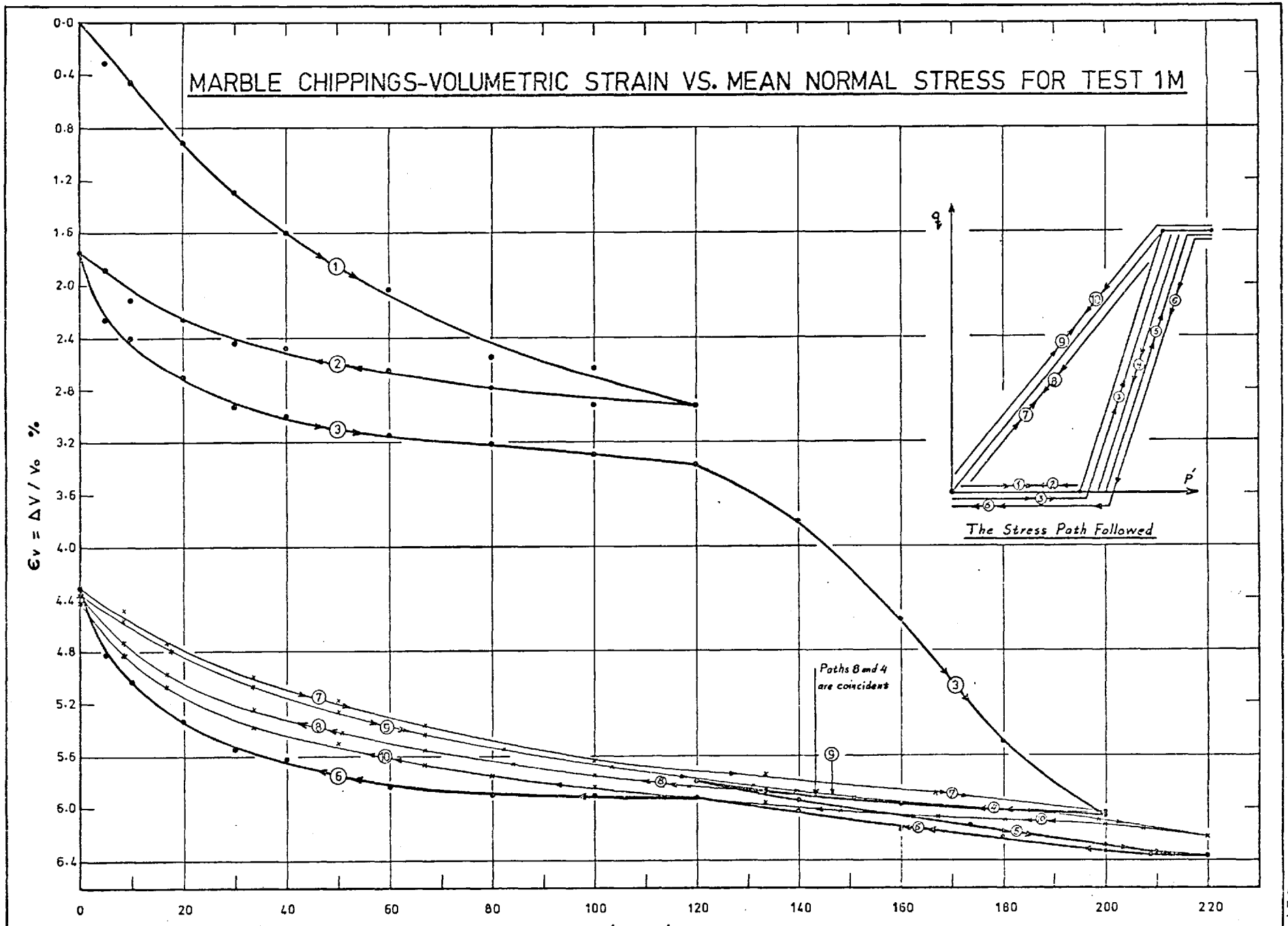
MARBLE CHIPPINGS-VOLUMETRIC STRAIN VS. MEAN NORMAL STRESS FOR TEST 1M
$\epsilon_v = \Delta V / V_o$ %
0·0
0·4
0·8
1·2
1·6
2·0
2·4
2·8
3·2
3·6
4·0
4·4
4·8
5·2
5·6
6·0
6·4
0
20
40
60
80
100
120
140
160
180
200
220
$p' = 1/3\ (\sigma'_1 + 2\sigma'_3)$ p. s.i.
Paths 8 and 4 are coincident
q
p'
The Stress Path Followed

FIG 7 - 34

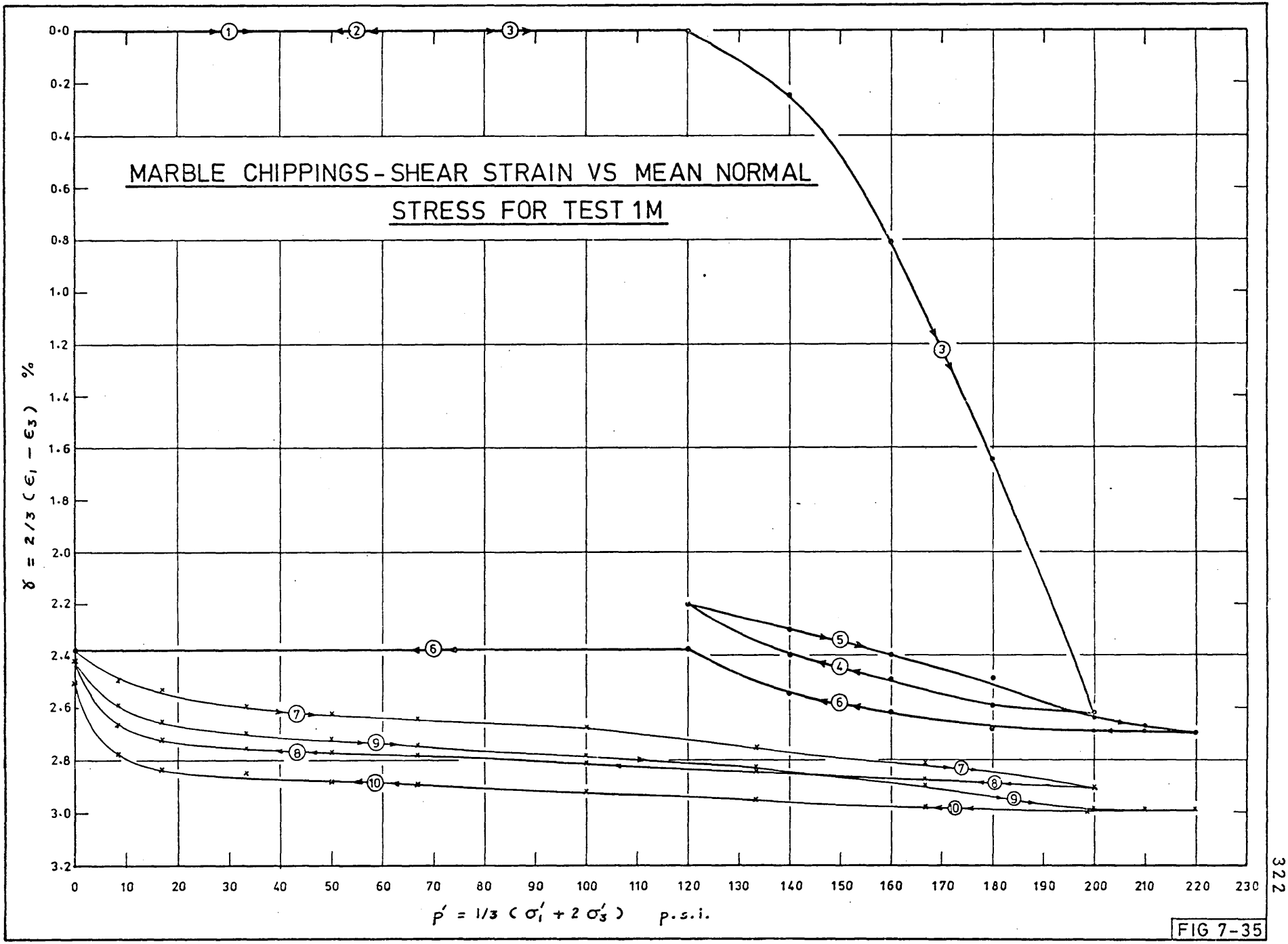
MARBLE CHIPPINGS - SHEAR STRAIN VS MEAN NORMAL STRESS FOR TEST 1M
γ = 2/3 (ε1 − ε3) %
p' = 1/3 (σ'1 + 2 σ'3) p.s.i.
0.0
0.2
0.4
0.6
0.8
1.0
1.2
1.4
1.6
1.8
2.0
2.2
2.4
2.6
2.8
3.0
3.2
0
10
20
30
40
50
60
70
80
90
100
110
120
130
140
150
160
170
180
190
200
210
220
230

FIG 7-35

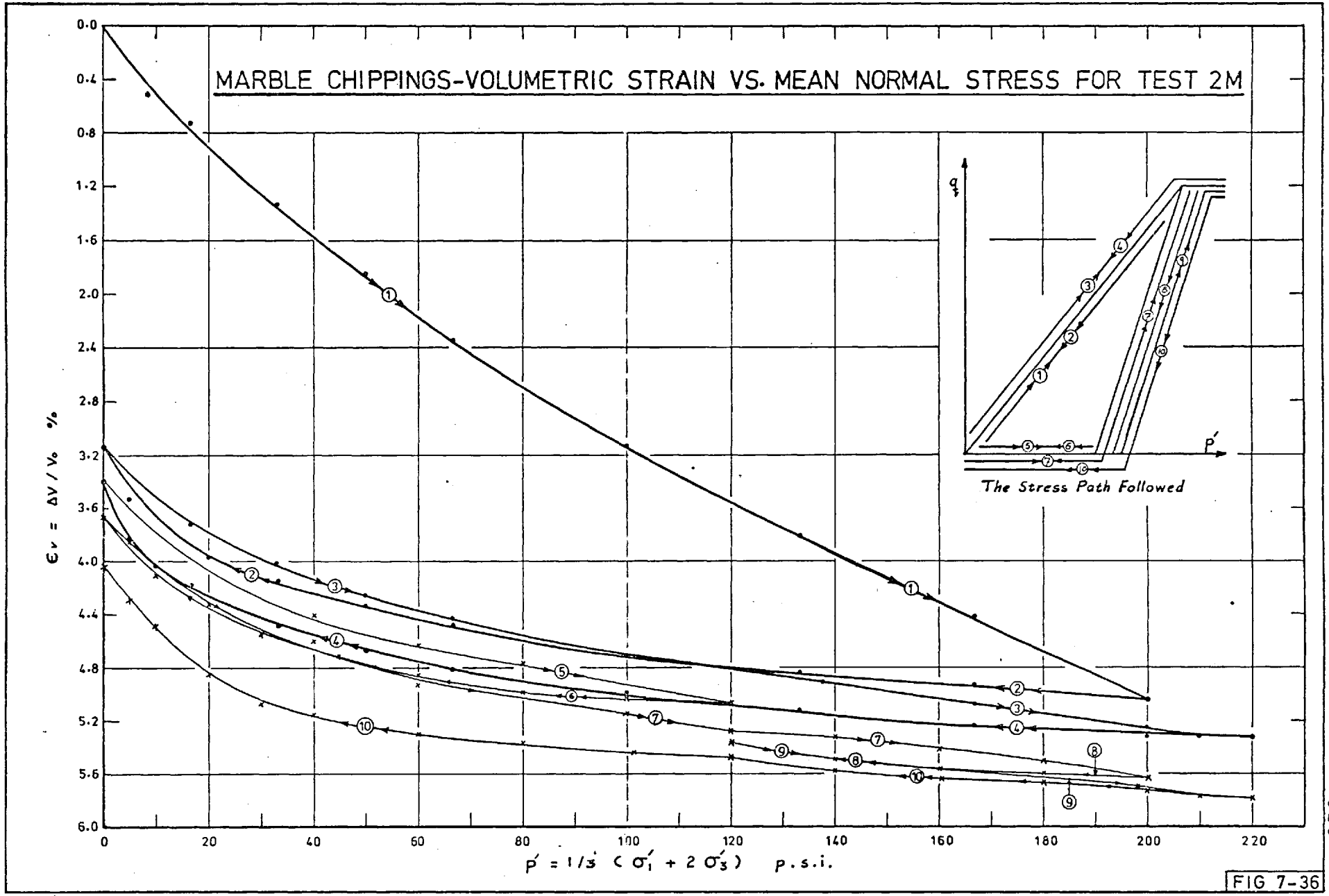
MARBLE CHIPPINGS-VOLUMETRIC STRAIN VS. MEAN NORMAL STRESS FOR TEST 2M
$\epsilon_v = \Delta V / V_0$ %
$p' = 1/3\ (\sigma'_1 + 2\sigma'_3)$ p.s.i.
0.0
0.4
0.8
1.2
1.6
2.0
2.4
2.8
3.2
3.6
4.0
4.4
4.8
5.2
5.6
6.0
0
20
40
60
80
100
120
140
160
180
200
220
q
P'
The Stress Path Followed

FIG 7-36

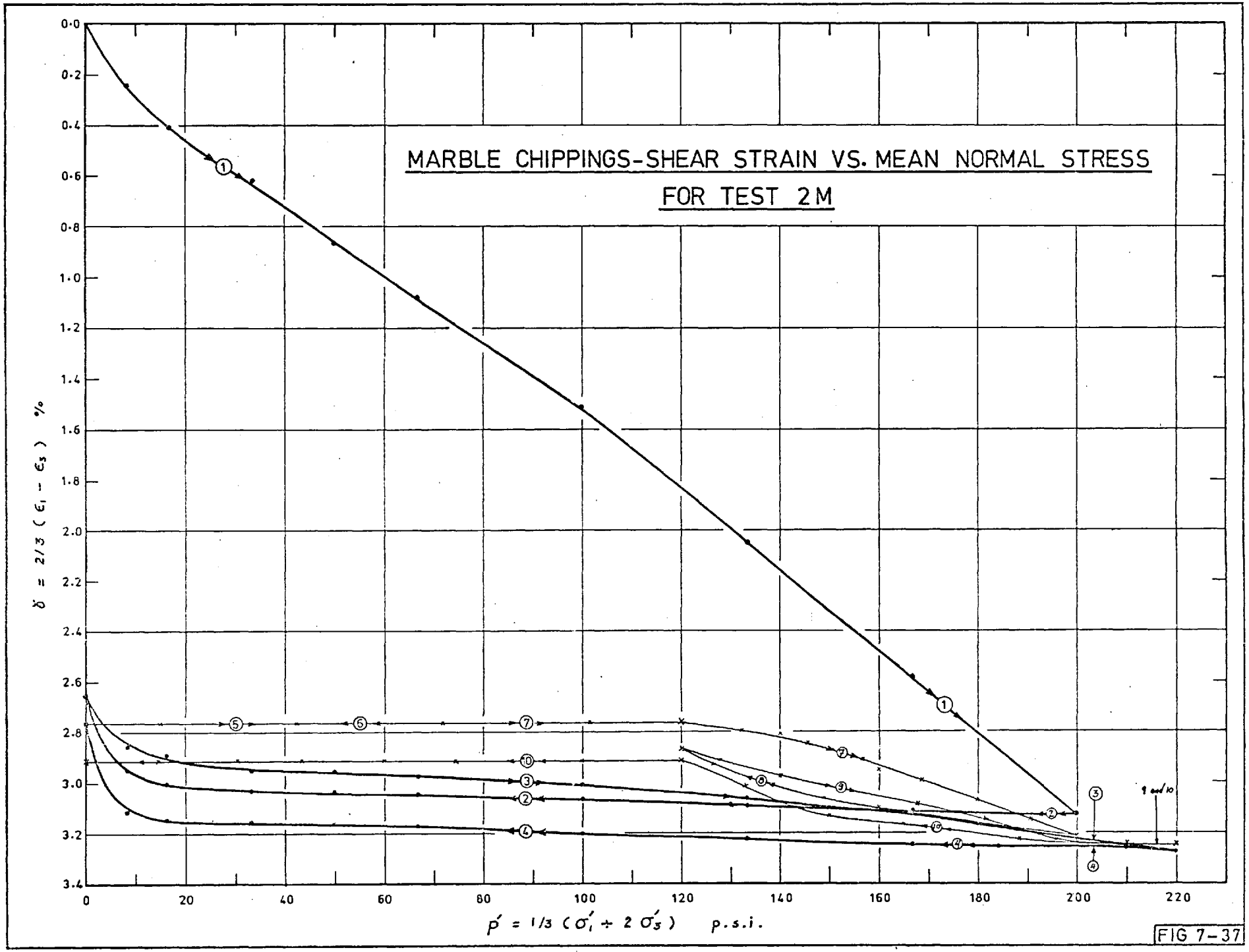
MARBLE CHIPPINGS-SHEAR STRAIN VS. MEAN NORMAL STRESS
FOR TEST 2M
δ' = 2/3 (ε1 - ε3) %
p' = 1/3 (σ'1 + 2 σ'3) p.s.i.
0.0
0.2
0.4
0.6
0.8
1.0
1.2
1.4
1.6
1.8
2.0
2.2
2.4
2.6
2.8
3.0
3.2
3.4
0
20
40
60
80
100
120
140
160
180
200
220
1 and 10

FIG 7-37

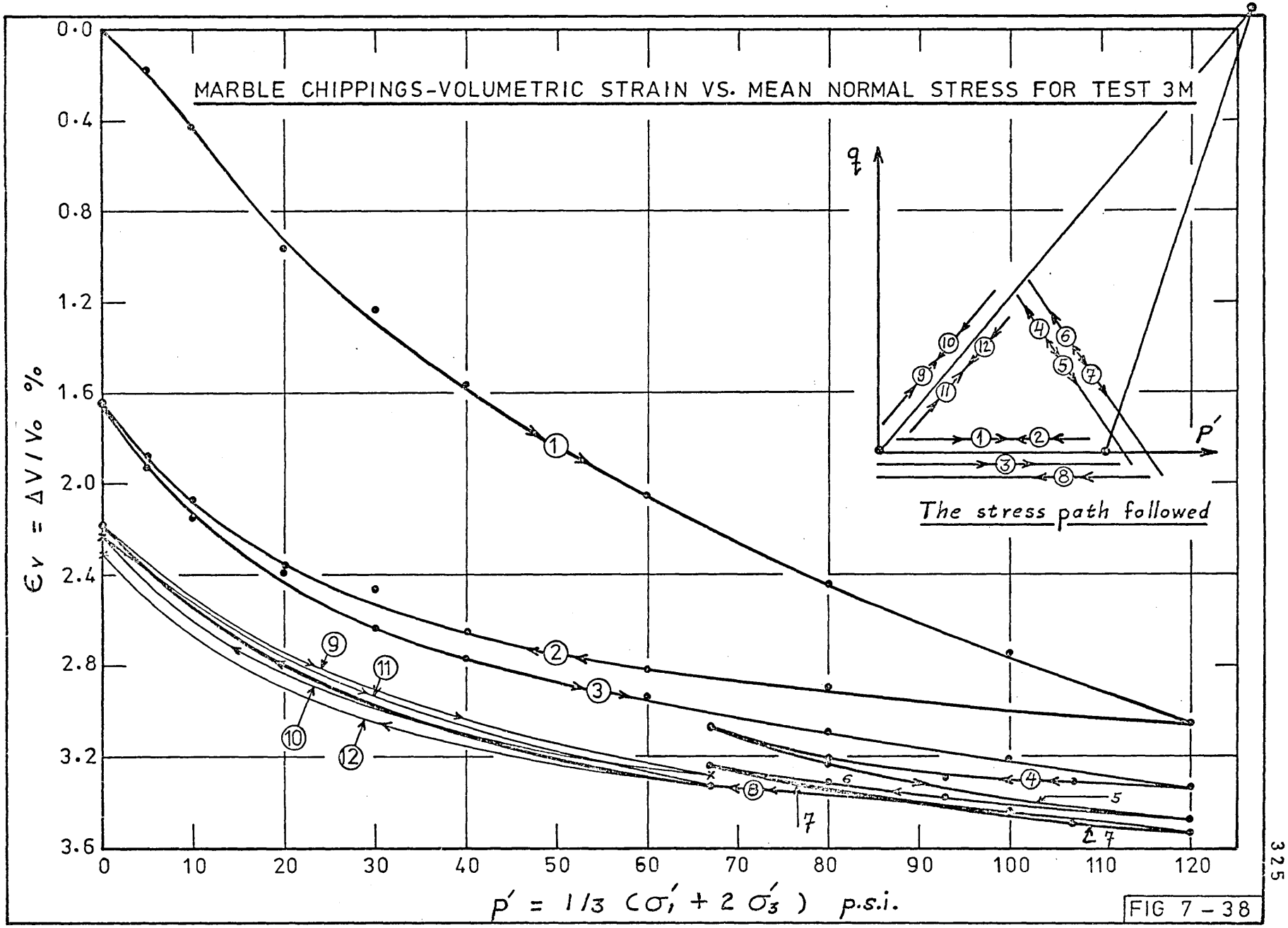
MARBLE CHIPPINGS-VOLUMETRIC STRAIN VS. MEAN NORMAL STRESS FOR TEST 3M
$\epsilon_v = \Delta V / V_o$ %
0.0
0.4
0.8
1.2
1.6
2.0
2.4
2.8
3.2
3.6
0
10
20
30
40
50
60
70
80
90
100
110
120
$p' = 1/3\ (\sigma_1' + 2\sigma_3')$ p.s.i.
q
p'
The stress path followed
FIG 7 - 38

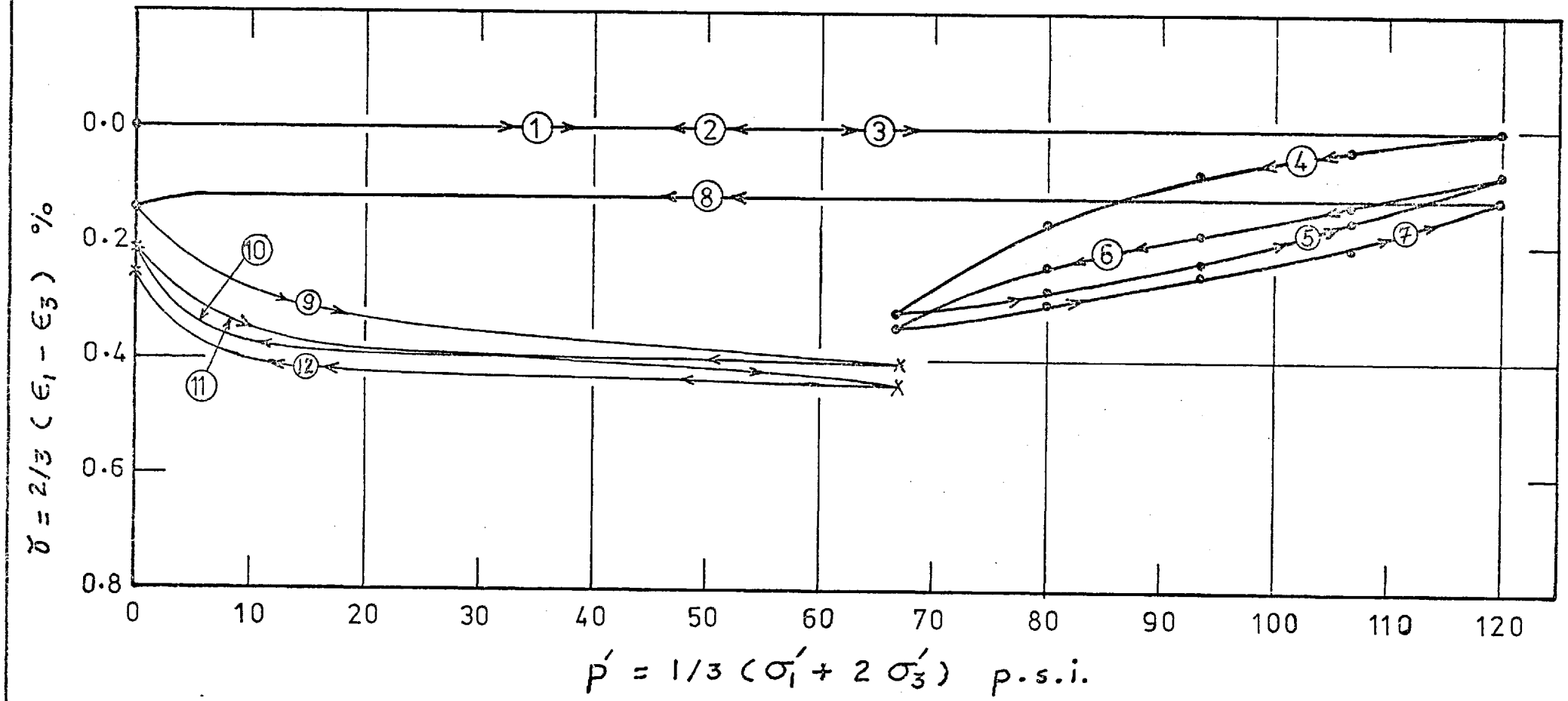

MARBLE CHIPPINGS-SHEAR STRAIN VS. MEAN NORMAL STRESS FOR TEST 3M

FIG 7 - 39

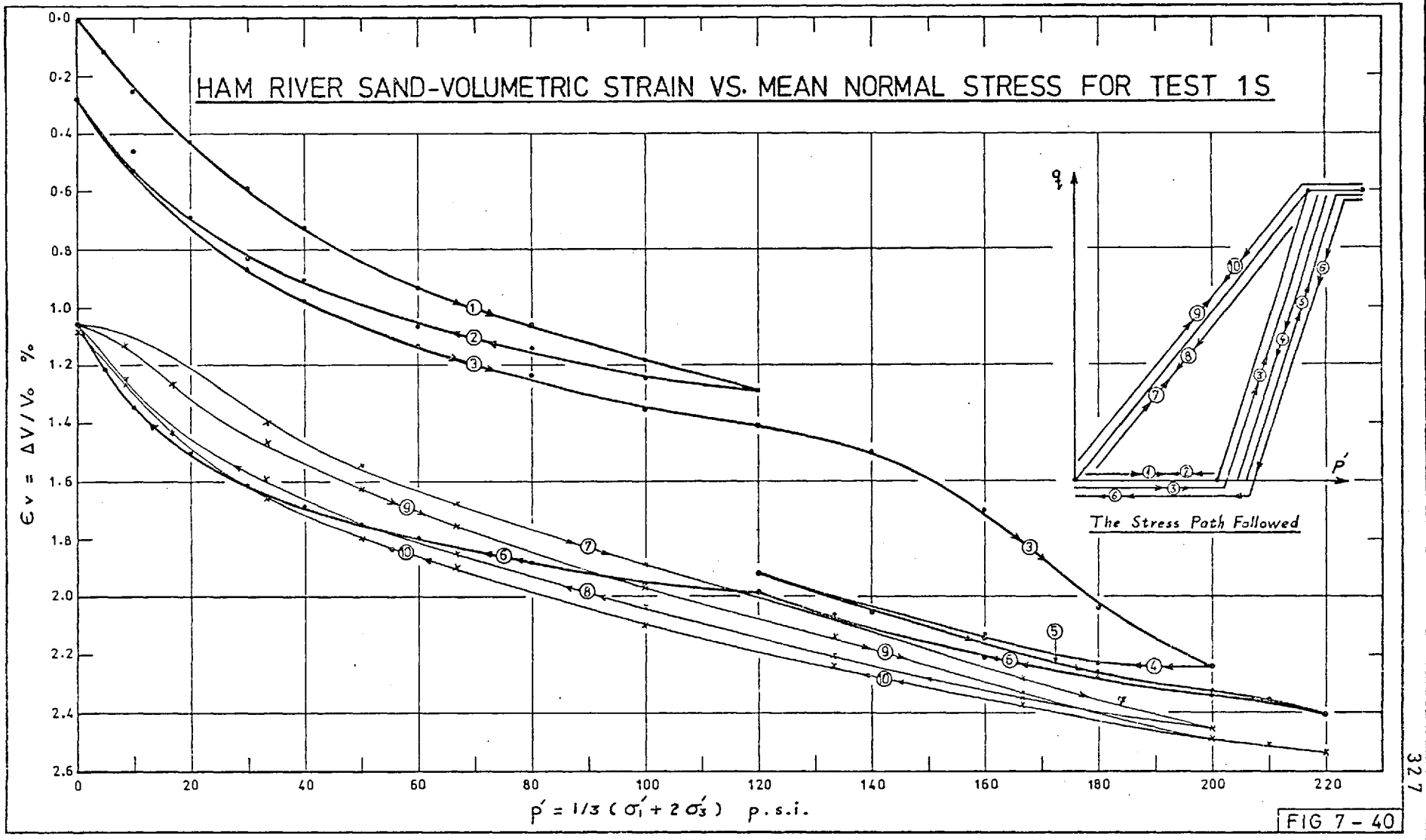
HAM RIVER SAND-VOLUMETRIC STRAIN VS. MEAN NORMAL STRESS FOR TEST 1S
$\epsilon v = \Delta V / V_o$ %
0·0
0·2
0·4
0·6
0·8
1·0
1·2
1·4
1·6
1·8
2·0
2·2
2·4
2·6
0
20
40
60
80
100
120
140
160
180
200
220
$p' = 1/3 (\sigma_1' + 2 \sigma_3')$ p.s.i.
q
p'
The Stress Path Followed

FIG 7 - 40

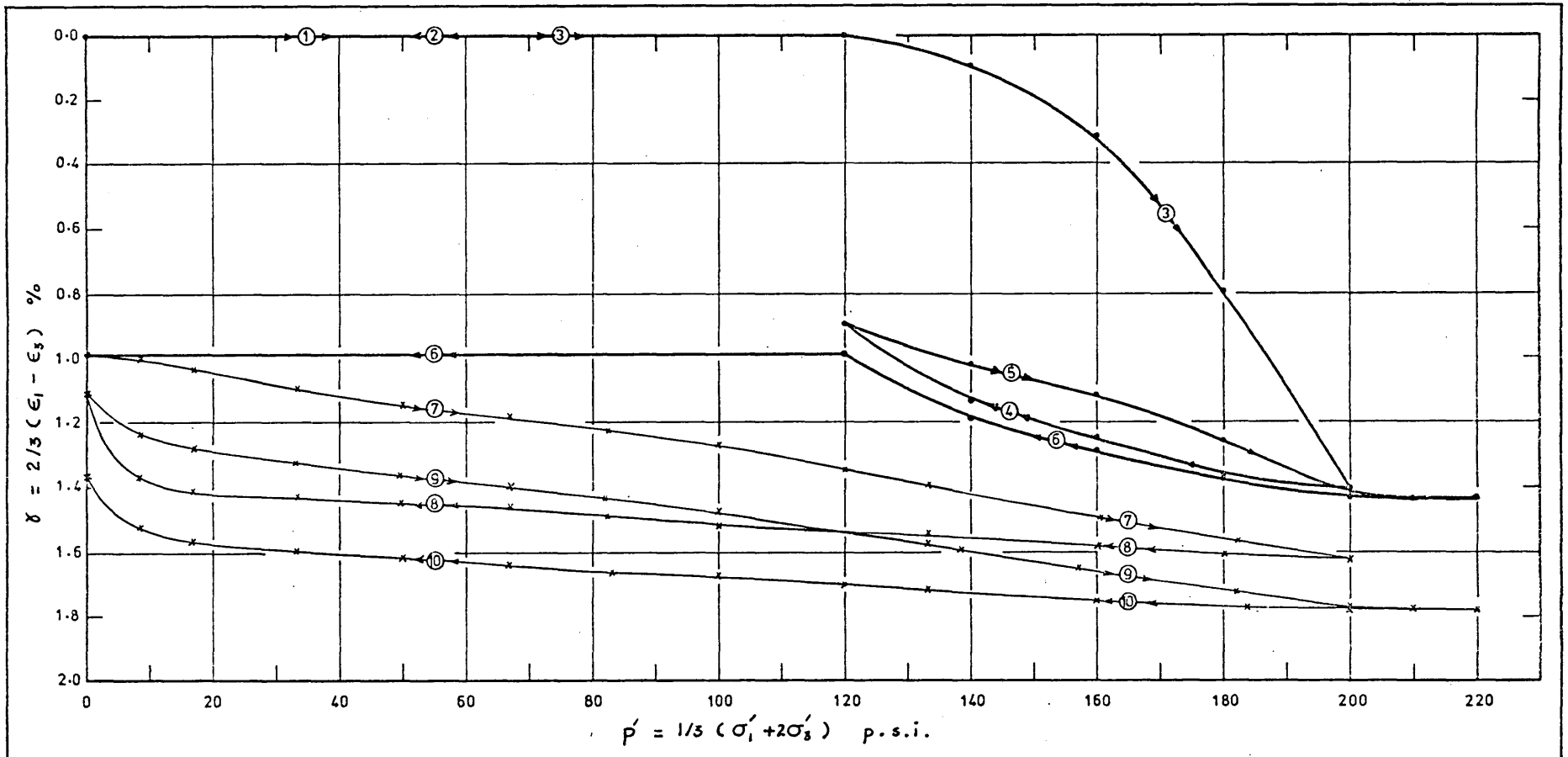

HAM RIVER SAND - SHEAR STRAIN VS. MEAN NORMAL STRESS FOR TEST 1S

FIG 7 - 41

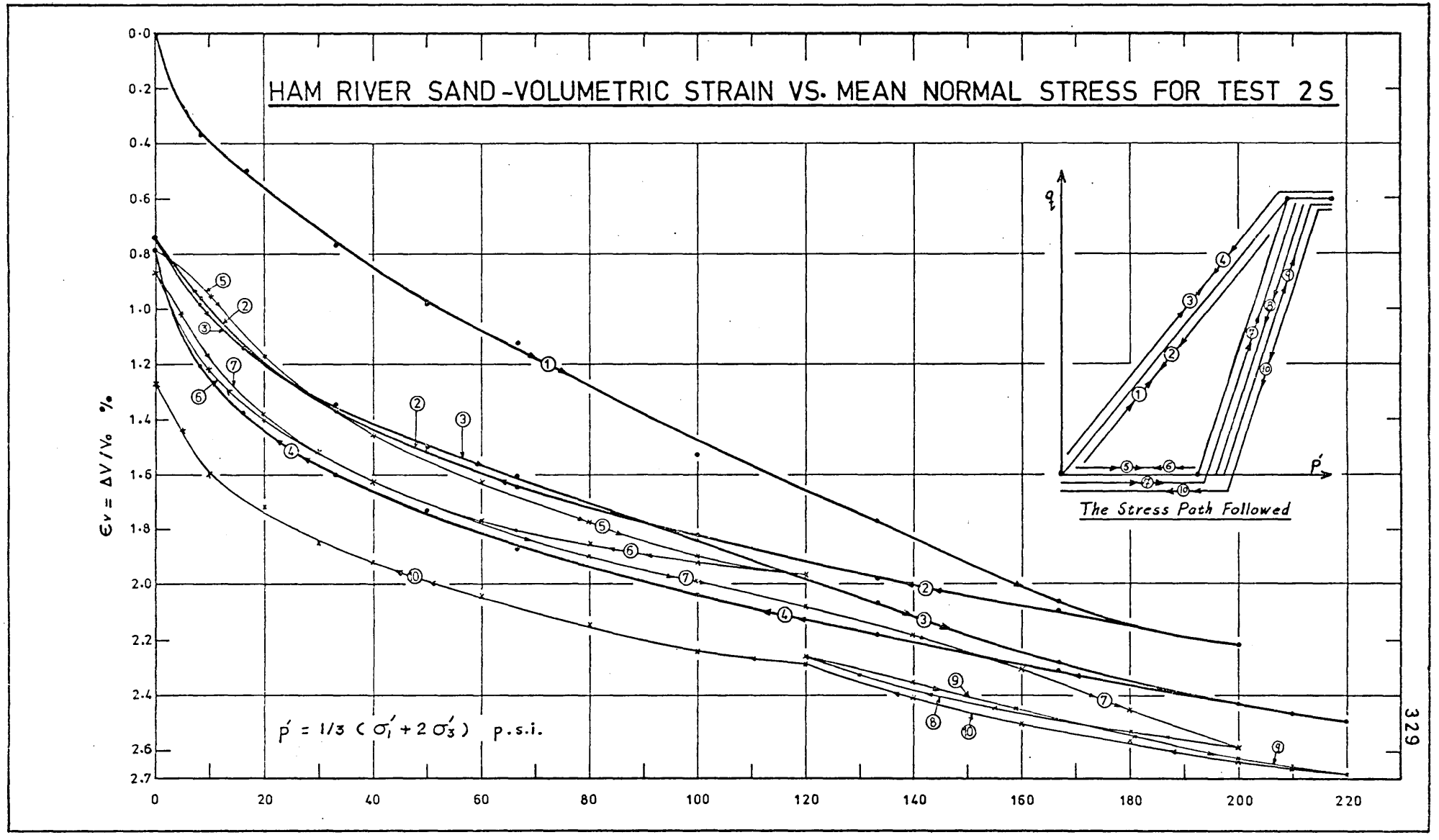
HAM RIVER SAND - VOLUMETRIC STRAIN VS. MEAN NORMAL STRESS FOR TEST 2S
$\epsilon_v = \Delta V / V_0$ %
$p' = 1/3 (\sigma_1' + 2\sigma_3')$ p.s.i.
0.0
0.2
0.4
0.6
0.8
1.0
1.2
1.4
1.6
1.8
2.0
2.2
2.4
2.6
2.7
0
20
40
60
80
100
120
140
160
180
200
220
q
p'
The Stress Path Followed

(FIG 7–42)

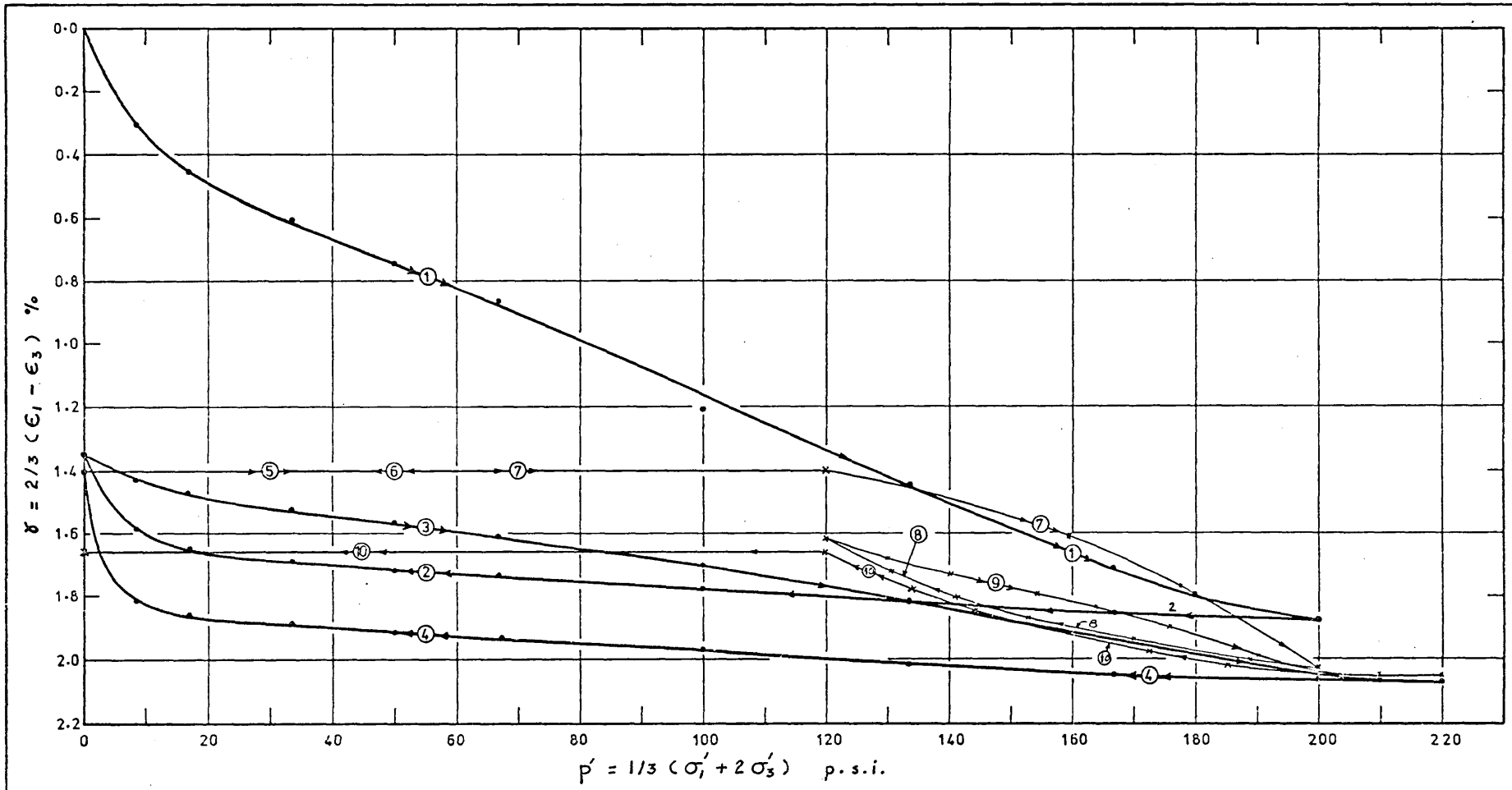

HAM RIVER SAND-SHEAR STRAIN VS. MEAN NORMAL STRESS FOR TEST 2S

FIG 7-43

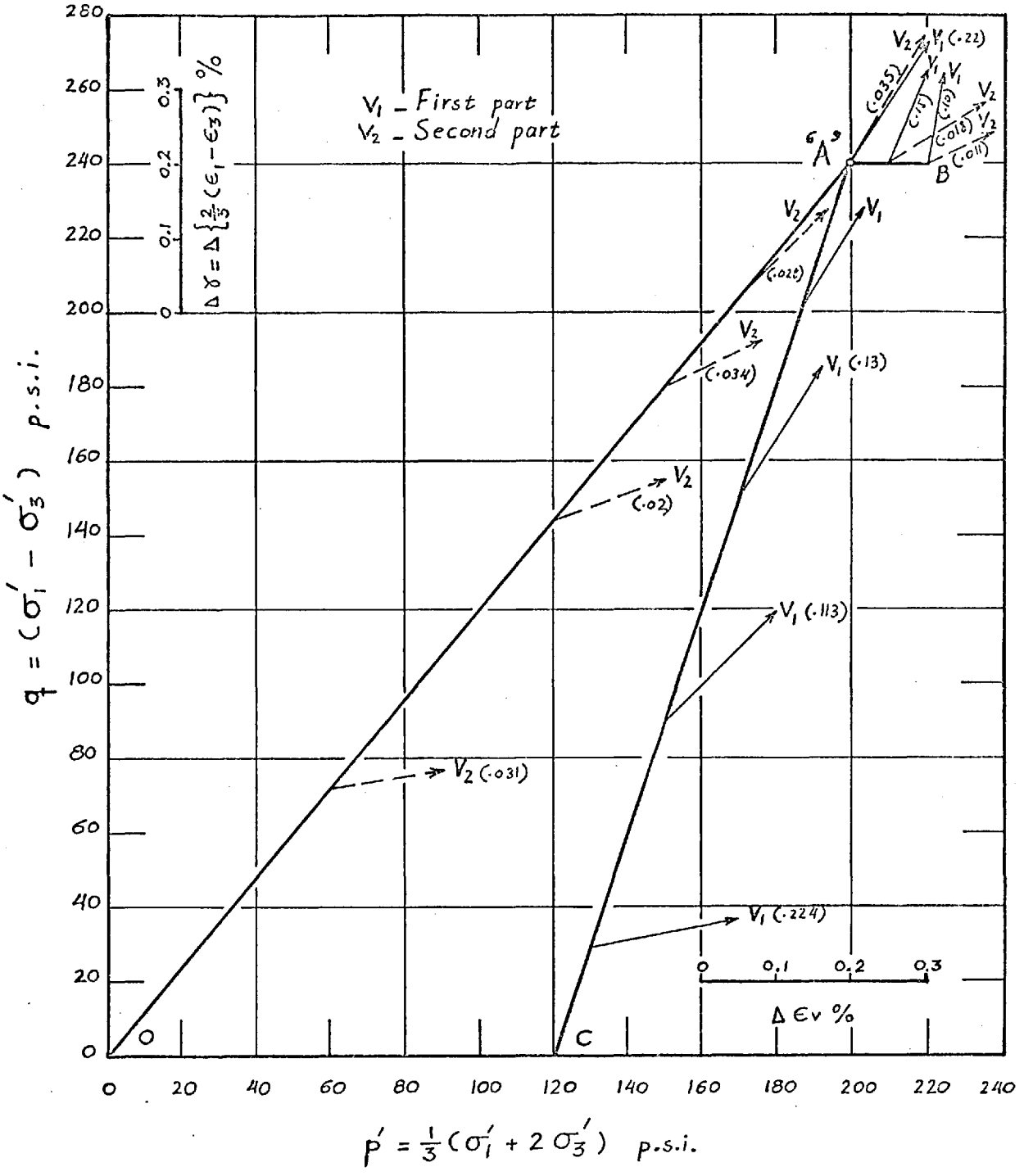

GRANITE ROCKFILL

THE PLASTIC STRAIN INCREMENT VECTORS FOR TEST 1G.

FIG 7–44

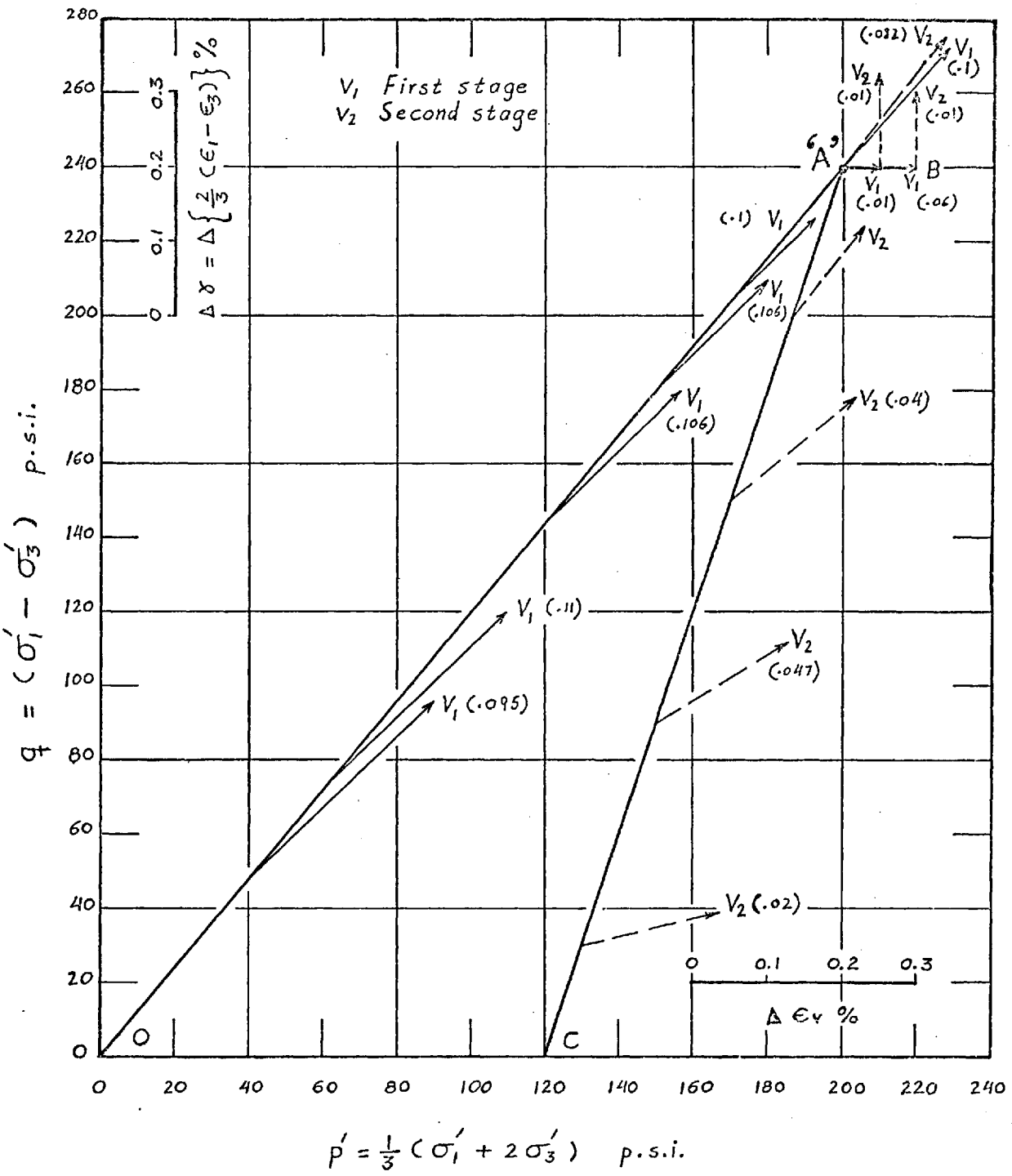

GRANITE ROCKFILL

THE PLASTIC STRAIN INCREMENT VECTORS FOR TEST 2G

FIG 7-45

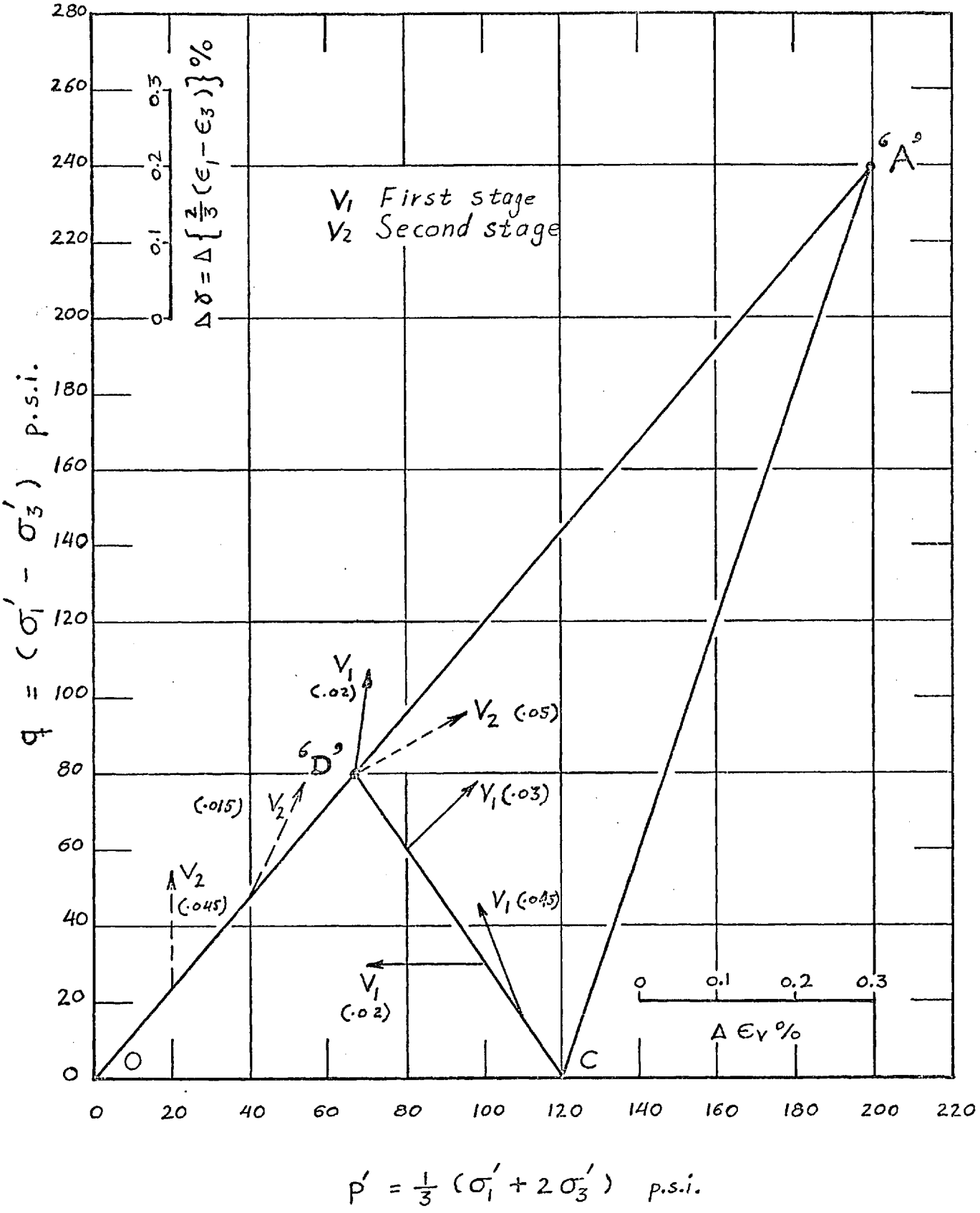

GRANITE ROCKFILL

THE PLASTIC STRAIN INCREMENT VECTORS FOR TEST 3G

FIG 7 - 46

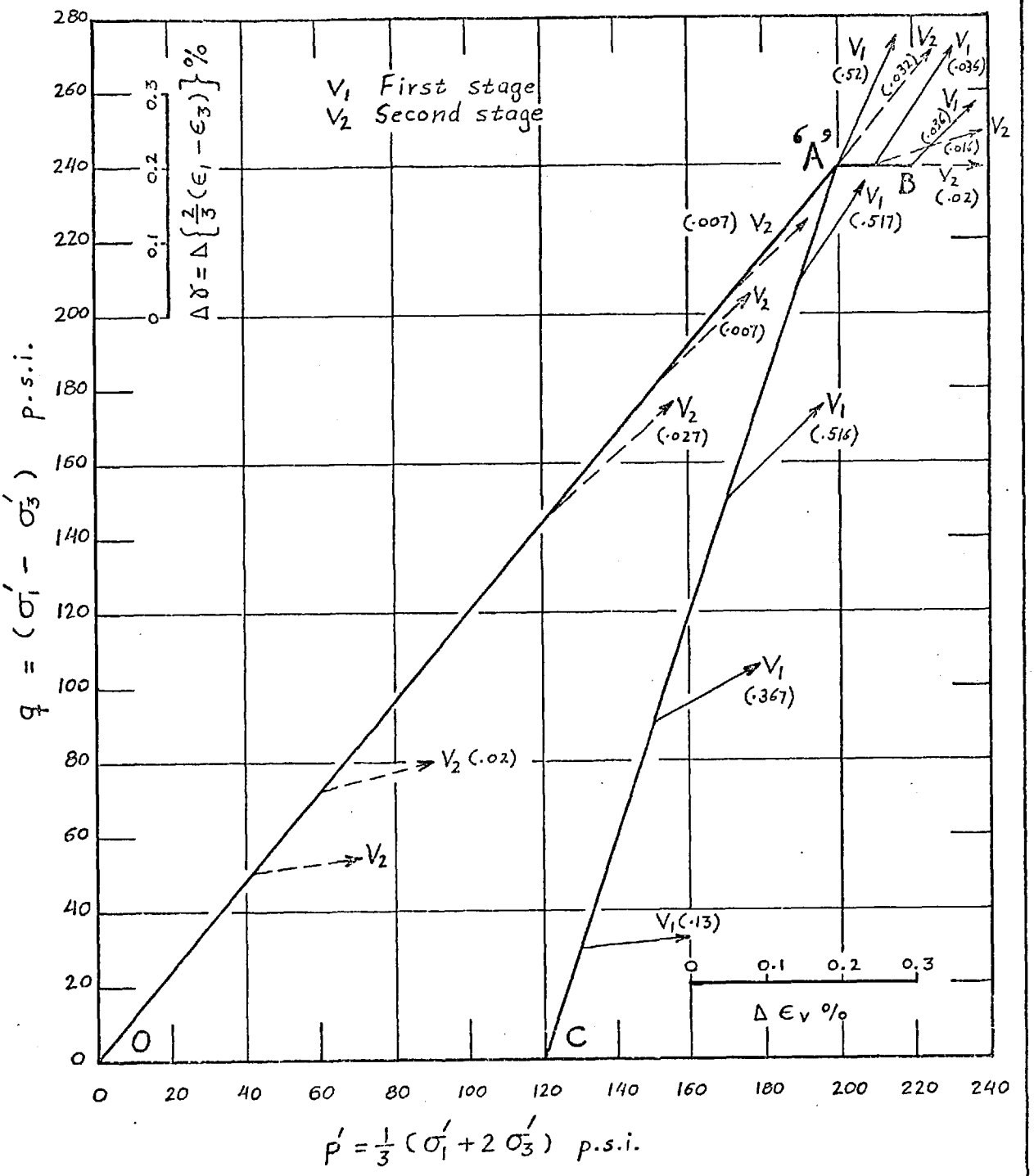

MARBLE CHIPPINGS

THE PLASTIC STRAIN INCREMENT VECTORS FOR TEST 1M

FIG 7 - 47

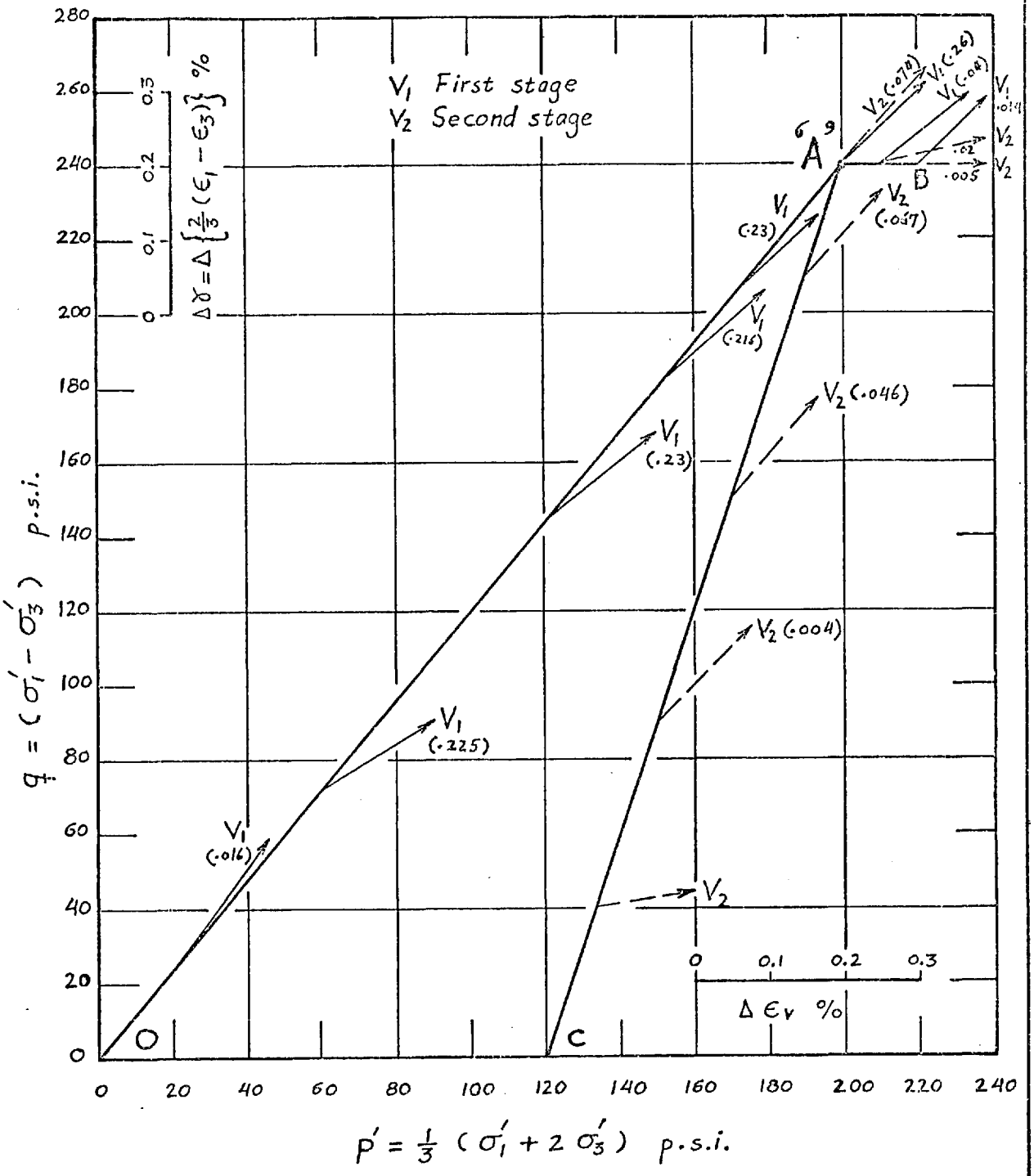

MARBLE CHIPPINGS

THE PLASTIC STRAIN INCREMENT VECTORS FOR TEST 2M

FIG 7-48

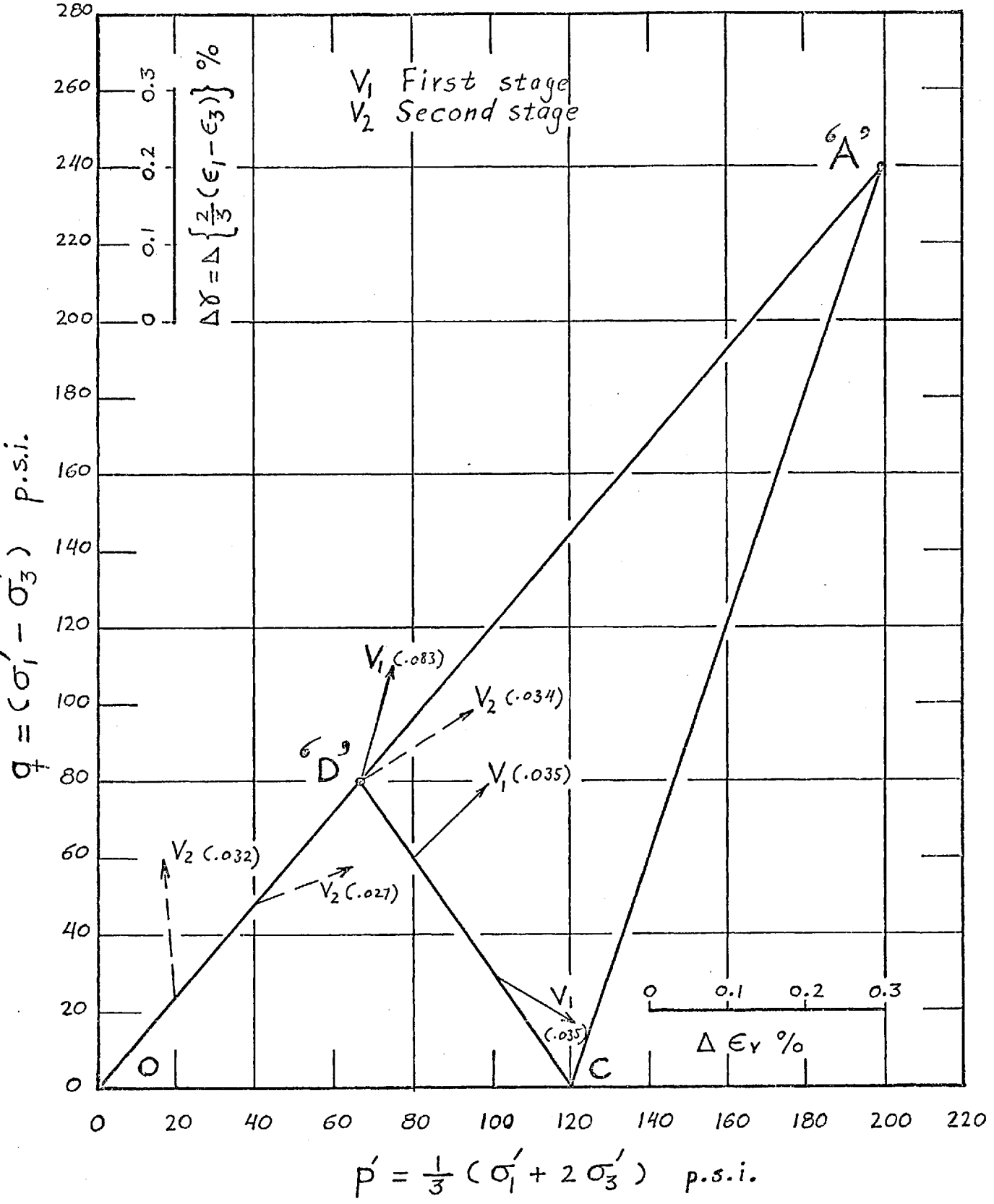

MARBLE CHIPPINGS

THE PLASTIC STRAIN INCREMENT VECTORS FOR TEST 3M

FIG 7-49

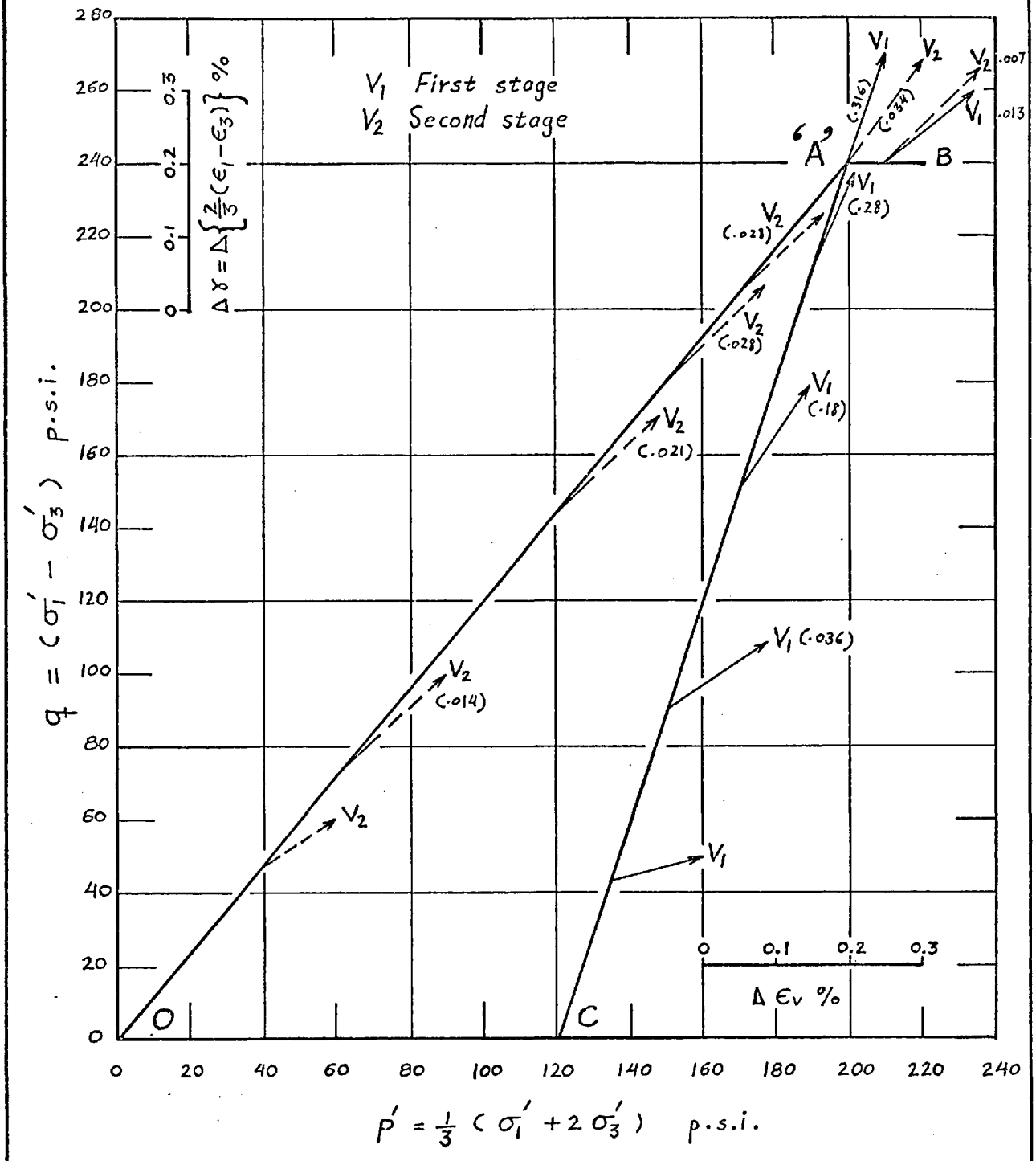

HAM RIVER SAND

THE PLASTIC STRAIN INCREMENT VECTORS FOR TEST 1S

FIG 7-50

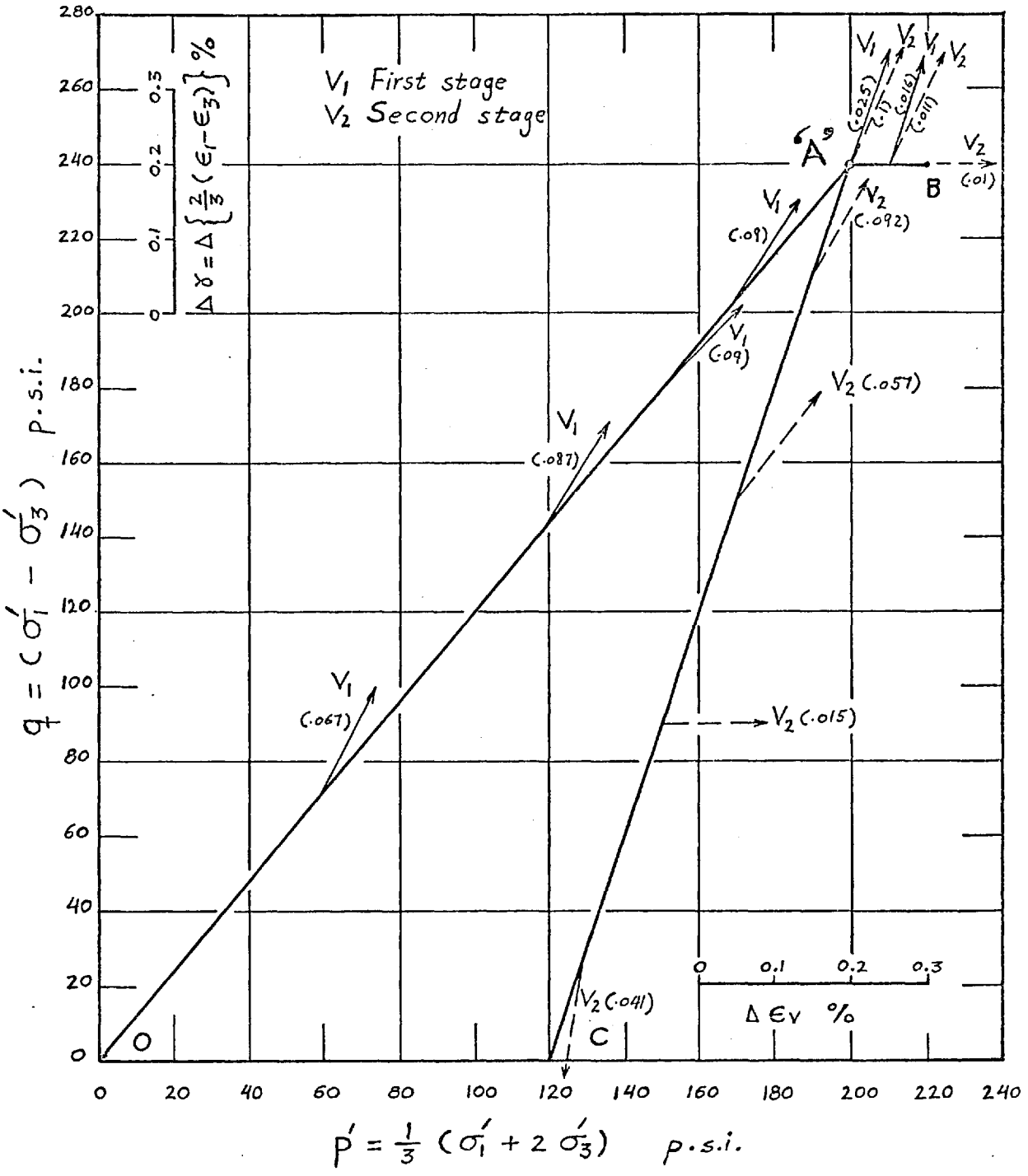

HAM RIVER SAND

THE PLASTIC STRAIN INCREMENT VECTORS FOR TEST 2S

FIG 7-51

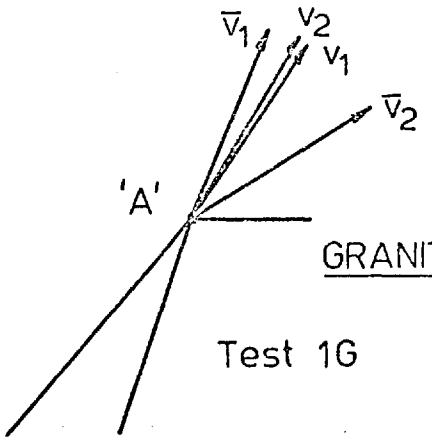

Fig. 7-52a

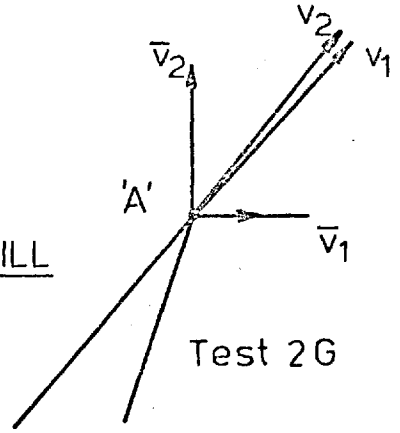

Fig. 7-52b

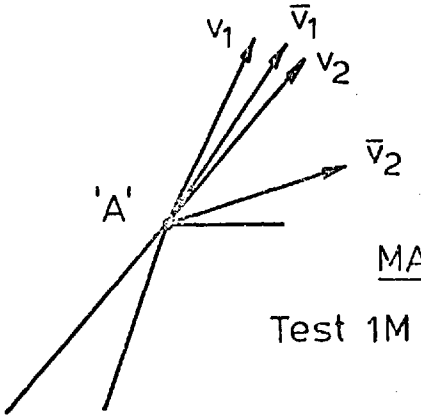

Fig. 7-52c

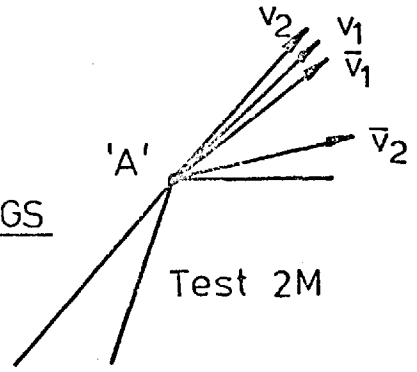

Fig. 7-52d

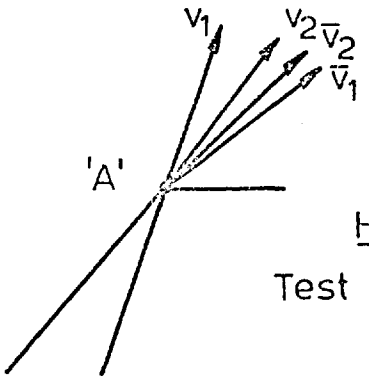

Fig. 7-52e

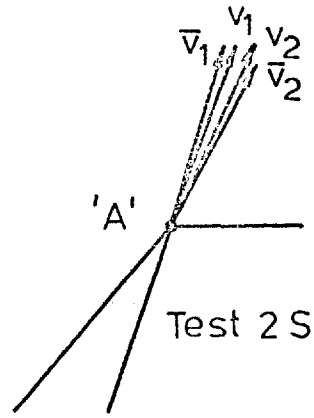

Fig. 7-52f

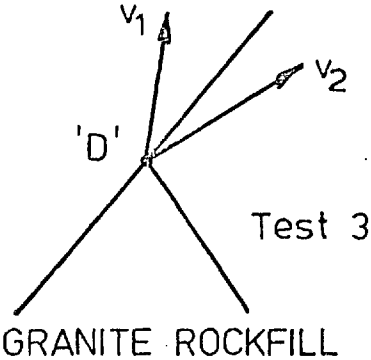

Fig. 7-52g

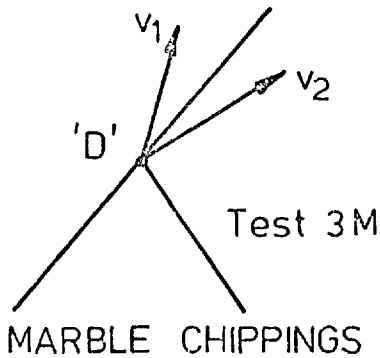

Fig. 7-52h

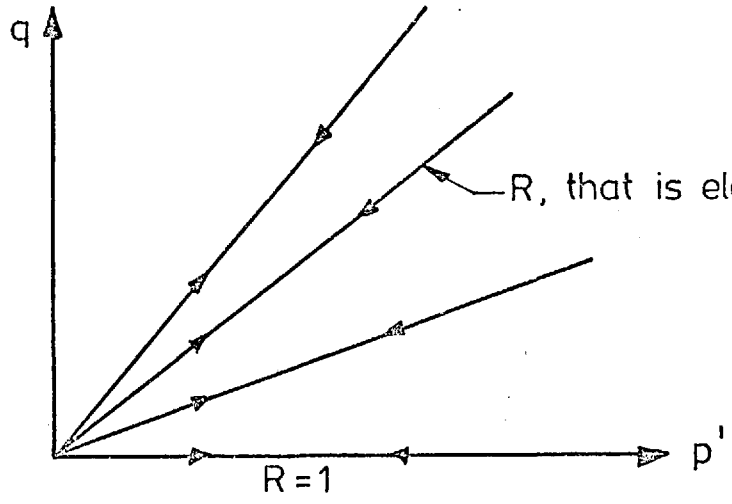

Fig. 7-53 a

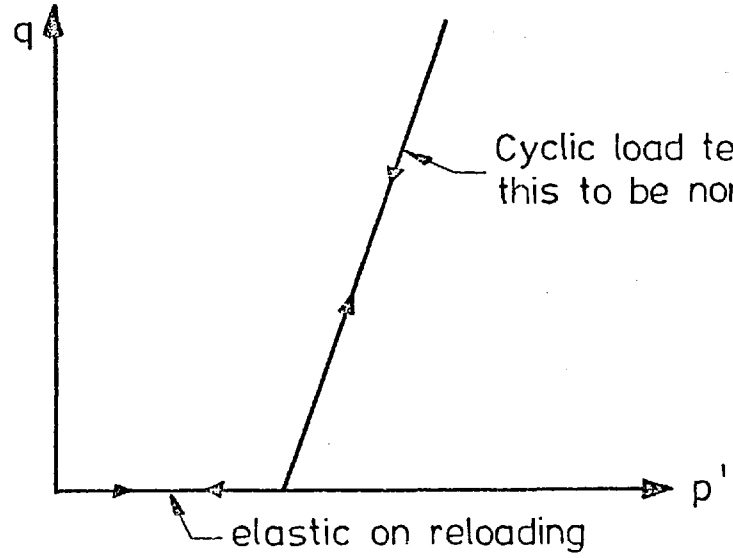

Fig. 7-53 b

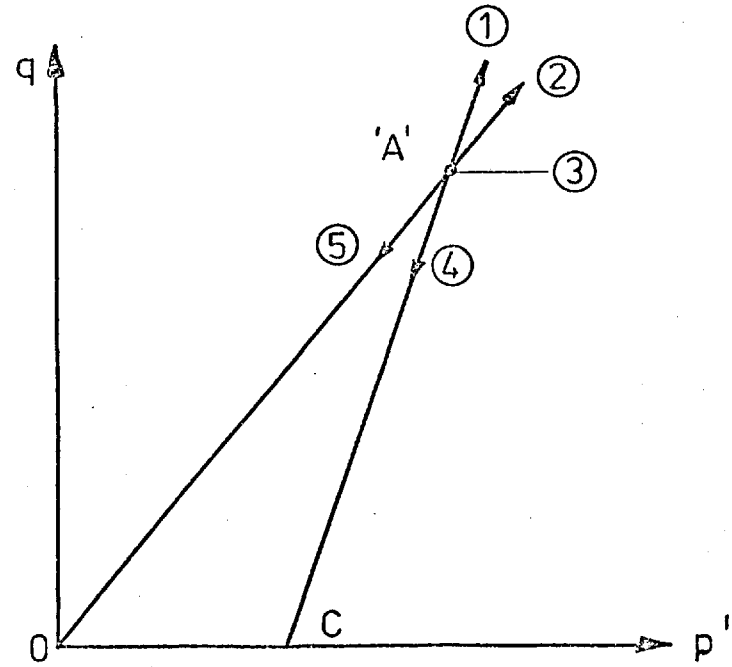

Fig. 7-53 c

Fig. 7-53

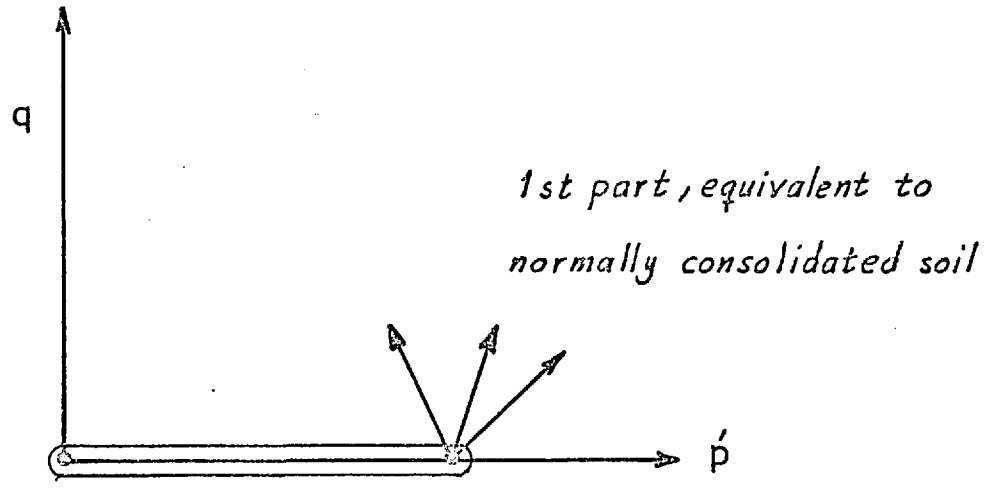
q
1st part, equivalent to
normally consolidated soil
p'

(a)

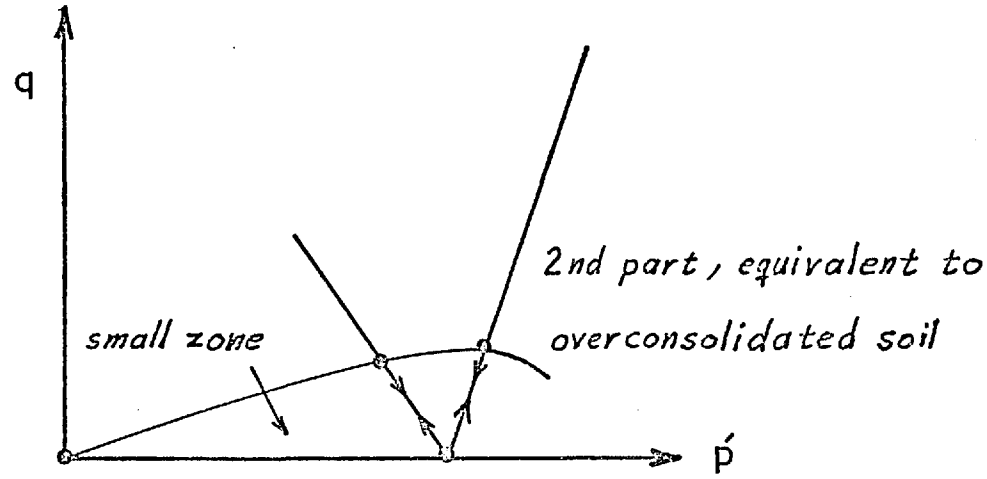
q
small zone
2nd part, equivalent to
overconsolidated soil
p'

(b)

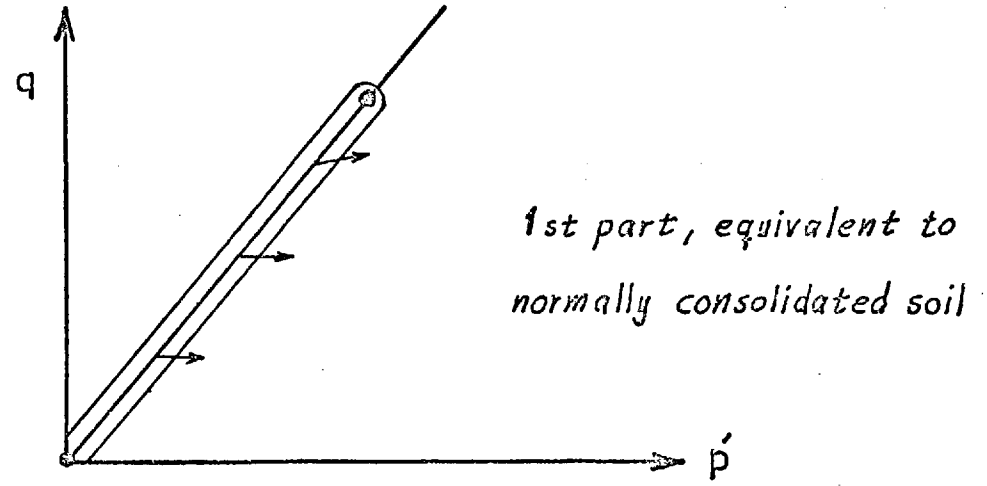
q
1st part, equivalent to
normally consolidated soil
p'

(c)

FIG 7—54

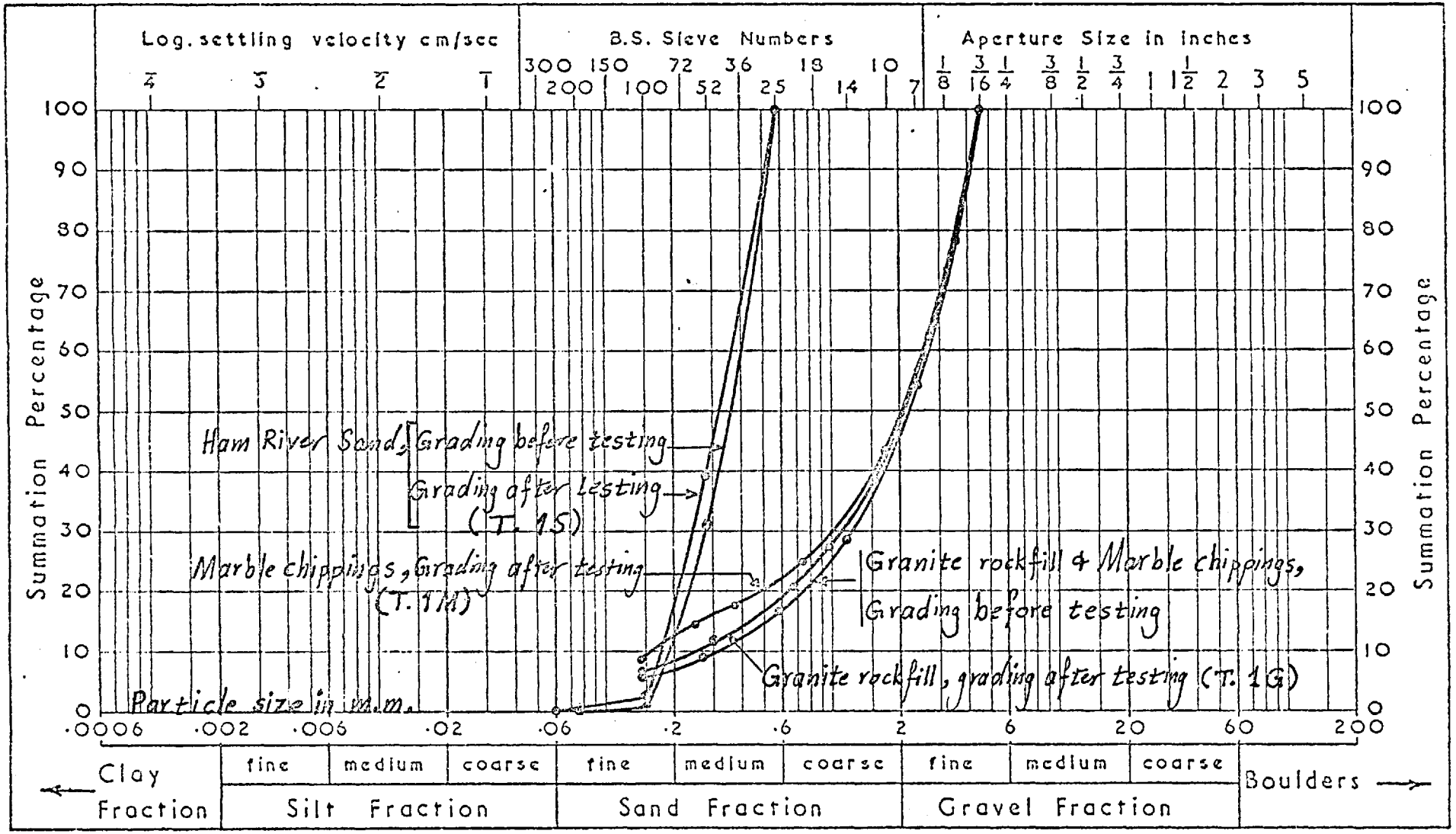

GRADINGS OF THE MATERIALS USED BEFORE AND AFTER LOADING (TESTS 1G, 1M AND 1S)

FIG 7 - 55

CHAPTER VIII

FINAL DISCUSSION AND CONCLUSIONS

8.1 Strength and Deformations of Rockfill Materials

In the initial section of Part I of this thesis a study was conducted to investigate the factors influencing the strength and deformation characteristics of rockfill materials, especially at failure. Although some theoretical considerations have been discussed, the study was mainly experimental. The conclusions arrived at will be summarised in the following sections.

8.1.1 Isotropic Consolidation

As expected, denser material showed a smaller compressibility for a given applied effective isotropic consolidation pressure range. If a dry rockfill material, no matter how dense, is compacted and consolidated it will undergo, while it is under constant effective stress, further consolidation on first wetting. For the granite rockfill tested, this further consolidation ranges from 19.8% to 30% for samples at 27.2% and 38.5% initial porosity respectively.

Tombs (1969) from tests on granite rockfill and cleaved mudstone observed a greater volume change at a given stress level, for the samples with greater maximum particle size while the test results on various rockfill materials reported by Marachi et al (1969) were mixed and did not show a similar trend. Thus the influence of particle size on the amount of consolidation needs more investigation.

8.1.2 The Stress-Strain Behaviour of the Samples Sheared Under Drained Conditions

Drained triaxial tests were performed with effective confining pressures as high as 850 psi, the results of which indicate that the effect of high confining pressures during shear is to reduce the effects of all other testing parameters. The stress-strain curves of the dense samples have a well-defined peak which occurs at an early stage of shearing,

especially at low confining pressure. At high confining pressures there is also a marked peak in the stress-strain curves but at higher axial strains. The stress-strain curves of the loose samples show less pronounced peaks than the dense samples and at high confining pressure, as high as 300 psi and 600 psi, the curves level off at the top. At higher confining pressure, up to 850 psi, the loose samples behaved similarly to the dense samples and showed a sharper peak than at lower confining pressures. Another interesting point that can be seen from these curves is that the stiffness of loose samples varies a lot under a wide range of confining pressures while the difference in stiffness is less for dense samples under the same range of confining pressures.

The main points that can be noted from the volumetric strain-axial strain curves are:

a) Dense samples at low confining pressures show a marked tendancy to dilate while at high confining pressures they decrease in volume during shear.

b) Loose samples at low confining pressures consolidate first then dilate moderately, while at high confining pressures they continue to decrease in volume during shear.

8.1.2.1 Variation of the Shear Strength of the Granite Rockfill

The angle of shearing resistance, ϕ', decreases as the initial porosity increases for the same confining pressure, Figure (6-8). Also the angle of shearing resistance for samples at different initial porosities varies significantly under low confining pressures while at higher pressures this variation becomes smaller. Samples tested under low confining pressures gave ϕ' higher than those tested at high confining pressures; the straight line relationship as shown in Figure (6-8) is a matter of approximation. Figure (6-8) also shows that the difference in ϕ' values for different cell pressures decreases as the initial porosity increases and approaches a state where this

difference in ϕ' values is very small for samples tested at low and high cell pressures.

The marked curvature of the envelopes at low effective stresses for the dense samples can be seen in Figure (6-9). Both Mohr envelopes for dense and loose samples at high stresses tend to converge. Bishop (1966) showed that Mohr envelopes for loose and dense Ham River sand converge at high stresses and are nearly coincident at σ'_3 = 1400 psi. The test results are summarised in Tables (6-2) and (6-4). The angle of shearing resistance ϕ' for dense samples decreased from 49.8° to 38.6° when the effective cell pressure σ'_3 increased from 20 psi to 850 psi. For loose samples ϕ' decreased from 43.5° to 37.2° when σ'_3 increased from 20 to 850 psi, Figure (6-10). The reduction in ϕ' values as σ'_3 increases is similar to the behaviour of Ham River sand reported by Bishop (1966) except for two points:

1. The magnitude of reduction in ϕ' values of Ham River sand is different from that of granite.

2. At high effective cell pressures (as high as 4000 psi) ϕ' value for Ham River sand increased with effective cell pressure after it had decreased to a minimum value at about 1000 psi effective cell pressure. In this research work there is no evidence that at high effective cell pressures (as high as 850 psi) the value of ϕ' for both dense and loose samples will be the same nor that they reach a minimum value and then subsequently increase at higher stresses as reported by Bishop (1966) for Ham River sand.

8.1.2.2 Variation of the Volumetric Strain at Failure

The amount of volumetric strain at failure increases with the increase of the effective cell pressure σ'_3 in the low and medium pressure range, but there is no significant change at high cell pressures especially with the dense samples, Figure (6-11). The volumetric strain - axial strain curves indicate that particles of loose samples continue crushing during shearing at high confining pressures while

the very dense samples showed almost a constant ϵ_v at failure as the shearing continued. But generally speaking, the decrease in volume at failure for both dense and loose samples when sheared at high confining pressures is not very significant. The influence of the initial porosity can be seen clearly in Figures (6-2) through (6-7). The dilatancy rate at failure will be discussed in Section 8.1.2.4.

8.1.2.3 Variation of the Axial Strain at Failure

As the confining pressure used is increased, the axial strain at failure increases to a maximum and then decreases, Figure (6-12). The decrease in the value of the axial strain at failure for dense samples at high pressures is more than that for the loose ones. Figure (6-13) shows the $\epsilon_{1f} - \sigma'_3$ relationships for a wide range of coarse granular materials. All the data show that the axial strain at failure increases as the confining pressure increases, and reaches a maximum value at a certain stress level above which it decreases. This decrease in the value of ϵ_{1f} may be related to the crushing of particles. The relative positions of the curves within the graph are a property of the particular granular material.

The influence of the density on the axial strain at failure is shown clearly in Figures (6-7) and (6-12). For a certain material sheared at a certain level of confining pressure, the axial strain at failure increases with the increase of porosity.

8.1.2.4 Rate of Dilatancy at Failure

For both the loose and the dense samples the rate of dilatancy at failure, $(d\epsilon_v/d\epsilon_1)_f$, decreased as the effective cell pressure increased, Figure (6-14). The general behaviour of granite rockfill is similar to that of Ham River sand except in the following points:

a) Dense samples of Ham River sand reached a minimum $(d\epsilon_v/d\epsilon_1)_f$ of -0.14 at σ'_3 of 1000 psi and it seems there is a tendancy to rise at higher effective cell pressures although no data are available.

b) $(d\epsilon_v/d\epsilon_1)_f$ values for loose sand samples reached a minimum value of approximately -0.18 at σ'_3 of 1000 psi then increased to -0.05 at σ'_3 of 4000 psi.

Tests on granite rockfill did not show such behaviour.

Figure (6-15) shows $(d\epsilon_v/d\epsilon_1)_f$ vs. σ'_3 relationship for a wide range of coarse granular materials. The effect of increasing the effective cell pressure at any porosity is to reduce the rate of dilatancy at failure as well as the angle of shearing resistance. This reduction is associated with an increase in particle crushing. The relative position and displacement of the curves in Figure (6-15) indicate the nature and strength of the particles under consideration.

The initial porosity plays a significant part at low pressures while at high pressures its significance diminishes and a stage may be reached where both dense and loose samples behave similarly.

The relationship between the angle of shearing resistance, ϕ', and the rate of dilatancy at failure for some of the tests is shown in Figure (6-16). It is seen from this figure that the variation of the porosity has no effect on the relationship. In general the departure from the mean curve is about 1.2° only. With increasing effective cell pressure the test results group around the zero rate of volume change axis, but with progressively lower values of ϕ'. This indicates that the parameter $\phi'cv$ is substantially more pressure-dependent in this type of rockfill material. The approximate $\phi'cv$ value is 40.2 degrees. Results of tests on different types of rockfill materials reported by many researchers are shown in Figure (6-17). It appears that particle crushing plays a major part in the behaviour of rockfill material during deformation.

8.1.3 The Stress-Strain Behaviour of Granite Rockfill Under Drained Cyclic Loading

A conventional drained triaxial test (No. 28) taken in a single loading cycle to failure is considered as a reference for comparison purposes and was called "The Reference Test".

The failure characteristics of the sample subjected to two loading-unloading cycles were similar to those of the reference test, while the samples subjected to ten loading-unloading cycles exhibited different behaviour at failure. The main differences are: increase in the shear strength, decrease in the axial strain at failure, decrease in volume and increase in the rate of dilatancy at failure. These differences may be attributed to the increase in the density of the samples after so many repeated loading and unloading cycles. The stress-strain curve of the 150 cycles test showsthat the sample had reached a quasi equilibrium state after it had been subjected to so many cycles.

8.1.3.1 Variation of the Axial Strain Under Cyclic Loading Conditions

In these cyclic loading tests it has been observed that there was an appreciable amount of irrecoverable axial strain during the first loading-unloading cycle. On subsequent loading and unloading the amount of the residual axial strain increased but at a decreasing rate until after about the 100th cycle the stress-strain curve formed almost closed hysteresis loops. This is shown in Figures (6-20) and (6-21).

Figure (6-22b) shows the final axial strain after each loading and unloading cycle as a function of the number of cycles for the 150 cycle test. From this figure it seems that the failure of the sample by excessive deformation does not occur. Two other interesting points can be noticed from this figure (6-22b):

1. The axial strain-log No. of cycles relationship is linear after the 2nd or 3rd cycle.

2. The straight line relationships mentioned above are parallel after both the loading and unloading stages.

8.1.3.2. Variation of the Volumetric Strain Under Cyclic Loading Conditions

After cyclic loading and unloading the volumetric strain had decreased and the changes for each successive cycle became progressively smaller. At about the 100th cycle the volumetric strain-axial strain curve formed a closed hysteresis loop with insignificant increase in overall volumetric strain. This is better shown in Figure (6-22a) which shows the variation of the volumetric strains against the log. number of cycles for loading and unloading cycles of test 36. Thus from these cyclic loading tests it appears that the state of the volumetric strains on loading and unloading depends on the material and sample properties, stress level and testing conditions.

8.1.3.3 Influence of Cyclic Loading on the Shear Strength, and Strains at Failure

The samples subjected to loading-unloading cycles showed higher strengths than that subjected to single loading to failure. Moreover, the shear strength increased with the increase of loading cycles Figure (6-23a). For example, the shear strength of the sample subjected to 150 loading-unloading cycles was 31% higher than that of the reference sample.

The axial and volumetric strains at failure decrease significantly with an increasing number of loading cycles, Figure (6-23b). The rate of dilatancy at failure for the sample subjected to 150 loading cycles was much higher than that of the reference sample and the other samples of the cyclic loading tests. These differences are mainly due to the increase of the density of the sample and the crushing of particles.

8.1.4. The Stress-Strain Behaviour of the Samples Sheared Under Undrained Conditions

The angle of shearing resistance, ϕ', at peak ($\sigma_1 - \sigma_3$) decreases as the effective consolidation pressure increases for both dense and loose samples. The value of ϕ' at peak ($\sigma_1 - \sigma_3$) obtained from one of the dense samples is close to $\phi'f$ corresponding to zero rate of dilatancy at failure for drained samples while the other tests gave slightly lower values of ϕ' at peak ($\sigma_1 - \sigma_3$), Table (6-7).

The stress paths for all the dense and loose samples are shown in Figure (6-26). These stress paths showed no tendancy to turn back on themselves. The stress paths for loose samples have a different shape from those for the dense samples. These results are in agreement with those reported by Tombs (1969) and Bros (1969) on the same type of material but with a different sample diameter. However, the stress paths for most of the samples (dense and loose) lie close to a line which corresponds to $\phi'f$ of 43.8°, Figure (6-26).

The influence of the effective consolidation pressure on the axial strain at peak ($\sigma_1 - \sigma_3$) is shown in Figures (6-24) and (6-25). The axial strain at peak ($\sigma_1 - \sigma_3$) increases with the increase of the effective consolidation pressure for both the loose and dense samples. Tombs (1969) reported similar behaviour for his 12 in. dia. samples of granite while Bros (1969) observed different behaviour for his 4 in. dia. samples.

8.1.5 Particle Breakage in Rockfill

The properties of the materials tested and the strength of the particles were discussed in Chapter 5 while analysis of the data concerning particle crushing throughout the testing was discussed in Chapter 6. During various types of loading it was observed that particle breakage increases with:

1. the increase in effective cell pressure
2. the increase in shear stress at a given effective cell pressure
3. the decrease in strength of individual particles
4. the increase in angularity of particles, and
5. the increase in uniformity of the soil sample.

Also, coarse particles undergo more crushing than fine ones. Other points of interest have been observed at each stage of the loading, and these will be mentioned below:

Particle breakage during compaction:

1. There is no significant difference between dry and wet compaction during sample preparation.
2. To achieve high density samples, more compaction is required which results in more particle breakage.

Particle breakage during isotropic consolidation:

Particle breakage is relatively small during isotropic consolidation compared to that during the shearing stage. Also it appears from the data obtained, that the particle breakage resulting from compaction is as much as, or more than, that resulting from application of the confining pressure.

Particle breakage during drained shearing to failure:

Visual observations showed that most of the particle breakage occurred in the middle part of the sample. In this part most of the particles had been fractured, whereas the particles in the rest of the sample were generally intact. The data presented in Section 6.6.3 showed that the amount of particle breakage during shearing is substantially larger than that caused during isotropic consolidation, Figure (6-30). Other points of interest drawn from the analysis of the data are:

1. The amount of particle breakage increased, at a decreasing rate, as the consolidation pressure increased, Figure (6-31).

2. The angle of shearing resistance, ϕ', decreases as particle breakage factor, B, increases, Figure (6-32).

3. The rate of dilatancy at failure decreases as the particle breakage factor, B, increases and at zero volume change the particle breakage factor rises considerably, Figure (6-33).

4. Samples consolidated to the same effective consolidation pressure show more particle breakage when sheared drained than when sheared undrained.

Thus the behaviour of a rockfill material in shear may be described by the parameter ϕ', rate of dilatancy at failure and particle breakage factor for first loading. These parameters appear to be directly interrelated.

Particle breakage during drained cyclic loading:

1. A few loading-unloading cycles (less than 5 cycles) do not cause excessive particle breakage when compared to the one cycle loading test provided they are under the same testing conditions.

2. As the number of loading cycles increases, the particle breakage increases, Figure (6-34).

Particle breakage during anisotropic consolidation:

Samples consolidated at a constant stress ratio σ_1' / σ_3' of 2.04 underwent more particle breakage than those consolidated at lower stress ratios. But when the stress ratio was increased to 3.0 the particle breakage was smaller than that when σ_1' / σ_3' was at 2.04. Thus it appears that the particle breakage increases in direct proportion to the increase in the value of the constant stress ratio during the consolidation stage, but at some stage reaches a peak, above which, for increasing stress ratio, the amount of breakage decreases.

Particle breakage for the special stress path tests:

1. When samples are loaded successively along two stress paths, these two stress paths being the same for all samples, the order in which the two paths are followed has only a small effect on the final amount of particle breakage.

2. The phenomenon of particle breakage has a marked influence on the direction of the plastic strain increment vector. Moreover the increase in breakage of particles during loading tends to cause increase in rotation of the plastic strain increment vector.

8.2. Pre-Failure Stress-Strain Characteristics of Granular Soils

In design and analysis in soil mechanics, attention has been increasingly focussed on deformations and the corresponding compatible stress distribution associated with them, rather than assuming a limiting equilibrium condition, and ignoring the displacements. The work undertaken for this part of the project has been directed towards evaluating the validity of the assumptions, for granular soils, on which current stress-strain theories are based.

These theories fall into two distinct categories. The first assumes that the behaviour is elastic, that is conservative, implying that all the stored energy is recoverable, whether the stress-strain characteristics are linear or non-linear. Secondly it is assumed that the material deforms plastically as a continuum and that various conditions are obeyed in so doing, but, if the stresses are reduced or if the material is overconsolidated, it behaves elastically.

8.2.1 The Plastic Behaviour of Granular Soils

As an example of this type of theory the Cambridge models will be considered. The fundamental idealisation, of all the variations of the basic model proposed, is that, the plastic strain increments are normal to plastic potentials which expand symmetrically as the stresses are increased. That is at a particular stress point on the current

plastic potential the plastic strain increment vector will have a unique direction if the associated stress increment is directed outward from the yield locus. That this is not true is observed in the tests on granite rockfill and marble chippings which showed that the plastic strain increment direction is influenced by the previous stress increment direction. For example at the stress point 'A' in Figure (8-1), the plastic strain increment directions for granite rockfill and marble chippings are shown. Similar variations were found for the Ham River sand.

Even more striking divergence is observed between tests where the mean normal stress is increasing and tests where the mean normal stress is decreasing. These types of test were conducted on the granite rockfill and marble chippings. The results can be summarised in Figure (8-2). This figure clearly shows that the plastic strain increment direction is not unique. It is howevever possible to criticise the stress directions chosen for comparison, as neither the locus of the yield surface nor the full shape of the plastic potential surface was determined. But near the stress point 'D' the plastic potential surface is evidently expanding for both paths*. So if the assumption of symmetrical expansion of these surfaces was valid, the plastic strain increment directions for both paths should have coincided. Though they do not, this does not in itself completely discredit the concept of isotropic hardening because it could be argued that the stress point being considered is always at a corner of the current yield locus, and so the vectors measured are just a pair of vectors within the fan of permitted vectors as shown in Figure (8-3). However, it is true to say that the angle 'θ', Figure (8-4), is slightly less than 90^{o} which is not possible if the concept of normality is valid. This is because path 2 (in Figure (8-4)) is necessarily within the expanding plastic potential surface as plastic strain increments are generated along it.

---

* Because the plastic strain increment vectors for both paths are directed away from the origin of stresses, and it is assumed that the material is strain hardening.

Another feature of the plastic strain increment vectors found was that along a constant stress ratio path the vector slowly rotated in an anticlockwise direction. This indicates that the local normal to the plastic potential surface also changes its inclination with respect to the stress axes as the stress point moves away from the origin of stress, or in other words that the inclination of the plastic potential surface is itself rotating, which would imply a non-symmetrical expansion of the plastic potential surfaces.

The conclusion that can be drawn is that a strain hardening process is followed by the granular materials tested, but it does not produce a symmetric expansion of the associated yield surface and the shape of the yield surface is probably path-dependant. Since the shape of the right hand boundary of the 'elastic' domain was not investigated, it is not possible to discuss the relationships for energy dissipation, postulated in the various Cambridge soil models. However, the shape of the possible state boundary surface was investigated for constant stress ratios up to 3.0 for a model rockfill material, Venemo granite.

The form of the relationship postulated for the Cambridge models for R = constant* is:

$$e = e_o - \lambda \ln p' \qquad \ldots\ldots (8.2.1)$$

where e denotes the void ratio

e_o denotes the initial void ratio which is taken to be the same for all the tests at $p' = 1$

λ denotes the slope of $e - \ln p'$ line,

p' denotes the effective mean normal stress.

It is taken that all constant stress ratio paths have the same coefficient λ, but are displaced along the e direction.

The tests on granite and marble materials showed that this relationship was not obeyed, a better description was given by the

---

* $R = \sigma'_1 / \sigma'_3$

following relationship:

$$\ln \epsilon_v = \ln D_1 + \bar{\lambda} \ln p' \quad \ldots\ldots (8.2.2)$$

i.e. $$\ln \frac{e_o - e}{1 + e_o} = \ln D_1 + \bar{\lambda} \ln p' \quad \ldots\ldots (8.2.3)$$

where ϵ_v denotes the volumetric strain

D_1 denotes the volumetric strain which corresponds to mean normal stress of 1 psi on loading

$\bar{\lambda}$ denotes the slope of the volumetric strain path on natural log. scale.

e and e_o as denoted in equation (8.2.1)

This relationship was found to be independent of stress ratio up to the maximum value of R = 3 for a particular initial void ratio. By varying the initial voids ratio a family of similar curves are formed all having the same $\bar{\lambda}$ but being displaced along the log ϵ_v axis as the initial voids ratio increased.

These results differ slightly from the published data of El-Sohby (1969) who found that for the same initial voids ratio and mean normal stress the volumetric strain increased and then decreased as the constant stress ratio was increased. This was found for some values of mean stress, but the opposite at other stress levels. In general the differences in strain were small and a good approximation would be to say that the volumetric strain relationship as a function of p' was independent of stress ratio.

During unloading at constant stress ratio a similar relationship is found, namely

$$\ln \epsilon_v = \ln D_2 + \bar{K} \ln p' \quad \ldots\ldots (8.2.4)$$

where D_2 denotes the volumetric strain which corresponds to mean normal stress of 1.0 psi on unloading

$\bar{K}$ denotes the slope of the volumetric strain path on natural log. scale

ϵ_v and p' as denoted previously.

It has been pointed out in Chapter 7 that the above relationship could be used to represent the elastic volumetric strain of rockfill material.

The shear strain for this series of tests was evaluated from volumetric and axial strain measurements. The shear strains are strongly dependent on stress ratio during loading but were very small during unloading. The influence of membrane penetration on these results is marked and emphasised the need for accurate strain measurements to be made directly.

To complete the plastic model for granular materials, it would be necessary to probe the shape of the right boundary and to determine its variability with stress increment direction. The investigation of this boundary should be undertaken with two aims in mind:

1. To find out if its shape is sensitive to the stress path used to set it up, as shown in Figure (8-5).

2. If the shape is not sensitive then the normality condition could be investigated.

Research along these lines has been attempted but with little success. The main problem in these research studies (for example Holubec, 1966) has been the very small strains that are produced for probing stresses as indicated. But the author believes that the measuring techniques developed for the work reported in this thesis are of suitable sensitivity to give a reasonable chance of success.

8.2.2 The Elastic Behaviour of Granular Soils

A complete description of the stress-strain characteristics of granular soil must include a description of its elastic behaviour. That is the behaviour within the current yield surface. All the Cambridge models assume that the material behaves isotropically and elastically within the yield surface. However, it is known that stress cycles in the elastic domain produce a certain amount of hysteresis, the associated

energy loss becomes larger as the stress change increases. It is difficult to understand why this happens if the material behaves isotropically*.

To probe the elastic characteristics an analysis of the behaviour of the marble chippings within the current yield surface will be made. To obtain a general understanding of the 'elastic' properties the strain measured for a particular stress path will be averaged. Even if the material behaves isotropically it is evident that the elastic response is non-linear, so the results will be analysed incrementally to produce values of tangent moduli and the corresponding Poisson's ratio. For this reason the results of the tests on marble chippings will be analysed in the following sections.

8.2.2.1 Analysis of Results of Test 1M

Although the material behaves non-linearly during loading and unloading after pre-stressing, it will be assumed here in the first instance that for a particular increment, the rules of isotropic elasticity can be applied.

Assuming isotropic elasticity case:

$$\Delta\epsilon_1 = \frac{\Delta\sigma'_1}{E} - \frac{2\nu}{E}\cdot\Delta\sigma'_3 \qquad \ldots\ldots (8.2.5)$$

and

$$\Delta\epsilon_3 = \frac{\Delta\sigma'_3}{E} - \frac{\nu}{E}\cdot\Delta\sigma'_3 - \frac{\nu}{E}\cdot\Delta\sigma'_1 \qquad \ldots\ldots (8.2.6)$$

For a drained shear path at a constant cell pressure $\Delta\sigma'_3 = 0$,

then

$$\Delta\epsilon_1 = \frac{\Delta\sigma'_1}{E} \qquad \ldots\ldots (8.2.7)$$

and

$$\Delta\epsilon_3 = -\frac{\nu}{E}\cdot\Delta\sigma'_1 \qquad \ldots\ldots (8.2.8)$$

For a particular constant stress ratio path (anisotropic consolidation path) as

---

* The stored and dissipated energy along the stress path of tests 1M and 2M will be discussed in Section 8.2.3.

$$\Delta\sigma'_3 = \frac{\Delta\sigma'_1}{3}, \quad \text{then}$$

$$\Delta\epsilon_1 = \frac{\Delta\sigma'_1}{E} - \frac{2\nu}{E} \cdot \frac{\Delta\sigma'_1}{3} = \frac{\Delta\sigma'_1}{E}\left[1 - \frac{2\nu}{3}\right] \quad \ldots\ (8.2.9)$$

and

$$\Delta\epsilon_3 = \frac{\Delta\sigma'_1}{3E} - \frac{\nu}{3E} \cdot \Delta\sigma'_1 - \frac{\nu}{E} \cdot \Delta\sigma'_1$$

$$= \frac{\Delta\sigma'_1}{E}\left[\frac{1}{3} - \frac{4\nu}{3}\right] \quad \ldots\ (8.2.10)$$

where $\Delta\epsilon_1$ denotes the incremental axial strain

$\Delta\epsilon_3$ denotes the incremental radial strain

$\Delta\sigma'_1$ denotes the incremental effective major principal stress,

$\Delta\sigma'_3$ denotes the incremental effective minor principal stress,

ν denotes the Poisson's ratio

E denotes the modulus of elasticity.

The values of E and ν for both drained shear path and anisotropic consolidation path are shown in Table (8-1).

For $\Delta\epsilon_3 = 0$ and finite E (equation 8.2.10):

$$1 - 4\nu = 0 \qquad \therefore \nu = 0.25.$$

If we average the strains in the first unload reload isotropic loop from $5 \rightarrow 0 \rightarrow 5$ psi, we get an average strain of 0.00114.

This would imply a ν of 0.17 for an E of 2894 lb/in^2. For the other end of the isotropic consolidation stage an average of $\epsilon_1 = 0.00051$ (σ'_1 is $120 \rightarrow 80$ then $80 \rightarrow 120$) which would imply an E $\simeq$ 52000 lb/in^2 for a $\nu = 0.17$.

If we take another approach and say that the material develops an elastic anisotropy during loading we have many more unknowns. Taking the sample as having axial symmetry gives the following equations:

$$\Delta\epsilon_1 = \frac{\Delta\sigma'_1}{E_1} - \frac{2\nu_{31}}{E_3} \cdot \Delta\sigma'_3 \qquad \ldots\ldots (8.2.11)$$

where E_1 denotes the modulus of elasticity in the (1) direction*
E_3 denotes the modulus of elasticity in the (3) direction*
ν_{31} denotes the Poisson's ratio for the effect of horizontal stress on axial strain.

and $$\Delta\epsilon_3 = \frac{\Delta\sigma'_3}{E_3} - \frac{\nu_{33}\,\Delta\sigma'_3}{E_3} - \frac{\nu_{13}\,\Delta\sigma'_1}{E_1} \qquad \ldots\ldots (8.2.12)$$

where ν_{13} denotes the Poisson's ratio for the effect of axial stress on horizontal strain†

But $$\frac{E_3}{E_1} = \frac{\nu_{31}}{\nu_{13}} \qquad \ldots\ldots (8.2.13)$$

thus $$\nu_{13} = \nu_{31} \cdot \frac{E_1}{E_3} \qquad \ldots\ldots (8.2.14)$$

The unknowns are E_1, E_3, ν_{13}, ν_{31} and ν_{33}. The first four are linked by equation (8.2.14).

Thus we have too many unknowns to sort out from the data available. But some insight might be obtained if we proceed in the analysis as follows:

The results of the drained shear stage where $\Delta\sigma'_3 = 0$ provides values of vertical modulus and they are the same as for the isotropic assumption. But in this case the ratio $-\frac{\Delta\epsilon_3}{\Delta\epsilon_1}$ gives ν_{13} which has the same numerical value as ν for the isotropic case, so we see that ν_{13} is positive and slowly decreases as the shear stress increases. So, we assume that for the anisotropic loading path the value of ν_{13} is also always positive and finally has a value of 0.12 where the two shearing stress paths intersect. If the material develops an elastic anisotropy during loading we would have to find a value near the origin. If we take the average strains during the isotropic loading and unloading stages, near the stress origin and assume that the modulus is close to that found for the first step of anisotropic

---

* 1 denotes the vertical axis. 3 denotes the horizontal axis.

† The other terms were defined earlier in this section.

loading we get a value of $\nu = 0.17$. As a first approximation we can assume that ν_{13} varies linearly from 0.17 at the stress origin to 0.12 at the highest stress reached.

The axial strain increments can now be written in terms of E_1, ν_{13}, $\Delta\sigma'_1$ and $\Delta\sigma'_3$. Also $\Delta\sigma'_3 = \frac{\Delta\sigma'_1}{3}$, so one stress can be eliminated:

$$\Delta\epsilon_1 = \frac{\Delta\sigma'_1}{E_1} - 2\Delta\sigma'_3 \cdot \frac{\nu_{13}}{E_1}$$

$$= \frac{\Delta\sigma'_1}{E_1}\left[1 - \frac{2}{3}\nu_{13}\right] \qquad \ldots\ldots (8.2.15)$$

On this basis the values of E_1 were calculated and shown in Table (8-2).

In this case, as shown in the table, E_1 progressively increases instead of increasing and then decreasing as was obtained by using the assumption of isotropy.

To calculate values of E_3 some assumption for the value of ν_{33} is necessary. For the isotropic case ν_{13} was 0.17. This would of course have been equal to ν_{33} for the low stress range, and for loading in drained shear from $\sigma'_1 = 120 \rightarrow 180$ psi. ν_{13} was 0.14, again in this case ν_{33} could not have been very different, so it would seem to be reasonable to take a value of about 0.15 for ν_{33}, and we will assume it to be constant.

$$\Delta\epsilon_3 + \frac{\nu_{13}}{E_1}\Delta\sigma'_1 = \frac{\Delta\sigma'_3}{E_3}\left[1 - \nu_{33}\right]$$

taking $\nu_{33} = 0.15$, $(1 - \nu_{33}) = 0.85$

$$\text{so} \quad E_3 = \frac{0.85\,\Delta\sigma'_3}{\Delta\epsilon_3 + \frac{\nu_{13}}{E_1}\Delta\sigma'_1} \qquad \ldots\ldots (8.2.16)$$

On this basis the values of E_3 were calculated and shown in Table (8-3). Finally the values of E_1/E_3 for both the anisotropic and drained shear paths were calculated and shown in Table (8-4).

8.2.2.2 Analysis of Results of Test 2M

The axial and radial strains along the 3 paths of unloading, reloading and unloading have been averaged for both the anisotropic consolidation stage and the drained shear stage. These final average strains are shown in Figure (8-7)

First: Assuming isotropic elastic properties: the values of E and ν for both drained shear path and anisotropic consolidation path were calculated and shown in Table (8-5).

Secondly: Assuming elastic anisotropy approach. For this test it appears that the analysis for developing elastic anisotropy can be conducted within the assumption that $\nu_{13} \simeq 0.18$ throughout. This results in the values of E_1 shown in Table (8-6) for the anisotropic consolidation stage. Equation (8.2.15) was used for the calculation:

$$\Delta\epsilon_1 = \frac{\Delta\sigma'_1}{E_1}\left[1 - \frac{2}{3}\nu_{13}\right] \qquad \ldots\ldots (8.2.15)\text{ bis}$$

In this case E_1 (Table (8-6)) does show a decrease with increasing stress, but the increase is much smaller than that for the isotropic elastic assumption. If we had assumed that the Poisson's ratio ν_{13} decreased with increasing stress, as was indicated for the test 1M, we would have had a consistently increasing modulus (i.e. if ν_{13} at highest stress level was 0.12, $E_1 = 58700$ lb/in^2). Of course at these higher stress levels, the material will be more susceptible to creep which would give rise to non-elastic strains and make our assumption of wholly elastic behaviour incorrect. It is interesting, however, that if the $\Delta\epsilon_1$ values are larger due to this effect, the measured ν_{13} values would be too high. However, accepting the values calculated in Table (8-6) and in this case taking $\nu_{33} \simeq 0.18$ as well, we can go on and calculate values of E_3. Values of E_3 are obtained from the following relationship:

$$E_3 = \frac{\Delta\sigma'_3[1 - \nu_{33}]}{\Delta\epsilon_3 + \frac{\nu_{13}}{E_1}\Delta\sigma'_1} \qquad \ldots\ldots (8.2.16)\text{ bis}$$

Take $\nu_{13} = \nu_{33} = 0.18$, as discussed above:

then $$E_3 = \frac{0.82\ \Delta\sigma'_3}{\Delta\epsilon_3 + \frac{\nu_{13}}{E}\Delta\sigma'_1} \qquad \ldots\ldots (8.2.17)$$

Using the above relationship, values of E_3 and E_1/E_3 for the anisotropic consolidation path are calculated in Table (8-7).

It is clear from the analysis of this test data (Tests 1M and 2M) that there is a strong case for accepting the hypothesis of a developed elastic anisotropy. Applying this to the drained shear path and taking E_3 constant because $\Delta\sigma'_3 = 0$ gives $E_3 = 32086$ lb/in^2, the values of E_1/E_3 for the drained shear path are calculated in Table (8-8).

8.2.2.3 Analysis of Results of Test 3M

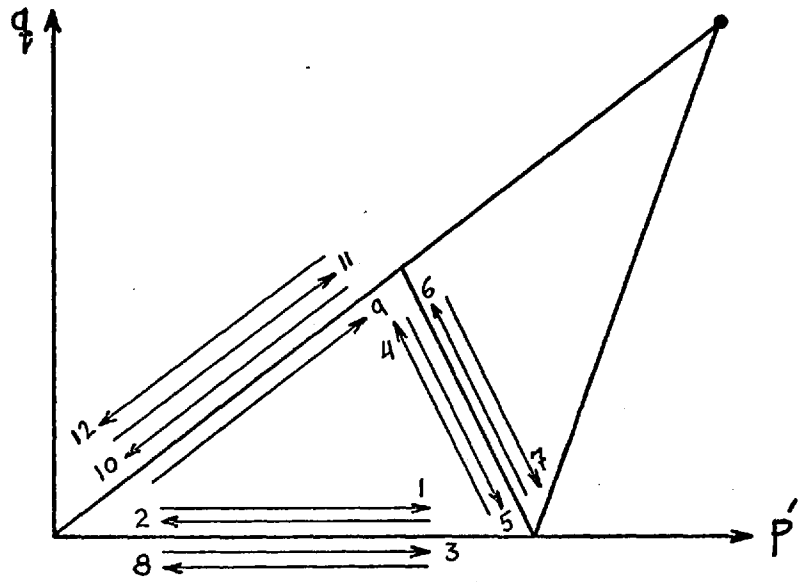

The assumption of isotropic elasticity: The average strains along the paths 5, 6 and 7 are shown in the above figure and are calculated and plotted in Figure (8-8). Assuming incremental isotropic elasticity, the values of E and ν were calculated using the following equations:

$$\Delta \epsilon_1 = \frac{\Delta \sigma'_1}{E} - \frac{2\nu}{E} \Delta \sigma'_3 \qquad \ldots\ldots (8.2.5)\text{ bis}$$

and $$\Delta \epsilon_3 = \frac{\Delta \sigma'_3}{E} (1 - \nu) - \frac{\nu}{E} \Delta \sigma'_1 \qquad \ldots\ldots (8.2.6)\text{ bis}$$

along these paths $\Delta \sigma'_1 = 0$

thus $$\nu = \frac{\frac{\Delta \epsilon_1}{\Delta \epsilon_3}}{\frac{\Delta \epsilon_1}{\Delta \epsilon_3} - 2} \qquad \ldots\ldots (8.2.18)$$

and $$E = \frac{-2\nu \Delta \sigma'_3}{\Delta \epsilon_1} \qquad \ldots\ldots (8.2.19)$$

The values of E and ν for paths 5, 6 and 7 are shown in Table (8-9).

The overall average strains along the anisotropic consolidation path (paths 9, 10, 11 and 12) were calculated and plotted in Figure (8-8). Assuming incremental isotropic elasticity, the values of E and ν are calculated in Table (8-10) for paths 9, 10, 11 and 12.

Averaging the strains in the isotropic loops near the origin gives an ϵ_1 of 0.00091 ($\Delta \sigma' = 0 \rightarrow 5$) and

$$\Delta \epsilon_1 = \frac{\Delta \sigma}{E} (1 - 2\nu) \qquad \ldots\ldots (8.20)$$

For an E = 4794 lb/in^2, $\nu = 0.06$.

This seems to be a rather low value of ν compared with those obtained for the previous cases, but the E = 4794 lb/in^2 is much larger than for the previous cases. If we look at the volumetric strains in the isotropic loops we see that they are much the same as the other two tests where the modulus near the origin was found to be about 3000 lb/in^2. If this value is used we get $\nu = 0.23$ which is much closer to the values obtained before (which were 0.19).

The assumption of elastic isotropy is again found to require negative ν-values for the constant stress ratio path while the isotropic

compression and radial stress release paths require positive ν-values to match the measured strains.

The assumption of elastic anisotropy:

This assumption will now be considered to see if it provides a more rational explanation, as it did previously. In this case the stress paths 4, 5, 6 and 7 will be considered first where $\Delta\sigma'_1 = 0$.

So $$\Delta\epsilon_1 = -\frac{2\nu_{31}}{E_3}\Delta\sigma'_3 \quad \ldots\ldots (8.2.21)$$

and $$\Delta\epsilon_3 = \frac{\Delta\sigma'_3}{E_3}\left[1 - \nu_{33}\right] \quad \ldots\ldots (8.2.22)$$

We have to assume a value of ν_{33}; looking at the incremental isotropic elastic analysis we see that $\nu = 0.36$ for the first increment and then decreases. ν_{33} cannot be very different from ν so let the value of ν be used as ν_{33}.

$$E_3 = \frac{\left[1 - \nu_{33}\right]\Delta\sigma'_3}{\Delta\epsilon_3} \quad \ldots\ldots (8.2.23)$$

and $$\nu_{31} = -\frac{\Delta\epsilon_1 . E_3}{2\,\Delta\sigma'_3} \quad \ldots\ldots (8.2.24)$$

The values of E_3, ν_{31}, E and ν are shown in Table (8-11). The incremental isotropy assumption gave E and ν values which are shown in the last two columns of Table (8-11) and are seen to be much larger than the E_3 values with the exception of the first radial unloading increment which could be compared with the values of 28,700 lb/in^2 and 32,000 lb/in^2 found for the standard drained shear loading path in the tests 1M and 2M respectively.

If we take the hypothesis of developed anisotropy as correct, we can say that the value of E_1 would stay approximately constant for this path where $\Delta\sigma'_1 = 0$. So accepting that $E_1 \simeq E_3$ initially, E = 25,400 lb/in^2 which would give the modulus ratios E_1/E_3 as shown

in Table (8-12). These results (Table (8-12)) give the same qualitative picture of the behaviour of the material as was obtained from the previous two tests. It remains to be seen whether the constant stress ratio paths 9, 10, 11 and 12 give as good an agreement as we have obtained so far.

But before going on to consider the constant stress ratio paths, one aspect of the results to date must be pointed out. That is the effect of developing anisotropy on the values of the Poisson's ratio ν_{13} and ν_{31}.

The results of tests with $\Delta \sigma'_3 = 0$ give values for ν_{13} which do not vary a great deal in an individual test. The values for test 1M were $0.14 > \nu_{13} > 0.12$ and for test 2M $0.20 > \nu_{13} > 0.17$. These values are incremental values. This of course implies that the values of ν_{31} had to vary with the varying elastic anisotropy, demonstrated by the changing modulus ratio.

This is because the modulus ratio is linked to the ratio of the two Poisson's ratios by the equation

$$\frac{E_1}{E_3} = \frac{\nu_{13}}{\nu_{31}} \qquad \ldots\ldots \text{(8.2.13) bis}$$

So for this test path where $\Delta \sigma'_3 = 0$, we deduced a modulus ratio variation for E_1/E_3 from 1 to 2.03 for test 1M and from 1 to 2.05 for test 2M. For test 1M ν_{31} varies between $0.14 \leftrightarrow 0.06$

ν_{13} " " $0.14 \leftrightarrow 0.12$

and E_1/E_3 " " $1.0 \leftrightarrow 2.03$

For test 2M these values are

ν_{31} varies between $0.17 \leftrightarrow 0.1$

ν_{13} " " $0.17 \leftrightarrow 0.20$

and E_1/E_3 " " $1.0 \leftrightarrow 2.05$

In the case of the test 3M where $\Delta\sigma'_1 = 0$, we obtained ν_{31} from the analysis and this gave

	ν_{31}	varying between	$0.37 \longleftrightarrow 0.27$
so	ν_{13}	" "	$0.37 \longleftrightarrow 0.1$
for	E_1/E_3	" "	$1.0 \longleftrightarrow 3.79$

This shows that for this test $\nu_{31} > \nu_{13}$ in general, which is opposite to that found for the stress paths with increasing σ'_1 and σ'_3.

However, too much significance must not be placed on this finding as in all cases the strains used are only average values since only a qualitative description of the elastic behaviour is being attempted. If a quantitative description was to be determined, the displacements should be determined for much smaller stress increments and should be of a greater precision. The approximate resolution of the lateral strain devices used in this work is 2.5×10^{-4} in. per division of the measuring meter. For a quantitative description as discussed above, higher sensitivity transducers have to be made.

Returning now to the constant stress ratio paths 9, 10, 11 and 12 of test 3M. The analysis of the σ'_1 constant path indicated a possible value of ν_{13} of 0.1 at the stress point on the constant stress ratio path, and the isotropic analysis gave a value of $\nu_{13} = \nu = 0.13$ near the stress origin for the constant stress ratio path and a value of $\nu = 0.23$ if the isotropic elastic behaviour was compared with that measured in the other tests. However, in the analysis we will use the values found for this particular sample and assume that the value varies as a linear function of stress. Thus the values of E_1 for the constant stress ratio path are calculated in Table (8-13).

To calculate E_3 the assumption for ν_{33} will be 0.13 at the origin to the value of $\nu_{33} = 0.23$ at $\sigma'_1 = 120$ psi and $\sigma'_3 = 40$ psi which is the same value used for the last stress decrement, in σ'_3 increasing and σ'_1 = constant stress path (paths 5, 6 and 7). On this basis the values of E_3 and the ratio of E_1/E_3 are calculated in Table (8-14).

8.2.2.4 Discussion of the Analysis and Conclusions

It is evident from the previous analyses that the elastic behaviour is compatible with the concept of a stress developed elastic anisotropy; furthermore the material appears to have only a small "memory" of the previous stresses operating on it. This is clear if one looks at the graphs of γ versus p' for the special stress path tests where it is seen that irrespective of the previous stress path, there is little or no shear strain for stress changes on the isotropic stress axis. The granite rockfill seemed to have a larger memory than the other two materials (see γ versus p' for granite rockfill, Figure (7-31)).

That there is a residual effect for other stress paths is seen from the diagram of energy expended versus p' (Figures(8-10) and (8-11)) because the slope of the E vs p' lines for the same stress changes along the same paths in the same sense is different before and after probing in other stress directions.

With the aid of this model for the elastic behaviour it is easier to understand why there is a hysteresis loss for cyclic stresses, because as the elastic anisotropy changes the individual grain contacts will be subjected to small shear displacements which will vary depending on the magnitude of the change in the degree of anisotropy and also as the magnitude of stress changes. A clear indication of this is seen if the shear strains for the R = constant path are compared with the σ'_3 constant and σ'_1 constant paths. For the former there is a very rapid change in the elastic anisotropy near the stress origin giving rise to rapid shear strain changes, whereas the latter two paths involve progressive changes in elastic anisotropy giving smoother shear strain curves.

If the sample had no memory then the elastic modulus in a particular direction should be related to the stress in that direction. To see if this is valid, the results of the analyses are plotted in Figure (8-9).

The moduli are plotted to a base of the average stress for the particular increment analysed; because of this there is a scattering effect at the low stress end. The moduli for all the samples are much the same for the same stress path, which is rather encouraging, however it must be remembered that the strains used in the analysis are average strains and if the strains during each portion of the stress cycles was considered a bigger variation would have been found.

Nevertheless, it is clear that design studies and analyses for structures founded on granular soils should take into account this very important aspect of their character.

In the case of an elastic design study it may be permissible to take as a first approximation the mean values for strains and perhaps use a linear log E_x versus log σ'_x relationship where (x) is the relevant direction. This of course ignores the influence of stress rotations which should be a major topic of a future research programme.

8.2.3 Energy Consideration for Various Stress Path Tests

The cyclic loading and the special stress path tests showed that on repeated loading small irrecoverable deformations occur. In some cases marked shear strains were associated with very small changes in volume. If the material is behaving elastically, then all the deformations (axial, shear and volumetric strains) that occur on loading should be recovered on unloading. It was thus decided to analyse the results of a few special stress path tests in terms of energy expended and recovered during the various stages of loading and unloading. Such calculations for most of the special stress path tests are shown in Table (8-15).

Comparing the energy recovered during unloading along stress paths 2 and 4 of test 2G, Table (8-15), one can see the energy recovered is decreasing with the repeating of the cycles, e.g. it decreased 5.7% during unloading along path 4. Similarly the recovered energy decreased during unloading along path 8 when compared with that along path 6 of the

same test. The comparison of the energy recovered should be made for the same type of stress path for the same test.

The results of the other tests shown in Table (8-15) appear to be of the same trend. In summary it can be seen that the recovered energy during the second unloading cycle is approximately equal or slightly less than that during the first unloading cycle for each path of the same test (e.g. paths 8 and 10 of test 1M; paths 2 and 4 of test 2M; paths 8 and 10 of test 1S and paths 2 and 4 of test 2S).

If the material behaviour on unloading is elastic then the energy recovered during the subsequent unloading cycles (on the same stress path) should be the same. However, the decrease in the amount of energy recovered is small; being always less than 12%. In fact to investigate whether the material behaviour on unloading is elastic, one should compare the energy expended during loading with that recovered during unloading. For a material behaving elastically the energy expended during loading should be equal to that recovered during unloading. To clarify this point the amount of energy expended or recovered per unit volume during the various stages of loading and unloading for tests 1M and 2M (marble chippings) is plotted in Figures (8-10) and (8-11).

It is seen from Figure (8-10) that the energy expended on loading along the first drained shear path is larger than that during the isotropic loading stage. On unloading along the drained shear path a small part of the energy was recovered which means a large part of the energy was dissipated due to plastic deformations. On reloading along the drained shear path the energy expended was slightly more than that recovered during the previous unloading cycle. This indicates that some plastic deformation occurred. This appears, from Figure (8-10), to be largely during the last stage of loading (180 - 200 psi).

During stress probing the amount of recovered energy is also less than that expended on loading. Again the dissipated energy indicates that plastic deformations occurred during stress probing. During subsequent constant stress ratio loading-unloading cycles (anisotropic

paths) there were small amounts of dissipated energy. At low stress levels, e.g. within p' of 100 psi, the amount of dissipated energy is relatively small, then as the loading continues to higher levels, the dissipated energy increases.

Figure (8-11) shows the energy expended and recovered for test 2M. The energy recovered and expended for paths other than that on first loading are nearly equal up to p' of 120 psi, then at higher stress levels the amount of dissipated energy increases. During the stress probing the energy balance is nearly similar to that of test 1M.

Thus it can be concluded that the behaviour of the materials tested is nearly elastic on unloading and reloading up to the previous maximum mean normal stress. This assumption has been used throughout the previous analysis of stresses and strains. Also this type of energy analysis for loading and unloading paths is a reasonable method to analyse the behaviour of granular materials instead of only examining the volumetric and shear strain paths.

8.2.4 Application of the Stress-Dilatancy Theory

The dilatancy factor, $D = 1 + d\epsilon_v / d\epsilon_1$, versus the stress ratio, σ'_1 / σ'_3, relationship for the stress path followed in test 2G (granite rockfill) is shown in Figure (8-12), together with the ϕ'_{cv} and ϕ_u lines. The results of the constant stress ratio section of the stress path lie on the line of R = 3 with negative values of dilatancy factor. The experimental points along the other sections of the stress path scatter widely on the positive side of the abscessa. From these results it is difficult to draw conclusions and it seems that the stress-dilatancy theory is not applicable here. It should be remembered here that the stress path followed in this test consists of many stages of loading and unloading. However, more results should be examined before the stress-dilatancy theory can be dismissed as inapplicable to this area of study.

Table (8-1)

Test 1M - Value of E and ν for both drained shear path and anisotropic consolidation path (on unloading) based on the assumption of isotropic elasticity.

σ'_1 lb/in^2	σ'_3 lb/in^2	E lb/in^2	ν
For drained shear path with constant σ'_3			
120 → 180	120	28,708	0.14
180 → 240	120	48,780	0.15
240 → 300	120	54,545	0.13
300 → 600	120	58,252	0.12
For anisotropic consolidation path			
0 → 15	0 → 5	2,894	0.19
15 → 30	5 → 10	15,528	-0.19
30 → 60	10 → 20	24,272	-0.21
60 → 90	20 → 30	37,994	-0.13
90 → 120	30 → 40	51,020	-0.39
120 → 180	40 → 60	58,275	-0.13
180 → 240	60 → 80	61,679	0.05
240 → 300	80 → 100	58,947	0.10
300 → 360	100 → 120	54,945	0.25

Table (8-2): Test 1M

σ'_1 lb/in^2	$\Delta\epsilon_1$	Assumed ν_{13}	E_1 lb/in^2
0 → 15	0.00454	0.17	2,941
15 → 30	0.00109	0.17	12,248
30 → 60	0.00141	0.16	18,936
60 → 90	0.00086	0.16	31,047
90 → 120	0.00074	0.16	36,081
120 → 180	0.00112	0.15	48,214
180 → 240	0.00094	0.13	58,085
240 → 300	0.00095	0.12	58,105
300 → 360	0.00091	0.12	60,659

Table (8-3): Test 1M

σ'_1 lb/in^2	σ'_3 lb/in^2	$\Delta \epsilon_3$	E_3 lb/in^2
0 → 15	0 → 5	0.00044	3,252
15 → 30	5 → 10	0.00057	5,461
20 → 60	10 → 20	0.00076	8,387
60 → 90	20 → 30	0.00044	14,295
90 → 120	30 → 40	0.00050	13,427
120 → 180	40 → 60	0.00057	22,467
180 → 240	60 → 80	0.00025	44,238*
240 → 300	80 → 100	0.00019	54,155*
300 → 360	100 → 120	0	143,223*

* Radial strains are very small here and discrimination and accuracy of radial strain transducers will introduce errors.

Table (8-4): Test 1M - Value of E_1/E_3 for both anisotropic and drained shear paths

For anisotropic path		For drained shear path †	
σ'_1 lb/in^2	E_1/E_3	σ'_1 lb/in^2	E_1/E_3
0 → 15	0.90	120 → 180	1.0
15 → 30	2.24	180 → 240	1.70
30 → 60	2.26	240 → 300	1.90
60 → 90	2.17	300 → 360	2.03
90 → 120	2.69		
120 → 180	2.15		
180 → 240	1.31		
240 → 300	1.07		
300 → 360	0.42		

† Assuming E_3 does not change from initial value at start of shear stage because $\Delta\epsilon_3 = 0$ gives $E_3 = 28,708$ lb/in^2.

Table (8-5): Test 2M - Values of E and ν for both drained shear path and anisotropic consolidation path (on unloading) based on the assumption of isotropic elasticity

σ'_1 lb/in^2	σ'_3 lb/in^2	E lb/in^2	ν
For drained shear path with constant σ'_3			
120 → 180	120	32,086	0.17
180 → 240	120	56,074	0.19
240 → 300	120	65,934	0.20
300 → 360	120	64,516	0.17
For anisotropic consolidation stage			
0 → 15	0 → 5	2,799	0.19
15 → 30	5 → 10	11,737	-0.03
30 → 60	10 → 20	27,322	-0.32
60 → 90	20 → 30	50,505	-0.60
90 → 120	30 → 40	55,556	-0.33
120 → 180	40 → 60	64,516	-0.29
180 → 240	60 → 80	73,529	-0.01
240 → 300	80 → 100	66,225	-0.01
300 → 360	100 → 120	59,172	0.11

Table (8-6): Test 2M - Values of E_1 for the anisotropic shear path

σ'_1 lb/in^2	$\Delta\epsilon_1$	E_1 lb/in^2
0 → 15	0.00468	2,820
15 → 30	0.00130	10,154
30 → 60	0.00133	19,850
60 → 90	0.00083	31,807
90 → 120	0.00066	40,000
120 → 180	0.00111	47,568
180 → 240	0.00082	64,390
240 → 300	0.00091	58,022
300 → 360	0.00094	56,170

Table (8-7): Test 2M - Values of E_3 and E_1/E_3 for the anisotropic shear path

σ'_1 lb/in^2	σ'_3 lb/in^2	E_3 lb/in^2	E_1/E_3
0 → 15	0 → 5	2,971	0.95
15 → 30	5 → 10	5,540	1.83
30 → 60	10 → 20	7,455	2.66
60 → 90	20 → 30	9,762	3.26
90 → 120	30 → 40	14,642	2.73
120 → 180	40 → 60	18,222	2.61
180 → 240	60 → 80	36,444	1.77
240 → 300	80 → 100	32,800	1.77
300 → 360	100 → 120	43,158	1.30

Table (8-8): Test 2M - Value of E_1/E_3 for the drained shear path based on the assumption that E_3 is constant

σ'_1 lb/in^2	E_1/E_3
120 → 180	1.0
180 → 240	1.75
240 → 300	2.05
300 → 360	2.01

Table (8-9): Test 3M - Values of E and ν for paths (5, 6, 7) based on the assumption of isotropic elasticity

σ'_1 lb/in^2	σ'_3 lb/in^2	E lb/in^2	ν
120	40	20,356	0.23
120	60	31,809	0.19
120	80	29,143	0.23
120	100	25,397	0.365
120	120		

Table (8-10): Test 3M - Values of E and ν for paths (9, 10, 11 and 12) based on the assumption of isotropic elasticity

σ'_1 lb/in^2	σ'_3 lb/in^2	E lb/in^2	ν
0 → 15	0 → 5	4,794	0.13
15 → 30	5 → 10	20,161	-0.35
30 → 45	10 → 15	23,901	-0.20
45 → 60	15 → 20	50,505	-0.82
60 → 90	20 → 30	53,191	-0.40
90 → 120	30 → 40	46,040	-0.08

Table (8-11): Test 3M - Values of E and ν for paths (5, 6 and 7).

σ'_1 psi	σ'_3 psi	anisotropic elasticity		isotropic elasticity	
		E_3 psi	ν_{31}	E psi	ν
120	120 → 100	25,400	0.37	25,397	0.365
120	100 → 80	14,951	0.33	29,143	0.23
120	80 → 60	10,520	0.30	31,809	0.19
120	60 → 40	6,710	0.27	20,386	0.23

Table (8-12): Test 3M - Values of E_1/E_3 for paths (5, 6 and 7)

σ'_1 lb/in^2	σ'_3 lb/in^2	E_1/E_3
120	120 → 100	1.0
120	100 → 80	1.70
120	80 → 60	2.41
120	60 → 40	3.79

Table (8-13): Test 3M Values of E_1 for paths (9, 10, 11 and 12) based on the assumption of anisotropic elasticity.

σ'_1 lb/in^2	assumed ν_{13}	E_1 lb/in^2
0 → 15	0.13	4,786
15 → 40	0.13	14,837
30 → 45	0.12	19,355
45 → 60	0.12	30,000
60 → 90	0.11	39,021
90 → 120	0.10	40,552

Table (8-14): Test 3M - Values of E_3 and E_1/E_3 for paths (9, 10, 11 and 12) based on the assumption of anisotropic elasticity

σ'_1 psi	σ'_3 psi	assumed $1-\nu_{33}$	E_3 psi	E_1/E_3
0 → 15	0 → 5	0.87	4,728	1.01
15 → 30	5 → 10	0.86	5,890	2.52
30 → 45	10 → 15	0.84	8,936	2.17
45 → 60	15 → 20	0.83	8,557	4.56
60 → 90	20 → 30	0.80	14,035	2.78
90 → 120	30 → 40	0.77	21,389	1.90

Table (8-15): Energy recovered along the unloading paths as described:

Material	Test No.	Stress Path No.	Description of the stress path (on unloading)	Energy Recovered lb. in.
Granite	2G	2	anisotropic	141.35
		4	anisotropic	133.26
		6	drained shear + isotropic	146.67
		8	drained shear + isotropic	129.41
Marble Chippings	1M	2	isotropic	37.66
		6	drained shear + isotropic	132.6
		8	anisotropic	114.76
		10	anisotropic	111.18
	2M	2	anisotropic	122.48
		4	anisotropic	120.45
		6	isotropic	45.46
		10	drained shear + isotropic	121.59
Ham River Sand	1S	2	isotropic	39.6
		6	drained shear + isotropic	135.44
		8	anisotropic	136.2
		10	anisotropic	131.62
	2S	2	anisotropic	130.40
		4	anisotropic	130.57
		6	isotropic	37.44
		10	drained shear + isotropic	138.20

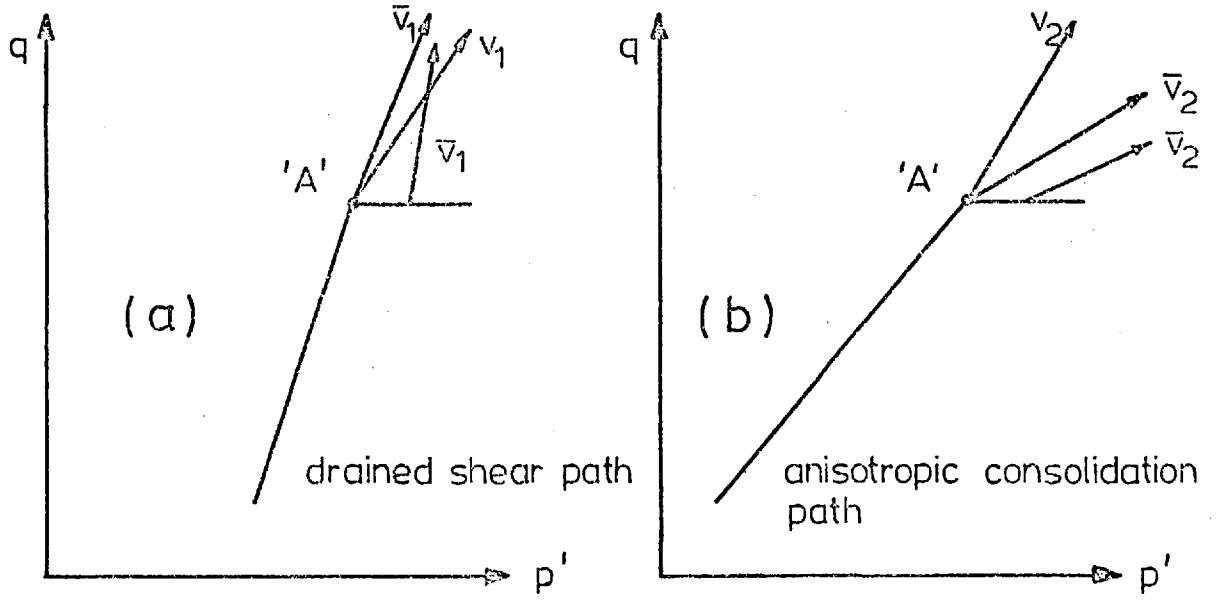

GRANITE ROCKFILL - T.1G

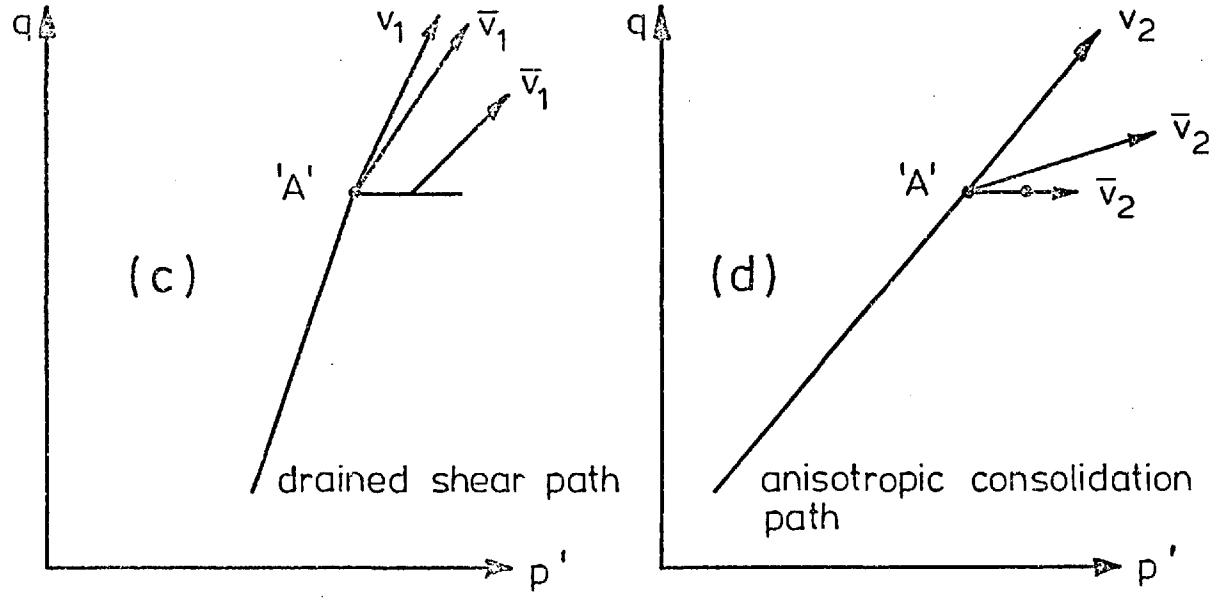

MARBLE CHIPPINGS - T. 1M

Fig. 8-1

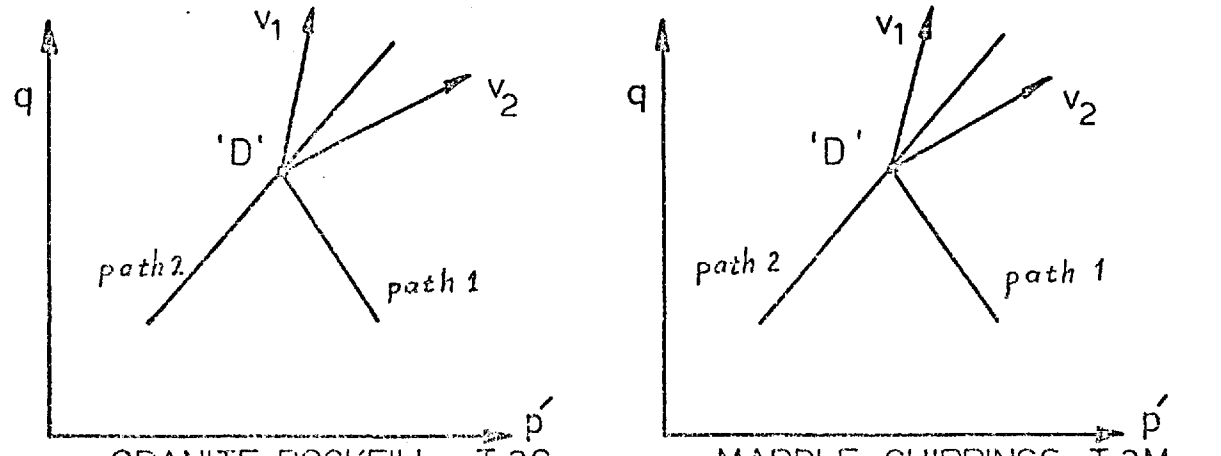

GRANITE ROCKFILL - T.3G

MARBLE CHIPPINGS - T.3M

Fig. 8-2

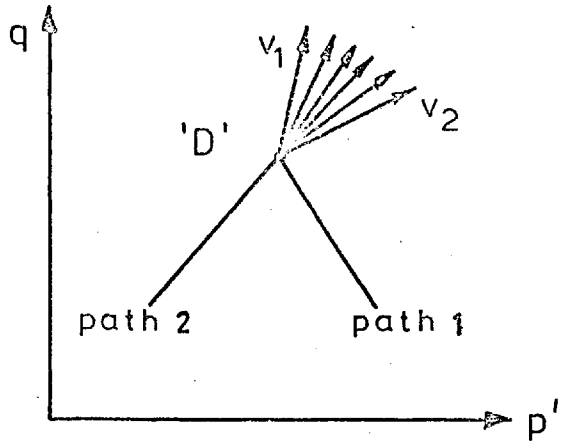

Fig. 8-3

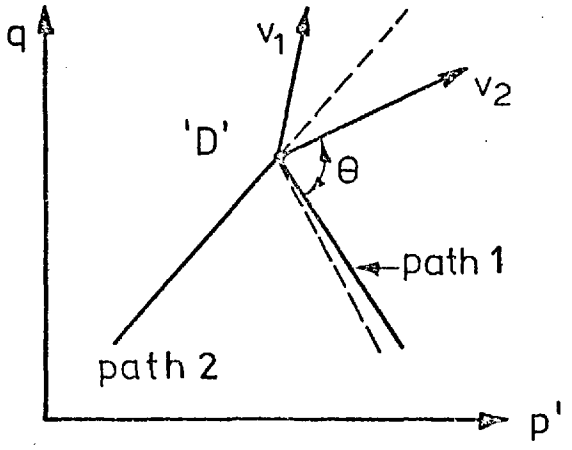

Fig. 8-4

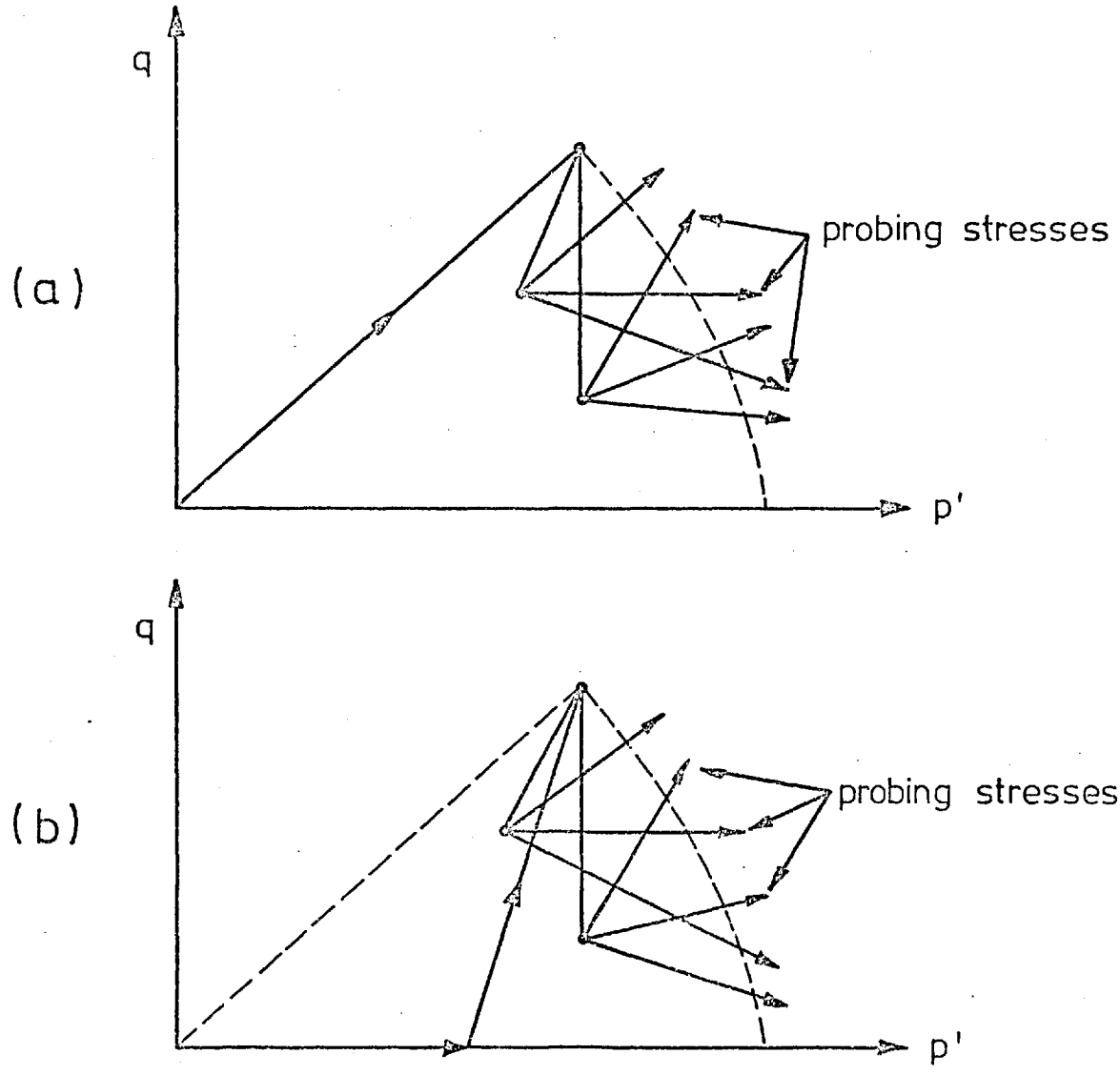

Fig. 8-5

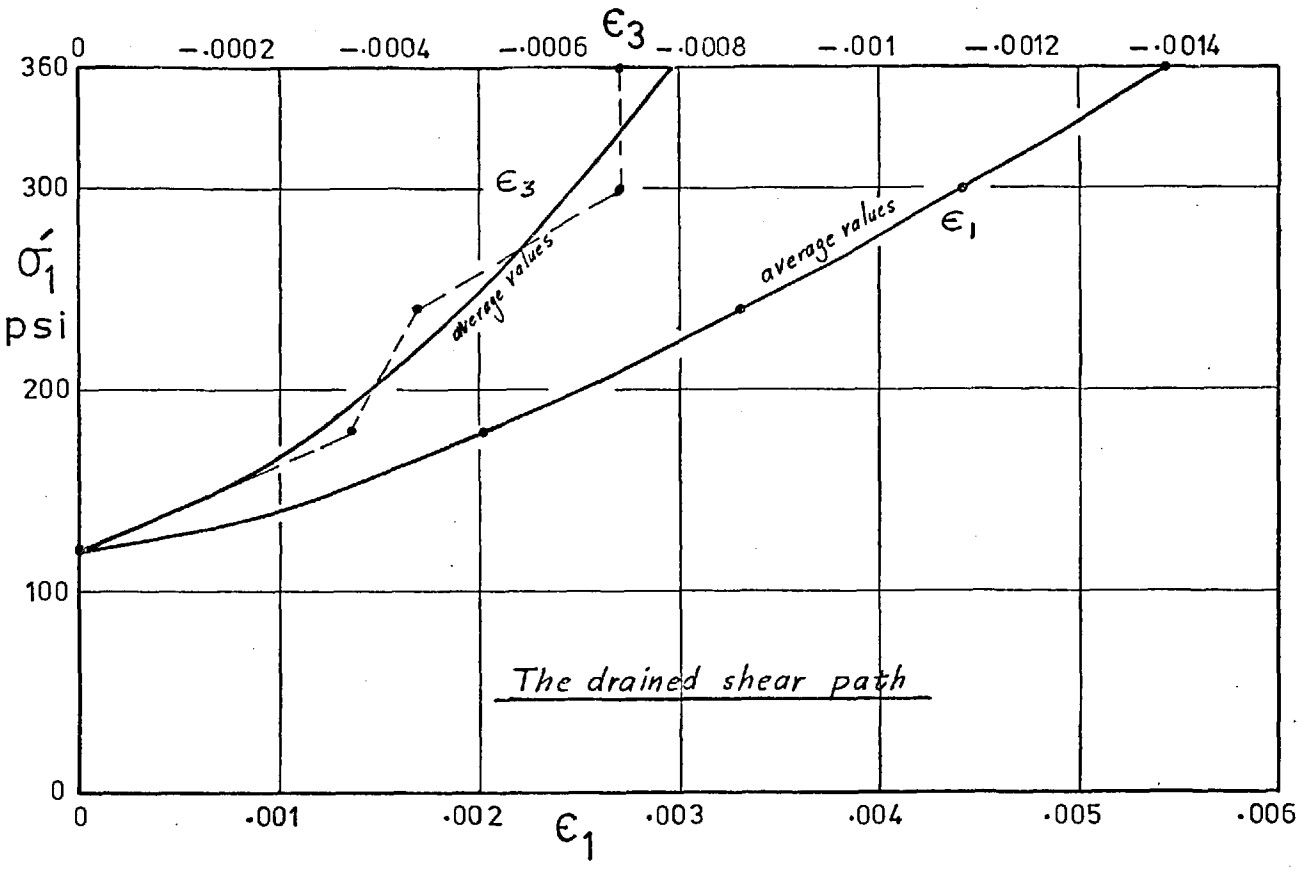

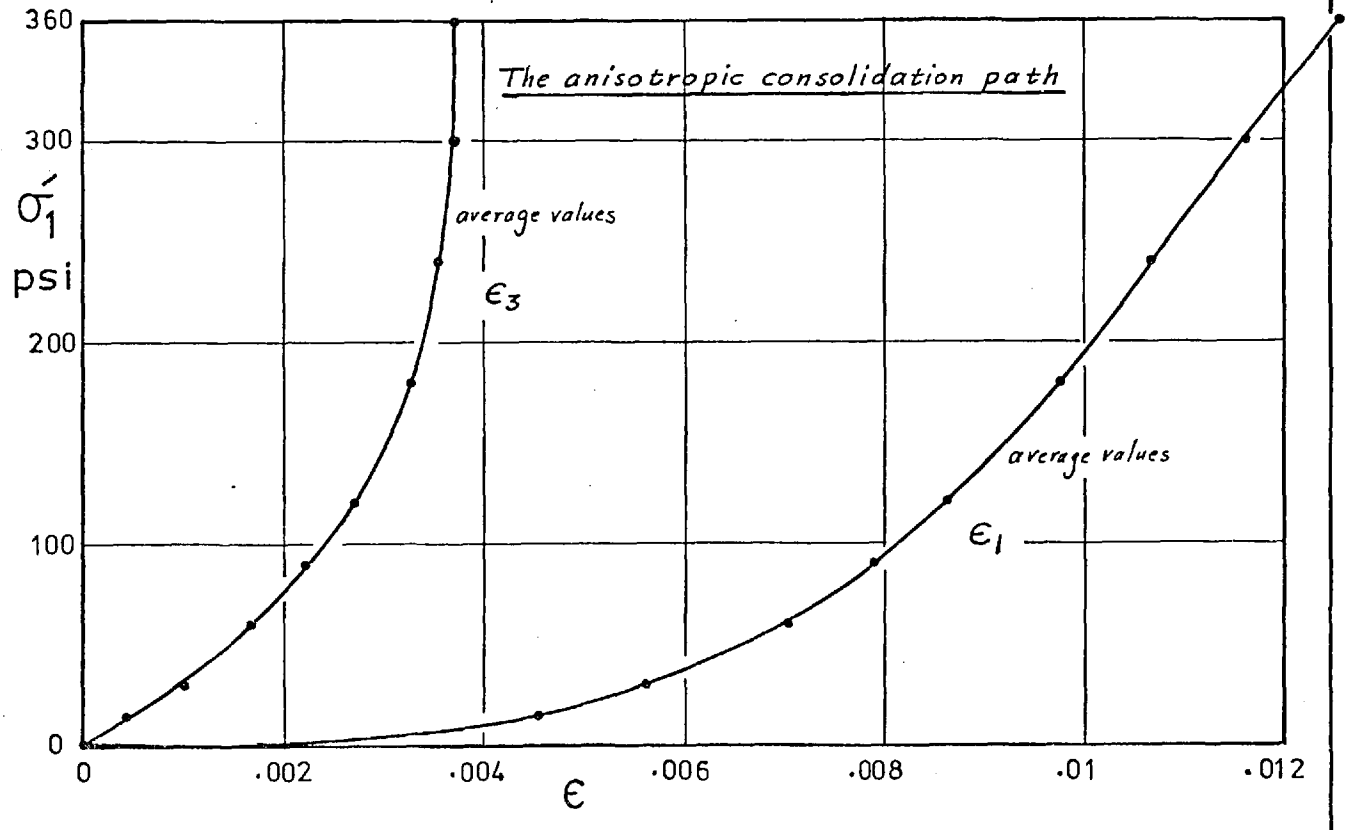

MARBLE CHIPPINGS - σ_1' VS. ϵ_1 & ϵ_3 FOR T. 1M

FIG 8-6

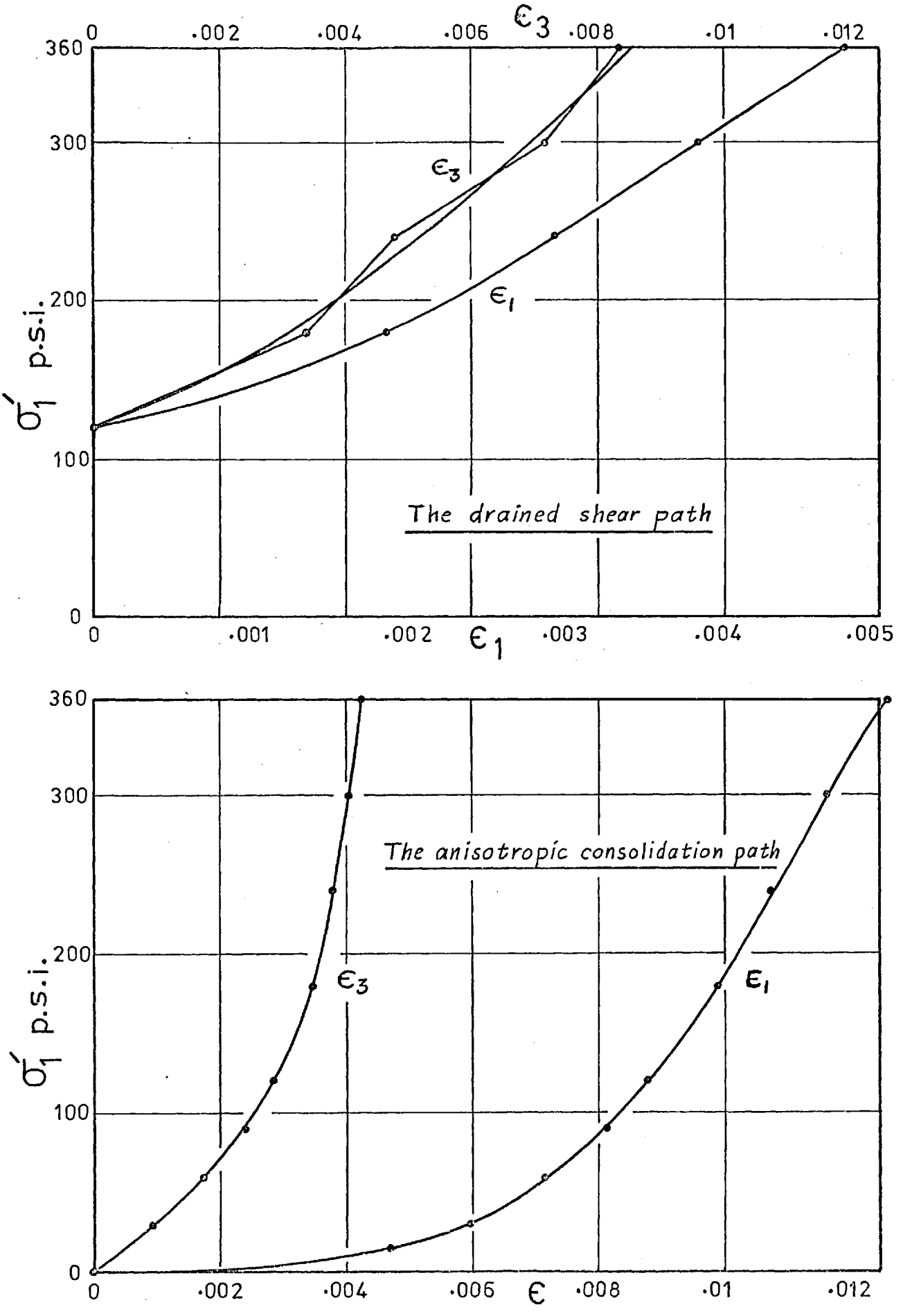

MARBLE CHIPPINGS – σ_1' VS. ϵ_1 & ϵ_3 FOR T. 2M

FIG 8 – 7

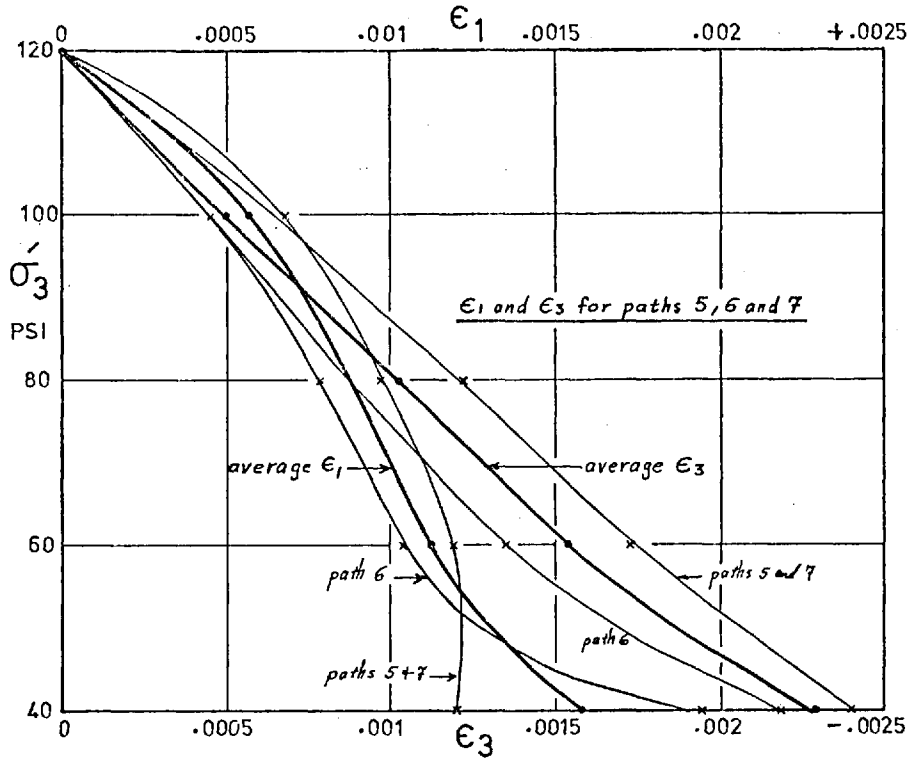

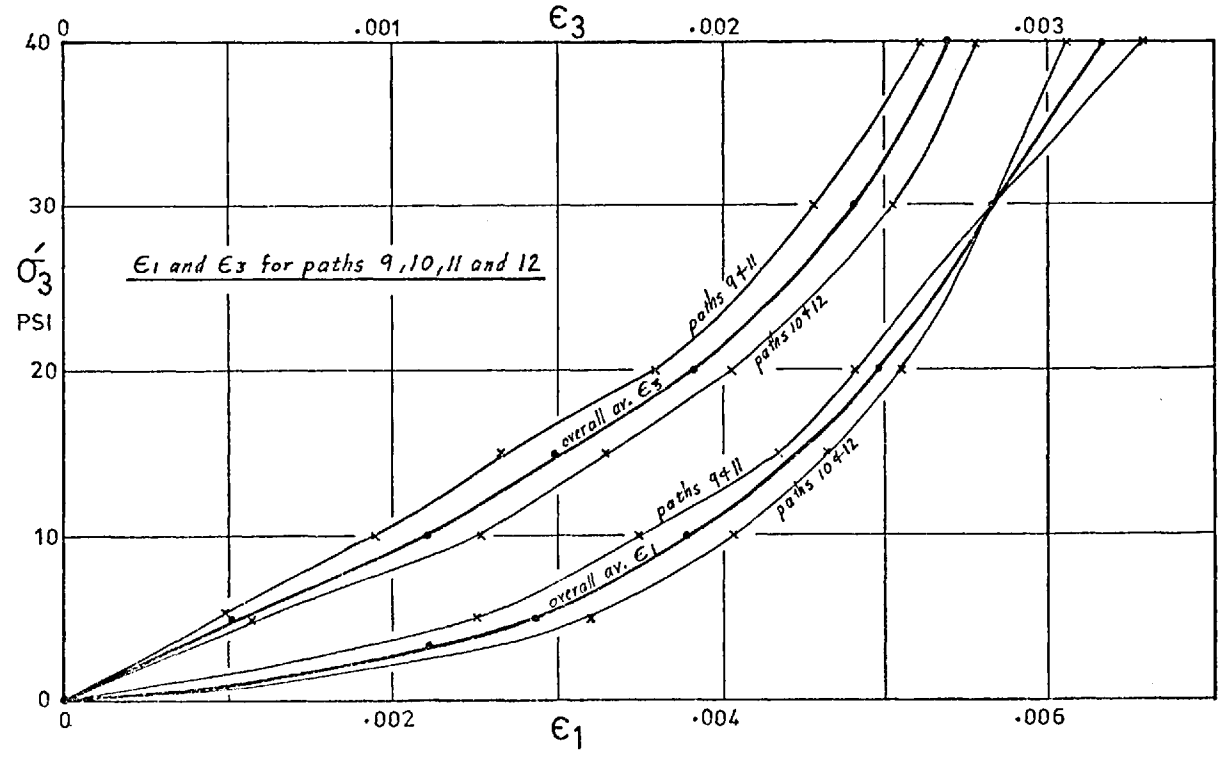

MARBLE CHIPPINGS – σ'_3 VS. ϵ_1 & ϵ_3 FOR T 3M

FIG 8–8

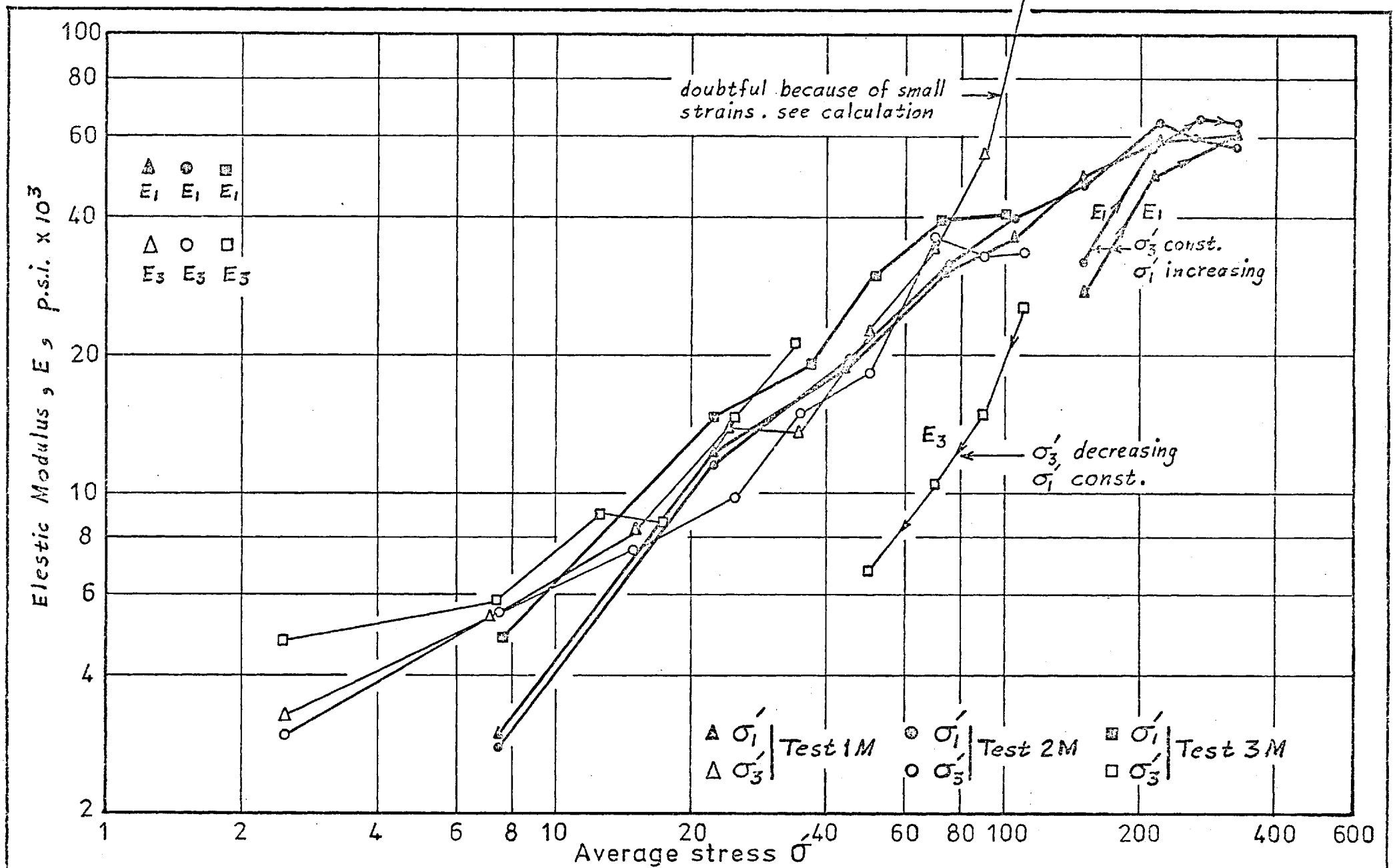

ELASTIC MODULII CALCULATED WITH THE ASSUMPTION THAT THE MATERIAL DEVELOPS ANISOTROPY_Plotted to a base of the current stress along the same axis as the moduli

FIG 8-9

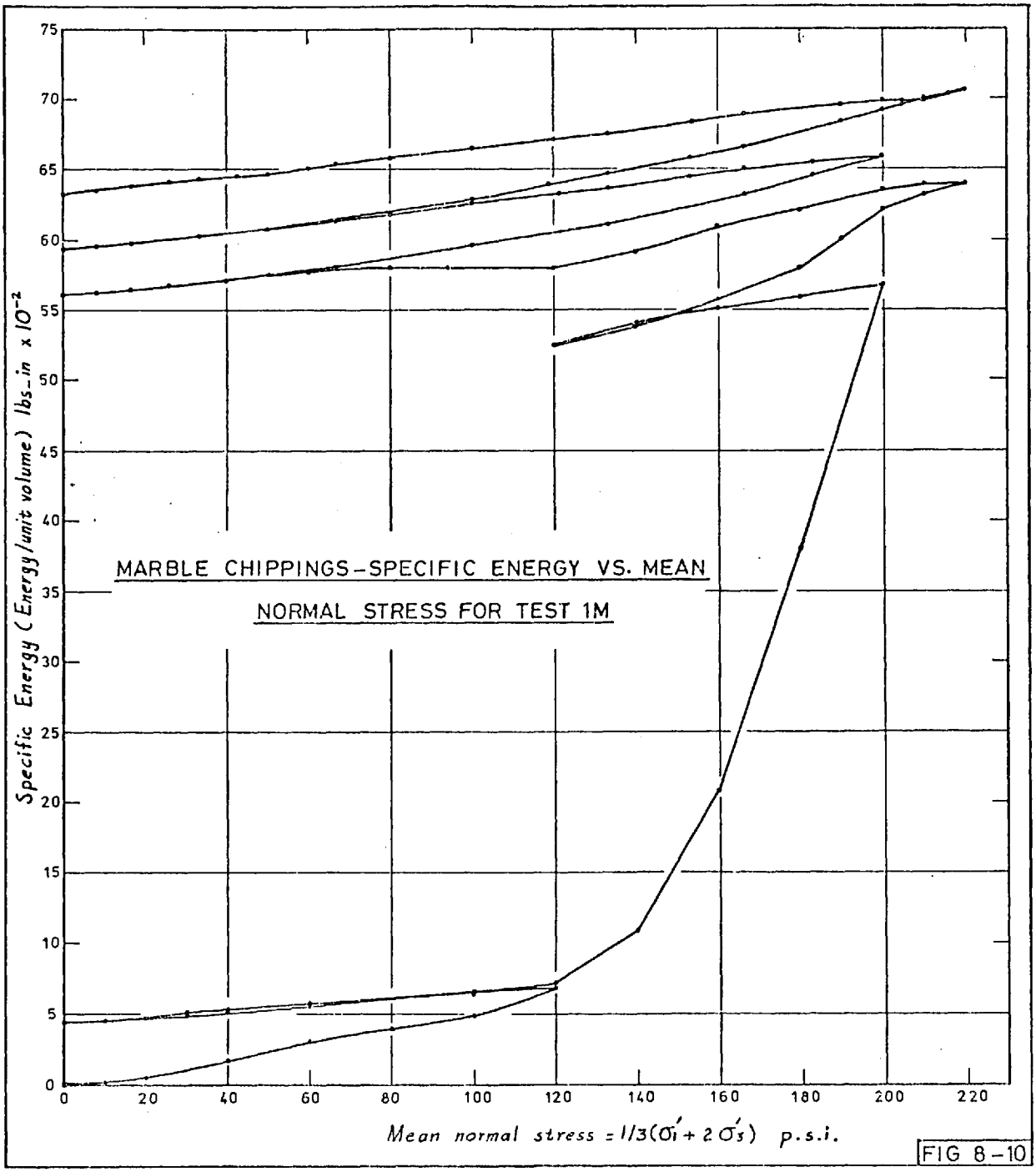
MARBLE CHIPPINGS-SPECIFIC ENERGY VS. MEAN
NORMAL STRESS FOR TEST 1M
Specific Energy (Energy/unit volume) lbs-in x 10⁻²
Mean normal stress = 1/3(σ'1 + 2σ'3) p.s.i.
0
5
10
15
20
25
30
35
40
45
50
55
60
65
70
75
0
20
40
60
80
100
120
140
160
180
200
220

FIG 8-10

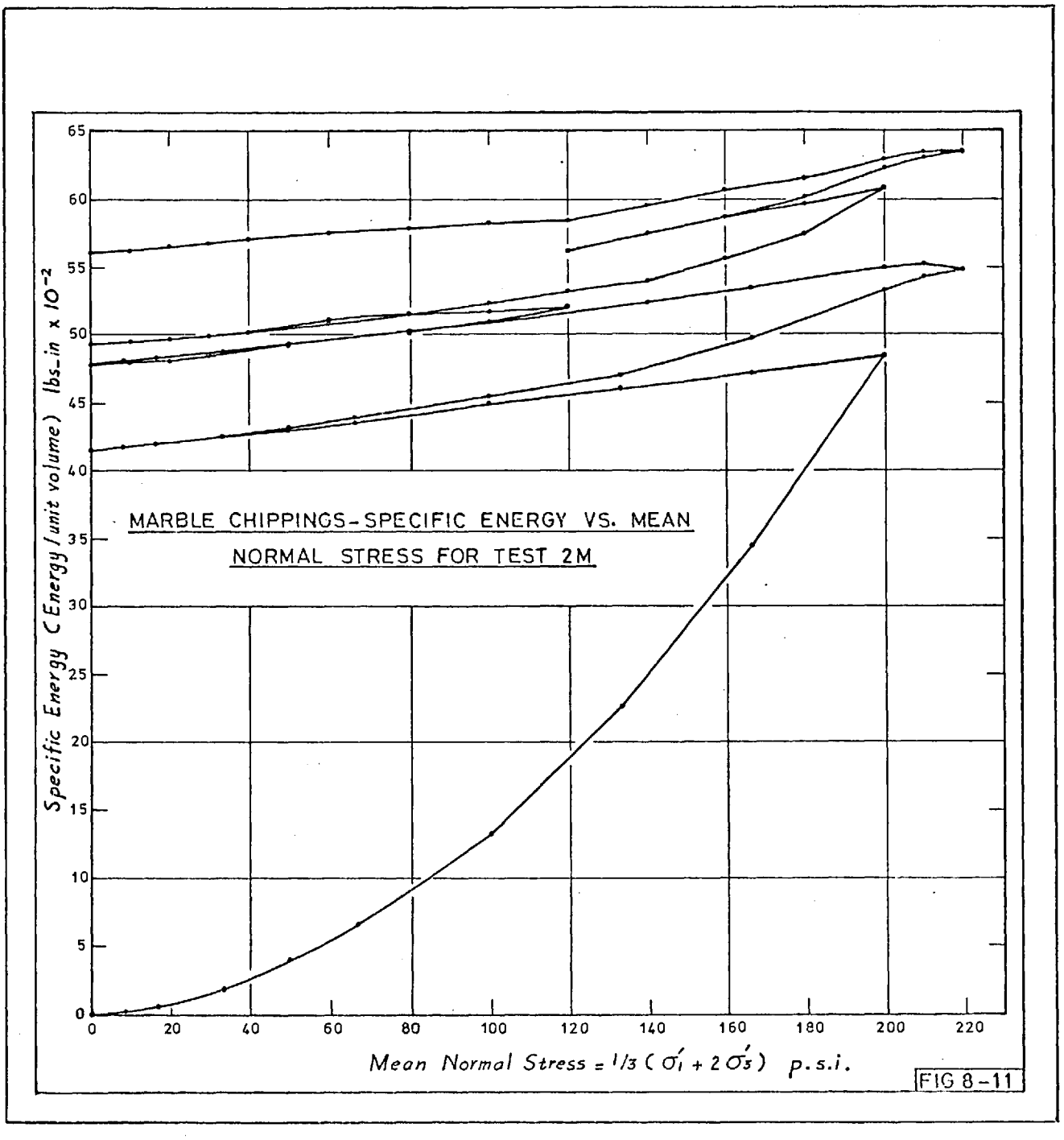
MARBLE CHIPPINGS-SPECIFIC ENERGY VS. MEAN NORMAL STRESS FOR TEST 2M
Specific Energy (Energy/unit volume) lbs-in x 10⁻²
Mean Normal Stress = 1/3 (σ'1 + 2σ'3) p.s.i.
0
5
10
15
20
25
30
35
40
45
50
55
60
65
0
20
40
60
80
100
120
140
160
180
200
220

FIG 8-11

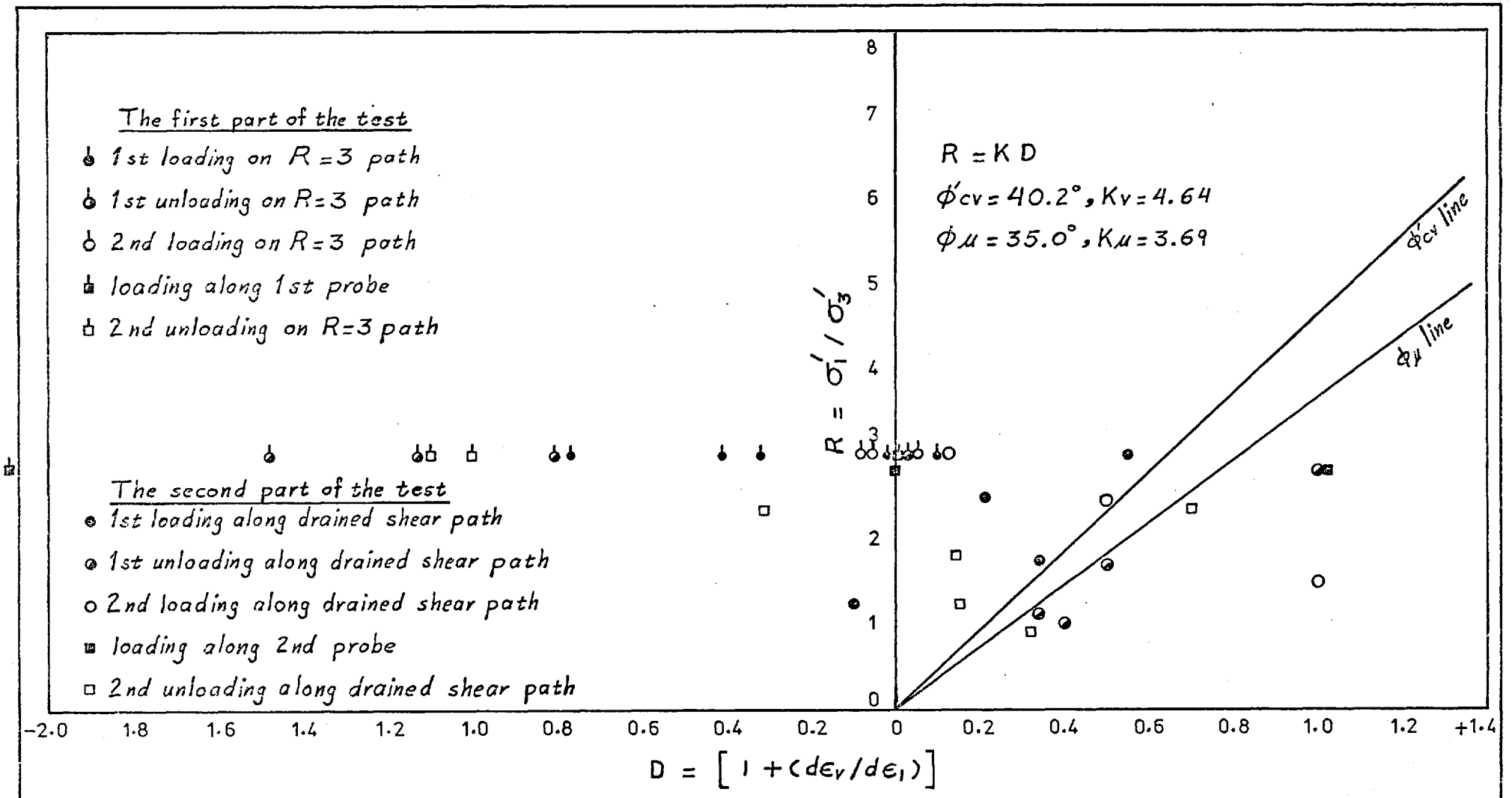

GRANITE ROCKFILL. STRESS-DILATANCY PLOT FOR TEST 2G

FIG 8-12

PART II

STRESS-STRAIN CHARACTERISTICS OF CLAYS UNDER HIGH PORE WATER TENSION

CHAPTER IX

INTRODUCTION, LITERATURE REVIEW AND THEORETICAL PRINCIPLES

9.1 Introduction

The prediction and measurement of the pore pressure set up due to changes in the state of stress under undrained conditions has received considerable attention in soil mechanics research. Although Terzaghi (1936) has introduced the effective stress equation ($\sigma' = \sigma - u$),* he did not analytically derive a relationship between Δu and $\Delta \sigma$, but assumed that the ratio of Δu to $\Delta \sigma$ was equal to unity.

From consideration of the physical model of a porous solid it is clear that the value of the pore pressure change must be a function of the relative compressibilities of the porous soil skeleton, of the pore fluid filling the voids and the solid grains, together with the porosity and probably the intergranular contact area between the soil grains (Bishop, 1973).

Bishop and Eldin (1950) introduced an expression for the ratio of the pore pressure change to the change in total normal stress in terms of the porosity and the relative compressibilities of the pore water and the solid skeleton only. This expression was later extended to include the compressibility of the solid material forming the skeleton of the soil (Bishop, 1966a and 1973).

Since then satisfactory results and explanations have been concluded during the application of this expression within low and medium confining pressure ranges. But at high confining pressure, no results are so far available. It is intended, in this part of the thesis, to examine this expression with regard to high confining pressures†.

It is accepted, in soil mechanics literature, that the undrained shear strength of saturated normally consolidated intact samples is independent of the applied confining pressure during shear. In fact this is the basic assumption of the $\phi = 0$ analysis (Skempton 1948).

---

* where σ denotes total normal stress and u denotes pore pressure.

† as high as 9000 psi.

This assumption has been confirmed by the negligible increase in undrained strength with increase in total normal stress reported from tests on saturated clays (Terzaghi, 1932 and 1936; Golder and Skempton, 1948; Bishop and Bjerrum, 1960) and from tests on saturated sand (Bishop and Eldin, 1950).

Many cases, for both sands and clays, have been reported which are at variance with the previous assumption. These cases will be discussed in detail in Section 9.3.2. In all these cases negative pore water pressures were noted though they have not been measured directly. Thus it appears that the ability of pore water to sustain tension is in doubt. Unfortunately the influence of negative pore water pressure on the shearing resistance of soils has not been investigated until the study reported by Kumaply (1969). His work will be reviewed briefly in the next section.

Results of tests to assess the ability of distilled water to sustain tension (maximum negative pore water pressure) vary from approximately 10 to 200 atmospheres (Dixon, 1909; Temperley, 1946 and Rees and Trevena, 1966)*. The pore water in soils is different from distilled water due to the presence of salts, gases, etc. Therefore the values of the maximum tension in water mentioned above cannot be assumed to represent the maximum negative pore water pressure in soils. In this thesis an attempt has been made to investigate the ability of pore water in cohesive soils to sustain tension and to determine the stress level above which the pore water will cavitate. Two types of cohesive soils were examined, London clay and Kaolin; their properties, the testing technique and the results obtained will be presented in the following chapters.

9.2 Literature Review

9.2.1 General

When the applied stresses to a saturated sample of clay which has reached an equilibrium water content, are reduced under undrained

---

* All these authors used the Berthelot method of measuring tensions in liquids.

conditions, the sample will expand and a decrease in pore pressure will occur simultaneously. A large negative pore pressure may be set up if the initial pore pressure was small or zero and the decrease in the applied pressures was large. If this negative pore pressure is less than one atmosphere (-14.7 psi at sea level) the pore water would be in absolute tension. Then if the pore water can sustain this tension the sample will stay saturated, otherwise bubbles of water vapour and air freed from solution will occur.* Therefore under such conditions, the decrease in pore water pressure is equal to the decrease in total applied stresses if $B = 1$. Now if Terzaghi's principle of effective stresses for fully saturated soils can be extrapolated into the range of negative pore pressures, then the effective stress on the sample remains unchanged during the change of the applied stresses. The validity of such assumption will be discussed in a later section.

The ability of distilled water and soil pore water to withstand high tensions without rupture has been examined and discussed by few researchers. The work done in this field can be split into two groups:

1. Work on the tensile strength of distilled water or ordinary water.

2. Work on the tensile strength of pore water in soils.

9.2.2 The Tensile Strength of Distilled Water

Many attempts have been made to estimate the critical tension (i.e. maximum tension before rupture) in liquids, but unfortunately varying results were reported. Berthelot (1850) developed a method for studying the behaviour of liquids under hydrostatic tension and since then it has been used and modified by many researchers, e.g. Dixon (1909); Temperley and Chambers (1946); and Rees and Trevena (1964 and 1966). Another method of applying tension to a liquid was introduced by Reynolds (1878). These two methods were examined by the above workers among others and different results were obtained.

---

* This state will be called in the future "cavitation".

The experimental procedure adopted in both methods will not be described here.

Dixon (1909), using Berthelot's method, had reported maximum tensions in water of up to 200 atmospheres. Temperley (1946) pointed out that one of Dixon's basic assumptions was that the pressure inside the Berthelot tube was zero at the filling temperature. Temperley claimed that this assumption was incorrect and suggested that it is necessary to develop pressures of the order of 50 to 100 atmospheres inside the tube in order to cause the gas bubble to disappear in a reasonable time. This was the reason why Dixon reported higher values for the tension in water. However, Temperley (1946) concluded that the maximum tension which can be sustained by water in the presence of glass is of the order of 30 - 50 atmospheres.

Temperley and Chambers (1946) studied the behaviour of water under hydrostatic tension and suggested a modification to the Berthelot method to give results in much better agreement with other methods. They concluded that if tension is applied statically, ordinary water can withstand tensions of up to 40 atmospheres, even if it is not perfectly air-free. On the other hand water nearly saturated with air is only able to withstand tensions of up to 6 atmospheres. Rees and Trevena (1966) carried out a few experiments, using a modified Berthelot method, to estimate the critical tension of distilled water in steel Berthelot tubes. They reported values for the critical tension in distilled water which vary from 9.4 - 77.6 atmospheres. Rees and Trevena suggested that these values of the critical tension might represent the adhesion of the water to the steel rather than the true tensile strength of the liquid.

Therefore it can be concluded that there is no agreed method for measuring the tensile strength of water and the reported experimental results vary widely.

9.2.3 The Tensile Strength in Soils Pore Water

Bolt and Miller (1958) suggested that soil water would have little tensile strength compared to de-aired water. They relate this conclusion to the release of bubbles of water vapour when the absolute pressure approached the vapour pressure of the water. They, therefore, concluded that soil water and the water in the measuring apparatus must have the same limitations on their strength.

Other researchers stated that soil water is different from the de-aired water because the former is under the influence of certain factors. The adsorption forces on the particle surface* and the osmotic pressures due to dissolved salts are some of these factors.

Olson and Langfeller (1965) measured low negative pore pressures† in compacted clays. They suggested that the total head (h) in the pores of a soil element is made up of of four components, a pressure head $(\frac{u}{\gamma_w})$, an osmotic head (ω), an adsorptive head (α) and a position head (Z). Hence:-

$$h = \frac{u}{\gamma_w} + \omega + \alpha + Z \qquad \ldots\ldots \quad (9.2.1)$$

They concluded that the actual negative pore pressure in the soil is one atmosphere, and if lower pore pressures+ were measured, it was because of the influence of the adsorptive and the osmotic heads.

Therefore it can be concluded that the ability of soil water to withstand high tensions without cavitation is still not clear. In fact measuring the tensile strength of soils water is merely a physical problem and not of direct interest to the soils engineer. From the engineering point of view an attempt was made by Kumapley (1969) to examine the influence of negative pore pressures on the shear strength of clays.

---

* Lambe (1953) and Winterkorn (1953)

† Less than -250 psi

\+ Less than -14.7 psi

9.2.4 The Shear Strength of Clays Under Negative Pore Water Pressures

Kumapley (1969) carried out two series of consolidated-undrained tests on two batches of remoulded London clay.*

Batch 1:

For samples consolidated isotropically under the same effective pressure (P'_c) and sheared undrained under various cell pressures ($\sigma_3)_s$ (less than or equal to P'_c), the undrained shear strength was seen to decrease with the increase of the difference between the consolidation pressure P'_c and the cell pressure ($\sigma_3)_s$ during shear, i.e. ($P'_c - \sigma_{3s}$). A non-dimensional plot of (c_u/c_{uo}) against the ratio (σ_{3s}/P'_c)$^{\neq}$ was presented which shows the points close to a unique curve, Figure (9-1a). The curve indicates that there was a decrease of 35% in the undrained shear strength between samples sheared unconfined, and samples sheared with the cell pressure equal to the effective consolidation pressure P'_c. However, the present author carried out a series of similar tests. The results, which will be presented in Chapter 11, showed no decrease in unconfined undrained strength, until a level of consolidation pressure, above which there was a decrease in the unconfined undrained strength. The reason for Kumapley's contrary results was due to take up of water by the sample, from the drainage system (porous stones, leads etc.) on unloading, in effect making the unloading partially drained^{+}. The present author took special precautions to prevent taking up water during unloading, and these are described in Chapter 10.

---

* It is the same clay which has been tested in this thesis.

$\neq$ Where: c_u denotes the undrained shear strength under any confining pressure ($\sigma_3)_s$ after it has been consolidated under P'_c.

c_{uo} denotes the undrained shear strength of the normally consolidated sample at P'_c then sheared at $\sigma_{3s} = P'_c$.

+ For example in the case of a sample of London clay consolidated at 1000 psi cell pressure with a time, between reducing the cell pressure to zero and achieving failure in compression, of 15 minutes then the consolidation ratio U, is about 12.5% due to swelling of the sample.

Batch 2:

The samples were consolidated against a back pressure of 500 psi and then the applied pressures were adjusted to give an over-consolidation ratio as marked on Figure (9-1b). It was noticed that the maximum decrease in undrained shear strength between the normally consolidated and the unconfined samples was only 17%. However Kumapley attributed this decrease in undrained shear strength to the release of dissolved gases from the pore water following the sudden decrease in confining pressure prior to shear. Therefore he concluded that the pore water may not be able to sustain large induced negative pressures.*

9.3 Theoretical Principles

9.3.1 The Pore Pressure Changes and Compressibility of Soils

When a saturated porous material is subjected to a pressure, the solid skeleton of the material will only take the whole of the load if the pore fluid is free to flow instantaneously out of the voids. If the out flow of the pore fluid is prevented, the load will be shared between the solid skeleton and the pore fluid in a proportion governed by their respective compressibilities. The flow would be prevented by a high rate of loading, the material having a low permeability, or by there being a long drainage path.

For a saturated porous material, Bishop and Eldin (1950) derived an expression for the ratio of the change in pore pressure Δu to the change in total normal stress $\Delta \sigma$ as follows:

$$\frac{\Delta u}{\Delta \sigma} = \frac{1}{1 + n \frac{C_w}{C}} \qquad \ldots\ldots (9.3.1)$$

where n denotes the porosity,

C_w denotes the compressibility of the pore fluid,

C denotes the compressibility of the solid skeleton under an all-round pressure due to the decrease in the void space.

---

* No magnitude has been given to this negative pore pressure.

In the derivation of the above expression it was assumed that:

(i) The compressibility C_s of the solid material forming the skeleton of a soil is negligible.

(ii) The effective stress equation ($\sigma' = \sigma - u$) is valid irrespective of the magnitude of the intergranular contact area.

A similar expression was given by Bruggeman et al (1939) for the case in which water is considered as compressible:

$$\frac{\Delta u}{\Delta \sigma} = \frac{1}{1 + n\,(K/K_w)} \qquad \ldots\ldots \qquad (9.3.2)$$

where: σ denotes the mean normal stress $= \frac{1}{3}(\sigma_1 + \sigma_2 + \sigma_3)$

n denotes the porosity

K denotes bulk modulus of the soil skeleton

K_w denotes bulk modulus of the water.

In deriving this expression Bruggeman et al (1939) assumed that the intergranular contact area between the soil particles is zero when the effective stress equation ($\sigma' = \sigma - u$) is applicable. In fact this is an unreasonable approximation at high stresses when the intergranular forces are large.

A more general expression which includes the effect of compressibility of the soil grains (or of the solid material of the skeleton) C_s has been given by Bishop (1966a, 1973)

$$\frac{\Delta u}{\Delta \sigma} = \frac{1}{1 + n\left(\frac{C_w - C_s}{C - C_s}\right)} \qquad \ldots\ldots \qquad (9.3.3)$$

Bishop (1973) derived the above expression from first principles which are based on the following assumptions:-

(i) the pores of the porous medium are inter-connecting

(ii) the solid material forming the skeleton of the porous medium is elastic and isotropic

(iii) the bulk behaviour of an element of the skeleton when subject to a change in boundary stress with zero change in pore pressure is that of an elastic isotropic material.

(iv) the distribution of pore space within the skeleton is statically random.

(v) the water filling the pore space is linearly compressible.

Bishop (1973) showed that equation (9.3.3) may also be derived by using the equation relating the change in volume of pore space to the changes in total stress and pore pressure, obtained by Geertsma(1957). Also equation (9.3.3) leads to the same expression for undrained compressibility as that obtained by Gassmann (1951). In conclusion the approaches adopted by Gassman (1951); Geertsma (1957) and Bishop (1973) lead to similar results.

However, for a soil saturated with water, $C_w = 49 \times 10^{-5}$ m^2/MN and $C_s = 2 - 3 \times 10^{-5}$ m^2/MN. The value of the compressibility of the solid skeleton C is much larger than those for C_s and C_w. For a sample of heavily over-consolidated London clay C is equal to 3000×10^{-5} m^2/MN. Therefore equation (9.3.3) is dominated by the ratio of C_w to C and, since C is much larger than C_w, the ratio $\Delta u / \Delta \sigma$ approximates to unity in the low and medium stress range. For the example mentioned above the $\Delta u / \Delta \sigma$ ratio is equal to 0.994.*

For soils and rocks under very high confining pressures, the value of C becomes low and may approach C_s; this will lead to a low value of $\Delta u / \Delta \sigma$. For example, in sandstone under a high confining pressure C is equal to 9×10^{-5} m^2/MN, which leads to $\Delta u / \Delta \sigma = 0.47$†. Thus the ratio $\Delta u / \Delta \sigma$ departs significantly from unity at high consolidation pressures.

---

* n assumed equal to 37%

† n assumed equal to 15.5%

However, the above conclusion, concerning soils in the low and medium stress range, is substantiated by direct measurements of pore pressure change in saturated Brasted sand (Bishop and Eldin 1950) and in saturated clay (Taylor 1944; Bishop 1960). In fact the best way to determine whether or not a soil sample is fully saturated is to measure the ratio $\Delta u / \Delta \sigma$ under undrained conditions.

The value of the compressibility C for a normally consolidated clay soil is approximately proportional to the reciprocal of the consolidation pressure. Thus in this thesis the compressibility C will be defined as the ratio of the volumetric strain to the consolidation pressure applied on the soil element. This is expressed as:-

$$C = \frac{\Delta \epsilon_v}{\Delta p} \qquad \ldots\ldots \qquad (9.3.4)$$

where ϵ_v and p are the volumetric strain and the consolidation pressure respectively.

In Chapter 11 results of tests on London clay samples at high confining pressures are presented and a summary of some of the results is shown in Table (11-3). The values of $\Delta u / \Delta \sigma$ obtained from this table are 0.97 and 0.80 for consolidation pressures of 3000 psi and 9000 psi respectively. On unloading the calculated values of $\Delta u / \Delta \sigma$ drop to 0.94 and 0.63 - 0.77 for swelling pressures of 3000 psi and 9000 psi respectively. This is because the soil structure is not elastic and therefore the rebound modulus is different from that observed on first loading. Few direct observations are currently available of $\Delta u / \Delta \sigma$ for porous materials of low compressibility, where the departure from the truly undrained condition due to the flow of water into the measuring system becomes important.*

---

* Bishop (1973) gave more details about this problem and examples of system compressibility are given by Wissa (1969) and Bruhn (1972).

9.3.2 Examination of the Effective Stress Equation

Consider an element of saturated soil which has been subjected to an all-round pressure , and has been able to drain freely at a constant pore pressure of u. The effective stress relationship, which controls the volume change and shear strength characteristics, is expressed for saturated soils by the equation*:

$$\sigma' = \sigma - ku \qquad \ldots\ldots \qquad (9.3.5)$$

where k is a parameter which differs only slightly from unity in the case of uncemented soils at low consolidation pressures.

In fact the value of k depends on whether equation (9.3.5) is used with respect to changes in volume or to changes in shear strength. For changes in volume Bishop (1953) gave the following expression:

$$k_v = (1 - \frac{C_s}{C}) \qquad \ldots\ldots \qquad (9.3.6)$$

For changes in shear strength Skempton (1960) gave the following expression:

$$k_s = (1 - a \frac{\tan \psi}{\tan \phi'}) \qquad \ldots\ldots \qquad (9.3.7)$$

where a denotes area of contact between the particles, per unit gross area of material

ψ denotes the angle of intrinsic friction of the solid material of the soil grains,

ϕ' denotes the angle of shearing resistance of the granular material.

The value of k_v is very much influenced by the level of the consolidation pressure applied to the soil element. For the values of the compressibility C for London clay used in the previous calculation† of the ratio $\Delta u / \Delta \sigma$

---

* Terzaghi (1936); Bishop and Eldin (1950); Bishop (1959); Skempton (1960); Bishop and Blight (1963) and Bishop (1966a).

† The examples given in Section (9.3.1).

values of k_v of 0.999, 0.994 and 0.939 are obtained for the over-consolidated sample, and the samples consolidated at pressures of 3000 psi and 9000 psi respectively.*

Estimation of the value of k_s is less accurate due to uncertainty about the value of $\underline{a}$, especially for clays. A very accurate experimental examination of Ham River sand in the low effective stress range ($\sigma - u = 52.6$ psi) using pore pressure changes of up to 4000 psi indicated that k_s did not differ from unity by more than 5×10^{-5}, which was the limit of accuracy of the test (Bishop, 1966a; Skinner, 1975)†. If it is assumed that, for small values, $\underline{a}$ increases linearly with the consolidation pressure (Skempton, 1960), thus it can be concluded from equation (9.3.7) that the difference between the actual value of k_s and unity increases linearly with the consolidation pressure. If the mentioned difference 5×10^{-5} (corresponding to σ'_3 of 52.6 psi) is taken as a basis for calculation then the difference between the actual value of k_s and unity would not exceed 2.8×10^{-3} at 3000 psi and 8.6×10^{-3} at 9000 psi. Therefore the values of k_s would not be lower than 0.997 and 0.991 for consolidation pressures of 3000 psi and 9000 psi respectively.

For clays there is no evidence that the values of k_s would be lower than those for sand, although the physical nature of the inter-particle contact and soil skeleton are very different. Kumapley (1969) carried out a series of similar tests on clay. The results are consistent with those on sand, but are not within the same limits of accuracy due to the lower pressures applied and to the problems of pore pressure equalisation in clay samples.

---

* Because the rebound modulus is lower than that of first loading.

† Bishop (1966a) described tests carried out by Mr. A.E.Skinner. In these tests the confining pressure and the pore pressure were changed simultaneously by nearly 4000 psi three times during the progress of a compression test while maintaining the difference ($\sigma_3 - u$) constant at only 52.6 psi. No significant influence on the strength was detected during this pressure change.

Now if the element of soil described at the beginning of this section (9.3.2) is subjected to a change in total normal stress $\Delta\sigma$ under undrained conditions, the pore pressure will change by Δu. Skempton (1954) expressed the ratio $\Delta u / \Delta\sigma$ by a parameter called 'B'. Thus the change in effective stress could be expressed as follows:

$$\begin{aligned}\Delta\sigma' &= \Delta\sigma - k\,\Delta u \\ &= \Delta\sigma - \Delta u + (1-k)\,\Delta u \\ &= (1-B)\,\Delta\sigma + (1-k)\,B.\,\Delta\sigma \qquad \ldots\ldots \qquad (9.3.8)\end{aligned}$$

At low and medium values of consolidation pressure the parameter B deviates from unity by less than 1% and, as shown previously, k differs from unity by less than 0.1%. Therefore the change in effective stress, and thus the volume change and strength, will be close to the direct measurement in the laboratory. This has been confirmed by the insignificant increase in undrained strength with increase in total normal stress reported on saturated clays (Terzaghi, 1932 and 1936; Jurgenson, 1934; Golder and Skempton, 1948; Bishop and Bjerrum, 1960) and on saturated sand (Bishop and Eldin, 1950).

There are two reported cases which deviate from the preceding discussion, namely:

(i) Strongly dilatant sands tested at low confining pressures (Tests carried out by Bishop and Eldin, 1950)

In these tests the application of the principal stress difference causing failure was associated with a significant decrease in pore pressure. In triaxial undrained tests on dense sand at low cell pressures this decrease resulted in negative pore pressures and the stress-strain curve terminated prematurely. Bishop and Eldin (1950) related this to the inability of the water in the pore space and in the measuring system to withstand the tension necessary to maintain full saturation.

(ii) Unconfined compression tests on some clay samples (Bishop, 1947; Golder and Skempton, 1948; Bishop and Henkel, 1962).

From tests on clay samples by the above authors, it has been observed that the unconfined compression strength is often lower than the average of the strengths at higher confining pressures, although the water content is the same and the testing was under undrained conditions. Since the samples are usually saturated this difference has been attributed to the presence of fissures (loc. cit.). However, it may be noted that throughout an unconfined compression test the pore water pressure is negative (Bishop, 1960), and from the high strength of some samples substantial pore water tensions may be set up, though they cannot be measured directly (for example, Croney and Coleman, 1960). Thus it was thought that the pore water cannot sustain high tension and that was the reason behind the lower strength.

Therefore, in this part of the thesis, it is intended to study the influence of the high pore-water tensions on the strength of clay tested at constant water content in the absence of fissures.

9.3.3 Prediction of Pore Water Tension on Stress Release

Consider an element of saturated soil which has been consolidated under a total normal stress σ_o with free drainage to atmospheric pressure. If the total normal stress is changed to σ under conditions of no drainage, the relationship between the normal stresses and the pore pressure set up is given by the following expression:

$$u = B(\sigma - \sigma_o) \quad \ldots\ldots \quad (9.3.9)$$

This relationship is illustrated in Figure (9-2) where the predicted pore pressure is plotted against the total normal stress. For an unconfined sample, where σ drops to zero, the initial pore pressure before shear would be equal to $-B.\sigma_o$. The part of this negative pore water pressure which falls below -1 atmosphere will represent the tension in the pore water.

Then if B is assumed equal to unity, then the pore water of undrained samples consolidated at a total normal stress in excess of +1 atmosphere should be in a state of tension when the cell pressures drop to zero (i.e. in unconfined state). Thus the value of the pore water tension at low and medium range of stress could be predicted from Figure (9-2).

Figure (9-3) shows the previous case in a more general form. Here in Figure (9-3) the sample drains against a back pressure u_o, instead of to atmospheric pressure, and thus the relationship between the total normal stress and the pore pressure is expressed as:

$$u = u_o + B(\sigma - \sigma_o) \quad \ldots\ldots \quad (9.3.10)$$

As will be seen later a consolidation pressure of up to 9000 psi was applied to a sample of London clay draining to atmospheric pressure. From equation (9.3.9) a theoretical maximum pore water tension of B(9000-15) psi could be set up in the pore water. If a value of B for unloading at this consolidation pressure is taken as 0.63* then a tension of 5670 psi could have been induced in the pore water at the end of the unloading stage. It will be seen in the following sections that a sample of London clay could not sustain such high pore water tension and remain saturated.

9.3.4. Prediction of Pore Water Tension at Failure in Unconfined Samples

The pore water pressure at failure for the unconfined sample discussed previously is equal to the sum of the negative pore pressure estimated prior to shear (due to stress release) and the change in pore pressure resulting from the application of the stress difference to cause undrained failure. This additional pore pressure resulting from the application of a stress difference is positive in most clays, unless they are heavily overconsolidated, while it is negative in the case of dilatant sands†.

---

* This value has been estimated in Section (9.3.1).

† For non-dilating sands this additional pore pressure is positive.

Skempton (1954) derived an expression for the change in pore pressure Δu resulting from the application of the stress difference as follows:

$$\Delta u = B \left[\Delta\sigma_3 + A \left(\Delta\sigma_1 - \Delta\sigma_3 \right) \right] \quad \ldots \quad (9.3.11)$$

where $\Delta\sigma_1$ denotes the change in major principal stress,
$\Delta\sigma_3$ denotes the change in minor principal stress,
A denotes a pore pressure parameter which varies with clay type and stress history.

For normally consolidated clays A is positive and approximately equal to unity at failure if the consolidation was under isotropic conditions (Bishop and Henkel, 1962). This is in contrast to overconsolidated clays where the A value at failure becomes negative only where the overconsolidation ratio exceeds 4 or 5 in typical cases of remoulded clay (Bishop and Henkel, 1962, Figure 82). Undisturbed samples of heavily overconsolidated London clay do not show a negative A value at maximum stress difference (Bishop, Webb and Lewin, 1965; Agarwal, 1967), although in undisturbed Weald clay a value as low as -0.62 has been observed (Bishop and Henkel, 1962). Tests on undisturbed Lias clay showed A value at failure of +0.35 (Maguire, 1975).

From equations (9.3.10) and (9.3.11) the pore pressure u for a triaxial sample could be expressed as:

$$u = u_o + B(\sigma - \sigma_o) + B.A_f(\Delta\sigma_1 - \Delta\sigma_3)_f \quad \ldots \quad (9.3.12)$$

The undrained shear strength c_u of a clay sample is equal to $\frac{1}{2}(\Delta\sigma_1 - \Delta\sigma_3)_f$ and the ratio c_u/p^* is approximately constant for normally consolidated samples of clay. Thus equation (9.3.12) may be arranged as:

$$u = u_o + B(\sigma - \sigma_o) + B.A_f.2\frac{c_u}{P}(\sigma_o - u_o) \quad \ldots \quad (9.3.13)$$

---

* Where p is the effective consolidation pressure.

It will be seen in Chapter 11 that c_u/p for London clay approximates to 0.20 for normally consolidated samples and A_f could be taken as approximately 1.25*. Then for the case where $u = 0$ and $B = 1$, the pore pressures are:

the initial pore pressure in the unconfined state is:

$$u = -\sigma_o \quad \ldots \quad (9.3.14)$$

the pore pressure at failure in the unconfined state is

$$u = -\sigma_o + 1.25 \times 2 \times 0.20\ \sigma_o = -0.50\ \sigma_o \quad \ldots \quad (9.3.15)$$

Therefore the pore water tension will be highest in the unconfined state before the application of the axial load and will decrease significantly before failure. This is in contrast to the case for dilatant sands, for which A_f may drop as low as -0.42 (Bishop and Eldin, 1950)†.

In the case where B or k differ from unity as explained previously, it is clear from equation (9.3.8) that a reduction in cell pressure will result in a decrease in effective stress. The unconfined sample will therefore behave as a slightly overconsolidated material, but as the overconsolidation ratio p_c/p is only marginally bigger than unity+ the value of A_f will not change significantly. Hence the conclusion of the previous paragraph is still appropriate.

However, this decrease in effective stress will be reflected in a reduction in the undrained strength of the sample. It will be seen in Chapter 11 that the relationship between the undrained strength c_u and the consolidation pressure p is approximately linear on first loading from a slurry, Figure (9-4). However, this relationship is not fully reversible. The results of the tests on London clay presented in Chapter 11 showed that on the reduction of the effective consolidation pressure before undrained shear the following relationship could be established.

---

* From the results of undrained tests at relatively high consolidation pressure reported by Bishop, Webb and Lewin (1965).

† For cohesionless soils where the angle of internal friction is ϕ', the theoretical lower limit of A_f is given by the expression (Bishop, 1952):

$$A_f = -\frac{1 - \sin\phi'}{2 \sin\phi'}$$

+ It is equal to $1/B$ if $k = 1$

$$\left[\frac{\Delta (c_u)}{\Delta p}\right]_{\text{unloading}} = m\left[\frac{c_u}{p}\right]_{\text{first loading.}}$$

$$= m \cdot n \qquad \ldots\ldots \qquad (9.3.16)$$

where m = 0.5 for London clay consolidated from a slurry,

for $-\Delta p/p_{max} = \frac{1}{2}$

n = a constant approximating to 0.2 for this batch of London clay.

Now if it is assumed that k = 1, then from equation (9.2.8):

$$\Delta p = \Delta \sigma' = (1 - B)\,\Delta \sigma \qquad \ldots\ldots \qquad (9.3.17)$$

Therefore the reduction in strength resulting from a reduction in total stress - $\Delta \sigma$ could be calculated from combining equations (9.3.16) and(9.3.17) as follows:

$$-\Delta(c_u) = (1 - B)(-\Delta \sigma) \cdot m \cdot n \qquad \ldots\ldots \qquad (9.3.18)$$

At the end of the consolidation stage, the effective consolidation pressure is $(\sigma_o - u_o)$ and the undrained strength $(c_u)_o$ is equal to $n \cdot (\sigma_o - u_o)$. Thus the proportional reduction in strength (r) is expressed as:

$$r = \frac{-\Delta (c_u)}{(c_u)_o}$$

then $$r = -\frac{m(1 - B)\Delta \sigma}{(\sigma_o - u_o)} \qquad \ldots\ldots \qquad (9.3.19)$$

The accuracy of predictions, using this expression, is subject to two conditions:

(i) The value of the stress decrement ratio - $\Delta p/p_{max}$ due to an undrained reduction in total stress is less than the values of the ratio used to obtain values of m. Values of m = 0.5 obtained from this clay and from earlier work on London clay by Donald (1961) could possibly be a slight overestimate.

(ii) In determining the value of B from the value of expansibility, volume changes associated with relatively large stress changes are used. However, a preliminary examination seems to indicate that the error involved is not important.

The previous theoretical predictions have been examined experimentally in two stages as follows:

(i) Tests to investigate the influence on undrained strength of large reductions in confining pressure which do not result in pore water tensions. Within this range of total stresses the samples do not depart from a fully saturated state. The experimental investigation will be discussed in the next section.

(ii) Tests to investigate the influence on undrained strength of reduction in confining pressure leading to pore water tensions of various magnitudes. In the limit these will result in departures from full saturation and thus from the assumption on which the predicted values of r are based. An experimental investigation has been carried out as part of this thesis and the results will be presented and discussed in Chapters 11 and 12.

9.3.5 Influence on Undrained Strength of Reductions in Confining Pressure Which do not Result in Pore Water Tensions

An experimental investigation has been carried out by Kumapley (1969) and will be reviewed briefly in this section. The material tested was London clay, the classification tests for which are shown in Table (9-1a). The initial water content of the slurry from which the batch was prepared was 112%. The material was consolidated in a 9 in. diameter oedometer under a maximum vertical stress of 40 psi and was not allowed to swell before unloading. The final water content after removing the material from the oedometer is 43%. A summary of the consolidation pressures and water contents is shown in Table (9-1b).

Samples for this series of tests were cut from the consolidated block of London clay and were consolidated with a cell pressure σ_3 = 1000 psi and an initial pore water pressure u = 500 psi. The samples were then tested in the triaxial cell, with the pedestal saturated under undrained conditions, at cell pressures of 1000, 900, 800, 700, 600 and 500 psi. Each sample was $\frac{3}{4}$ in. diameter and $1\frac{1}{2}$ in. high as will be described in the next chapter. The rate of axial strain was approximately $1\frac{1}{2}$% per minute.

The results of these tests are summarised in Table (9-2) and are plotted in Figure (9-5). Although there is some scatter in the test results it will be seen that there is a small but significant decrease in strength, reaching to about 2.1% for a decrease in total stress of 500 psi which is equal to the effective consolidation pressure p. This decrease corresponds to a slope of 0.2^{o} for the Mohr envelope for undrained strength plotted against total stress.

Comparison may be made between this reduction in strength and the value predicted by using equation (9.3.19). The predicted value is obtained by substituting the following values:

$$m = 0.5 \quad \text{and} \quad B = 0.983$$

$$-\Delta\sigma = \sigma_o - u_o = 500 \text{ psi}$$

$$r = -\frac{m(1-B)\Delta\sigma}{\sigma_o - u_o}$$

hence $r = 0.86\%$.

This predicted value is smaller than the observed decrease in strength which is 2.1%. As the predicted and observed absolute values of r, with respect to the scatter of the test results as shown in Figure (9-5), are small this difference is probably not significant.

Thus it can be concluded that for saturated samples of clay the influence on undrained strength of large reductions in confining pressures is very small. This is in general agreement with predictions based on the relative expansibilities of the soil structure and of the pore water.

Table (9-1a) Classification Tests

Material	Liquid Limit %	Plastic Limit %	Plasticity Index %	Clay Fraction % 2	Activity PI/% Clay	Specific Gravity of Particles
London Clay	74	28	46	57	0.81	2.81

Mineralogy of London Clay: illite with kaolinite, montmorillonite and chlorite

Table (9-1b) Consolidation of Clay Before Sampling

Material	Maximum Vertical Stress: lb/sq.in.	Final Vertical Stress: lb/sq.in.	Water Content Initial %	Water Content Final %
London Clay	41	41	112	43

TABLE (9 - 2)

RESULTS OF TESTS ON LONDON CLAY

AFTER KUMAPLEY, (1969)

Test No	Consolidation Pressures σ_3 lb/sq inch	u lb/sq inch	Value of σ_3 during compression test lb/sq inch	Undrained strength c_u lb/sq inch	c_u/p
1	1000	500	1000	97.6	0.195
2	1000	500	900	96.4	0.193
3	1000	500	800	96.5	0.193
4	1000	500	700	96.8	0.194
5	1000	500	600	95.3	0.191
6	1000	500	500	95.3	0.191

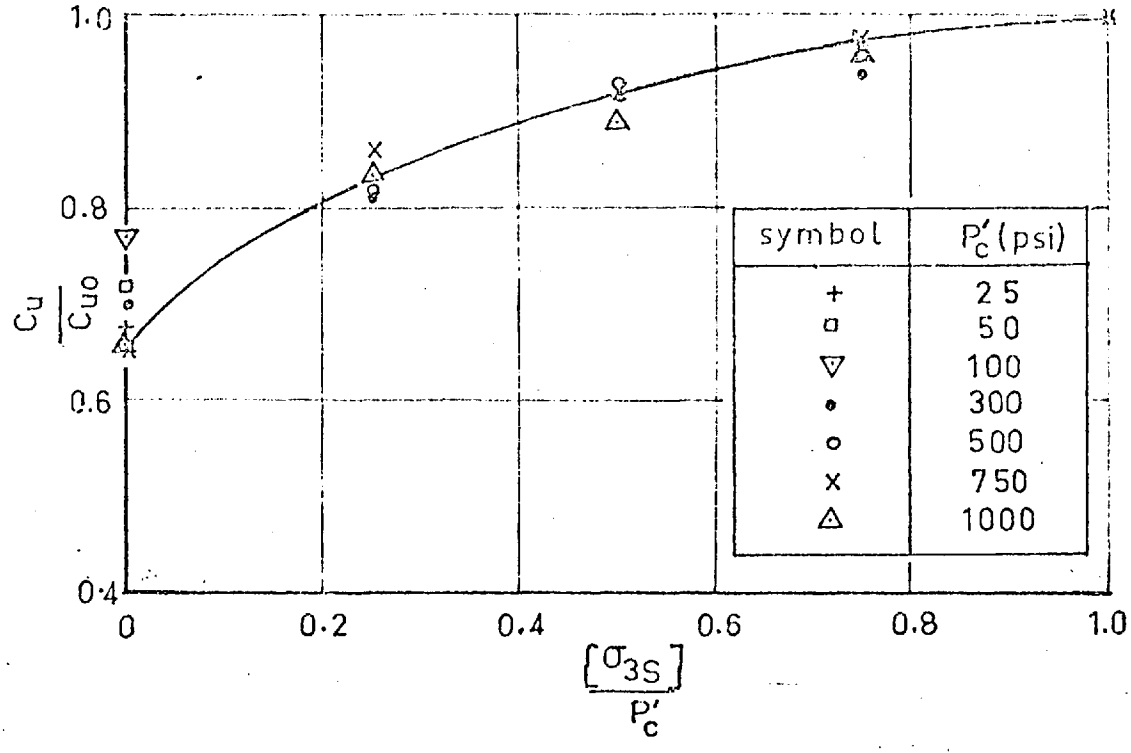

(a) Undrained Tests on Remoulded London Clay Batch 1

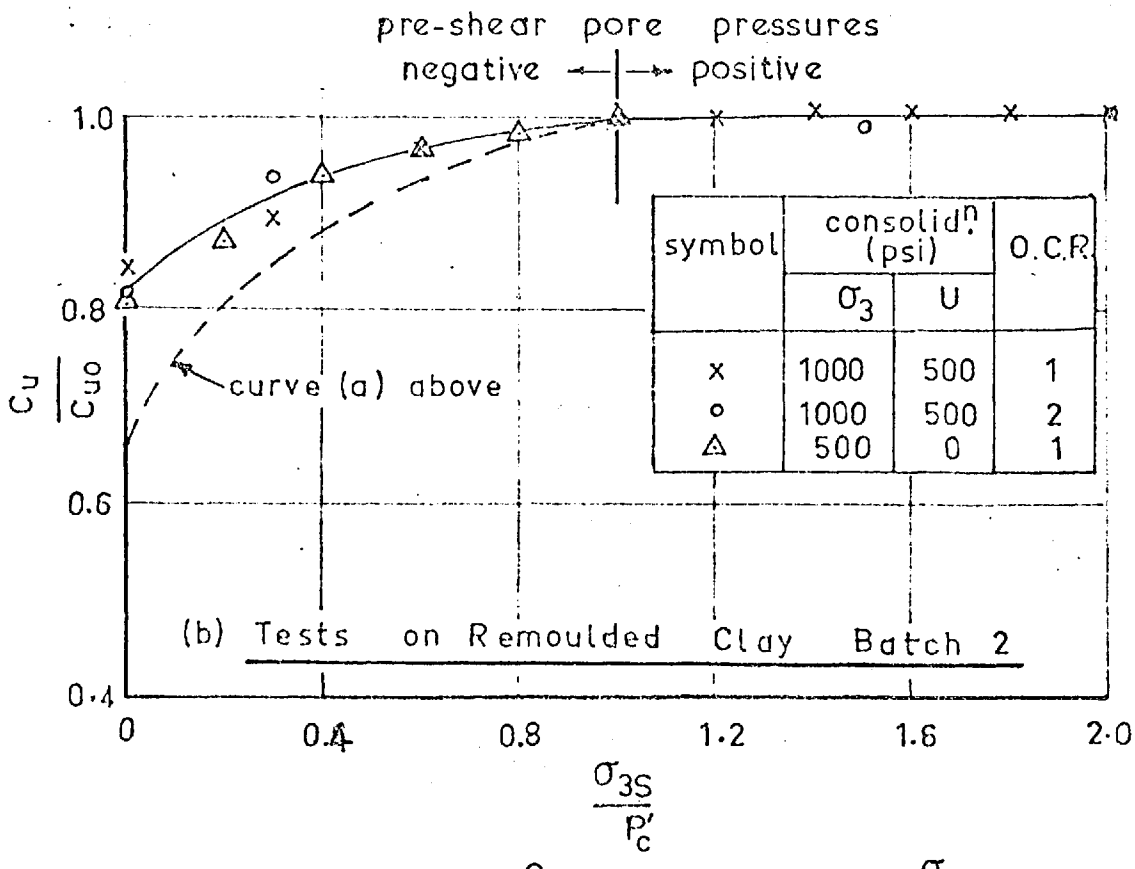

(b) Tests on Remoulded Clay Batch 2

(b) GRAPHS OF $\frac{C_u}{C_{uo}}$ AGAINST $\frac{\sigma_{3S}}{P'_c}$.

(after Kumapley 1969)

FIG 9-1

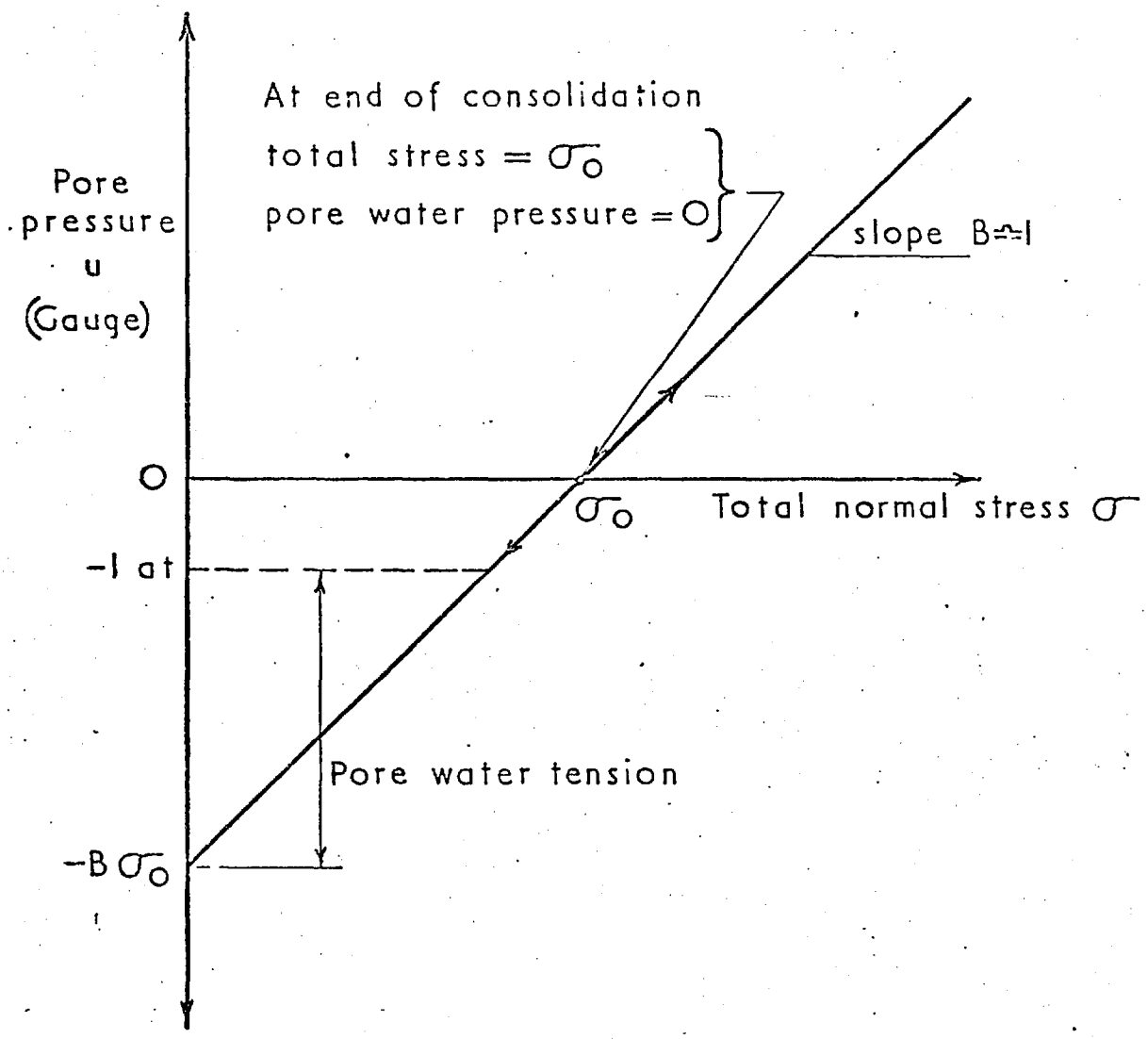

RELATIONSHIP BETWEEN PORE WATER PRESSURE & TOTAL NORMAL STRESS FOR AN UNDRAINED CHANGE IN STRESS AFTER CONSOLIDATION WITH THE TOTAL STRESS = σ_o & THE PORE WATER FREE TO DRAIN TO ATMOSPHERE. FULL SATURATION ASSUMED.

FIG 9-2

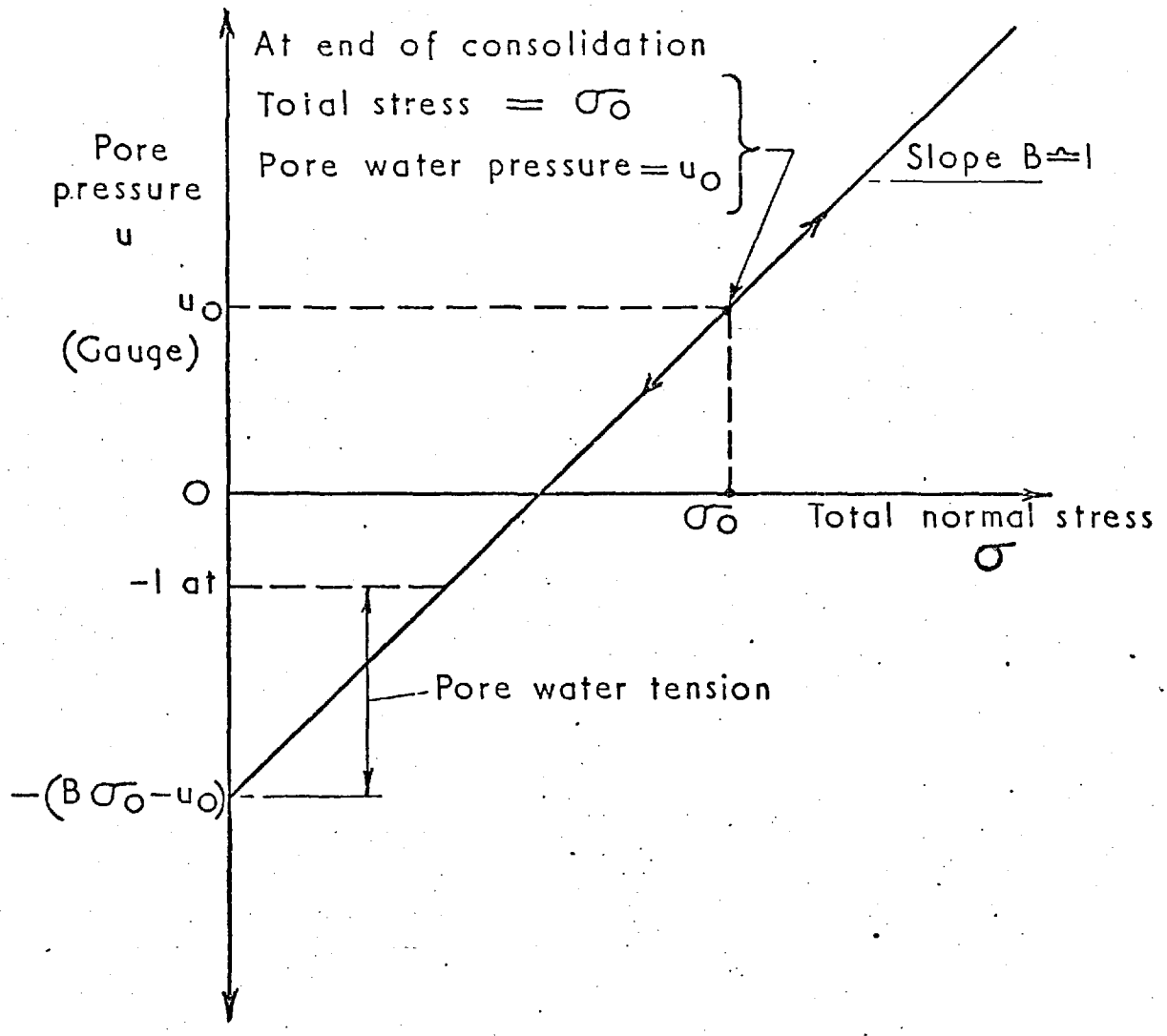

RELATIONSHIP BETWEEN PORE WATER PRESSURE & TOTAL NORMAL STRESS FOR AN UNDRAINED CHANGE IN STRESS AFTER CONSOLIDATION WITH THE TOTAL STRESS = σ_o & THE PORE PRESSURE = u_o
FULL SATURATION ASSUMED

FIG 9 - 3

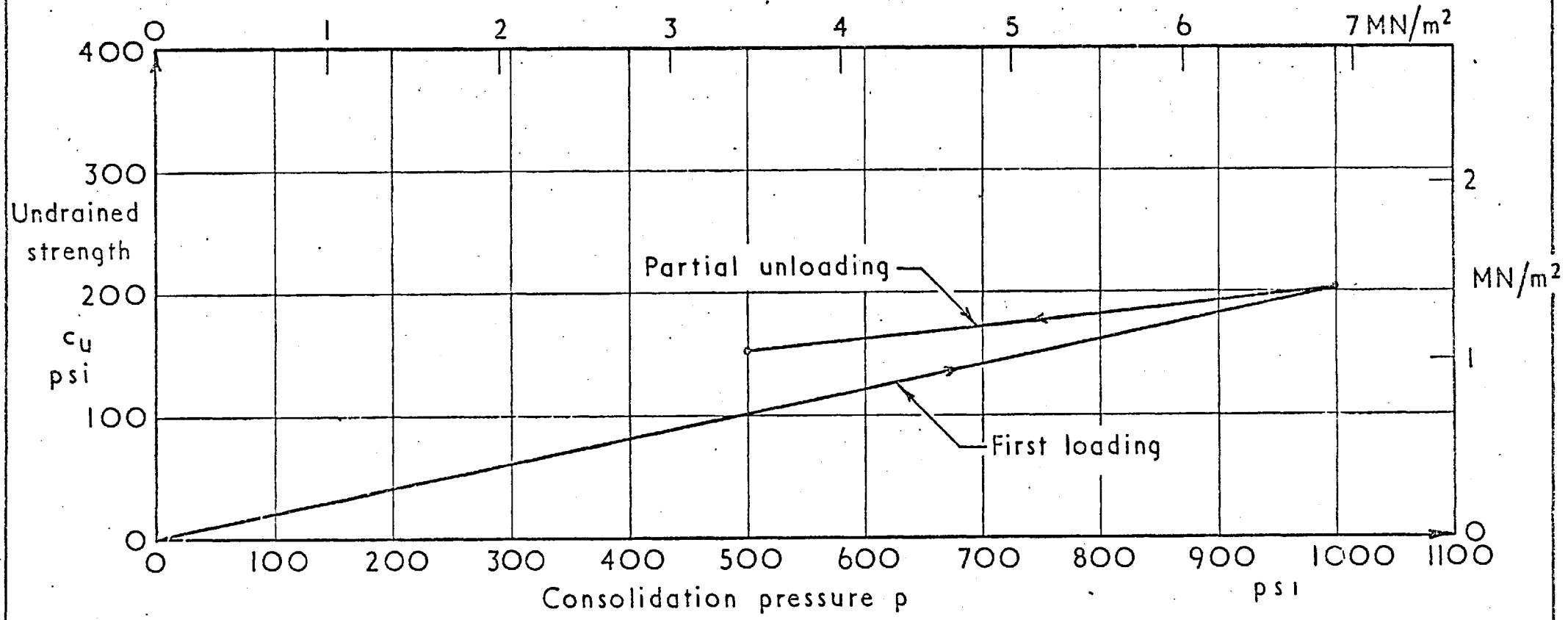

FIG 9-4

THE RELATIONSHIP BETWEEN UNDRAINED STRENGTH c_u & CONSOLIDATION PRESSURE p ON FIRST LOADING & ON PARTIAL UNLOADING. DATA FROM TESTS ON LONDON CLAY.

4-14

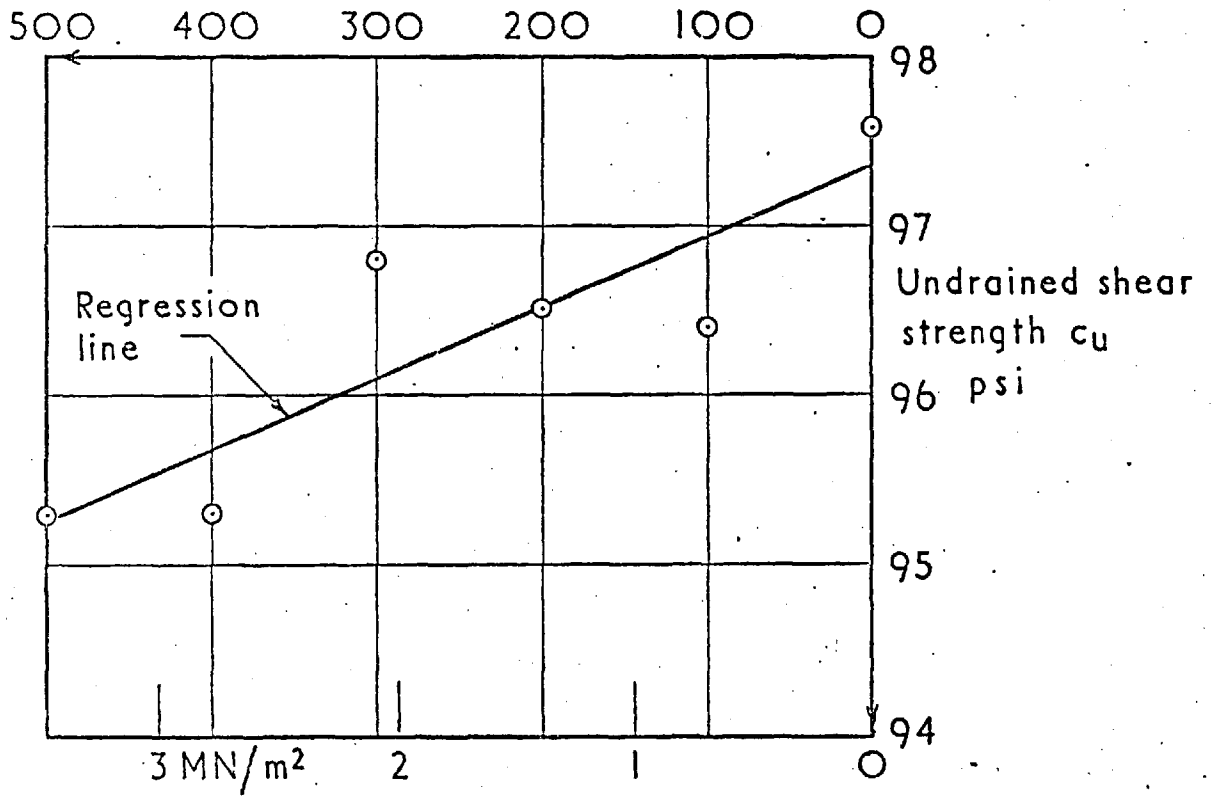

RELATIONSHIP BETWEEN UNDRAINED SHEAR STRENGTH & DECREASE IN CELL PRESSURE AFTER COMPLETION OF CONSOLIDATION STAGE: BLUE LONDON CLAY, CONSOLIDATED UNDER $\sigma_3 = 1000$ P.S.I., $u = 500$ psi

FIG 9 - 5

CHAPTER X

APPARATUS, MATERIAL PREPARATION AND TESTING TECHNIQUES

10.1 Apparatus

10.1.1 Description and Layout of the 9 in. dia. Oedometer

The apparatus consists of a stout frame, built of steel plate. The loading beam consists of a pair of channels bolted together and suspended longitudinally through the uprights of the frame. One end of the beam rests against a jack which is fixed to the top of the frame. This jack is operated with an oil pump fixed to the floor and can be locked in any position with a threaded brass sleeve. This arrangement permits the adjustment of the level of the beam at any stage of the loading. At the other end of the loading beam a counter-weight is hung to balance the weight of the beam and the hangers. The sample is loaded through a steel yoke which consists of two cross-pieces connected by two tie-bars. The dial gauge is held on the top of the loading yoke by a separate frame fixed to the mould containing the sample.

The mould is made of plated bronze and rests on a Dowty sealing ring fitted into the top of the base plate. The mould is fixed to the base with six studs. The inside diameter and height of the mould are 9 inches and 5.01 inches respectively, and it can be loaded up to 16 tons/sq. ft. A porous stone is fitted to the base of the mould and connected to the outside by a drainage lead.

The top cap of the mould consists of a circular bronze disc with a porous stone fixed to its bottom. The load is applied through a steel ball bearing placed in a recess on the upper side of the cap.

10.1.2 General Layout of the Triaxial Apparatus

Two triaxial cells have been used in this testing programme, one for tests with confining pressures up to 1000 psi and the other for confining pressures up to 10 000 psi. The general layout of the two cells is the same although they are different in detail.

The 1000 psi triaxial cell rests in a 6 ton frame; the arrangement being similar to that discussed in Chapter 4 for the rockfill tests. Pressure was supplied from a hydraulic pump by a lead through the base of the cell. The pedestal for the sample was connected to two drainage paths, which will be described in detail in a later section. During the consolidation stage the two drainage leads are connected to a glass burette for volume change measurements. For the purpose of drying the base of the sample, one lead is connected to a steel bottle containing dry oxygen free nitrogen under 3000 psi pressure, and the other lead is connected to a vacuum system. The pressure from the nitrogen bottle is monitored by a distributor with two gauges, one for controlling the pressure coming out of the bottle and the other to indicate the pressure inside the bottle. Thus the pressure and the time required for blowing the bottom of the sample could be controlled. There is a 'Hoke' valve between the sample base and the nitrogen bottle.

The vacuum system consists of an electrical vacuum pump capable of creating a suction of 12 psi, a glass desiccator and a mercury manometer. The suction is applied to the base of the sample by a polythene tube, with an in-line a hoke valve to turn the suction on and off. The mercury manometer is connected to the glass desiccator and the suction could be read at any time. The arrangement of the nitrogen supply and the suction, was the same for both the 1000 psi and the 10 000 psi triaxial cells. The general layout of the 1000 psi triaxial cell is shown in Plate (10-1).

The 10 000 triaxial cell rests on a Duff Norton screw jack of 100 tons capacity. The jack is designed to push or pull and bronze bushes are provided to take any eccentric loads which may be applied. The drive mechanism consists of main drive motor, Kopp variator, reduction gearbox and worm gear reduction. Between the worm gear box and the 'Jacuator' is an Oldhams coupling, which can take up any small misalignment of the shafts and can be readily disconnected prior to operating the rapid return motor.

The loading frame is of 100 tons capacity and consists of 2 tie-bars of 4 in. dia. and 3/8 in. square thread. The loading frame stands on a 1 in. thick mild steel plate which is anchored to the concrete slab with four internal expanding Rawl bolts.

A moving crosshead is mounted on the tie-bars. This crosshead is rectangular in section and is of mild steel, 12 in. wide and 9 in. thick and is powered by a geared motor with an output speed of 30 r.p.m., and can be adjusted to any desired level.

These are the main parts of the apparatus, but there are other fittings and accessories which are necessary for testing. The general layout of the 10 000 psi triaxial cell is shown in Plate (10-2).

In fact this loading frame and jack were designed and built for 12 in. dia. triaxial cell for rockfill testing, but due to shortage of loading frames in the Soils laboratory, it was used in this programme. A detailed description and diagrams are presented by Tombs (1969).

10.1.3 Description of the 1000 psi Triaxial Cell

The 1000 psi triaxial stainless steel cell for this testing programme is the same cell used for testing rockfill material and it was described in detail in Section 4.1. A few modifications were made to suit the present testing requirements. Figure (10-1) shows diagrammatically the details of the cell with the modified pedestal of the sample. The new modified pedestal was designed to seat a $\frac{3}{4}$ in. dia. sample and will be described in detail in Section 10.1.5.

The axial loads were measured by a proving ring which rests on a $\frac{1}{2}$ in. dia. ball bearing seated on the upper end of the stainless steel ram. Different proving rings were used to suit the maximum confining pressure applied to the samples. The calibration of the proving rings is shown in Appendix A.

10.1.4 Description of the 10 000 psi Triaxial Cell

This cell is another alternative of a previous 10 000 psi stainless steel triaxial cell described by Bishop, Webb and Skinner (1965). The new 10 000 psi triaxial cell basically consists of three parts, base, cylindrical cell and top cap, Figure (10-2). Each part is fixed to the other by a split steel ring of three segments enclosed in a mild steel ring 1/2 inches thick and $1\frac{1}{2}$ in. wide. No screws or bolts are used to tighten the parts. Rubber O-rings are used to seal the moving parts against leakage. All the parts are made of EN25 high tensile steel except the ram, which is EN26 steel, and other parts made of stainless steel. The parts made of high tensile steel were phosphate processed to make them withstand rust and corrosion. Plate (10-3) shows the general feature of this high pressure triaxial cell seated on the jack ready for testing.

The base of the cell is a 5.8 in. dia. solid cylinder with steps machined in it to enable it to fit onto the cylindrical cell. There are 12 outlets through the base for drainage leads, strain gauge wires and other probes. In the present testing programme three outlets were used; one for sample drainage and the other two for pressure supply. The remaining nine outlets were blocked by 0.365 in. dia. stainless steel nipples. The pedestal of the sample is screwed to the base and a rubber O-ring is used to seal it against leakage. Details of the pedestal will be described in a later section.

The cylindrical cell is 4 inches inside diameter, 0.9 in. thick and 16 in. high, and has two collars at the ends for placing the split rings. A steel handle is fitted around the upper neck for lifting the cell.

The top cap is a 5.8 in. diameter solid cylinder with a collar at the bottom and a 2 in. dia. hole for passing the ram through.

A 4 in. dia. stainless steel annular plug is fitted around the ram at the bottom and is used to plug in the cell. An outlet in the top cap is provided for air release as in the standard triaxial cells.

The ram is a EN26 high tensile steel bar 2 in. dia. and 10 in. long with a hole through it for the load cell wires. A brass extension $1\frac{1}{2}$ in. dia. and $2\frac{3}{4}$ in. long is fitted to the bottom end to which an electrical resistance load cell is screwed.

The axial load was measured by a 6000 lb. electrical resistance load transducer which will be called the "load cell" in the following description and discussion.

There are two interesting features incorporated in the 10 000 psi triaxial cell; these are:

1) The hydraulically balanced loading ram

Fig. (10-3) shows details of the head of the triaxial cell with hydraulically balanced loading ram. The central section of the loading ram is enlarged to form a piston having a diameter 2 times that of the ram, sliding with an appropriate oil seal in a cylinder formed in the head of the triaxial cell. Oil at pressure communicates through passages drilled in the ram with the annular upper surface of the piston. The cylinder below the piston is bled to atmospheric pressure.

If σ_3 is the fluid pressure in the cell, and d the diameter of the ram, then the upthrust on the ram due to the cell pressure is $(\pi d^2/4) \times (\sigma_3)$. The downthrust on the piston is $\pi/4 \left[(\sqrt{2} \cdot d)^2 - d^2 \right] \sigma_3$ and thus also equals $(\pi d^2/4) \times (\sigma_3)$. However high the cell pressure, the axial load applied to the ram is equal only to the compression strength of the sample together with the ram friction.

Furthermore, there is no change in the total volume of oil in the triaxial cell and loading head as the ram enters the cell. Thus the use of a high strain rate does not lead to a build-up of pressure

in the cell due to hydraulic resistance in the small bore pressure tubing or to the characteristics of the pressure control system. It should be noted here that the triaxial cell was filled with Dynobear L oil supplied by Shell Ltd. For testing in mineral oil a special membrane had to be manufactured to protect the original natural rubber membrane enclosing the sample. This will be discussed in a later section.

2) The internal electrical resistance load transducer

The internal load transducer is the standard Imperial College load cell which has been designed by Dr. A.E. Skinner. The load transducer consists of three triangular cantilevers of uniform thickness radiating from a common boss and bearing on the edge of a groove in the cylindrical loading cap, Fig. (10-4)†. As the bending moment and moment of resistance both increase linearly from the apex of each triangular cantilever the surface strains are almost uniform, and the calibration is therefore insensitive to the location of the electrical resistance strain gauges.

The cylindrical loading cap is filled with oil and sealed with a flexible nitrile rubber cover. Therefore any change in cell pressure has no significant influence on the zero or on the calibration.

Twelve strain gauges* type (EA-06 - 125 MG - 120) are mounted on the cantilevers, two in each of the three cantilevers on both the top and bottom surfaces of the element. The strain gauges are connected electrically to act as a full bridge configuration. Therefore the strain gauges give complete insensitivity to eccentricity of loading and to the horizontal component of load.

The maximum capacity of the load cell is 6000 lb. and showed a good performance throughout the testing programme. It was calibrated before and after each test and a typical calibration curve is shown in Appendix A.

* The strain gauges were made by "Micro-Measurements, Romulus, Michigan".
† Fig (10–4) and (4–3) are identical; refer to Fig (4 – 3).

10.1.5 The Modified Triaxial Cell Base

The samples tested were 0.75 in. in diameter and 1.5 in. in height and were allowed to consolidate by drainage through the base. In the standard triaxial cell (Bishop and Henkel, 1962) the sample stands on a porous ceramic disc, the lower side of which communicates through passages drilled in the pedestal to the valves controlling drainage. Undrained tests on saturated samples can be carried out satisfactorily with this system provided the cell pressure is maintained at a high enough value to ensure that the pore pressure in the sample remains positive (or at least does not drop below −12 psi). At lower pressures, and in all tests at the stage when the cell pressure is dropped to zero to remove the sample for water content determination, the water in the drainage passages will cavitate and the sample will start to suck water from the porous ceramic disc.

This effect leads to an error in the final water content determination in all consolidated undrained tests, the magnitude of which depends on the dimensions of the sample, the coefficient of swelling of the clay and the time taken to strip down the triaxial cell. This influence also leads to an error, which is of more importance in the present investigation, in the undrained strength of all samples in which significant pore water tensions are created by reducing the cell pressure. Even the use of a very short duration test, together with the use of high air entry ceramic discs and a reduction in the volume of the passages between the disc and the valves, could not bring the magnitude of this influence within acceptable limits.

Therefore the triaxial cell base was modified, so that, when required, all free water could be removed from below the base of the sample by blowing dry, oxygen free, nitrogen through the drainage passages*. Schematic details of the 1000 psi triaxial cell base are

* A similar method was used by Westman (1932) in studying the influence of mechanical pressure on the moisture content of some ceramic clays. He used two porous pistons within a rigid cylinder, and removed the water from the pistons with compressed air.

shown in Figure (10-5). The porous ceramic disc is replaced by a disc of filter paper resting on a disc of fine wire gauze cut from a sieve No. 200, which is recessed into the top of the pedestal so that the strands of the gauze do not puncture the rubber membrane enclosing the sample. The depth of the recess is 1/16 in. and the outside diameter of the pedestal is 0.75 in. The general layout of the connections to the triaxial base is illustrated in Figure (10-6).

Drainage is through two groups of small diameter holes (1.6 mm dia. in the intermediate pressure range and 0.8 mm dia. in the high pressure range). One group of holes is in the stainless steel collar forming the outer annulus of the pedestal and connects with the drainage passage A on one side of the cell base, Figure (10-6). The other group of holes is in the stainless steel disc forming the centre of the pedestal and connects with the drainage passage B leading to the other side of the cell base. The stainless steel disc. is 0.375 in. dia. and 0.187 in. thick seated in a recess in the centre of the pedestal.

It is seen that nitrogen could be circulated from valve 1, through the holes in the collar then through the holes in the centre disc after passing under the bottom of the sample and finally through valve 3 to the desiccator. During the nitrogen circulation, valves 2 and 4 are closed. The procedure of blowing out the water from the drainage passages will be described in a later section. This arrangement has been adopted for both the 1000 psi and the 10 000 psi triaxial cells with minor differences in the type and size of the outside connections.

10.1.6 Cell Pressures Supply

Cell pressures up to 150 psi were supplied by a self-compensating mercury control system and pressures above that level were given by a hydraulic pump. The mercury control system is described in detail by Bishop and Henkel (1962).

The high pressure unit consists of an electric motor operating a hydraulic pump which is fitted inside an oil tank. The pump generates the pressure and supplies it to the cell through a system of steel tubes,

the pressure being controlled by a spring loaded Amsler bleed valve. This unit has been used to supply a 9000 psi cell pressure without any significant fluctuation such as happens with other hydraulic pumps. Oil used in this hydraulic constant pressure unit is Dynobear L oil supplied by Shell Ltd. and it is the same oil used in filling the high pressure triaxial cell.

10.2.7 The Nitryle Rubber Membranes

In tests at confining pressures in excess of 1000 psi, the hydraulically balanced ram cell was used. The cell fluid used in this cell was Dynobear oil grade L. For these tests in the 10 000 psi triaxial cell, two membranes were used, one natural rubber and the other a nitryle rubber for protecting the first one from the effects of the oil in the cell.

The procedure of manufacturing nitryle rubber membranes was described in Section 4.3 and will not be repeated here. The only difference between these membranes and those which were used for rockfill testing is the size.

The rubber membranes used here are 0.75 in. dia. and 5 in. long. Mild steel bars 0.80 in. dia. and 7 in. long each were used as formers for the dipping process. The final pealed membranes were approximately 0.75 in. dia. and 0.010 in. thick. They provided excellent protection for the natural rubber membranes throughout the testing programme.

10.1.8 The Shrinkage Limit Apparatus

A standard electric shrinkage limit device was tried but unfortunately the accuracy of the volume change measurements was not adequate for the present research*. Another shrinkage apparatus has been brought from the Building Research Station at Garston working

---

* This device was manufactured originally for volume measurements on 1.5 in. dia. and 3 in. high samples.

on the same basis* as the first one and the results were also unsatisfactory. Therefore a direct measurement of the sample dimensions was used to determine the volume changes.

For the sample height measurement a special device was assembled. This consists of a dial gauge reading to 0.0001 in. fitted on a steel frame of inverted U-shape. The sample was placed on a glass plate and the height was measured at the centre of the sample each time.

For the diameter measurement a rotating steel semi-circular gauge and adjustable platform were used. The rotating semi-circular gauge stands on a stainless steel stand and rotates freely. A dial gauge reading to 0.0001 in. was fitted to one end of the semi-circle and a brass disc 3/8 in. dia. was screwed to the other end. The level of the platform is adjusted by a rotating handle to permit sample diameter measurements by the dial gauge and at the required levels.

10.2 Material Preparation

10.2.1 Slurry Preparation

London Clay: The slurry was thoroughly mixed by hand for several hours then left to cure overnight. Next day the slurry was transferred into a Hobart Mixer and mixed continuously for a further 12 hours. It was intended to pour the mixed material into the oedometer at a water content approximately equal to the liquid limit, therefore the initial water content during mixing had to be higher than the liquid limit . During preparation, care was taken to achieve a uniform water content throughout the slurry and to get rid of all the air bubbles and lumps. The water content of the slurry during placing in the oedometer was 77.5%. The classification tests will be presented in Chapter 11.

---

* Both apparatus work on the basis of using mercury as a part of an electric circuit. The change in the mercury level due to change in volume of a sample is measured by an attached micrometer to which an electric bulb is wired to indicate the mercury level.

Kaolin: Exactly the same procedure was followed in preparing the Kaolin paste except the water content was different. Here the final water content of the Kaolin paste during placing it in the oedometer was 71.5% which is 1.5% higher than the liquid limit.

10.2.2 Oedometer Consolidation Stage

The porous stones of the oedometer were saturated with water then covered with 9 in. dia. filter paper. After each slurry (London clay and Kaolin) had been prepared as described in the previous section, it was placed in the oedometer to the upper edge level. Care was taken not to leave any air bubbles inside the sample while levelling off the surface with steel edge. Samples for water content were taken at this stage to determine the initial water content of the sample. Then the top cap was placed on the sample and the dial gauges were fixed in place for height measurements.

The normal loads were added to give pressure levels of 10, 45, 85 and 160 psi. The sample was permitted to achieve full consolidation before adding the next increment. For London clay the normal pressure was reduced to 10 psi and the sample was allowed to swell at this normal pressure.

Then the drainage lead was disconnected and the extra water was removed from the top of the mould. The normal load was lifted and the mould was transferred to a triaxial apparatus frame for jacking the sample out of the mould. The same procedure was followed for the Kaolin except that the unloading was in two stages, first to 10 psi normal stress at which the sample was allowed to swell, and secondly to 3 psi normal stress at which the sample was removed from the oedometer as described for London clay.

The high consolidation pressures used (160 psi) were chosen to reduce the volume changes in the subsequent triaxial consolidation stage which might otherwise result in sample distortion when very high consolidation pressures were applied.

The material after jacking out of the mould was in the form of a disc of clay about 2.3 in. in thickness and of a strength and water content convenient for sample preparation.

10.2.3 Material Storage for Future Testing

The clay disc was then cut into 4 equal sectors and samples from the inside corners were taken for water content measurements. Then each quarter was painted twice with thin films of melted paraffin wax. A layer of aluminium foil was wrapped around each portion and again three coats of paraffin wax were applied to provide a good protection for the sample. After 2 years in the store the water content was measured and found to have decreased by only about 3%. The same procedure was followed for the Kaolin material. Then all the material pieces were stored in a steel box at a constant temperature until required for testing.

10.3 Testing Techniques

10.3.1 Sample Preparation and Set-up.

The triaxial samples were taken by a $\frac{3}{4}$ in. inside diameter thin walled brass tube having a sharp edge. The block sample was seated on the steel platform of a drill and the brass tube was pushed by the handle of the drill. This method ensured a vertical smooth sampling without disturbing the rest of the block sample. The exposed surface of the block sample was then waxed and stored as described earlier.

The sample inside the brass tube was then extruded with a wooden cylinder. It was then trimmed to approximately 1.5 in. in length and two samples from top and bottom of the remaining part were taken for water content determination. The sample dimensions were measured by a Vernier calliper to an accuracy of 0.0005 in.

The triaxial cell was prepared for operation and water was circulated through all the leads and the drainage passages to ensure the de-airing of the system. The gauze and the filter paper were

placed on top of the pedestal as described earlier. Then the sample was seated on the top of the pedestal and a brass top cap was placed on it. A latex rubber membrane 0.015 in. thick was fitted around it using a membrane stretcher. Four O-rings were used, two on the bottom and two on the upper end.

The sample which was tested in the 10 000 psi triaxial cell, was covered with nitryle rubber membrane to protect it from the oil in the cell.

Finally the cell was assembled ready for the consolidation stage. It should be noted here that the 1000 psi triaxial cell was filled with water while the 10 000 psi one was filled with Dynobear oil grade L, as described in a previous section.

10.3.2 Triaxial Consolidation of the Samples

As has been pointed out in Section 10.1.6, cell pressures in excess of 150 psi were supplied by constant pressure pumps. This made no difference for the consolidation or shearing of the samples other than at 3000 psi and 9000 psi, it took 1.5 minutes and 2 minutes respectively to increase the pressure to those levels.

In the Kaolin tests, pressures at which the samples were consolidated were: 125 psi, 250 psi, 500 psi and 1000 psi. The consolidation pressure was applied in one stage in these tests and the samples were allowed to consolidate at zero pore water pressure.

In the London clay tests, the consolidation pressures of 500 psi, 1000 psi and 3000 psi were applied in one stage and the samples were allowed to consolidate fully before the shearing stage. Confining pressures of 6000 psi and 9000 psi were applied in two stages. First a confining pressure of 1000 psi was applied and the sample was allowed to consolidate, then the cell pressure was increased to either 6000 psi or 9000 psi, the sample being allowed to fully consolidate. A one stage consolidation was tried (6000 psi or 9000 psi) but it was not successful.

10.3.3 Sample Base Drying

The modified triaxial cell base was described in Section 10.1.5 and the layout of the apparatus is shown in Figure (10-6). Water removal from the pedestal and sample base drying were carried out in two circumstances. One before releasing the cell pressure in the consolidated-unconfined compression tests and the other at the end of consolidated-undrained compression tests in the positive pore pressure range.

In the first case, after the completion of the consolidation stage, which is carried out with a saturated pedestal and zero back pressure, the water is blown out of the connections and burette used to measure volume change during consolidation by admitting dry oxygen free nitrogen through valve 1 with valves 2 and 4 open, Figure (10-6). With valves 2 and 4 closed, dry nitrogen is circulated through valve 1 to the outer annulus of the base of the sample and exhausted through the central disc to valve 3 which is opened to a reservoir connected to a vacuum pump. By admitting the nitrogen at a pressure of a little under one atmosphere at valve 1, the base of the sample is maintained at atmospheric pressure.

The time required to remove all free water from the connecting passages and from the gauze and filter paper was determined by trial and error, and proved to be about 6 minutes. It was found that this time is enough to clear all the drainage passages of water without damaging the sample. Water content measurements of the sample proved the successfulness of this method. It was considered preferable to risk slight drying of the base of the samples, which would not increase the measured compression strength due to the ratio of height to diameter of 2, rather than to leave free water at the base which would initiate base failure at a reduced strength.

After removing the water from connecting passages as explained above, valve 1 was first closed, followed by valve 3. At this stage the cell pressure was reduced to zero and the sample was ready for unconfined compression testing.

In the second case consolidated-undrained compression tests with positive pore pressure were carried out and accurate moisture content determinations were required. In order to obtain the correct water content values for the samples tested in the positive pore pressure range (for which undrained testing necessitated a saturated pedestal with valves 1, 2, 3 and 4 closed), an estimate of the final pore pressure was made by using equation (9.3.12) and an assumed value of A_f. The cell pressure was then dropped by an equal amount after failure, to bring the final pore pressure to zero (for B = 1). The system (sample base and the connecting passages) was then de-watered with dry nitrogen as explained in the first case before dropping the cell pressure to zero for the removal of the sample. The close agreement apparent in Table (11-2) between the water contents observed in the high pressure range on the unconfined samples (base de-watered before the compression test) and the confined samples (base de-watered after the compression test) indicates the success of this technique.

At the end of the testing the sample was taken out of the base and the shape of the failure was sketched and the water content was measured. To determine the water content the sample was generally cut into 5 horizontal slices, and the value of the bottom slice recorded but not included in the average.

10.3.4 Rate of Axial Strain and Total Strains

Both London clay and Kaolin samples were sheared at an axial strain rate of approximately 2.0% per minute which gave a deformation rate of 0.025 inches per minute. Thus the time required to complete the shearing of a sample was approximately 6 minutes. This rate of strain is high compared to the conventional undrained tests on London clay.*

* The standard rate for commercial tests without pore water pressure measurement is 1% per minute; 2% per minute is the maximum rate at which the results can still be recorded. Tests in which the pore water pressure is measured need to be run at slower speed.

It was intended to shear the samples at a very high rate of axial strain to overcome the water migration problem while at the same time the rate of axial strain being slow enough to permit reading the strain dial gauge and the load cell meter. The rate of 0.025 in. per minute was found reasonable for this purpose.

Originally it was intended to stop all the tests at the same axial strain but the variation in the failure strains prevented this. Therefore the axial strain at which the tests were stopped varied from 17.50% to 24% over a confining pressure range from 1000 psi to 9000 psi. However, at these axial strain levels, a clear picture of the failure plane was obtained and further distortion of the samples was avoided.

10.3.5 Shrinkage Limit Test Procedure

Two shrinkage limit tests were carried out on London clay, one on a sample taken from the block which had been consolidated in the oedometer and the other one on a sample consolidated in the high pressure triaxial apparatus at 9000 psi cell pressure.

The sample taken from the block was cut to approximately $1\frac{1}{2}$ in. length and weighed to an accuracy of 0.0001 gram. The sample height and diameter were measured by the devices described in Section 10.1.8. Three readings at different levels were taken for the diameter and the average was considered as the sample diameter. With regard to the height, only one reading was taken at the centre of the sample. The accuracy of dimension measurement was 0.00005 inches. Then the sample was dried in stages and at each stage the weight and dimensions were recorded. Finally the sample was dried in the oven to zero water content and the weight and dimensions were again recorded. The results were plotted in terms of water content versus the volume in c.c. per 100 grams of dry soil. Also variation of the height and diameter of the sample were plotted against the water content.

The second sample was consolidated in the high pressure triaxial cell under 9000 psi confining pressure in the same way used for the triaxial tests. After achieving full consolidation, the water was blown out of the base and the drainage passages in the way described earlier. Then all the drainage valves were closed and the cell pressure was reduced to zero. The sample was removed from the cell, weighed and its dimensions recorded. Then the shrinkage limit test continued as in the first one.

Two shrinkage limit tests were also carried out on two samples of Kaolin following the above procedure except that the consolidation pressure applied in the triaxial test was 1000 psi instead of 9000 psi; the results were plotted in the same way.

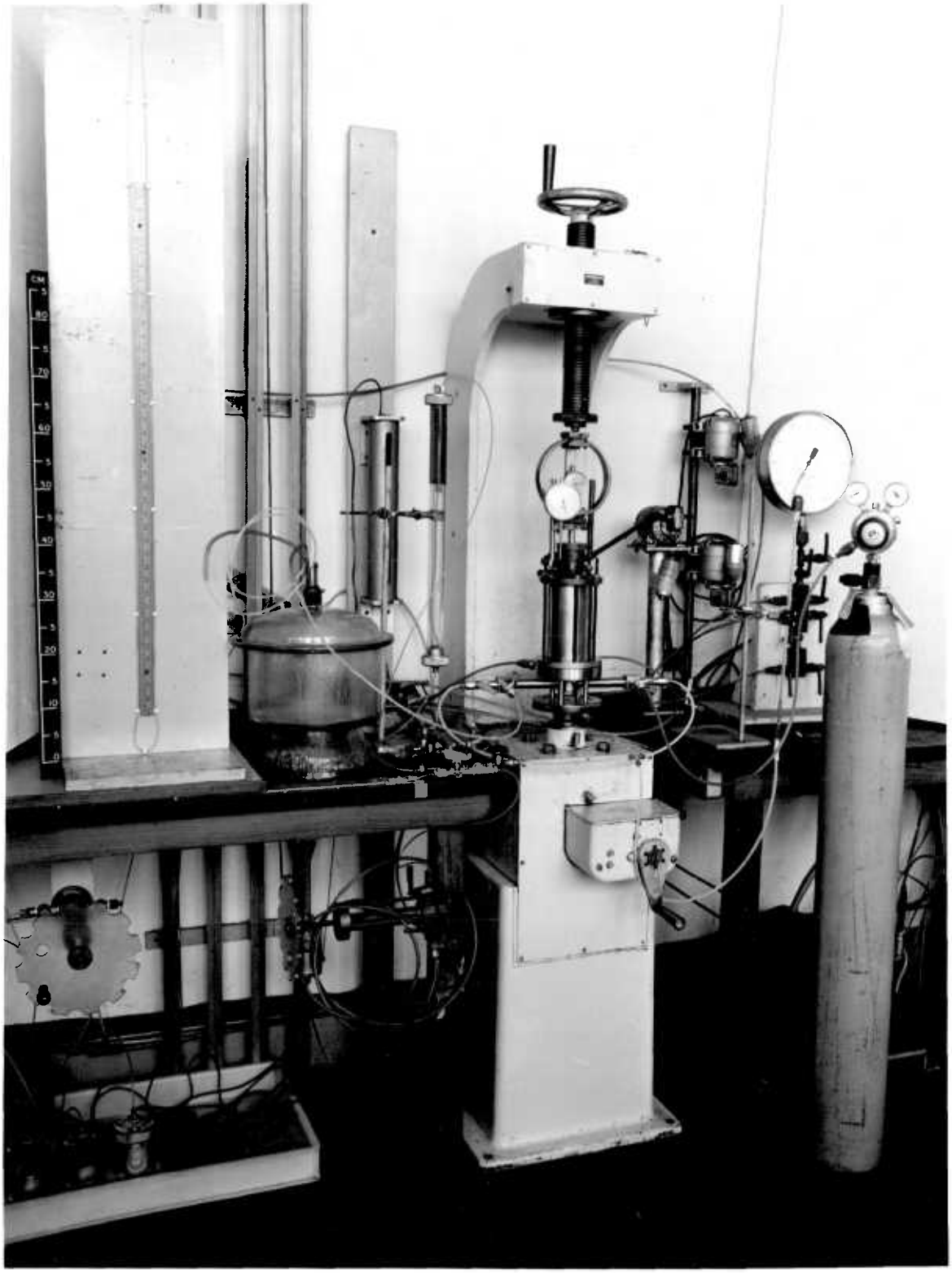

Plate (10-1) The General Layout of the 1000 psi Triaxial Cell.

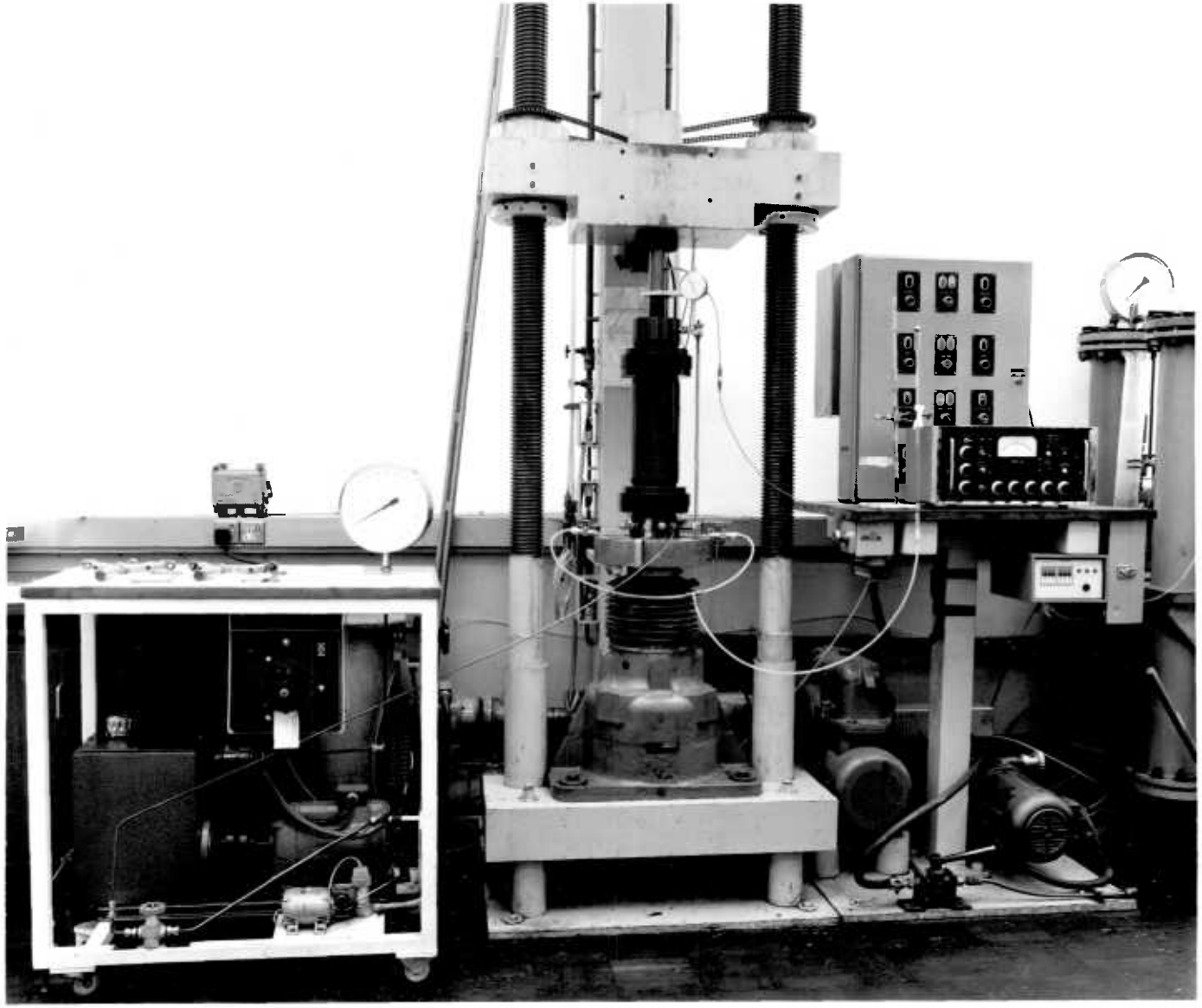

Plate (10-2) **The General Layout of the 10 000 psi Triaxial Cell.**

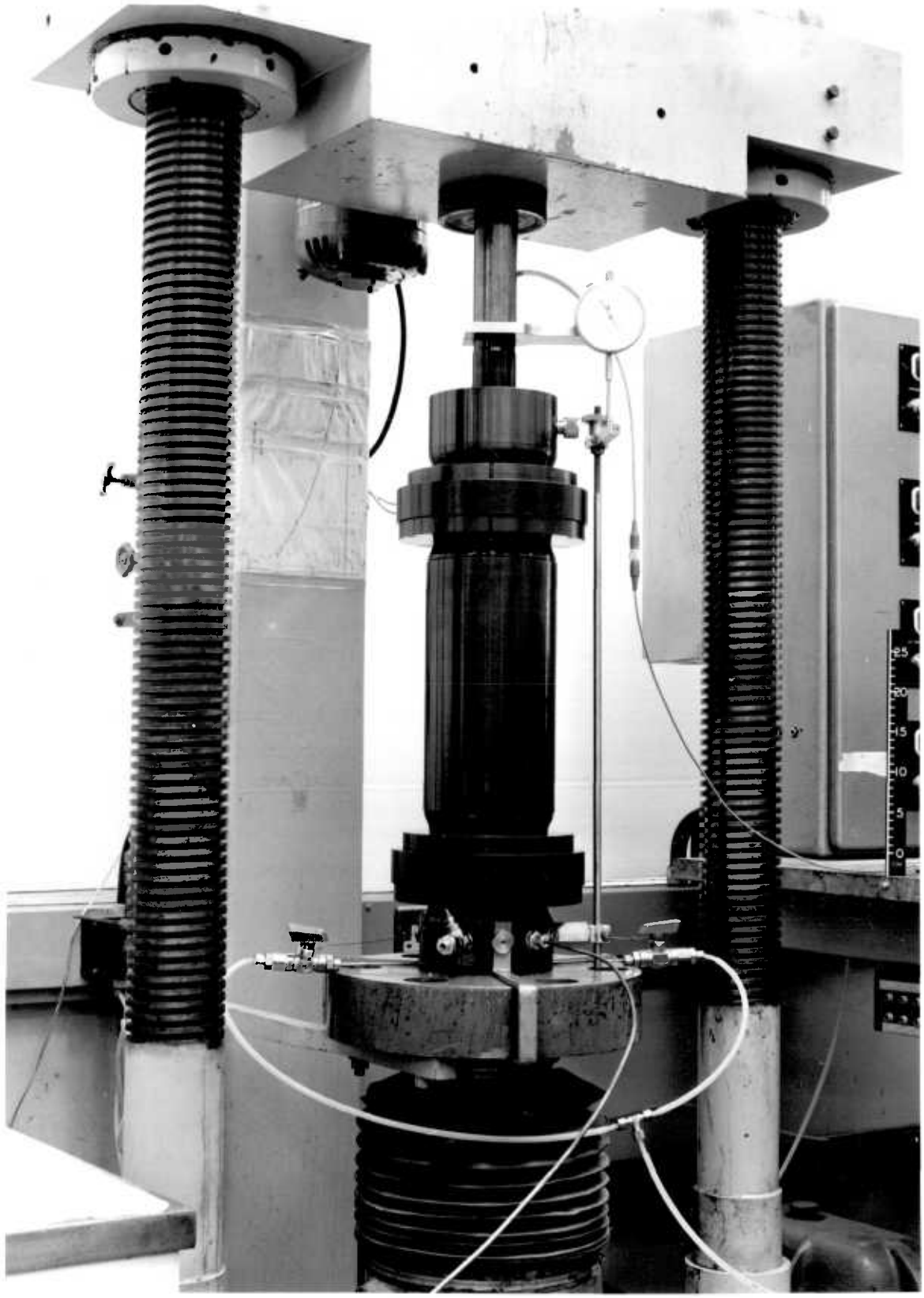

Plate (10-3) The 10 000 psi **Triaxial Cell.**

Sample Base

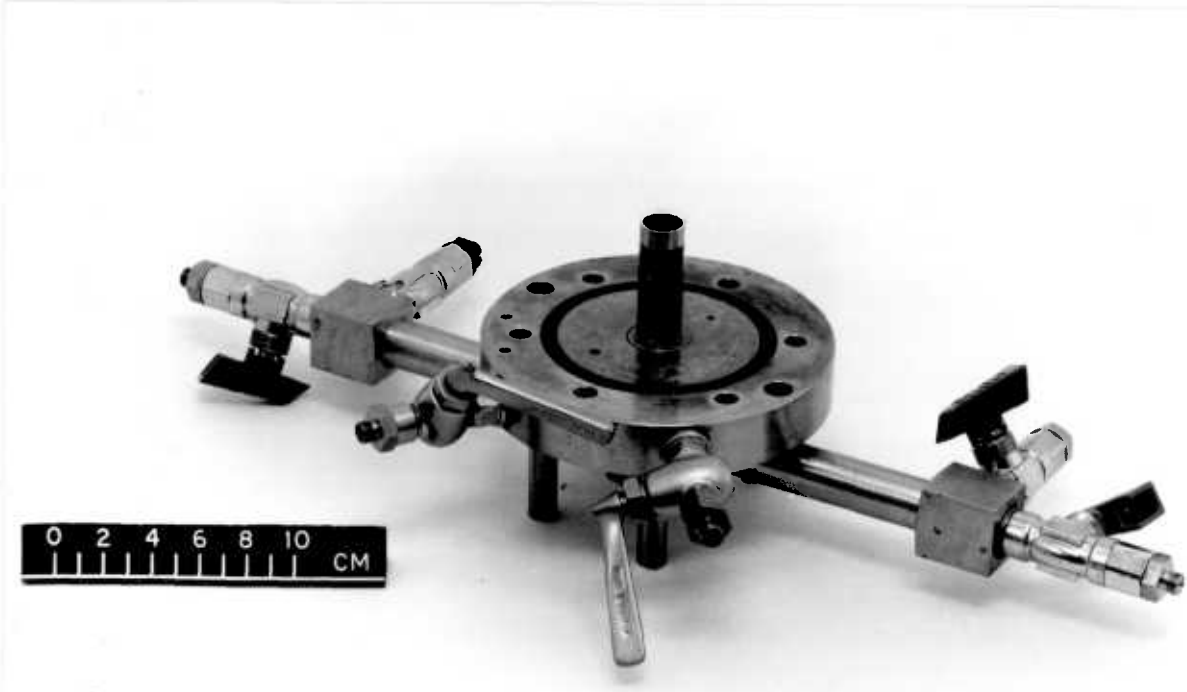

Plate (10-4): The Modified Base of the 1000 psi Triaxial Cell

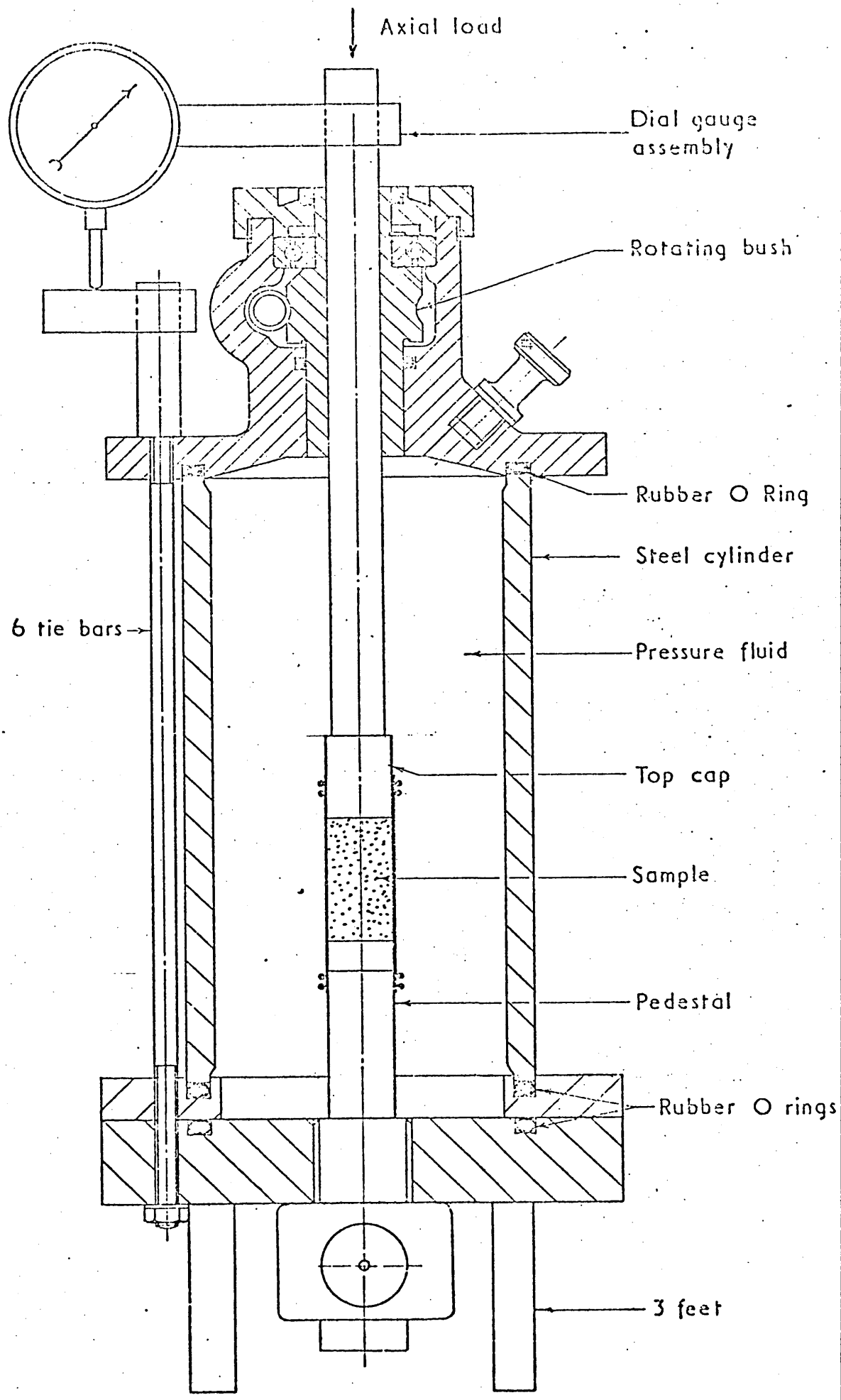

GENERAL ASSEMBLY OF HIGH PRESSURE CELL

FIG 10-1

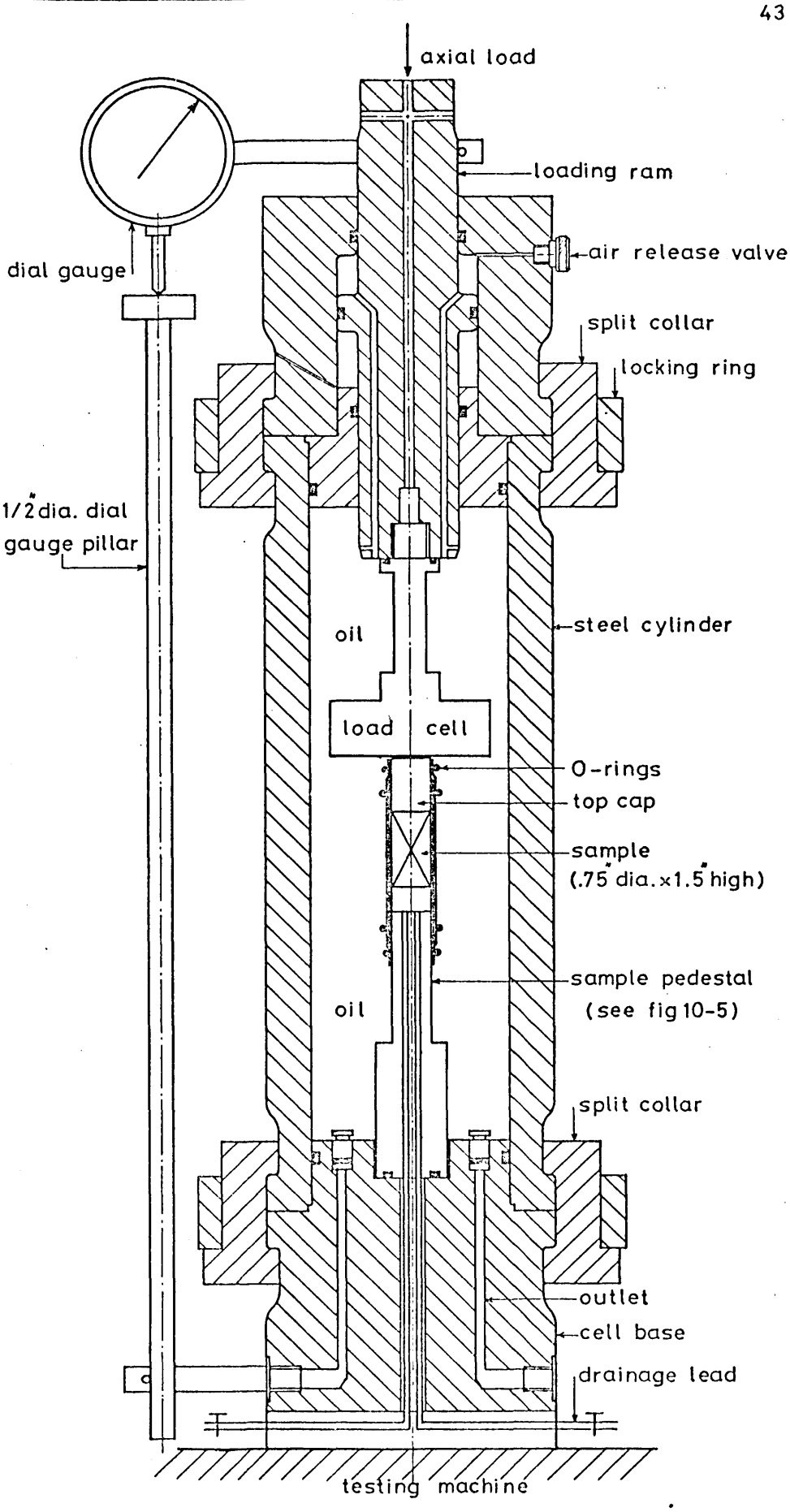

THE 10,000 P.S.I. TRIAXIAL CELL

Scale 1 1/2 0 1 2 3 4 IN.

FIG. 10-2

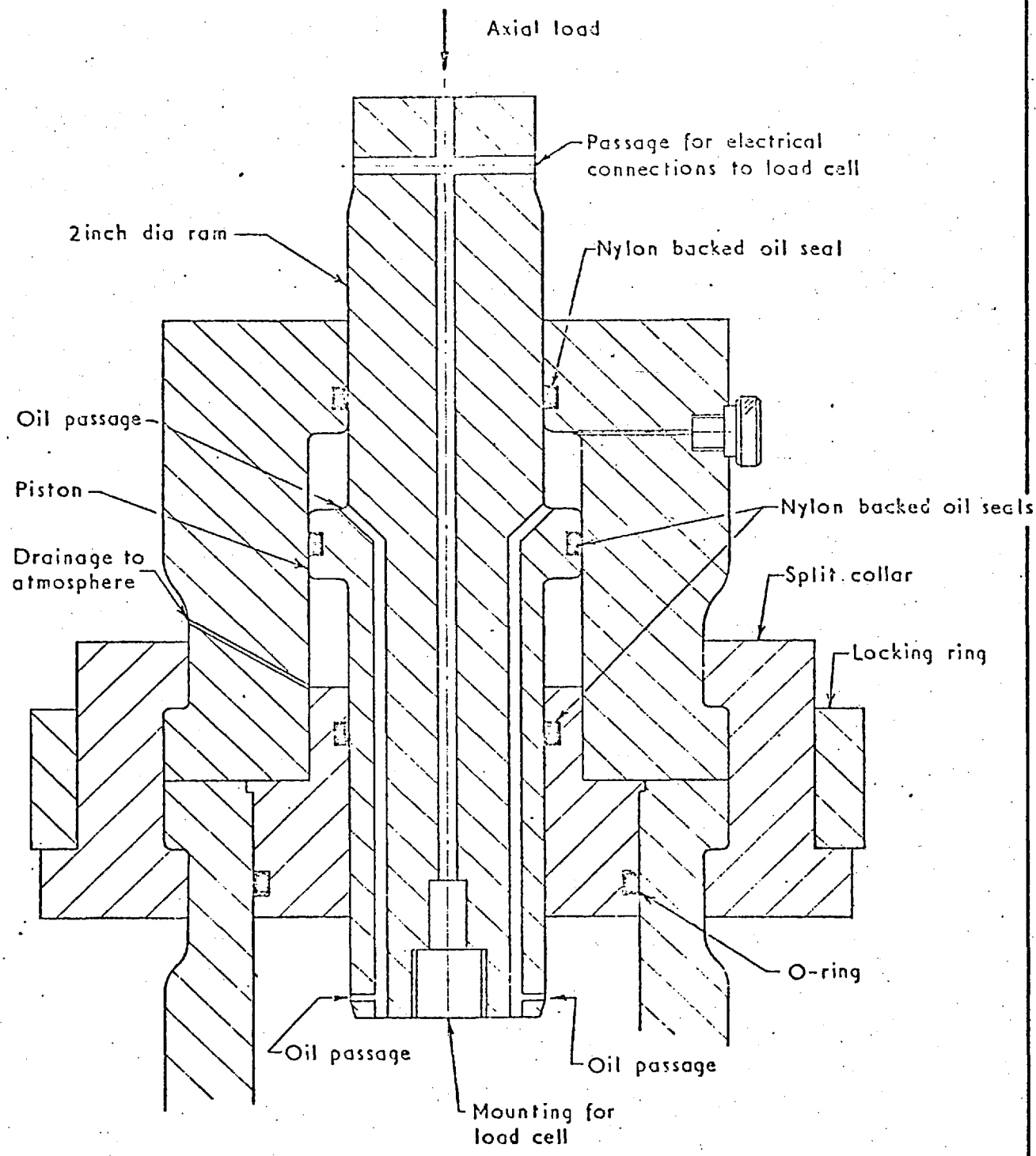

HEAD OF TRIAXIAL CELL WITH HYDRAULICALLY BALANCED RAM

FIG 10-3

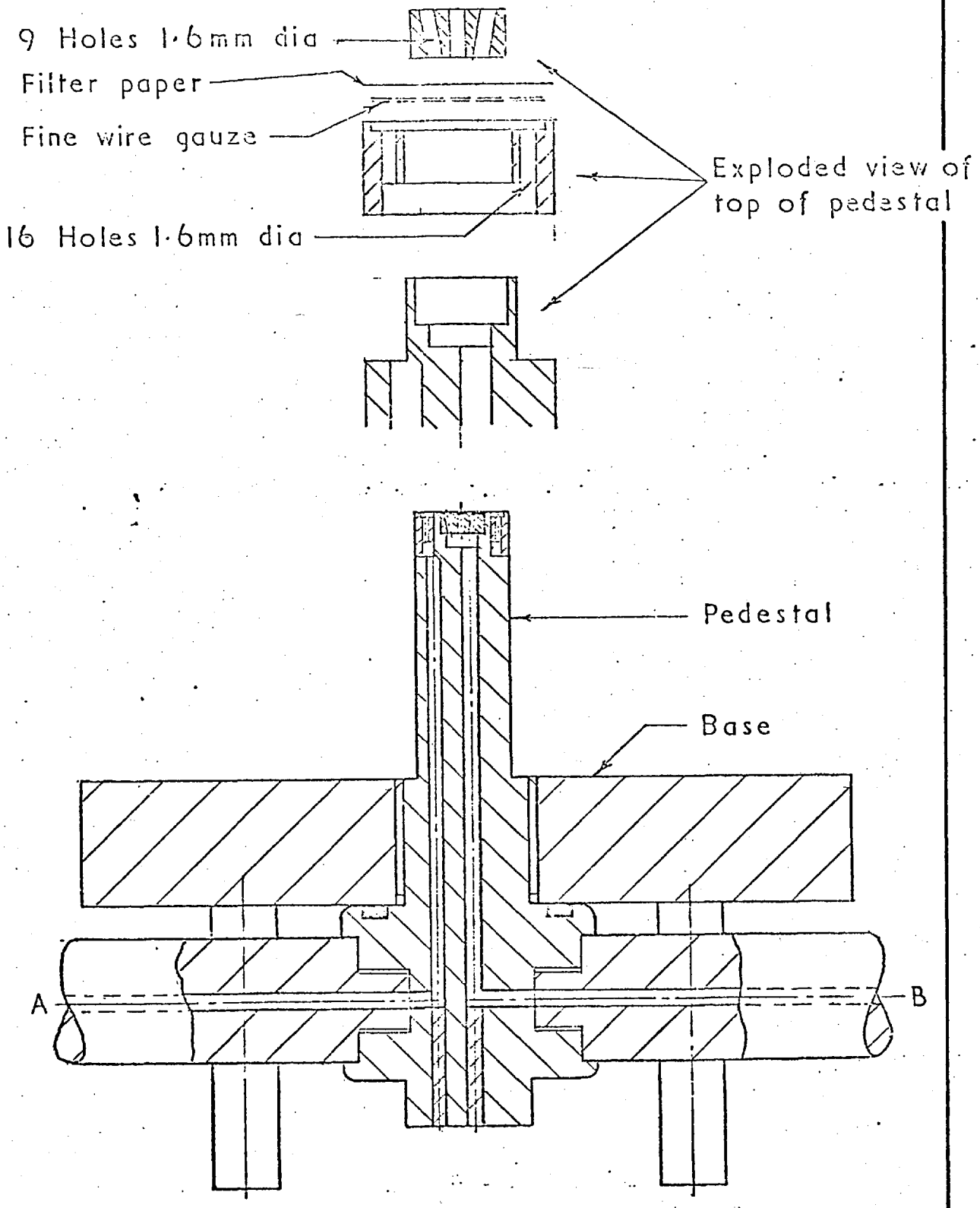

MODIFIED TRIAXIAL CELL BASE

FIG 10-5

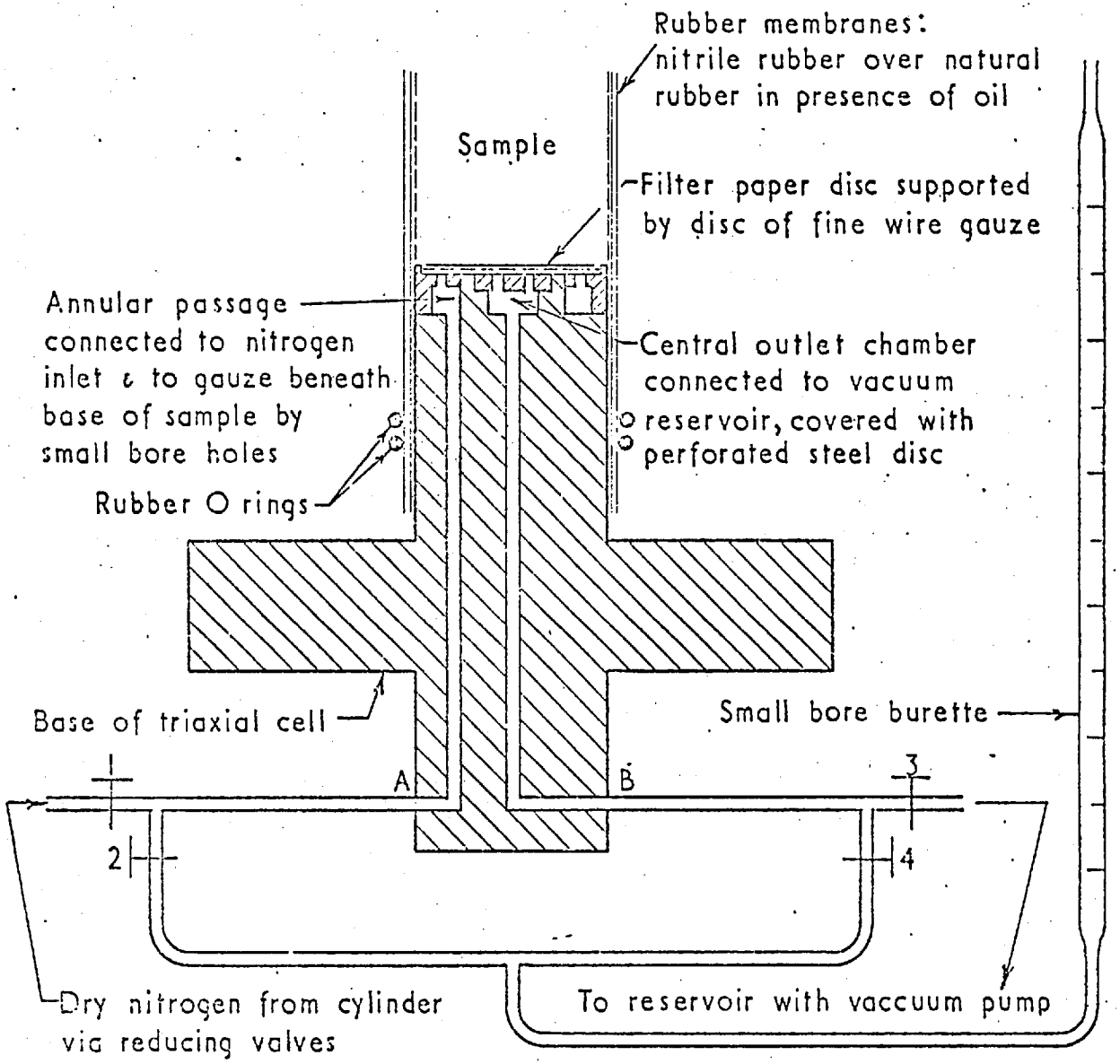

FIG 10-6

LAYOUT OF CONNECTIONS TO TRIAXIAL CELL BASE FOR TESTS WITH HIGH PORE WATER TENSIONS (Diagrammatic)

CHAPTER XI

MATERIALS TESTED AND TEST RESULTS

11.1 Materials Tested

The materials used in this experimental investigation were remoulded blue London clay and Kaolin. In this section a brief description of these materials will be given. Their preparation for testing was presented in Chapter 10.

The blue London clay was from a depth of about 20 feet in the borrow pit for Wraysbury Reservoir in Middlesex. The London clay was deposited under marine conditions in the Eocene period. Tests reported by Bishop, Webb and Lewin (1965) suggest a preconsolidation load in this area of 600 psi. The natural water content of the clay at this level was around 29%. The results of various classification tests on London clay used in this thesis are given in Table (11-1 a).

The Kaolin was a commercially prepared product mined in Cornwall and marked as English China Clay, Spestone powder. The results of various classification tests are given in Table (11-1 a). A slurry was prepared from this powder at a water content near to the liquid limit.

The initial water contents of the slurries from which the batches of the material were prepared are given in Table (11-1 b), together with the consolidation pressures applied in the 9 inches diameter oedometer. To reduce the pore water tensions and any consequent tendency towards partial saturation, the batches of London clay and the Kaolin were allowed to swell to relatively low effective stresses before storage*.

---

* The London clay and the Kaolin were allowed to swell to 10 psi and 3 psi respectively.

The high consolidation pressures used were chosen to reduce the volume changes in the subsequent triaxial consolidation stage which might otherwise result in sample distortion when very high consolidation pressures were used.

11.2 Oedometer Consolidation

Both the London clay and the Kaolin slurries were consolidated in a 9 in. diameter oedometer as described in Chapter 10. The relationship between the water content and the effective normal stress for both materials is shown in Figure (11-1). The maximum normal stress applied on each material was 160 psi then they were allowed to swell at normal stresses of 10 psi in the case of the London clay and 3 psi in the case of the Kaolin. It can be seen from this figure that the experimental points for London clay and Kaolin lay on parallel straight lines on both loading and unloading.

11.3 Testing Programme

Samples for this programme were cut and prepared as described in Chapter 10. All the samples are $\frac{3}{4}$ in. diameter and 1.5 in. high. The samples were consolidated isotropically with a range of cell pressures (1000 - 9000 psi for London clay and 125 - 1000 psi for the Kaolin) but with zero back pressure in all cases.

The samples were then tested either with the cell pressure equal to the consolidation pressure ($\sigma_3 = p$) or unconfined ($\sigma_3 = 0$), the pedestal being de-watered at the appropriate stage, as described earlier in Chapter 10. Most of the tests were repeated to make sure that no experimental errors were involved during the testing. The test results are given in Tables (11-2) and (11-4), and will be described separately in the following sections.

Another series of unconfined compression tests was carried out on samples of the London clay consolidated by slow shrinkage from the same initial water content as those consolidated by a confining pressure. A summary of the test results is given in Table (11-5).

Finally a series of shrinkage limit tests was carried out on samples of London clay and Kaolin. For the London clay a sample was consolidated at a cell pressure of 9000 psi then removed from the cell before testing. A series of dimension measurements was taken while the sample was left to dry in the air. A second sample was cut from the stored block and left to dry in the air. A series of volume change measurements was taken as the water content was reduced during drying.

Similar shrinkage limit tests were carried out on samples of Kaolin except that a confining pressure of 1000 psi was applied to the first sample instead of the 9000 psi which was applied to the London clay sample.

11.4 Results of Triaxial Tests

11.4.1 Tests on London Clay

Two preliminary tests on remoulded London clay (1B and 2B, Table 11-2) had indicated that the ratio c_u/p for unconfined samples did not differ significantly from that for confined samples for a consolidation pressure of 1000 psi, and that much higher consolidation pressures must therefore be used for this kind of investigation. The stress-strain curves for these tests are shown in Figure (11-2) together with a schematic diagram for the shape of the failure planes.

Subsequent tests were carried out on samples of London clay with a lower initial water content, in order to reduce the magnitude of the volume change and associated distortion, on subsequent consolidation in the triaxial cell.

The two most recognizable effects of high pore-water tensions on the strength and deformation characteristics of clay are the shape of the stress-strain curves and the failure mechanisms of the samples. These are illustrated very clearly by the series of stress-strain curves for progressively increasing consolidation pressure, Figures (11-2) to (11-10).

The stress-strain curves for samples consolidated with a cell pressure σ_o = 1000 psi and a pore water pressure u_o = 0 are illustrated in Figures (11-3), (11-4) and (11-5). It will be seen that the samples tested with the cell pressure maintained at 1000 psi (and thus with the pore pressure zero at the beginning of the test and positive at failure) show a rounded stress-strain curve with a relatively gradual reduction in stress after failure, Figures (11-3) and (11-5). In contrast the samples tested after reducing the cell pressure to zero (and thus inducing a negative pore pressure of approximately 1000 psi before the beginning of the undrained compression test) retained approximately the same peak value of strength but showed a rapid reduction in strength after failure amounting almost to brittle failure, Figure (11-4).

The fractured samples fell apart on removal from the enclosing rubber membrane in the case of all samples tested under high negative pore pressures, whereas those tested under positive pore pressures could not be separated by hand along the rupture plane which was visible on the surface of the sample. The inclination of the rupture planes for all these tests is marked on the above figures. The failure mechanisms are illustrated in Plate (11-1) by photographs of samples subjected to the highest consolidation pressure.

The corresponding curves for a consolidation pressure of 3000 psi show the same general trends in behaviour, Figures (11-6) and (11-7), although there is a small but significant reduction in peak strength accompanied by a marked increase in the brittleness of the samples tested under the condition of high negative pore pressure. Samples 14B and 16B, Figure (11-7), fell apart in 3 pieces which indicated the brittle mechanism of failure.

The stress-strain curves for a consolidation pressure of 6000 psi show a very substantial reduction in peak strength in the sample tested with a high induced negative pore pressure (B x 6000 psi), accompanied again by a very brittle type of failure, Figure (11-8). The unconfined sample (24B) fell into 2 pieces after removal from the enclosing rubber

membrane which is similar to that described for the 1000 psi consolidation pressure. Another notable feature is the sharpness of the stress-strain curve at peak for test (24B) compared to the previous tests.

The stress-strain curves for a consolidation pressure of 9000 psi (the maximum pressure at which the load cell could be used) show an even larger percentage reduction in compression strength (about 42%) and a very brittle failure, Figure (11-9). The fractured sample is illustrated in Plate (11-1). The sharpness of the stress-strain curves at peak for tests 21B and 22B is most marked and similar to that for test (24B) at the 6000 psi consolidation pressure range.

It has been pointed out in Chapter 10 that each sample after testing, was sliced into 5 horizontal pieces for water content determination and the base slice was recorded but not included in the average. In Figure (11-10) the distribution of the water content throughout the samples tested is plotted diagramatically. The uniform distribution of the water content can be seen in this figure and the influence of drying the base in some of the samples is clear*. However this influence did not affect the behaviour of the samples nor the interpretations which will be made later.

Another three special triaxial tests were carried out and the results are also shown in Table (11-2). A sample of London clay (12B) was consolidated at σ_3 = 1000 psi then allowed to swell at σ_3 = 500 psi, then sheared undrained with σ_3 = 0. The sample showed a rounded stress-strain curve, Figure (11-11), with a relatively rapid reduction in strength after 14% axial strain amounting to a brittle failure. It should be noted here that the sample is overconsolidated (OCR = 2) prior to shearing.

---

* For tests 24B and 25B the water content distribution is shown on the stress-strain plot, Figure (11-8).

The second sample of London clay (15B) was consolidated in stages to σ_3 = 1000 psi, then permitted to swell. Then it was reconsolidated to σ_3 = 1000 psi and u = 0, and finally it was sheared undrained with σ_3 = 1000 psi. The general shape of the stress-strain curve, Figure (11-12), is similar to those normally consolidated at σ_3 = 1000 psi then sheared undrained with σ_3 = 1000 psi, Figure (11-3), except here sample (15B) exhibited higher shear strength.

The third sample (20B) was consolidated at σ_3 = 1000 psi and u = 0, then it was left for 35 minutes under σ_3 = 0 before shearing undrained with σ_3 = 0. The stress-strain curve is shown in Figure (11-13) with a peak shear strength similar to those sheared straight away after reducing the cell pressure to zero.

The results of the previous tests are summarized on graphs relating undrained shear strength c_u and consolidation pressure p, Figure(11-14), undrained shear strength c_u and water content as tested w, Figure (11-15) and percentage loss in strength r against reduction in confining pressure, Figure (11-16). It is quite clear from all three sets of curves that a major change in behaviour is beginning at a reduction in cell pressure of about 3000 psi.

A theoretical relationship between the reduction in strength r, the reduction in confining pressure - $\Delta\sigma$ and the consolidation pressure $\sigma_o - u_o$ was obtained in Section 9.3.4, equation (9.3.19). In the present series of tests u_o = 0, and for the samples tested unconfined (i.e. σ_3 = 0) the reduction in confining pressure - $\Delta\sigma = \sigma_o$. Therefore equation (9.3.19) reduces to the expression:

$$r = m(1 - B) \qquad \ldots\ldots \qquad (11.3.1)$$

In the present series of tests a very wide range of confining pressures was used for both London clay and Kaolin. The relationship between the void ratio e calculated from the final water content and the logarithm of consolidation pressure p is shown in Figure (11-17). This relationship departs substantially from a straight line and the compressibility falls to a value less than that of water. Therefore no simple relationship

can be established between r and p, and the values of r should be calculated for each stress level, using the general expression for B (equation (9.3.3)) for the higher consolidation pressures.

In the calculation of B for unloading it is assumed that the ratio of the expansibility of the soil structure C_e to the compressibility C is equal to λ. In the lower stress range the value of λ is approximately 0.45 for London clay consolidated from a slurry and allowed to swell under an equal all-round pressure. At high consolidation pressure (3000 psi and more) this value is expected to rise.

The values of r for the four values of consolidation pressure used (1000 psi, 3000 psi, 6000 psi and 9000 psi) and for two assumptions about λ are given in Table (11-3) and are plotted in Figure (11-16). It will be seen that the theoretical relationships between r and the reduction in confining pressure for samples remaining fully saturated are smooth curves which do not depart to any marked extent from straight lines except at the highest cell pressures (9000 psi). The departure of the observed line, Figure (11-16), relating loss in strength to reduction in total stress from the shape of the theoretical lines at a pressure of a little below 3000 psi suggests that a breakdown in the condition of full saturation occurs at this point*. It can be seen from Table (11-3) that on the assumption of full saturation the theoretical value of r for a reduction in total stress of 1000 psi lies in the range of 1.22 to 1.40%. The observed value lies in the range of 0.5% to 2.0%,

---

* If a departure from unity of the value of k in equation (9.3.8) had been assumed to cause the loss of strength, then there would not be a significant change in the slope of curves II and III. Using equation (9.3.7) gives us:

$$1 - k_s = a \frac{\tan \psi}{\tan \phi'}$$

where a is the contact area between the particles per unit area. It had been indicated earlier that this area is almost directly proportional to consolidation pressure (Skempton, 1960), therefore the component of r involving $1 - k_s$ would likewise be almost linearly related to consolidation pressure.

the latter value being obtained if one exceptionally high value is included in the average of the confined test results, see Tables (11-2) and (12-2). The agreement obtained is therefore well within the limits set by experimental error.

It can also be seen from the stress-strain curves, Figures (11-6) and (11-7) that a major change in the mechanism of failure is beginning to take place at this stress level. As the induced pore water tension in the unconfined samples at this consolidation pressure (3000 psi), if fully saturated, is equal approximately to 0.94 x 3000 = 2820 psi, the breakdown might be due either to tensile failure in the pore water or due to failure of capillary miniscii to prevent the invasion of the pore space by air or nitrogen in contact with the sample or released from solution in the pore water.

Therefore a series of tests were carried out on Kaolin, which has a radically different pore size, as is indicated by a permeability some two orders of magnitude greater than that of London clay although the percentage of clay size particles is greater in the Kaolin, see Table (11-1a).

11.4.2 Tests on Kaolin

Test 2D, Table (11-4) on Kaolin showed clearly that the breakdown pressure for Kaolin was well below 1000 psi. Therefore the series of tests on Kaolin was carried out for consolidation pressures in the range 125 psi to 1000 psi. The samples generally showed substantially larger strains at failure than observed for London clay, and several samples showed a tendancy to tilt associated with a reduced strength at failure. These later tests have been assumed to be unrepresentative.

As was the case in London clay most of the tests on Kaolin were repeated to avoid any doubt about the experimental results. It will be seen later that the stress-strain curves for the repeated tests do not lie close to each other as was observed for London clay. It appears that Kaolin is a less stable material and is more sensitive to test conditions.

The stress-strain curves of all the tests are presented in Figures (11-18) to (11-25) and the test results are summarised in Table (11-4). It should be noted that the lowest consolidation pressure σ_3 = 125 psi lies a little below the maximum vertical stress applied to the material during preparation in the oedometer (the maximum vertical stress applied was 160 psi). Samples consolidated at this pressure are therefore lightly overconsolidated, though the increase in the value of c_u/p is small (a maximum value of 0.290 for one unconfined test as against a maximum value of 0.284 at a consolidation pressure of 250 psi). The unconfined samples at the lowest consolidation pressure (125 psi) do not show a significant decrease in undrained strength (or in the ratio c_u/p), but the rapid drop in strength after failure observed with London clay is not apparent at this low stress level. It should be noted that the unconfined Kaolin samples after shearing have higher water contents than the London clay samples. The stress-strain curves and water content distribution throughout the Kaolin samples consolidated at σ_3 = 125 psi then sheared undrained are shown in Figures (11-18) and (11-19).

At a consolidation pressure of 250 psi a reduction in strength in the unconfined samples is already becoming apparent, Figures (11-20) and (11-21). The rapid post-peak drop in strength has also appeared. The kink in the stress-strain curve of test 6D, Figure (11-21), is due to tilting of the sample during the compression test.

As the consolidation pressure is increased to 500 psi, the divergence in strength becomes very pronounced and the brittle failure of the unconfined samples is becoming more like that observed on the London clay samples with a consolidation pressure an order of magnitude higher, Figures (11-22) and (11-23). Test 11D was repeated twice but the stress strain curves show some scatter, Figure (11-22).

At a consolidation pressure of 1000 psi, which is the maximum pressure applied, the divergence in strength is even more pronounced, the loss of strength on the removal of the confining pressure being 65%,

Figures (11-24) and (11-25). The brittleness of the relatively low strength unconfined samples is, however, not quite as marked as that of the unconfined samples of London clay, which have been subjected to higher consolidation pressures, Figures (11-8) and (11-9).

The test results are summarised, as for the London clay, on curves relating c_u and p, Figure (11-26), c_u and w, Figure (11-27), and percentage loss in strength r and reduction in confining pressure, Figure (11-28). It can be seen from the three sets of curves that the divergence in strength begins at a reduction in confining pressure of about 200 psi.

11.5 Results of Unconfined Tests on Air-Dried Samples

A series of unconfined compression tests was carried out on samples of the London clay consolidated by slow air-drying from the same initial water content (approximately equal to 34.6%) as those consolidated by a confining pressure. A summary of the test results is given in Table (11-5) and the stress-strain curves are plotted in Figures (11-29) and (11-30).

Sample (1E) which was sheared unconfined at a water content of 31.2% failed by one shear plane but the two pieces of the sample remained together. The strength of the sample decreased a little, gradually after peak; the stress-strain curve is nearly flat at peak.

Samples (2E, 3E and 5E) sheared unconfined at lower water contents (as low as 16.8%) fell apart into two pieces; the failure being of a brittle nature. The stress-strain curves at peak are round, then they fall rapidly due to the brittle failure of the samples.

Samples 4E and 6E sheared unconfined at water contents of 12.3% and 7.6% respectively, were crushed into many pieces at peak stress difference. The strength decreased rapidly after peak due to the brittle failure mechanism, Figure (11-30).

Sample (8E) was air-dried in the laboratory to 4.5% water content (the minimum water content could be achieved), then sheared unconfined. The sample exhibited higher strength than the previous samples and the failure mechanism was a brittle type, Figure (11-30). The sample was crushed into pieces at the peak stress difference.

Sample (7E) was oven-dried at 105°C to zero water content then sheared unconfined. It achieved higher strength than the previous samples and the failure was of a brittle nature. The sample was shattered into many pieces at the peak stress difference.

The relationship between the strength c_u and the water content w is plotted in Figure (11-15). This relationship will be discussed in detail in the next chapter.

11.6 Results of Shrinkage Limit Tests

11.6.1 Tests on London Clay

A sample of London clay which had been stored after initial consolidation and swelling in the 9 in. diameter oedometer, but had not been heavily consolidated, was subjected to a shrinkage test. In this test the sample was allowed to dry slowly in the air, and a series of very accurate height and diameter observations were taken. Then a final set of observations was taken after oven-drying at 105°C. The procedure of height and diameter measurement has already been described in Chapter 10. The variation of the diameter and height of the sample with the change of the water content during drying is given in Figure (11-31).

Another shrinkage limit test was carried out. In this test the sample was consolidated at the highest confining pressure (9000 psi) and then removed from the cell without testing (i.e. without shearing), for immediate volume determination based on a series of very accurate height and diameter observations. A series of such observations was continued while the sample was allowed to dry slowly in the air, and a

final set of readings was taken after oven-drying at 105°C as in the previous shrinkage test.

The variation of the diameter and the height of this sample with the change of water content during drying is shown in Figure (11-32).

11.6.2 Tests on Kaolin

A sample of Kaolin which had been stored after initial consolidation and swelling in the 9 in. diameter oedometer was subjected to a shrinkage test in a way similar to that for the London clay sample described in the previous section. The variation of the diameter and height of the sample with the change in water content during drying is shown in Figure (11.33).

A second shrinkage limit test was carried out on a sample of Kaolin which had been consolidated in the triaxial cell at a confining pressure of 1000 psi then removed from the cell without shearing, for volume determination. The test is similar to that for the second London clay sample described in the previous section except that the consolidation pressure applied to the Kaolin is 1000 psi while that for the London clay was 9000 psi. The variation of the dimensions of the sample with the change in water content during drying is shown in Figure (11-34).

Table (11-1a) Classification Tests

Material	Liquid Limit %	Plastic Limit %	Plasticity Index %	Clay Fraction % 2	Activity PI/% clay	Specific Gravity of Particles
Kaolin	70	40	30	68	0.44	2.64
London Clay	78	28	50	55	0.91	2.81

Mineralogy of London Clay: illite with kaolinite, montmorillonite and chlorite

Table (11-1b) Consolidation of Clay Before Sampling

Material	Maximum Vertical Stress: lb/sq. in.	Final Vertical Stress: lb/sq.in.	Water Content Initial %	Water Content Final %
Kaolin	160	3	71.5	42.6
London Clay	160	10	77.5	34.2

TABLE (11 - 2): RESULTS OF TESTS ON LONDON CLAY

Test No	Consolidation pressures σ_3 lb/sq inch	u	Water Contents Initial w %	Final w %	Tests with $\sigma_3 = p$ C_u lb/sq inch	C_u/p	Tests with $\sigma_3 = 0$ C_u lb/sq inch	C_u/p
1 B_1^1	1000	0	54.6	19.5			209	0.209
2 B_1^1	1000	0	53	19.3			210	0.210
3 B	1000	0	36.2	19.7			198	0.198
4 B	1000	0	32.4	19.9	201	0.201		
5 B								
6 B	1000	0	35.4	19.5			206	0.206
7 B	1000	0	34.8	19.8	221	0.221		
8 B	1000	0	35.5	19.6	200	0.200		
9 B								
10 B	1000	0	33.4	20.0	203	0.203		
11 B_2	1000	0	33.5	19.5	207	0.207		
12 B^2	1000	0	33.6					
	500	0		21.8[5]			151	0.302
13 B	3000	0	33.6	13.8	638	0.213		
14 B_3	3000	0	34.5	13.8			580	0.193
15 B^3	1000	0	33.1					
		0						
	1000	0		17.8[7]	241	0.241		
16 B	3000	0	36.7	13.9			593	0.198
17 B	3000	0	34.7	13.4	590	0.197		
18 B	3000	0	33.5	13.4	640	02.13		
19 B_4	9000	0	33.5	10.2[5]	1723	0.191		
20 B^4	1000	0	33.9	19.7[5]			196	0.196
21 B	9000	0	33.9	10.1			980[6]	0.109
22 B	9000	0	33	10.1			1020[6]	0.113
23 B								
24 B	6000	0	33.2	11.0			825[6]	0.137
25 B	6000		33.5	10.8	1325	0.221		

1 Preliminary series with higher initial water content.
2 Sample consolidated to 1000 lb/sq inch and allowed to swell under 500 lb/sq inch before testing.
3 Sample allowed to swell and then reconsolidated before testing.
4 Sample allowed to stand unconfined for 35 minutes before testing.
5 Calculated from volume change.
6 The expansion on stress release and reduction in volume under the axial stress were not measured during these tests and are significant only for the samples which departed from full saturation. At the maximum consolidation pressure the tabulated value may represent an over-estimate of the strength by about 2½%.
7 The final water content determination appears to be in error and should approximate to that of 26B.

TABLE (11 - 3)

The basis for the determination of the values of the parameter r.

Consolidation pressure		Compressibility C from p-e curves	Expansibility C_e from p-e curves	$\lambda = \frac{C_e}{C}$	Expansibility C_e in m^2/MN units on basis of 3 assumptions			Porosity n	Values of r for assumptions II and III	
lb/sq inch	MN/m^2	m^2/MN	M^2/MN		I	II	III		II	III
1000	6.9	15.8×10^{-3}	6.2×10^{-3} (1)	0.39	6.2×10^{-3}	7.1×10^{-3}	6.2×10^{-3}	0.357	1.22%	1.40%
3000	20.7	45.0×10^{-4}	24.0×10^{-4} (2)	0.53	23.7×10^{-4}	20.2×10^{-4}	24.0×10^{-4}	0.277	3.10%	2.80%
6000	41.4	14.8×10^{-4}			12.4×10^{-4}	6.6×10^{-4}	10.0×10^{-4}	0.235	7.20%	5.05%
9000	62.1	45.0×10^{-5}			84.3×10^{-5}	20.2×10^{-5}	36.0×10^{-5}	0.222	18.5%	11.7%

Assumption I - Unloading p - e curves are straight parallel lines on e - log p plot.

II - The value of λ is constant and equal to 0.45

III - Extrapolating observed C_e values using a value of λ increasing with p

(1) Assuming a linear relationship between e and log p on unloading from 1000 lb/sq inch to 100 lb/sq inch.

(2) Extrapolated from volume change observed over range 2854 lb/sq inch to 2554 lb/sq inch.

Test No	Consolidation pressures σ_3 lb/sq inch	u	Water Contents Initial w %	Final w %	Tests with $\sigma_3 = p$ C_u lb/sq inch	C_u/p	Tests with $\sigma_3 = 0$ C_u^2 lb/sq inch	C_u/p
1 D	1000	0	44.2	20.0	243	0.243		
2 D	1000	0	43	19.9			93	0.093
3 D	1000	0	43.2	20.1			78	0.078
4 D	500	0	42.2	23.2			75	0.150
5 D	1000	0	42.7	19.6			88	0.088
6 D[1]	250	0	42.9	27.2			55.5	0.222
7 D	250	0	43.0	26.9			61.0	0.244
8 D	250	0	42.0	27.0	71.0	0.284		
9 D	250	0	41.2	27.1	62.5	0.250		
10 D	250	0	42.0	26.8	71.0	0.284		
11 D[1]	500	0	42.8	22.5	108	0.216		
12 D[1]	500	0	42.9	23.2	101	0.202		
13 D								
14 D								
15 D	500	0	42.8	23.1	130	0.260		
16 D	125	0	42.5	30.8			36.3	0.290
17 D	125	0	42.1	30.5	35.0	0.280		
18 D	125	0	42.6	31.3			32.0	0.256

1 Samples tilted during compression test.

2 The expansion on stress release and reduction in volume under the axial stress were not measured during these tests and are significant only for the samples which departed from full saturation. At the maximum consolidation pressure the tabulated value may represent an over-estimate of the strength by about 7%.

Table (11-5) : Results of Unconfined Tests on Air-Dried Samples of London Clay .

Test No.	Water Content Initial w%	Water Content Final w%	c_u psi	ϵ_1% at Failure	Type of Failure
1E	34.3	31.2	21.9	12.3	One failure plane
2E	34.8	21.4	112.9	10.3	One failure plane
3E	34.7	16.8	237.0	7.7	One failure plane
4E	34.1	12.3	415.6	5.1	Multiple failure planes
5E	34.6	22.8	89.5	11.6	One failure plane
6E	34.3	7.6	844.0	4.7	Sample crushed
7E	34.2	0.0	1557.0	8.6	Oven-dried. Sample crushed
8E	34.4	4.5	979.5	2.6	Air-dried. Sample crushed

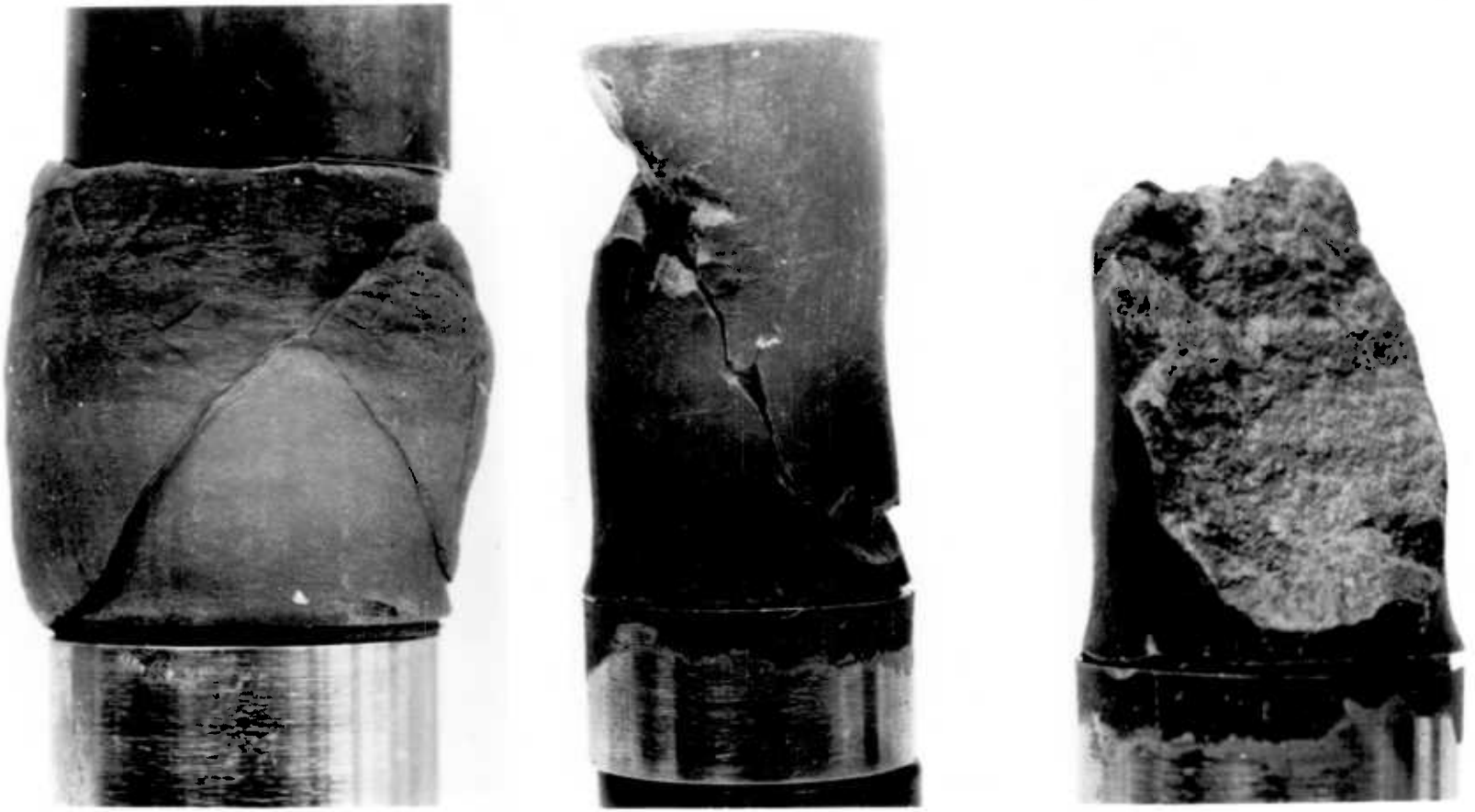

Plate (11-1) Samples Consolidated at 9000 psi and Tested (a) With Cell Pressure Equal to Consolidation Pressure - Test 19B and (b) Unconfined - Test 21B. Surface Texture shown in (c) for Unconfined Test.

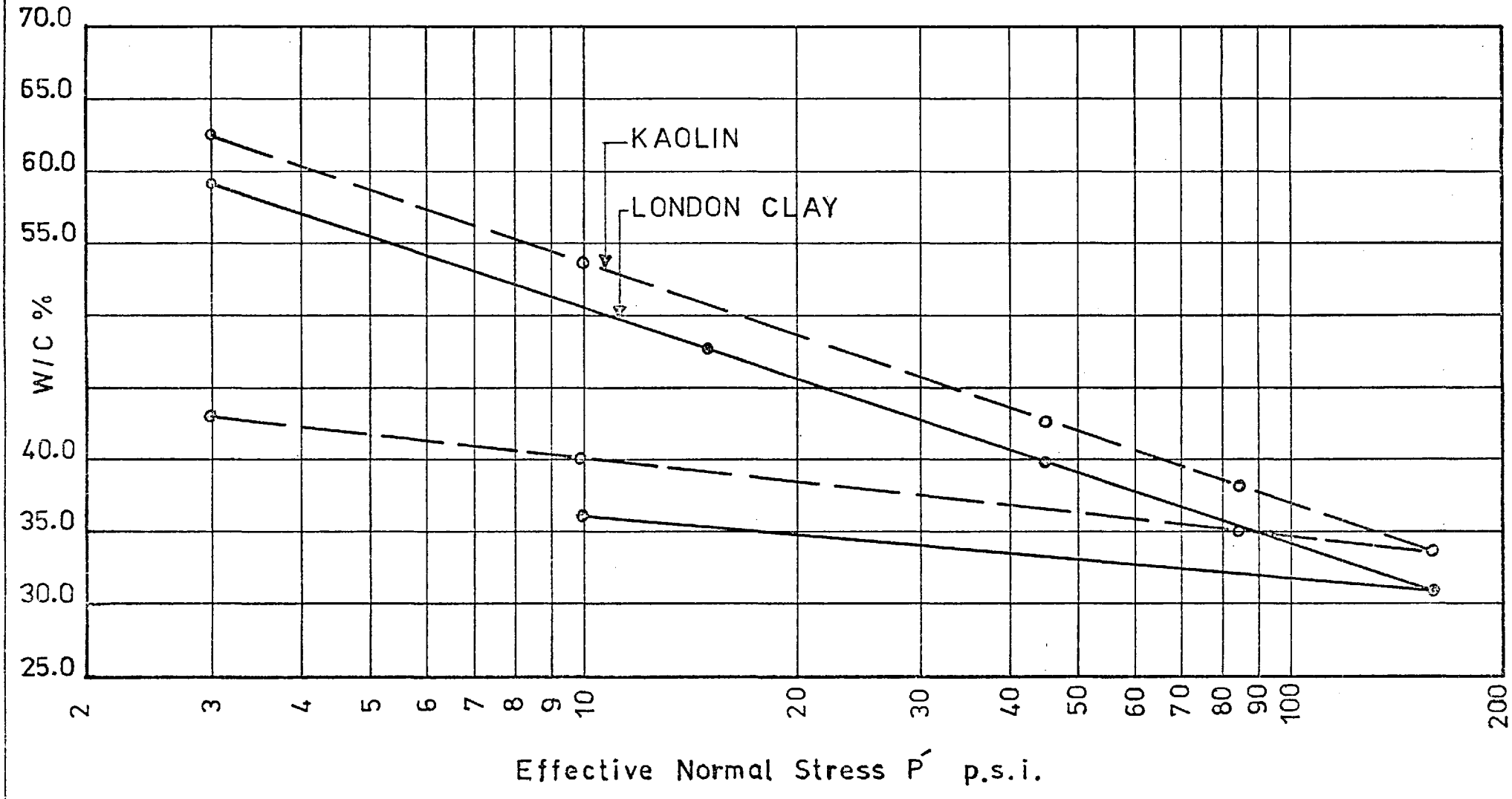

CONSOLIDATION OF LONDON CLAY & KAOLIN IN 9 IN. DIA. OEDOMETER

FIG 11-1

TEST NO.	INITIAL W/C	FINAL W/C	$\frac{C_u}{P}$
1 B	54.6 %	19.5 %	0.21
2 B	53.0%	19.3 %	0.208

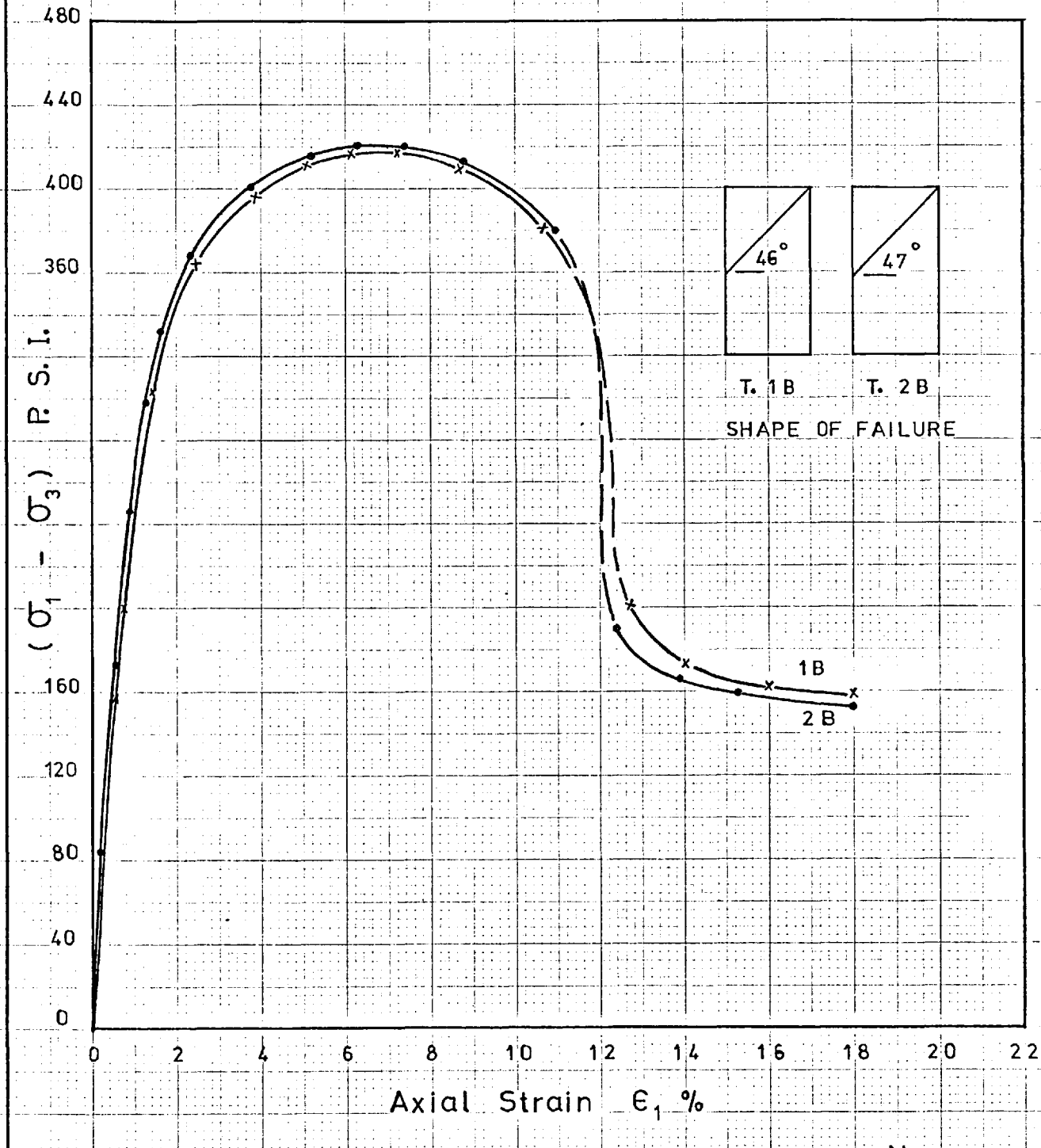

TESTS (1 B & 2 B). REMOULDED LONDON CLAY CONSOLIDATED AT σ_3 = 1000 P. S. I. & U = 0 , THEN SHEARED UNDRAINED WITH σ_3 = 0 .

FIG 11 - 2

TEST NO.	INITIAL W/C	FINAL W/C	C_u/P
4 B	32.4 %	19.95 %	0.201
8 B	35.5 %	19.6 %	0.20
10 B	33.4 %	19.95 %	0.203
11 B	33.5 %	19.5 %	0.207

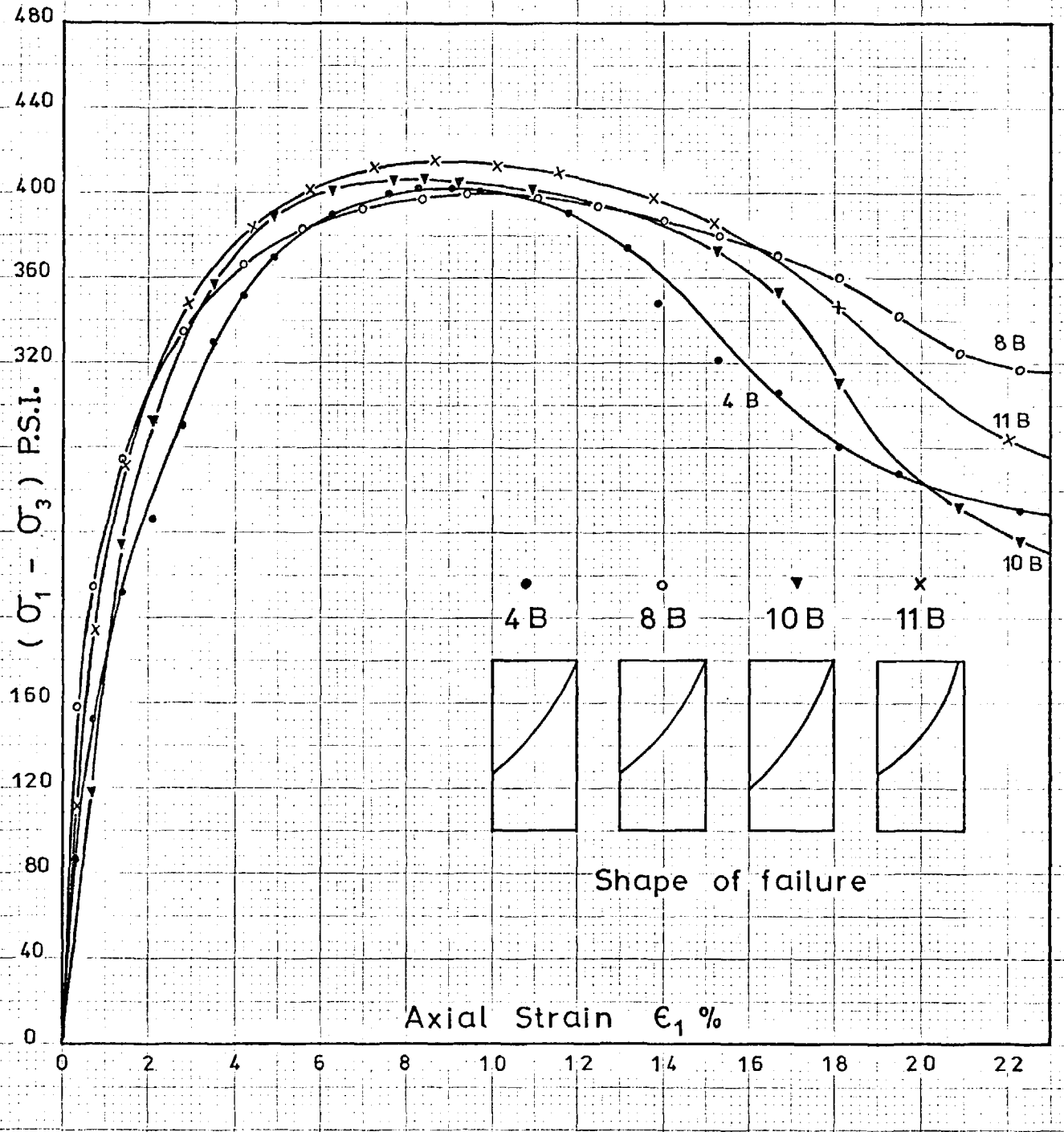

TESTS 4B, 8B, 10B & 11B. LONDON CLAY CONSOLIDATED AT σ_3 = 1000 P.S.I & U = 0, THEN SHEARED UNDRAINED WITH σ_3 = 1000 P.S.I.

FIG 11 - 3

TEST NO.	INITIAL W/C	FINAL W/C	C_u/P
3 B	36.2 %	19.7 %	0.198
6 B	35.4 %	19.14 %	0.206

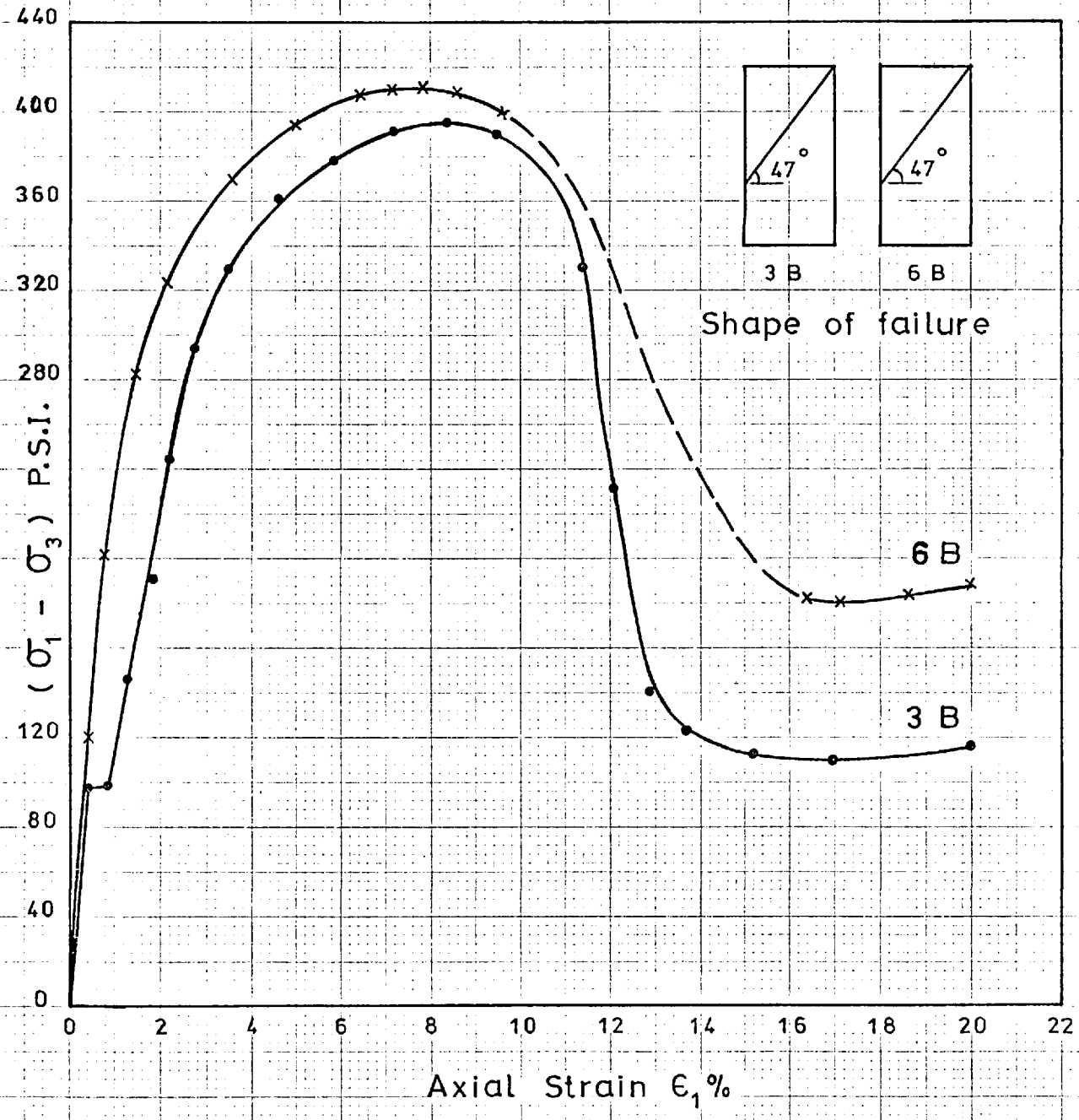

TESTS 3B & 6B. LONDON CLAY CONSOLIDATED AT σ_3=1000 P.S.I. & U=0, THEN SHEARED UNDRAINED WITH σ_3 = 0.

FIG 11 - 4

INITIAL W/C	34.8 %
FINAL W/C	19.75 %
C_u/P	0.221

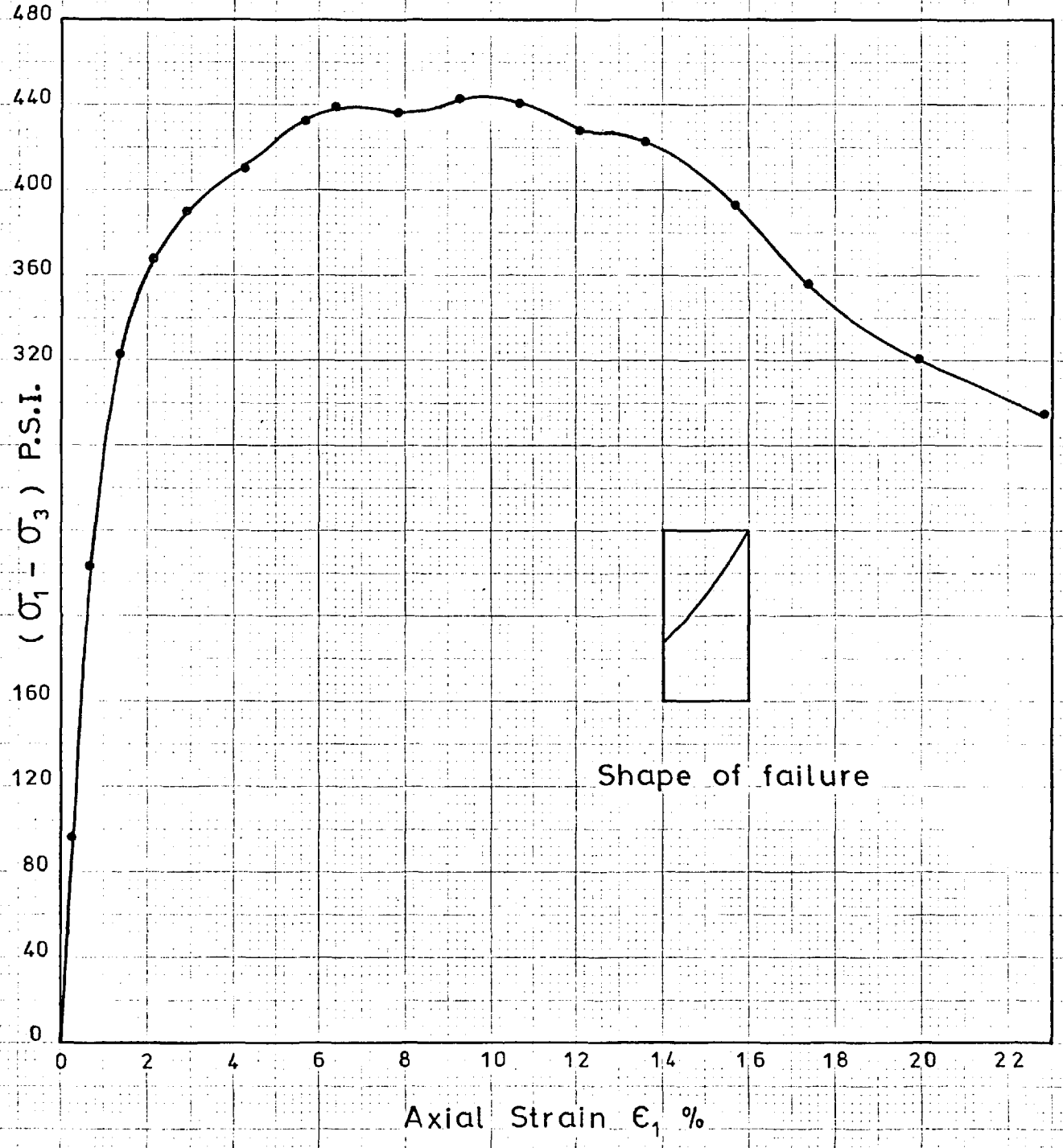

TEST 7B. LONDON CLAY CONSOLIDATED AT σ_3 = 1000 P.S.I. & U = 0, THEN SHEARED UNDRAINED WITH σ_3 = 1000 P.S.I.

FIG 11 – 5

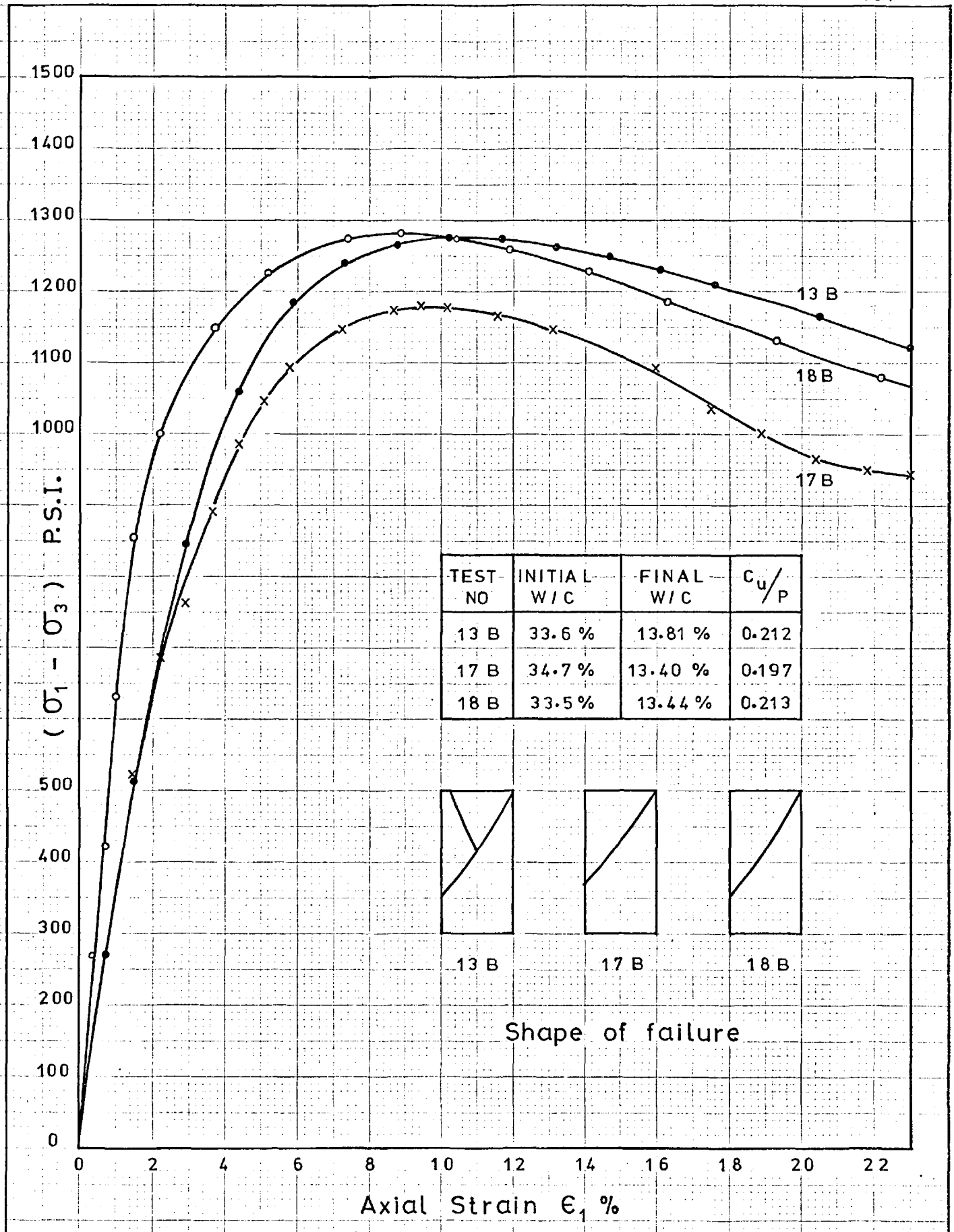

TEST NO	INITIAL W/C	FINAL W/C	C_u/P
13 B	33.6 %	13.81 %	0.212
17 B	34.7 %	13.40 %	0.197
18 B	33.5 %	13.44 %	0.213

Shape of failure

TESTS 13 B, 17 B & 18 B. LONDON CLAY CONSOLIDATED AT σ_3 = 3000 P S I & U = 0, THEN SHEARED UNDRAINED WITH σ_3 = 3000 P.S.I.

FIG 11 - 6

TEST NO.	INITIAL W/C	FINAL W/C	C_u/P
14 B	34.5 %	13.83 %	0.193
16 B	36.72%	13.90 %	0.198

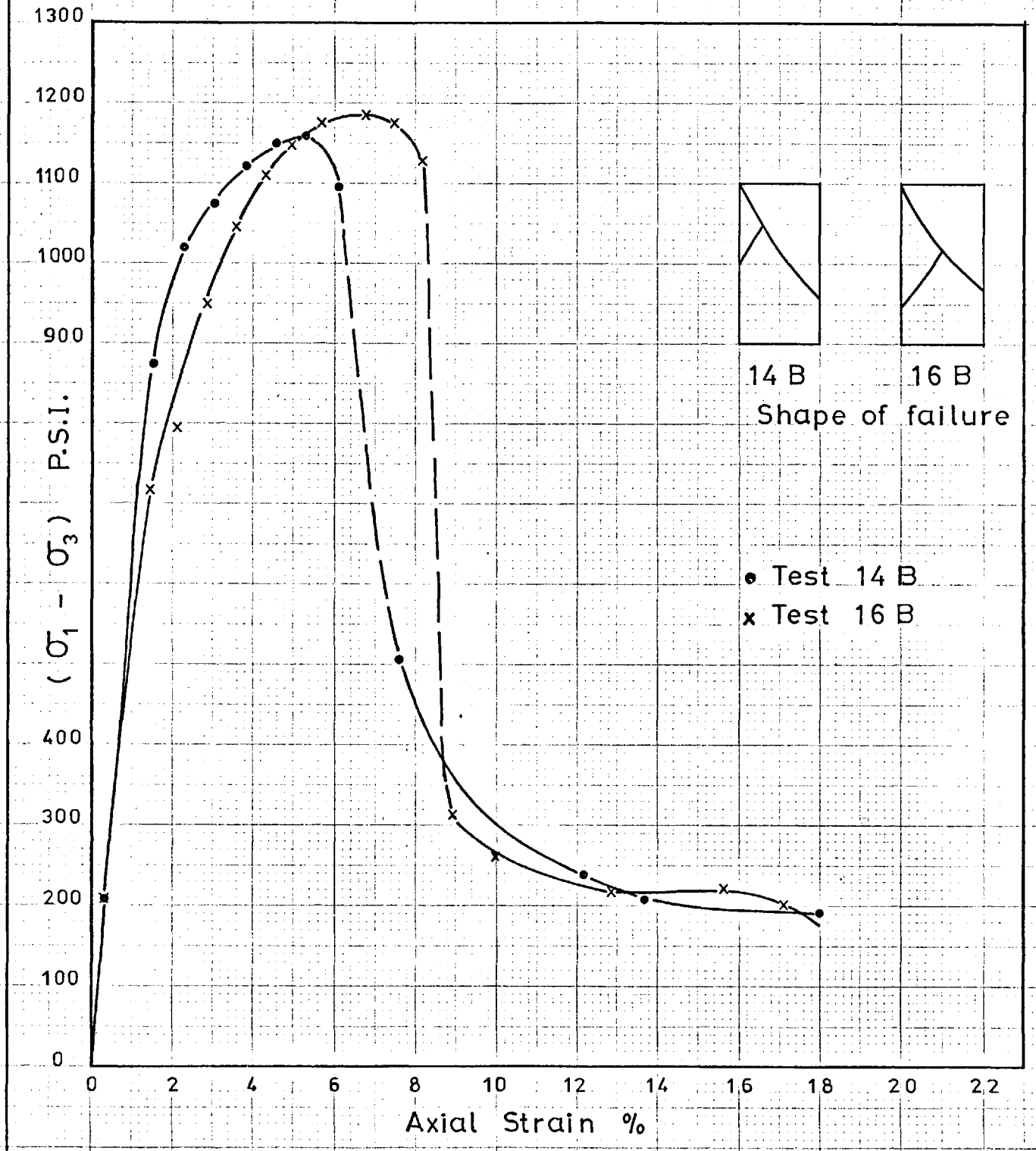

TESTS 14 B & 16 B. LONDON CLAY CONSOLIDATED AT σ_3 = 3000 P.S.I. AND U = 0, THEN SHEARED UNDRAINED WITH σ_3 = 0.

FIG 11 - 7

TESTS NO.	INITIAL W/C	FINAL W/C	C_u/P
24 B	33.24 %	11.0 %	0.138
25 B	33.5 %	10.81 %	0.22

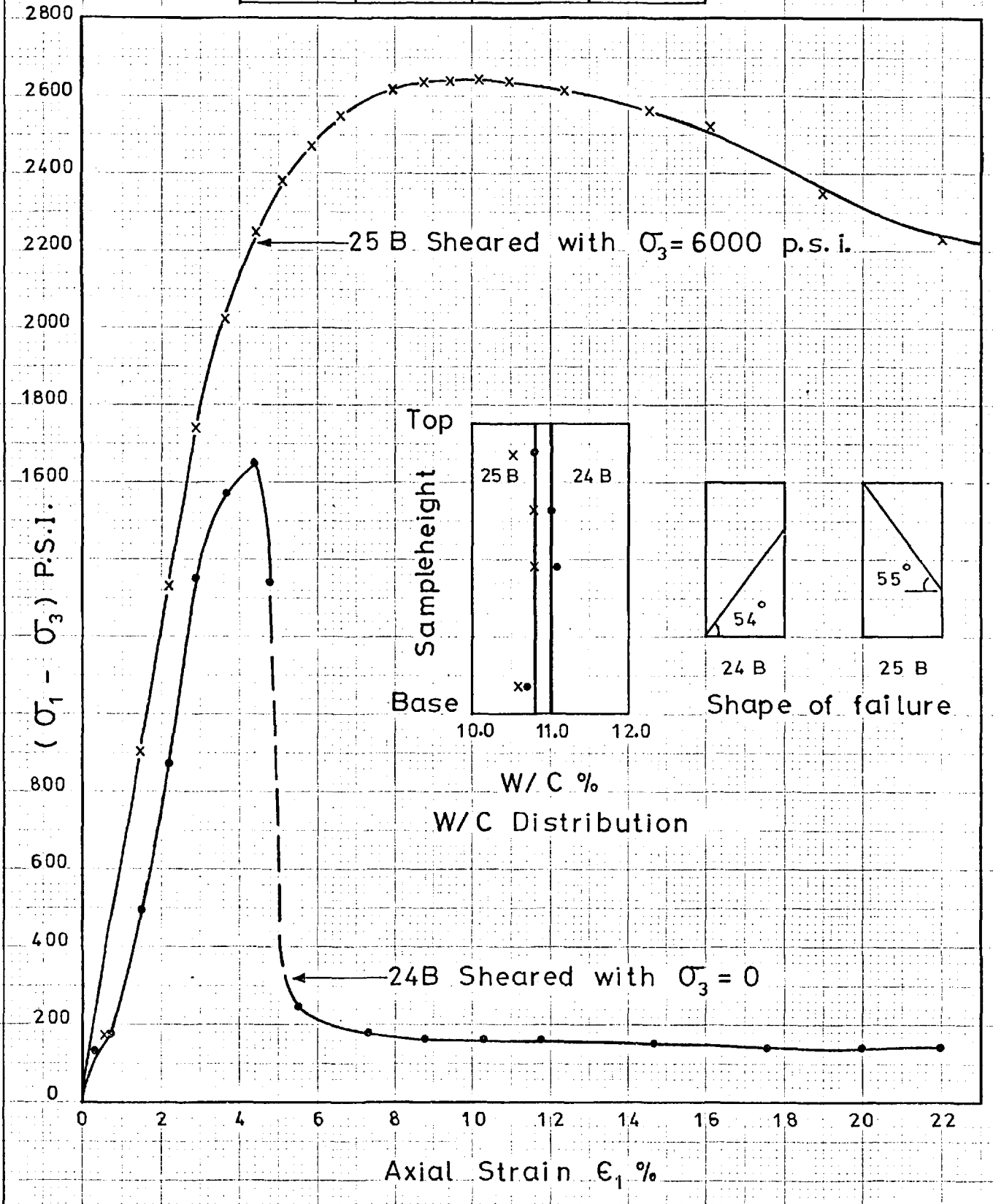

TESTS 24 B & 25 B. LONDON CLAY CONSOLIDATED AT σ_3 = 6000 P.S.I. & U = 0, THEN SHEARED UNDRAINED

FIG 11 - 8

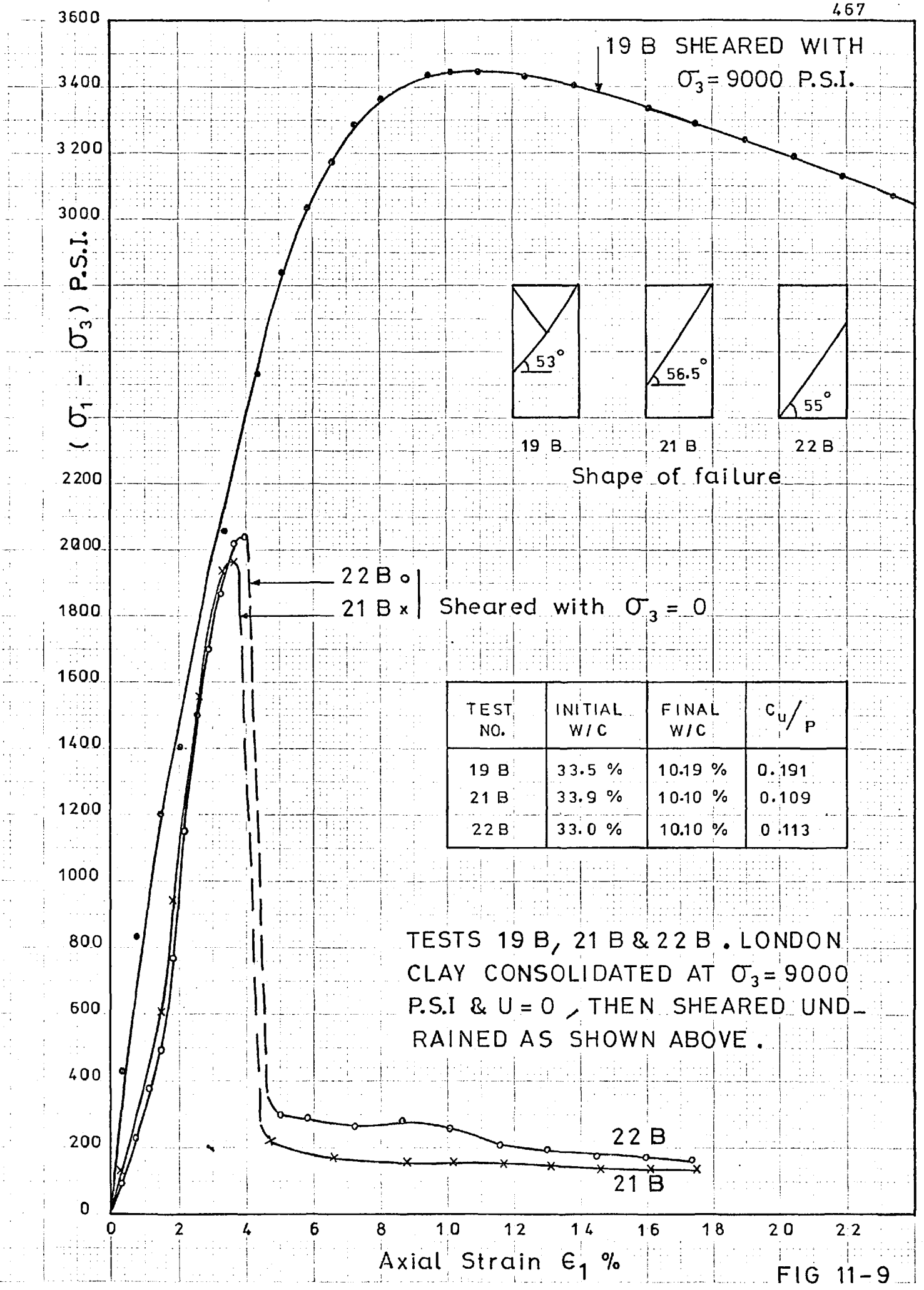

TEST NO.	INITIAL W/C	FINAL W/C	C_u/P
19 B	33.5 %	10.19 %	0.191
21 B	33.9 %	10.10 %	0.109
22 B	33.0 %	10.10 %	0.113

TESTS 19 B, 21 B & 22 B . LONDON CLAY CONSOLIDATED AT σ_3 = 9000 P.S.I & U = 0 , THEN SHEARED UNDRAINED AS SHOWN ABOVE .

FIG 11-9

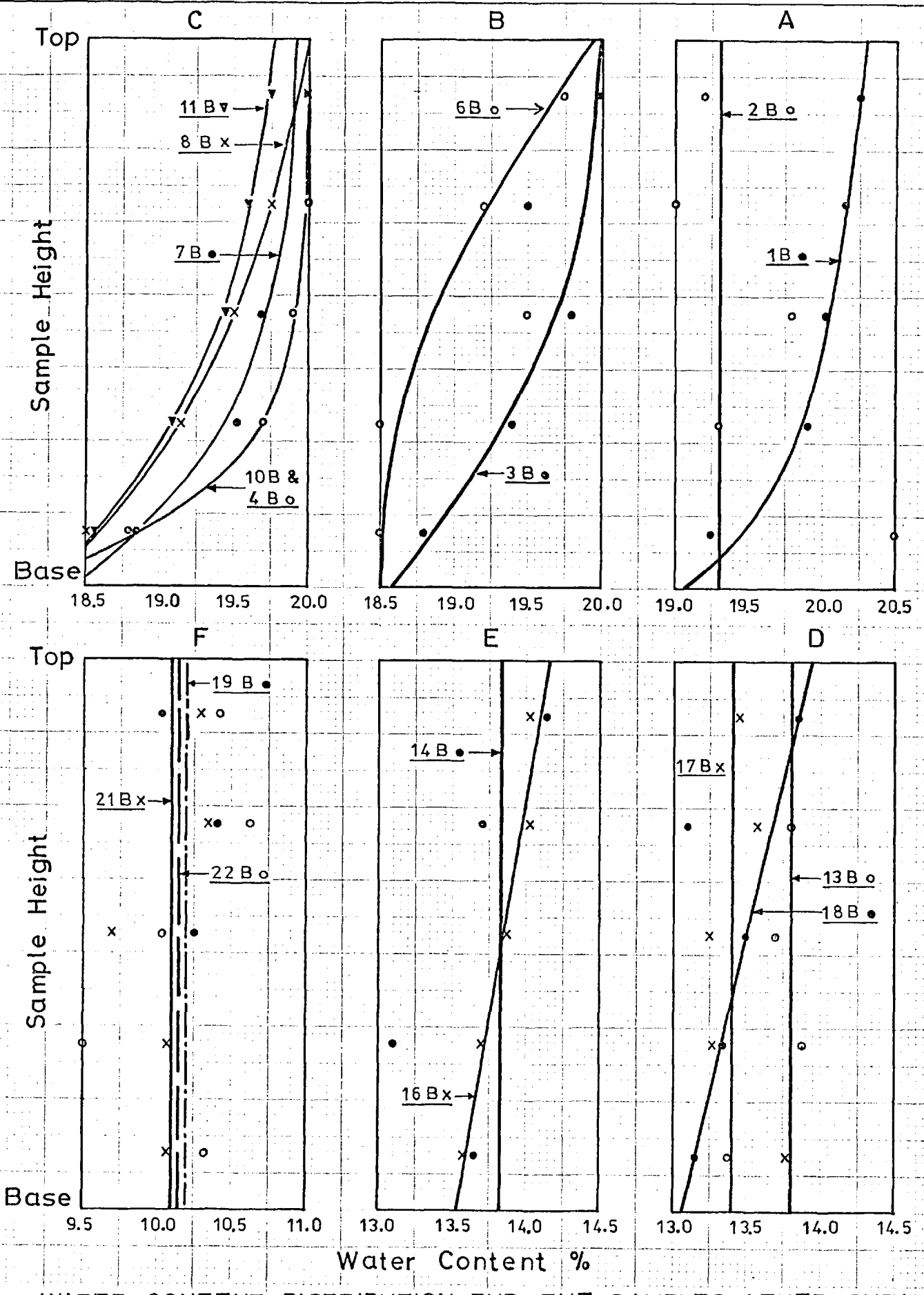

WATER CONTENT DISTRIBUTION THR. THE SAMPLES AFTER SHEARING. (TESTS 1B, 2B, 3B, 4B, 6B, 7B, 8B, 10B, 11B, 13B, 14B, 16B, 17B, 18B, 19B, 21B & 22B).

FIG 11-10

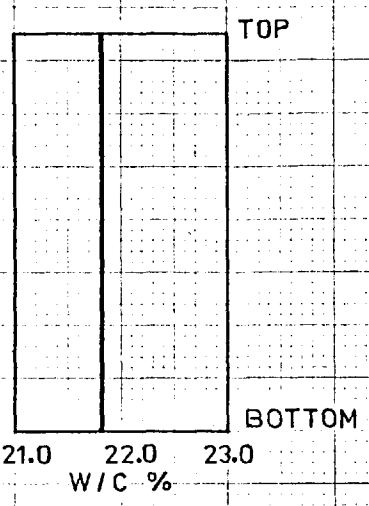

W/C Distribution

INITIAL W/C	33.6 %
FINAL W/C	21.8 %
C_u/P	0.30

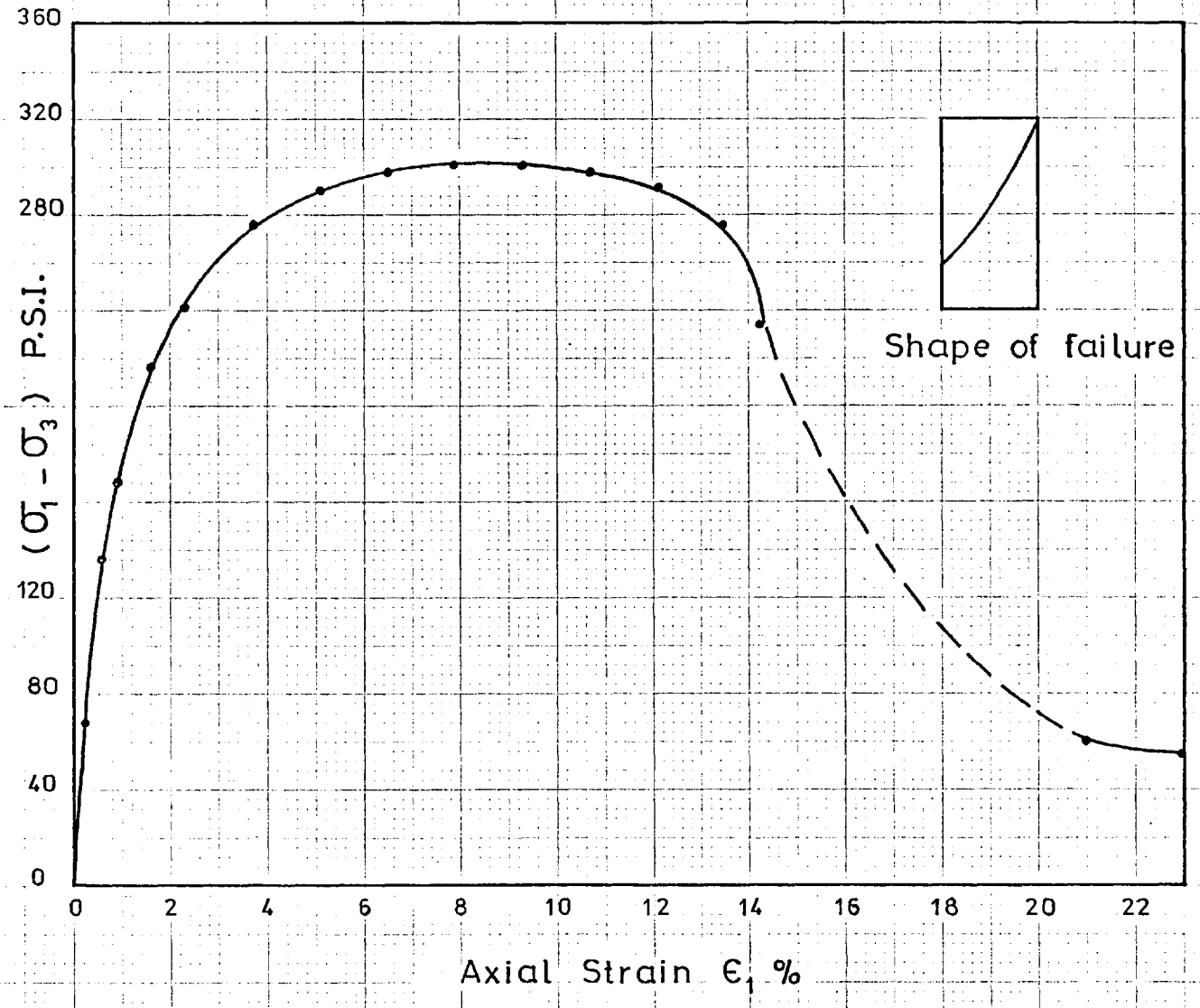

TEST (12 B). LONDON CLAY CONSOLIDATED AT σ_3 = 1000 P.S.I. THEN ALLOWED TO SWELL AT σ_3 = 500 P.S.I., THEN SHEARED UNDRAINED WITH σ_3 = 0.

FIG 11 - 11

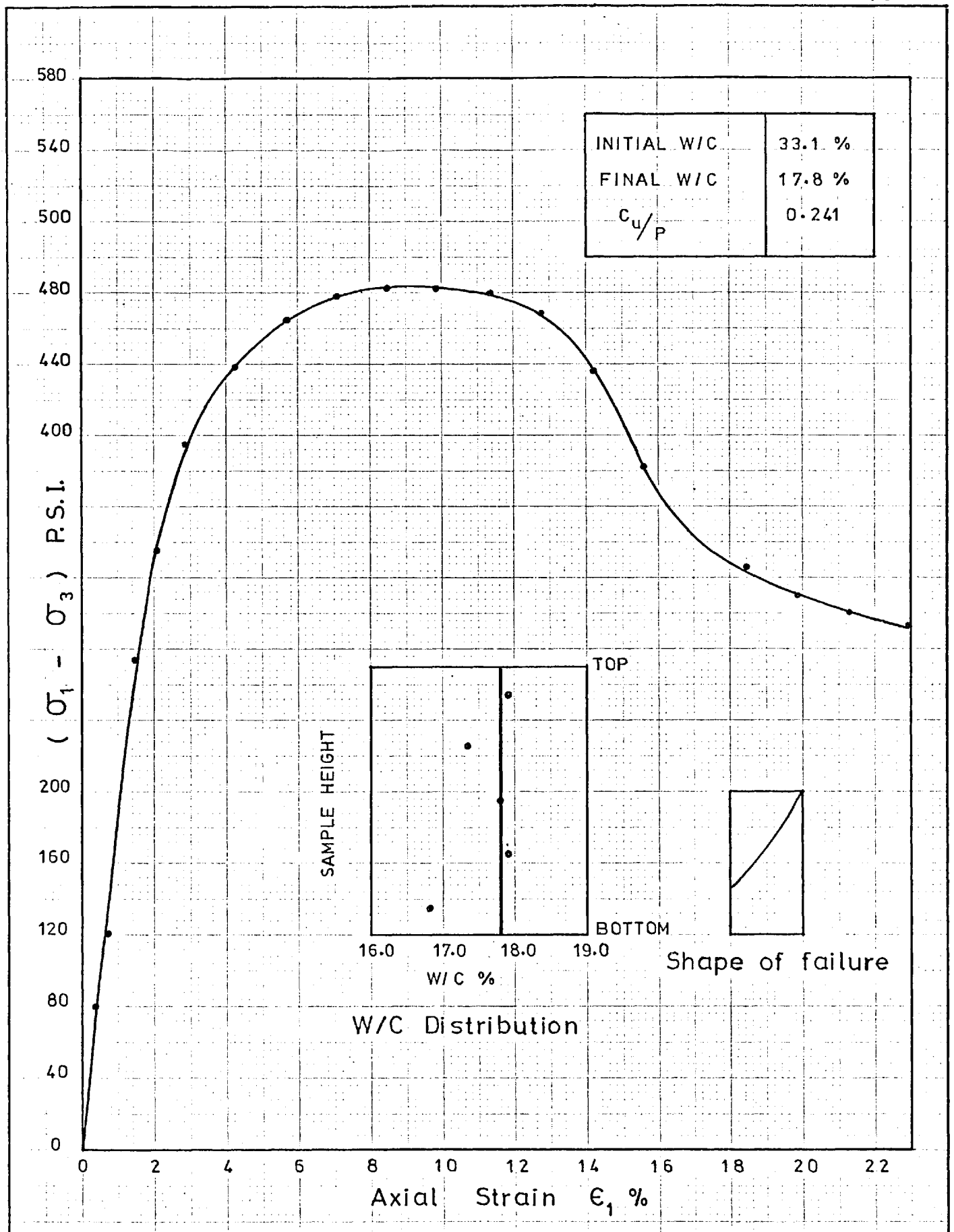

TEST (15 B). LONDON CLAY CONSOLIDATED IN STAGES TO σ_3 =1000 P.S.I., THEN ALLOWED TO SWELL. RECONSOLIDATED AT σ_3 =1000 P.S.I. AND U=0 THEN SHEARED UNDRAINED WITH σ_3 =1000 P.S.I.

FIG 11-12

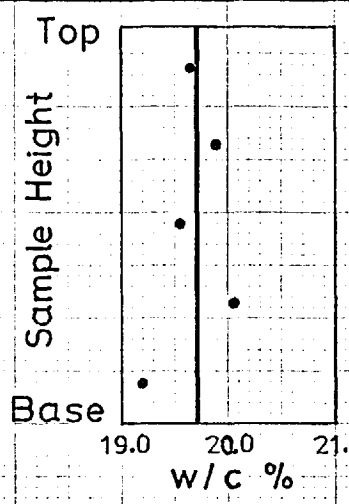

INITIAL W/C	33.85 %
FINAL W/C	19.7 %
$c_u/_P$	0.196

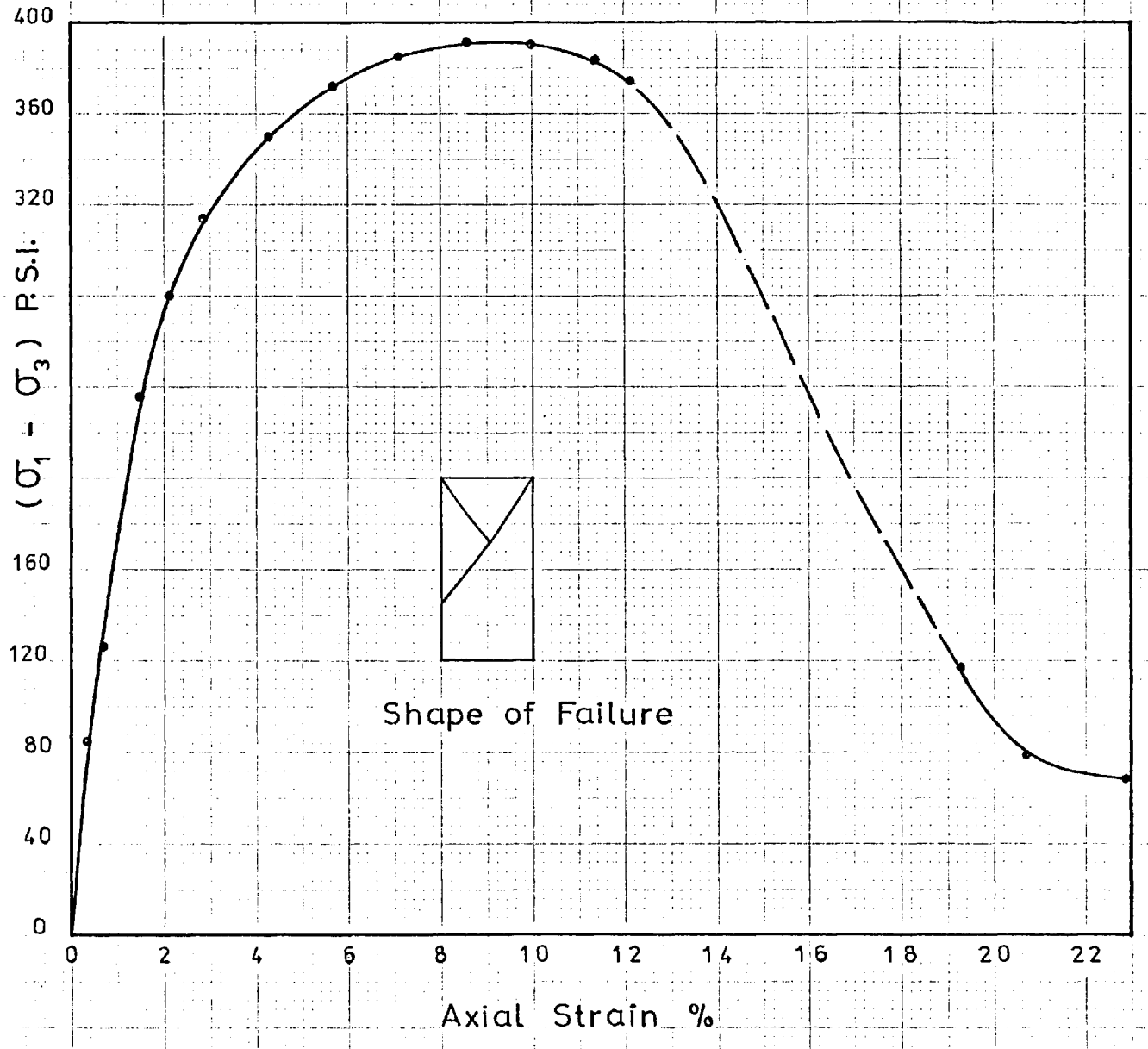

TEST 20B - LONDON CLAY CONSOLIDATED AT $\sigma_3 = 1000$ P.S.I. AND U = 0, THEN THE SAMPLE LEFT FOR 35 MINUTES UNDER $\sigma_3 = 0$ BEFORE SHEARED UNDRAINED UNCONFINED.

FIG 11-13

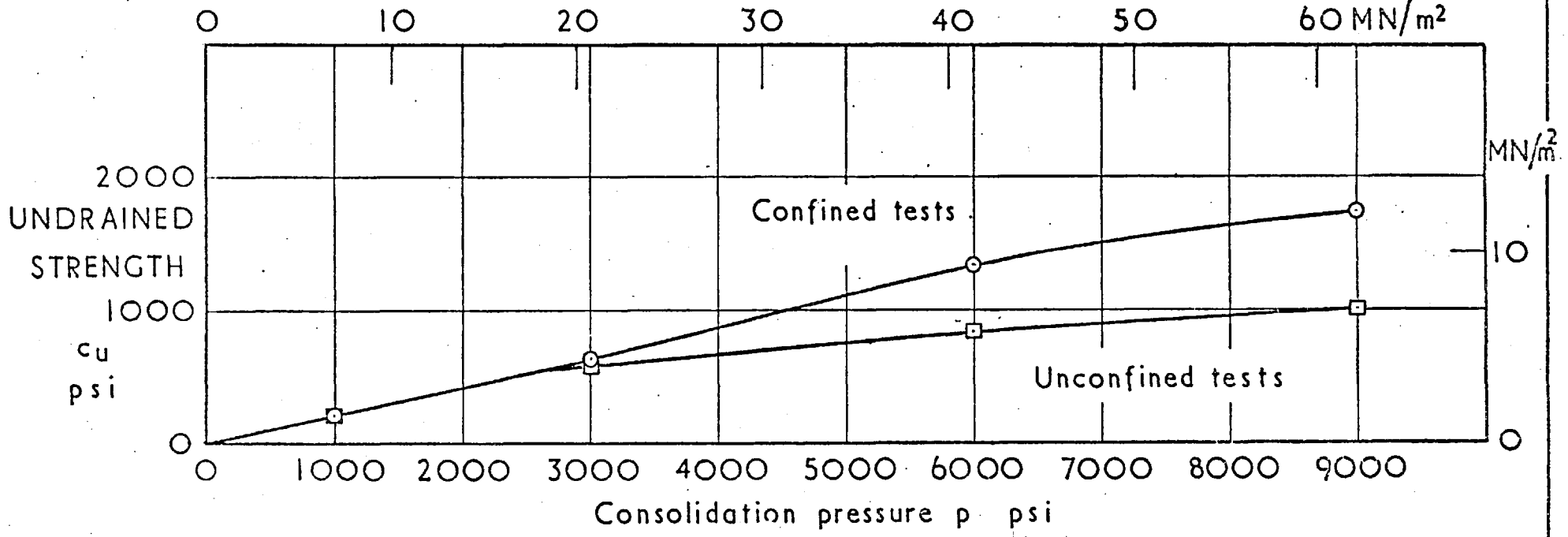

RELATIONSHIPS BETWEEN UNDRAINED STRENGTH c_u & CONSOLIDATION PRESSURE p FOR CONFINED & UNCONFINED TESTS ON LONDON CLAY. WHERE A NUMBER OF TESTS WERE PERFORMED AT A PARTICULAR PRESSURE THE AVERAGE VALUE IS PLOTTED

FIG 11-14

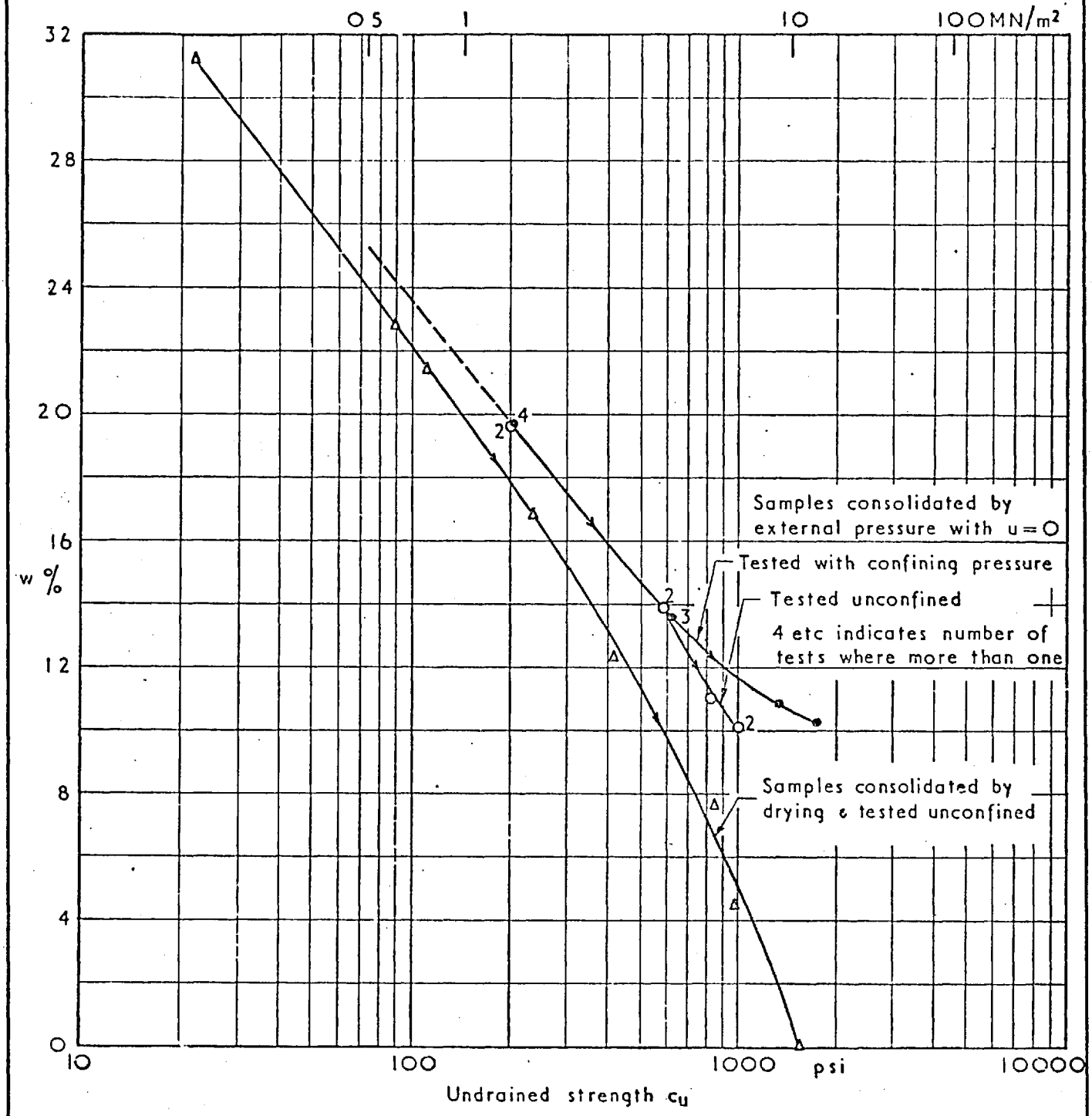

RELATIONSHIPS BETWEEN UNDRAINED STRENGTH c_u & WATER CONTENT w FOR CONFINED TESTS & UNCONFINED TESTS ON SAMPLES CONSOLIDATED BY EXTERNAL PRESSURE & UNCONFINED TESTS ON SAMPLES CONSOLIDATED BY DRYING: LONDON CLAY

FIG 11-15

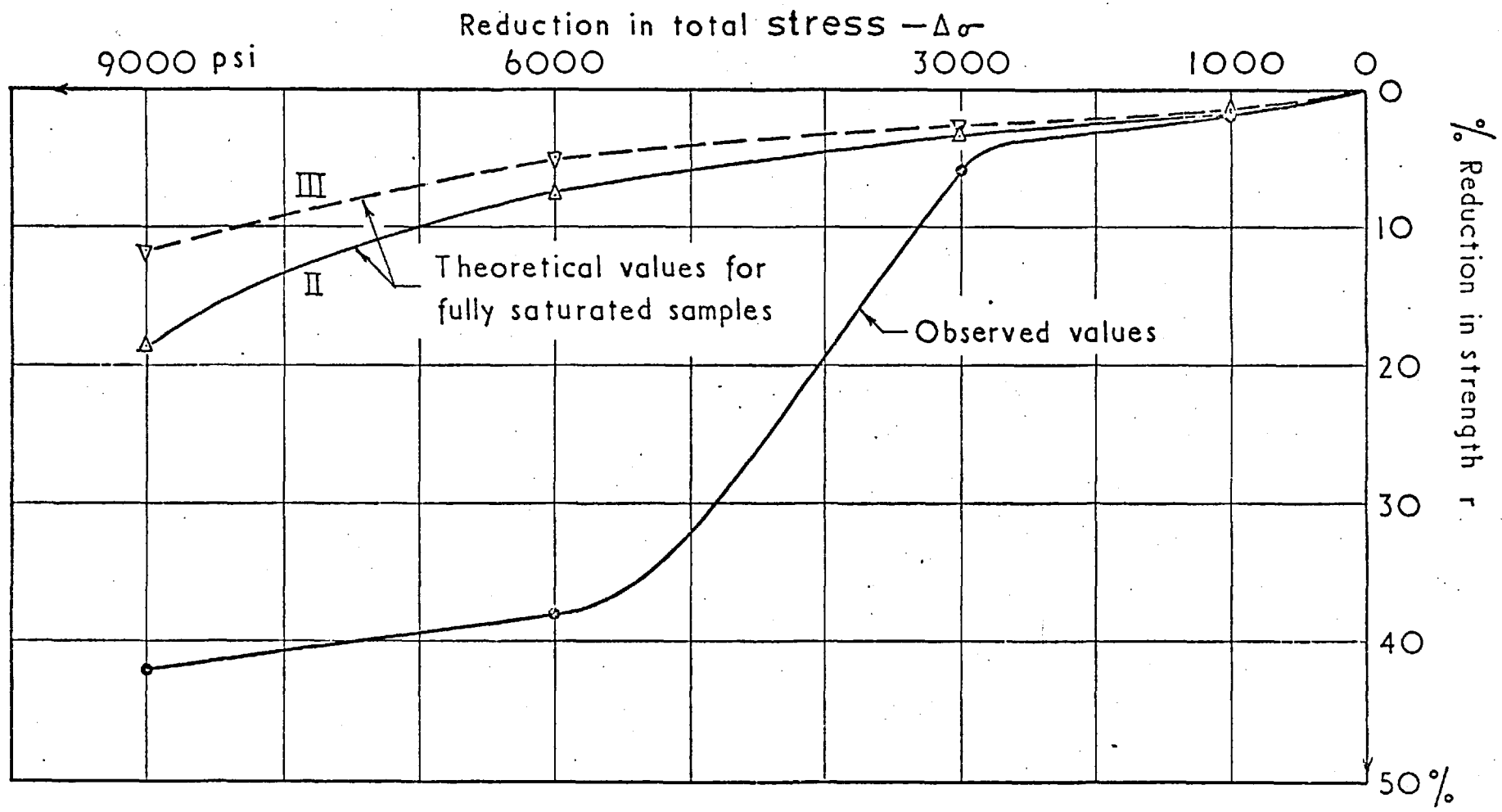

FIG 11-16

RELATIONSHIPS BETWEEN REDUCTION IN STRENGTH r & REDUCTION IN TOTAL STRESS $-\Delta\sigma$: A COMPARISON BETWEEN THE OBSERVED VALUES & THE THEORETICAL VALUES BASED ON THE ASSUMPTION OF FULL SATURATION. NORMALLY CONSOLIDATED LONDON CLAY; INITIAL PORE WATER PRESSURE = O

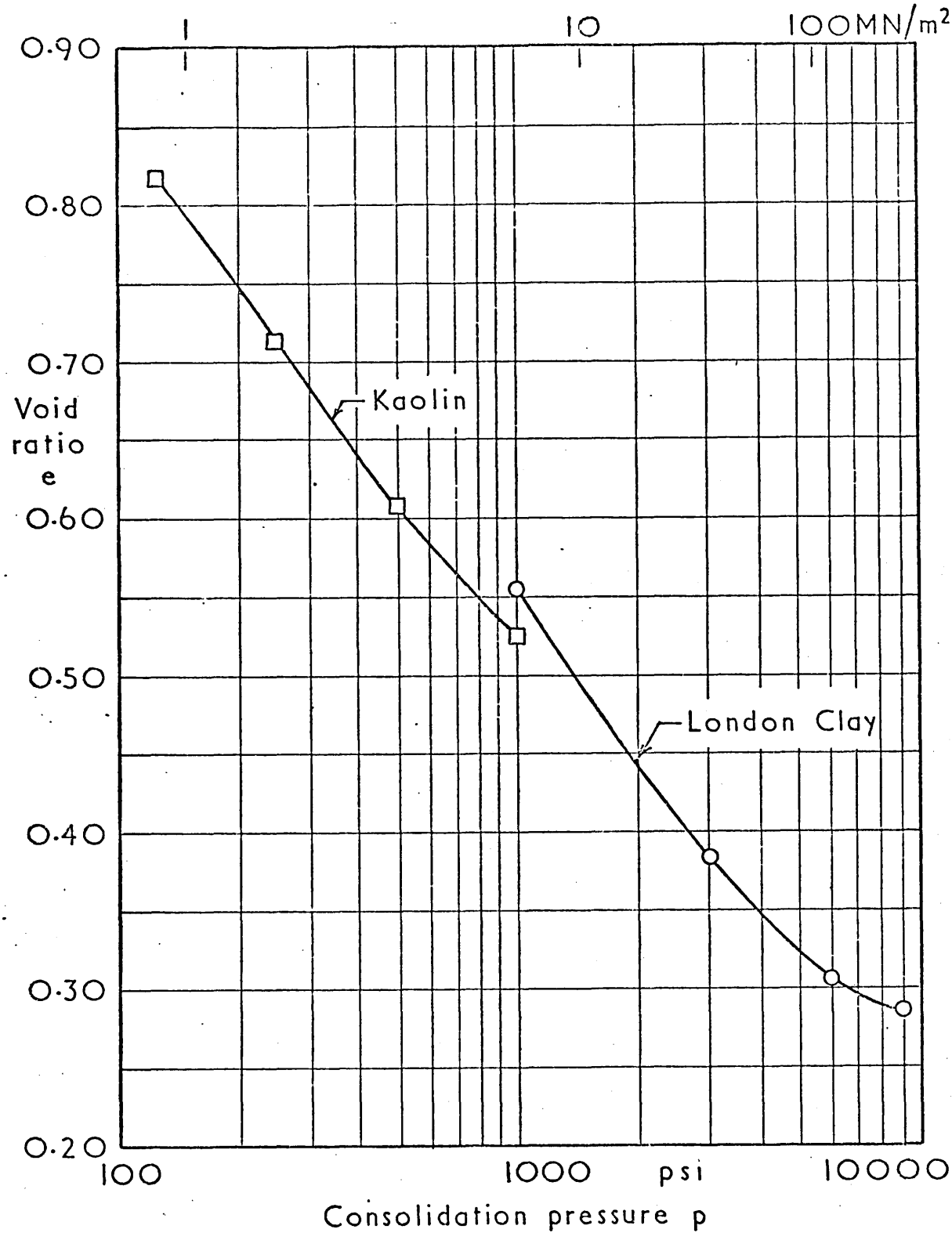

RELATIONSHIPS BETWEEN THE VOID RATIO e CALCULATED FROM THE FINAL WATER CONTENT & THE CONSOLIDATION PRESSURE p FOR LONDON CLAY & KAOLIN

FIG 11-17

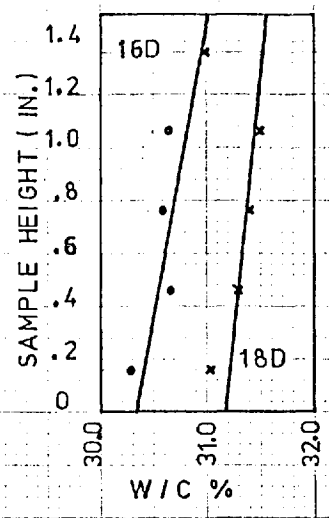

W/C DISTRIBUTION THR. THE SAMPLE

TEST NO.	INITIAL W/C	FINAL W/C	C_u/P
16D	42.5%	30.8%	0.29
18D	42.6%	31.3%	0.26

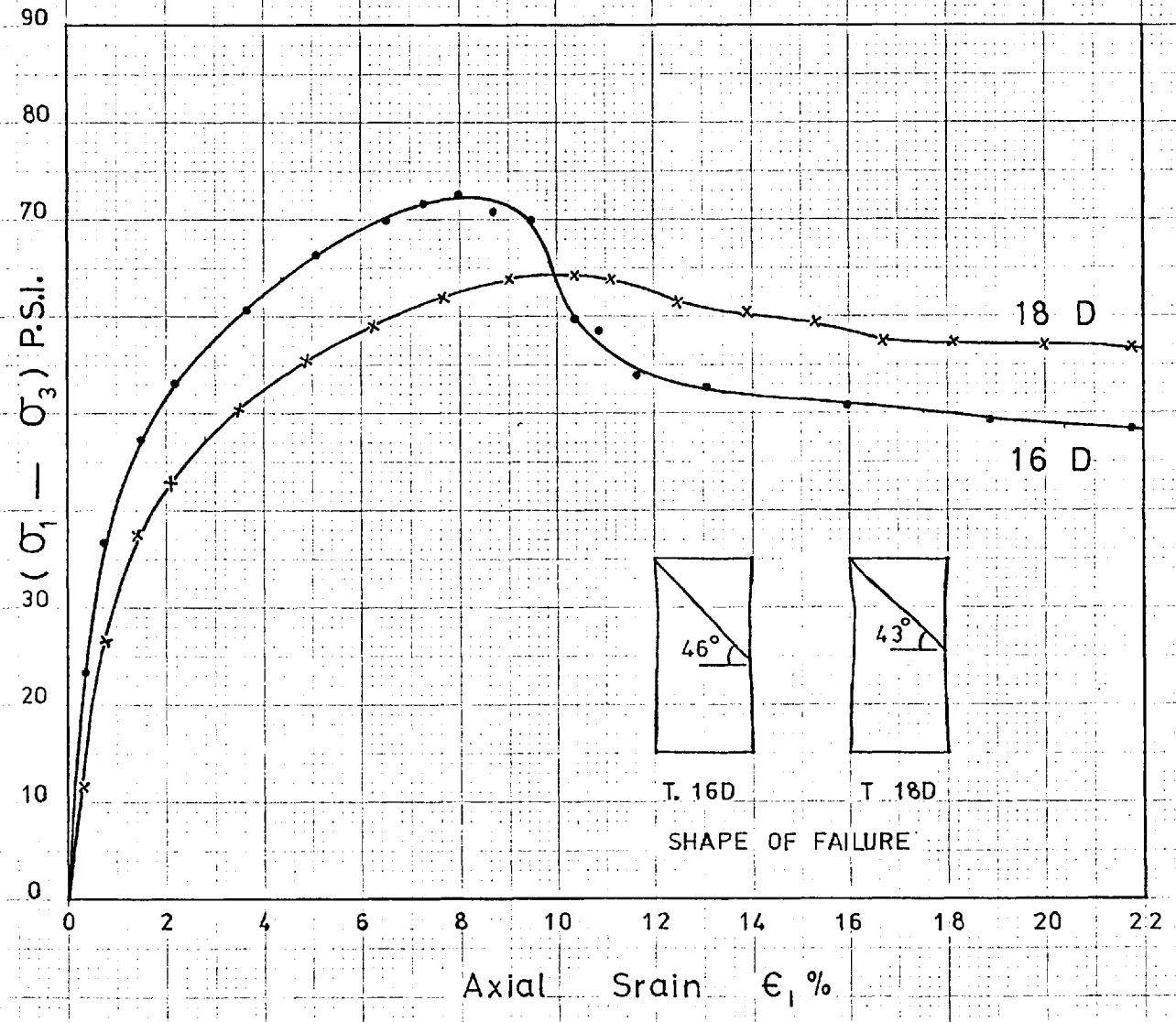

FIG. (11-18) _ TESTS (16 D & 18 D). KAOLIN CONSOLIDATED AT σ_3 = 125 P.S.I. & U = 0, THEN SHEARED UNDRAIN_ED WITH σ_3 = 0 P.S.I.

TEST NO.	INITIAL W/C	FINAL W/C	C_u/P
17 D	42.1%	30.5%	0.28

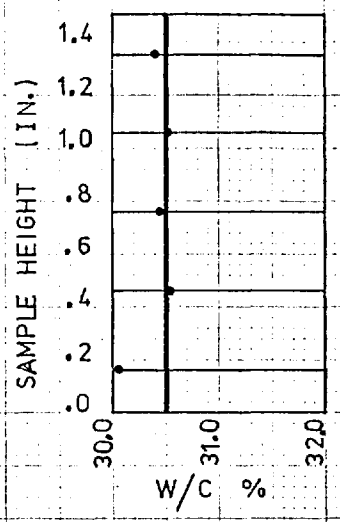

W/C DISTRIBUTION THROUGH THE SAMPLE

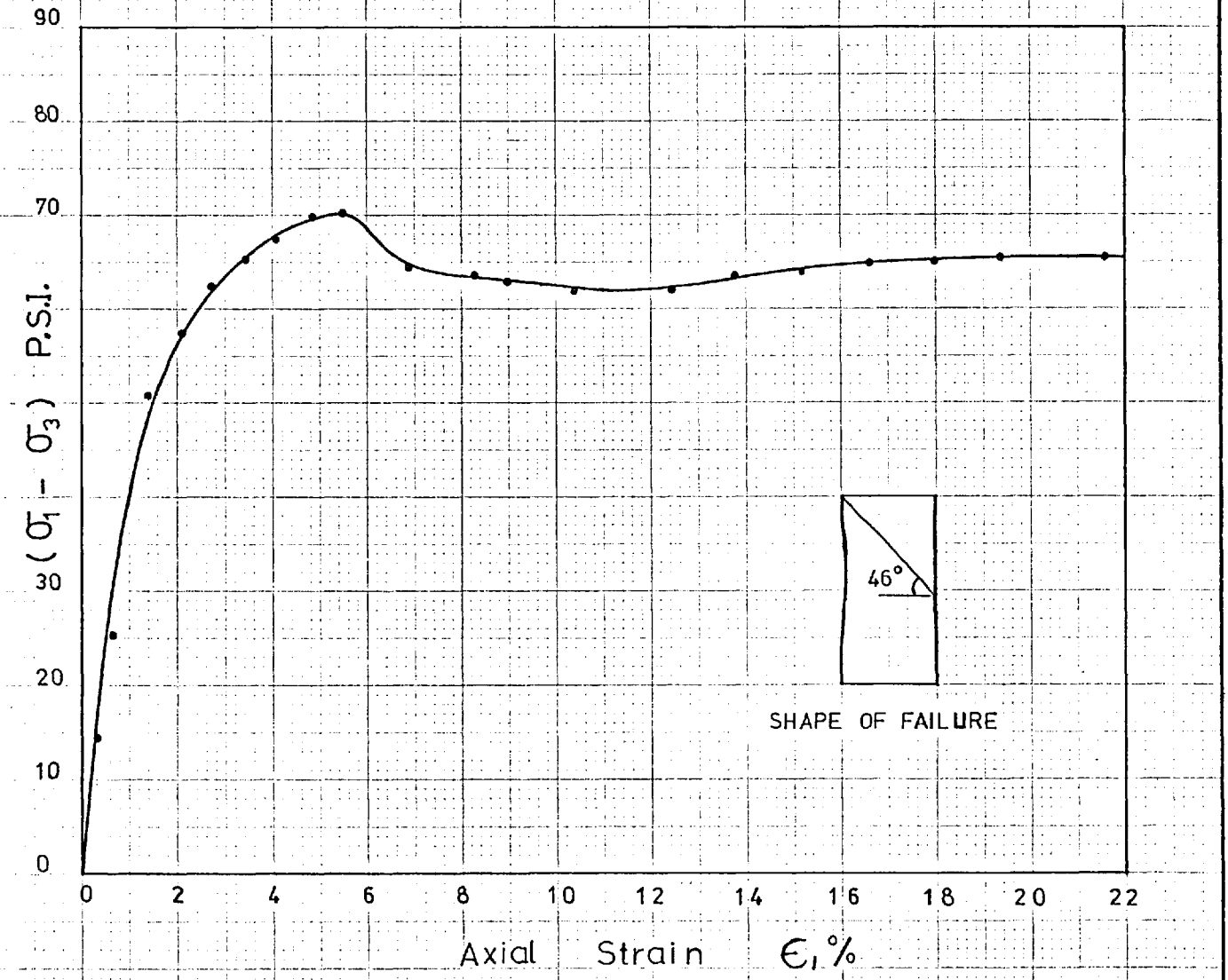

FIG(11-19)–TEST (17 D). KAOLIN CONSOLIDATED AT σ_3 = 125 PSI AND U = 0, THEN SHEARED UNDRAINED WITH σ_3 = 125 PSI.

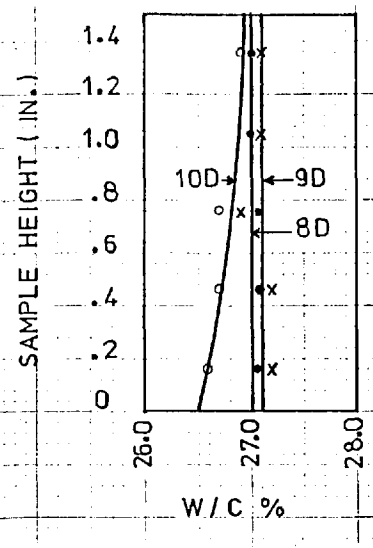

W/C DISTRIBUTION THR. THE SAMPLE

TEST NO.	INITIAL W/C	FINAL W/C	C_u/P
8D	42.0%	27.0%	.285
9D	41.8%	27.1%	.250
10D	42.0%	26.8%	.283

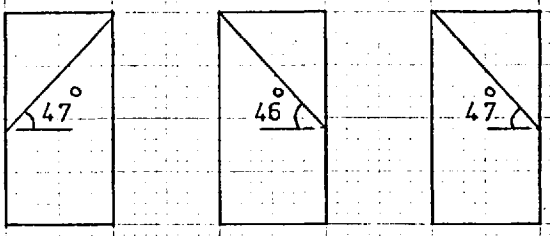

T 8D T 9D T 10D

SHAPE OF FAILURE

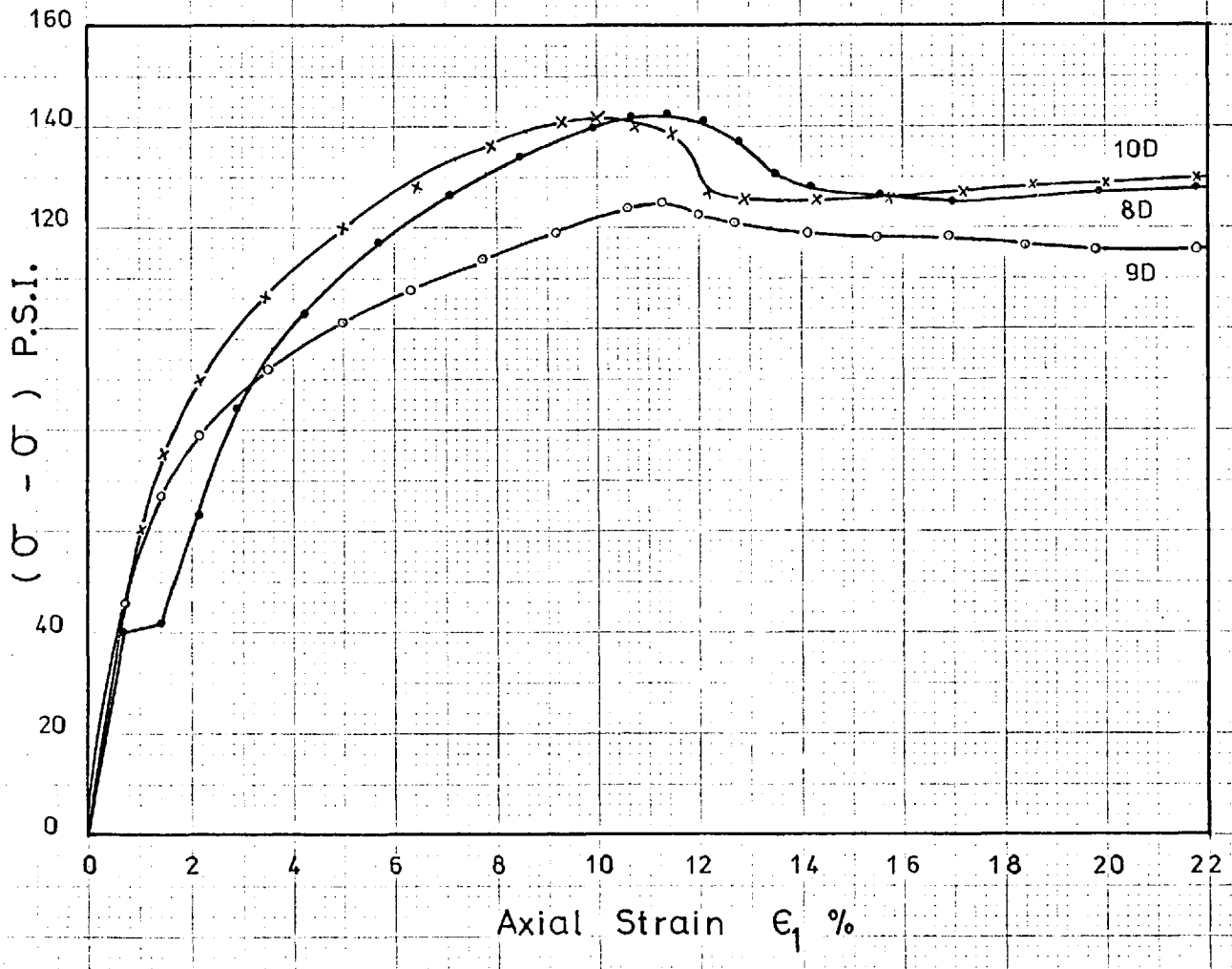

10D

TESTS (8D & 9D). KAOLIN CONSOLIDATED AT σ_3 = 250 P.S.I. AND U = 0 , THEN SHEARED UNDRAINED WITH σ_3 = 250 P.S.I

FIG 11 - 20

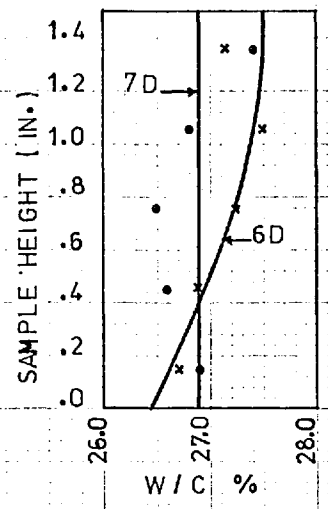

W/C DISTRIBUTION THR. THE SAMPLES

TEST NO.	INITIAL W/C	FINAL W/C	C_U/P
6 D	42.9 %	27.2%	.222
7 D	43.0%	26.9%	.244

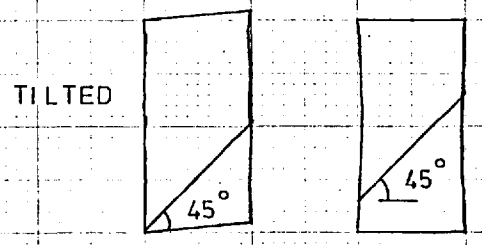

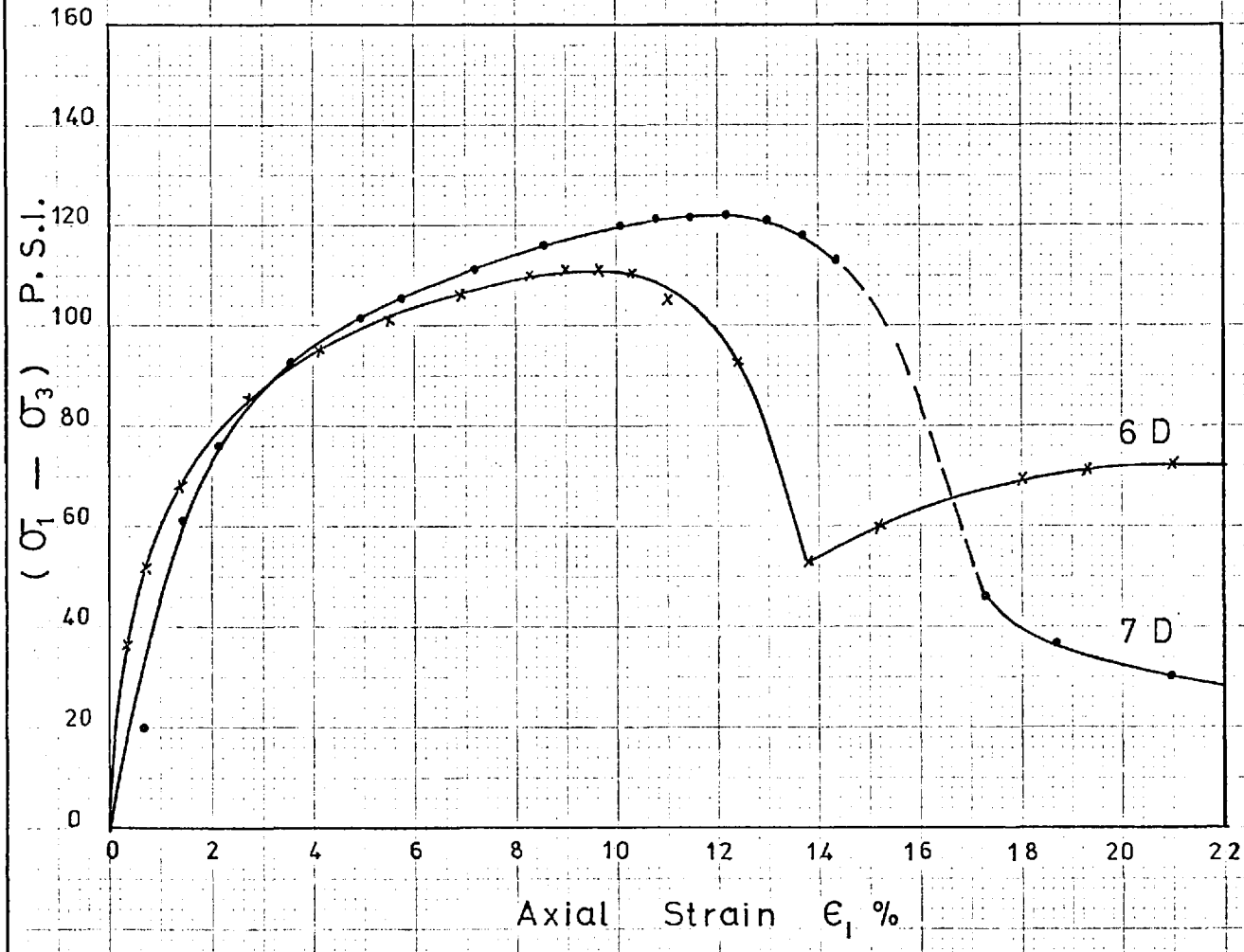

FIG. (11-21) - TESTS (6 D & 7 D). KAOLIN CONSOLIDATED AT σ_3 = 250 P.S.I. & U = 0, THEN SHEARED UNDRAINED WITH σ_3 = 0 P.S.I.

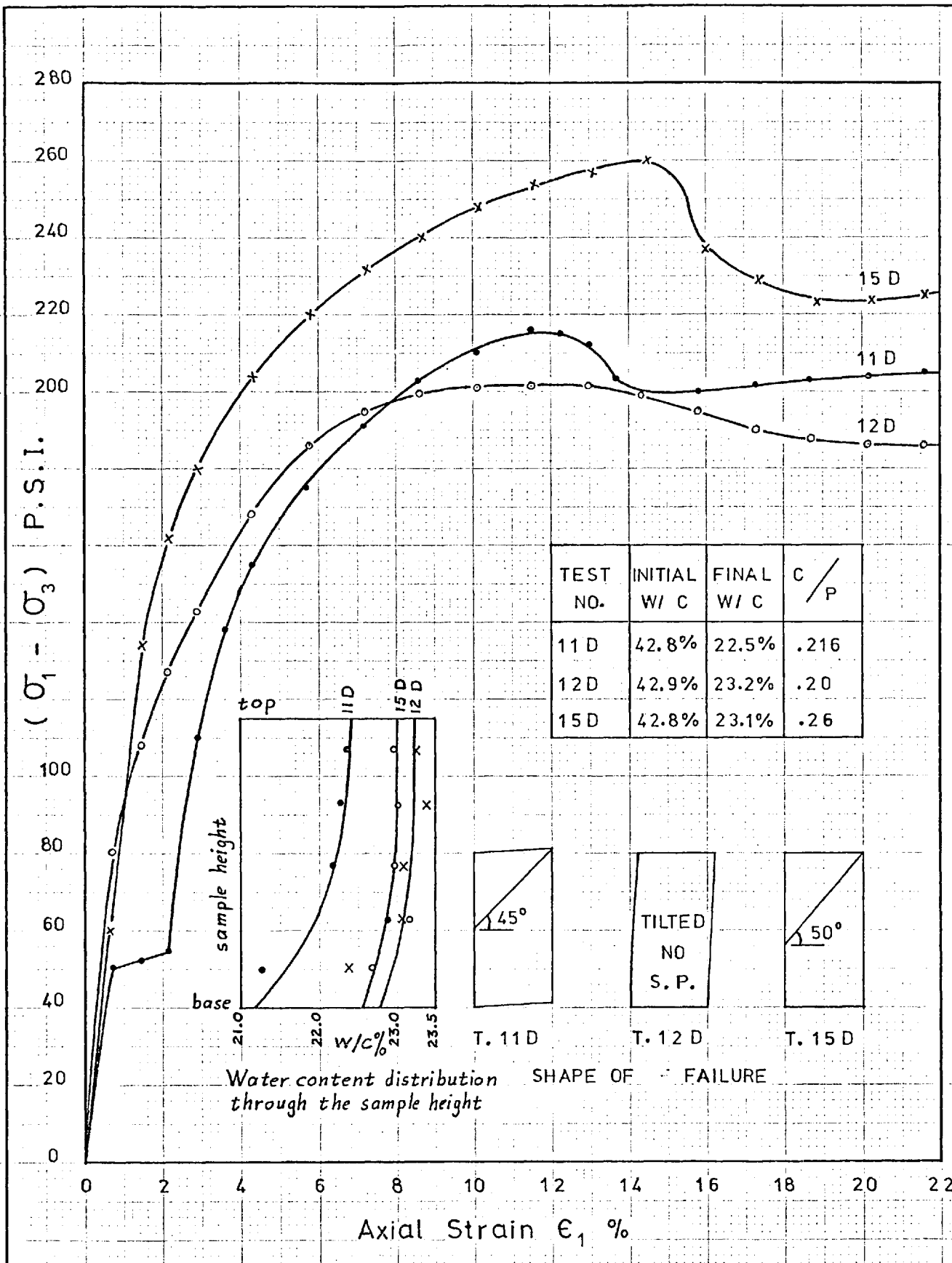

TESTS (11D, 12D & 15D) · KAOLIN CONSOLIDATED AT σ_3=500 P.S.I. & U = 0, THEN SHEARED UNDRAINED WITH σ_3 = 500 P.S.I.

FIG 11-22

INITIAL W/C	42.2 %
FINAL W/C	23.2 %
c_u/p	0.15

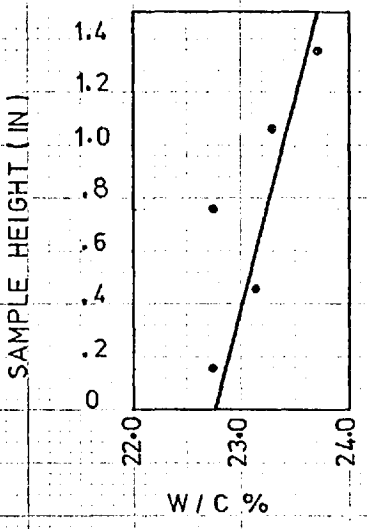

W/C DISTRIBUTION THR. THE SAMPLE

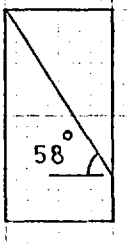

SHAPE OF FAILURE

TEST (4D). KAOLIN CONSOLIDATED AT $\sigma_3 = 500$ P.S.I AND U = 0, THEN SHEARED UNDRAINED WITH $\sigma_3 = 0$ P.S.I.

FIG 11 - 23

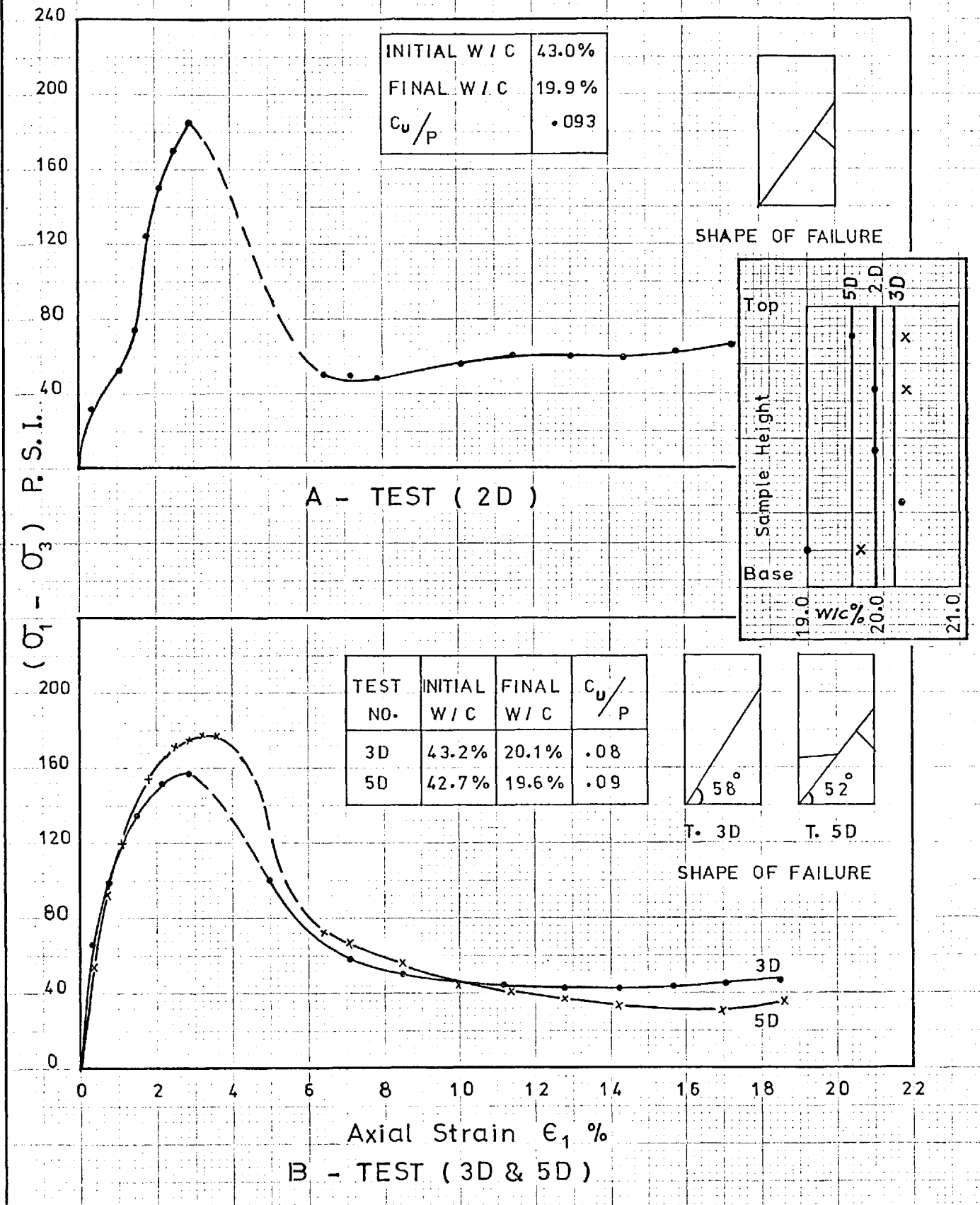

TESTS (2D, 3D & 5D). KAOLIN CONSOLIDATED AT σ_3=1000 P.S.I. & U = 0, THEN SHEARED UNDRAINED WITH σ_3 = 0 P.S.I.

FIG 11 - 24

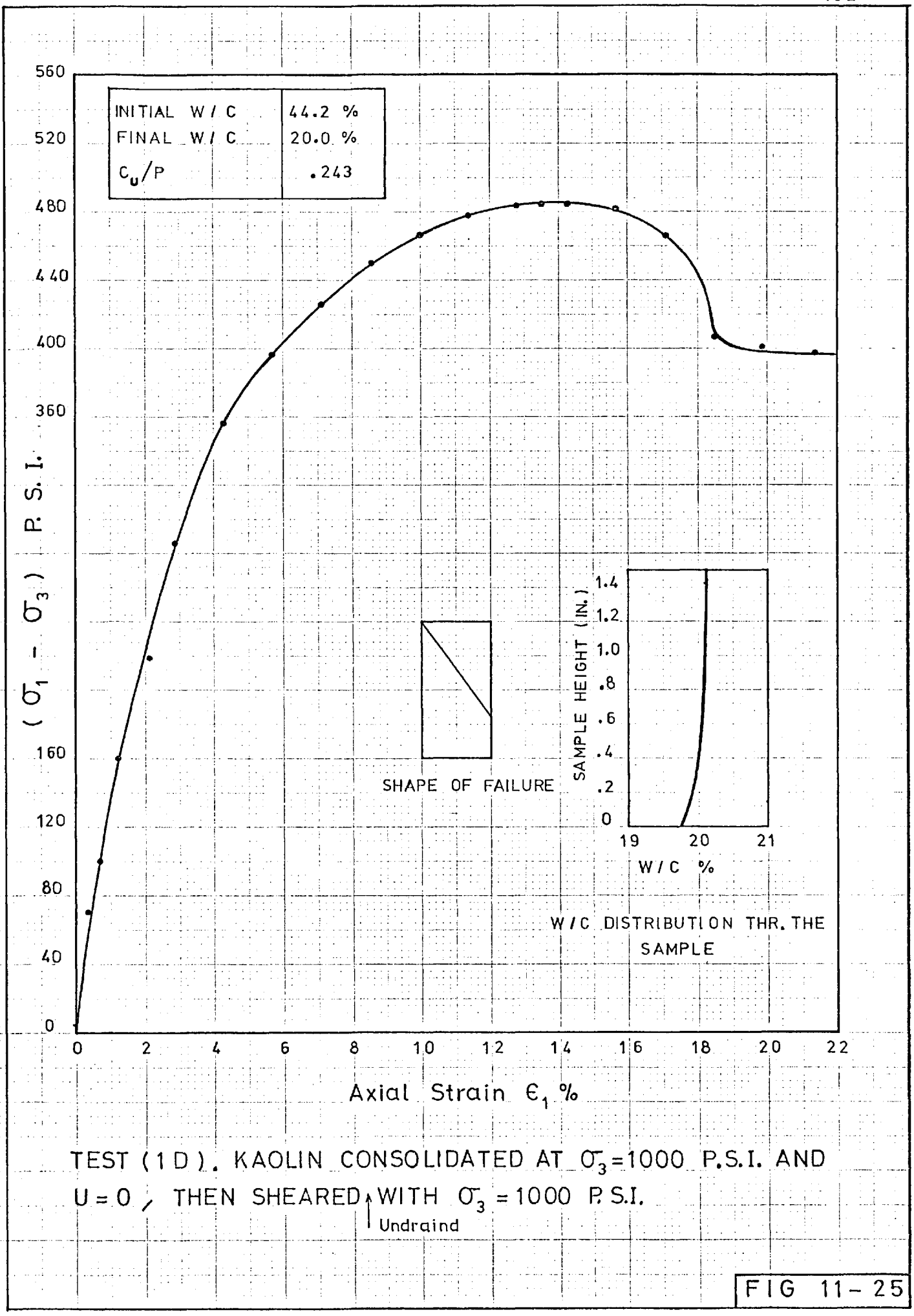

TEST (1D). KAOLIN CONSOLIDATED AT σ_3=1000 P.S.I. AND U=0, THEN SHEARED ↑ WITH σ_3 = 1000 P.S.I.
Undraind

FIG 11-25

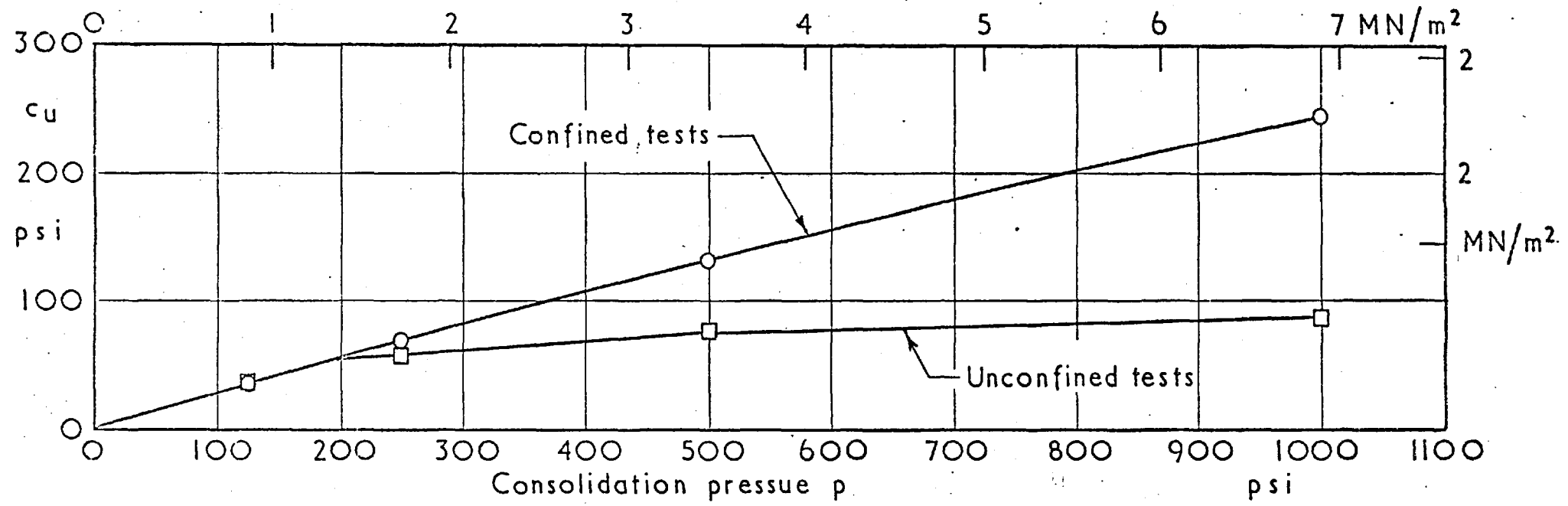

RELATIONSHIP BETWEEN UNDRAINED STRENGTH c_u & CONSOLIDATION PRESSURE p FOR CONFINED & UNCONFINED TESTS ON KAOLIN. WHERE A NUMBER OF TESTS WERE PERFORMED AT A PARTICULAR PRESSURE THE AVERAGE VALUE IS PLOTTED

FIG 11-26

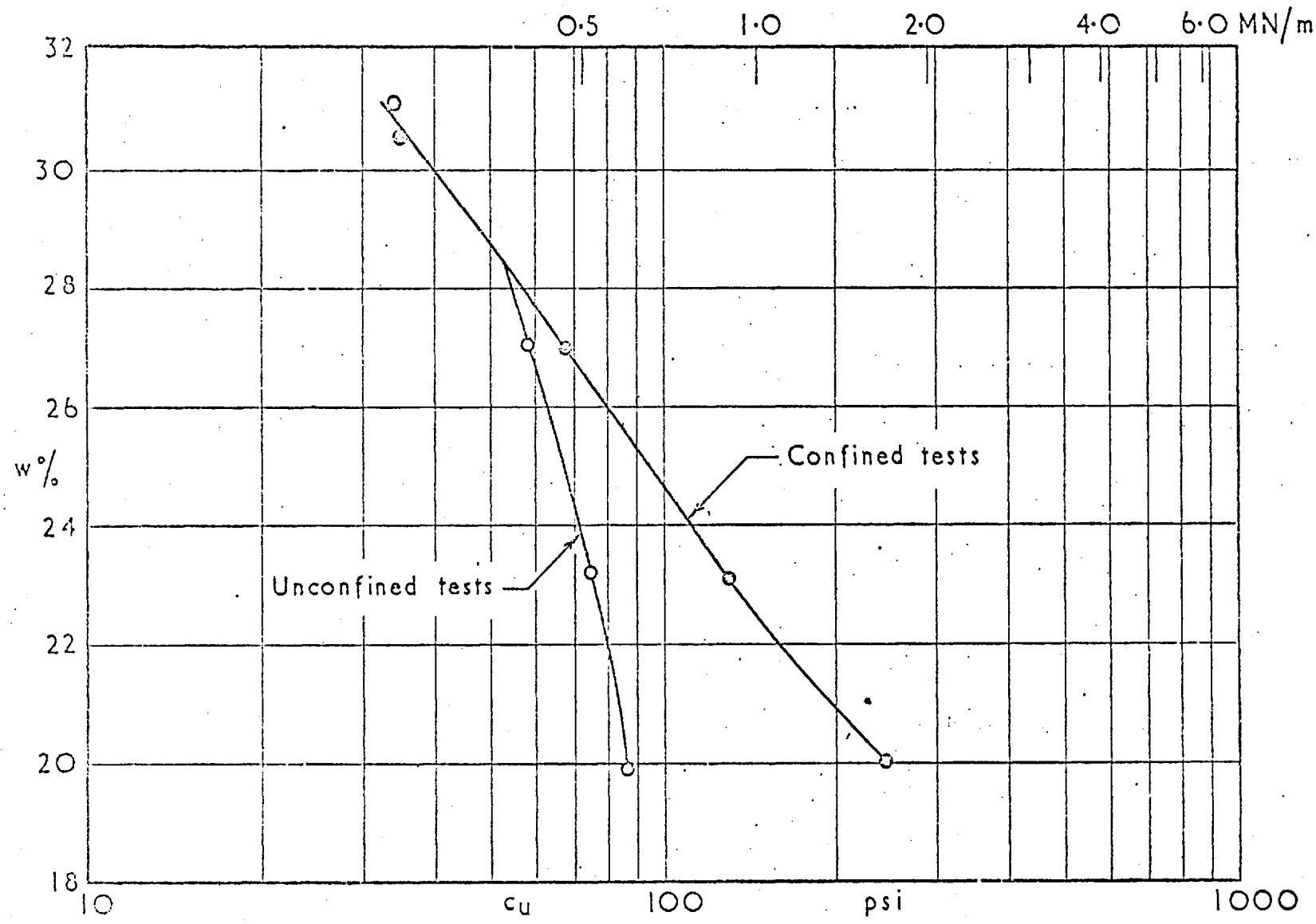

FIG 11-27

RELATIONSHIP BETWEEN UNDRAINED STRENGTH c_u & WATER CONTENT w FOR CONFINED TESTS & UNCONFINED TESTS ON SAMPLES CONSOLIDATED BY EXTERNAL PRESSURE: KAOLIN

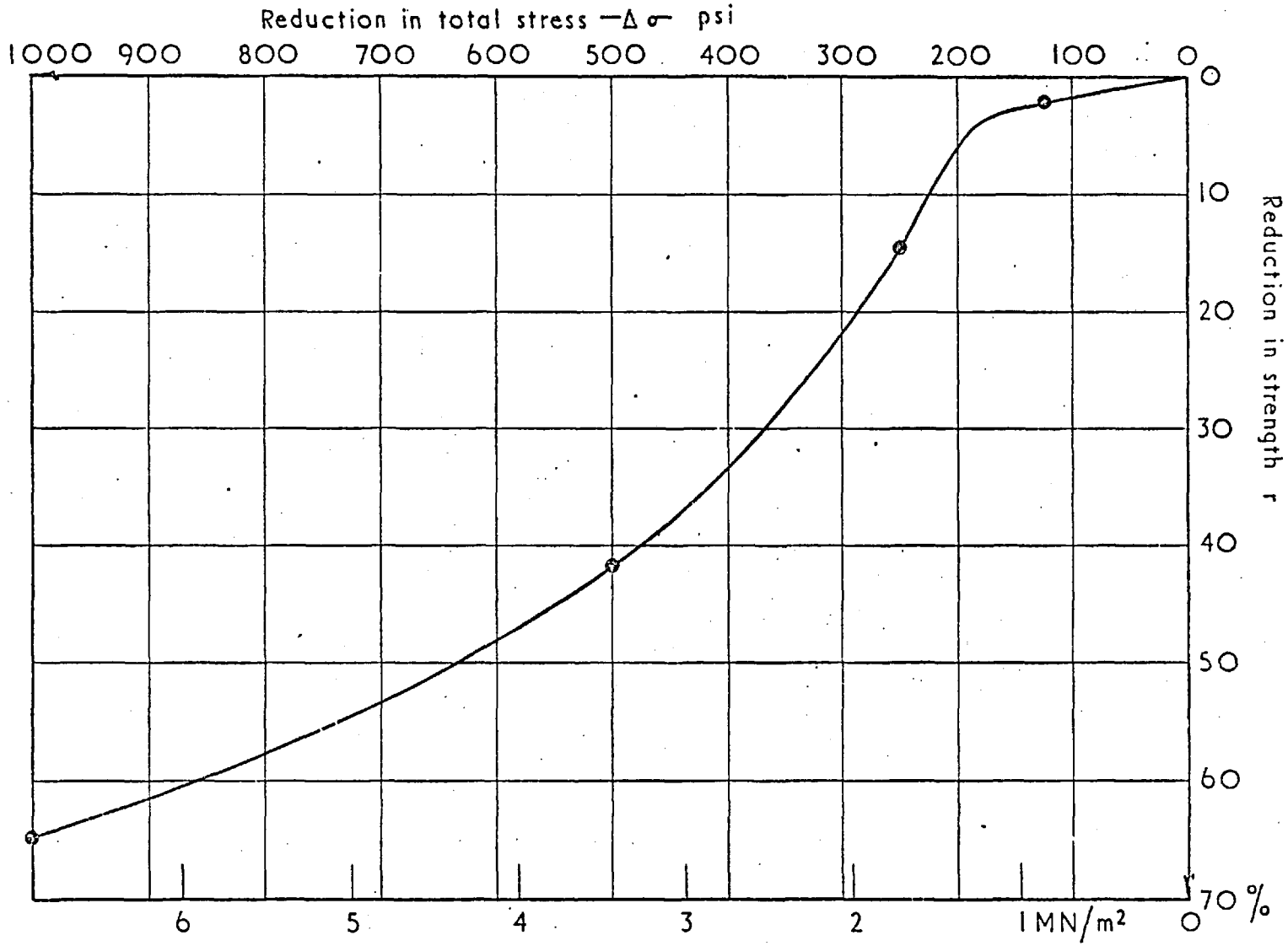

FIG 11-28

RELATIONSHIP BETWEEN REDUCTION IN STRENGTH r & REDUCTION IN TOTAL STRESS —Δσ:
OBSERVED VALUE FROM TESTS ON KAOLIN; INITIAL PORE WATER PRESSURE = 0

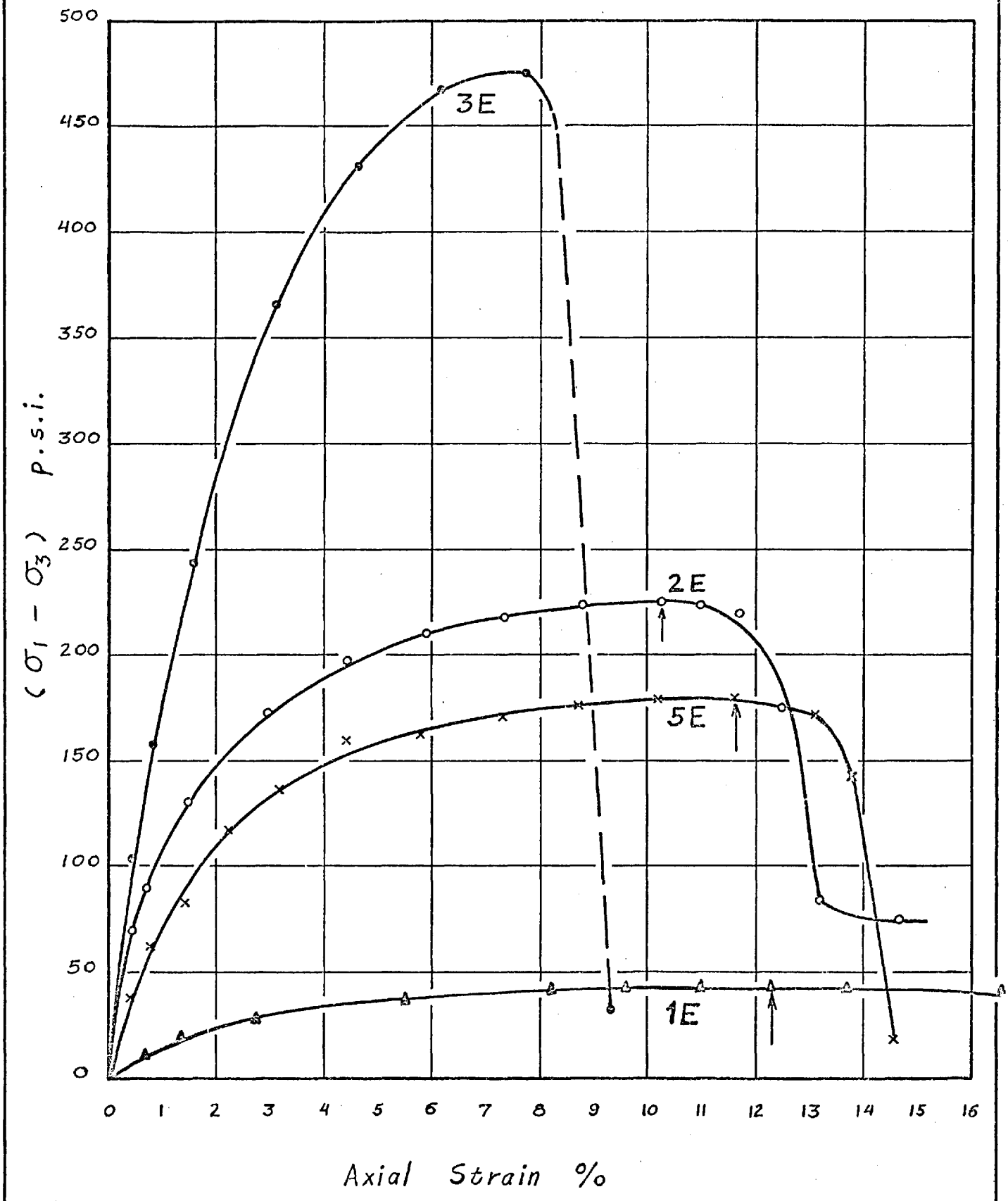

LONDON CLAY – UNCONFINED COMPRESSION TESTS

1E, 2E, 3E AND 5E

FIG 11 - 29

* Oven dry sample

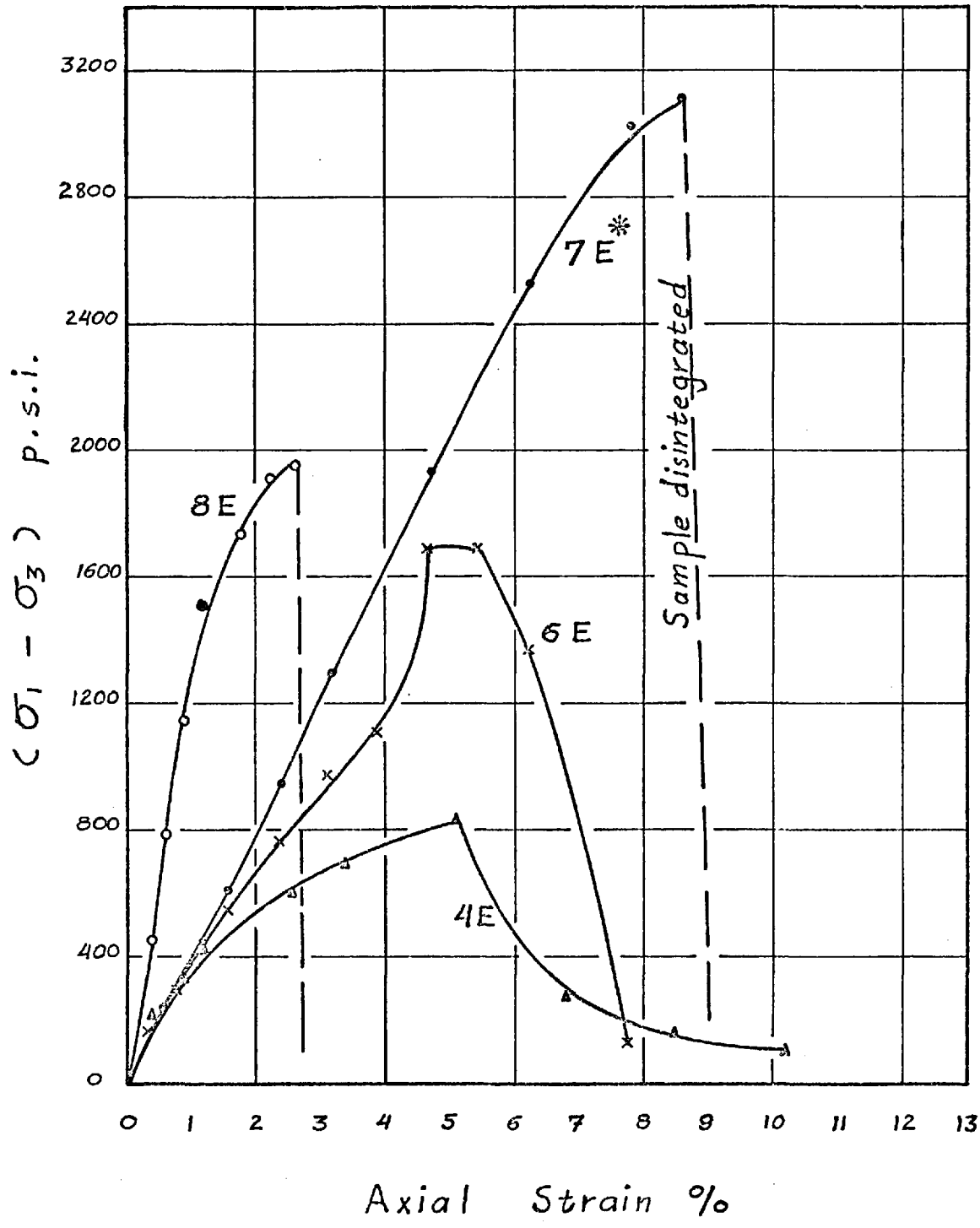

LONDON CLAY — UNCONFINED COMPRESSION TESTS

4E, 6E, 7E AND 8E

FIG 11-30

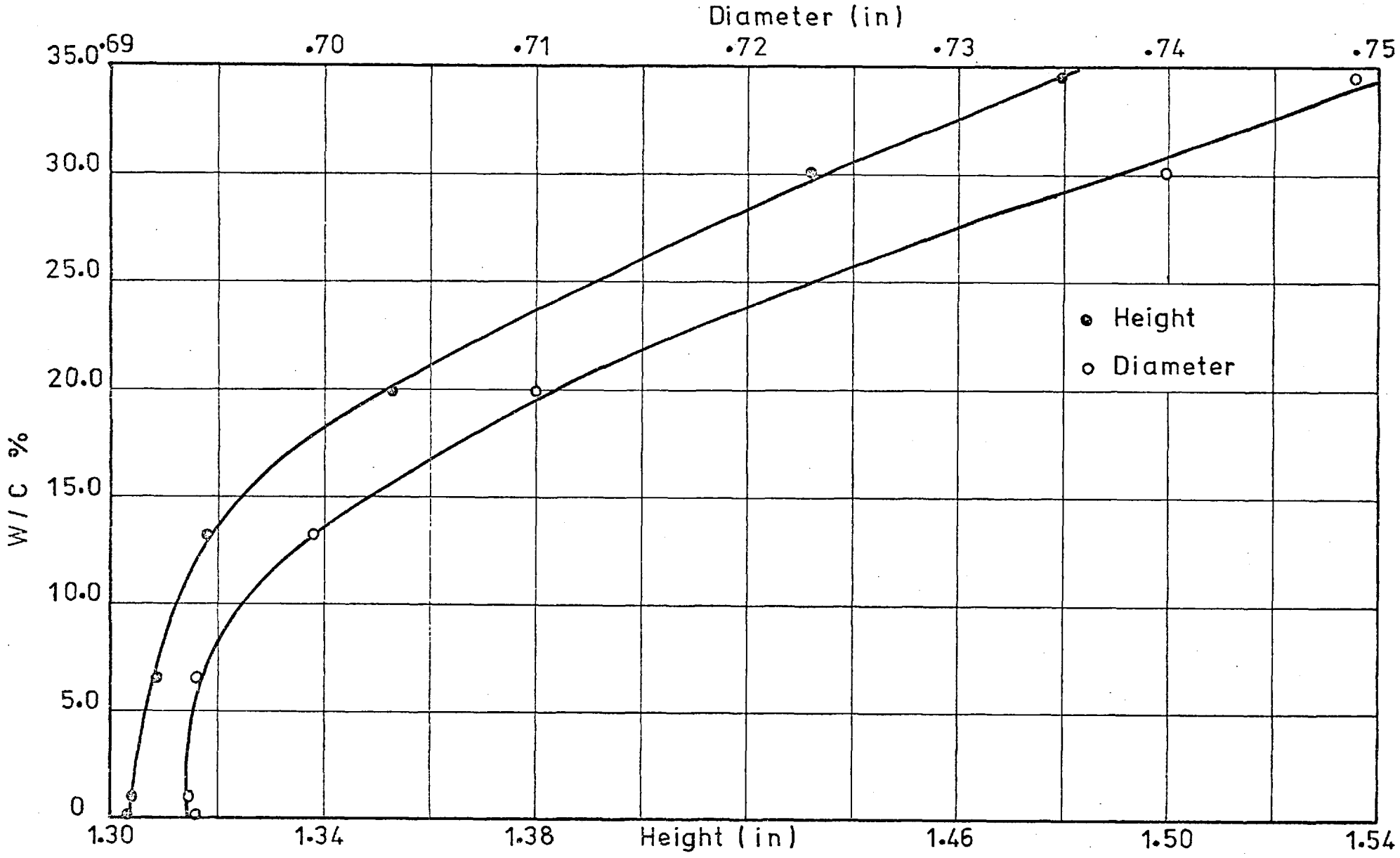

TEST 25B _ LONDON CLAY

FIG 11 - 31

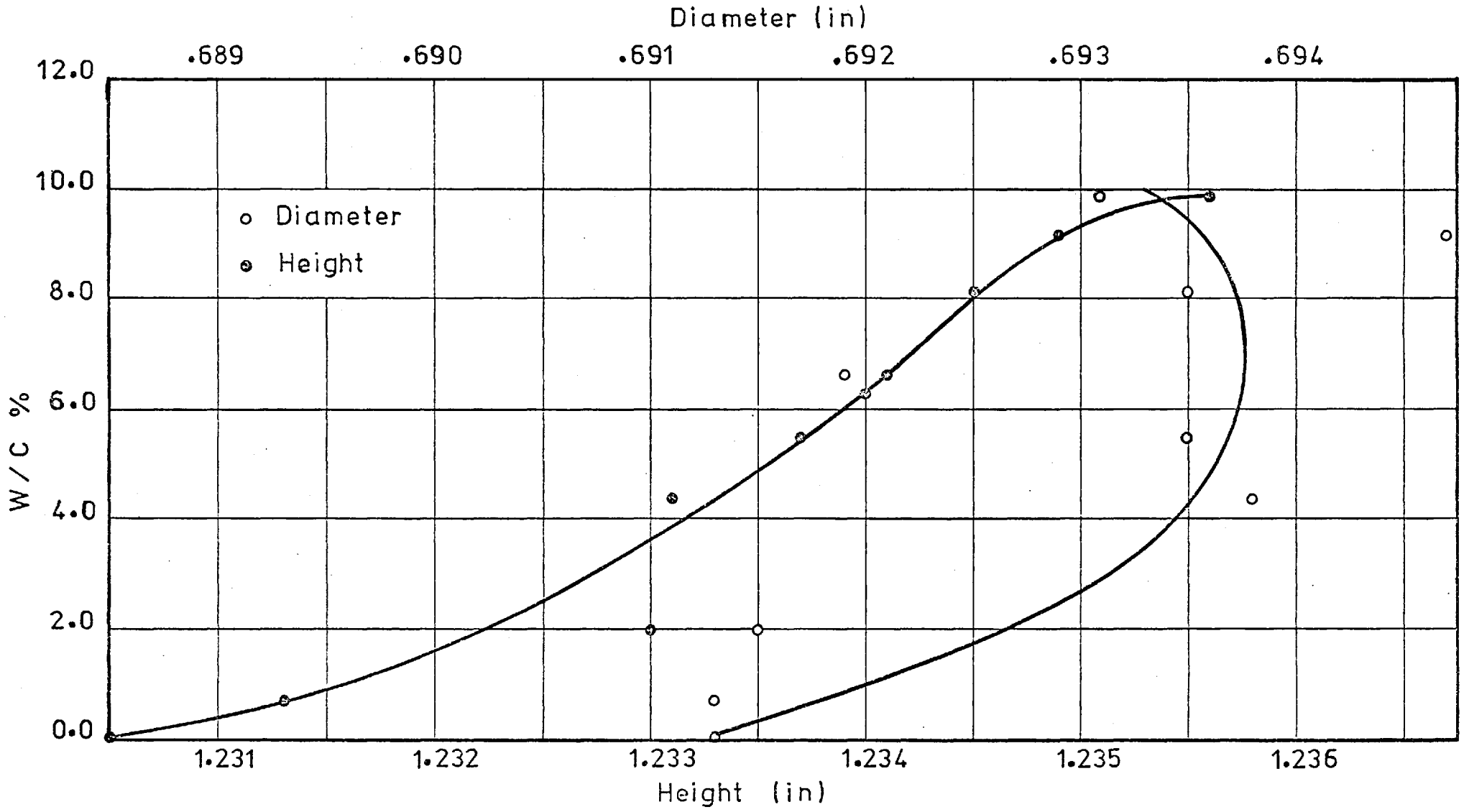

TEST 23B_ LONDON CLAY PRECONSOLIDATED IN THE TRIAXIAL CELL AT σ'_3 = 9000 P.S.I.

FIG 11 - 32

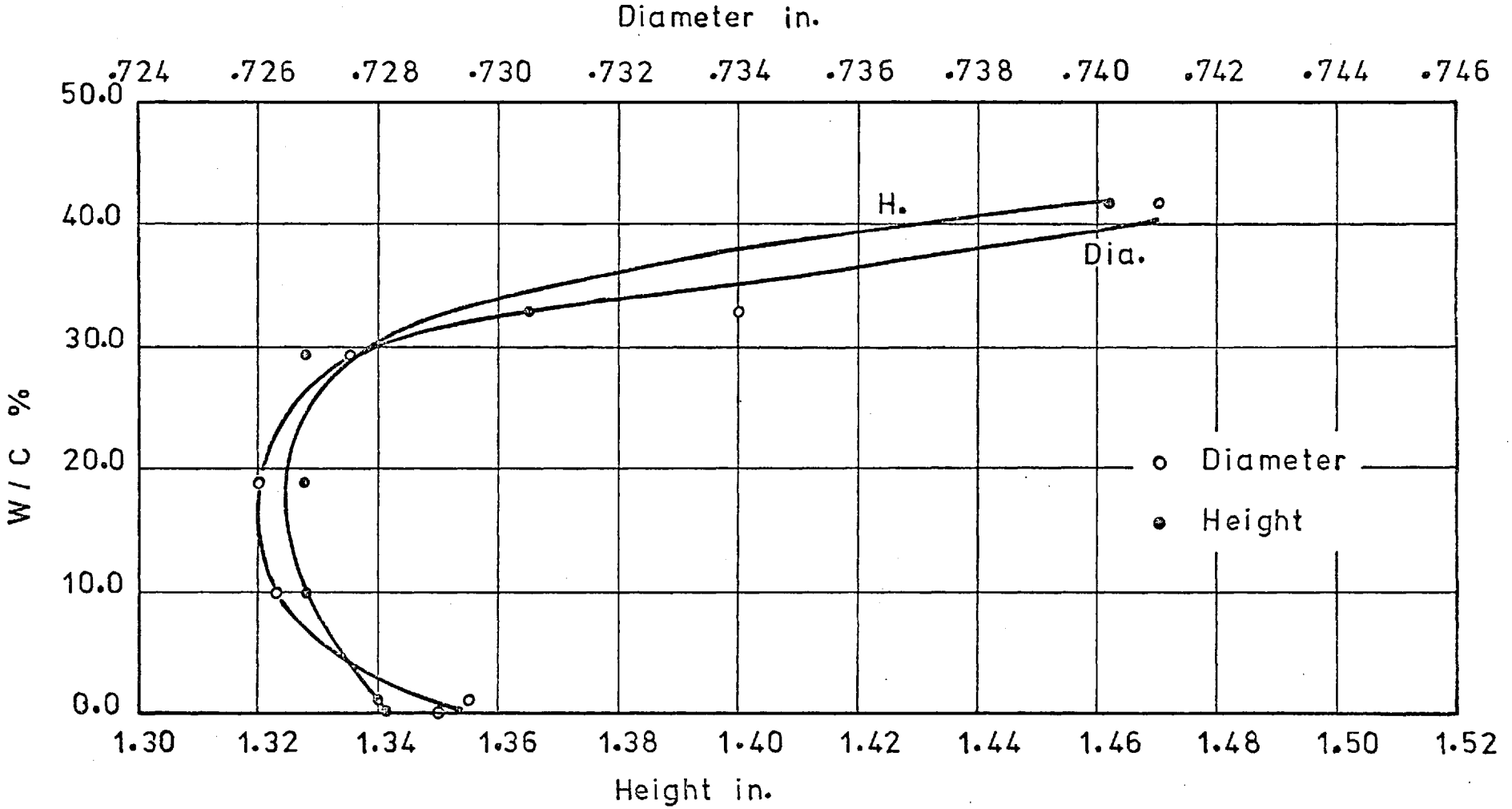

TEST 14D _ KAOLIN

FIG 11 - 33

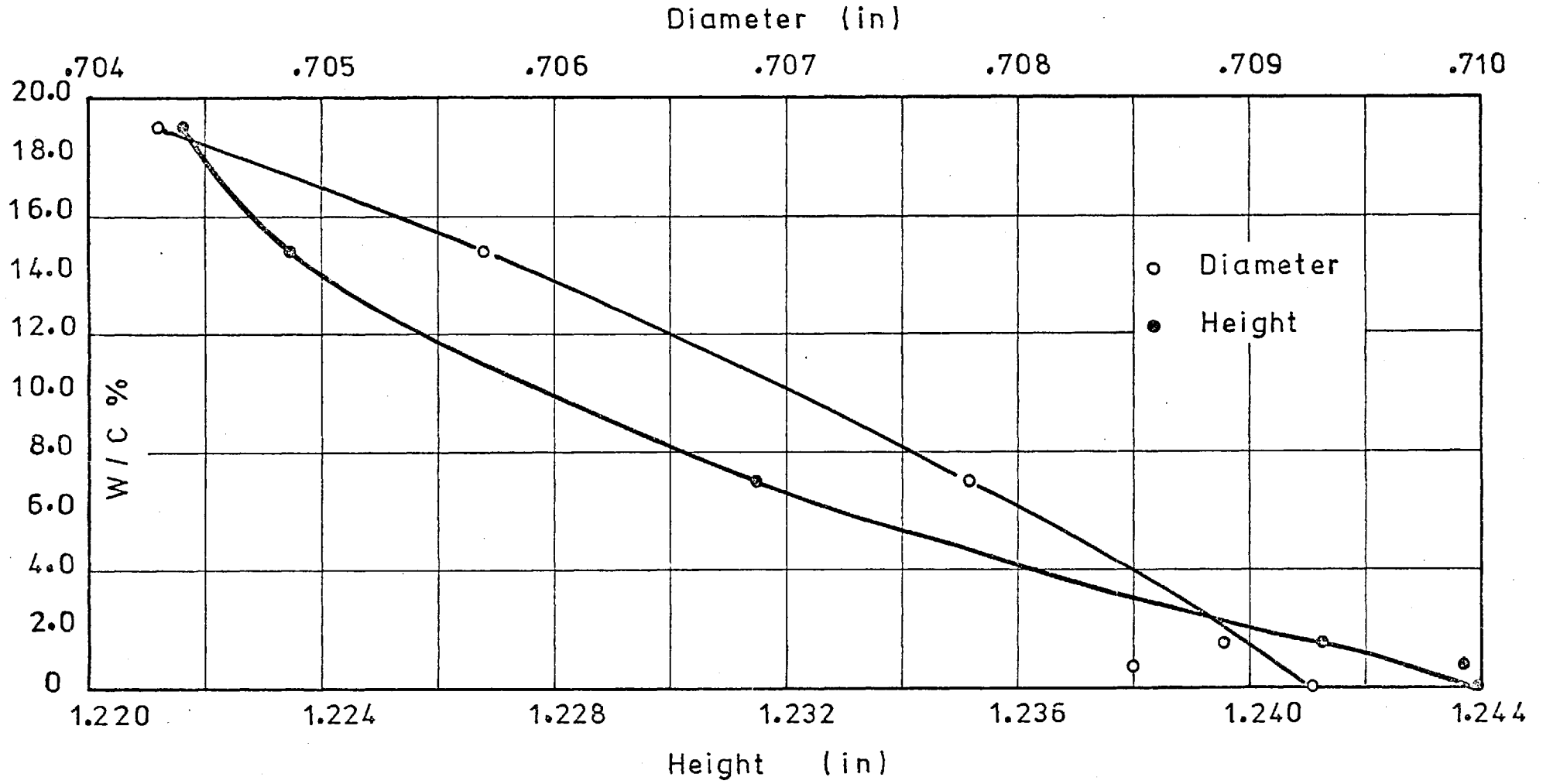

TEST 13D - KAOLIN PRECONSOLIDATED IN THE TRIAXIAL CELL AT σ'_3 = 1000 P.S.I.

FIG 11-34

CHAPTER XII

DISCUSSION OF RESULTS AND CONCLUSIONS

12.1 The Influence of Pore Water Tensions on the Undrained Strength of Clays

In this section the results dealing with the influence of pore water tensions on the undrained strength of clays will be discussed, while in a subsequent section further effects of pore water tensions on the strength properties will be commented on.

The results of tests presented in the previous chapter in which reductions in confining pressure resulted in pore water tensions of various magnitudes showed clearly that a tensile component in the pore-water pressure is capable of replacing, with respect to its mechanical effects, an externally applied confining pressure up to a value of about 3000 psi in the case of London clay and about 200 psi in the case of Kaolin.

At pore water tensions smaller than these limiting values the reduction in peak strength with confining pressure is a minor effect, of a similar order of magnitude to that noted by Kumapley (1969), for saturated soils in the positive pore pressure range (this was discussed in Section 9.3.5). However, there is a very significant change in the shape of the stress-strain curve after the peak (for example, London clay with an induced pore water tension of 965 psi before shear, Figures (11-3) and(11-4)). This indicates that high pore water tensions result in greatly increased brittleness. As the value of the induced pore water tension becomes higher, the failure mechanism of the sample becomes more brittle. Then at the highest induced pore water tension of 7200 psi (Bx 9000 psi) the sample was crushed like a piece of solid rock.

The loss in strength at larger cell pressure reductions (i.e. larger than the limiting values mentioned earlier) indicates a failure of the pore water to sustain higher tensions without a departure from the condition of full saturation. This will be confirmed, in a subsequent section, by the observed volume changes in a number of special tests.

In the case of London clay the implied tensile stress in the pore water was above any value obtained by direct experimental measurement (for example, Temperley and Chambers, 1946; Temperley, 1946)*. If this were the case the pore water would have failed in tension although its value is below the theoretical value of tensile strength of water†. However, the low value of breakdown pressure obtained for Kaolin, 200 psi, suggests that it is not a case of tensile failure in the pore water, but of the rupture of a miniscus in a capillary whose diameter is related to the effective pore size of the clay. Thus it is necessary to examine the pore size of the material tested.

The capillary rise hc is given by the expression (e.g. Terzaghi and Peck, 1967):

$$hc = \frac{2Ts}{r\,\gamma_w} \cdot \cos\alpha \qquad \ldots\ldots \qquad (12.1.1.)$$

where γ_w denotes unit weight of water

Ts denotes surface tension

α denotes contact angle

r denotes radius of capillary.

Thus the capillary pressure is inversely proportional to the equivalent pore diameter, and the equivalent pore diameters for Kaolin and London clay would therefore be expected to have a ratio of approximately 2820: 200 which is equivalent to 14 to 1.

The equivalent pore diameters can be calculated from the permeabilities of the clays at the appropriate stress levels. The permeability K can be calculated from the coefficient of consolidation c_v

---

* It has been shown in Section 9.2.2 that Temperley (1946), measured the tensile strength of water using Berthelot tubes. He obtained values between 20 and 60 atmospheres with an average value of 32 atmospheres (470 psi).

† Temperley (1946), suggests a theoretical value for the tensile strength of water between 500 and 1000 atmospheres while Green (1951) suggests a lower theoretical value of only 2800 psi.

and the compressibility observed during the consolidation stage. This could be done by using the Terzaghi expression (Terzaghi, 1943):

$$c_v = \frac{K}{\gamma_w m_v} \quad \ldots\ldots \quad (12.1.2)$$

where c_v denotes coefficient of consolidation

m_v denotes compressibility and is replaced by C for equal all-round stress change.

Thus the permeability of the clay can be calculated at the required stress level from the values of c_v available from the consolidation tests. For this reason the values of c_v and m_v for both London clay and Kaolin are plotted in Figures (12-1) and (12-2) respectively. The previous method of calculation yields values of permeability of $2.55 - 2.80 \times 10^{-8}$ cm/sec for Kaolin at a consolidation pressure of 200 psi and 0.49×10^{-10} cm/sec for London clay at a consolidation pressure of 3000 psi.

A relationship between the permeability K and the equivalent pore diameter was suggested by Taylor (1948), in a short form, as follows:

$$K = \beta \cdot D^2 n \quad \ldots\ldots \quad (12.1.3)$$

where β is a constant which includes a shape factor

D denotes the equivalent pore diameter

n denotes the porosity of the material.

At the limiting pressures under discussion (200 psi and 3000 psi) the values of the porosity for both Kaolin and London clay are 0.43 and 0.28 respectively. Assuming β to be the same for the two materials, thus the ratio of the equivalent pore diameter of the Kaolin to that of London clay is approximately 19 to 1 (in the range 18.4 to 19.3). This is in reasonably close agreement with the ratio of 14 to 1 obtained by the assumption that the breakdown pressure is controlled by capillarity as explained earlier. However it is not expected to reach a very close agreement between the results of the two approaches, since

(i) the relationship between equivalent pore diameter and permeability will be subject to the influence of surface forces and thus dependent on clay mineralogy and stress level,

(ii) for a given pore size distribution the "equivalent diameter" controlling the two phenomena need not necessarily be the same.

The equivalent pore diameter can be estimated from equation (12.1.1) for both Kaolin and London clay. In the cases under consideration the values of equivalent pore diameter obtained are $2.06 \times 10^{-1}\,\mu$ and $1.46 \times 10^{-2}\,\mu$ for both Kaolin and London clay respectively. The value of the equivalent pore diameter obtained above is in the range of values obtained from shrinkage tests by Holmes (1955), who gives $2.3 \times 10^{-2}\,\mu$ and $0.9 \times 10^{-2}\,\mu$ for two clays with marked swelling characteristics and of similar clay mineralogy to London clay.*

In summary, it has so far been shown that up to a limiting pore water tension, the sign of the pore water pressure has little influence on the shear strength, but a pronounced influence on the shape of the post-peak part of the stress-strain curve. The value of the limiting pore water tension varies with the type of clay and correlates with equivalent pore diameter in a way similar to capillary tension.

---

* The clay minerals in London clay consist mainly of illite and kaolinite, with small amounts of montmorillonite. The clay fraction of the two clays tested by Holmes ranges from 64% to 65%.

12.2 Volume Changes and Water Contents of Samples Subjected to Consolidation, Undrained Stress Release and Drying

It has already been pointed out, Section 11.4 that many samples were subjected to reduction in total stress large enough to cause partial saturation. For samples under such testing conditions, passages filled with water vapour and gas will propagate within the sample. In a clay with a relatively high expansibility there is no reason to believe that there will be a macroscopic migration of water relative to the sample boundaries and there is no significant experimental evidence of migration from the water content determinations at the end of the tests. In fact it is difficult to find whether the passages propagate from the external boundaries of the sample or from internal nuclei as well, especially with small samples.

There is no doubt that some air will have been in solution in the pore water in all the tests during the preparation of the samples. The total volume of the gas-filled voids can be calculated from the volume of the sample and its water content after the release of the stress applied to the sample. But after compression testing the samples were fractured into pieces, especially at very high confining pressures, and therefore accurate volume change measurements are almost impossible under such conditions. For this reason samples of London clay and Kaolin were consolidated in the triaxial cells (London clay samples at 9000 psi and the Kaolin at 1000 psi) then removed from the cells without testing, for immediate volume determination. A series of such observations was continued while the samples were allowed to dry slowly. These are the shrinkage limit tests described earlier and the results were presented in Section 11.6. Those results are summarized in Figures (12-3) and (12-4).

The void ratio and degree of saturation of the samples at the end of consolidation and after release of the cell pressure can be calculated using expressions given in standard text books on soil

mechanics (e.g. Lambe and Whitman, 1969). The expressions used are:

$$\gamma_d = \frac{G \cdot \gamma_w}{1 + w \cdot G/S} \quad \ldots\ldots \quad (12.2.1)$$

$$\gamma_d = \frac{G \cdot \gamma_w}{1 + e} \quad \ldots\ldots \quad (12.2.2)$$

$$G.w = S.e \quad \ldots\ldots \quad (12.2.3)$$

where γ_d denotes the dry unit weight of the sample,
G denotes the specific gravity of the particles,
e denotes the void ratio
S denotes the degree of saturation,
γ_w denotes the unit weight of water at the relevant temperature,
w denotes the water content of the sample.

From these expressions the void ratio of the saturated sample at the end of consolidation can be obtained from the final water content, and the dry unit weight on removal from the cell can be used to calculate the void ratio after release of the cell pressure.

The above expressions were used to calculate the state of the samples immediately on the release of the cell pressure after the consolidation stage. The sample of London clay consolidated at 9000 psi, expanded approximately by 6.0%, and the percentage air voids was 5.7% and the degree of saturation was 78%. For the sample of Kaolin consolidated at 1000 psi, the corresponding values are: expansion 12.7%, air voids 11.3% and degree of saturation 73%*. Westman (1932) reported comparable results of one dimensional consolidation tests on Georgia Kaolin consolidated to 8280 psi. Westman's results are: expansion 11.6%, air voids 10.4% and degree of saturation 66%.

---

* The calculation of degree of saturation and percentage air voids are subject to a small error due to the variation of γ_w with the induced tensile stress in the water. This error will be discussed in Appendix C.

After the cell pressure had been released and the samples removed from the cell, they showed no significant change in volume with time (before drying started). This would seem to indicate that once cavitation has begun the process is fast and complete.

From Figure (12-3), it can be seen that the London clay sample consolidated at 9000 psi then removed from the cell to dry underwent a small decrease in volume of about 1% which occurred mainly on the removal of the last 5% of water content. While drying from 10% to 5% water content the sample volume was almost constant. In contrast to this, the Kaolin sample showed expansion of 3% on drying, Figure (12-4). These results are consistent with those reported by Westman (1932) on ceramic clays. Westman explained this behaviour by stating that "..., the data obtained could be readily explained by specifying a system of flexible, mechanically weak, solid particles in solid contact with each other." This view of the role of water layers in soil mechanics was also emphasised by Lambe and Whitman (1969).

12.3 Further Examination of the Effect of Undrained Stress Release on the Degree of Saturation.

An assumption made in using equations (12.2.1), (12.2.2) and (12.2.3) was that the specific gravity G of the soil particles remain constant, for the stress range under consideration. On the basis of elastic behaviour, a maximum increase of 0.2 to 0.3% in the unit weight of the solid material would be expected at an effective stress of 9000 psi and $u = 0$*. This increase is not significant as far as the present work is concerned. However, Rieke and Chilingarian (1974) found substantial decreases in the unit weight of soil particles with increasing consolidation pressure. Their method of testing and determining the results has been described by Cebell and Chilingarian (1972), who carried out a series of high pressure consolidation tests.

---

*This is from equation (9) of Bishop (1973).

They assumed that whatever the reduction in total stress, (larger than the reductions in total stress in the present work) the soil remained fully saturated. From the results of the present thesis this assumption must be regarded as incorrect.

Rewriting equation (12.2.1) we get the following relationship:

$$\frac{1}{\gamma_d} = \frac{1}{G\,\gamma_w} + \frac{w}{S\,\gamma_w} \qquad (12.3.1)$$

It can be seen that $G.\gamma_w$ can only be determined from measurements of γ_d and w if assumptions are made about S and γ_w. Assuming S = 1, and γ_w = 1.00 g/cc gives $G.\gamma_w$ = 2.59 g/cc for London clay and 2.22 g/cc for Kaolin at consolidation pressures of 9000 psi and 1000 psi respectively. If instead the values of $G.\gamma_w$ measured at low pressures, of 2.81 and 2.64 are taken to be applicable it leads to values of $S\gamma_w$ of 0.78 and 0.73 g/cc for London clay and Kaolin respectively. If the soil was saturated it would mean that the density of water in the soil voids differed from that of bulk water by 22% for London clay and 27% for Kaolin. This is hardly likely, although the value of γ_w for the 9.8% water content in the London clay and the 19.0% water content in the Kaolin is arguable. Therefore the assumption of partial saturation on stress release is much more acceptable.

12.4 Further Effects of the Pore Water Tensions on Strength Properties of Clays

12.4.1 The Rate of Increase of Unconfined Strength with Consolidation Pressure Above the Limiting Pressure at which Partial Saturation Occurs

Above the limiting pressure discussed earlier (approximately 2820 psi for London clay and 200 psi for Kaolin) a substantial volume increase occurs and the samples behave as an overconsolidated and partly saturated soil. Thus it is difficult to estimate the rate of increase of unconfined strength with consolidation pressure above the limiting pressure. However, several points of interest may be noted.

Bishop (1971) reported results of tests on normally consolidated and lightly overconsolidated remoulded saturated samples of London clay which indicate an almost unique relationship between undrained strength and water content and hence with void ratio. The existence of such relationship could be used to estimate the strength of saturated samples, in the present series of tests, at any given void ratio. In Table (12-1) undrained strengths are given for saturated samples assumed to be tested at the void ratios observed on removal of the confining pressure for both London clay and Kaolin (samples consolidated at the maximum consolidation pressures only, i.e. 9000 psi for London clay and 1000 psi for Kaolin). For London clay this estimated undrained strength is much less than the observed unconfined strength at this void ratio while for Kaolin the estimated and observed strengths are in close agreement.

This difference in strength reflects the importance of the contribution made by true cohesion (as defined by Hvorslev, 1937) to the strength of the two clays. In Table (12-1) values are given of Hvorslev's parameter K^* taken from typical values given by Gibson (1953), together with values of the activity of the clay.†

In Table (12-1) the values of the ratio of the change in the unconfined strength to the change in consolidation pressure $d(c_u)/dp$ are given. It is noted that this ratio is almost linearly related to the value of activity of the clay, if based on average values over the full range of partial saturation observed.

A correlation of the unconfined strength of the samples consolidated in this pressure range with cohesion is also consistent with the work of Schmertmann and Osterberg (1960) who pointed out that the cohesion term reached a peak very early in the tests, while the friction

---

* Hvorslev's parameter K is the ratio of true cohesion to the consolidation pressure.

† The activity of the clay was defined by Skempton (1953).

term required 10 - 20 times the strain to reach its full mobilisation. For London clay the failure axial strains of the unconfined samples* 24B, 21B and 22B (Figures (11-8) and (11-9)) drop to 35 - 45% of the failure strains of the samples tested in the positive pore pressure range. For Kaolin the failure axial strains of the unconfined samples* 4D, 2D, 3D and 5D (Figures (11-23) and (11-24)) drop to 20 - 25% of the failure strains of the samples tested in the positive pore pressure range. This indicates that the contribution of the friction term is reduced in the unconfined tests in which full saturation is not maintained not only due to the reduction in effective stress but due to the reduction in failure strain.

12.4.2 The Increase in Brittleness Associated with Pore Water Tensions

It has been shown in Chapter 11 that both samples of London clay and Kaolin tested after reducing the cell pressure to zero (and thus inducing a negative pore pressure before the beginning of the undrained compression test) showed a rapid reduction in strength after failure amounting almost to brittle failure. This rapid change in the shape of the post-peak part of the stress-strain curve is more pronounced when the pore water tension exceeds the limit at which the samples are no longer fully saturated. It can also be seen from Figures (11-8); (11-9); (11-23) and (11-24) that the unconfined samples show a sudden loss of strength occurring mainly within an additional 1% to 2% of axial strain after the failure. It is also of interest to note (Table (12-2)) that this sudden reduction in strength is more pronounced in the London clay than in the Kaolin. In the London clay this reduction in strength reaches approximately 63% for a cell pressure reduction of 3000 psi while in the Kaolin the reduction in strength does not reach 63% until the limiting pressure has been exceeded by more than 100%.

In contrast to these unconfined samples, the samples tested with the cell pressure maintained equal to the consolidation pressure (and thus the pore pressure is zero at the beginning of the test and positive at failure)

---

* It should be noted that the state of full saturation was not maintained in these unconfined samples.

show a relatively small reduction in strength after failure at the final axial strain achieved in the test, Figures (11-3); (11-6); (11-8); (11-9); (11-19); (11-20); (11-22) and (11-25).

Bishop (1971) defined the brittleness index I_B for undrained tests as:

$$I_B = \frac{(c_u)_f - (c_u)_r}{(c_u)_f} \quad \ldots \quad (12.4.1)$$

where the suffices f and r denote failure (peak) and residual states respectively. The actual value of the brittleness index I_B cannot be found out from triaxial tests due to the limited strains imposed. Furthermore, the top of the sample is not free to move sideways during shearing the sample. The highest value of I_B observed was for London clay samples at 9000 psi consolidation pressure, which was 92.5%, Figure (11-9). On removal of this sample from the rubber membrane after the unconfined testing it fell apart along the rupture surface. This suggests that the true value of I_B was very close to 100% for this sample. Also all the samples with high pore water tensions, and which fell apart after testing, have a brittleness index close to 100%.

12.4.3 The Consolidation of Samples by the Pore Water Tension Associated with Drying

In Section 11.5 there are presented results of unconfined compression tests on samples of London clay consolidated by slow shrinkage and a summary of these results is shown in Figure (11-15). From this figure it is seen that the strengths are lower, for a given water content, than those of samples consolidated by a confining pressure, and tested unconfined (i.e. cell pressure is zero).

At a water content of 19.7% (corresponding to a consolidation pressure of 1000 psi) the strength of a sample consolidated by shrinkage is 75% of that consolidated by a confining pressure. At 13.6% water content (corresponding to 3000 psi) the strength is 61% of that of the sample consolidated by a confining pressure. At a water content of 10.1% (corresponding to 9000 psi consolidation pressure) the strength

is 59% of that of a sample consolidated by a confining pressure and tested unconfined, and only 33% of that of a sample tested under a confining pressure equal to the consolidation pressure.

From the above estimated values it appears that there is no unique relationship between the strength and the water content, even for the unconfined samples at water contents corresponding to consolidation pressures less than the limiting pressure discussed in earlier sections, Figure (11-15). This difference in strength discussed above may be examined with respect to the shrinkage limit test results shown in Figure (12-3). The equation for the saturation lines shown on this figure can be obtained from equation (12.2.1) as follows:

$$\frac{\gamma_w}{\gamma_d} = \frac{1}{G} + \frac{w}{S} \qquad \ldots\ldots \qquad (12.4.2)$$

From Figure (12-3) it is seen that the degree of saturation for a sample following the shrinkage path is 92% at 19.7% water content, 73% at 13.6% water content and 57% at 10.2% water content. These values of the degree of saturation may be compared with 100%, 98% and 78% respectively* for the samples consolidated under a confining pressure and released to zero value. Therefore it seems that the void ratio of the sample following the shrinkage path is higher, at each reference water content, than that of a sample consolidated by a confining pressure and then tested unconfined.

The relationships between the undrained strength (c_u) and the void ratio (e) at the beginning of the compression test for all the London clay samples tested in this programme are shown in Figure (12-5). Two main points of interest can be noticed from this figure:

(i) There is no unique relationship between undrained strength and void ratio at the beginning of the compression test, and that uniqueness is unlikely to be obtained even after correcting for the volume change before reaching failure in compression.

---

* The first two values were estimated from strength changes, Figure (11-15), and the third was measured.

(ii) The sample on the drying curve has a strength of 1557 psi for an initial void ratio of 0.484 and zero water content, while the confined sample consolidated at 9000 psi confining pressure gives nearly the same strength (1723 psi) for an initial void ratio of 0.287 and a water content of 10.2%. If a Poisson's ratio of 0.2 is assumed for the dry sample the void ratio at failure will drop only to 0.407. Thus the difference between the values of the void ratio of the two samples is obvious.

The results of the present unconfined tests on the dry samples can be compared with the data given by Croney and Coleman (1960) who carried out unconfined compression tests on samples of undisturbed London clay dried to known initial suctions. The maximum value of c_u observed was about 550 psi at an implied suction of 100,000 psi and nearly zero water content. This observed value of c_u is only about 35% of the value obtained in the present series of unconfined tests on remoulded London clay of similar index properties. Croney and Coleman's observed low value of c_u may be attributed to the non-uniformity of particle size distribution in natural soil, and to the effects of sample size on strength in an undisturbed soil with a fissured structure.

The high pore water tensions associated with drying in the range of water contents under consideration will not be discussed here; it is outside the scope of this thesis. The behaviour of partly saturated soils has been discussed by many researchers, e.g. Holmes (1955); Bishop (1959); Croney and Coleman (1960); Aitchison (1960); Bishop et al (1960) and Bishop and Blight (1963).

12.5 Implications of the Test Results to Field Behaviour of Clays Subject to Undrained Stress Reductions and to the Choice of Laboratory Test Conditions

In general the state of stress in the ground is not isotropic, and therefore the pore water tensions created due to stress release do not equal the vertical effective stress, even for a B value of one. In normally consolidated clays K_o lies in the range 0.4 to 0.7, depending on the plasticity index. These values are from both laboratory (Bishop, 1959; Simons, 1958) and field determinations (Bjerrum et al, 1972). Using the elastic theory the following relationship is obtained for B = 1:

$$-\frac{u_s}{\sigma'_v} = \frac{(1 + 2 K_o)}{3} \qquad .. \quad .. \qquad (12.5.1)$$

where u_s denotes the pore water tension
σ'_v denotes the vertical effective stress, and
K_o denotes the ratio of the horizontal effective stress to the vertical effective stress.

Substituing the above values of K_o perfect sampling would be expected to give values of $-u_s / \sigma'_v$ of 0.6 to 0.8.

Normally consolidated clay does not behave as a perfectly elastic soil however. Laboratory tests with samples subjected to the stress changes occurring during perfect sampling give lower pore pressure changes, especially in soils of low plasticity (Bishop and Henkel, 1953; Skempton and Sowa, 1963; Ladd and Lambe, 1963). From these results values of $-u_s / \sigma'_v$ in the range 0.35 to 0.75 might be expected for soils obtained from the field.

A far greater reduction in $-u_s / \sigma'_v$ for normally consolidated clay can result from sampling disturbance. Laboratory tests have shown that one application and removal of a shear stress equal to the strength can reduce this ratio by more than 50% (Bishop and Henkel, 1953) while complete remoulding can lead to losses in excess of an order of magnitude (Croney and Coleman, 1960; Bishop, 1960; Skempton and Sowa, 1963). A drop of 80% from the value expected from perfect sampling is suggested

by Ladd and Lambe (1963) to be typical, on the basis of field data using conventional sampling methods.

Heavily overconsolidated clays are in marked contrast however, with values of K_o exceeding unity. Their behaviour approximates more closely that of the assumed ideal elastic material and in fact does not show a significant drop in pore water tensions on remoulding. A single application and removal of shear stress may increase the pore water tensions in a heavily overconsolidated sample (Bishop and Henkel, 1953) which is in contrast to normally consolidated clay. Remoulding may also increase the pore water tensions (Croney and Coleman, 1960). A small but not insignificant reduction in pore water tensions occurs in cutting a small sample from a large block (Skinner, 1975).

Field data from overconsolidated London clay shows the ratio $-u_s/\sigma'_v$ varying from 2.3 to 1.3 east of London (Skempton, 1961) and 2.7 to 1.7 west of London (Bishop et al, 1965). Values of K_o based on these values are 2.8 to 1.5 and 3.4 to 1.7 respectively. Blight (1967) reported higher values of $-u_s/\sigma'_v$ for an expansive clay.

The largest value of pore water tension reported from any of these sites is -110* psi from west London at a depth of 138 ft. For a sample of normally consolidated clay taken in the conventional manner to have a value this high it would need to come from a depth of nearly 1000 metres.

Thus in homogeneous clay of pore size similar to the London clay, or even the Kaolin no difficulty should be found in maintaining full saturation under the residual pore water tensions normally found in practice. However in macrovoids in the clay, or in zones of coarser material, the pore water very probably cavitates. This will also be the case for the pore water in discontinuities such as fissures, joints and bedding planes. Cavitation may result in a substantial reduction in strength or even a complete loss for the unconfined case (Bishop and Henkel, 1962, Figure 66).

* It is measured indirectly.

The reduction in pore water tensions in the more disturbed zones of a borehole sample will result in migration of pore water, at constant overall volume, to the least disturbed zones and thus to a general reduction in strength.

As far as the field behaviour of clay masses is concerned, the two most significant effects of undrained stress release are the increased brittleness and the reduction in strength when the pore water tension causes discontinuity of the pore water in fissures, joints and silty partings.

12.6 Conclusions

(i) The influence on undrained strength of large reductions in confining pressure which result in pore water tensions is very small until a limiting tension is reached above which a departure from full saturation occurs. The value of this limiting tension is about 2820 psi (i.e. 0.94 x 3000) for the London clay and about 200 psi for the Kaolin. This value correlates with equivalent pore diameter in the same way as the limiting capillary tension.

Reductions in confining pressure larger than the limiting tension mentioned above lead initially to rapidly increasing reductions in undrained strength which reach 42% for the London clay and 65% for the Kaolin with the ranges of pressure investigated in this thesis. It should be noted here that the limiting pore water tension and the percentage reduction in undrained strength for a given reduction in total stress are not unique soil characteristics, but will depend on the stress history of the samples. For instance, reductions in confining pressure of 3000 psi and 6000 psi will not lead to the same reduction in undrained strength when applied to a sample consolidated to 9000 psi as when applied to samples consolidated only to 3000 psi and 6000 psi respectively. This is due to initial differences in expansibility and in equivalent pore diameter.

(ii) The increase in unconfined strength with consolidation pressure above the limiting pressure correlates both with the activity of the clay and with the Hvorslev cohesion parameter.

(iii) Samples under high pore water tensions at failure have a very pronounced change in the shape of the post-peak section of the stress-strain curves. The unconfined samples of London clay in particular show a very brittle behaviour and negligible cohesion after rupture. This indicates that undrained residual strength is a function of total normal stress, as suggested by Bishop (1971).

(iv) Samples consolidated by drying do not show the same strength - water content or strength - void ratio relationships as those consolidated by applied pressure at the relatively high pore water tensions examined. This seems to be due, partly, to a departure from full saturation at a much higher water content and thus at a smaller pore water tension than that implied for samples consolidated by an applied cell pressure and tested unconfined. It may also reflect the influence of residual stresses resulting from pore pressure gradients during drying.

(v) The implications of the test results presented in this thesis with regard to the stress release associated with sampling from deep boreholes and shafts in clay strata were discussed in Section 12.5. It can be concluded that the maintenance of full saturation under the residual pore water tensions encountered in normal sampling work should present no difficulty in homogeneous clays of pore size similar to the London clay or even the Kaolin tested in this experimental work. However, the pore water in zones of coarser particles such as silty partings, fissures and joints is likely to cavitate and drain into the adjacent

clay. This could possibly lead to a substantial reduction in strength or a complete loss of the unconfined strength.

(vi) As far as the field behaviour of clay masses is concerned the most significant effects of undrained stress release are the increased brittleness and the reduction in strength when the pore water tension causes discontinuity of the pore water in fissures, joints and silty partings.

TABLE (12 _ 1)

Relationships between the increase in unconfined strength above the limiting pressure, the activity of the clay, and Hvorslev's cohesion parameter.

Material	Consolidation pressure lb/sq inch	Consolidation pressure MN/m^2	Unconfined value of c_u lb/sq inch	Unconfined value of c_u MN/m^2	Strength of saturated sample at same void ratio lb/sq inch	Strength of saturated sample at same void ratio MN/m^2	$d/c_u)/dp$	Activity PI/% clay	Hvorslev κ
London Clay	3000	20.7	586	4.04	-	-	0.069	0.91	0.10*
	9000	62.1	1000	6.89	760	5.24			
Kaolin	250	1.72	58.2	0.40	-	-	0.037	0.44	0.02*
	1000	6.9	86.3	0.60	85.0	0.59			

* Approximate, based on typical values given by Gibson (1953) for the low pressure range.

TABLE (12 _ 2)

Loss in strength for 2% post-peak strain for confined and unconfined tests.

Material	Consolidation pressure		Loss in peak strength when tested unconfined	Confined test - loss in strength for 2% post peak strain	Unconfined test - loss in strength for 2% post peak strain
	lb/sq inch	MN/m^2	%	%	%
London Clay	1000	6.9	0.5 (2)*	1.3	3.2
	3000	20.7	6	0.9	63
	6000	41.4	38	0.4	88
	9000	62.1	42	0.6	87
Kaolin	125	0.86	3	8.6	7.5
	250	1.72	11	6.0	6.6
	500	3.45	42	7.1	63
	1000	6.89	65	1.4	42

* The value of 2% is obtained if the fifth test, which differs substantially from the average, is included.

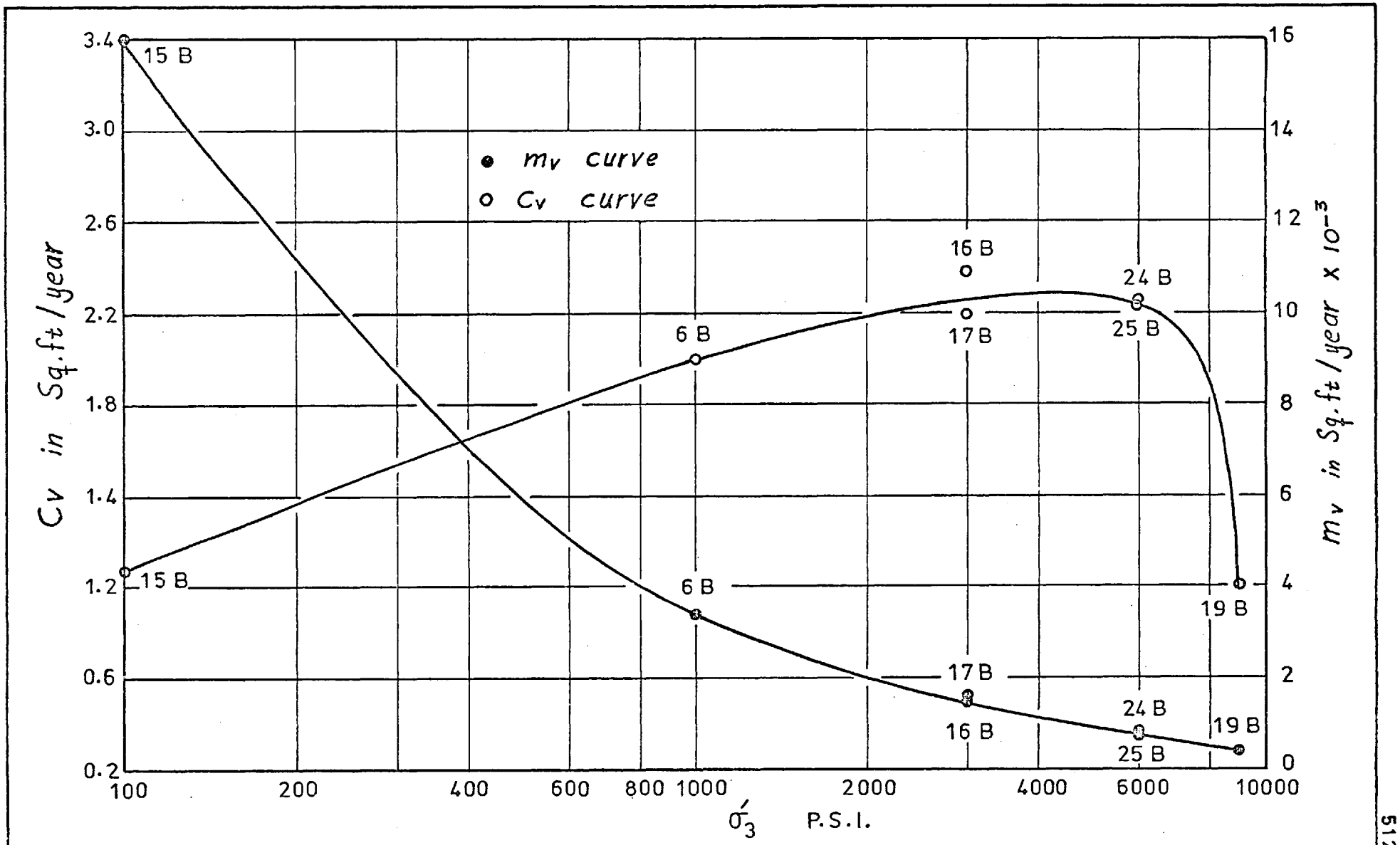

LONDON CLAY — VARIATION OF C_v AND m_v WITH EFFECTIVE CELL PRESSURE

FIG 12-1

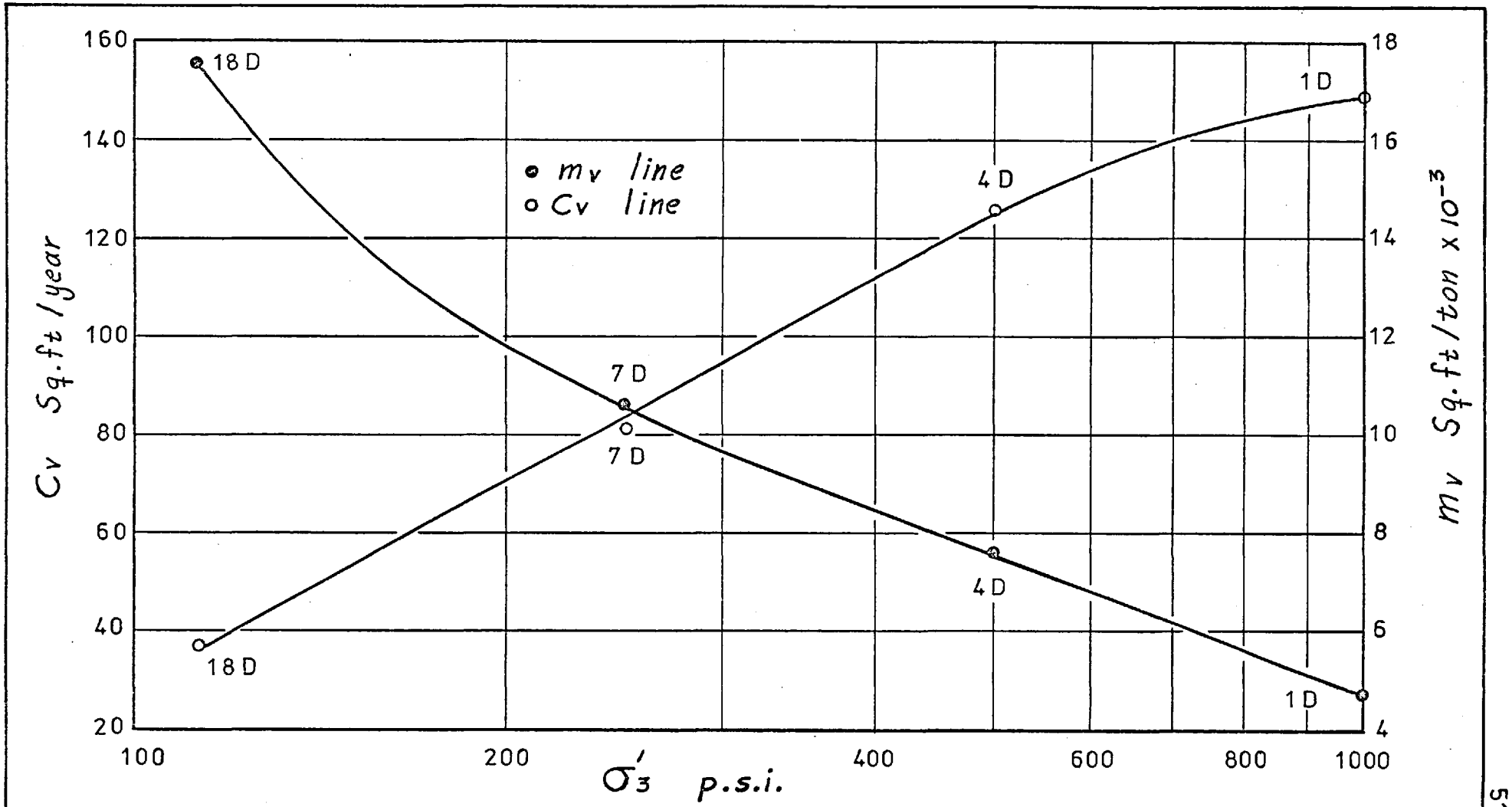

KAOLIN — VARIATION OF C_v AND m_v WITH EFFECTIVE CELL PRESSURE

FIG 12 - 2

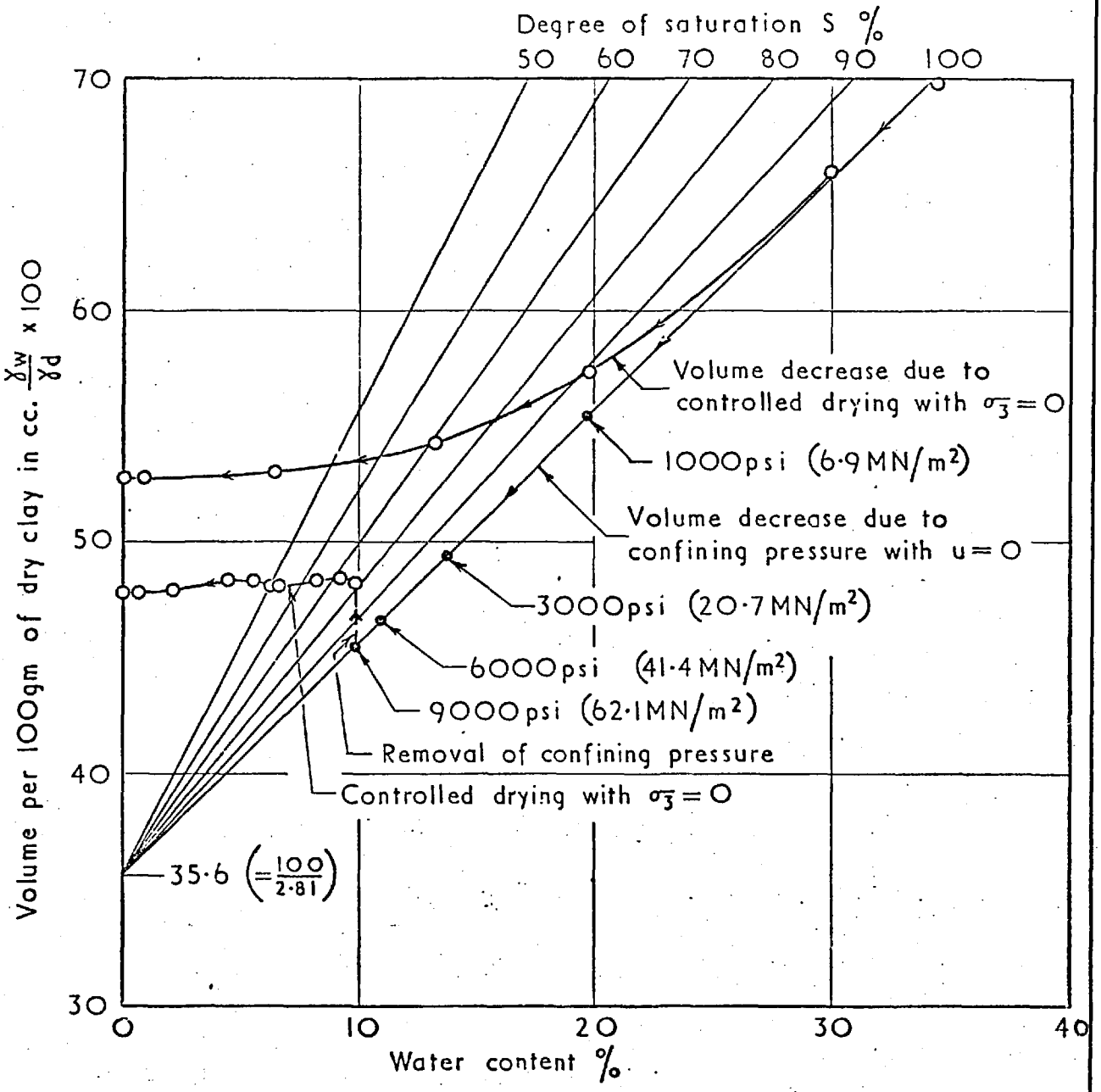

RELATIONSHIPS BETWEEN VOLUME CHANGE & WATER CONTENT DURING CONSOLIDATION, UNDRAINED STRESS RELEASE & DRYING LONDON CLAY; SPECIFIC GRAVITY G ASSUMED CONSTANT AT 2·81 THROUGHOUT PRESSURE RANGE

FIG 12 – 3

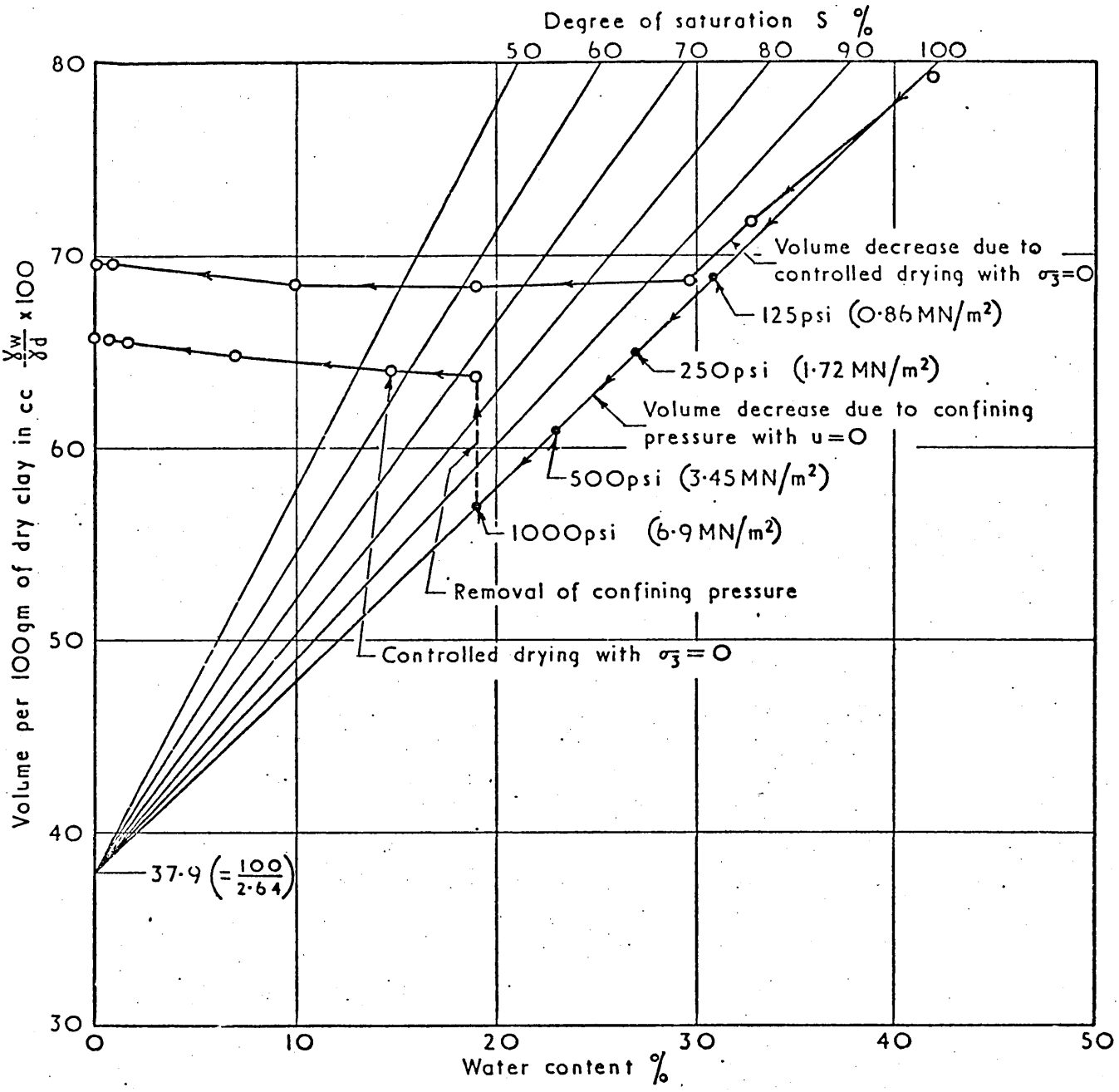

RELATIONSHIPS BETWEEN VOLUME CHANGE & WATER CONTENT DURING CONSOLIDATION, UNDRAINED STRESS RELEASE & DRYING; KAOLIN; SPECIFIC GRAVITY G ASSUMED CONSTANT AT 2·64 THROUGHOUT PRESSURE RANGE

FIG 12-4

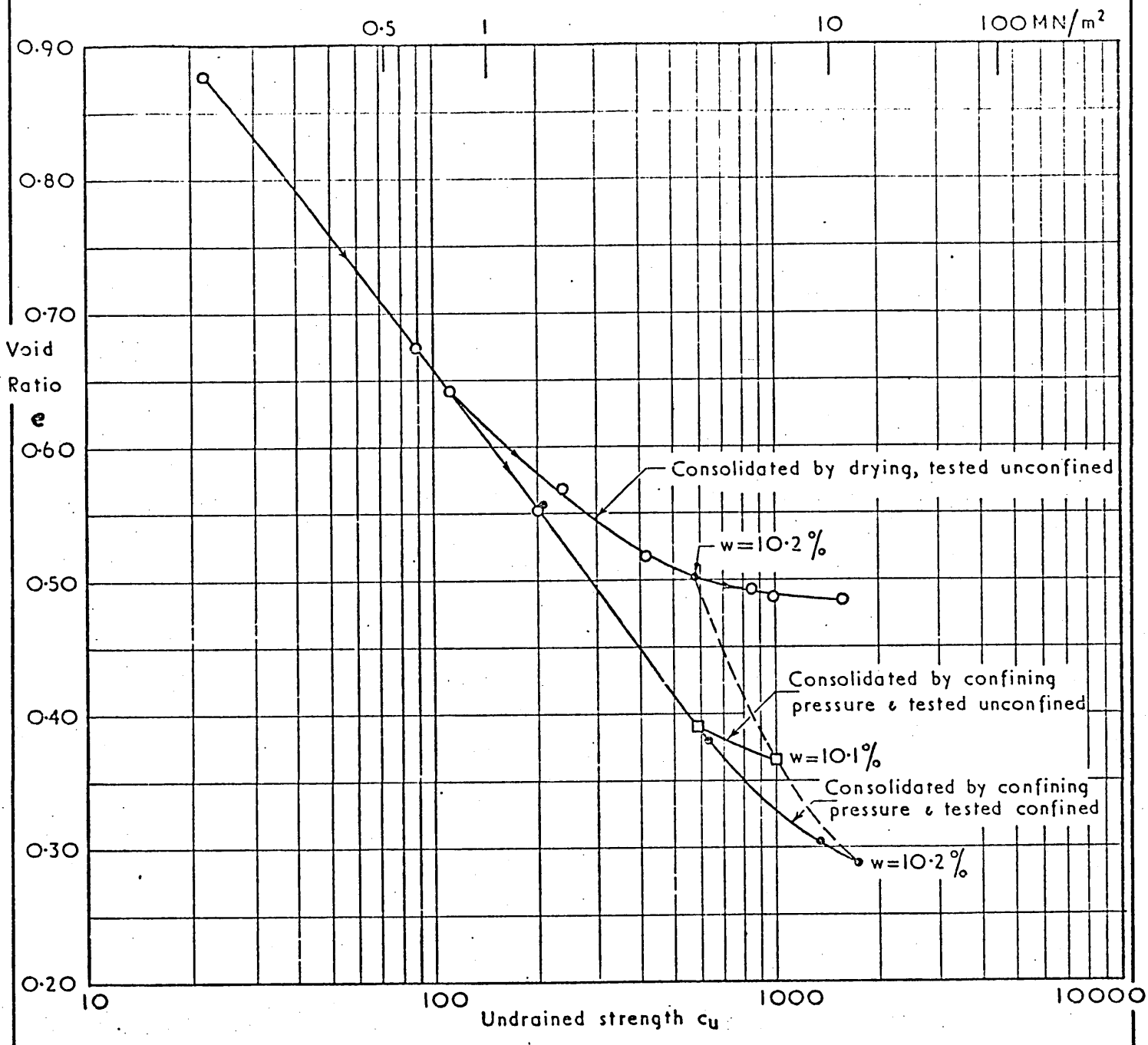

RELATIONSHIPS BETWEEN UNDRAINED STRENGTH c_u & VOID RATIO e AT THE BEGINING OF THE COMPRESSION TEST FOR CONFINED TESTS, UNCONFINED TESTS ON SAMPLES CONSOLIDATED BY EXTERNAL PRESSURE & UNCONFINED TESTS ON SAMPLES CONSOLIDATED BY DRYING: LONDON CLAY

FIG 12-5

APPENDIX A

CALIBRATION OF PROVING RINGS, LOAD CELLS, LATERAL STRAIN DEVICES AND PRESSURE GAUGES

A.1. Method of Calibration

In order to obtain consistent data over a long period of time it is necessary periodically to calibrate the load and strain measuring devices against a relatively invariant standard. This has been done throughout the present testing programme. In the case of the high confining pressure tests (above 1000 psi) the load cell was calibrated before and after each test.

For the proving ring and load cell calibrations, a 2 in. diameter honed stainless steel piston, running in a phosphor bronze bushing, provided the basic component of the calibrator (Bishop and Green, 1965, p. 249). The pressure was supplied to the calibrator by a Budenberg dead weight tester. A motor had been installed to rotate the piston of the tester at about 30 rpm to ensure that friction was minimised. The method of calibration has been described by Green (1969). The proving rings and the load cells were calibrated for loading and unloading; depending on the type of test under consideration. This type of calibrating system has been used to calibrate proving rings and load cells of maximum capacity up to 1850 lb. while those of higher capacities were calibrated in an Amsler compression machine installed in the Concrete Laboratory of Imperial College.

The effective loads for the levels of pressure used are shown in the following table. The same figures were used by Reades (1972):

Budenberg pressure lb/in^2	Effective load lb.
10	25.648
15	41.236
25	72.410
50	150.345
75	228.280
100	306.214
150	462.084
200	617.954
250	773.829
300	929.694
350	1085.564
400	1241.434
450	1379.304
500	1553.174
550	1709.044
600	1864.914

A.2 Calibration of the Proving Rings

Four proving rings were used of 300, 1000, 3000 and 6000 lb. capacity each. The 3000 lb. proving ring was calibrated using the proving ring calibrator and an Amsler test machine as explained earlier. A reasonable agreement was obtained as shown in Figure (A-1c). The calibration curves of the other proving rings are shown in Figures (A-1a), (A-1b) and (A-1d). The calibrations were checked using dead weights up to a level of 80 lb. In all cases a very good agreement between the two methods of calibration was obtained.

A.3 Calibration of the Load Cells

The procedure explained in Section A.1. was used in calibrating all the load cells. One 1000 lb. high sensitivity load cell was needed and it was calibrated by dead weights up to 50 lb. load and then the calibration was continued using the proving ring calibrator as previously explained.

The 10 ton load cell was calibrated in an Amsler compression machine as mentioned in Section A.1. The calibration curves are shown in Figures (A-2a), (A-2b) and (A-2c).

A.4 Calibration of the Lateral Strain Measuring Devices

These transducers were calibrated using a mild steel cylinder as shown in Plate (4_2). The steps shown on the steel cylinder are 0.2 in. width. These lateral strain measuring devices produced a linear relationship between read-out and diameter change and no measurable hysteresis was found. Furthermore, no visible creep or temperature effects were found.

Three devices were used for each sample tested, as described in Section (4.4). The calibration curves for the three lateral strain devices are shown in Figure (A-3). The sensitivity of these devices is quite satisfactory for the present work, as pointed out earlier in the text.

A.5 Calibration of the Pressure Gauge

All the pressure gauges used in this work were calibrated through a pot having an oil-water interface. One of the Bourdon gauges showed an error of about 0.2 psi up to 150 psi which is the maximum pressure which could be obtained from the mercury pressure system. The other Bourdon gauges were accurate and they were calibrated periodically throughout the testing programme.

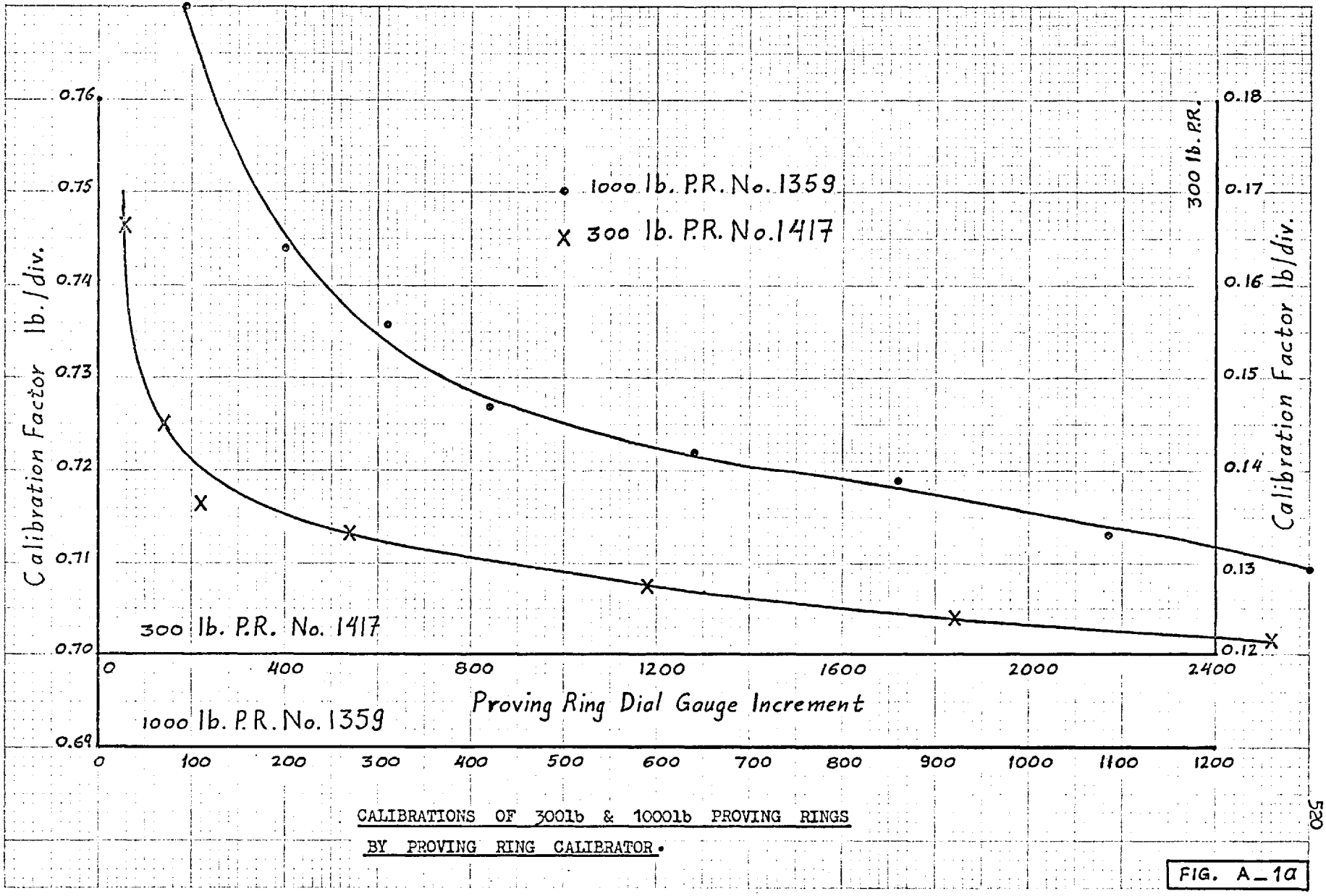

CALIBRATIONS OF 300lb & 1000lb PROVING RINGS
BY PROVING RING CALIBRATOR.

FIG. A_1a

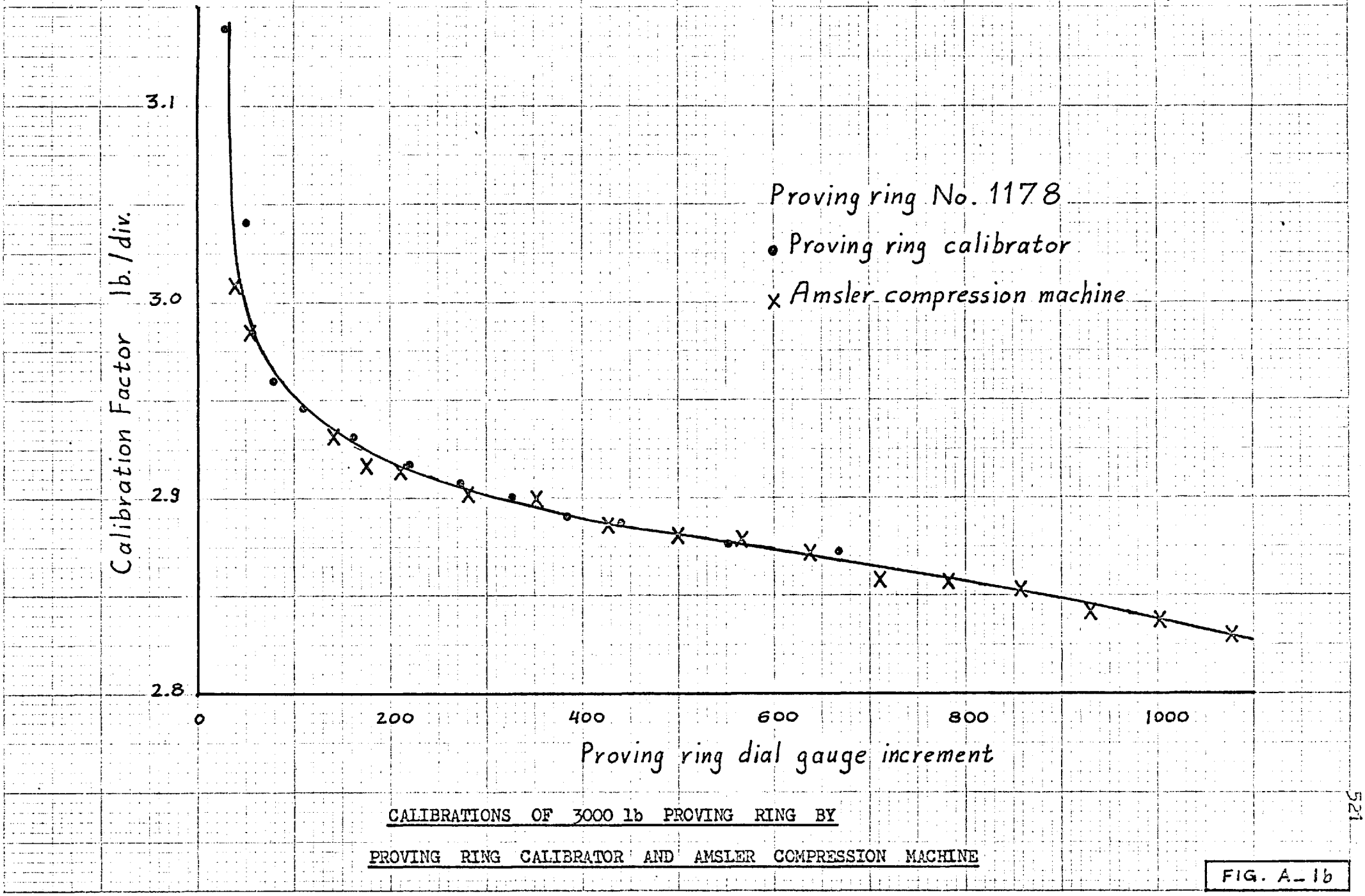

CALIBRATIONS OF 3000 lb PROVING RING BY

PROVING RING CALIBRATOR AND AMSLER COMPRESSION MACHINE

FIG. A-1b

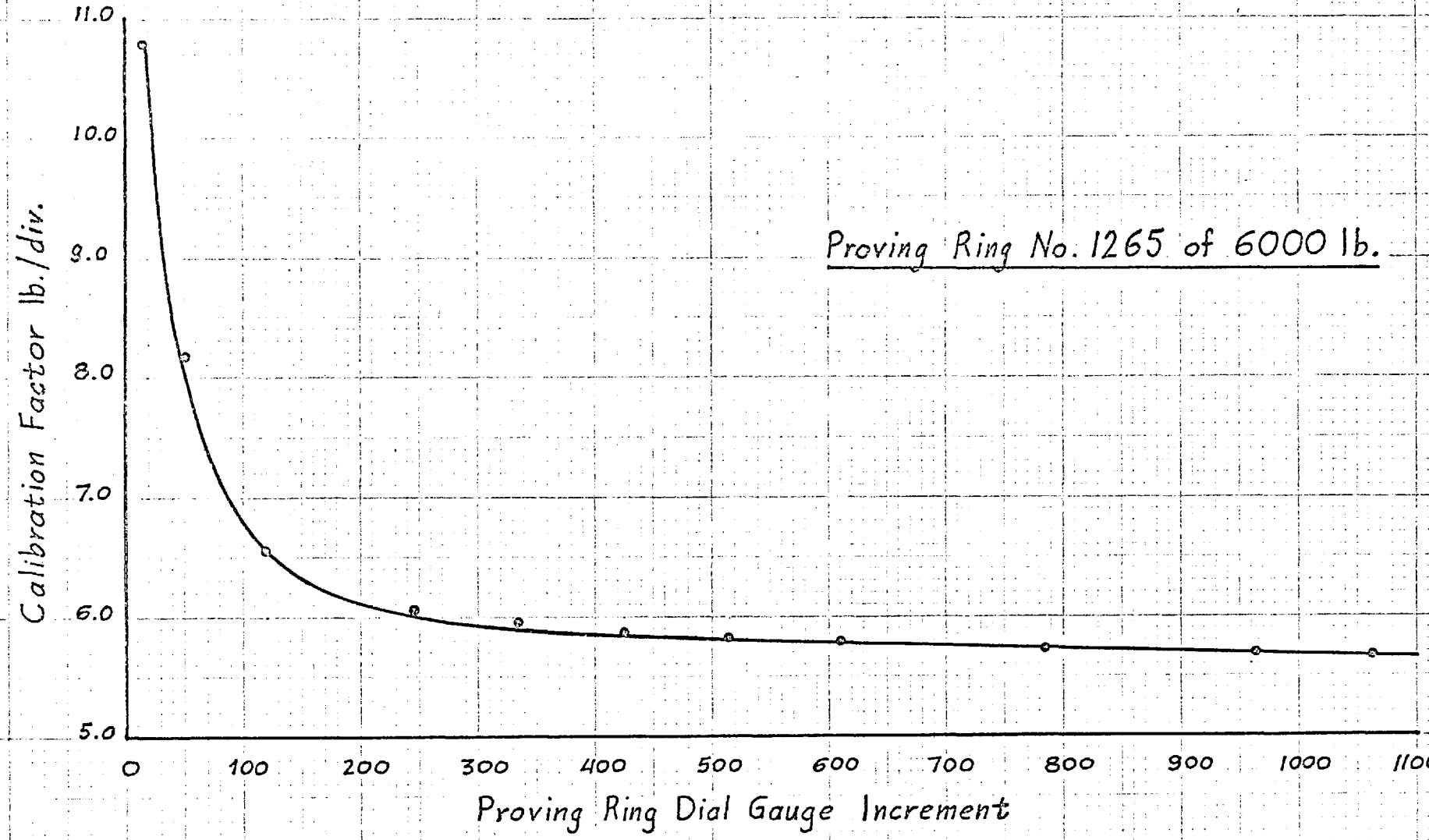

CALIBRATION OF 6000 lb PROVING RING BY AMSLER COMPRESSION MACHINE.

FIG. A-1C

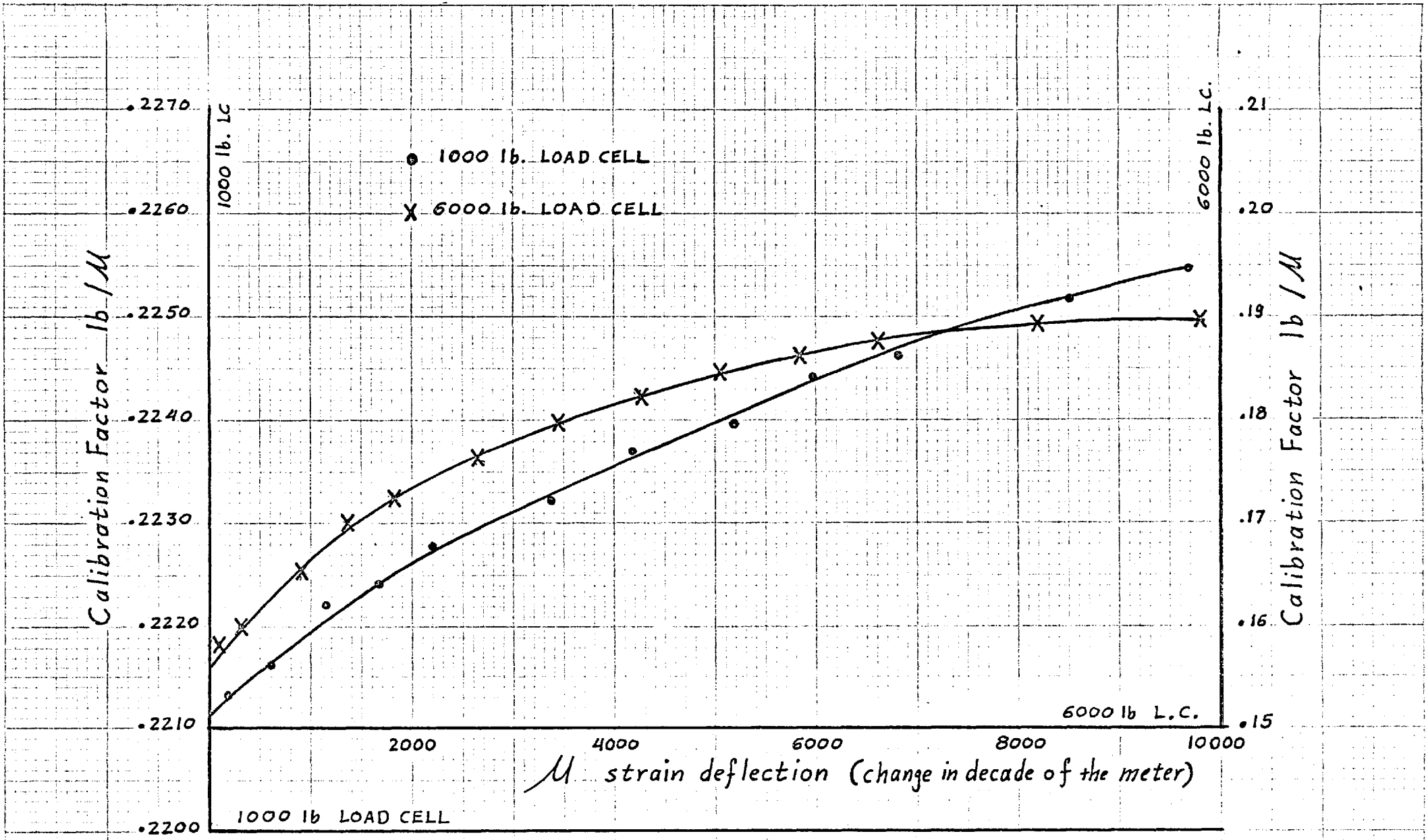

CALIBRATIONS OF 1000 lb & 6000 lb LOAD CELLS USING C-61 METRE.

FIG. A-2α

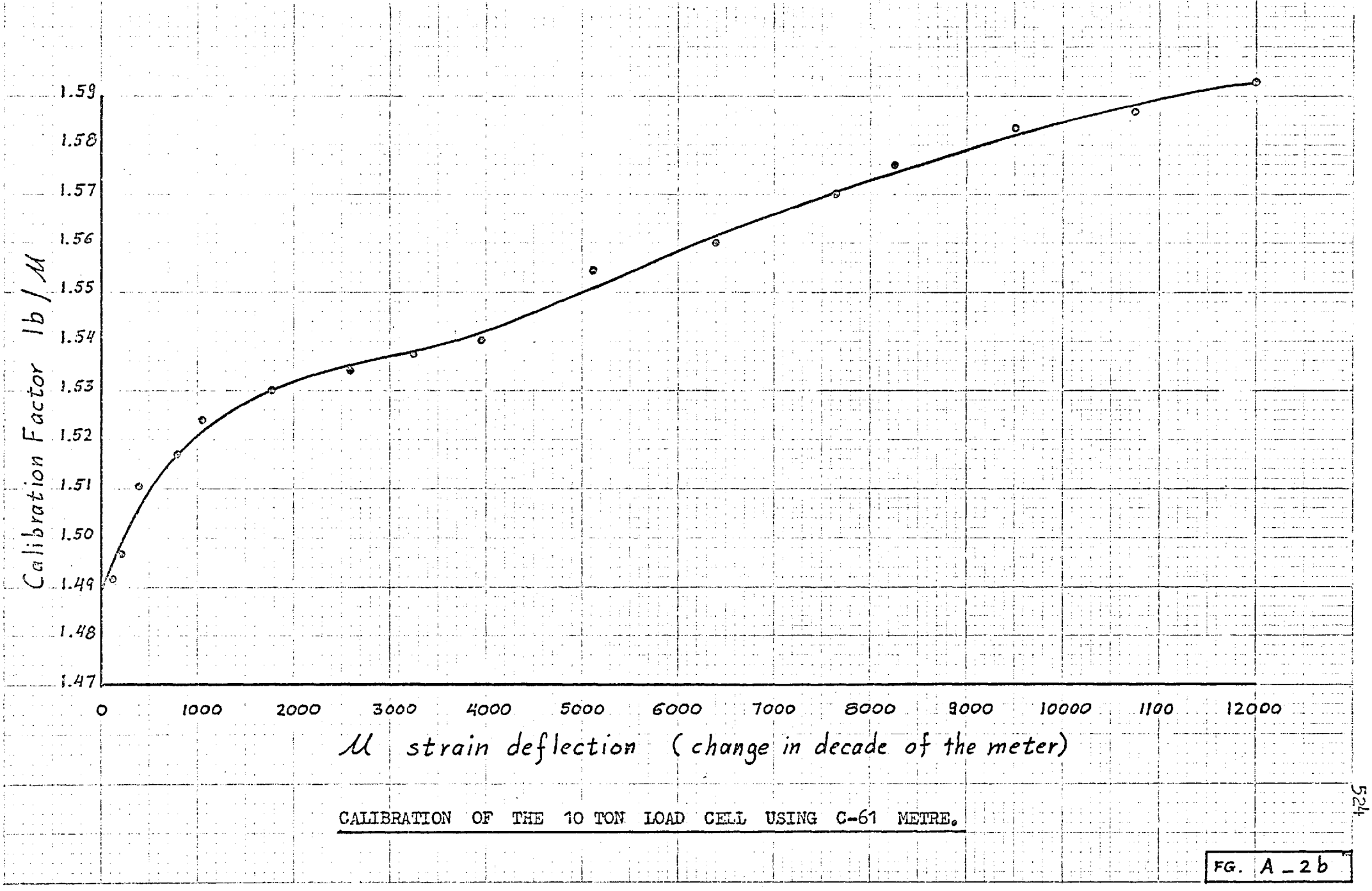

CALIBRATION OF THE 10 TON LOAD CELL USING C-61 METRE.

FG. A_2b

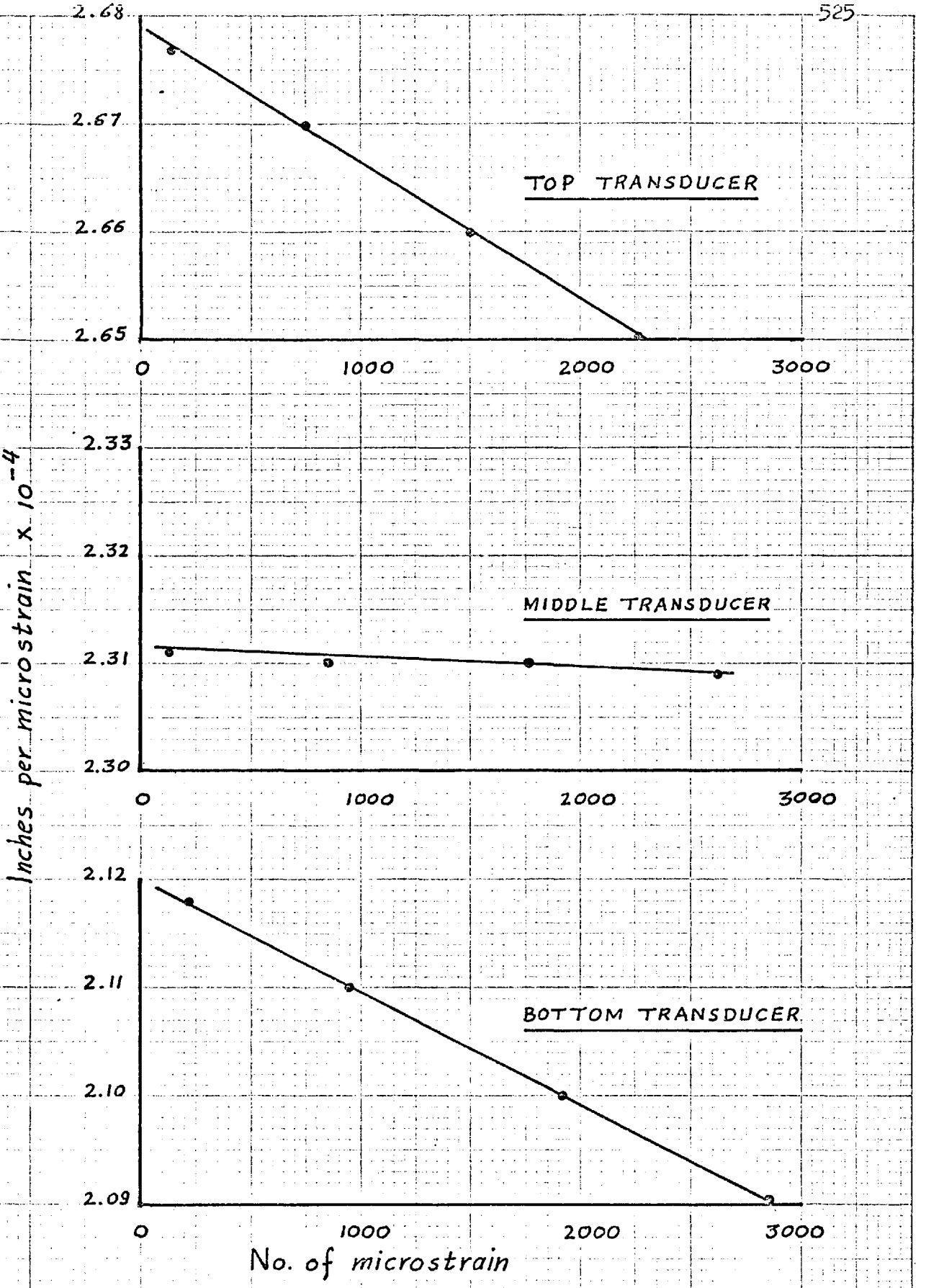

CALIBRATIONS OF THE LATERAL STRAIN MEASURING DEVICES.

USING C-61 METRE.

FIG. A_3

APPENDIX B

DRAINED TESTS ON SATURATED HAM RIVER SAND

As has been pointed out in Chapter 6 a series of drained triaxial tests on $1\frac{1}{2}$ in. dia. samples of saturated Ham River sand was carried out to check the apparatus and testing techniques and to permit correlation of the subsequent test results of rockfill with other published data. A summary of this series of tests on Ham River sand is shown in Table (A-1). The stress, strain and volume change curves are shown in Figures (A-4) through (A-6). The effective cell pressure used ranges from 14 psi to 1005 psi. The marked effect of the confining pressure on the volume change during shear can be clearly seen. The results obtained from this series of tests are in close agreement with those reported by Bishop et al (1965), Bishop (1966) and Reeds (1972). The sand used in this investigation is the same as that used by those authors but from a different patch. It should be noted here that a fresh sample was used for each test to ensure similar material gradation for each test.

TABLE (A-1)

Drained Triaxial Tests on $1\frac{1}{2}$ in. dia. samples of saturated Ham River sand

Test No.	1	2	3	4	5	6	7	8
σ'_3 (psi)	14	14	100	145	300	500	1000	1005
n_i %	44.5	35.1	37.8	39.6	39.5	37.5	37.5	37.1
density (pcf)	92.7	108.4	103.9	100.8	101.2	104.7	104.7	104.4
$\phi'_f{}^o$	34.8	45.5	37.5	37.0	33.5	32.5	30.5	31.3
$(\sigma'_1 - \sigma'_3)_f$	37	70	313	436	736	1161	2069	2192
$(\sigma'_1 + \sigma'_3)_f$	65	98	513	726	1336	2161	4069	4202
σ'_{1f}	51	84	413	581	1036	1661	3069	3197
ϵ_{1f}%	7.1	4.0	7.9	7.1	10.5	12.6	17.4	19.4
ϵv_f%	+.82	+2.7	+1.8	+.62	-.52	-1.9	-5.5	-5.6
$(d\epsilon v/d\epsilon_1)_f$	+.19	+.86	+.42	+.26	-.15	-.006	-.18	-.18
Final Strain	19.4	16.6	28.4	25.8	30.7	28.4	28.4	30.6

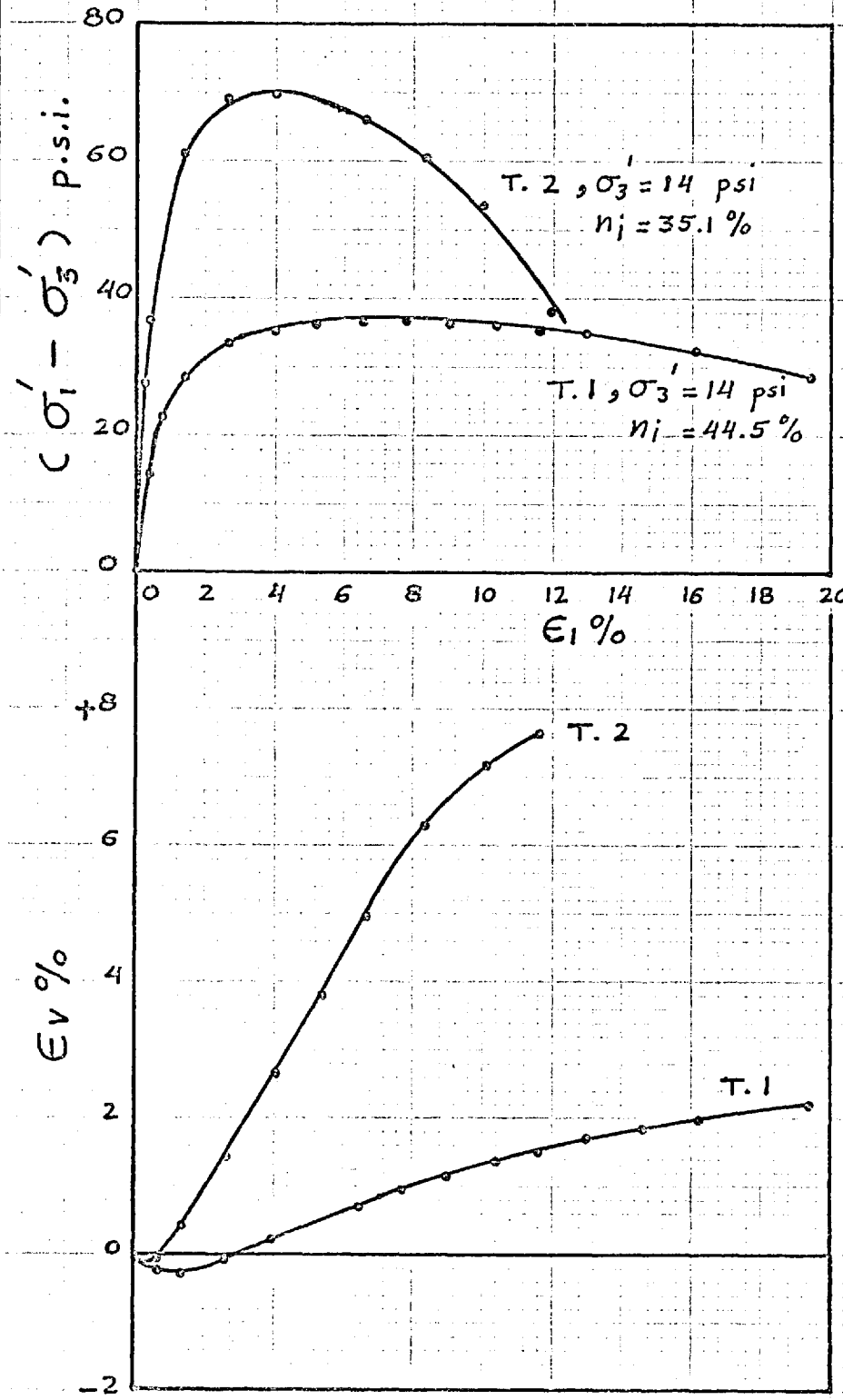

Results of Drained Tests on Saturated Ham River Sand

FIG A-4

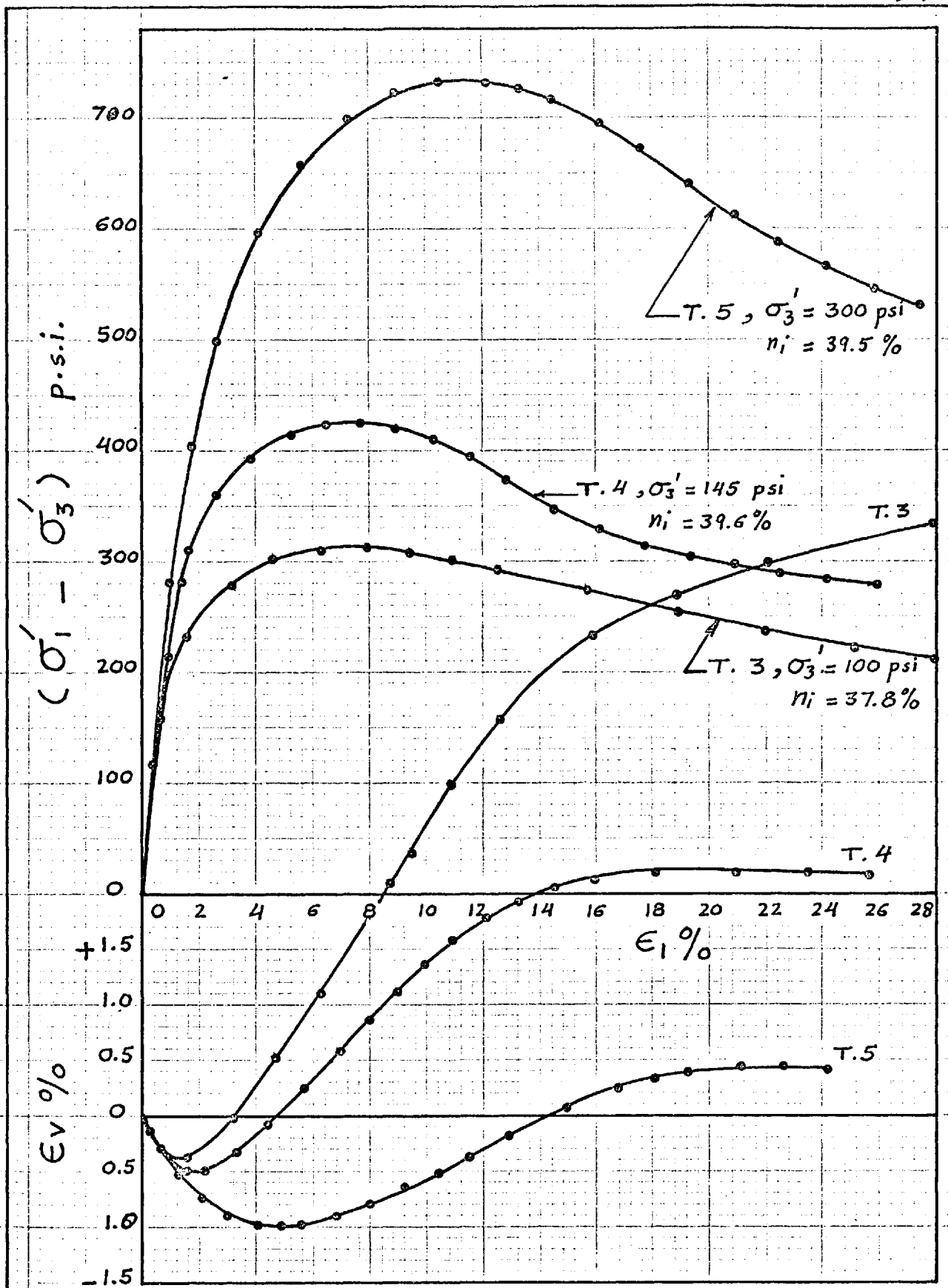

Results of Drained Tests on Saturated Ham River Sand

FIG. A – 5

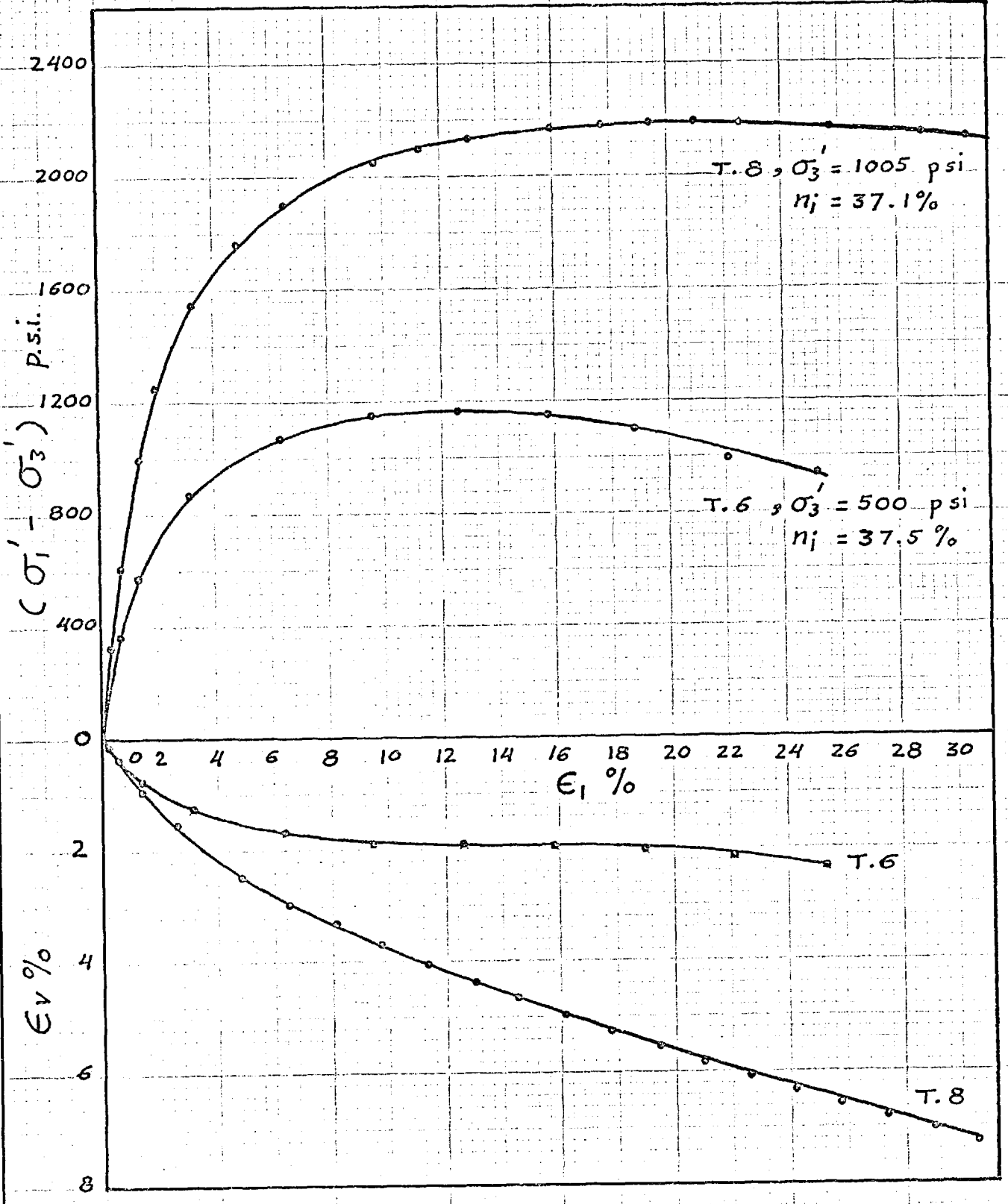

Results of Drained Tests on Saturated Ham River Sand

FIG A-6

APPENDIX C

VARIATION OF THE UNIT WEIGHT OF WATER WITH TENSILE STRESS IN THE WATER

The assumption that the unit weight of water in the soil voids is equal to the value* used as the reference for calculating the specific gravity, was made in deriving equations (12.2.1), (12.2.2) and (12.2.3). Taylor (1948) realised this point, however it is not mentioned in the standard method for assessing the specific gravity of soils, BS 1377 (1967). There is also a difference due to temperature, at 20°C (the usual standard laboratory temperature) the unit weight of water is 0.9982 grammes per millilitre.

There will be a considerably larger difference at high pore water pressures (or tensions) due to the compressibility (or expansibility) of water. This difference will be significant, in the tests reported here, where substantial tensions were induced in the pore water. Assuming that the coefficient Cw is the same in tension as in compression (Temperley and Chambers, 1946) then for water at a tension of 3000 psi the unit weight of water would decrease by 1.01%, and at a tension of 9000 psi it would decrease by 3.03%.

Although an accurate estimate cannot be made of the pore water tensions in samples in which partial saturation has occurred, they will be larger than the breakdown value (2820 psi for London clay) but smaller than the values estimated for the particular consolidation pressure on the assumption of full saturation. This gives a range of the unit weight of water from 0.9888 to 0.9750 grammes per millilitre for highest consolidation pressure. The possible error in the calculated degree of saturation is 1 to 2 ½%, and in the percentage of air voids 4% to 9%; again for the 9000 psi consolidation pressure†.

---

* This value is at 4°C

† The original values are stated in Section 12.2.

For a sample consolidated to 9000 psi the expansion occurring due to undrained stress release, assuming full saturation, can be calculated using the expression for undrained compressibility, $\overline{C}$, given by Bishop (1966a, 1973):

$$\overline{C} = \frac{nCw + (1-n)\,C_s - C_s^2/C}{1+n\,.\,Cw/C - (1-n)\,C_s/C} \qquad \ldots\ldots \quad (A\cdot C\cdot 1)$$

This equation gives a value of the expansion as 0.60%

This equation is based on the assumption that the compressibility of the pore water is the same as that of bulk water, the same assumption as for equation (9.3.3). The accuracy of equation (A.C.1) can be checked from the actual measurements made on the samples. The present triaxial cell was not designed to measure volume changes of undrained samples directly, however if the sample is assumed to have behaved isotropically then the axial deformation can be used to calculate the volume changes. Although the observations were affected by a time-dependent flow of water between the sample and the rubber membrane occurring as the pore water tension was changed; corrected instantaneous values for two porosities suggest that equation (A.C.1) is reasonably correct.

REFERENCES

AGARWAL, K.B. (1967). The influence of size and orientation of samples on the undrained strength of London clay. Ph.D. Thesis, University of London.

AITCHISON, G.D. (1960). Relationships of moisture content and effective stress functions in unsaturated soils. Proc. Conf. Pore Pressure and Suction in Soils, London, 47-52.

AKROYD, T.N.W. (1964) Laboratory Testing in Soil Engineering. Geotechnical Monograph No. 1., Soil Mechanics Ltd.

ALBERRO, J. (1972) Stress-Strain Analysis of El Infiernillo Dam. Proc. of the Speciality Conf. on 'Performance of Earth and Earth-Supported Structures' Vol. 1, Part I, pp 837-852.

ASCE Symposium on Rockfill Dams, Portland, Oregon, June 1958. Papers published in Proc. of the ASCE, Vol 84, Journal of the Power Division, 1958.

ANAGNOSTI, P. (1967). Shear Strength of Soil other than Clay. Proc. of Geotech. Conf., Oslo, Vol. 2, 73-76.

ATKINSON, J.H. (1973). The Deformation of Undisturbed London Clay. Ph.D. Thesis, University of London.

AUDIBERT, J.M.E. (1972). Prediction and Measurement of Strain Fields in Soils. Ph.D. Thesis, Duke University, 1972.

BARDEN, L. (1969) A quantitative Treatment of the Deformation Behaviour of Granular Material in Terms of Particulate Mechanics. Int. Conf. on Structures, Solid. Mech. & Eng. Design, Southampton University, Paper 56.

BARDEN, L. and KHAYATT, A.J. (1966). Incremental Strain Rate Ratios and Strength of Sand in Triaxial Test. Geotechnique, Vol. 16, No. 4, pp 338-357.

BARDEN, L. and KHAYATT, A.J. (1968) Incremental Stress-Strain Relations for Sand. Research Report No. 5., Dept. of Civil Engineering, University of Manchester.

BARDEN, L. and PROCTER, D.C. (1971) The Drained Strength of Granular Material. Canadian Geotech. Journal, Vol. 8, No.3. pp 372-383.

BARDEN, L., ISMAIL, H. and TONG, P. (1969). Plane Strain Deformation of Granular Material at Low and High Pressures. Geotechnique, Vol. 19, No.4, pp 441-452.

BARDEN, L, KHAYATT, A.J. and WIGHTMAN, A. (1969). Elastic and Slip Components of the Deformation of Sand. Canadian Geotech. Journal, Vol. 6, No.3.

BARNES, J. (1960). Experimental Evidence for the Stress Dilatancy Theory. M.Sc. Thesis, University of Manchester.

BERTHELOT, M. (1850). Ann. Chim. (Phys.), 30, 232-9.

BILLAM, J. (1967). The Behaviour of Granular Materials at High Pressures. Ph.D. Thesis, University of Birmingham.

BILLAM, J. (1971) Some Aspects of the Behaviour of Granular Materials at High Pressure. Proc. of Roscoe Memorial Symposium, Cambridge. pp 69-80.

BISHOP, A.W. (1947) Strength Variations in London Clay. Silicates Industriels, 13, 109-113.

BISHOP, A.W. (1948) A large Shear Box for Testing Sands and Gravel. Proc. of 2nd ICSMFE, Vol.1, pp 207-211.

BISHOP, A.W. (1952) The Stability of Earth Dams. Ph.D. Thesis, University of London.

BISHOP, A.W. (1953) Private communication to Dr. A.S. Laughton. See Skempton, 1960.

BISHOP, A.W. (1954). Shear Characteristics of a Saturated Silt, Measured in Triaxial Compression. British Geotech. Vol.4, pp 43-45.

BISHOP, A.W. (1958). Test Requirements for Measuring the Coefficient of Earth Pressure at Rest. Proc. Brussels Conf. on Earth Pressure Problems, 1, 2-14.

BISHOP, A. W. (1959) The Principal of Effective Stress. Teknisk Ukeblad No. 39, 859-863.

BISHOP, A. W. (1960) The Measurement of Pore Pressure in the Triaxial Test. Proc. Conf. Pore Pressure and Suction in Soils, London, 38-46.

BISHOP, A.W. (1963) General Reporter: Compressibility of Soils, Stress-Strain Properties, Pore Pressure Prediction. European Conf. SMFE, Wiesbaden, Vol. 2.

BISHOP, A.W. (1965). Shear-Strength Behaviour of Soils Under High Confining Pressures. Panel Discussion, 6th ICSMFE, Vol. 3, p. 306.

BISHOP, A. W. (1966) The Strength of Soils as Engineering Materials. Sixth Rankine Lecture. Geotechnique 10: 2, pp. 89-129.

BISHOP, A. W. (1966a) Soils and Soft Rocks as Engineering Materials. Inaugural Lecture, Imperial College of Science & Technology, 6, 289-313.

BISHOP, A. W. (1967) Progressive Failure With Special Reference to the Mechanism Causing It. Proc. Geotech. Conf. Oslo, Vol. 2, pp. 142-150.

BISHOP, A.W. (1971). Shear Strength Parameters for Undisturbed and Remoulded Soil Specimens. From: Stress-Strain Behaviour of Soils. Proc. Roscoe Memorial Sumposium, Cambridge, 3-58, 134-139.

BISHOP, A.W. (1973) The Influence of an Undrained Change in Stress on the Pore Pressure in Porous Media of Low Compressibility. Geotechnique, 23, 435-442.

BISHOP, A.W., and BJERRUM, L. (1960) The Relevance of the Triaxial Test to the Solution of Stability Problems. Proc. Res. Conf. Shear Strength of Cohesive Soils, Boulder, 437-501.

BISHOP, A.W., and BLIGHT, G.E. (1963). Some Aspects of Effective Stress in Saturated and Partly Saturated Soils. Geotechnique, Vol. 13, pp 177-197.

BISHOP, A.W. and ELDIN, G. (1950) Undrained Triaxial Tests on Saturated Sands and Their Significance in the General Theory of Shear Strength. Geotechnique, 2, 13-32.

BISHOP, A.W. and GREEN, G.E. (1965). The Influence of End Restraint on the Compression Strength of a Cohesionless Soil. Geotechnique, Vol. 15, No.3, pp 243-266.

BISHOP, A.W. and HENKEL, D.J. (1953) Pore Pressure Changes during Shear in Two Undisturbed Clays. Proc. of 3rd Int. Conf. on Soil Mech. & Found. Eng., Switzerland, 1, 94-99.

BISHOP, A.W. and HENKEL, D.J. (1962). The Measurement of Soil Properties in the Triaxial Test. Publisher: Edward Arnold, London, 1962 (2nd Edn.)

BISHOP, A.W., WEBB, D.L. and LEWIN, P.I. (1965). Undisturbed Samples of London Clay from the Ashford Common Shaft: Strength - Effective Stress Relationships. Geotechnique, 15, 1-31.

BISHOP, A.W., WEBB, D.L. and SKINNER, A.E. (1965). Triaxial Tests on Soil at Elevated Cell Pressures. Proc. Sixth Int. Conf. Soil Mech. & Found. Eng. Toronto, 1, 170-174.

BISHOP, A.W., ALPAN, I., BLIGHT, G.E. and DONALD, I.B. Factors Controlling the Strength of Partly Saturated Cohesive Soils. Proc. Res. Conf. on Shear Strength of Cohesive Soils, Boulder, 503-532.

BJERRUM, L., and ANDERSON, K.H. (1972). In-situ Measurement of Lateral Pressures in Clay. Proc. 5th Europ. Conf. Soil Mech., Madrid, 1, 11-20.

BLIGHT, G.E. (1967) Horizontal Stresses in Stiff and Fissured Lacustrine Clays. Proc. 4th Regional Conf. Soil Mech., Capetown.

BOLT, G.H. and MILLER, R.O. (1958). Calculation of Component and Total Potentials in Soils. Trans. Amer. Geophys. Union. 30.

BOROWICKA, H. 1963. Vienna Method of Shear Testing. Laboratory Shear Testing of Soils. ASTM, STP, 361, p.306.

BRAUNS, J. and LEUSSINK, H. (1967) Discussion on Marsal, 1967. Proc. ASCE, 93: SM6: 383-388.

BRACE, W.F. (1963). Behaviour of Quartz During Indentation. The Journal of Geology, 71: 5: 581-595.

BS 1377 (1967). Methods of Testing Soils for Civil Engineering Purposes. British Standards Institution, London, W1.

BROMWELL, L. (1966). The Friction of Quartz in High Vacuum. Research Report R66-18. MIT, Civil Engineering, May.

BROS, (1969) Undrained Tests on Granite Rockfill. Unpublished data, see Tombs (1969).

BRUGGEMAN, J.R., ZANGER, C.N. and BRAHTZ, J.H.A. (1939). Memorandum to Chief Designing Engineer: Notes on Analytical Soil Mechanics. US Dept. of the Interior Technical Memorandum No. 592.

BRUHN, R.W. (1972) A Study of the Effects of Pore Pressure on the Strength and Deformability of Berea Sandstone in Triaxial Compression. US Dept. of the Army, Technical Report - Eng. Study No. 52.

*

BURLAND, J.B. (1965). Correspondence on the Yielding and Dilation of Clay. Geotech. Vol. 15, No.2., pp 211-214.

BURLAND, J.B. (1967) Deformation of Soft Clay. Ph.D. Thesis, Cambridge University.

BURLAND, J.B. (1971). A Method of Estimating the Pore Pressure and Displacements Beneath Embankments on Soft Natural Clay Deposits. From: Stress-Strain Behaviour of Soils. Proc. Roscoe Memorial Symposium, Cambridge, 505-536.

CALABRESI, G. (1968). Deformazioni Plastiche di una Terra Argillosa. Riv. Ital. di Geotecn. No.4.

CALLADINE, C.R. (1963). Correspondence on the Yielding of Clay. Geotech. Vol. 13, No.3., pp 250-255.

---

* Burland, J.B. (1964). Correspondence on effective stresses in partly saturated soils. Geotech. Vol. 14, pp 64 - 68.

CAQUOT, A. (1934). Equilibre des Massifs a Frattement Interne. Stabilite des Terres Pulverents et Coherentes. Paris: Gauthier Villars.

CASAGRANDE, A. (1936). Characteristics of Cohesionless Soils Affecting the Stability of Slopes and Earth Fills. Journal, Boston Society of Civil Engineers, Jan 1936, pp 257-276.

CASAGRANDE, A. (1965). Hohe Staudamme. Communication No. 6., Institute for Foundation Engineering and Soil. Mech. Technische Hochschule, Vienna, Dec. 1965, p 32.

CASTRO, G. (1969). Liquefaction of Soils. Ph.D. Thesis, Harvard University.

CEBELL, W.A. and CHILINGARIAN, G.V. (1972). Some Data on Compressibility and Density Anomalies in Halloysite, Hectorite and Illite Clays. Amer. Assoc. Petroleum Geol. Bull. 56, 796-821.

CHARLES, J.A. (1973). Correlation Between Laboratory Behaviour of Rockfill and Field Performance with Particular Reference to Scammonden Dam. Ph.D. Thesis, University of London.

CHEN, L.S. (1948). An Investigation of Stress-Strain and Strength Characteristics of Cohesionless Soils by Triaxial Compression Tests. Proc. 2nd Int. Conf. on SMFE, Vol. 5, pp 35-43.

COON, M.D., and EVANS, R.J. (1969). Discussion on Elastic Behaviour of Cohesionless Soil. Journal of Soil Mech. Found. Div. ASCE, 95, SM5, 1281-1283.

CORNFORTH, D.H. (1964). Some Experiments on the Influence of Strain Conditions on the Strength of Sand. Geotech. 14: 2, 143-167.

CRONEY, D. and COLMAN, J.D. (1960). Pore Pressure and Suction in Soil. Proc. Conf. Pore Pressure and Suction in Soils, London, 31-37.

DAVIS, E.H. (1968) Theories of Soil Plasticity and the Failure of Soil Masses. Soil Mechanics; Selected Topics (ed. I.K. Lee) London: Butterworths.

DIXON, H.H. (1909). Sci. Proc. Roy. Soc., Dublin, 12, 60-5.

DONALD, I.B. (1961). The Mechanical Properties of Saturated and Partly Saturated Soils with Special Reference to the Influence of Negative Pore Water Pressure. Ph.D. Thesis, University of London.

DRUCKER, D.C. (1951). A More Fundamental Approach to Plastic Stress-Strain Relations. Proc. of the First US National Congress on Applied Mechanics, ASME, 487-491.

DRUCKER, D.C. (1964a). On the Postulate of Stability of Material in the Mechanics of Continua. Journal de Mecanique, 3.

DRUCKER, D.C. and PRAGER, W. (1952). Soil Mechanics and Plastic Analysis or Limit Design. Quarterley of Applied Mathematics, V.10, pp 157-165.

DRUCKER, Daniel C, GIBSON, Robert E. and HENKEL, David J. (1957) Soil Mechanics and Work-Hardening Theories of Plasticity. Trans. ASCE, Vol. 122, p 338.

EL-SOHBY, A.A.K. (1969). Deformation of Sands Under Constant Stress Ratio. Proc. 7th Int. Conf. Soil Mech., Mexico, Vol.1, 111-119.

EVANS, I. and POMEROY, C.D. (1966). The Strength, Fracture and Workability of Coal. Pergamon Press, London, 277.

FAROUKI, Omar T., and WINTERKORN, Hans F. (1964). Mechanical Properties of Granular Systems. Highway Research Record No.52 - Mechanical and Physico-Chemical Properties of Soils. National Research Council, Washington, pp 10-42.

FELT, E.J. (1958) Laboratory Methods of Compacting Granular Soils. Symposium on Application of Soil Testing in Highway Design and Construction, ASTM, STP 239, 89-110.

FRASER, A.M. (1957). The Influence of Stress Ratio on Compressibility and Pore Pressure Coefficients in Compacted Soils. Ph.D. Thesis, University of London.

FRYDMAN, S. (1972). An Inquiry into the Stress-Strain Behaviour of Particulate Media. Ph.D. Thesis, Israel Institute of Technology, Haifa.

FUMAGALLI, E. (1969). Tests on Cohesionless Materials for Rockfill Dams. Proc. of ASCE, Soil Mech. Div., Vol. 95, No. SM1, p 313-330.

GASSMANN, F. (1951). Über die Elastizität Poröser Medien. Mitteilungen aus dem Institut für Geophysik, No. 17.

GEERTSMA, J. (1957). The Effect of Fluid Pressure Decline on Volumetric Changes of Porous Rocks. Soc. Petrol. Engrs., Los Angeles, 14-17.

GIBSON, R.E. (1953). Experimental Determination of the True Cohesion and True Angle of Internal Friction in Clays. Proc. 3rd Int. Conf. Soil Mech., Zurich, 1, 126-130.

GIBSON, R.E. and MORGENSTERN, N.R. (1963). Discussion on 'Stress-Dilatancy, Earth Pressures and Slopes' by P.W.Rowe, JSMFD, ASCE, Vol. 89, SM6, pp 127-129.

GOLDER, H.Q. and SKEMPTON, A.W. (1948). The Angle of Shearing Resistance in Cohesive Soils for Tests at Constant Water Content. Proc. 2nd Int. Conf. Soil Mech., Rotterdam, 1, 185-192.

GREEN, G.E. (1969). Strength and Compressibility of Granular Materials under Generalised Strain Conditions. Ph.D. Thesis, University of London.

GREEN, G.E. (1971). Strength and Deformation of Sand Measured in Independent Stress Control Cell. Roscoe Memorial Symposium, Cambridge.

GREEN, R.B. (1951). Ordinary Liquid Water-substance, Its Thermodynamic Properties, Dynamic Behaviour and Tensile Strength. D.Sc. Thesis, Massachusetts Institute of Technology.

GRIFFITHS, J.C. (1967). Scientific Method in Analysis of Sediments. International Series in the Earth and Planetary Sciences, McGraw Hill, New York, p 508.

HAFIZ, M.A. (1950). Strength Characteristics of Sands and Gravels in Direct Shear. Ph.D. Thesis, University of London.

HALL, E.B. and GORDON, B.B. (1963). Triaxial Testing with Large-Scale High Pressure Equipment. Proc. of ASTM Symposium on Lab. Shear Testing of Soils. ASTM Special Technical Publication No. 361, p.315.

HARKNESS, R.M. (1971). The Implications of 'Mohr-Coulomb' as a Failure Criterion. Roscoe Memorial Symposium, Cambridge.

HENKEL, D.J. (1959). The Relationships Between the Strength, Pore-Water Pressure, and Volume Change Characteristics of Saturated Clays. Geotechnique, Vol. 9, pp 119-135.

HENKEL, D.J. (1960). The Relationships Between the Effective Stresses and Water Content in Saturated Clays. Geotechnique, Vol. 10, pp 41-54.

HILL, R. (1950). The Mathematical Theory of Plasticity. Oxford University Press.

HILLIS, S.F. and SKERMER, N.A. (1968). Discussion on Large-Scale Testing of Rockfill Materials. Journal of ASCE, Soil Mech. & Found Div. Vol. 94, No. SM1, pp 326-328.

HIRSCHFELD, R.C. and POULOS, S.J. (1963). High-Pressure Triaxial Tests on a Compacted Sand and an Undisturbed Silt. Proc. of ASTM Symposium on Lab. Shear Testing of Soils. ASTM Special Technical Publication No. 361, p 329.

HIRSHFELD, R.C. and POULOS, S.J. (1973) Embankment-Dam Engineering: Casagrande Volume. New York: Wiley,

HOBBS, D.W. (1963) A Simple Method for Assessing the Uniaxial Compressive Strength of Rock. Int. J. Rock Mech. Mining Sci., Vol. 1, 5-15.

HOLESTØL, K, KJAERNSLI, B., and TORBLAA, I., (1965). Compression of Tunnel Spoil at Venemo Dam. Proc. 6th ICSMFE, Montreal, Vol. 2, p.490.

HOLMES, J.W. (1955). Water Sorption and Swelling of Clay Blocks. J. Soil Sci., 6, 200-208.

HOLTZ, W.G., and GIBBS, H. (1956). Shear Characteristics of Pervious Gravelly Soils. Proc. ASCE, Jan. 1956, p1.

HOLUBEC, I. (1966). The Yielding of Cohesionless Soils. Ph.D. Thesis, University of Waterloo, Canada.

HOLUBEC, I. (1968). Elastic Behaviour of Cohesionless Soil. J. Soil Mech. Found. Div., ASCE, 94, SM6, 1215-1231.

HORN, H.M. and DEERE, D.U. (1962). Frictional Characteristics of Minerals. Geotechnique, 12: 4: 319-355.

HORNE, M.R. (1965). The Behaviour of an Assembly of Rotund Cohesionless Particles. Proc. Royal Soc., Series A, Vol. 286, pp 62-78 Part I, A, Vol. 286, pp 79-97, Part II.

HORNE, M.R. (1969). The Behaviour of an Assembly of Rotund Cohesionless Particles. Proc. Royal Soc., Series A, Vol. 310, pp 21-34 Part III.

HOWKINS, W. (1966). Report on 9" dia. Oedometer Tests on Rockfill, Carried out at Imperial College. Internal Report, Binnie and Partners.

HUDER, J. and FETZ, L.B. (1967). Shear Strength and Density of Talus Material used in the Geoschenenalp Dam. Proc. Geotechnical Conf., Oslo, Vol. 1, pp 205-207.

HVORSLEV, M.J. (1937). Uber die Fesigkeitseigenschaften gestörter bindiger Böden. Ingvidensk. Skr. A, No. 45, (English translation No. 69-5, Waterways Experiment Station, Vicksburg, Miss., 1969).

IDEL, K.H. (1960). Die Scherfestigkeit Rolliger Erdstoffe. Veröffenlichungen des Instituts für Bodenmechanik und Grundbauder Technischen Hocshschule Fridericiana in Karlsruhe, Nr. 2.

INSLEY, A.E. and HILLIS, S.F. (1963). Discussion. Proc. of ASTM Symposium on Lab Shear Testing of Soils. ASTM Special Technical Publication No. 361, p. 328.

JACKOBSON, B. (1957). Some Fundamental Properties of Sand. Proc. 4th Int. Conf. Soil Mech., London, Vol. 1, 167-171.

JAEGER, J.C. (1969). Elasticity, Fracture and Flow. (2nd Edn.) London: Methuen.

JOHNSON, K.L. (1955). Surface Interaction Between Elastically Loaded Bodies Under Tangential Forces. Proc. Royal Soc. of London, Series A 230, 531-548.

De JONG, G. De Josselin, (1958) The Undefiniteness in Kinematics for Frictional Materials. Conf. on Earth Pressure Problems, Brussels.

JURGENSON, L. (1934). The Shearing Resistance of Soils. J. Boston, Soc. Civ. Engrs., 21, 242-275.

KING, G.J.W. and DICKIN, E.A. (1970). Comparison of Stress Dilatancy Theories. J. Soil Mech. Found. Div. ASCE, 96, SM5, 1697-1714.

KIRKPATRICK, W.M. (1957). The Condition of Failure of Sands. Proc. 4th Int. Conf. Soil Mech. & Found. Eng., Vol. 1, pp 172-178.

KJAERNSLI, B. and SANDE, A. (1963). Compressibility of Some Coarse-Grained Materials. Norwegian Geotechnical Institute, Publication No. 66.

KJELLMAN, W. and JAKOBSON, B. (1955). Some Relations Between Stress and Strain in Coarse Grained, Cohesionless materials. Royal Swedish Geotechnical Inst. Proc. No. 9, Stockholm.

KO, H.Y. and SCOTT, R.F. (1967a). Deformation of Sand in Hydrostatic Compression. J. Soil Mech. Found. Div. ASCE, 93, SM3, 137-157.

KO, H.Y. and Scott, R.F. (1967b). Deformation of Sand in Shear. J. Soil. Mech. Found Div., ASCE, 93, SM5, 283-310.

KOIZUMI, Y. and ITO, K. (1969). On the Mechanism of Liquefaction of Saturated Sands During Earthquakes. 1st Nat. Symp. on Seismology and Earthquake Eng., Peru.

KOLBUSZEWSKI, J.J. (1948). An Experimental Study of the Maximum and Minimum Porosities of Sands. Proc. 2nd Int. Conf. Soil Mech. and Found. Eng., Vol. 1, 158-165.

KOLBUSZEWSKI, J.J. and JONES, R.H. (1961). The Preparation of Sand Samples for Laboratory Testing. Proc. Midland SMFE Soc., Vol. 4, 107-123.

KRUMBEIN, W.C. (1941). Measurement and Geological Significance of Shape and Roundness of Sedimentary Particles. Jour. Sediment Petrol., 11: 64-72.

KUMAPLEY, N.K. (1969). Triaxial Tests on Clays and Silts at Elevated Cell Pressures. Ph.D. Thesis, University of London.

LADANYI, B. (1960). Etude des Relations entre les Contraintes et les Deformations lors du Cisaillement des Zols Pulverulents. Annales des Trauvaux Publics de Belgique, 3: 241-170.

LADANYI, B. (1967). Discussion on 'Compressibility and Crushing of Granular Soils in Anisotropic Triaxial Consolidations' by Lee, K.L. and Farhoomand, I. Canadian Geotechnical Journal, February, p. 87-88.

LADANYI, B., LA ROCHELLE, P., and TANGUAY, L. (1964). Some Factors Controlling the Predictability of Stress-Strain Behaviour of Clay. 18th Canadian Soil Mechanics Conf.

LADE, P.V. and DUNCAN, J.M. (1973). Cubical Triaxial Tests on Cohesionless Soil. Journal of the Soil Mech. & Foundations Div. ASCE, Vol. 99, No. SM 10, pp 793-812.

LADD, C.C. and LAMBE, T.W. (1963). Shear Strength of Saturated Clays. Symp. on Laboratory Shear Testing of Soils, Ottawa, ASTM STP 361, 342-271.

LAMBE, T.W. (1953). The Structure of Inorganic Soil. Proc. Amer. Soc. of Civil. Eng., 79, Sept.

LAMBE, T.W. and WHITMAN, R.V. (1969). Soil Mechanics. New York: John Wiley.

LAREW, H.G. and LEONARDS, G.A. (1962). A Repeated Load Strength Criterion. Proc. Hwy. Res. Bd. No. 41, p. 529.

LEE, K.L. and FARHOOMAND, I. (1967). Compressibility and Crushing of Granular Soil in Anisotropic Triaxial Compression. Canadian Geotechnical Journal, 4: 1: 68-86.

LEE, K.L. and SEED, M.B. (1967). Cyclic Stress Conditions Causing Liquefaction of Sand. JSMFD, ASCE, Vol. 93, SM1, 47-70.

LESLIE, D.D. (1963). Large Scale Triaxial Tests on Gravelly Soils. Proc. 2nd Pan Am. Conf. on SMFE, Vol. 1, p. 181, Brazil.

LESLIE, D.D. (1969). Relationship Between Shear Strength, Gradation and Index Properties of Rockfill Materials. SS13, 7th Int. Conf. SMFE, Mexico, p. 201.

LEUSSINK, H. (1965). Effect of Specimen Size on the Shear Strength of Granular Materials. Panel discussion, 6th Int. Conf. on SMFE, Vol. 3, p. 316.

LEUSSINK, H. and BLINDE, A. (1964). Scherverhalten Körniger Erdstoffe bei Hohen Normalspannungen. Vorträge der Baugrundtagung. Berlin. Herausgeber: Deutsche Gesellschaft für Erd-und Grundbau. Essen.

LEUSSINK, H. and BRAUNS, J. (1969). On Regular Sphere Packings as Models for Cohesionless Soils. Contribution and Discussion on Mechanical Properties of Rockfill and Gravel Materials. Proc. Speciality Session No. 13, 7th ICSM and FE, pp 111-113.

LEUSSINK, H. and WITTKE, W. (1963). Difference in Triaxial and Plain Strain Shear Strength. ASTM Symposium on Laboratory Shear Testing of Soils. STP No. 361, p 77-89.

LEWIN, P.I. (1970). Stress Deformation Characteristics of a Saturated Soil. M.Sc. Thesis, University of London.

LEWIN, I.P. (1972). Three-dimensional Anisotropic Consolidation of Clay and the Relationship Between Plane Strain and Triaxial Test Data. Proc. of RILEM Symposium on 'The Deformation and Failure of Solids Subjected to Multiaxial Stress', Cannes.

LEWIN, P.I. (1973). The Influence of Stress History on the Plastic Potential. Proc. of Symp. on Plas. and Soil Mech., Cambridge, 96-107.

LEWIN, P.I. and BURLAND, J.B. (1970). Stress-probe Experiments on Saturated N.C. Clays. Geotech., 20: 1, 38-56.

LEWIS, J.G. (1956). Shear Strength of Rockfill. Proc. 2nd Australia-New Zealand CSMFE, Vol. 1,

LE LIEVRE, B. and POOROOSHASB, H.B. (1967) Strains in Triaxial Compression of N.C. Clays. Proc. of 3rd Pan Am Conf. on SM and FE, Venezuela, pp 398-409.

LOUDON, A.G. (1952). The Computation of Permeability from Simple Soil Tests. Geotechnique, 3: 4: 165-183.

LOVE, A.E.H. (1892). A Treatise on the Mathematical Theory of Elasticity. Cambridge University Press.

LOWE, J. (1964). Shear Strength of Coarse Embankment Dam Materials, R.II Q.31, Vol. 3, p 745, 8th ICOLD, Edinburgh.

MAGUIRE, W. M. (1975). The Shear Strength of Upper Lias Clay. Ph. D. Thesis, University of London (in preparation).

MAKHLOUF, H. M. and STEWART, J. J. (1965). Factors Influencing the Modulus of Elasticity of Dry Sand. Proc. 6th Int. Conf. Soil Mech., Montreal, Vol. 1, 298-302.

MARACHI, N. Dean, CHAN, C.K., SEED, H. Bolton and DUNCAN, J. M.(1969) Strength and Deformation Characteristics of Rockfill Materials. Report No. TE 69-5, Dept of Civil Engineering, University of California, Berkeley.

MARSAL, Raúl J. (1963a). Contact Forces in Soils and Rockfill Materials. Proc. 2nd Pan Am. Conf. Soil Mech. Found. Eng., Brazil, Vol. 2, 67-98.

MARSAL, R. J. (1965a). Research on the Behaviour of Granular Materials and Rockfill Samples. Report: Comision Federal de Electricidad, Mexico.

MARSAL, R. J. (1965b) Plane Strain Triaxial Tests of Rockfill Samples. Panel discussion, 6th ICSMFE, Vol. 3, p. 306.

MARSAL, R. J. (1965c) Stochastic Processes in the Grain Skeleton of Soils. Proc. of 6th Int. Conf. SMFE, Montreal, Vol. 1, p. 303.

MARSAL, R. J. (1965d) Contribution to panel discussion, Division 2. Proc. 6th Int. Conf. Soil Mech, Vol. 3: 310-316.

MARSAL, R. J.,, ARELLANO, L.R. De and NUNEZ, A. (1967). Plane Strain Testing of Rockfill Materials. Proc. of 3rd Pan Am. Conf. on SMFE, Caracas, Vol. 1, p. 249-271.

MARSAL, Raúl J. (1967a). Large Scale Testing of Rockfill Materials. Journal of SM and FD, ASCE, Vol. 93, No. SM2, p. 27-43.

MARSAL, R. J. (1967b). Grain Forces in Non-cohesive Soils. Proc. of 3rd Pan Am. Conf on SMFE, Caracas, Vol. 1, p 227-248.

MARSAL, R. J. (1968). Discussion: Large Scale Testing of Rockfill Materials. Proc. ASCE, Vol. 94, No. SM4, p. 1042.

MARSAL, R.J. (1972). Eight Years of Observations at El Infiernillo Dam. Proc. of the Speciality Conf. on 'Performance of Earth and Earth-Supported Structures', Vol. 1, Part I, pp 703-722.

MERKLE, J.G. and MERKLE, D.H. (1969). Discussion on Elastic Behaviour of Cohesionless Soil. J. Soil Mech. Found. Div., ASCE, 95, SM5, 1276-1280.

MOGAMI, T. (1969). Panel Discussion. Proc. of 7th Int. Conf. on SMFE, Mexico, Vol. 3, pp 169-171.

NADAI, A.L. (1963). Theory of Flow and Fracture of Solids. McGraw-Hill.

NAMY, D. (1970). An Investigation of Certain Aspects of Stress-Strain Relationships for Clay Soils. Ph.D. Thesis, Cornell University.

NASH, David, (1971). The Shear Strength and Compressibility of Rockfill. M.Sc. Thesis, University of London.

NITCHIPOROVITCH, A.A. (1964). Deformations and Stability of Rockfill Dams. R.19, Q31, Vol. 3, p.879, 8th ICOLD, Edinburgh.

NITCHIPOROVITCH, A.A. and RASSKAZOV, L.N. (1967). Shear Strength of Coarse Fragmental Materials. Proc. Geotechnical Conf., Oslo, Vol.1, pp 225-229.

NOBARI, E.S. and DUNCAN, J.M. (1972). Movements in Dams due to Reservoir Filling. Proc. of the Speciality Conf. on 'Performance of Earth and Earth-Supported Structures', Vol. 1, Part 1, pp797-815.

OLSON, R.E. and LANGFELLER, L.J. (1965). Pore Water Pressures in Unsaturated Soils. Journal of the Soil Mech and Found. Div. of ASCE, Vol. 91.

PALMER, A.C. (1965). Stress-Strain Relations for Soils. Brown University, Div. of Eng. Tech. Report, GP 1115/19 to the National Science Foundation.

PARKIN, A.K., GERRARD, C.M. and WILLOUGHBY, D.R. (1968). Discussion on 'Deformation of Sand in Hydrostatic Compression' by H.Y.Ko and A.F.Scott. J. Soil Mech. Found. Div. ASCE, Vol. 94, SM1, 336-340.

PEARCE, J.A. (1970) The Behaviour of a Soft Clay in a New True Triaxial Apparatus. Ph.D. Thesis, University of Cambridge.

PENMAN, A.D.M. and CHARLES, J.A. (1971). Measuring Movements of Engineering Structures. Building Research Station Current Paper 32/71, Watford.

PENMAN, A.D.M. and CHARLES, J.A. (1972a). Effect of the Position of the Core on the Behaviour of Two Rockfill Dams. Building Research Station Current Paper 18/72, Watford.

PENMAN, A.D.M. and CHARLES, J.A. (1972b) Constructional Deformations in a Rockfill Dam. Building Research Station Current Paper 19/72, Watford.

PENMAN, A.D.M., BURLAND, J.B. and CHARLES, J.A. (1971). Observed and Predicted Deformations in a Large Embankment Dam During Construction. Building Research Station Current Paper 18/71, Watford.

PIGEON, Y. (1969). The Compressibility of Rockfill. Ph.D. Thesis, University of London.

POOROOSHASB, H.B. and ROSCOE, K.H. (1961). The Correlation of the Results of Shear Tests with Varying Degrees of Dilation. Proc. 5th Int. Conf. Soil Mech. and F.E., Vol. 1, pp 297-304.

POOROOSHASB, H.B., HOLUBEC, I. and SHERBOURNE, A.N. (1966). Yielding and Flow of Sand in Triaxial Compression: Part I. Canadian Geotech. Journal, Vol. 3, No. 4.

POOROOSHASB, H.B., HOLUBEC, I. and SHERBOURNE, A.N. (1967). Yielding and Flow of Sand in Triaxial Compression: Parts II and III, Canadian Geotech. Journal, Vol. 4, No.4.

POPE, R.J. (1967). Evaluation of Cougar Dam Embankment Performance. Journal of the Soil Mech. and Found. Div. ASCE, Vol. 93, No. SM4, pp 231-250.

POWERS, T.C. (1964). Topics in Concrete Technology. Part I: Geometric Properties of Particles and Aggregates. Jour. PCA Res. and Development, January, 2-15.

READES, D.W. (1972). Stress-Strain Characteristics of a Sand Under Three Dimensional Loading. Ph.D. Thesis, University of London.

REES, E.P. and TREVENA, D.H. (1964). Brit. J. Appl. Phys. 15, 337-9.

REES, E.P. and TRAVENA, D.H. (1966). A Study of the Berthelot Method of Measuring Tensions in Liquids. Brit. J. Phys. Vol. 17.

RENDULIC, L. (1936). Poreuziffer und Poreuwasserdruck. Bauingenieur, Vol. 17 - 559.

RENDULIC, L. (1937). Ein Grundgesetz der Ton-mechanik und Sein Experimentaller Beweiss. Bauingenieur, Vol. 18, 459-467.

REYNOLDS, (1878). Mem. Manchr. Lit. Phil. Soc., 17, 159.

RIEKE, H.H. and CHILINGARIAN, G.V. (1974). Developments in Sedimentology. London: Elsevier.

RITTENHOUSE, G. (1943). A Visual Method of Estimating Two Dimensional Sphericity. Journ. Sediment. Petrol., 13: 79-81.

ROBERTS, J.E. and De SOUZA, J.M. (1958). The Compressibility of Sands. Proc. ASTM, Vol. 58, pp 1269-1277.

ROSCOE, K.H. and BURLAND, J.B. (1968). On the Generalized Stress-Strain Behaviour of 'Wet' Clay. Eng. Plasticity, Ed. by J. Heyman and F.A. Leckie, Cambridge University Press, p 535 - 609.

ROSCOE, K.H. and POOROOSHASB, H.B. (1963). A Theoretical and Experimental Study of Strains in Triaxial Compression Tests on Normally Consolidated Clays. Geotechnique, Vol. 13, No. 1, p. 12-38.

ROSCOE, K.H. and SCHOFIELD, A.N. (1964). Stress Dilatancy, Earth Pressure and Slopes - Discussion. Journal of SMFD, ASCE, Vol. 90, SM1, January.

ROSCOE, K.H., SCHOFIELD, A.N. and WROTH, C.P. (1958). On the Yielding of Soils. Geotechnique, 8, 22-53.

ROSCOE, K.H., SCHOFIELD, A.N. and THURAIRAJAH, A. (1963a) Yielding of Clays in States Wetter than Critical. Geotech. Vol. 13, No. 3, pp 211-240, September.

ROWE, P.W. (1962). The Stress-Dilatancy Relation for Static Equilibrium of an Assembly of Particles in Contact. Proc. of Royal Soc. of London, Vol. 269, pp 500-527.

ROWE, P.W. (1963a) Stress-Dilatancy, Earth Pressures, and Slopes. JSMFD, ASCE, Vol. 89, SM3, 37-61.

ROWE, P.W. (1963b) Discussion. Proc. of ASTM Symposium on Lab. Shear Testing of Soils. ASTM Special Technical Publication No. 361, p. 340.

ROWE, P.W. (1969). The Relation Between the Shear Strength of Sands in Triaxial Compression, Plane Strain and Direct Shear. Geotch. Vol. 19, No. 1, pp 75-86.

ROWE, P.W. (1971a). Theoretical Meaning and Observed Values of Deformation Parameters for Soil. Roscoe Memorial Symposium, Cambridge.

ROWE, P.W. (1971b). Discussion on 'Comparison of Stress-Dilatancy Theories' by G.J.W. King and E.A. Dickin. JSMFD, ASCE, Vol. 97, SM4, pp 704-709.

ROWE, P.W., OATES, D.B. and SKERMER, N.A. (1963). The Stress-Dilatancy Performance of Two Clays. Proc. of Symp on Lab. Shear Testing of Soils. ASTM STP No. 361, p. 134.

SANGREY, D.A., HENKEL, D.J. and ESRIG, M.I. (1969). The Effective Stress Response of a Saturated Clay Soil to Repeated Loading. Proc. of the Canadian Geotechnical Journal Vol. 6, pp 241 - 252.

SCHMERTMANN, J.H. and OSTERBERG, J.O. (1960). An Experimental Study of the Development of Cohesion and Friction with Axial Strain in Saturated Soils. Proc. Res. Conf. Shear Strength of Cohesive Soils, Boulder, 643-694.

SCHOFIELD, A.N. and WROTH, C.P. (1968). Critical State Soil Mechanics. McGraw-Hill, London.

SCHULTZE, E. (1957). Large Scale Shear Tests. Proc. of 4th Int. Conf. SMFE, Vol. 1, pp 193-199.

SEED, H.B. and CHAN, C.K. (1966). Clay Strength under Earthquake Loading Conditions. Proc. ASCE, JSMFD, Vol. 92, SM2, pp 53-78.

SEED, H.B. and LEE, K.L. (1966). Liquefaction of Saturated Sands during Cyclic Loading, JSFMD, ASCE, Vol. 92, SM6, 105-134.

SEED, H.B., CHAN, C.K. and MONISMITH, C.L. (1955). Effects of Repeated Loading on the Strength and Deformation of Compacted Clays. Proc. Hwy. Res. Bd. No. 34, pp 541-558.

SHA'AL, B.Z. (1972). The Behaviour of Cohesionless Soils in Simple Shear under Cyclic Loading. Ph.D. Thesis, University of London.

SHARMA, Y.K. (1975). The Particulate Mechanics of Granular Soils. Ph.D. Thesis, University of London.

SHERARD, J.L. et al (1963). Earth and Earth Rock Dams, Engineering Problems of Design and Construction. John Wiley.

SIMONS, N. (1958). Discussion on 'Test Requirements for Measuring the Coefficient of Earth Pressure at Rest. Proc. Brussels Conf. on Earth Pressure Problems, 3, 50-53.

SKEMPTON, A.W. (1948). The Effective Stresses in Saturated Clays Strained At Constant Volume. Proc. of 7th Int. Cong. on Applied Mechanics, London, 378-392.

SKEMPTON, A.W. (1953). Soil Mechanics in Relation to Geology. Proc. Yorkshire Geol. Soc., 29, No.3.

SKEMPTON, A.W. (1954). The Pore Pressure Coefficients A and B. Geotechnique, Vol. 4, No. 4, 143-147.

SKEMPTON, A.W. (1960). Effective Stresses in Soils, Concrete and Rocks. Proc. of Pore Pressure and Suction in Soils, 4-16.

SKEMPTON, A.W. (1961). Horizontal Stresses in an Over-Consolidated Eocene Clay. Proc. 5th Int. Conf. Soil Mech. Paris, 1, 351-357.

SKEMPTON, A.W. and SOWA, V.A. (1963). The Behaviour of Saturated Clays During Sampling and Testing. Geotechnique, Vol. 13, 269-290.

SKINNER, A.E. (1969). A Note On The Influence of Interparticle Friction On The Shearing Strength of a Random Assembly of Spherical Particles. Geotech. Vol. 19, No. 1, pp 150-157.

SKINNER, A.E. (1975). The Effect of High Pore Water Pressure on the Mechanical Behaviour of Sediments. Ph.D. Thesis, University of London.

SOWERS, G.F., WILLIAMS, R.C. and wallace, T.S. (1965). Compressibility of Broken Rock and the Settlement. Proc. 6th Int. Conf. Soil Mech. Found. Eng. Montreal, Vol. 2, 561-565.

SULTAN, H.A. and SEED, H.B. (1967). Stability of Sloping Core Earth Dam. Journal, Soil Mech. and Found Div. ASCE, Vol. 93, SM4, pp 45-67.

TATSUOKA, F. and ISHIHARA, K. (1974). Yielding of Sand in Triaxial Compression. J. Japanese Soc. Soil Mech. Found. Eng. Vol. 14, No. 2, 63-76.

TAYLOR, D.W. (1944). Cylindrical Compression Research Programme on Stress-Deformation and Strength Characteristics of Soils. MIT 10th Progress Report to US Engineers Department.

TAYLOR, D.W. (1948). Fundamentals of Soil Mechanics. New York: John Wiley.

TAYLOR, G.I. and QUINNEY, H. (1931). The Plastic Distortion of Metals. Phil. Trans. Roy. Soc. A. 230.

TEMPERLEY, H.N.V. (1946). The Behaviour of Water under Hydrostatic Tension, II. Proc. Phys. Soc. 58, 436.

TEMPERLEY, H.N.V. and CHAMBERS, L.L.G. (1946). The Behaviour of Water under Hydrostatic Tension, I. Proc. Phys. Soc. 58, 420.

TERZAGHI, K. (1932). Tragfahigkeit der Flachgründungen. Int. Assoc. Bridge Struct. Eng. Prelim. Publ. 659-683.

TERZAGHI, K. (1936). The Shearing Resistance of Saturated Soils and the Angle Between the Planes of Shear. Proc. 1st Int. Conf. Soil Mech., 1, 54-56.

TERZAGHI, K. (1943). Theoretical Soil Mechanics. New York: John Wiley.

TERZAGHI, K. (1960). Discussion of Steele and Cooke, 1958. Proc. ASCE, Vol. 86, PO1, February, p.65.

TERZAGHI and PECK (1967). Soil Mechanics in Engineering Practice. 2nd Edn. John Wiley & Sons, London.

TOMBS, S.G. (1969). Strength and Deformation Characteristics of Rockfill. Ph.D. Thesis, University of London.

TROLLOPE, D.H. and PARKIN, A.K. (1963). Discussion on 'Stress-Dilatancy, Earth Pressure and Slopes' by P.W. ROWE. JSMFD, ASCE, Vol. 89, SM6, pp 129-133.

U.S. Army Corps of Engineers (1967). Shear Strength of Rockfill. USA Army Engineer. Div. Laboratory, South Pacific, Engineering Study 526.

U.S. Bureau of Reclamation (1963). Earth Manual. pp 783.

VESIC, A. and BARKSDALE, R.D. (1963). Discussion on Testing Methods and New Equipment. ASTM Symposium on Laboratory Shear Testing of Soils, STP No. 361, pp 301-305.

VESIC, A.S. and CLOUGH, G.W. (1968). Behaviour of Granular Materials Under High Stresses. Journal of Soil Mech. and Found. Eng. ASCE, pp 661-688.

WESTMAN, A.E.R. (1932). The Effect of Mechanical Pressure on the Imbibitional and Drying Properties of Some Ceramic Clays, I, II. J. Amer. Ceramic Soc. 15, 552-563, and 16, 256-264.

WILSON, G. and SUTTON, J.L.E. (1948). A Contribution to the Study of the Elastic Properties of Sand. Proc. 2nd Int. Conf. Soil Mech., Rotterdam, Vol. 1, 197-202.

WINTERKORN, H.F. (1953). The Condition of Water in Porous Systems. Soil Sci., Vol. 55.

WISSA, A.E.Z. (1969). Pore Pressure Measurement in Saturated Stiff Soils. J. Soil Mech. Found. Div. ASCE, 95, SM4, 1063-1073.

WROTH, C.P. (1971). Some Aspects of the Elastic Behaviour of Overconsolidated Clay. Roscoe Memorial Symposium, Cambridge.

WROTH, C.P. and BASSETT, R.H. (1965). A Stress-Strain Relationship for the Shearing Behaviour of a Sand. Geotechnique, Vol. 15, No. 1, pp 32-56.

YEE, Hsu Chueh (1972). Some Characteristics of Creep and Strength of Granular Soil at High Pressure. M.Sc. Thesis, University of Birmingham.

ZELLER, J. and WULLIMANN, R. (1957). The Shear Strength of Shell Materials for the Goeschenenalp Dam, Switzerland. Proc. 4th Int. ICSMFE, London, Vol. 2, p 399.